

NHC-supported Disilavinylidenes and Oxysilylenes: Synthesis, Characterization and Reactivity Studies

Dissertation

Submitted in fulfillment of the degree
doctor rerum naturalium
(Dr. rer. nat.)

of the
Faculty of Mathematics and Natural Sciences
of the
University of Bonn

by
Simon Schwarzwald, M.Sc.
née Krämer, born in Bonn, Germany

Bonn, 2022

Prepared with the consent of the Faculty of Mathematics and Natural Sciences of the University of Bonn.

Members of the doctoral committee:

1st Examiner: Prof. Dr. Alexander C. Filippou
2nd Examiner: Prof. Dr. Rainer Streubel
3rd Examiner: Prof. Dr. Arne Lützen
4th Examiner: Prof. Dr. Nikolaus Froitzheim

Date of viva: 4.4.2023

Year of publication: 2023

“In the fields of observation chance favours only the prepared mind.”

– Louis Pasteur, Lille, 1854

Acknowledgments

First and foremost, I would like to express my gratitude to Prof. Dr. Alexander C. Filippou for his invaluable guidance and trust during my doctoral studies and constructive feedback on this work. Additionally, I am very thankful for the chance to pursue the challenging research topic in a suitable, well-equipped inert-gas chemistry laboratory.

Furthermore, I would like to thank Prof. Dr. Rainer Streubel for his co-mentorship within the framework of the Bonn International Graduate School of Chemistry.

The important contributions of several people crucially facilitated the preparation of this doctoral thesis. Therefore, I would like to thank in particular:

- Dr. Priyabrata Ghana for his pioneering work in disilavinylidene chemistry and kind advice throughout the years
- Dr. Ujjal Das for his advice and proofreading the first draft of this work
- Dr. Gregor Schnakenburg for the single-crystal X-ray diffraction analyses, quantum-chemical calculations and correcting the theoretical parts of this work
- Jens Rump for quantum-chemical calculations and and, even more, for enduring patience in discussions resulting thereof
- Dr. Jürgen Tirrée for his experience and continuous efforts to keep the lab running
- My B.Sc. project students Christian Lippmann, Lucar Rothe and Marvin Schumacher for their enthusiasm, thirst for knowledge and new perspectives
- Katrin Werthmann and Joana Tewes for the synthesis of precious starting materials and great company
- Charlotte Rödde for the single-crystal X-ray diffraction analyses
- Dr. Andreas Lülldorf, Marcel Krumpholz and Leonard Maurer for the UV-Vis measurements
- Dr. Senada Nozinovic, Dipl.-Ing. Karin Prochnicki, Hannelore Spitz, and Ulrike Weynand for the recording of countless NMR spectra

I am also grateful to all current and former group members for productive scientific and non-scientific discussions both in the lab and in our free time. I very much appreciate your kindness and help throughout the years.

Finally, I would like to thank my wife Babsi, my family and good friends for the constant emotional support. Without you, this work would not have been possible.

Contents

1	Introduction	1
1.1	Low-coordinate silicon chemistry	2
1.2	General structure and objective of this work	11
2	Part I: Disilavinylidene Chemistry	13
2.1	Introduction	13
2.2	Substitution of the Si-Br bond.....	20
2.2.1	Lithiation attempts	20
2.2.2	Alkylation of 1	25
2.2.3	Unexpected role of the alkali metal	31
2.2.4	Proposed reaction mechanisms	36
2.3	Diastereoselective reaction with acetone	41
2.4	Synthesis of zinco-silylenes	46
2.5	An aromatic {Si ₂ P ₂ C} five-membered ring	52
2.6	Coinage metal complexes.....	64
2.6.1	Fluxional complexes of Cu(I) and Ag(I)	66
2.6.2	Push-pull complex of a disilyne.....	74
2.6.3	Cationic Cu ⁺ complexes	81
2.6.4	Liberation of an NHC-stabilized disilyne	83
2.6.5	Disilyne-Disilavinylidene-Isomerization.....	85
2.7	Summary & Outlook: Disilavinylidene Chemistry	95
2.7.1	Summary	95
2.7.2	Outlook	100
3	Part II: Oxysilylenes	103
3.1	Introduction	103
3.1.1	Heavier di(oxy)tetrylenes E(OR) ₂	104
3.1.2	Oxysilylenes.....	106
3.2	Synthesis of Base-stabilized Oxysilylenes	108

3.3	Synthesis of Cp*Si(OAr ^{Mes})	113
3.4	Excursus: Synthesis of Si{N(Me)Ar ^{Mes} } ₂	117
3.5	The first di(aryloxy)silylene	122
3.6	Reactivity of Si(OAr ^{Mes}) ₂	128
3.6.1	Thermolysis of Si(OAr ^{Mes}) ₂	129
3.6.2	Base coordination	130
3.6.3	Protonation	132
3.6.4	Silane activation	136
3.6.5	Reactions with BX ₃ and PCl ₃	146
3.6.6	Addition of ZnMe ₂	152
3.6.7	Ambiphilic reaction with a diazoalkane	156
3.7	Summary & Outlook: Oxysilylene chemistry	164
3.7.1	Summary	164
3.7.2	Outlook	170
4	Experimental Part	173
4.1	General Part	173
4.2	Analytical Methods	175
4.3	Commercially available starting materials	180
4.4	Literature-known starting materials	181
4.5	Additional spectroscopic data and improved syntheses of known compounds...	183
4.5.1	(E)-(SIDipp)Si=Si(Br)Tbb (1)	183
4.5.2	Cp*SiBr ₃	185
4.5.3	Benzyl lithium (LiCH ₂ Ph·(thf) _{1.25})	187
4.5.4	Benzyl sodium (NaCH ₂ Ph)	187
4.6	Syntheses of novel Compounds	188
4.6.1	[(SIDipp)Si(Li·dme)Si(H){C(SiMe ₃) ₂ -C ₆ H ₂ -4-tBu,6-(CH)(SiMe ₃) ₂ }] (2)	188
4.6.2	(E)-(SIDipp)Si=Si(CH ₂ Ph)Tbb (1-Me)	189
4.6.3	(E)-(SIDipp)Si=Si(CH ₃)Tbb (1-CH ₂ Ph)	190
4.6.4	cyclo-{Si(SIDipp)(SiHTbb)(CHPh)} (3)	192

4.6.5	SiH[SiBr{OC(CH ₂)Me}Tbb](SIDipp) (4)	195
4.6.6	Si(ZnBr)(SiCl ₂ Tbb)(SIDipp) (5-Cl)	196
4.6.7	Si(ZnBr)(SiBr ₂ Tbb)(SIDipp) (5-Br).....	197
4.6.8	Si(ZnBr)(SiBrCH ₂ PhTbb)(SIDipp) (6)	198
4.6.9	cyclo-Si[C{ONa(thf)}PSi(Tbb)P](SIDipp) (7).....	199
4.6.10	[Ag{η ¹ -(Z)-(SIDipp)Si=Si(Br)Tbb}][OTf] (9)	201
4.6.11	CuBr{η ² -(Z)-(SIDipp)Si=Si(Br)Tbb} (10)	202
4.6.12	[Cu{(Z)-(SIDipp)Si=Si(Br)Tbb}][B(Ar ^F -CF ₃) ₄] (11)	203
4.6.13	CuBr{η ² -(Z)-(SIDipp)(OtBu)Si=SiTbb} (12).....	206
4.6.14	[Cu{η ² -(Z)-(SIDipp)(OtBu)Si=SiTbb}][BAr ^F ₄] (13).....	207
4.6.15	(Z)-TbbSi=Si(OtBu)(SIDipp) (14).....	209
4.6.16	(Z)-SIDippSi=Si(OtBu)Tbb (15)	210
4.6.17	SiBr(OtBu)(SIDipp) (16-Br)	210
4.6.18	SiI(OtBu)(IDipp) (16-I).....	211
4.6.19	Cp*SiOAr ^{Mes} (17)	212
4.6.20	Si{N(Me)Ar ^{Mes} } ₂ (18)	213
4.6.21	Si(OAr ^{Mes}) ₂ (19)	214
4.6.22	Attempted synthesis of Si nanoparticles from 19.....	216
4.6.23	Si(OAr ^{Mes}) ₂ (IMe ₄) (19-IMe ₄)	217
4.6.24	SiHCl(OAr ^{Mes}) ₂ (19-HCl).....	218
4.6.25	SiH(OC(CF ₃) ₃)(OAr ^{Mes}) ₂ (19-HOtBu ^F)	219
4.6.26	SiI(SiH ₂ I)(OAr ^{Mes}) ₂ (19-SiH ₂ I ₂)	220
4.6.27	SiI{SiH ₂ (OC ₄ H ₈ I)}(OAr ^{Mes}) ₂ (20).....	222
4.6.28	SiCl(SiHCl ₂)(OAr ^{Mes}) ₂ (19-SiHCl ₃).....	223
4.6.29	SiCl ₂ (OAr ^{Mes}) ₂ (19-Cl ₂).....	224
4.6.30	SiBr ₂ (OAr ^{Mes}) ₂ (19-Br ₂)	225
4.6.31	SiI ₂ (OAr ^{Mes}) ₂ (19-I ₂).....	226
4.6.32	SiCl ₃ (OAr ^{Mes}) (21-Cl)	227
4.6.33	SiBr ₃ OAr ^{Mes} (21-Br).....	228

4.6.34	SiI ₃ OAr ^{Mes} (21-I).....	229
4.6.35	Attempted syntheses of SiX(BX ₂)(OAr ^{Mes}) (19-BX ₃)	230
4.6.36	SiCl(PCl ₂)(OAr ^{Mes}) ₂ (19-PCl ₃).....	231
4.6.37	SiMe(ZnMe)(OAr ^{Mes}) ₂ (19-ZnMe ₂)	232
4.6.38	Si(HN=NC(H)Tips)(NN≡CTips)(OAr ^{Mes}) ₂ (22)	233
4.6.39	[Cu(LiPr ₂ Me ₂)(SIDipp)]Br	234
4.6.40	[Cu(LiPr ₂ Me ₂) ₂ Br]	235
4.6.41	[iPrO(H)C{N(Dipp)CH} ₂]	236
5	Appendices.....	237
5.1	Determination of symmetry from ¹ H NMR spectra	237
5.2	Crystallographic data files of novel compounds	239
5.3	Supporting Crystal structures	250
5.3.1	SiH[SiBr{OC(CH ₂)Me}Tbb](SIDipp) (4).....	250
5.3.2	Si(ZnBr)(SiBrCH ₂ PhTbb)(SIDipp) (6).....	251
5.3.3	SiHBr(OAr ^{Mes}) ₂ (19-HBr) and SiHI(OAr ^{Mes}) ₂ (19-HI)	252
5.3.4	SiBr ₃ OAr ^{Mes} and SiI ₃ OAr ^{Mes} (21-Br and 21-I)	253
5.3.5	S(SO ₃)(IDipp)·C ₆ H ₆ and SO ₃ (IDipp)	254
5.3.6	[Cu(LiPr ₂ Me ₂)(SIDipp)]Br and [CuBr(LiPr ₂ Me ₂)(SIDipp)].....	255
5.3.7	[H(IMe ₄)](OAr ^{Mes})·C ₆ H ₆	257
5.3.8	Ar ^{pToi} Br.....	258
5.3.9	Ar ^{pToi} SiCl ₃	258
5.3.10	[H(SIDipp)] ₄ [Sb ₄ I ₁₆]·C ₆ H ₆	260
5.4	Supporting Crystallographic data files	262
5.5	UV-vis-NIR spectra	265
5.5.1	(Z)-(SIDipp)Si=Si(Br)Tbb (1).....	265
5.5.2	(E)-(SIDipp)Si=Si(Me)Tbb (1-Me).....	266
5.5.3	(E)-(SIDipp)Si=Si(CH ₂ Ph)Tbb (1-CH ₂ Ph)	267
5.5.4	cyclo-Si[C{ONa(thf)}PSi(Tbb)P](SIDipp) (7)	268
5.5.5	CuBr{η ² -(Z)-(SIDipp)Si=Si(Br)Tbb} (10).....	269

5.5.6	CuBr{(Z)-(SIDipp)(OtBu)Si=SiTbb} (12).....	270
5.5.7	Si(OAr ^{Mes}) ₂ (19).....	271
5.6	Kinetic- and variable temperature NMR studies.....	273
5.6.1	SiH[SiBr{OC(CH ₂)Me}Tbb](SIDipp) (4).....	274
5.6.2	Isomerization of 14 into 15.....	275
5.7	Results of quantum chemical calculations.....	276
5.7.1	(SIDipp)Si=Si(Br)Tbb and (SIDipp)Si=Si(CH ₂ Ph)Tbb (1 and 1-CH ₂ Ph)....	276
5.7.2	SiH[SiBr{OC(CH ₂)Me}Tbb](SIDipp) (4).....	276
5.7.3	Si(ZnBr)(SiBrCH ₂ PhTbb)(SIDipp) (6).....	278
5.7.4	CuBr{(Z)-(SIDipp)Si=Si(Br)Tbb} (10) and CuBr{(Z)-(SIDipp)(OtBu)Si=SiTbb} (12).....	279
5.7.5	(SIDipp)(tBuO)Si=SiTbb and (SIDipp)Si=Si(OtBu)Tbb (14 and 15).....	280
5.7.6	cyclo-Si[C{ONa(thf)}PSi(Tbb)P](SIDipp) (7 _{calc} ⁻).....	281
5.7.7	Si{N(Me)Ar ^{Mes} } ₂ (18).....	283
5.7.8	Si(OAr ^{Mes}) ₂ (19).....	284
5.7.9	SiX(BX ₂)(OAr ^{Mes}) ₂ or Si(BX ₃)(OAr ^{Mes}) ₃ : 19-BX ₃ or 19·BX ₃ ?.....	286
5.8	Indices.....	288
5.8.1	List of abbreviations.....	288
5.8.2	Enumeration of compounds discussed in this work.....	290
5.8.3	Abbreviation of Substituents.....	293
5.8.4	Enumeration of literature-known compounds.....	294
5.8.5	List of tables.....	295
5.8.6	List of figures.....	297
5.8.7	List of schemes.....	300
5.9	Curriculum vitae.....	303
5.10	Oath of Compliance with the Principles of Scientific Integrity.....	304
6	References.....	305

1 Introduction

Among all elements of the periodic table, carbon, the “element of life”, takes an outstanding importance. Its unique combination of versatility and controllability is the common basis of all biological systems and driving force of the innumerable accomplishments of organic chemistry. Its next heavier homologue is of literally fundamental importance: accounting for about 26 % of the earth’s crusts mass, silicon is the second most abundant element after oxygen and usually found in form of silicates and silica.^[1] Modern society utilizes these ubiquitous minerals with wide-ranging applications. With a consumption of 28.6 gigatons in 2018, sand and gravel are the world’s most commonly used resource after air and water and essential for building construction e.g. as concrete, asphalt, glass or mortar.^[2,3] Elemental silicon has importance in metallurgy and ultrapure, crystalline silicon is effectively employed as semiconductor materials in microelectronics taking advantage of its diamond like network structure whereas applications of polymeric silicones in everyday life include rubber, oils, grease or resins.^[1] But when it comes to molecular compounds, the unique versatility of carbon chemistry cannot be achieved.

Although chemical elements belonging to the same group of the Periodic Table often exhibit similar properties and reactivities, the vastly different physical properties of carbon and silicon and of famous simple compounds such as CO₂ and SiO₂ are commonly known. The reasoning behind this discrepancy mostly lies in the anomalously lower electronegativity of silicon (C: 2.55, Si: 1.90; Pauling scale), its larger atomic radius (C: 77 pm, Si: 117 pm) and the substantial difference in the size of the s- and p-valence orbitals (Figure 1) which, in turn, is responsible for diminished propensity of silicon to form hybrid orbitals.^[1,4,5]

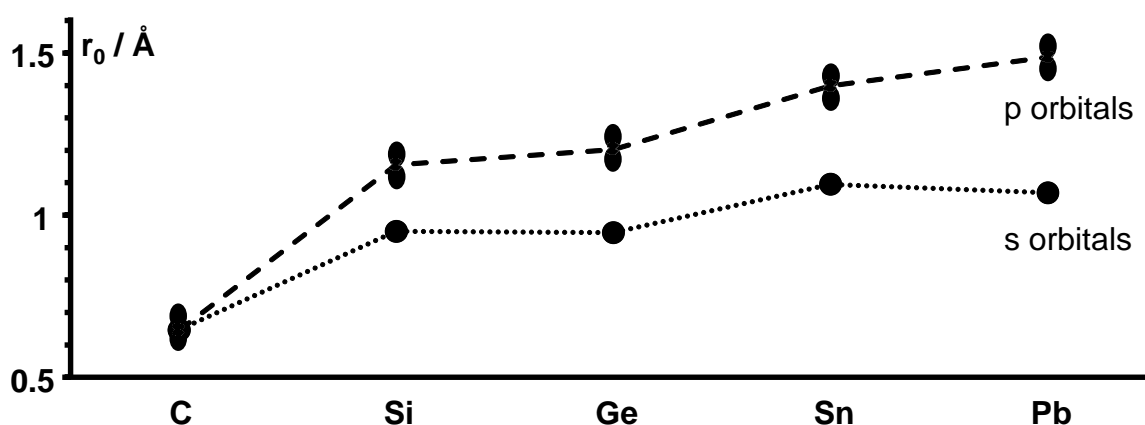


Figure 1. Expected radii (Å) of maximum radial density r_0 of the respective s- and p-valence orbitals of group 14 elements. The values were taken from the literature.^[6]

In a valence bond picture, a C=C double bond is formed between two sp² hybridised carbon atoms by overlapping of the sp² hybrid orbitals (σ bond) and 2p orbitals (π bond). The reluctance of silicon to form these hybrid orbitals therefore hampers the formation of classical

multiple bonds and was historically summarized in the empirical “multiple bond rule”, that declared the formation of stable $(np-p(n+1))\pi$ ($n \geq 2$) bonds between main group elements beyond the second period impossible.^[6] This rule was first debunked by Lappert in the 1970s by isolation of the distannene $(\text{dsi})_2\text{Sn}=\text{Sn}(\text{dsi})_2$ ($\text{dsi} = \text{CH}(\text{SiMe}_3)_2$) which dissociates in solution but features a weak $\text{Sn}=\text{Sn}$ double bond in the solid state.^[7,8] Weak nonclassical attractive effects between the substituents are nowadays known to play a vital role in the bonding of E_2R_4 and E_2R_2 (vide infra, $\text{E} = \text{Sn}$ or Pb , $\text{R} =$ bulky substituent).^[9]

1.1 Low-coordinate silicon chemistry

The earliest milestone of modern low-coordinate molecular silicon chemistry is the year 1981, which marks the isolation of the first thermally stable¹ silene (silaalkene) $(\text{Me}_3\text{Si})_2\text{Si}=\text{C}(\text{OSiMe}_3)\text{Ad}$ ($\text{Ad} = 1\text{-adamantyl}$) as well as the first disilene $\text{Mes}_2\text{Si}=\text{SiMes}_2$ ($\text{Mes} =$ mesityl) each of them synthesized by photolysis reactions in the group of Brook and West, respectively (Figure 2).^{[10–13], 2}

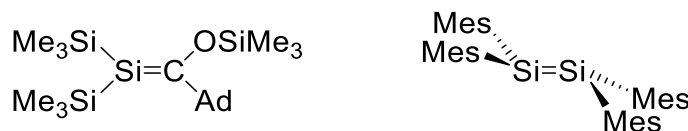


Figure 2. The first isolable silene (left) and disilene (right) are kinetically stabilized by large substituents.^[10–13]

While silenes typically adopt the expected planar structure of alkenes, heavier ditetrylenes usually feature a pyramidalization of the tetrel atoms that leads to trans-bending of the substituents (from $\theta \approx 15^\circ$ for $\text{E} = \text{Si}$ to 70° for $\text{E} = \text{Pb}$).^[16,6,17,18]

In the Carter–Goddard–Malrieu–Trinquier (CGMT) model, the $\text{E}=\text{E}$ double bonding is essentially described as a double donor-acceptor interaction (or Lewis acid/base adduct formation) between two ambiphilic tetrylenes $\{:\text{ER}_2\}$, see page 6} in their electronic singlet ground state due to the aforementioned insufficient hybridization of the heavier tetrel atoms (Figure 3). The greater the hybridization (corresponding to a smaller energy difference between the singlet- and triplet state $\Delta E_{\text{S-T}}$), the less are the trans-bending and twisting deformations. Moreover, the CGMT model correlates the trans-bending with $\text{E}=\text{E}$ bond cleavage energy and singlet-triplet energy gaps of the tetrylene fragments. Once the value of the bond cleavage energy (total intrinsic interaction energy, BCE) is higher than the double of energy difference

¹ In this work, the term „stable“ refers to compounds that can be isolated in absence of air under an atmosphere of protecting gas without thermal decomposition within a reasonable time. Most compounds described here will readily react with traces of air, moisture and/or aggressive solvents such as CHCl_3 .

² Transient disilenes were studied under matrix isolation conditions by Peddle since the early 1970s.^[14,15]

between the singlet- and triplet states of the tetrylene fragments ($BCE > 2 \cdot \Delta E_{s-t}$), no trans-bending is expected.^[19,20,4]

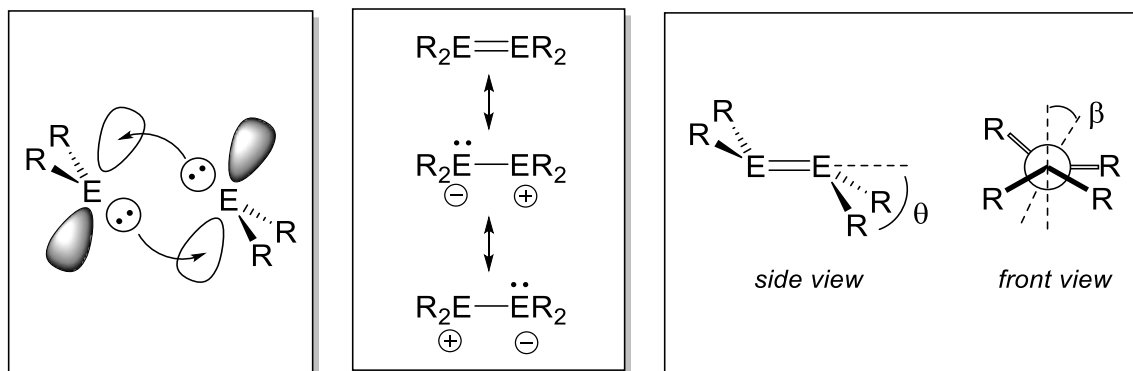


Figure 3. Double donor-acceptor bonding model (left) and valence-bond description (middle) of heavy ditetrylenes.^[18,21,22] The trans-bent angle θ is measured between the E=E bond vector and the plane defined by the substituents; the twisting angle (β) highly depends on the E=E distance, steric bulk and nonclassical interactions between the individual substituents.^[9] For example $\text{Mes}_2\text{Si}=\text{SiMes}_2$: $d = 2.160 \text{ \AA}$, $\theta = 18^\circ$ and $\beta = 5^\circ$;^[12] $\text{Mes}_2\text{Ge}=\text{GeMes}_2$: $d = 2.2856(8) \text{ \AA}$, $\theta = 33^\circ$ and $\beta = 3^\circ$.^[23] For the electronic structure of tetrylenes, see also Figure 6 on page 6.

Another approach based on molecular orbital (MO) theory is the second order Jahn-Teller effect (SOJT). Mixing bonding σ - and π -orbitals (a_g and b_{2u}) with the of symmetry related antibonding counterparts, b_{1g} and b_{3u} , respectively, leads to an overall reduced energy and symmetry reduction from D_{2h} (planar E_2R_4) to C_{2h} (trans-bent E_2R_4) (Figure 4). This model not only rationalizes the trans-bending of the substituents but also correctly predicts the weakening of the E-E σ -bond, which is also observed experimentally for the tin- and lead homologues.^[18,21,22]

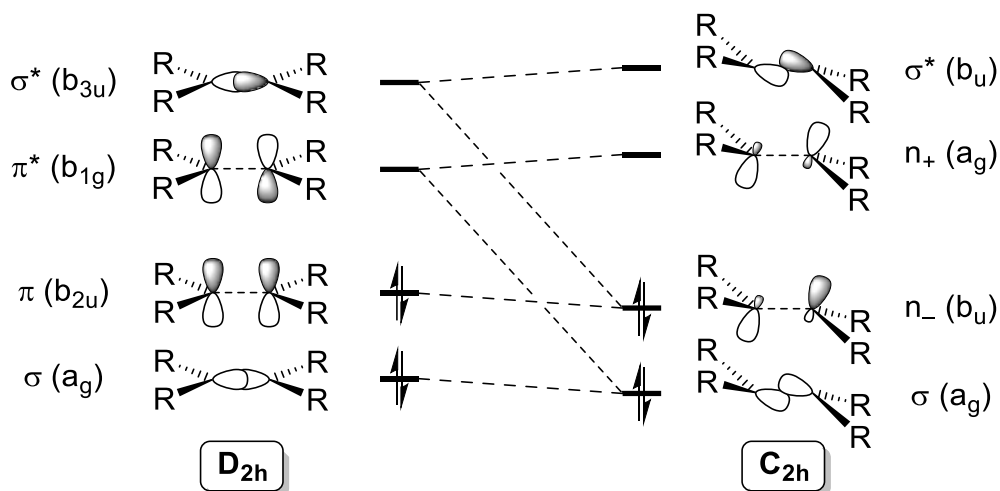


Figure 4. Second-order Jahn-Teller distortion in heavier ditetrylenes.^[18,21,22]

Presently, Wests $\text{Mes}_2\text{Si}=\text{SiMes}_2$ is the first among plethora of derivatives which have been reported so far (Figure 5).^[16,24-27] Stable disilenes are typically obtained by reductive coupling of substituted halosilanes $\text{R}_n\text{SiX}_{3-n}$ ($n = 1$ or 2). They often readily react with oxidizing or reducing

agents and can undergo both electrophilic and nucleophilic 1,2-additions or cycloaddition reactions.^[16,24-27] A particularly fruitful subclass are nucleophilic disilenides (or metalladisilenes $R_2Si=Si(M)R$),^[28-33] which were used as starting materials for substituted disilenes including linked bis(disilenes) or in various transmetallation experiments.^[34-39] The most famous $Trip_2Si=Si(Li)Trip$ ($Trip = 2,4,6$ -triisopropylphenyl) was first mentioned as a reactive intermediate by Weidenbruch in 1997^[28] and isolated by Scheschkewitz in 2004 after reduction of $SiCl_2Trip_2$ by lithium power.^[29] Examples of highly reactive dimetalladisilenes $Ar(M)Si=Si(M)Ar$ coordinated by K^+ or $[Cu(PMe_3)]^+$ were recently synthesized in the Filippou group^[40-42] and a magnesium derivative was obtained by Cui from $SiBr_3(boryl)$,^[43] but disilenides can also be obtained in situ from silyl-substituted disilenes by silyl abstraction using $KOtBu$ under relatively mild conditions.^[44] A counterpart are the electrophilic 1,2-dihalodisilenes. The first silyl-substituted derivative was mentioned by Wiberg in 2004^[45] and examples with large aryl groups were later isolated by Tokitoh and Tamao.^[46-48] Monomerization of 1,2-dibromodisilenes has been discussed in the literature^[40,47,49] and they have been utilized as sources for base-stabilized silylenes ($SiR_2(carbene)$)^[40,48,50,51] or for the generation of silicon-transition metal multiple bonds in silylidene ($L_nM=SiR_2$) and silylidyne ($L_nM\equiv SiR$) complexes by the groups of Tokitoh and Filippou.^[40,52-55,51]

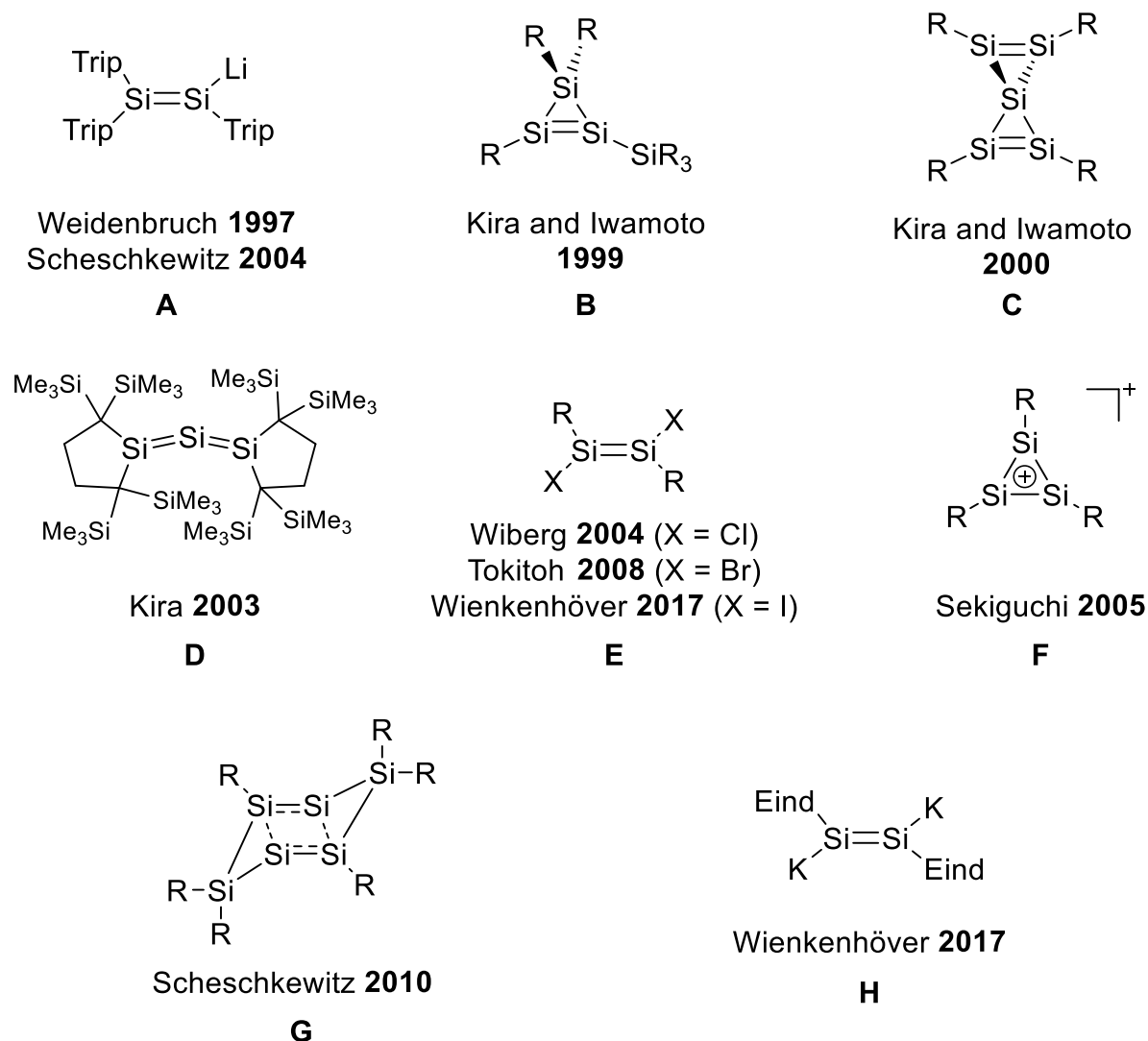
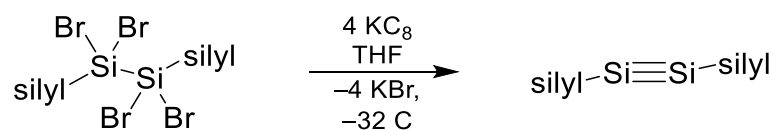


Figure 5. Selected examples of compounds containing Si=Si double bonds: a metalladisilene (**A**, Trip = 2,4,6-triisopropylphenyl),^[28,29] a cyclotrisilene (**B**) and its spirocyclic congener (**C**, R=Si(tBu)Me₂),^[56,57] a trisilaallene (**D**),^[58] 1,2-dihalodisilenes (**E**; X = Cl,^[59] Br,^[46] I^[40]; R = silyl or aryl), an aromatic cyclotrisilenylium ion (**F**, R = SiMe(tBu)₂, anion = B{2,3,5,6-F₄,C₆H₃}₃),^[60] an aromatic dismutational isomer of hexasilabenzene (**G**, R = 2,4,6-triisopropylphenyl),^[61] and a dimetalladisilene (**H**, Eind = 1,1,3,3,5,5,7,7-octa-ethyl-*s*-hydrindacen-4-yl).^[40]

The first spectroscopic characterization of a compound with a Si≡Si triple bond was achieved by Wiberg and coworkers in 2002^[59] but the group of Sekiguchi was the first to isolate a stable disilyne (R-Si≡Si-R) after reduction of a tetrabromodisilane in 2004 (Scheme 1).^[62] Other methods for the synthesis of disilynes are reduction of 1,2-halodisilenes, oxidation of disilene dianions or synproportionation of a mixture.^[45,63,42]



Scheme 1. Synthesis of the first isolable disilyne by Sekiguchi. silyl = Si(iPr)dsi₂; dsi = CH(SiMe₃).^[62]

Silylenes ($:\text{SiR}_2$) are the formal dissociation products of disilenes: molecular, neutral, divalent and two-coordinated congeners of carbenes with six valence electrons. In contrast to carbenes, silylenes generally adopt an electronic singlet ground state³ (see Figure 7 on page 7) due to the larger relative size difference of the valence orbitals of silicon which decreases the electron-electron repulsion of the electron lone pair.^[68,67] This electronic structure directly explains the ambiphilic nature of silylenes: they can act as strong electrophiles (Lewis acids) due to the unoccupied p-orbital or as nucleophiles (Lewis bases) via their free electron lone pair.^[69]

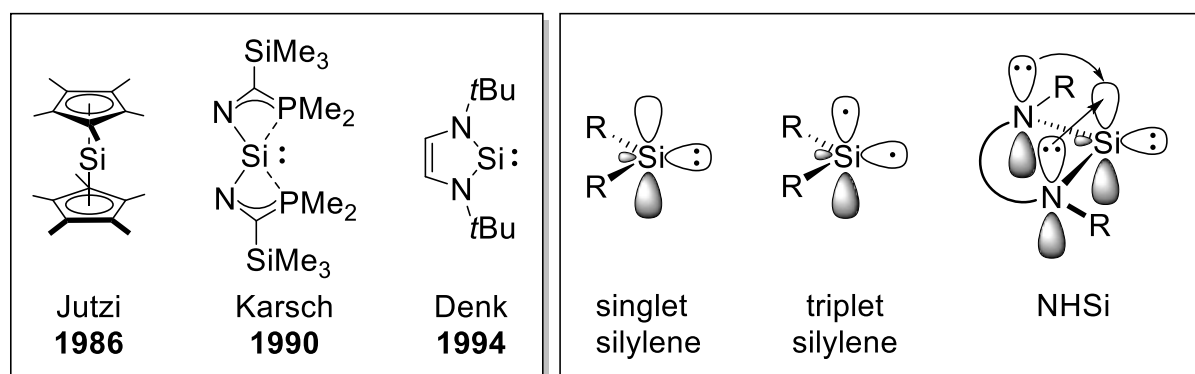


Figure 6. Selected monomeric Si(II) compounds (left); schematic orbital depiction of singlet- and triplet silylenes as well as π -donation in NHSis (right). Formal charges are omitted for simplicity.

The first isolable monomeric molecular Si(II) compounds are Jutzi's decamethylsilicocene (SiCp^{*2} , $\text{Cp}^* = 1,2,3,4,5$ -pentamethylcyclopentadienyl) and Karsch's spirocyclic bis(diphosphino) silicon(II) compound $\text{Si}\{\eta^2\text{-(Me}_2\text{P)}_2\text{C(SiMe}_3)\}_2$, which were published in 1986 and 1990, respectively.^[70,71] However, both exhibit hypercoordinated Si atoms and are hence not considered silylenes. Only after the pioneering invention of N-heterocyclic carbenes (NHCs) by Arduengo in 1991,^[72] an analogous stable N-heterocyclic silylene (NHSi) was synthesized by Denk and West only three years later (Figure 6).^[73] Parallel to the rise of the omnipresent NHCs in molecular chemistry,^[74–76] the chemistry of NHSis has flourished since the 1990s. They've found some application as ligands in catalysis and their reactivity has been recently covered in several review articles.^[69,77–82] Akin to the aforementioned monomeric Si(II) compounds, their electrophilicity is reduced by the combination of electronic σ -accepting and π -donating properties of the adjacent N-atoms which greatly increases their stability (Figure 6, right). These “tamed” silylenes can often still react ambiphilic but are mostly considered as nucleophiles. Thermodynamic stabilization was refined over the years and popular motifs are depicted in Figure 7. Especially the use of 1,3-diketimine (nacnac-type) ligands (**B**)^[83] by Driess

³ The singlet ground state can be destabilized by large, electropositive silyl substituents to decrease $\Delta E_{s-\tau}$. A first candidate of a triplet silylene, $\text{Si}\{\text{Si}(\text{iPr})_3\}_2$, was discussed in 2001 based on its reactivity but rejected by theory.^[64,65] Two years later, Sekiguchi et. al. described the direct characterization of the triplet-silylene $\text{Si}\{\text{Si}(\text{tBu})_3\}_2$ by electron spin resonance (ESR) spectroscopy below 80 K.^[66] But until today, no stable derivative is known to literature.^[67]

since 2006 as well as the discovery of a chlorosilylene $\text{Si}(\text{Cl})\{\text{N}_2(\text{tBu})_2\text{CPh}\}$ stabilized by a benzamidinate ligand (**C**)^[84] by Roesky in the same year gave access to a plethora of functionalized silylenes that found application as ligands or in small molecule activation.^[85,69]

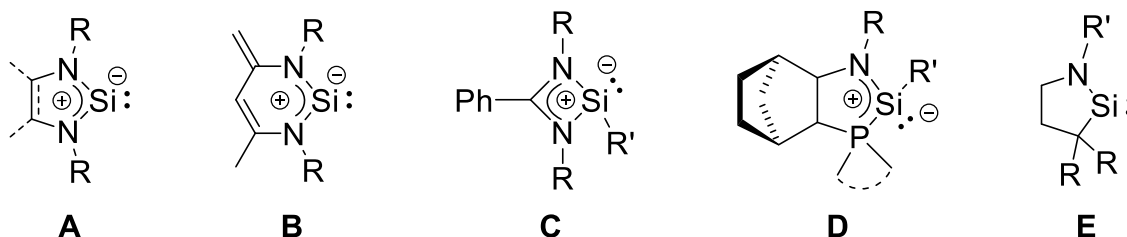


Figure 7. General formulae of classical divalent N-heterocyclic silylenes (**A**)^[73] and **B**)^[83] as well as three-coordinated amidinato-silylenes (**C**)^[84], N,P-phosponium-silylenes (**D**)^[86] and cyclic alkyl(amino)silylenes (**E**)^[87].

In this context, it should be noted that formally neutral donating groups such as the aforementioned nacnac- and benzamidinato-substituents or external Lewis bases are often depicted in the donor-acceptor notation using arrows ($\text{base} \rightarrow \text{SiR}_2$) instead of zwitterionic Lewis formulae ($^+\text{base}-\text{SiR}_2^-$). Both notations can be of equal value when it comes to conceptual presentation, but the classical Lewis formulae are used in this work following the recommendations by Krossing and Schnepf.^[88]

The heavier acyclic di(amino)tetrylenes $\text{E}(\text{NR}_2)_2$ ($\text{E} = \text{Ge}, \text{Sn}, \text{Pb}$; $\text{R} = \text{alkyl}, \text{aryl}, \text{silyl}$) have already been established by the groups of Lappert and Harris in the 1970s.^[89-91] But in sharp contrast, the isolation of acyclic silylenes is very challenging due to their tendency to dimerize or undergo insertion reactions, which is caused by their smaller HOMO/LUMO and singlet/triplet energy gaps when compared to their cyclic congeners.^[92] The Kira group was able to observe the di(amino)silylene $\text{Si}\{\text{N}(\text{iPr})_2\}_2$ by UV- and NMR spectroscopy at room temperature in 1998 and the larger derivative $\text{Si}\{\text{N}(\text{SiMe}_3)_2\}_2$ was found to undergo rapid decomposition above 0°C by West and Müller in 2003.^[93,94] Only in 2012, the groups of Power and Aldridge independently succeeded in the isolation of the first stable, acyclic silylenes after reduction of bromosilanes with $[\text{Mg}(\text{nacnac})]_2$ or an excess of the substitution agent $\text{LiB}\{\text{N}(\text{Dipp})\text{CH}\}_2$, respectively (Figure 8).^[95,96] Within the last decade, another handful of acyclic silylenes has been published^[95-104] and their capabilities of small molecule activation have recently been covered in a review paper.^[105]

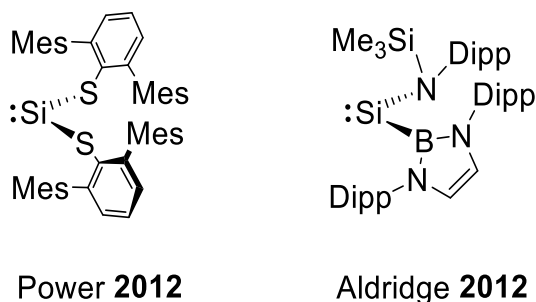


Figure 8. The first stable acyclic silylenes.

Another major breakthrough was undoubtedly achieved by Robinson and coworkers who were the first to stabilize low-valent silicon by NHC ligands upon reduction of the chlorosilane adduct $\text{SiCl}_4(\text{IDipp})$ ($\text{IDipp} = \text{:C}\{\text{N}(\text{Dipp})\text{CH}\}_2$, $\text{Dipp} = 2,6\text{-diisopropylphenyl}$) with potassium graphite (KC_8).^{[106], 4} The spectacular disilicon(0) compound $\text{Si}_2(\text{IDipp})_2$ (**I**, Figure 16) combines the $\text{Si}=\text{Si}$ π -bond of disilenes with features of silylenes: two-coordinated Si atoms in the singlet-state and free electron pairs.

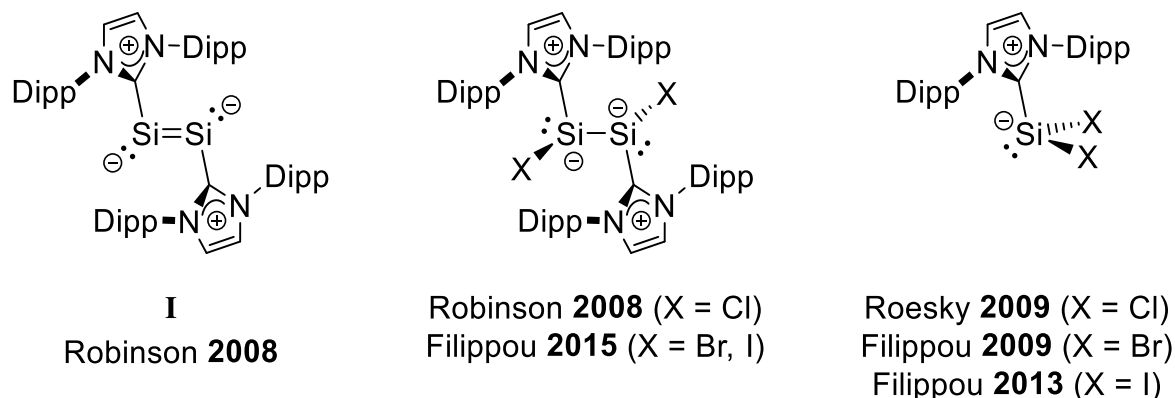


Figure 9. The first NHC-stabilized examples of base-stabilized disilicon(0),^[106] disilicon(I)^[106,111] and silicon dihalides^[112–114] each coordinated by the bulky NHC IDipp.

In addition, the synthetic strategy itself was quickly amended by the community. Soon Roesky and Filippou independently reported on the isolation of base-stabilized dihalosilylenes $\text{SiX}_2(\text{IDipp})$ obtained by dehydrohalogenation of SiHCl_3 using two equivalents of the NHC, that also reacts as a Brønsted base in this case, or reductive dehalogenation of $\text{SiBr}_4(\text{IDipp})$ and $\text{SiI}_4(\text{IDipp})$ with two equivalents of KC_8 , respectively.^[112–114] The $\text{SiX}_2(\text{NHC})$ derivatives are bottleable base-adducts of dihalosilylenes. They have proven to be powerful synthons in

⁴ The first Silylene-NHC adduct with a very weak Si-C bond ($\text{BDE} \approx 13 \text{ kJ}\cdot\text{mol}^{-1}$) was reported by Lappert in 1999.^[107] By that time, Robinson and coworkers had already reported on the isolation of $\text{EMe}_3(\text{NHC})$ ($\text{E} = \text{Al}, \text{Ga}$; $\text{NHC} = \text{:C}\{\text{N}(\text{iPr})\text{CH}\}_2$), the first examples of main group elements stabilized by an NHC, in 1996^[108] as well as $(\text{IDipp})\text{HB}=\text{BH}(\text{IDipp})$ in 2007, which is the first compound with a $\text{B}=\text{B}$ double bond.^[109] In the following years, multiple mono- and diatomic “allotropes” stabilized by two NHC- or cAAC ligands were published.^[110]

academic research leading to numerous novel products, some of which have been depicted in Figure 10.

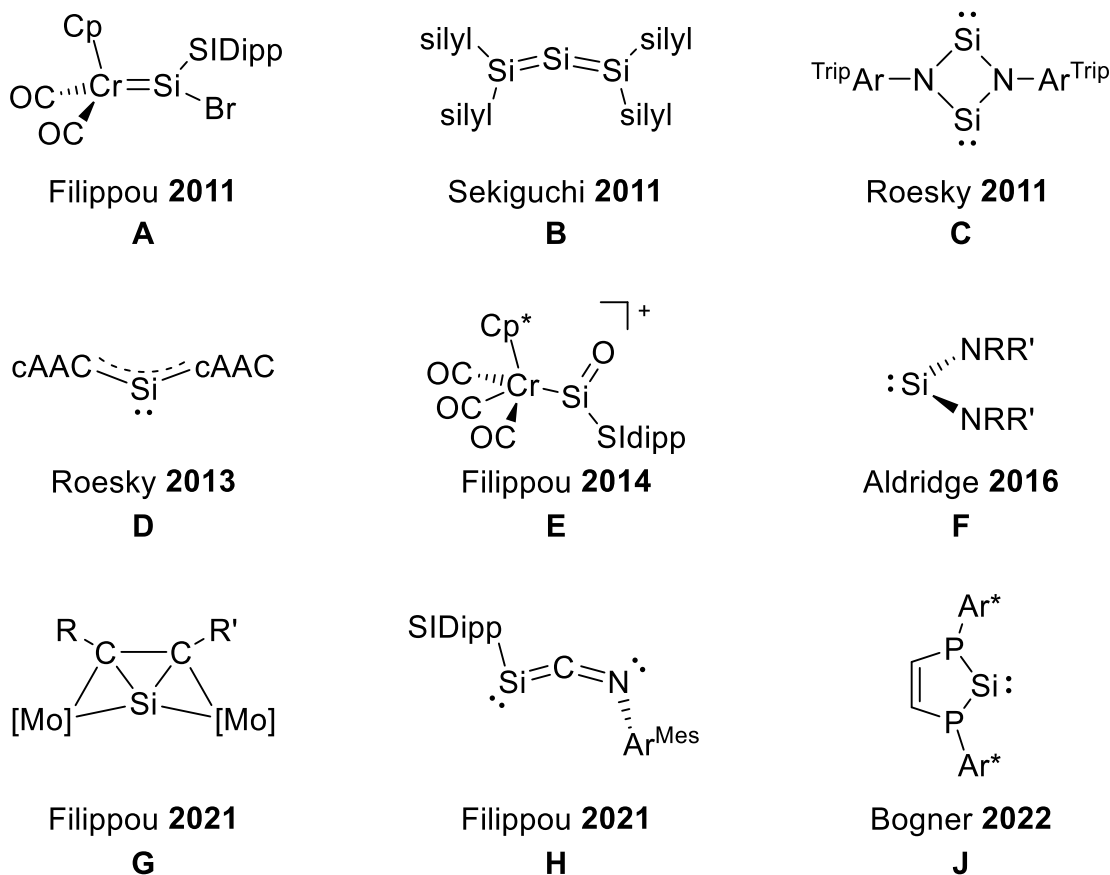


Figure 10. Selected compounds obtained from NHC-stabilized di(halo)silylenes. The first bromosilylidene complex (**A**, SIDipp = :C{N(Dipp)CH₂}₂), a trisilaallene (**B**, silyl = SiMetBu₂), a dimer of silaisonitrile (**C**, Ar^{Trip} = 2,6-Trip₂-C₆H₃), a cAAC-stabilized silylone (**D**, cAAC = :C(CH₂)(CMe₂)₂N(Dipp)), a metallasilanone (**E**, anion = [B{C₆H₃-3,5-(CF₃)₂}₄]⁻), an acyclic di(amino)silylene (**F**, NRR' = N(SiMe₃)boryl, boryl = B{N(Dipp)CH₂}₂), a complex with a planar, four-coordinated Si atom (**G**, [Mo] = Tp'Mo(CO)₂, Tp' = κ³-N,N',N''-hydridotris(3,5-dimethylpyrazolyl)borate, R/R' = Me/Me, H/SiMe₃, H/Ph), a Si(0)-isocyanide complex (**H**, Ar^{Mes} = 2,6-dimesitylphenyl) and a P-heterocyclic silylene (PHSi) (**J**, Ar* = Mes* or Eind). Formal charges are omitted for simplicity.

Early reactivity studies include the reactions with diazoalkanes and azides leading to coordination products (NHC)SiX₂(N₂CR₂), zwitterionic dichlorosilaimines (NHC)SiX₂(NR) and Roesky's dimer of a silaisonitrile (**C**).^[115-117] The group of Sekiguchi reported on the formation of a trisilaallene (**B**) after salt metathesis with Li₃Si(silyl)₂ and subsequent thermal isomerization to a cyclotrisilene^[118] whereas Filippou and coworkers later used their bromosilylidene complex (**A**) as a precursor for the synthesis of the first metalla(silanone) (**E**) after halide abstraction, carbonylation of the resulting cationic silylidyne complex and oxidation.^[119,120] In 2012, Rivard obtained so-called push-pull-complexes of the parent silylene in the form of (IDipp)SiH₂(LA) (LA = W(CO)₅ or BH₃) after chloride/hydride exchange with LiAlH₄,^[121] whereas NHC substitution in favor of chelating bis(NHC)s or cyclic alkyl(amino)carbenes (cAACs) lead the

groups of Roesky und Driess to the isolation of Silylones, neutral monosilicon(0) Si(carbene)₂ compounds (**D**) in 2013.^[122,123] At the same time, Filippou and coworkers explored the substitution of halides by small NHCs such as IMe₄, leading to the dication [Si(IMe₄)₂(IDipp)]I₂.^[114] Substitution with a phosphanide and subsequent elimination of Me₃SiCl led to an NHC-stabilized phosphasilenyliene (IDipp)Si=PMes* in 2015 and one year later,^[124] Aldridge reported on the isolation of a base-free acyclic di(amino)silylene (**F**), that was obtained from a non-stoichiometric redox reaction with LiTBoN (TBoN = N(SiMe₃)boryl, boryl = B{N(Dipp)CH₂})₂.^[125,126] The SiX₂(NHC) compounds were also pivotal as starting materials for more effective synthetic routes to Jutzi's SiCp*₂ or fused derivatives,^[127,128] and are generally utilized as easily accessible source for Si(II) in e.g. cAAC chemistry to access SiX₂(cAAC)_n or Si₂X₂(cAAC)₂ (n = 1,2).^[123,129,130] Very recently, substitution reactions led to the isolation of a planar, tetracoordinated silicon compounds (**G**) as well as a Si(0)-isocyanide complex (SIDipp)Si=C=NAr^{Mes} (**H**, SIDipp = "saturated IDipp" = :C{N(Dipp)CH₂})₂, Ar^{Mes} = 2,6-dimesitylphenyl) and a P-heterocyclic silylene (PHSi).^[131-133] But more importantly for this work, an NHC-stabilized disilavinylidene (E)-(SIDipp)Si=Si(Br)Tbb (**1**, Tbb = 2,6-dsi₂-4-tBu-C₆H₃, dsi = CH(SiMe₃)₂) was isolated by Dr. P. Ghana from the Filippou group in 2015.^[134]

1.2 General structure and objective of this work

The fascinating chemistry of low-coordinate silicon has flourished in recent years. Progress in the synthesis of Si-based compounds in unprecedented bonding modes has attracted much attention, culminating in the isolation of the NHC-stabilized disilavinylidene (E)-(SIDipp)Si=Si(Br)Tbb in 2015.^[134] The experimental work presented in this thesis was performed in the timespan between 2016 and 2021 and covers two major parts:

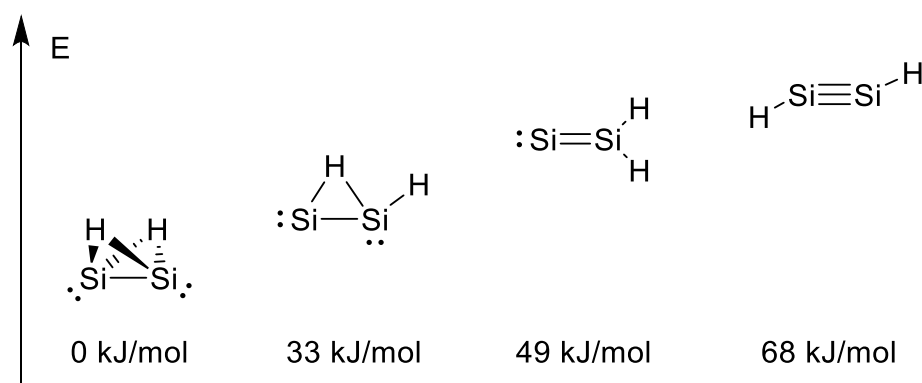
- In part I the versatile reactivity of (E)-(SIDipp)Si=Si(Br)Tbb is explored in a detailed reactivity study. The NHC-stabilized disilavinylidene features four reactive sites (the NHC, the Si(0) electron lone pair, the Si-Br bond and the Si=Si π -bond) of which the latter two will be paid special attention. The discussion part will also pick up some of the research findings from the preceding master thesis whose completion is now aspired.^[135]
- In part II synthetic access to acyclic silylenes with oxygen-based substituents is aimed for. Potential synthetic routes include the reduction of Si(IV) precursors and the substitution of existing base-stabilized halosilylenes. At the beginning of the experimental work presented in this thesis, only very rare examples of cyclic, amidinato-substituted oxysilylenes and not a single compound with a 2-coordinated silicon with a Si-O bond were known, but intermediate progress in the literature is taken into account.

Difficulties lie within the extreme sensitivity of most low-coordinate Si-based compounds towards air- and moisture as well as their generally high reactivity that can often lead to unselective reactions and complicates the prediction of reaction outcomes. Isolable reaction products should be fully characterized by analytical methods (typically NMR spectroscopy, elemental analysis, melting point and XRD) whereas instable species should be appropriately characterized by spectroscopic methods. Depending on the respective compounds, additional characterization methods like IR-, Raman- and UV-vis spectroscopy as well as DFT calculations are also to be performed.

2 Part I: Disilavinylidene Chemistry

2.1 Introduction

Vinylidenes (:C=CR_2) are transient, unsaturated carbenes and readily tautomerize to the respective alkynes ($\text{RC}\equiv\text{CR}$). Yet of all things, their instability is likely their most utilized trait with the Fritsch-Buttenberg-Wiechell rearrangement^[136–139] being a key step in both the Corey-Fuchs-reaction^[140] and the Seyferth–Gilbert homologation.^[141] And while vinylidenes can only be isolated in frozen argon matrices, their stable transition metal complexes $[\text{L}_n\text{M=C=CR}_2]$, containing an electrophilic α -carbon and nucleophilic β -carbon atom, have been extensively studied in a variety of stoichiometric and catalytic transformations.^[142–145]



Scheme 2. Calculated (CCSD(T)) respective energies of different Si_2H_2 isomers (linear $\text{HSi}\equiv\text{SiH}$ is not a minimum structure). The values were taken from the literature.^[146,147]

In sharp contrast to carbon chemistry, the parent disilavinylidene isomer (:Si=SiH_2) was predicted to be more stable than the trans-bent disilyne ($\text{HSi}\equiv\text{SiH}$, Scheme 2)^[146–148] and was detected in the gas phase by the groups of Kaiser and Stanton after reaction of ground-state atomic silicon with SiH_4 .^[149] Substituents have a considerable impact on the energetic order of the Si_2R_2 minimum structures. For example, in case of Si_2Me_2 , the disilavinylidene :Si=SiMe_2 was predicted by theory to be the minimum structure followed by the disilyne $\text{MeSi}\equiv\text{SiMe}$. Unsurprisingly, increasing steric congestion in Si_2R_2 favors the disilyne over the disilavinylidene isomer.^[145,150–153]

Nevertheless it were disilynes that attracted considerable interest in theoretical and experimental chemistry^[154,155] with a handful of stable derivatives known since the isolation of the first stable derivative in 2004 by the group of Sekiguchi.^[45,46,62,63,156,157] Only within the last decade, several remarkable examples of heavier base-stabilized vinylidenes could be isolated (Figure 11): Scheschkewitz et al. reported mixed NHC-stabilized silagermenylidenes $(\text{NHC})\text{Ge=SiRR}'$ (**III-R**; $\text{NHC} = \text{iPr}_2\text{Me}_2$; $\text{R} = \text{Tip}$; $\text{R}' = \text{Tip, SiClTip}_2, \text{NMe}_2$),^[158–160] the group of Aldridge succeeded in the isolation of a base free-digermavinylidene (**VI**) in 2016,^[161] and recently Wesemann et al. proceeded with a phosphane-stabilized digermavinylidene (**V**) as well

as with its germasilylenylidene (**IV**) derivative.^[162,163] Apart from these congeners, disilavinylidenes remain an academic rarity with only two examples reported in the literature: One was published by the group of Iwamoto in 2021 (**II**), and the other one by our group back in 2015 (**1**).^[134,164]

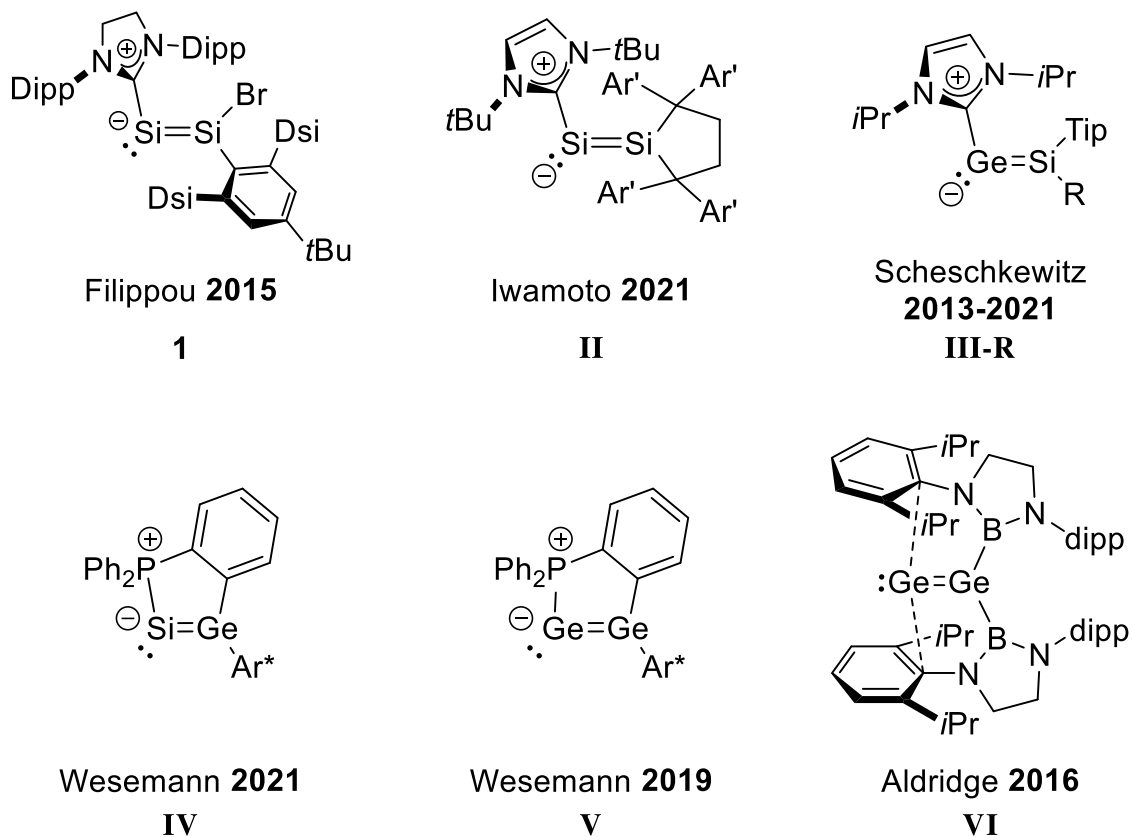
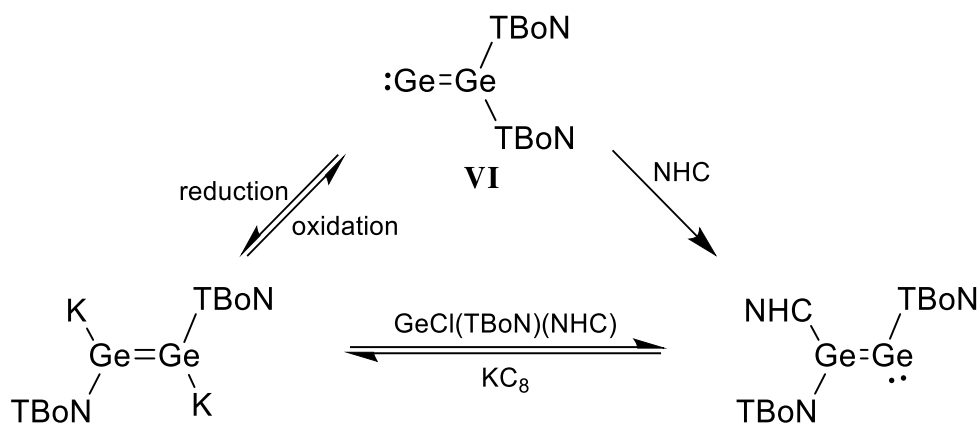


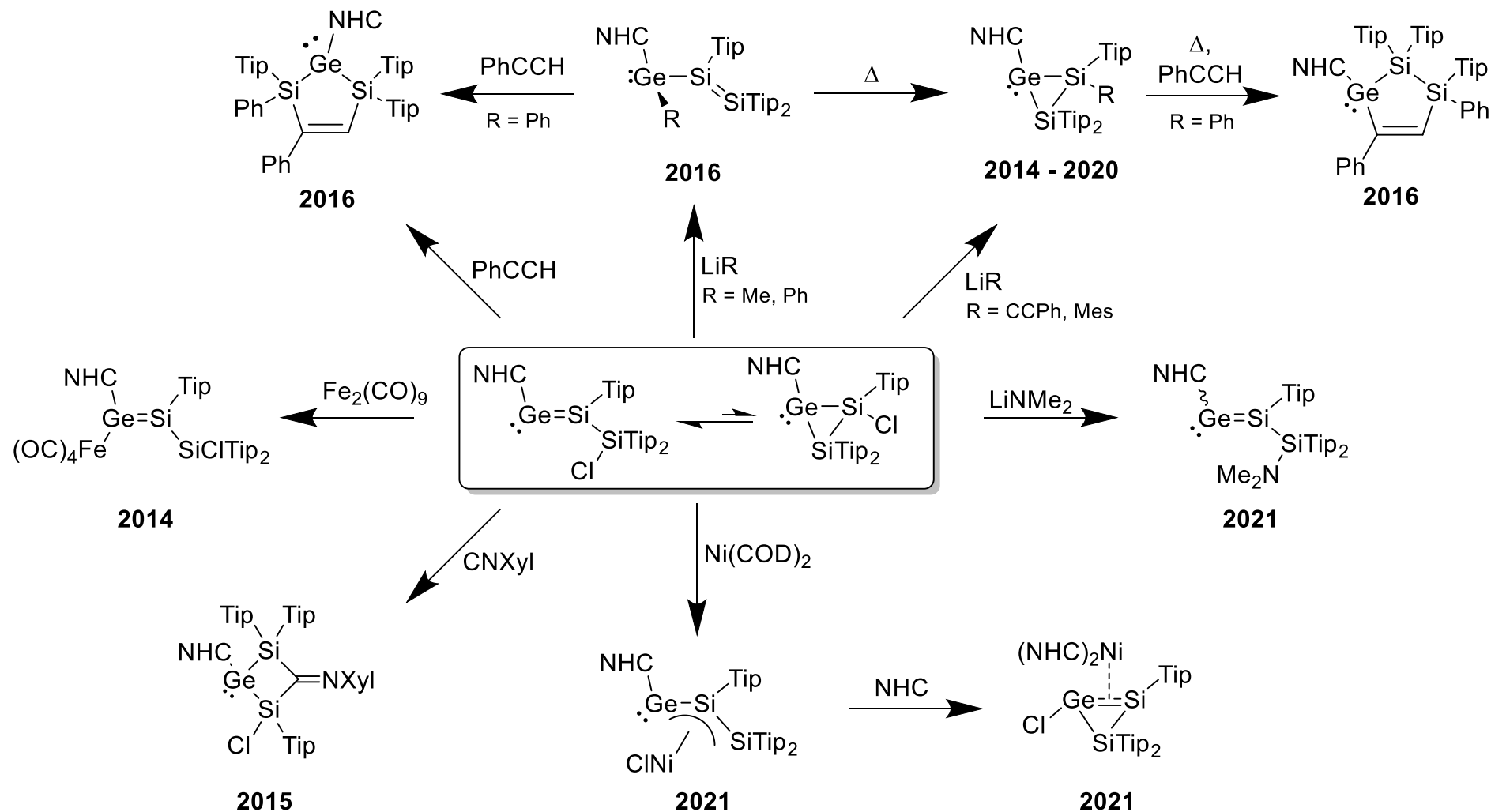
Figure 11. Isolable base-stabilized vinylidene analogues of the heavier Group 14 elements (Dsi = CH(SiMe₃)₂, Ar' = C₆H₃-3,5-tBu₂-4-OMe; Tip = C₆H₃-2,4,6-iPr₃; R = Tip, SiClR₂ or Si(NMe₂)R₂; Ar* = C₆H₃-2,6-Tip₂).

In this context, it should be mentioned that a derivative stabilized by a cyclic alkyl(amino)carbene (cAAC) was recently prepared by F. Gstrein in the Filippou group. (cAAC)Si=Si(Br)Tbb is currently under investigation and its reactivity will soon be discussed as part of his dissertation.^[165] Accordingly, reactivity studies of the heavier vinylidene compounds are scarce. In their 2016 paper, Aldridge and coworkers described the addition of a small NHC to **VI** yielding an NHC-stabilized di(boryl)digermene as well as 2-electron reduction to a digermene dianion using KC₈ (Scheme 3). Additionally, hydrogenation of **VI** was shown to afford a 1,2-diboryldigermene. The migration of one boryl substituent to the second Ge atom in either reaction highlights the fragility of the vinylidene moiety and the importance of the electronic stabilization of the Ge(0) atom by the ipso-carbon atoms of the Dipp groups in **VI**.^[166]



Scheme 3. Reactivity of Aldridge's digermavinylidene **VI**. Reduction was achieved by excess KC_8 ; oxidation by $[\text{Cp}_2\text{Fe}][\text{BAr}^{\text{F}}_4]$ or $[\text{Ph}_3\text{C}][\text{B}(\text{C}_6\text{F}_5)_4]$. $\text{Ar}^{\text{F}} = 3,5\text{-(CF}_3)_2\text{-C}_6\text{H}_3$; $\text{NHC} = \text{IiPr}_2\text{Me}_2 = \text{:C}\{\text{N}(\text{iPr})\text{CMe}\}_2$.

Recently, Wesemann demonstrated the synthetic potential of **V** and **IV** as Si(0) or Ge(0) atom transfer reagents: simple addition of 1,4-diazabutadienes cleaves the E=E bond, affording the known N-heterocyclic silylene or -germylene, respectively.^[167,163] Conversely, the behavior of Scheschkewitz's derivatives has been explored to a certain extent (see Scheme 4 on page 16). Compounds **III-R** have been shown to undergo various reactions including cycloadditions of an alkyne to the Ge=Si bond,^[168] addition of isonitriles,^[169] coordination to transition metals via the lone pair of the dicoordinated Ge atom^[159] or the Ge=Si π -bond and reactions with nucleophiles.^[158–160,169–173] Yet almost all reactions have been performed using the chlorosilyl-substituted derivative **III-SiTip₂Cl**, which not only offers a Si-Cl bond that is involved in almost every reaction, but was also shown to lie in an equilibrium with an NHC-stabilized disilacyclogermeneylidene. It is hence not clear, if the unquestionably rich chemistry of **III-SiTip₂Cl** provides insight in the “true” properties of silagermeneylidenes, or if the key steps involve mere disilacyclogermeneylidene- and chlorosilane reactivity in this case.

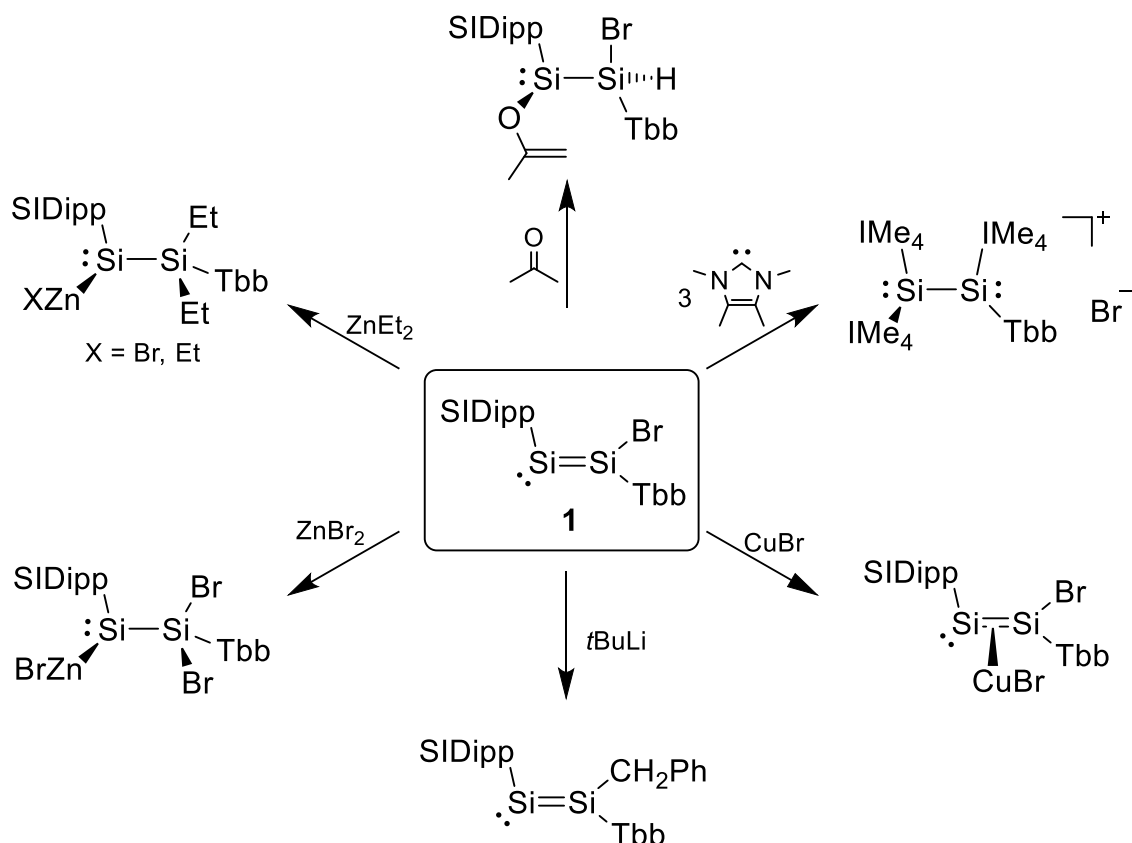


Scheme 4. Reactivity of Scheschkewitz's NHC-stabilized silagermenylidene **III-SiTip₂Cl**.^[158–160,169–173]

By contrast, reactivity studies of NHC-stabilized disilavinylidenes have not been reported yet, with the only exception being the oxidation of Iwamotos **II** with N₂O in presence of B(C₆F₅)₃ yielding (NHC){(F₅C₆)₃BO}Si(μ²-O)SiR₂, a silicon analog of an acetolactone.^[164]

The NHC-stabilized disilavinylidene **1** can be seen as a hybrid of the NHC-stabilized disilicon(0) compounds (NHC)Si=Si(NHC)^[106] and the 1,2-dibromodisilenes (E)-R(Br)Si=Si(Br)R^[25,27,47,48] with multiple reactive sites: the NHC or the bromine atom can be substituted while the Si=Si π-bond is an objective for addition of polar substrates and cyclization reactions and has potential for metal coordination like the electron lone pair at the 2-coordinated Si atom. Displaying both nucleophilic and electrophilic character, an auspicious synthetic chemistry is expected. Owing to the versatility of **1**, initial experiments performed by Dr. P. Ghana were diversified but quickly proved to be challenging due to their low selectivity.^[174] Promising results were obtained from attempts to abstract the bromide atom, leading to a mixed Ag- and AgBr-complex with coordination via both the Si=Si π-bond and the free electron lone pair that was identified by X-ray diffraction (XRD) analysis of single crystals grown from a mixture (for details see Scheme 21 on page 66). Likewise, a C,H-activated compound was characterized by XRD after reduction with elemental lithium and Ghana observed a mostly selective reaction with tBuLi, that was eventually followed in the master thesis in direct preparation of this work.^[135]

In the context of that thesis, multiple compounds could be obtained in a variety of reactions summarized in Scheme 5 on page 18. The reactions include NHC replacement, activation of the Si=Si π-bond by formal 1,2-addition of ZnBr₂ or HOC(Me)CH₂ (from acetone) and coordination to CuBr. The aforementioned reaction with tBuLi was found to give a substitution product, where the Br is replaced with a benzyl group (CH₂Ph) after activation of the toluene solvent. Due to time limitations as well as renovations of the universities analytical department in 2015, some of those compounds could not be fully characterized and will again be addressed in this work. Additional insights as well as quantum-chemical calculations performed by Dr. G. Schnakenburg and J. Rump from the Filippou group will thus be included in the following.

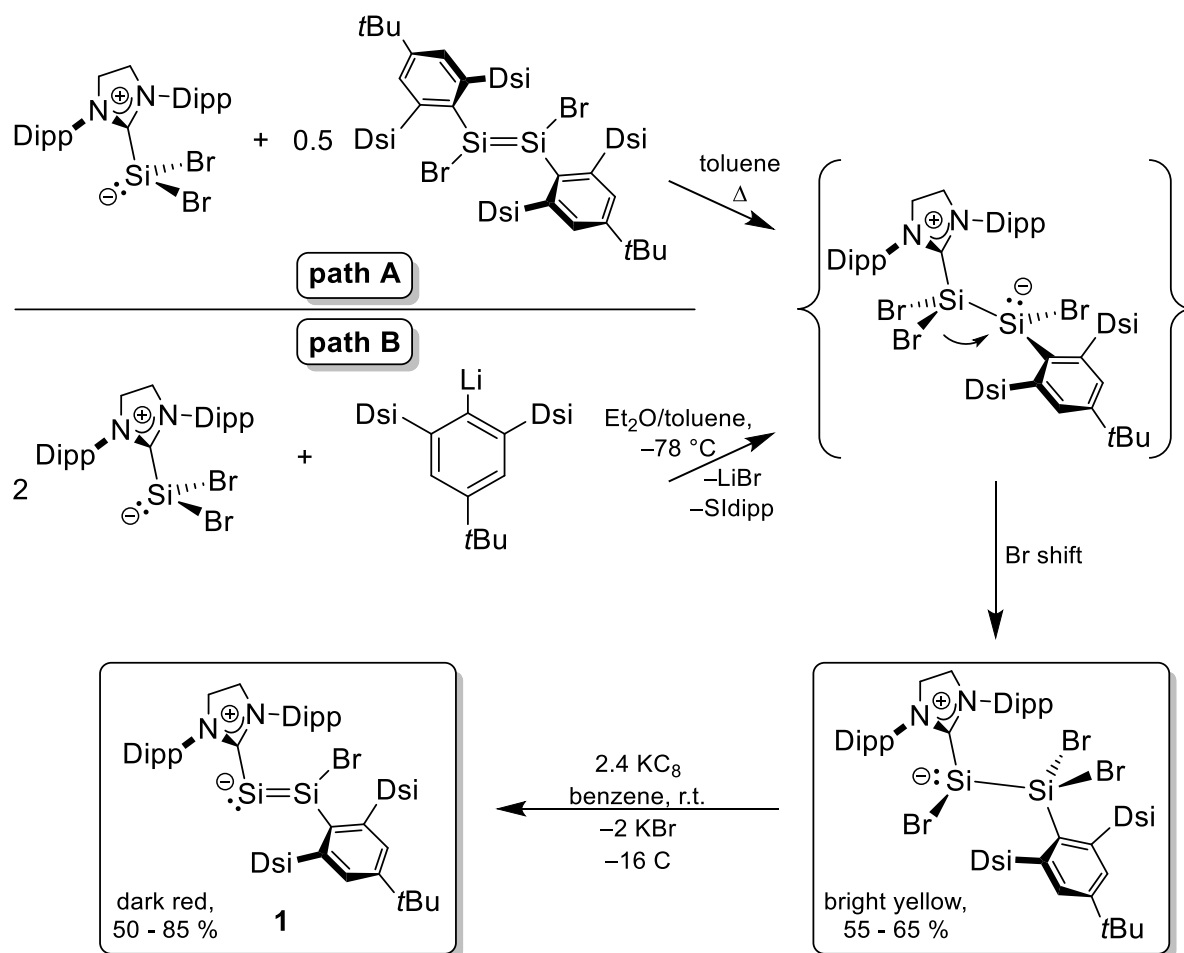


Scheme 5. Results of the preparatory master thesis preceding to this work. $\text{IME}_4 = \text{:C}\{\text{NMeCMe}\}_2$.

In this work, compound **1** was synthesized by two different methods following established literature procedures, both of which are based on the NHC-stabilized dibromosilylene $\text{SiBr}_2(\text{SIDipp})$. First, SiBr_4 was made from elemental silicon,^[175] treated with free SIDipp ^[176] in petrol ether and finally reduced to $\text{SiBr}_2(\text{SIDipp})$ using 2.4 equiv. of potassium graphite in benzene overnight.^[119] By this route, approximately 15 g of extremely air sensitive $\text{SiBr}_2(\text{SIDipp})$ can be made at once. For the Tbb substituent (Tbb = 2,6-dsi-4-tBu-C₆H₂; dsi = CH(SiMe₃)₂), TbbBr was synthesized in ~40 g scales (60 – 65 % overall yield) in three steps from 4-tertbutyl-meta-xylene following internal group protocols that mostly follow the published procedures.^[177] From there, metalation with *t*BuLi afforded TbbLi that is only stable up to about –40 °C and is therefore only generated in situ. Subsequent silylation with $\text{SiH}(\text{OR})_3$ (R = Me, Et), hydrogenation and bromination yielded the tribromosilane in a satisfying overall yield of ca. 60 %. Finally, reduction with sodium naphthalenide in thf at –60 °C gave the disilene (E)-Tbb(Br)Si=Si(Br)Tbb as a bright yellow, relatively robust solid in yields between 60 and 70 % on a 5 g scale.^[48,134]

Heating a solution of the disilene and 2 equiv. $\text{SiBr}_2(\text{SIDipp})$ in toluene to about 80 °C overnight (literature: 100 °C for 5 h)^[134] results in the formation of the extremely sensitive NHC-stabilized silylsilylene $\text{SiBr}(\text{SiBr}_2\text{Tbb})(\text{SIDipp})$ (path A in Scheme 6). The reaction is

believed to proceed via a nucleophilic attack of the silylene precursor which monomerizes the disilene to form the Lewis acid/base pair $\{(\text{SIDipp})\text{SiBr}_2\}\{\text{SiBrTbb}\}$ and a subsequent 1,2 bromide shift. This assumption is based on the existence of the related mixed adduct $\{(\text{SIDipp})\text{SiBr}_2\}\{\text{GeBrAr}^{\text{Mes}}\}$ [51,134] ($\text{Ar}^{\text{Mes}} = 2,6\text{-dimesitylphenyl}$) and the cationic adduct $\{[(\text{SIDipp})\text{SiBr}]\{\text{SiBr}_2(\text{SIDipp})\}\}[\text{BAR}^{\text{F}}_4]$ ($\text{Ar}^{\text{F}} = 3,5\text{-(CF}_3)_2\text{-C}_6\text{H}_3$) that was recently isolated by Filippou and coworkers.^[132]



Scheme 6. Synthesis of $\text{SiBr}(\text{SiBr:Tbb})(\text{SIDipp})$ starting from $\text{SiBr}_2(\text{SIDipp})$ and $(E)\text{-Tbb}(\text{Br})\text{Si}=\text{Si}(\text{Br})\text{Tbb}$ (path A) or TbbLi (path B) as well as the subsequent reduction to $(\text{SIDipp})\text{Si}=\text{Si}(\text{Br})\text{Tbb}$ (**1**).^[134]

Finally, disilavinylidene **1** was obtained by reduction closely following the literature procedure on a 3 g scale. In this work, it was interchangeably used as dark red, crystalline 1:1 toluene solvate or, after rigorous drying, as a solvent-free brick red powder.

Alternatively and preferably, $\text{SiBr}(\text{SiBr:Tbb})(\text{SIDipp})$ can also be synthesized directly from 2 equiv. $\text{SiBr}_2(\text{SIDipp})$ and TbbLi (path B in Scheme 6). This route was already discovered in 2015 but gave mixtures of irreproducible content and therefore not used by the authors until the reason was discovered and eliminated in the preceding master thesis: a side reaction of the generated silylene with isobutene from the tBuLi that can be prevented by evaporation of the

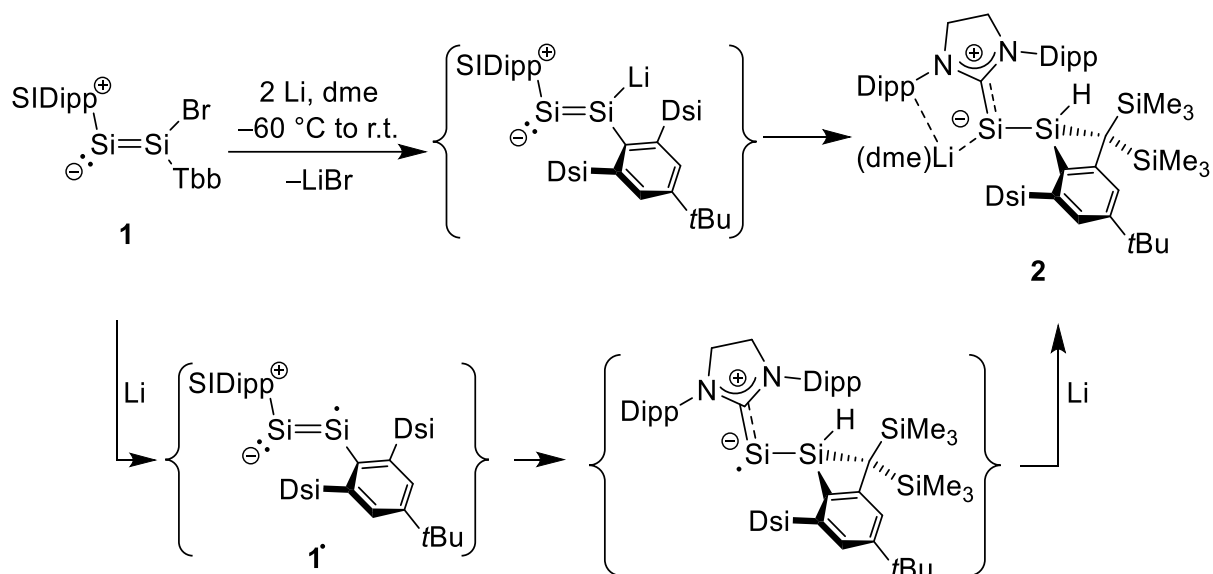
alkene in vacuo during the lithiation step.^[135] After additional adjustments of the reaction conditions as well as optimization of the workup procedure, a reliable procedure with yields between 50 and 65 % (about 5 g) is now finally given in this work on page 183.

2.2 Substitution of the Si-Br bond

The Si-Br bond of **1** is predestined for further functionalization. For the related bromodisilenes, rare examples of single nucleophilic substitutions using organolithium- or Grignard reagents have been described by the groups of Tokitoh and Tamao but the isolated yields are mediocre at best.^[46,47] More efficiently, stepwise electrophilic substitution is made possible by metalation to disilenides,^[27-29] with Scheschkewitz's $\text{LiTipSi}=\text{SiTip}_2$ being a particular fruitful example.^[159,178-188] In fact, this strategy also led to the only known twofold substitution from (E)-Eind(Br)Si=Si(Br)Eind to (E)-Eind(R)Si=Si(R)Eind (E = SiMe₃ or I) via the dianion (E)-Eind(K)Si=Si(K)Eind by Wienkenhöver in 2017.^[40]

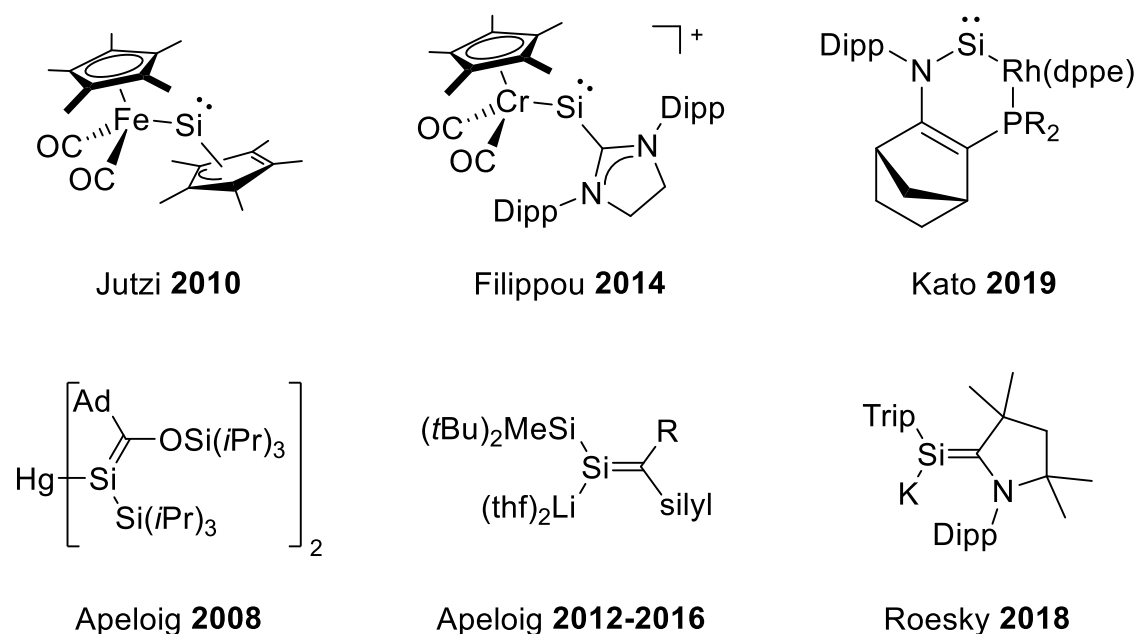
2.2.1 Lithiation attempts

Reacting disilavinylidene **1** with 2.5 equiv. of lithium sand in freezing di(methoxy)ethane (dme) at about -60 °C resulted in a color change from dark red to red-brown over a period of 3 h. No intermediates could be observed by in situ ¹H NMR spectroscopy from the reaction solution at about -30 °C, and after warming to ambient temperature, the complete consumption of the starting material into the C-H insertion product [(SIDipp)Si(Li·dme)Si(H){C(SiMe₃)₂-C₆H₂-4-tBu,6-(CH)(SiMe₃)₂}] (**2**, ca. 75 % selectivity by ¹H NMR spectroscopy), that was first identified by Ghana, was verified. The compound could be isolated in 52 % yield as dark red crystals after thorough extractions from the salt byproducts and twofold crystallization from n-hexane at -30 °C. It was found to be extremely sensitive towards air or moisture (immediate discoloration) but can be handled under an argon atmosphere. Compound **2** is well soluble in typical solvents (diethyl ether, toluene, benzene, aliphatic hydrocarbons) but slowly decomposes in thf. Upon heating, the solid deteriorates to a dark mass at 171 °C.



Scheme 7. Synthesis of the NHC-stabilized metalla(silyl)silylene **2** by C-H activation of the proposed lithiation intermediate (SIDipp)Si=Si(Li)Tbb (top) or by activation of a radical species **1**[•] (bottom).

Single crystals were grown from *n*-pentane or dme and the XRD analysis confirmed the identity of **2** as a base-stabilized metallasilylene. This is an extremely rare class of very reactive compounds and only three representative examples have been reported in the literature (Figure 12).^[120,189,190] ⁵ Additionally, F. Gstrein from the Filippou group very recently obtained an analogous compound by reacting his cAAC-stabilized disilavinylidene (cAAC^{Me})Si=Si(Br)Tbb with potassium, which will be described in his thesis.^[194]



⁵ Metallasilylenes (Si(ML_n)R) are not to be confused with silylene metal complexes (L_nM⁺SiR₂) or silyl radicals (L_nM[•]SiR₂) (M = Na, K; L_n = solvent or crown ether).^[191–193]

Figure 12. Top row: a hypervalent ferrosilylene,^[189] a cationic chromiosilylene^[120] and an N-hetero-Rh-metallacyclic silylene (PR₂ = cyclo-P{N(tBu)₂SiMe₂}, dppe = Ph₂PC₂H₄PPh₂).^[195] Bottom row: a mercury bis(silenide),^[196] lithium silenides (R = adamantyl or SiMe₂tBu; silyl = SiMe(tBu)₂ or SiMe₂tBu)^[197,198] and a cAAC-substituted potassium silenide.^[199] For the synthesis of the related zinc(silyl)silylenes from **1**, see Scheme 17 on page 46.

The molecular structure of **2** (Figure 13) reveals some characteristic features of NHC-stabilized silylsilylenes with a central Si1-Si2 distance (2.332(6) Å) that lies in between those of the starting material (**1**: 2.167(2) Å) and the silylsilylene SiBr(SiBr₂Tbb)(SIDipp) (2.391(1) Å) and corresponds to a typical single bond. Surprisingly, the coordination sphere of the Si2^{NHC} atom is almost perfectly trigonal planar (Σ_{Si} : 356.2(1)°), which is different from pyramidalized silylenes (for example SiBr(SiBr₂Tbb)(SIDipp): 287.4(1)°^[134]) or silyl anions that typically have high inversion barriers of ~100 kJ/mol.^[68] The planarization can be explained by an unusually strong Si2→C1^{NHC} back donation, which also noticeably reduces the bond length (1.830(2) Å) in respect to **1** (1.937(4) Å), SiBr(SiBr₂Tbb)(SIDipp) (1.978(3) Å)^[134] or SiBr₂(SIDipp) (2.007(5) Å) by 10 – 17 pm.^[119] The resulting distance is thereby almost as short as the distinct Si=C double bonds in silenes (about 1.7 – 1.8 Å) or silenides (Table 1), which are also planar.

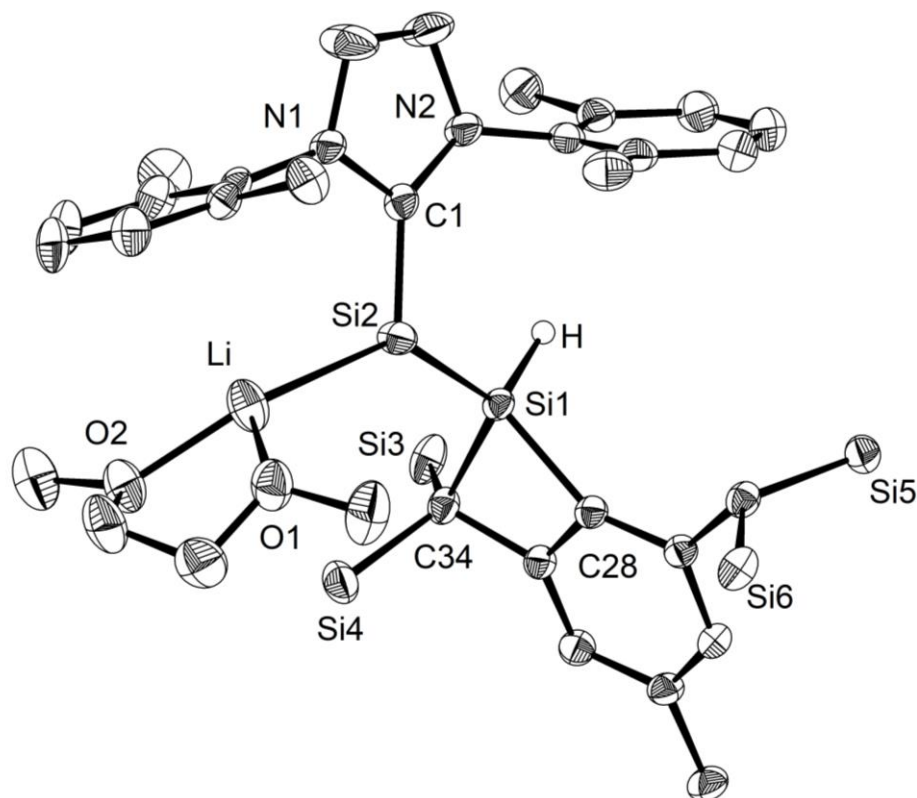


Figure 13. Molecular structures of $2 \cdot C_3H_7$. Thermal ellipsoids are set to 50 % probability; methyl groups, hydrogen atoms except for the Si-bonded atom and the solvent molecule are omitted for simplicity. Selected bond lengths (\AA) and angles ($^\circ$): Si1-Si2 2.332(6), Si2-C1 1.830(2), Si2-Li 2.554(3), Li-O1 1.979(4), Li-O2 1.985(4), Si1-C28, Si1-C34 1.913(2), Si1-C34 1.976(2); C1-Si2-Li 114.1(1), C1-Si2-Si1 109.00(5), Li-Si2-Si1 133.13(9), Si2-Si1-C28 130.74(5), Si1-Si2-C34 119.20(5), C28-Si1-C34 74.86(7). The position of the Si1-bonded hydrogen atom was not directly verified by XRD.

The shrinkage of the Si2-C1^{NHC} bond is further accompanied by a rotation of the NHC: whereas the double-bonded starting material **1** as well as the related Si₂(IDipp)₂ and (IDipp)Si=PMes* all show perpendicular orientations in respect to their Si=E π -bonds,^[106,124,164] the imidazolium ring in compound **2** is almost in plane with the moiety around the Si2^{NHC} atom ($\approx 6.67(9)^\circ$, Li-Si2-C1-N1: $3.1(2)^\circ$), allowing for an additional coordination of the Li atom by the N1-bonded Dipp group (Li \cdots centroid: 2.935(4) \AA , Li \cdots C_{ipso}: 2.984(4) \AA). This matches the close Si-Li contact (2.554(3) \AA), which is closer than those found in typical lithium silanides (around 2.7 \AA),^[200,201] disilenides such as Li(Tip)Si=SiTip₂ (2.853(3) \AA)^[29] or Apeloigs silenide Li(R¹)Si=CR¹R² (2.71(2) \AA ; R¹ = SiMetBu₂, R² = SiMe₂tBu) that is known for its vivid color change from violet-red to green-blue upon Si \cdots Li dissociation).^[198]

Table 1. Selected bond distances in disilenides $M(R^1)Si=CR^2R^3$ (with R^1 being Z to R^3).

M	R ¹	R ²	R ³	$\Sigma_{Si} / ^\circ$	$d_{Si=C} / \text{Å}$	$d_{Si-M} / \text{Å}$	Ref
Hg ^A	Si(iPr) ₃	Adamantyl	OSi(iPr) ₃	359.8	1.770	Ø2.447	[196]
Li(thf) ₂	SiMetBu ₂	Adamantyl	SiMe(tBu) ₂	359.6	1.773	2.613	[197]
Li(thf) ₂	SiMetBu ₂	Adamantyl	SiMe ₂ tBu	359.6	1.778	2.618	[197]
Li(thf) ₂	SiMe(tBu) ₂	SiMe ₂ tBu	SiMetBu ₂	359.8	1.763	2.714	[198]
K ^B	Tip	cAAC ^{Me}		-	1.793	3.284	[199]

A: the linear Hg{silenide}₂ complex; **B:** dimeric K(Tip)Si=cAAC^{Me} with bridging potassium cations coordinated by the Si atom and the Tip groups. This compound can also be seen as a cAAC^{Me}-stabilized metallasilylene.

Concurrently, ¹H- and ¹³C{¹H} NMR spectroscopy in benzene-d₆ solution are consistent with an overall C₁ symmetry of both the SIDipp and the activated Tbb group (for details on the determination of local point groups by NMR spectroscopy see page 237 in the appendix). As for all novel compounds presented in this work, comprehensive ¹H/¹³C as well as ¹H/²⁹Si correlation spectroscopic experiments were performed to ensure correct assignment of all signals. The low symmetry of the substituents is in agreement with the solid state structure, even though the locked rotation around the Si-NHC bond can be explained both by the presence of a Si=C double bond, by the strong π -coordination of the adjacent Li atom via a dipp group, that locks the NHC in place or simply by collisions with the bulky activated Tbb group at the second Si atom. The signal of the Si-H atom is found at $\delta_H = 5.09$ ppm (¹J_{Si,H} = 172 Hz), and the NCN atom resonates at $\delta_C = 197.9$ ppm. This, in turn, compares well with the carbene resonances of **1** (204.6 ppm) and SiBr(SiBr₂Tbb)(SIDipp) (190.9 ppm), whereas Apeloigs Li(R)Si=CRR' (143.5 ppm) experiences a much stronger shift to higher fields.^[198]

In the proton-coupled ²⁹Si NMR spectrum (Figure 14), independent signals are found for all Si atoms of which the four SiMe₃ groups resonate in the standard region around $\delta_{Si} = 0$ ppm. The Si^{Tbb}-H resonance at -14.7 ppm lies well within the range of hydridosilanes (about 0 to -30 ppm)^[202] and so does the ¹J_{Si,H} coupling constant of 173 Hz (bulky hydridosilanes: 150 – 200 Hz).^[203] Finally, the signal of the Li-coordinated Si^{NHC} atom is considerably shifted and appears as a quartet (¹J_{Si,Li} = 70 Hz) in the high field at -62.3 ppm. The pronounced Si,Li coupling is a clear sign for the presence of contact ion pairs of **2** in benzene solution, whereas no Si,Li couplings were reported by Apeloig and coworkers for their lithium silenides in thf solutions.^[197,198] The Si^{NHC} resonance (-62.3 ppm) is shielded in respect to the starting material (**1**: 34.6 ppm) which is caused by the electropositive lithium atom and is in excellent agreement with the zinco-silylenes **5-X** and **6** ($\delta_{Si} = -63.9$ ppm to -81.8 ppm vide infra, page 46ff). In comparison, Apeloigs lithium silenides resonate at much lower fields between 240 and 406 ppm whereby ion separation is accompanied with a low-field shift of approximately 50 ppm.^[197,198]

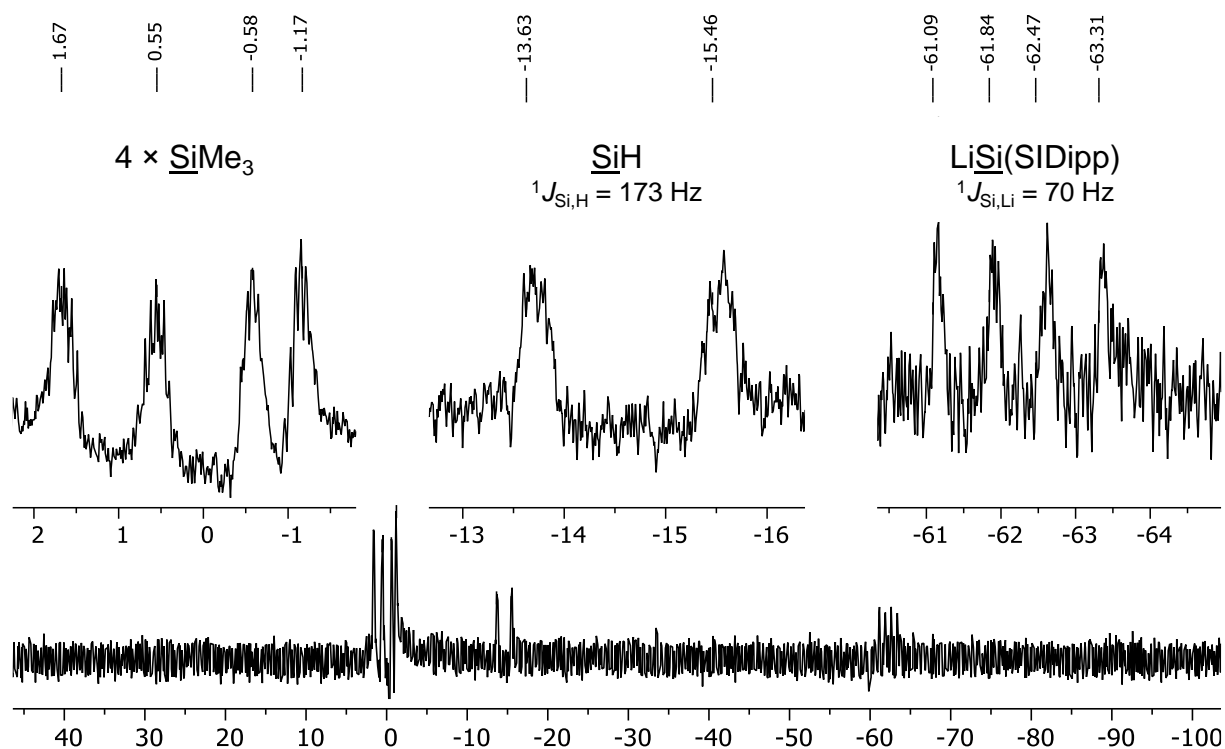
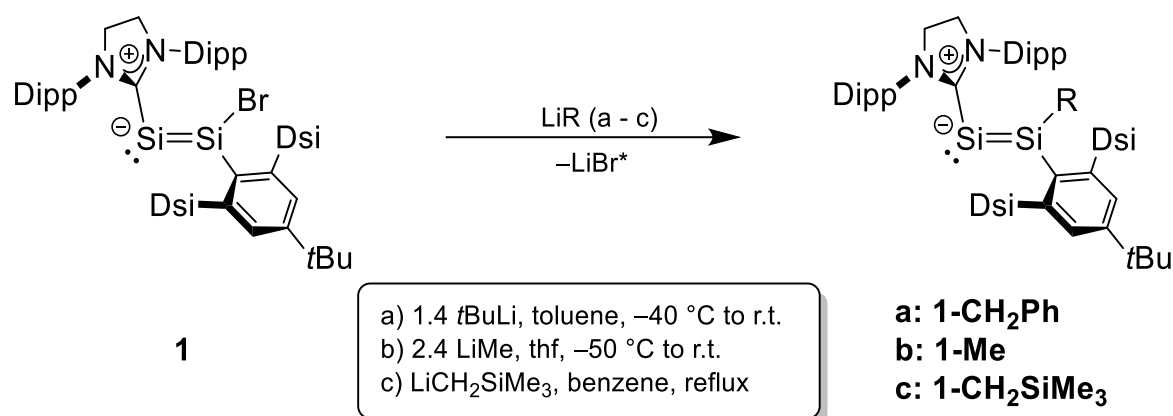


Figure 14. Proton-coupled ^{29}Si NMR (99.34 MHz) zg30 spectrum of compound **2** in benzene- d_6 at 298 K; the $^2J_{\text{Si,H}}$ coupling of the Si^{NHC} atom (approx. 10 Hz) as well as the fine coupling to the methyl protons are not fully resolved. Enlarged excerpts of the signals are given in the insets.

2.2.2 Alkylation of **1**

As mentioned in the introduction, the reaction of **1** with 2 equiv. of $t\text{BuLi}$ was also expected to yield the lithiation product “(E)-(SIDipp)Si=Si(Li)Tbb”. But when a toluene solution of compound **1** was treated with a solution of $t\text{BuLi}$ in n -pentane at $-40\text{ }^\circ\text{C}$ and slowly warmed to ambient temperature, ^1H NMR spectroscopic analysis instead revealed a slow but selective incorporation of a benzyl group (CH_2Ph) that originates from the solvent molecule.^[135] Further stirring of the orange-red mixture for ca. 12 h at ambient temperature resulted in a complete conversion of **1** to (E)-(SIDipp)Si=Si(CH_2Ph)Tbb (**1-CH₂Ph**), which after workup was isolated as a dark red solid (λ_{max} in n -hexane: 524 nm, see page 267 in the appendix) in 71 % yield (Scheme 8). Compound **1-CH₂Ph** is very air-sensitive but stable in common solvents such as thf, diethyl ether, toluene or n -hexane, where it readily dissolves; the disilavinylidenes are insoluble in acetonitrile but quickly decompose in acetonitrile-containing solutions. The solid is thermally robust and decomposes upon melting at $206\text{ }^\circ\text{C}$ to a dark brown oil (**1**: $237\text{--}238\text{ }^\circ\text{C}$).



Scheme 8. Bromide substitution of the NHC-stabilized disilavinylidene **1**. Compound **1-CH₂Ph** can also be obtained from **1** and LiCH_2Ph (see page 31f). In case of reaction a, HCMe_3 arises as a second byproduct.

Treatment of disilavinylidene **1** with methyl lithium in Et₂O or dme solution resulted in no conversion even at elevated temperatures and after addition of TMEDA. In sharp contrast, a fast reaction was observed in thf. To circumvent the decomposition of the methyl lithium ($t_{1/2}$ in thf at 298 K: 10 min),^[204] the synthesis was performed with a slight excess at $-50\text{ }^\circ\text{C}$ with subsequent warming to ambient temperature overnight. After monitoring the progress by ¹H NMR spectroscopy an additional 1.2 equiv. were added in the cold to complete the very selective (>95 %) conversion into the anticipated methylated derivative (E)-(SIDipp)Si=Si(CH₃)Tbb (**1-Me**). The product was isolated in 72 % yield as hemisolvate **1-Me**·0.5 Et₂O after extraction with n-hexane and subsequent crystallization from Et₂O as a dark red solid (λ_{max} in n-hexane: 520 nm, see page 266 in the appendix). Much like the starting material or **1-CH₂Ph**, **1-Me** is extremely air- and moisture sensitive but stable in common aromatic, ethereal or aliphatic solvents even at elevated temperatures. It quickly decomposes in dichloromethane or acetonitrile. When heated as a solid, **1-Me** melts at $233\text{ }^\circ\text{C}$. Encouraged by this success, compound **1** was treated with a variety of different organolithium reagents such as LiPh, LiMes, LiCp, LiOtBu, Li(thf)₃Si(pTol)₃ or LiPPh₂·Et₂O but found to be remarkably unreactive. Only heating a benzene solution of **1** with 1.4 equiv. of $\text{LiCH}_2\text{SiMe}_3$ to $80\text{ }^\circ\text{C}$ for 3 h was accompanied by a color change from dark red to purple-red, presumably caused by the formation of (E)-(SIDipp)Si=Si(CH₂SiMe₃)Tbb (**1-CH₂SiMe₃**, Scheme 8). However, compound **1-CH₂SiMe₃** could not be isolated due to its immense hydrophilicity as well as its sensitivity towards air and moisture. The crude product (about 75 % purity) was thus only characterized by ¹H NMR spectroscopy and will not be discussed any further.

¹H- and ¹³C{¹H} NMR spectroscopy of compounds **1-Me** and **1-CH₂Ph** in benzene-d₆ solution are consistent with local C_{2v} symmetry of both the SIDipp and the Tbb group, indicating a mirror plane within the central moiety as well as free rotations around the respective Si-C bonds. Overall, the spectra resemble those of **1** with additional characteristic signals of the respective alkyl substituents: in the ¹H NMR spectra, the Si-Me group of **1-Me** is found at $\delta_{\text{H}} = 1.33\text{ ppm}$

while the CH_2Ph group of **1-CH₂Ph** causes a singlet signal at $\delta_{\text{H}} = 1.18$ ppm as well as three signals in the aromatic region. In the $^{13}\text{C}\{^1\text{H}\}$ NMR spectrum, the most characteristic $\text{N}\underline{\text{C}}\text{N}$ carbene resonances at $\delta_{\text{C}} = 208.7$ ppm (**1-Me**) and 208.8 ppm (**1-CH₂Ph**) are almost identical. They appear in between the starting material **1** (204.6 ppm) and the disilicon(0) compound $\text{Si}_2(\text{SIDipp})_2$ (217.0 ppm)^[205] but considerably high field from free SIDipp (244.7 ppm),^[176] which is a first indication of similar acceptor strengths of the central Si_2 units in all disilavinylidene derivatives.

The $^{29}\text{Si}\{^1\text{H}\}$ NMR spectra of **1-Me** and **1-CH₂Ph** each display three signals, of which the most intense⁶ at $\delta_{\text{Si}} = 1.5$ ppm (**1-Me**) or 1.8 ppm (**1-CH₂Ph**) correspond to the four chemically equivalent $\underline{\text{Si}}\text{Me}_3$ groups of the Tbb substituent. More distinctive, the signals of the two-coordinated Si^{NHC} atoms are found at 50.4 ppm (**1-Me**) and 65.5 ppm (**1-CH₂Ph**) and each emerge at a lower field compared to those of **1** (34.6 ppm).^[134] This shift can be rationalized by the shielding effect of the bromine atom in **1** and consequently the values compare well to the two-coordinate Si^{NHC} atom in Iwamotos derivative **II** ($\delta_{\text{Si}} = 65.0$ ppm).^[164] The remaining three-coordinated Si^{Tbb} atom resonates as singlet signal at $\delta_{\text{Si}} = 127.9$ (**1-Me**) or at $\delta_{\text{Si}} = 123.7$ ppm as a triplet signal with a $^2J_{\text{Si,H}} = 10.3$ Hz coupling to the methylene protons of the adjacent CH_2Ph group (**1-CH₂Ph**, see Figure 15). This is low-field from **1** ($\delta_{\text{Si}} = 86.0$ ppm) or the dibromodisilene $\text{Tbb}(\text{Br})\text{Si}=\text{Si}(\text{Br})\text{Tbb}$ (84.1 ppm)^[48] but still within the range of typical disilenes (~60 to 150 ppm).^[16]

⁶ ^{29}Si has a small, negative gyromagnetic ratio γ that reduces the intensity of some signals in typical ^1H decoupled NMR spectra due to the nuclear Overhauser effect (most unsaturated Si atoms of compounds presented in this work are affected). To enhance the intensity, inverse-gated decoupling is applied (“zgig” spectra), which, in turn, often leads to a lower intensity of other signals (here: $\underline{\text{Si}}\text{Me}_3$ groups). For an example, see Figure 15.

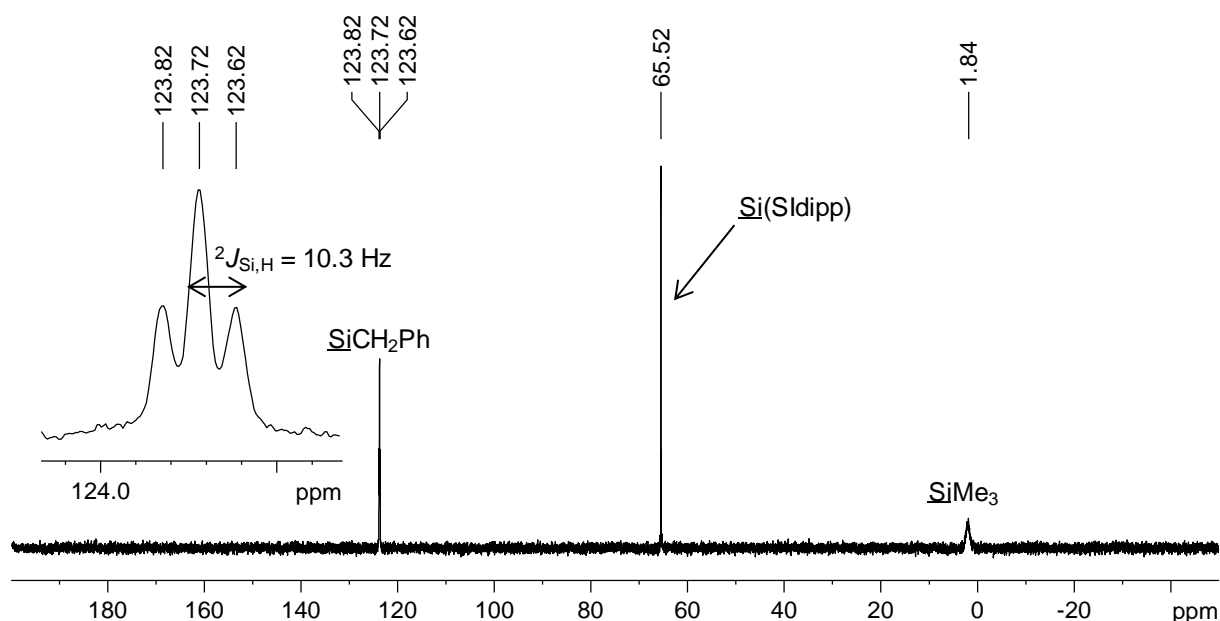


Figure 15. ^{29}Si NMR (99.37 MHz) zgig spectrum of **1-CHLPh** in benzene- d_6 at 298 K; the triplet signal of the SiCH_2Ph is shown as enlarged excerpt in the inset.⁶

Single crystals suitable for XRD analysis were obtained from toluene solution at $-30\text{ }^\circ\text{C}$ (**1-Me**) and slow evaporation of a saturated benzene solution (**1-CHLPh**· C_6H_6) at ambient temperature. Essentially, the molecular structures of **1-Me** and **1-CHLPh** are isotopic to that of the precursor (Figure 16), featuring Si=Si double bonds ($d_{\text{Si-Si}}$: 2.171(1) Å and 2.190(2) Å) that compare very well to those of the known disilavinylidenes **1** (2.167(2) Å)^[134] and **II** (2.1789(8) Å).^[164] Akin to **1**, the bulky Tbb and SIDipp substituents of **1-Me** and **1-CHLPh** are trans-oriented as evidenced by the $\text{C}^{\text{Tbb}}\text{-Si1-Si2-C}^{\text{NHC}}$ torsion angles (180.0° and $177.3(2)^\circ$) and the SIDipp substituents are twisted with respect to the central least-square plane of the central {Si1, Si2, C^{Tbb} , C^{NHC} , C^{rest} } moiety by 90° and $57.2(2)^\circ$, respectively. The di-coordinate Si2^{NHC} atoms are angled due to the presence of a free electron lone pair (**1-Me**: $101.66(7)^\circ$, **1-CHLPh**: $104.7(1)^\circ$). Despite the bending, that is a little bit larger when compared to **1** ($97.6(1)^\circ$)^[134] due to slight differences in hybridization after the Br/alkyl exchange, the three-coordinated Si^{Tbb} atoms remain planar in both **1-Me** ($\Sigma_{\text{Si}} = 360.0(1)^\circ$) and **1-CHLPh** ($359.8(2)^\circ$). The Si2-Si1-C1^{Tbb} angles in **1-Me** ($117.10(7)^\circ$) and **1-CHLPh** ($118.8(1)^\circ$) are marginally more narrow than that in the starting material **1** ($123.4(1)^\circ$)^[134] which can be caused by smaller contribution of triple-bonded mesomeric formulae in the alkyl-substituted derivatives.

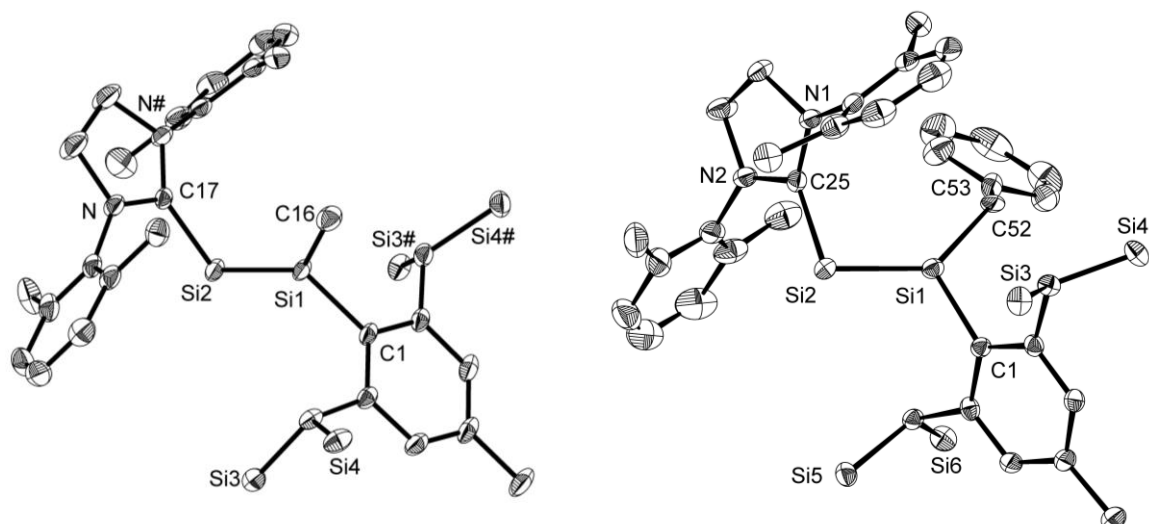


Figure 16. Molecular structures of **1-Me** (left) and **1-CH₂Ph** (C₆H₅) (right). Thermal ellipsoids are set to 50 % probability; peripheral methyl groups as well as hydrogen atoms and the solvent molecule are omitted for simplicity. The structural data of **1-Me** contain a crystallographic site occupancy (50 % disorder at the rotating tBu group of the Tbb) which was solved independently. Selected bond lengths (*f*Å) and angles (*f*°): **1-Me**: Si1-Si2 2.171(1), Si1-C1 1.905(3), Si1-C16 1.888(3), Si2-C17 1.932(3); C1-Si1-Si2 117.10(7), C1-Si1-C16 109.0(1), Si2-Si1-C16 133.9(1), Si1-Si2-C17 101.66(7); C1-Si1-Si2-C25, C25-Si2-Si1-C17 180.0. **1-CH₂Ph** (C₆H₅): Si1-Si2 2.190(2), Si1-C1 1.898(4), Si1-C52 1.922(4), Si2-C25 1.942(4); C1-Si1-Si2 118.8(1), C1-Si1-C52 108.7(2), Si2-Si1-C52 132.3(2), Si1-Si2-C25 104.8(1); C1-Si1-Si2-C25 -177.3(2), C25-Si2-Si1-C52 -3.1(3).

The characterization of Si=Si bonds by Raman spectroscopy has a long tradition since the report on the first disilene by West,^[11] but Raman data of disilavinylidenes have not been reported yet. Although the exact wavelengths of the vibrational bands strongly depend on the mass of the substituents (the range reported for disilenes is 454 – 592 cm⁻¹),^[206] comparison of related systems can give valuable information about the relative bonding strength. The Raman spectrum of a solid sample of **1-CH₂Ph** displays numerous signals in the finger print region of which a very strong vibrational band at $\tilde{\nu} = 525$ cm⁻¹ was assigned by comparison with the calculated value (527 cm⁻¹) to the $\nu(\text{Si}=\text{Si})$ stretching vibration. This is almost identical to the aforementioned $\text{Me}_2\text{Si}=\text{SiMe}_2$ ($\tilde{\nu}(\text{Si}=\text{Si}) = 529$ cm⁻¹)^[11] and at significant lower wavenumber compared to that of **1** ($\tilde{\nu}(\text{Si}=\text{Si})_{\text{exp}} = 573$ cm⁻¹; $\tilde{\nu}(\text{Si}=\text{Si})_{\text{calc}} = 574$ cm⁻¹). These findings are in line with the longer Si=Si bond observed in the solid state structure of **1-CH₂Ph** and again indicate a weaker Si=Si bond in **1-CH₂Ph** than in **1**.

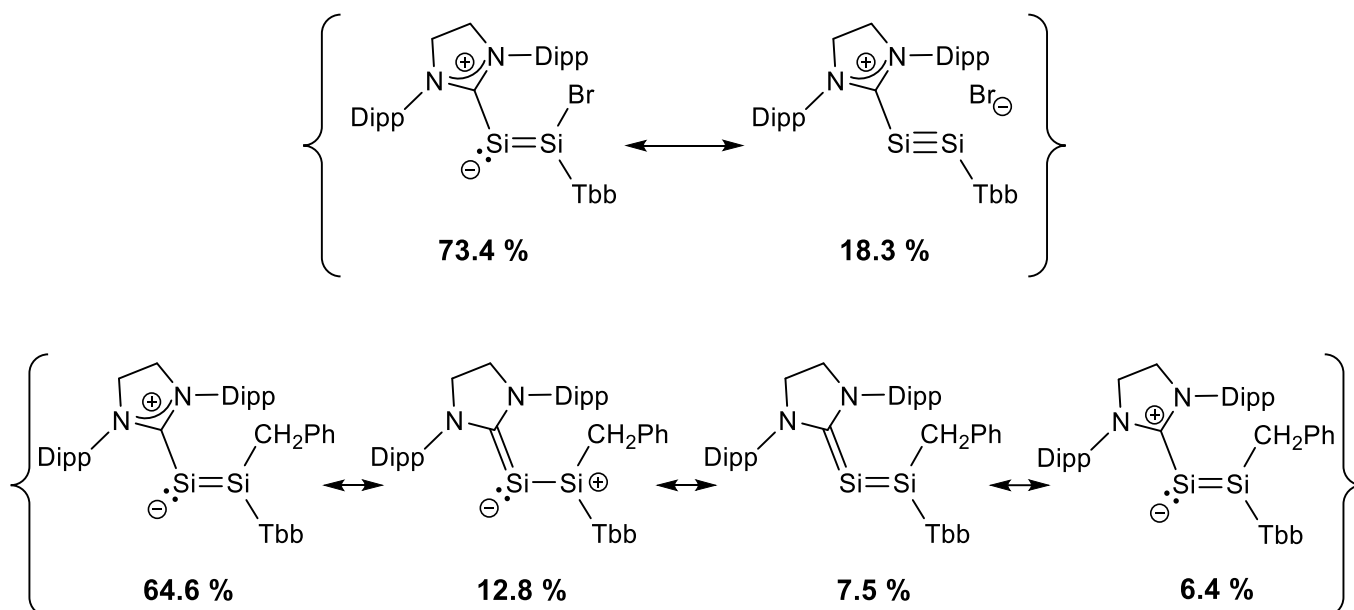
Table 2. Experimental and calculated Si=Si bonding parameters of the disilavinylidenes **1** and **1-CH₂Ph**.

	d(Si-Si)^A /Å	$\tilde{\nu}(\text{Si}=\text{Si})^B$ /cm ⁻¹	Occ(Si=Si)^C /e	Occ(LP)^D /e	WBI^E	NRT^F tot./cov./ion.
1	2.167(2) ^[134]	573	1.89	1.76	1.80	2.09/1.81/0.28
1-CH₂Ph	2.190(2)	525	1.74	1.77	1.70	1.8/1.60/0.21

A: crystallographic bond distance; **B:** Raman stretching vibration; **C:** Natural Lewis occupancy of the Si=Si π -bond pair according to NBO; **D:** occupancy of the electron lone pair at the Si^{NHC} atom according to NBO; **E:** Wiberg bond index; **F:** NRT bond order (total/covalent/ionic). RI-B97-D3/def2-TZVP level of theory. The calculated data of **1** differ slightly from the ones reported by Ghana et al., where the triply bonded ionic structure [SIDipp-Si=Si-Tbb]Br (14.2 %) was underrepresented, resulting in a lower Si-Si bond order of only 1.91. This can

presumably be addressed to the fact that those calculations were performed on a model compound which features SiH_3 groups instead of SiMe_3 groups and no electron donating tBu group on the Tbb substituent.^[134] For more details see Table 44 on page 276.

Additional evidence for slightly weaker $\text{Si}=\text{Si}$ bonds after alkyl substitution is provided by the natural bond orbital (NBO) analysis. Here, substitution of the bromide against the more electropositive benzyl group is accompanied by an increase of electron density used for that bond by the $\text{Si}1$ atom (from 17.5 % in **1** to 28.2 % in **1-CH₂Ph**). In turn, this results in an increase of the p -character of the hybrid orbital used for the $\text{Si}1\text{-Si}2$ σ bond from 48.7 % in **1** to 57.3 % in **1-CH₂Ph** and consequently both a lesser occupancy of the $\text{Si}=\text{Si}$ π -bond as well as a smaller Wiberg bond index (Table 2, for details see Table 44 on page 276 in the appendix).



Scheme 9. Leading natural Lewis structures (NLS) of **1** (top row) and **1-CH₂Ph** (below) and their respective percentage contributions to the resonance hybrid according to local NRT analysis (N1, N2, Si1, Si2, C^{NHC}, C^{Tbb}, Br; CH₂Ph; RI-B97-D3/def2-TZVP level of theory).

This is consistent with the results of the natural resonance theory (NRT) analysis which also predicts a considerable reduction in Si-Si bond order of about 0.3 (Scheme 9). Here, about 18 % of triple-bonded structures were calculated for compound **1**, whereas no major contributions were found for **1-CH₂Ph**. This matches both the slight elongation of the $\text{Si}=\text{Si}$ bond distance (**1-CH₂Ph**: **1**: 2.167(2) Å^[134]) as well as the slightly larger $\text{Si}2\text{-Si}1\text{-C}1^{\text{Tbb}}$ angle (**1-CH₂Ph**: 118.8(1)°, **1**: 123.4(1)°^[134]) that were found by XRD. Whereas the ca. 65 % leading structures of the NRT undoubtedly justify the description of **1-CH₂Ph** as an NHC-stabilized disilavinylidene, ca. 19 % suggest π -backbonding from the $\text{Si}1$ atom to the SiDipp , that was not observed as a major resonance structure for compound **1** (several minor contributions sum up to a total of 7 % with a $\text{Si}=\text{C}^{\text{NHC}}$ double bond). Consequently, the Si-C^{NHC} NRT bonding order is higher for **1-CH₂Ph** (1.20) than for **1** (1.07).

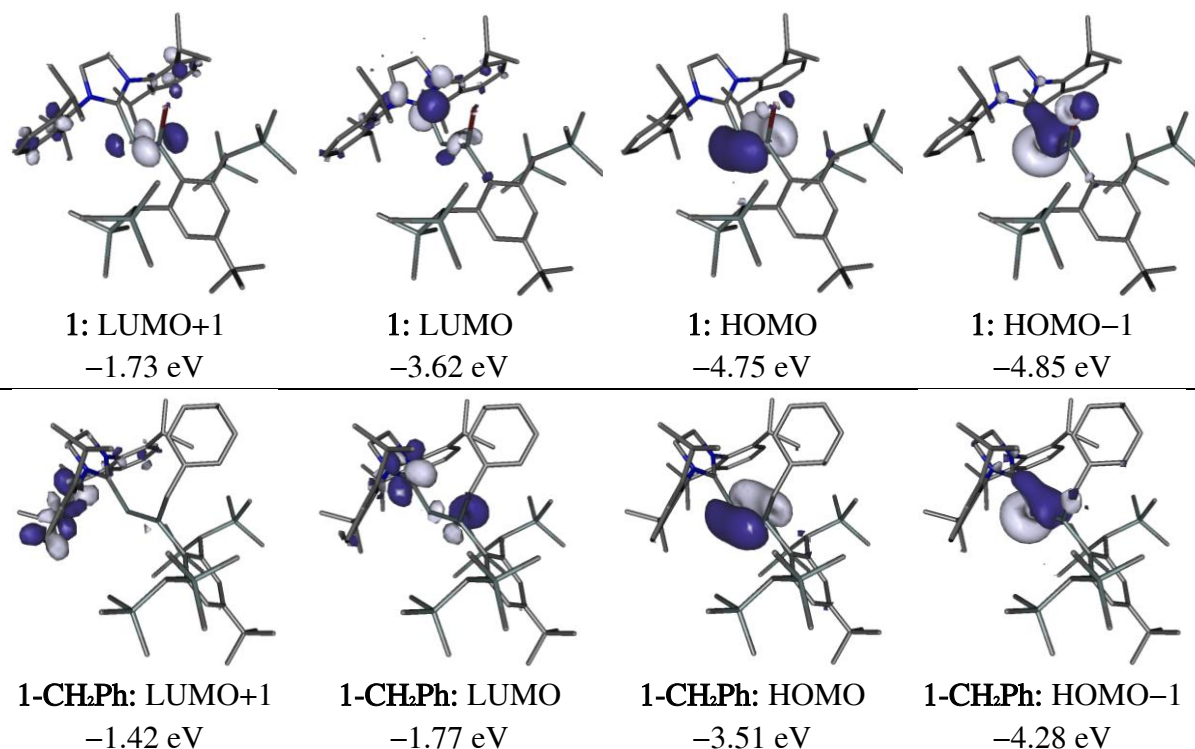


Figure 17. Selected Kohn-Sham orbitals (RI-B97-D3/def2-TZVP level of theory) of **1**^{calc} (top row) and **1-CH₂Ph**^{calc} (bottom row) and their corresponding energy eigenvalues; isosurface value: 0.05 e⁻bohr⁻³.

A look at the frontier Kohn-Sham orbitals illustrates the notable electronic similarities (Figure 17). In both derivatives, the HOMO corresponds to the Si=Si π -bonding orbital while the HOMO-1 represents the lone-pair orbital at the two-coordinate Si^{NHC} atom. The latter also display some electron density between the Si^{NHC} and the C^{NHC} atom, resembling minor π -backbonding that was also found by the NRT analysis. However, the effect should not be overestimated since the contribution of the C^{NHC} atom to the respective HOMO-1 is rather small (**1**: 6.8 %, **1-CH₂Ph**: 8.3 %).

2.2.3 Unexpected role of the alkali metal

As outlined, the reaction of **1** with tBuLi resulted in the incorporation of a benzyl group in **1-CH₂Ph**, that originates from the solvent toluene. The exact reaction sequence remained unknown for the moment with several plausible pathways:

1. Metalation of **1** and subsequent alkylation of “(SIDipp)Si=Si(Li)Tbb” (“**1-Li**”)
2. One-electron reduction of **1** and a subsequent radical reaction with toluene
3. Metallation of toluene and a subsequent substitution alkylation reaction

The first pathway, an in situ formation and subsequent alkylation of the desired “(SIDipp)Si=Si(Li)Tbb”, was ruled out since **1** was found to be unreactive towards tBuLi in inert solvents such as benzene or n-pentane and the metalation product would easily undergo

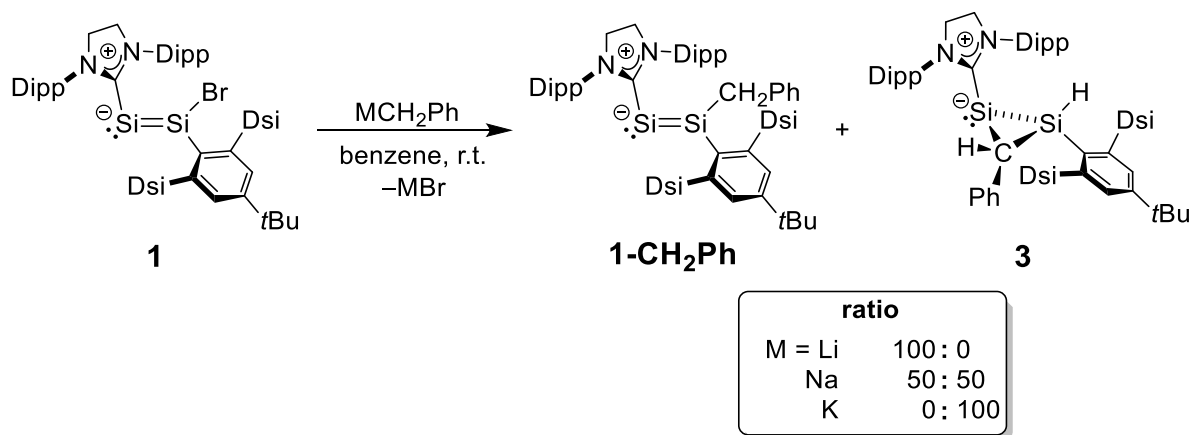
C-H activation as already observed during the synthesis of compound **2**. Further, the electrochemical potentials obtained by cyclic voltammetry suggest, that reduction of **1** requires extremely strong reducing agents. The disilavinylidene should thus be inert towards direct reduction by LiR (Table 3). Likewise, potential 1-electron reduction of **1** by tBuLi followed by a radical step (pathway 2) has to be queried.^[207]

Table 3. Reduction potentials of **1** and **1-CH₂Ph** and radical reduction potentials of organolithium compounds.

Compound	Ep _r /V ^A	Conditions	Conductivity salt	Reference
1	-2.41	THF, -11 °C	[NBu ₄]PF ₆	This work
1-CH₂Ph	-2.42	THF, -11 °C	[NBu ₄]PF ₆	This work
LiCH ₂ Ph	-1.55	THF, 25 °C	[NBu ₄]ClO ₄	[208]
tBuLi	-2.29	DME, 25 °C	None (5 mM solution)	[207]

A: Potentials are given in respect to Cp^{*}·Fe⁺⁰. Values taken from the literature were originally reported vs the saturated calomel electrode (SCE) and were converted using standard factors.^[209] The electrochemical reductions of **1** and **1-CH₂Ph** are mostly irreversible.

The third pathway is thus most likely: initial deprotonation of toluene by tBuLi to benzyl lithium (LiCH₂Ph) and subsequent reaction with **1**. For verification, compound **1** was reacted with more easily accessible KCH₂Ph in benzene at ambient temperature and the conversion was monitored by ¹H NMR spectroscopy. Surprisingly a mixture of several compounds was formed over the period of two days, that contained no **1-CH₂Ph**.⁷

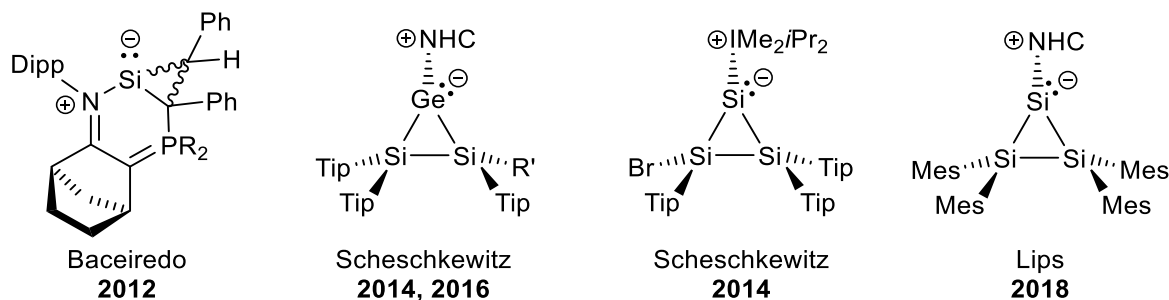


Scheme 10. Alkali metal dependent formation of **1-CH₂Ph** and/or **3** from **1** and MCH₂Ph (M = Li, Na, K). For the proposed reaction mechanisms, see chapter 2.2.4 on page 36ff.

Instead, the NHC-stabilized disilacyclopropylidene cyclo-Si(SiDipp)(SiHTbb)(CHPh) (**3**) was identified as the major component of the reaction mixture (Scheme 10) and was isolated in 26 % yield after extraction with n-pentane and subsequent crystallization at -30 °C. It should

⁷ Test reactions on a smaller scale (25 mg of **1** with approx. 1.5 equiv. of KCH₂Ph) were completed within 16 h of vigorous stirring at ambient temperature leading to ca. 70 % crude **3** with some unknown impurities and trace amounts of compound **1-CH₂Ph** (< 3%).

be mentioned, that reactions of **1** with KCH_3 and $\text{KCH}_2\text{SiMe}_3$ under identical conditions instead lead to slow and unselective decomposition. Compound **3** is an extremely air-sensitive, yellow solid; it is moderately soluble in aliphatic and aromatic solvents and decomposes upon heating at $221\text{ }^\circ\text{C}$. The formation of **3** is fully diastereoselective, leading to the (S,S,S)/((R,R,R)) racemate, which features the two exocyclic aryl substituents in cis orientation to each other and in trans orientation to the NHC substituent.



Scheme 11. Heavier silacyclopropylidenes described in the literature. PR_2 = cyclo-[P(NtBu)₂SiMe₂]; R' = Cl, Ph, mesityl; NHC = IMe_2iPr_2 or IMe_3 .^[170,171,210,211]

Although a handful of base-stabilized silacyclopropylidenes were reported recently (Scheme 11),^[170,171,210,211] compound **3** represents the first example of an NHC-stabilized disilacyclopropylidene. The parent disilacyclopropylidene cyclo-(Si)(SiH₂)(CH₂) has been predicted to be the global minimum structure on the PES of the {Si₂CH₄} molecule, with its yet unknown disilaallene isomer H₂C=Si=SiH₂ being higher in energy. Disilaallenes R₂C=Si=SiR₂, in turn, have been proposed as key intermediates in the formation of substituted silenes R₂C=SiR₂ by Sekiguchi.^[212,213] Thus, compound **3** could be a suitable precursor for the synthesis of elusive disilaallenes with bulky substituents in the future.^[214,215]

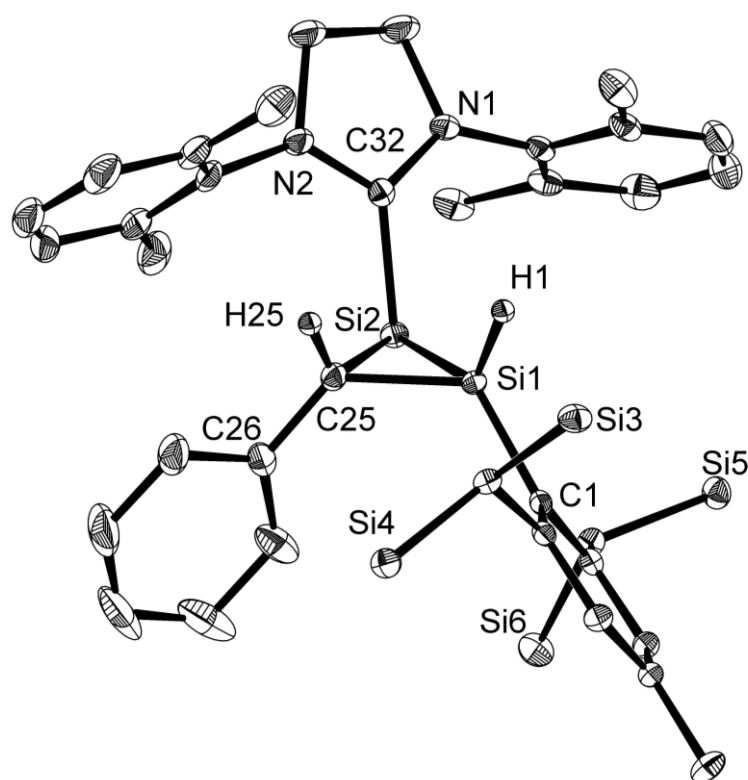


Figure 18. Molecular structure of **3**·(C₆H₆). Thermal ellipsoids are set to 50 % probability; methyl groups as well as hydrogen atoms (except for the Si-bonded H1 atom) and the solvent molecule are omitted for simplicity. Selected bond lengths (Å) and angles (°): Si1–Si2 2.2876(6), Si1–C1 1.892(2), Si1–C25 1.900(2), Si2–C25 1.929(2), Si2–C25 1.983(2); C1–Si1–Si2 129.69(5), C1–Si1–C25 121.89(7), Si2–Si1–C25 55.59(5), C32–Si2–C25 99.99(7), C32–Si2–Si1 104.59(5), Si1–Si2–C25 52.26(5), Si1–C25–Si2 72.15(6), Si1–C25–C26 128.5(1), Si2–C25–C26 117.3(1); C1–Si1–Si2–C32 –163.27(9), C32–Si2–C25–C26 –134.4(4), C1–Si1–C25–C26 7.9(2).

Yellow blocks of **3**·(C₆H₆) suitable for XRD analysis were obtained upon evaporation of a saturated solution of **3** in benzene at ambient temperature (Figure 18). The molecular structure displays a three-membered {Si1, Si2, C25} ring with a pyramidalized Si2^{NHC} atom ($\Sigma_{\text{Si2}}: 256.84^\circ$), which indicates the presence of a stereochemically active lone pair at Si2^{NHC}. The Si₂C ring forms a nearly isosceles triangle with a Si1–C25–Si2 vertex angle of 72.15(6)° and two C25–Si1–Si2 and C25–Si2–Si1 base angles of 55.59(5)° and 52.26(5)°, respectively. The bulky Tbb and SIDipp groups adopt a trans orientation (C1^{Tbb}–Si1–Si2–C32^{NHC}: –163.27(9)°), whereas the Tbb and the phenyl groups are cis oriented (C1^{Tbb}–Si1–C25–C26^{Ph}: 7.9(2)°). The Si1^{Tbb}-bonded H1 atom was located on the difference Fourier map and refined isotropically without normalization. The Si1–Si2 bond of **3** (2.2876(6) Å) is significantly longer than the Si=Si bond in the disilavinylidenes **1** (2.167(2) Å),^[134] **1-Me** (2.171(1) Å) or **1-CH₂Ph** (2.190(2) Å), but shorter than the single bond in the NHC-stabilized silylsilylene Si(SiBr₂Tbb)(SIDipp) (2.391(1) Å).^[134] This Si–Si bond shortening is not unusual for three-membered rings and has for example also been observed for Scheschkewitz’s NHC-stabilized trisilacyclopropylidene (2.2950(12) Å),^[170] the NHC-adduct of a trisilacyclopropene cyclo-{Cp*Si(LiPr₂Me₂)}{SiTip₂}{:SiTip} (2.2700(5) Å)^[216] or the neutral cyclotrisilane cyclo-SiCl(Tip)(SiMe₂)(SiTip₂) (2.307(1) Å).^[180]

Notably, one of the two endocyclic Si-C bonds of the Si₂C ring (Si1^{Tbb}-C25^{Ring} 1.900(2) Å, Si2^{NHC}-C25^{Ring} 1.983(2) Å) is slightly longer than a typical Si-C bond. This is not a direct effect of the ring structure (for example, the endocyclic Si-C bonds in cyclo-(Mes₂Si)₂CH₂ amount to 1.888 Å and 1.885 Å, respectively),^[217] but a similar elongation was also observed in Scheschkewitz's aforementioned NHC-stabilized trisilacyclopropylidene (Si-C: 1.993(3) Å, 1.920(3) Å).^[170] A possible explanation could be the increased p character of the hybrid orbital of the Si2^{NHC} atom employed for the Si2-C25^{Ring} σ bond due to the presence of the lone pair at Si2^{NHC}.^[218]

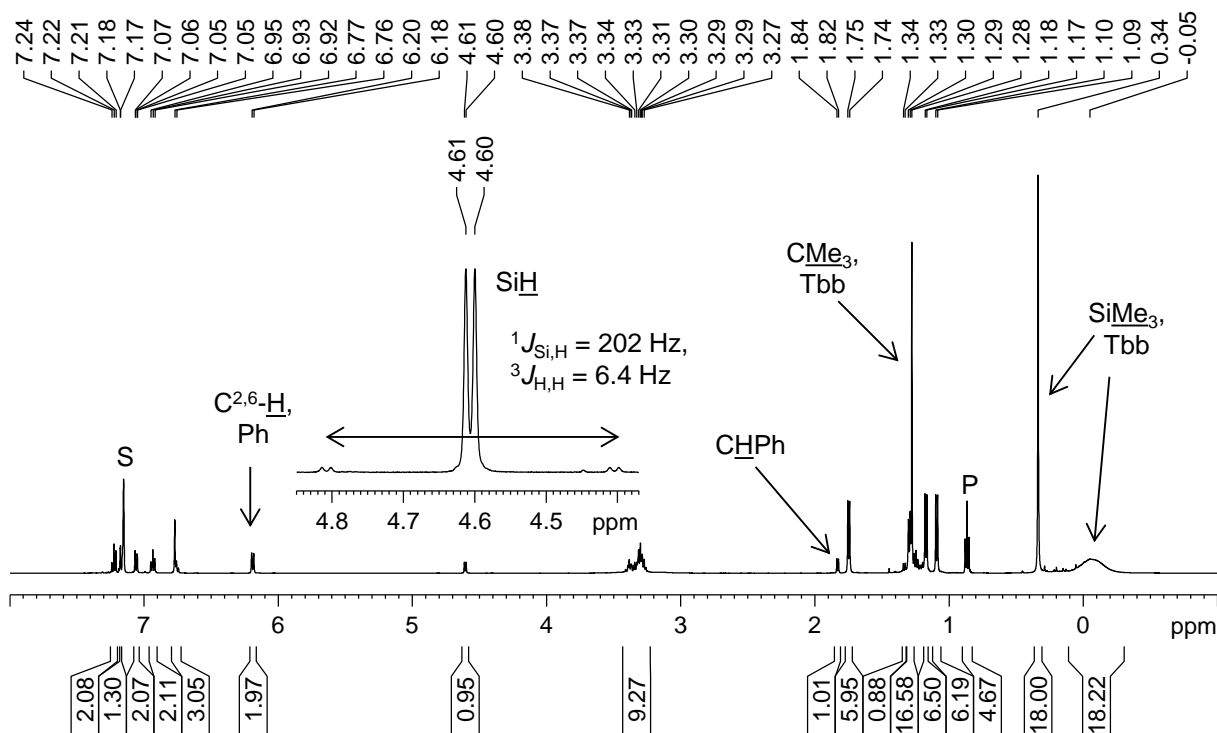


Figure 19. ¹H NMR (500.2 MHz) spectrum of **3** in benzene-d₆ at 298 K; the residual proton signal of the deuterated solvent is marked with the character S. The signal marked with the character P originates from some residual n-pentane (ca. 0.75 equiv.) present in the sample.

Consistent with the solid state structure, the ¹H, ¹³C and ²⁹Si NMR spectra of **3** in benzene-d₆ indicate an overall C₁-symmetric structure in solution with a fast rotation of the SIDipp (local C₂ symmetry) but a hindered rotation of the bulky Tbb group about the respective Si-C bond (Figure 19). Consequently, a broad as well as a sharp singlet signal in the ¹H and ¹³C NMR spectra as well as a very broad signal (δ_{Si} = 1.4 ppm) in the ²⁹Si NMR spectrum were observed for the SiMe₃ groups of the Tbb substituent, whereas the disilavinylidenes **1** or **1-CH₂Ph** each display one sharp singlet signal. The thermodynamic parameters for the hindered rotation of the Tbb substituent were determined by line shape analysis of the variable temperature ¹H NMR spectra in toluene-d₈ between 203 and 303 K, according to which the hindered rotation is endothermic with a positive ΔH[‡] (57(±1) kJ/mol) and a very small ΔS[‡] value (-1(±5) kJ/mol).

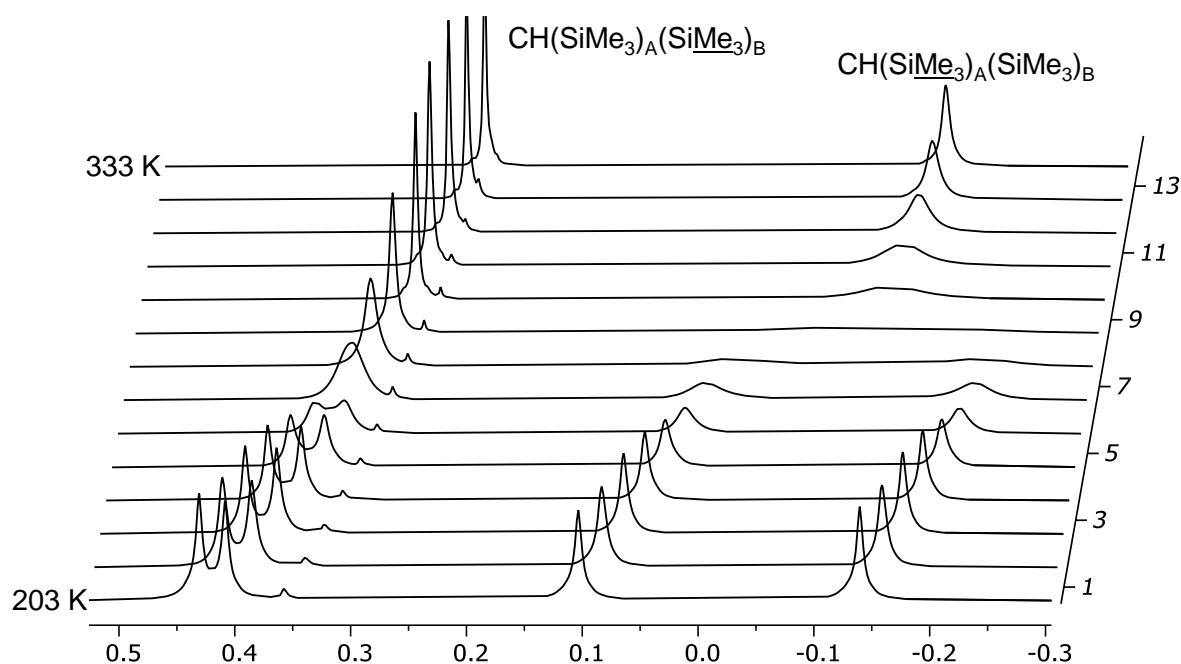


Figure 20. Stack-plot of the ^1H NMR (300.1 MHz) spectra of the SiMe_3 signals of **3** in in toluene- d_6 from 203 – 333 K in steps of 10 K each.

The remaining ^{29}Si NMR signals were assigned by ^1H - ^{29}Si correlation spectroscopy to the Si^{NHC} atom at $\delta_{\text{Si}} = -116.4$ ppm and the four-coordinated Si^{Tbb} atom at $\delta_{\text{Si}} = -75.6$ ppm. The chemical shift of the three-coordinate Si^{NHC} atom in **3** hereby compares very well with that of Scheschkewitz's NHC-stabilized trisilacyclopropylidene ($\delta_{\text{Si}} = -110.5$ ppm)^[170] or Lips' derivatives cyclo- $\{\text{Si}(\text{NHC})\}\{\text{SiMe}_2\}\{\text{SiMe}_2\}$ (NHC = iPr_2Me_2 : -132.2 ppm; NHC = IME_2 : -136.6 ppm).^[211] For the Si^{Tbb} signal, a coupling to the adjacent hydride atom ($^1J_{\text{Si,H}} = 202$ Hz) was observed, again confirming the unaltered connectivity in solution. In the ATR FT-IR spectrum, a solid-state sample of **3** displays a weak absorption band at $\tilde{\nu} = 2101$ cm^{-1} . This is characteristic for stretching vibrations of terminal Si–H bonds and at slightly lower wavenumbers than hydrosilanes (e.g. $\text{Ar}^{\text{Trip}}\text{SiH}_n\text{Cl}_{3-n}$ with $n = 1 - 3$: $\tilde{\nu}_{\text{Si-H}} = 2171 - 2240$ cm^{-1}).^[203,219]

2.2.4 Proposed reaction mechanisms

To sum up, the reaction of **1** with tBuLi in toluene clearly proceeds via LiCH_2Ph and results in the substitution product **1-CH₂Ph**, whereas reaction with isolated KCH_2Ph in benzene yields the NHC-stabilized disilacyclopropylidene **3** (see Scheme 10 on page 32). To further elucidate the reaction mechanism, **1** was also reacted with LiCH_2Ph and NaCH_2Ph . Additionally, a conceivable interconversion of **1-CH₂Ph** to **3** in presence of KBr and/or KCH_2Ph in refluxing benzene was excluded.

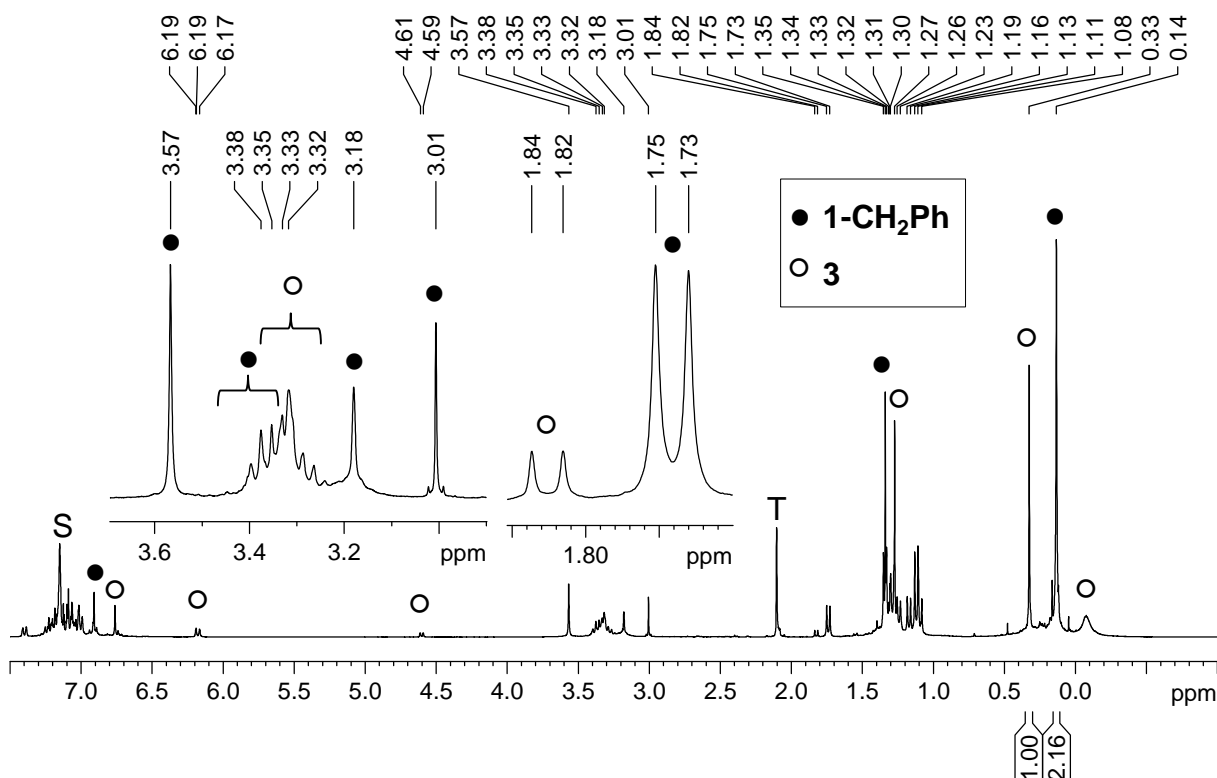


Figure 21. ^1H NMR (300.1 MHz) spectrum of the crude product of the reaction of **1** with NaCH_2Ph in benzene- d_6 at 298 K. Compound **1-CH₂Ph** is marked in black (●) and compound **3** in white (○). The characters S and T mark the residual signal of the deuterated solvent as well as some toluene present the crude product.

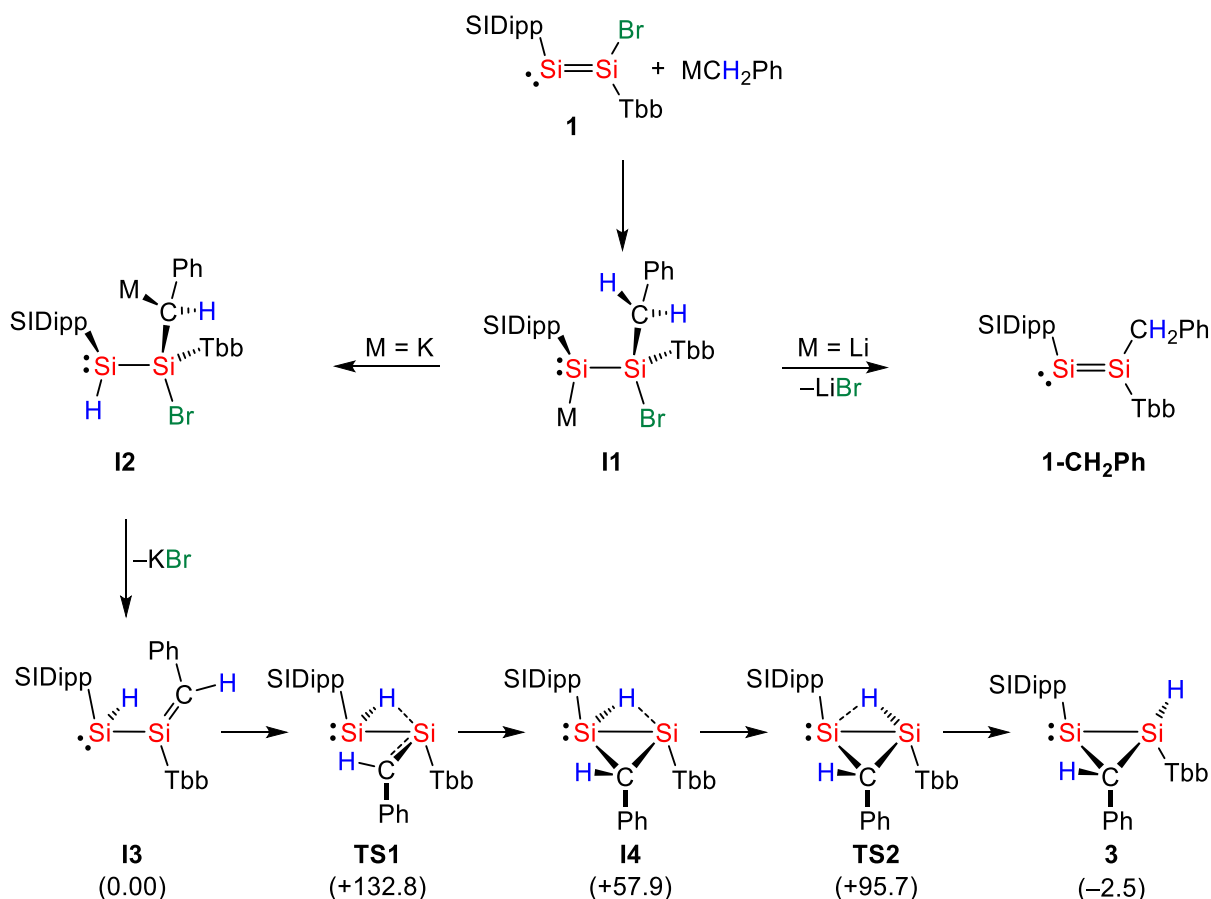
Corroborating the expectations, the reaction with LiCH_2Ph selectively afforded compound **1-CH₂Ph** in the same isolated yield that was obtained from the reaction with $t\text{BuLi}$ (71 % and 69 %). In contrast, addition of NaCH_2Ph led to a mixture of both **1-CH₂Ph** and **3** in a ratio of ca. 50 : 50 that was analyzed by NMR spectroscopy (Figure 21).⁸ This outcome is surprising, since alkyl sodium compounds usually display physical properties and reactivity comparable to their potassium derivatives. On the other hand, sodium has an intermediate electronegativity (Li: 1.0, Na: 0.9, K: 0.8), ionic radius (69, 97 and 133 pm) and MBr lattice energy (807, 747 and 682 kJ/mol) when compared to lithium or potassium.^[68,220,221]

A potential mechanism for the competing formation of the cyclic product **3** instead of the benzyl disilavinylidene **1-CH₂Ph** is described in Scheme 12. In the initial step of the reaction, a charge-controlled 1,2-carbometalation of MCH_2Ph (M = Li, K) along the Si=Si bond of **1** is suggested: the Si^{NHC} atom with a more negative charge (NPA charge -0.02) in comparison to the Si^{Tbb} atom (NPA charge $+0.59$) is considered nucleophilic and the $\sigma(\text{Si}-\text{Si})$ bond is polarized

⁸ Since the reaction of **1** with KCH_2Ph was much slower than the reaction with LiCH_2Ph or $t\text{BuLi}$, the reaction time with NaCH_2Ph was prolonged to 2 days (ca. 70 % conversion of **1**; note that NaCH_2Ph is insoluble in benzene- d_6 and decomposes in tetrahydrofuran- d_5). After that time, another 0.3 equiv. NaCH_2Ph were added, resulting in a full conversion of **1** without any significant changes in the ratio of the produced **1-CH₂Ph** and **3** after a total reaction time of 4 days. The conversion rate of similar heterogenous reactions was later found to highly depend on the set speed of the magnetic stirrer.

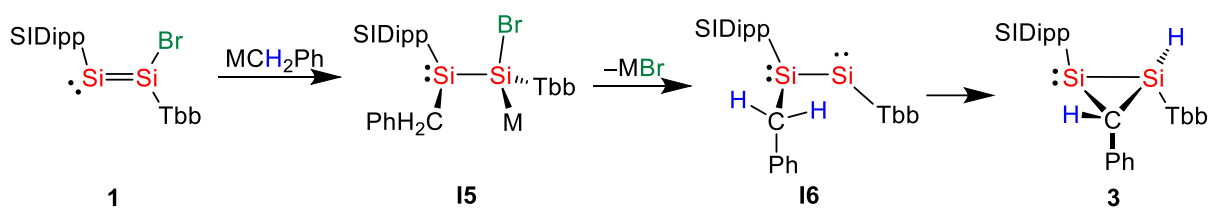
towards the Si^{NHC} atom as well (57.4 %) while the π -bond (the HOMO orbital) is nearly unpolarized. Additionally, pre-coordination of the Li atom by the electron lone pair at the Si^{NHC} atom (HOMO-1) is plausible. This addition would initially lead to the NHC-stabilized metalla(silyl)silylenes [Si(M){(Tbb)(CH₂Ph)(Br)Si}(SIDipp)] (**I1**). 1,2-additions of alkyllithium to Si-Si- π -bonds have been reported for both disilenes and disilynes,^[222,223] and the existence of such species (**I1**) is further supported by the isolation of related NHC-stabilized zinco(silyl)silylenes (**5-X**, see page 46ff). In the second step, two different follow-up reactions are plausible starting from **I1**. In the case of M = Li, a rapid LiBr elimination leads to the reformation of the Si=Si π -bond, directly resulting in the formation of **1-CH₂Ph**.

For the formation of disilacyclopropylidene **3**, a conversion of **I1** to **I2** via K⁺/H⁺ exchange with the acidic benzylic protons is proposed. This step is encouraged by the weak Si-K bond (resulting in a strongly basic metallasilylene) and the considerably smaller lattice energy of KBr (682 kJ/mol) when compared to LiBr (807 kJ/mol).^[221] A related metathesis between a Si(sp²)-M and a C-H bond was also reported for the reaction of MeLi with a disilyne by Sekiguchi and coworkers.^[223] Subsequent KBr elimination from **I2** then leads to the putative NHC-stabilized silenylsilylene **I3** and further rearrangement through a 1,2-H shift followed by ring closure finally affords the NHC-stabilized disilacyclopropylidene **3**. A similar rearrangement of an NHC-stabilized disilenylsilylene has been suggested to lead to an NHC-stabilized trisilacyclopropylidene.^[170]



Scheme 12. Proposed mechanism for the formation of **1-CH₂Ph** and **3** from the reactions of **1** and **MCH₂Ph** (M = Li, Na, K). The energies of the calculated structures **I3** – **3** (bottom row, ΔE in kJ·mol⁻¹) are given in parentheses and formal charges are omitted for simplicity.

Overall this cascade was found to be too complex to be calculated on an appropriate level of theory, especially due to the **MBr** elimination step. Therefore, only the isomerization starting from **I3** to **3** has been examined on the RI-B97-D3/def2-TZVP level of theory. The reaction is initiated by a back-side attack of the **Si^{NHC}**-bonded H atom to the **Si^{Tbb}** atom, which bends the {**CHPh**} moiety to the opposite direction and weakens the **C=Si^{Tbb}** bond. The respective transition state **TS1** is of very high energy (+132.8 kJ/mol), which, at first glance, contradicts the observation of a reaction that slowly proceeds at ambient temperature. Yet, the strongly exothermic **KBr** elimination was not considered in the calculations and energies of highly polar transition states are often overestimated in gas-phase calculations. Experimentally, considerable amounts of unknown byproducts were observed during the reaction, but the presence of intermediate **I3** could be neither confirmed nor disproved by NMR or IR spectroscopy. The resulting intermediate **I4** features a **Si^{NHC}-C⁵²** bond as well as a bridging hydrogen atom in between the two Si atoms, and then completes the H transfer to result in the final product **3**. Although all described species were identified as energy minima, the reaction barrier **I3** to **TS1** (132.8 kJ/mol) still appears very high even for a slow reaction at ambient temperature.

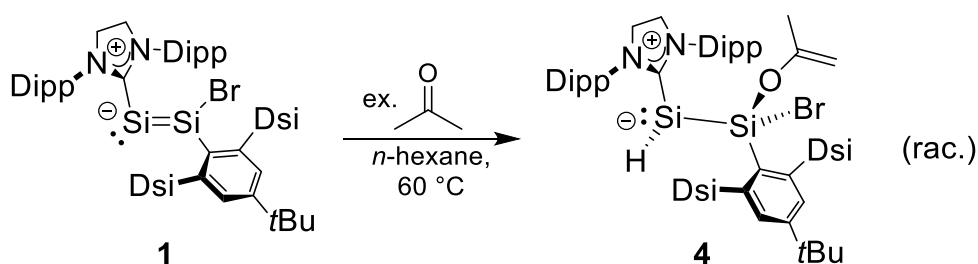


Scheme 13. Alternative, orbital-controlled mechanism for the formation of **3**. Formal charges are omitted for simplicity.

An alternative, more straight-forward approach would start with a reverse, orbital-controlled 1,2-addition of the heavier MCH_2Ph to the $\text{Si}=\text{Si}$ double bond via the p^* -orbital (Figure 17 on page 31), which is mostly located at the Si^{Tbb} atom (Scheme 13). This addition would then lead to the opposite regioselectivity when compared to the intermediate **I1** suggested for the charge-controlled pathway in Scheme 12, with the formation of a $\text{Si}^{\text{NHC}}-\text{CH}_2\text{Ph}$ bond and an alkali metal cation located at the Si^{Tbb} silylenoid atom (**I5**). From here, a 1,1-elimination of MBr hypothetically leads to a transient NHC-stabilized bis-silylene (or NHC-stabilized disilyne) $(\text{SIDipp})\text{PhCH}_2\text{Si}-\text{SiTbb}$ (**I6**) and, after subsequent C-H-activation, compound **3** is obtained. However, the chemoselectivity cannot be explained by this mechanism alone: It is not clear why in the case of $\text{M} = \text{Li}$ a 1,2-shift of the benzyl group in **I6** should be favored over the proposed oxidative addition leading to **3**. Lastly, it should be mentioned that Scheschkewitz's NHC-stabilized (2-chlorosilyl)silagermenylidene **III-SiTip₂Cl** lies in an equilibrium with its cyclopropylidene isomer and that substitution of the Cl atom or replacement of the medium-sized NHC with IME_4 stabilize the cyclic form.^[171,224]

2.3 Diastereoselective reaction with acetone

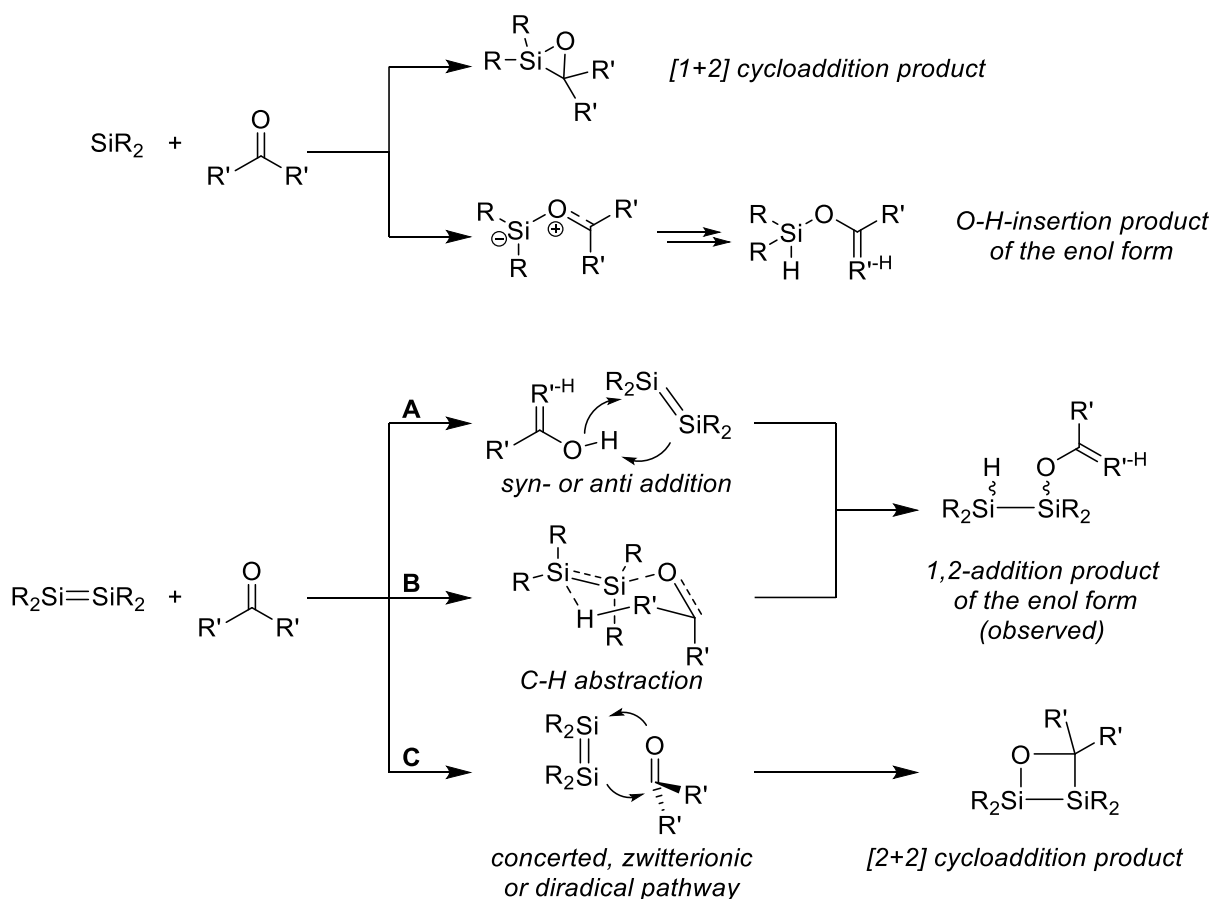
The reaction of **1** with an excess of acetone in *n*-hexane at 60 °C in a small, closed reaction vessel (due to the high volatility of acetone at that temperature) afforded diastereoselectively the formal 1,2-addition product of the enolic form, the NHC-stabilized hydrido(silyl)silylene $\text{SiH}[\text{SiBr}\{\text{OC}(\text{Me})\text{CH}_2\}\text{Tbb}](\text{SIDipp})$ (**4**). The formation of the (R,S) and (S,R) racemate was deduced from NOESY experiments: no correlation between the Si–H group and the $\{\text{OC}(\text{Me})\text{CH}_2\}$ substituent was found, indicating an antiperiplanar orientation in solution that was also found in solid state (see Figure 116 and Figure 117 in the appendix on page 274). Compound **4** was isolated as a highly air-sensitive, yellow solid in 55 % yield (Scheme 14). When heated as a solid, compound **4** gradually turns brown between 147 – 153 °C and melts under decomposition at 240 °C.



Scheme 14. Diastereoselective reaction of **1** with acetone to the NHC-stabilized hydrido(silyl)silylene **4**.

The spectroscopic properties as well as the solid state structure of **4** have already been reported in the master thesis preceding to this work (see Figure 91 on page 250 in the appendix for a higher quality X-ray structure and page 195 for an improved synthesis procedure), but the corresponding reaction mechanism remained elusive.^[135]

Reactions between unsaturated Si compounds and ketones give access to a variety of different functionalized products (Scheme 15) and the [2+2] cycloadditions to Si=Si π -bonds of disilenes were among the very first reported reactivity studies.^[225,226] Their general reaction pathway (concerted, zwitterionic or via a diradical) has been discussed in the literature,^[227,228] whereas silylenes are known to undergo either [1+2] cycloadditions or formal O-H insertions. Notably, rhodium silylidene- and silylene complexes have been identified as key intermediates in the hydrosilylation of ketones.^[229]



Scheme 15. General reaction products of silylenes (top) or disilenes (below) with (non-)enolizable ketones.^[24,27,227,230,231]

Initially, the reaction of **1** with acetone was believed to proceed via a 1,2-addition of the enol form $\text{HOC}(\text{Me})\text{CH}_2$ (path A)^[27] as evidenced by the high reaction temperature and slow conversion, that was attributed to the low enolization rate of acetone in n-hexane.^[232,233]⁹ Quantum chemical studies on disilenes already demonstrated that the addition of alcohols to $\text{Si}=\text{Si}$ bonds can be either syn selective via a regular electrophilic attack or anti selective via an initial nucleophilic attack and subsequent silyl rotation 20 years ago by Kira.^[231] Here, a formal anti-selective addition across the $\text{Si}=\text{Si}$ double bond of **1** was confirmed by both 2D NOE-experiments in solution and XRD of isolated **4**. Yet the observation of exclusively the (R,S) and (S,R) racemate of **4** does not necessarily require an anti selective alcohol addition in this case as quantum chemical calculations on the RI-B97-D3/def2-TZVP level of theory revealed that the observed (S,R) diastereomer is favored by $\Delta G = 7.7$ kJ/mol compared to the (S,S) stereoisomer, the product of a formal syn-addition. Considering the low interconversion barrier ($\Delta G^\ddagger = 46.9$ kJ/mol) which is already below the overall exergonicity of the reaction (ΔG

⁹ The enol is higher in energy by 49 kJ/mol with a calculated tautomerization barrier of approx. 240 kJ/mol in the gas phase. The equilibrium constant of the enolization of acetone highly depends on solvent, concentration and temperature. Interconversion can proceed via an intra- or intermolecular mechanism, which is why it can be catalyzed by bases, reducing the reaction barrier in e.g. water to about 160 kJ/mol.^[232,233]

= -75.1 kJ/mol, vide infra) as well as the high reaction temperature, no conclusion regarding the initial step mechanism can be gathered experimentally since a kinetic product of the syn-addition would inevitably be transformed to the thermodynamic anti-product under the reaction conditions.

Indirect evidence for path B was gathered from the reactions of **1** with the closely related isopropanol. Addition of the alcohol directly led to a cleavage of the Si=Si bond as a result of overreaction and the precipitation of a colorless, insoluble SIDipp-containing part (presumably the imidazolium salt [SIDippH]Br).¹⁰ Here, ¹H- and ²⁹Si NMR spectroscopy of the soluble part revealed the selective formation of a single Tbb-containing product that was identified as TbbSiH(OiPr)₂ based on spectroscopic trends and the ¹J_{Si,H} coupling constants in comparison to the known derivatives TbbSiH(OEt)₂ and TbbSiH(OMe)₂.¹¹ Since the reaction proceeded smoothly at ambient temperature over the timespan of several hours and no silylene intermediates were detected by NMR spectroscopy, this means that addition of a second equivalent isopropanol to the putative “SIDippSi(H)-SiBr(OiPr)Tbb” intermediate is much faster than the initial 1,2-addition. This, in turn, implies that the reaction of **1** with acetone is very unlikely to proceed via the enol form.

The complete mechanism of the addition reaction of acetone to the disilavinylidene **1** following path B in Scheme 15 was thus calculated on the RI-B97-D3/def2-TZVP level of theory, which revealed that the reaction follows an initial oxygen coordination to the electrophilic Si^{II} atom (Scheme 16). This is followed by a C-H activation at the nucleophilic Si⁰ center, initially leading to the (S,S)-isomer as the kinetic product. In an subsequent step, the (S,S)-isomer rearranges to the more stable (S,R/R,S)-isomers. Interestingly, this interconversion was computed to traverse a transition state with a planarized three-coordinate silicon atom, which is stabilized by a significant C_{NHC}=Si silene-type bonding interaction (see Figure 22 and Table 45 on page 277 in the appendix).

¹⁰ The reaction of free SIDipp and isopropanol instead leads to the molecular O,H-insertion product iPrO(H)C{N(Dipp)CH}₂ that was synthesized independently. This compound is well soluble in benzene and was not detected in the reaction mixture obtained from **1** and isopropanol (see page 247).

¹¹ **TbbSiH(OiPr)₂**: ¹H NMR (400.1 MHz, benzene-d₆, 298 K): δ /ppm = 0.23 (s, 36H, 4 × SiMe₃, Tbb), 1.19 (d, ³J_{H,H} = 8.2 Hz, 12H, 2 × OCH(CH₃)₂), 1.32 (s, 9H, CMe₃, Tbb), 2.67 (s, 2H, 2 × CH(SiMe₃)₂, Tbb), 4.12 (sept, ³J_{H,H} = 8.2 Hz, 2H, 2 × OCH(CH₃)₂), 5.59 (s, ¹J_{Si,H} = 223 Hz, 1H, Si-H), 6.89 (s, 2H, C^{3,5}-H, Tbb). ²⁹Si{¹H} NMR (99.34 MHz, benzene-d₆, 298 K): δ /ppm = -33.0 (s, Si-H), 2.1 (s, 4 × SiMe₃).

TbbSiH(OEt)₂: ¹H NMR (300.1 MHz, benzene-d₆, 298 K): δ /ppm = 0.21 (s, 36H, 4 × SiMe₃, Tbb), 1.18 (t, ³J_{H,H} = 7.0 Hz, 6H, 2 × OCH₂CH₃), 1.32 (s, 9H, CMe₃, Tbb), 2.68 (s, 2H, 2 × CH(SiMe₃)₂, Tbb), 3.72 – 3.85(m, 4H, 2 × OCH₂CH₃), 5.50 (s, ¹J_{Si,H} = 226 Hz, 1H, Si-H), 6.89 (s, 2H, C^{3,5}-H, Tbb). ²⁹Si{¹H} NMR (59.63 MHz, benzene-d₆, 298 K): δ /ppm = -28.1 (s, Si-H), 1.6 (s, 4 × SiMe₃).

TbbSiH(OMe)₂: ¹H NMR (300.1 MHz, benzene-d₆, 298 K): δ /ppm = 0.20 (s, 36H, 4 × SiMe₃, Tbb), 1.31 (s, 9H, CMe₃, Tbb), 2.60 (s, 2H, 2 × CH(SiMe₃)₂, Tbb), 3.46 (s, 6H, 2 × OCH₃), 5.41 (s, ¹J_{Si,H} = 227 Hz, 1H, Si-H), 6.88 (s, 2H, C^{3,5}-H, Tbb). ²⁹Si{¹H} NMR (59.63 MHz, benzene-d₆, 298 K): δ /ppm = -22.7 (s, Si-H), 2.0 (s, 4 × SiMe₃).

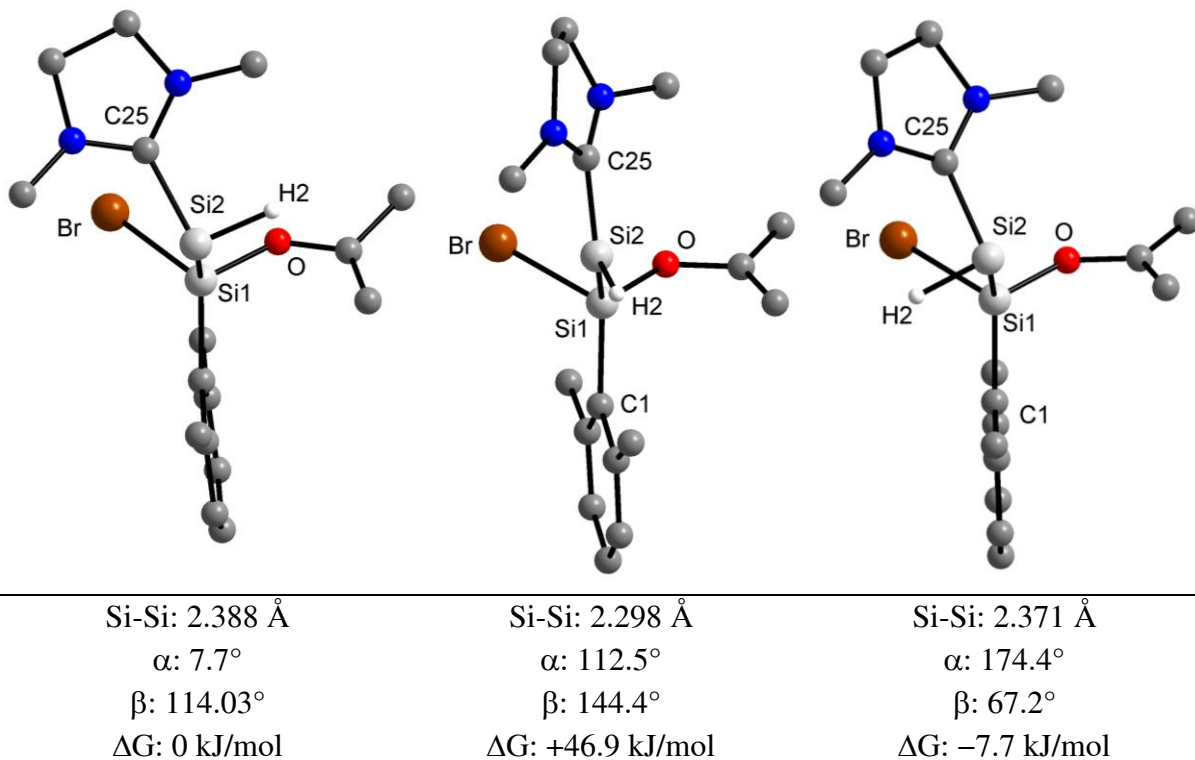
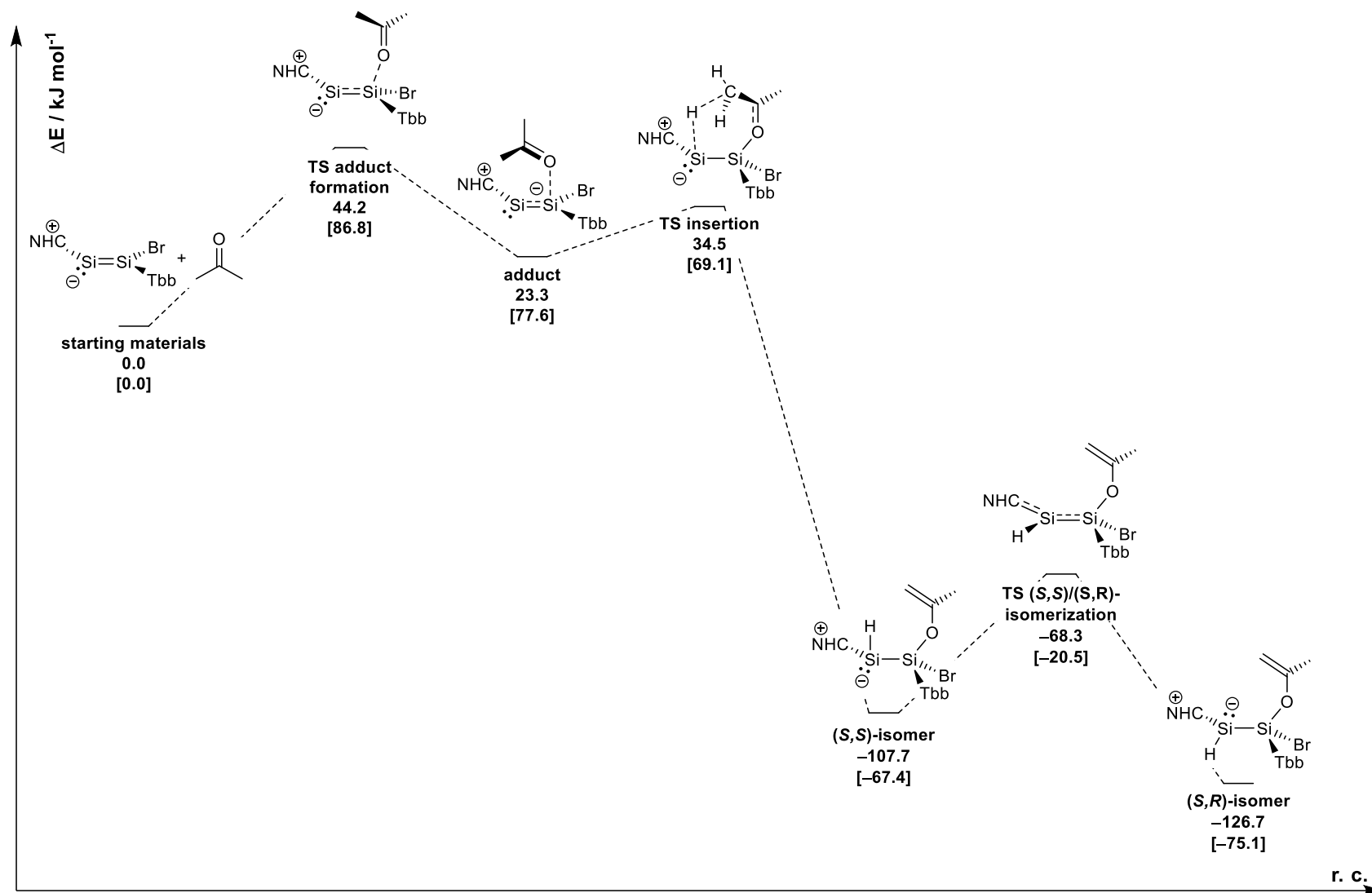


Figure 22. Interconversion of the (S,S)- isomer to the (S,R) isomer of **4** by a planar transition state (sawhorse projection). Peripheral Dipp-, tBu- and SiMe₃ groups are not depicted for clarity but have been included in the calculation. α = H2-Si2-Si1-O torsion angle, β = H2-Si2-Si1-Br torsion angle.

A similar reaction mechanism has already been proposed by Kira for the addition of acetone to a trisilaallene (R₂Si=Si=SiR₂)^[234] and recently been studied in depth from quantum chemical calculations by Braunschweig for the activation of acetone by the iminoborane (R₂N)B=NAr* (R₂N = 2,2,6,6-tetramethylpiperidyl, Ar* = 2,6-(CHPh₂)-4-tBu-C₆H₃) and the NHC-stabilized diboryne B₂(SIDep)₂ (SIDep = C[N(Dep)CH]₂, Dep = 2,6-diethylphenyl).^[235]

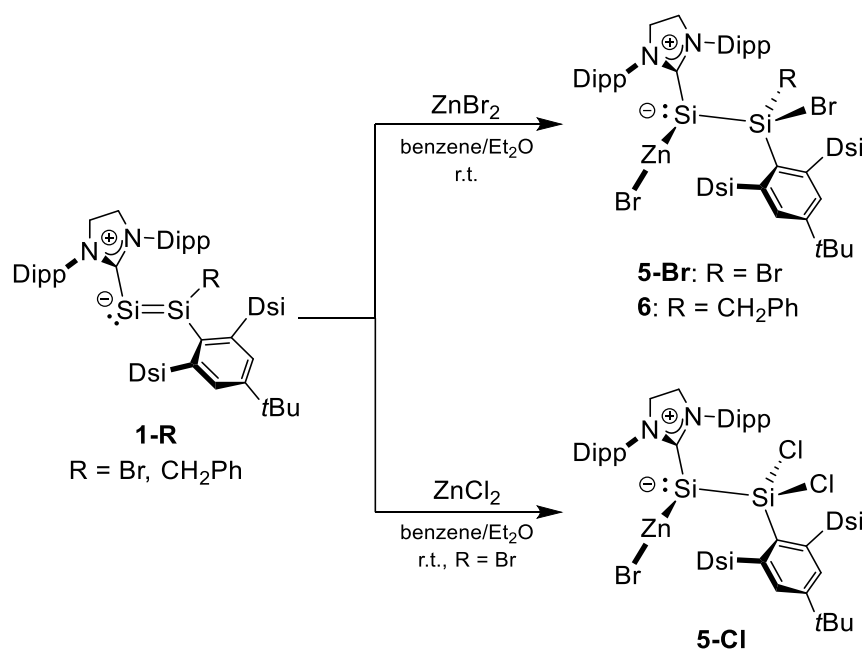


Scheme 16. Calculated (RI-B97-D3/def2-TZVP) mechanism of the reaction between 1 and acetone leading to 4. The (S,S)-configured diastereomer was identified as kinetic product but readily isomerizes at the reaction conditions. ΔG (in kJ/mol) is given in brackets.

2.4 Synthesis of zinco-silylenes

The presence of the polarized Si=Si π -bond as well as the lone pair at the two-coordinate silicon atom in compounds **1** and **1-CH₂Ph** prompted us to study their reactivity towards Lewis acids, such as ZnX₂ (X = Cl, Br), which could either lead to a simple coordination of ZnX₂ by the Si lone pair or a 1,2-addition of a Zn–X bond of ZnX₂ at the Si=Si bond.

Remarkably, a regioselective 1,2-addition occurs upon reaction of the NHC-stabilized disilavinylidenes **1** and **1-CH₂Ph** with an excess of ZnBr₂ at ambient temperature in benzene containing a small amount of diethyl ether, leading to the NHC-stabilized zinco(silyl)silylenes Si(ZnBr)[SiBr(R)Tbb](SIDipp) (**5-Br**: R = Br; **6**: R = CH₂Ph), which were isolated as extremely air-sensitive, yellow solids in yields of 94 % (**5-Br**) and 52 % (**6**) (Scheme 17). Similarly, the reaction of **1** with an excess of ZnCl₂·(1,4-dioxane)₂ in benzene led to the formation of the NHC-stabilized zinco(silyl)silylene Si(ZnBr)[SiCl₂Tbb](SIDipp) (**5-Cl**), which after work up was also isolated as a highly air-sensitive yellow solid in 98 % yield (Scheme 17).



Scheme 17. Syntheses of NHC-stabilized zincosilylenes **5-X** and **6** starting from the NHC-stabilized disilavinylidenes **1** or **1-CH₂Ph** and ZnCl₂ or ZnBr₂.

Monitoring of the reactions by ¹H NMR spectroscopy revealed selective conversions in all cases. However, whereas analytically pure samples of **5-Cl** and **6** could be isolated, the extreme sensitivity of compound **5-Br** towards air and its slow decomposition at room temperature in solution prevented its isolation in analytically pure form. In contrast, compounds **5-Cl** and **6** are thermally quite stable in the solid state and decompose upon heating at 219 °C and 158 °C, respectively. Compounds **5-X** and **6** are the first examples of NHC-stabilized zincosilylenes to be reported and were fully characterized. As mentioned already, metallasilylenes are extremely

rare (see Figure 12 on page 22)^[120,189,190] and although the synthesis of the first zincogermylene $\text{Ge}\{\text{ZnN}[\text{Si}(\text{iPr})_3]\text{Ar}\}(\text{TBoN})$ ($\text{Ar} = 2,6\text{-}(\text{CHPh}_2)_2\text{-}4\text{-Me-C}_6\text{H}_3$) was reported 2017 by the group of Jones,^[236] zincosilylenes are unknown and were also not described theoretically.

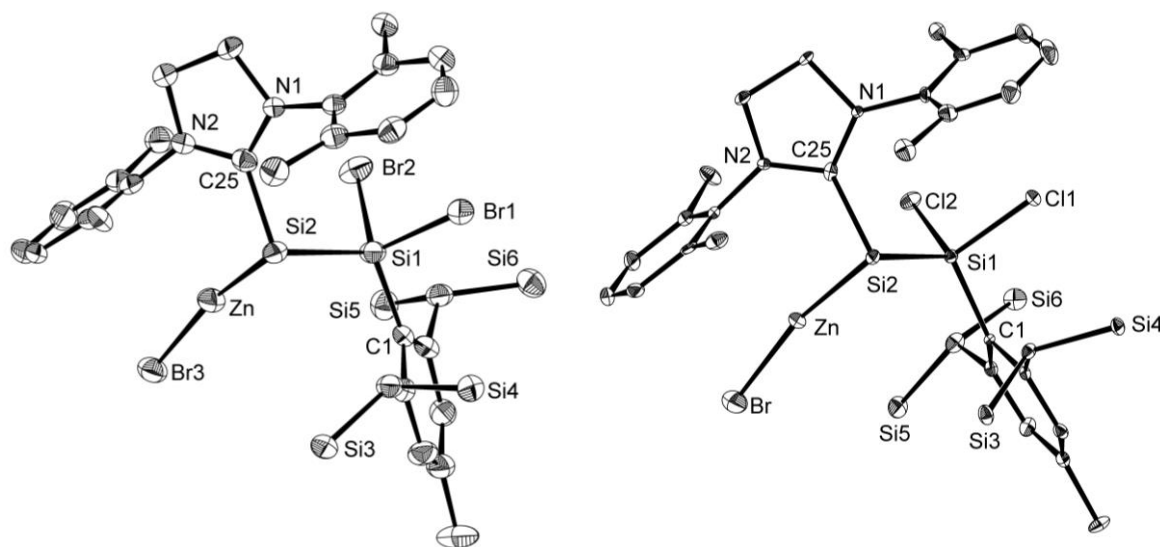


Figure 23. Molecular structure of the monomeric moiety **5-Br**·(C_6H_6)·($n\text{-C}_5\text{H}_{12}$) (left) and **5-Cl** (right). Thermal ellipsoids are set to 50 % probability; methyl groups as well as hydrogen atoms are omitted for simplicity. Selected bond lengths (\AA) and angles ($^\circ$): **5-Br**·(C_6H_6)·($n\text{-C}_5\text{H}_{12}$): Si1-Si2 2.341(3), Si1-Br2 2.286(2), Si1-Br1 2.256(2), Si1-C1 1.916(7), Si2-C25 1.951(7), Zn-Si2 2.335(2), Zn-Br3 2.288(1); Si1-Si2-Zn 93.94(9), Zn-Si2-C25 101.2(2), Si1-Si2-C25 104.1(2), Si2-Si1-Br2 103.95(9), Br1-Si1-Br2 101.12(8), Si2-Si1-Br1 112.7(1), C1-Si1-Br2 116.5(2), C1-Si1-Br1 104.1(2), C1-Si1-Si2 117.5(2), Br3-Zn-Si2 166.17(7); C1-Si1-Si2-C25 $-160.1(3)$, C1-Si1-Si2-Zn $-57.6(3)$, Zn-Si2-Si1-Br2 72.76(8), Zn-Si2-Si1-Br1 $-178.62(6)$. **6**·0.5($n\text{-C}_6\text{H}_{14}$): Si1-Si2 2.342(1), Si1-Br1 2.3041(9), Si1-C1 1.923(3), Si1-C52 1.888(3), Zn-Si2 2.3256(8), Zn-Br2 2.2809(5), Si2-C25 1.923(3); Si2-Zn-Br2 168.13(3), Si1-Si2-Zn 90.63(3), Zn-Si2-C25 101.12(8), Si1-Si2-C25 107.67(8), Br1-Si1-Si2 102.45(4), C1-Si1-Br1 110.18(8), Br1-Si1-C52 102.9(1), Si2-Si1-C52 111.9(1), C1-Si1-C52 119.1(1), C1-Si1-Si2 108.84(8); Zn-Si2-Si1-C52 $-171.62(9)$, C1-Si1-Si2-C25 156.5(1). **5-Cl**: Zn-Si2 2.326(2), Zn-Br 2.2749(8), Si2-C25 1.927(5), Si1-Si2 2.330(2), Si1-Cl1 2.086(2), Si1-Cl2 2.106(2), Si1-C1 1.903(5); Br-Zn-Si2 167.29(5), Zn-Si2-Si1 93.80(6), Zn-Si2-C25 100.2(2), Si1-Si2-C25 104.8(2), Cl1-Si1-Cl2 100.17(7), Cl1-Si1-Si2 111.86(7), Cl1-Si1-C1 103.4(2), Cl2-Si1-Si2 107.18(7), Cl2-Si1-C1 116.3(2), C1-Si1-Si2 116.7(2); C1-Si1-Si2-Zn 176.13(7), C1-Si1-Si2-C25 $-166.7(2)$. For a depiction of **6**·0.5($n\text{-C}_6\text{H}_{14}$) see Figure 92 on page 251 in the appendix.

The solid-state structures of compounds **5-Br**·(C_6H_6)·($n\text{-C}_5\text{H}_{12}$), **6**·0.5($n\text{-C}_6\text{H}_{14}$) (Figure 23) and **5-Cl** (see Figure 92 on page 251 in the appendix) were determined by XRD, which confirmed the identity of the NHC-stabilized zincosilylenes. All compounds adopt C_i symmetry in the solid state and are isotopic with compound **4** and $\text{SiBr}(\text{SiBr}_2\text{Tbb})(\text{SIDipp})$,^[134] featuring a stereogenic three-coordinate trigonal-pyramidal silicon atom with a lone pair and a four-coordinate tetrahedral silicon center, which is also stereogenic in compound **6**. Only the (*S,S*)/(*R,R*) enantiomeric pair was structurally found for **6** in the solid state, suggesting a syn-selective 1,2-addition of ZnBr_2 to the Si=Si bond of **1-CH₂Ph**. The sum of angles at the three-coordinate silicon centers of **5-Cl** ($\Sigma\text{Si} = 298.8^\circ$), **5-Br** ($\Sigma\text{Si} = 299.2^\circ$) and **6** ($\Sigma\text{Si} = 299.5^\circ$) are almost identical, but higher than that of **4** ($\Sigma\text{Si} = 293.27^\circ$), $\text{SiBr}(\text{SiBr}_2\text{Tbb})(\text{SIDipp})$ ($\Sigma\text{Si} = 287.4^\circ$)^[134] or $\text{SiBr}_2(\text{SIDipp})$ ($\Sigma\text{Si} = 290^\circ$),^[119] showing that the degree of pyramidalization decreases from 74 % in **4** or 81 % in $\text{SiBr}(\text{SiBr}_2\text{Tbb})(\text{SIDipp})$ to 67 – 68 % in **5-X** and **6**. This

can be rationalized by the lower *s* character of the lone pair orbital at silicon in **5-X** and **6** due to bonding to an electropositive zinc substituent. In all zinco(silyl)silylenes the Zn atoms are almost linearly coordinated (Si-Zn-Br angles vary from 166.17(7) to 168.14(3)°) and the Si-Zn bonds are almost identical (**5-Cl** (2.326(2) Å), **5-Br** (2.335(2) Å) and **6** (2.3253(8) Å)). Notably, the Si-Zn bond lengths are shorter than the dative Si(II)→Zn(II) bonds of Zn(II)-silylene complexes (2.3750(9) Å – 2.4939(7) Å)^[237-240] or the bonds in the more bulky disilylzinc(II) complex Zn{Si(SiMe₃)₃}₂ (2.342(4) Å)).^[241,242] The Si1–Si2 bond lengths in **5-X** and **6** (2.330(2) to 2.342(1) Å) compare well with those of **4** (2.355(2) Å) and SiBr(SiBr₂Tbb)(SIDipp) (2.391(1) Å)^[134] as well as the value found in α-Si (2.352 Å).^[11]

Table 4. Selected bonding parameters and ²⁹Si NMR spectroscopic data of compounds **1** and **5-Br** – **5-Cl**.

Comp.	Si-Si /Å	Si-C ^{Tbb} /Å	Si-C ^{NHC} /Å	∠(NHC-Tbb) ^A /°	∠(NHC-Tbb) ^B /°	δ(Si ^{Tbb}) ^C /ppm	δ(Si ^{NHC}) ^C /ppm
5-Cl	2.330(2)	1.903(5)	1.927(5)	166.6(3)	73.5(2)	29.4	-81.6
5-Br	2.341(3)	1.916(7)	1.951(7)	-160.1(4)	82.8(3)	6.6	-63.9
6	2.342(1)	1.924(3)	1.922(3)	156.5(1)	88.2(2)	15.0	-67.0
D ^[134]	2.330(2)	1.903(5)	1.927(5)	166.6(3)	73.5(2)	29.4	-81.6
1 ^[134]	2.167(2)	1.882(4)	1.937(4)	-177.3(2)	12.1(2)	86.0	34.6

A: torsion angle C^{NHC}-Si-Si-C^{Tbb}; **B:** angle between the least-square planes of the central rings of the NHC and the Tbb-substituents; **C:** ²⁹Si{¹H} NMR resonances in benzene-d₆ at 298 K; **D:** SiBr(SiBr₂Tbb)(SIDipp).

In the ²⁹Si{¹H} NMR spectra of **5-X** and **6** in benzene-d₆, the signals of the zinc-bonded Si^{II} atoms appear at δ_{Si} = -81.6 ppm (**5-Cl**), 63.9 (**5-Br**) and -67.0 (**6**). The chemical shifts of these signals are comparable with the SiH resonance signal of the hydrido(silyl)silylene **4** (94.2 ppm) but appear at considerably higher field compared to those of the corresponding bromo(silyl)silylene SiBr(SiBr₂Tbb)(SIDipp) (1.9 ppm),^[134] or the zinc(II)-silylene complexes **A** (60.5 ppm), **B** (R = Et: 55.3 ppm; R = Ph: 58.9 ppm; R = C₆F₅: 59.4 ppm) and **C** (X = Cl: 51.6 ppm; X = I: 50.7 ppm) depicted in Figure 23.^[238-240,243] In contrast to the three-coordinated Si^{NHC} atoms, the tetrahedral Si^{Tbb} atoms of **5-X** and **6** resonate at significantly lower field (**5-Cl**: 29.4 ppm, **5-Br**: 6.6 ppm and **6**: 15.0 ppm), and the values appear close to that of the isostructural SiBr(SiBr₂Tbb)(SIDipp) (11.3 ppm)^[134] or hydrido(silyl)silylene **4** (9.8 ppm).

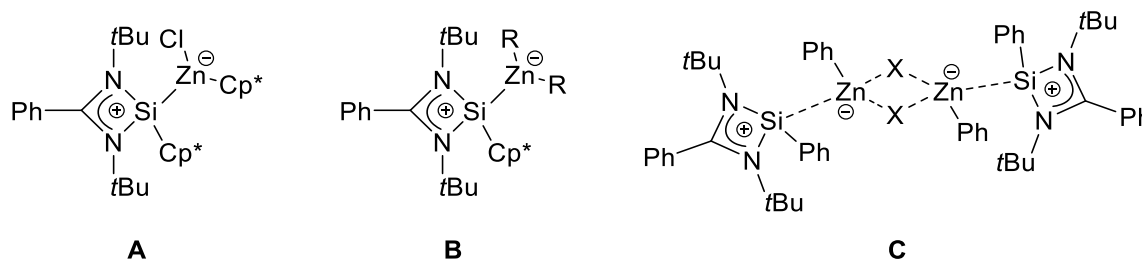


Figure 24. Zn(II) complexes of amidinato-stabilized silylenes. R = Et, Ph or C₆F₅; X = Cl or I.

Although the NHC-stabilized zinco(silyl)silylenes **5-Cl** and **5-Br** each display one stereogenic Si^{NHC} atom, local C_{2v} symmetry is observed for both the Tbb and the SIDipp substituents in the ¹H, ¹³C and ²⁹Si NMR spectra. The chemical equivalence of the ortho and meta positions suggests a dynamic process that involves the loss of the chiral information at the stereocenter. Indeed, cooling of the NMR samples of **5-Cl** and **5-Br** in toluene-d₈ to 203 K leads to splitting of the signals into two sets of signals as expected from the solid-state structures, but severe broadening of the signals hampered a further analysis of the dynamic process.¹² Instead, thorough ¹H VT-NMR measurements of the CH₂Ph-substituted compound **6** with an additional stereocenter at the Si^{Tbb} atom were performed to elucidate the process. In this case, two sets of signals are observed at ambient temperature in the ¹H, ¹³C and ²⁹Si NMR spectra in toluene-d₈, except for the ¹H signals of the SiMe₃ groups, which show only one instead of two singlets. Upon cooling to 253 K, the SiMe₃ signal splits into two separate singlets (T_c: 290 K, Δν: 4.4 Hz), whereas heating of the sample to 333 K leads to a coalescence of the four doublet signals of the diastereotopic isopropyl groups of the NHC substituent into two signals (T_c: 300 K, Δν: 7 Hz). As for compounds **5-Cl** and **5-Br**, this proves the presence of a dynamic process of **6** in solution, which leads to a loss of the stereoinformation on the chiral silicon atoms (Figure 25). Using standard methods, the Gibbs energy of activation (ΔG[‡]) for this dynamic process was estimated to be 65.5 kJ/mol. Additional cooling to 203 K led to significant broadening of all signals as it was also observed for **5-Cl** and **5-Br**. This indicates hindered rotations of the substituents at very low temperatures but prevented a full lineshape analysis of the processes.

¹² The additional broadening can probably be explained by hindered rotations of the Tbb and SIDipp at very low temperatures. As these processes overlap with the more interesting stereoisomerization for compound **5-Cl** and **5-Br**, no independent examination was possible. However, the same behaviour was found for compound **6**, where the dynamic processes trigger one after the other (vide infra).

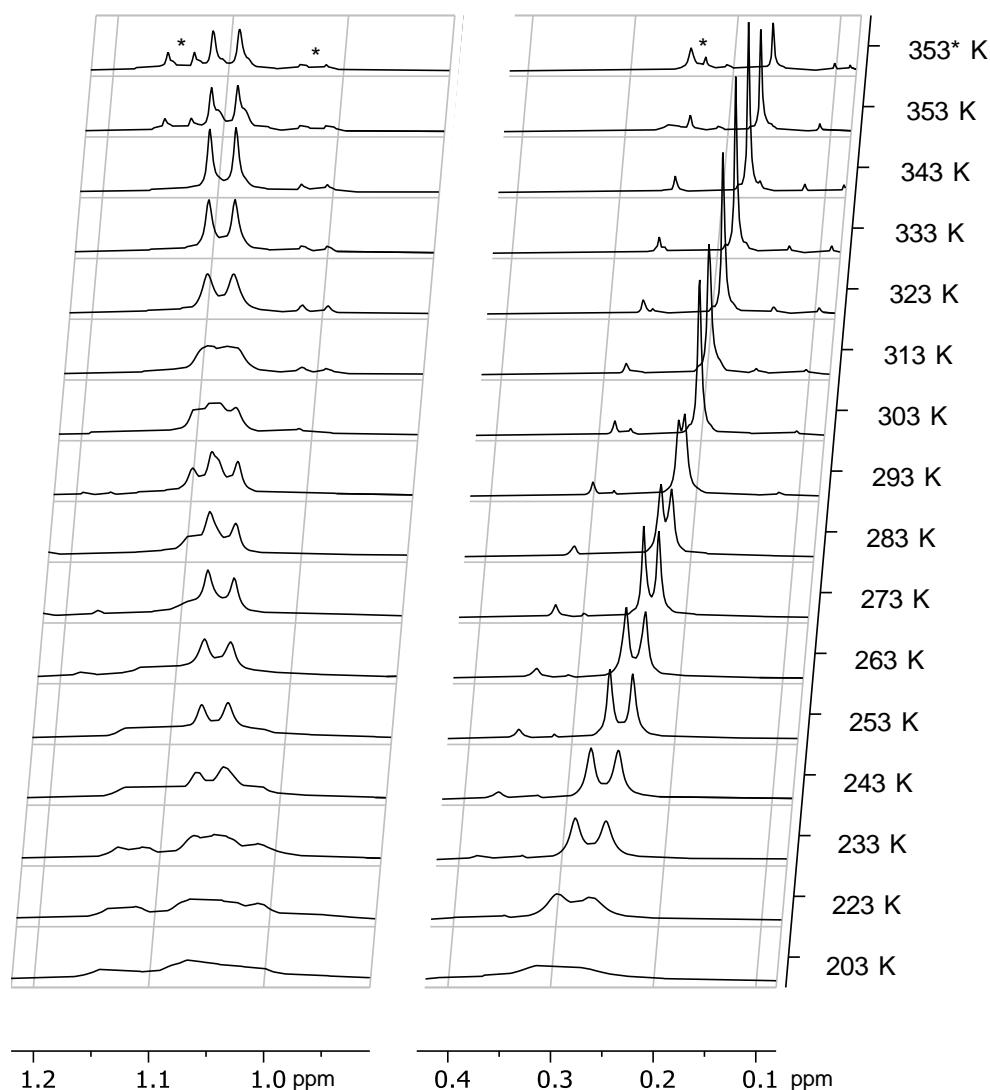
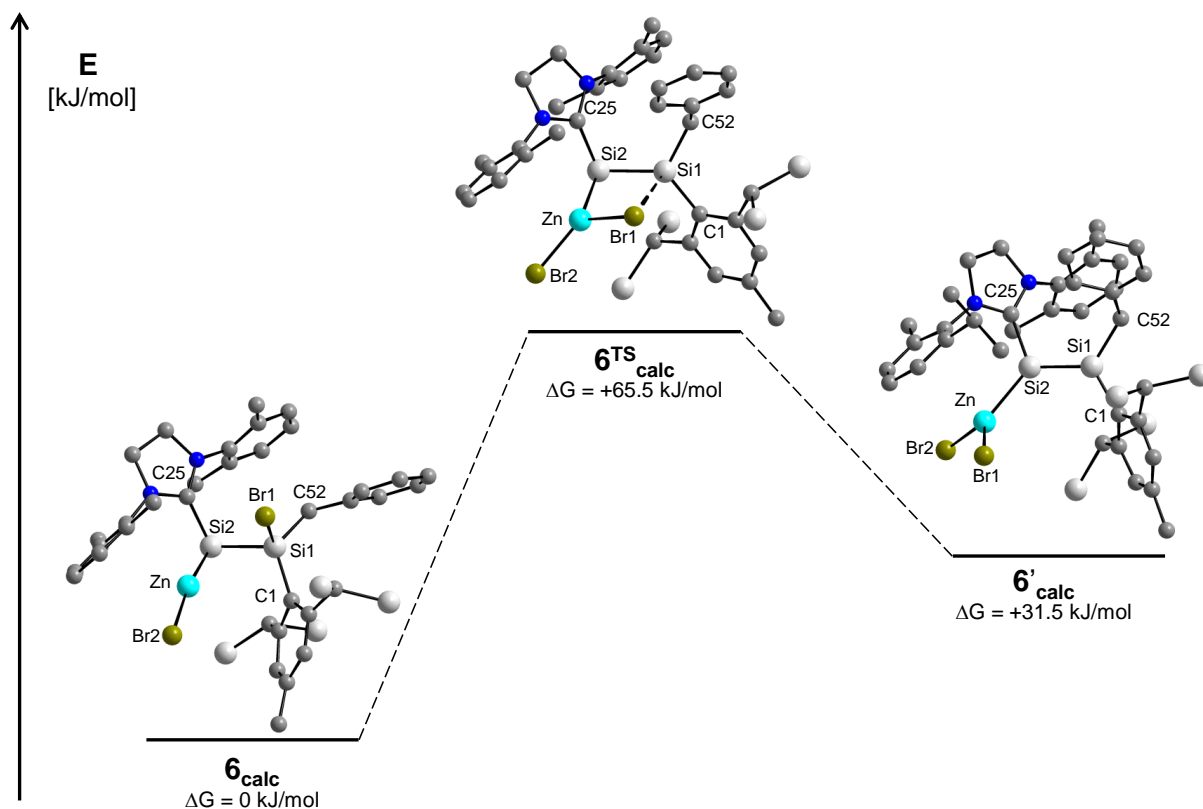


Figure 25. Excerpts of the variable temperature ^1H NMR (300.1 MHz) spectra of **6** in toluene- d_6 from 203 – 353 K and after 30 minutes at 353 K (marked with an asterisk). Right: signals of the SiH_2 groups of the Tbb substituent; left: $\text{C}^{2,6}\text{-CH}_2\text{Me}$, signal of the Dipp substituent. The spectra show thermal decomposition to unknown products at elevated temperatures.

DFT calculations of compound **6** on the RI-B97-D3/def2-TZVP level of theory shed further light on the nature of the aforementioned stereoisomerization: A scan of the potential energy surface (PES) revealed that in addition to the zincosilylene structure of **6**, a second local minimum is present: the η^1 -complex of disilavinylidene **1** and ZnBr_2 where the Zn atom is coordinated to the Si^{NHC} atom via the lone pair (**6'**, for structural details and the NBO analysis see Table 46 on page 278 in the appendix). According to the calculations, **6'** lies higher in energy by +37 kJ/mol and both minimum structures are interconnected via a transition state (**6^{TS}**), which displays one bromine atom in bridging position between the zinc and the divalent silicon atom. The corresponding energy barrier for the rearrangement of **6** via **6^{TS}** ($\Delta G_{\text{calc}}^\ddagger = +65.5$ kJ/mol) is in excellent agreement with the barrier determined by variable temperature NMR experiments ($\Delta G_{\text{exp}}^\ddagger = 65.5$ kJ/mol), suggesting that the computed migration of the Br

atom and the rehybridization of the Si^{tbh} atom are the rate-determining step of the dynamic process in solution (Scheme 18).



Scheme 18. Potential energy surface (RI-B97-D3/def2-TZVP) for the dynamic process of **6** showing the global minimum structure **6_{calc}**, the transition state **6^{TS}_{calc}** and the local minimum structure **6'_{calc}** with their respective relative energies ΔG in kJ/mol. Methyl groups as well as hydrogen atoms are omitted for clarity.

2.5 An aromatic {Si₂P₂C} five-membered ring

The 2-phosphaethynolate anion [P≡C-O]⁻ (Figure 26) is a heavier analogue of the cyanate anion and was first described as {LiOCP·(dme)₂}₂ by Becker et al. nearly 30 years ago.^[244,245] In 2011, the group of Grützmacher established a convenient synthetic access to the more stable sodium and potassium salts,^[246,247] initiating an impetus to organic and organometallic chemistry. By today, more than 70 research articles have been published and recent review papers cover reactivity studies as well as different synthetic approaches.^[248,249]

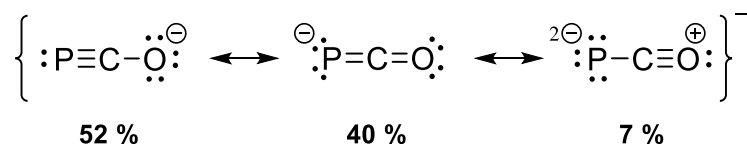
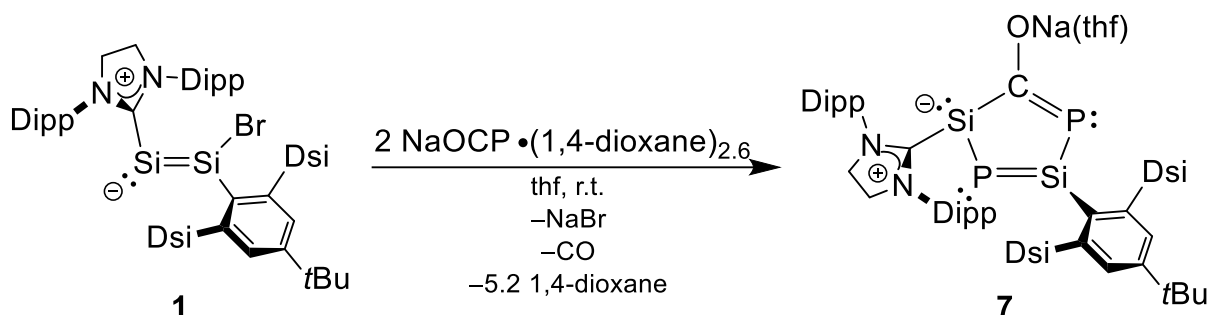


Figure 26. Resonance formula of the 2-phosphaethynolate anion [P≡C-O]⁻. The weights of the individual forms have been taken from the reference (B3LYP/6-31+G*).^[248]

The PCO⁻ anion has shown a tendency for cyclo reactions or can transfer a P atom or P⁻ unit after decarbonylation.^[250,251] Reactions with heavier tetrel compounds include ring expansion of a cyclotrisilene to the anionic cyclophosphasilene cyclo-{P=SiTip-SiTip-SiTips₂}⁻,^[252] substitution of base-stabilized halogermynes with subsequent dimerization to 2,4-Digerma-1,3-diphospha-cyclobutadienes^[253–256] and a bis(germyliumylidene)diphosphene (L)Ge-P=P-Ge(L) (L = anionic NHC).^[255] Thus, a reaction between this versatile building block with disilavinylidene **1** is extremely appealing: While a nucleophilic bromine substitution by PCO⁻ appears to be a reasonable first step, the Si=Si π-bond and the free electron pair at the Si(O) atom putatively give access to [2+2] or [2+1] cyclo reactions, respectively. Alternatively, another 1,2-addition to the Si=Si π-bond might form an NHC-supported sodium(silyl)silylene akin to the zincosilylenes **5-X** and **6** described above. Such a species could be less sensitive towards C-H activations when compared to the Li congener **2** and, after NaBr elimination, lead to follow-up chemistry likewise to the cyclization reaction observed for compound **3** (see Scheme 10 on page 32).

In practice, stirring a suspension of **1** and NaOCP·(1,4-dioxane)_{2.6} in thf was accompanied by a gradual color change from dark red to dark brown-blue. Monitoring of the reaction progress by in situ ¹H NMR and ³¹P{¹H} spectroscopy revealed a slow but selective conversion of **1** into an unknown C_{2v} symmetric compound **7**. Further, the ³¹P{¹H} NMR spectrum suggested the incorporation of two phosphorous atoms. Unfortunately, the slow reaction progress was accompanied by the simultaneous decomposition of the generated product in solution, ultimately limiting the content of **7** to about 30 %. This decomposition was much faster at 50 °C, where only traces of **7** could be detected in the reaction mixtures. Changing the solvent to methylated thf, Et₂O, or dme only led to lower yields; when fluorobenzene or mixtures of benzene and etheral solvents were used, no reaction occurred at all. Surprisingly, addition of a

small amount of dry 18-c-6 crown ether to increase the solubility had no visible effect as well. Large scale reactions (up to 500 mg of **1**) were hence performed in thf using a small excess of NaOCP·(1,4-dioxane)_{2,6} and eventually led to a nearly complete conversion after 3 – 8 days.¹³



Scheme 19. Synthesis of compound **7** from **1** and NaOCP·(1,4-dioxane)_{2,6}.

Surprisingly, the molecular structure obtained by XRD analysis (vide infra) revealed the complete cleavage of the Si=Si bond. Instead, a five-membered ring system was formed, where a {P≡C-ONa} moiety has formally inserted into the Si=Si bond of **1**. The molecules core is completed by an additional phosphorous atom, which originates from the second equivalent of NaOCP. Compound **7** can therefore be described either as the first NHC-stabilized cyclic alkenyl(phosphino)silylene or as a heavier, zwitterionic congener of the famous cyclopentadiene ligand. Known unsaturated Si,P-containing ring systems are depicted in Figure 27. The first examples, two phosphasilirenes **A**^R, were obtained as early as 1987 by Weidenbruch and Schäfer by [2+1] cyclo additions of in situ-generated :Si(tBu)₂ to phosphalkynes (:P≡C-R, R = tBu, Ad).^[257] But after these initial examples, only a handful of related compounds were introduced by the groups of Driess, Scheer, Roesky and Stalke, Goicoechea, Scheschkewitz and Lips in the 2010s, often as part of collaboration programs.^[187,252,258–263] Also, M. Bogner from the Filippou group very recently succeeded in the isolation of a cyclic diphosphinosilylene **J**.^[133]

¹³ The conversion rate was highly dependent on the exact stoichiometry and the speed of the magnetic stirrer. Faster stirring increases the reaction speed, but NaOCP was found to persistently settle at the glass wall in this case. Also, older batches of NaOCP gave lower conversion rates presumably due to partial polymerization.

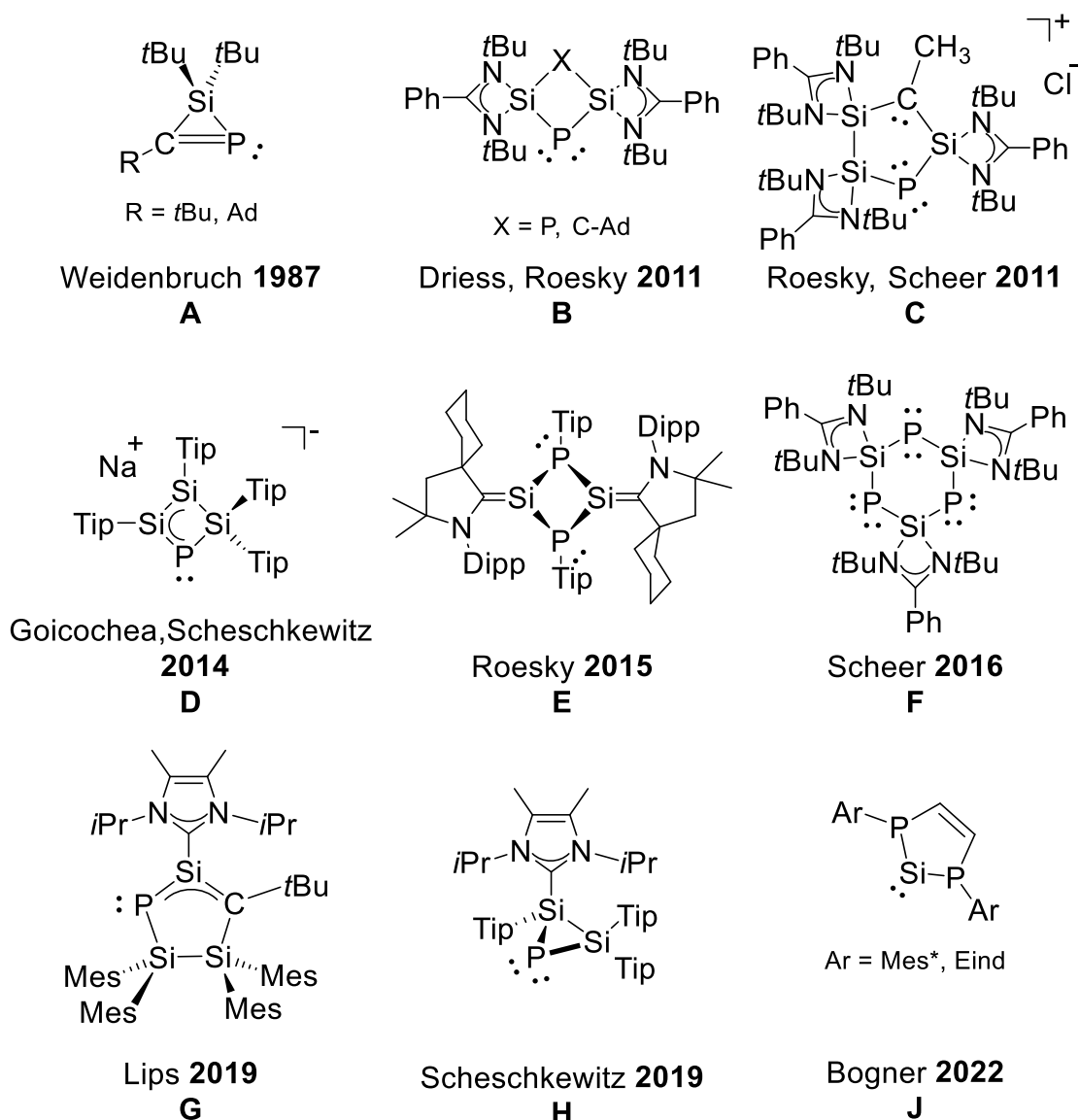


Figure 27. Literature-known cyclic compounds featuring Si-P bonds. Formal charges are omitted for simplicity.

A,^[257] **B**,^[258,259] **C**,^[260] **D**,^[252] **E**,^[261] **F**,^[262] **G**,^[263] **H**^[187] and **J**.^[133]

Purification was achieved by extraction with n-hexane and subsequent slow crystallization from a mixture of toluene and thf (5:1) at $-30\text{ }^{\circ}\text{C}$. Compound **7** was obtained as very dark, dichroic reddish/green to black, analytically pure microcrystalline solid. The low but reproducible yield (20 to 25 %) is thereby satisfactory given the amount of inevitable decomposition during the prolonged reaction time.

Even very diluted solutions of **7** appear deeply blue-green, which is caused by broad adsorption bands in the UV-vis NIR spectrum in thf between 300 and 500 nm as well as a very strong band at $\lambda_{\text{max}} = 593\text{ nm}$ ($\epsilon = 16435\text{ l}\cdot\text{mol}^{-1}\cdot\text{cm}^{-1}$; see Figure 107 on page 268 in the appendix). The compound is well soluble in ethereal or aromatic solvents and less soluble in aliphatic hydrocarbons. Exposure to air was accompanied by an instantaneous color change to

yellow-brown, followed by discolorization. Even after isolation, solid samples slowly decompose at ambient temperature to the same unknown, brown product that was also present during the synthesis. Solutions are stable for about a day when protected from direct light. Comprehensive ¹H and ¹³C{¹H} NMR spectroscopy of compound **7** in tetrahydrofuran-*d*₈ solution revealed local C_{2v} symmetry with free rotations around the respective Si-C bonds of either substituents. No unusual chemical shifts were observed, except for the carbene resonance (δ = 179.5 ppm), which is considerably highfield shifted from **1** (204.6 ppm) or free SIDipp (244.7 ppm) but is not quite at the level of an imidazolium salt such as [H(SIDipp)]Br (147.6 ppm, *vide infra*).

In the ³¹P{¹H} NMR spectrum (Figure 28), two doublet signals with coupling constants of ²J_{P,P} = 40.6 Hz are found at -81.7 ppm and +94.9 ppm, respectively. The former was assigned to the SiPC atom by ¹H-³¹P correlation spectroscopy, which is expectedly low field shifted from the starting material NaOCP (-392.0 ppm)^[246] and also notably low field shifted in respect to **G** (-195.0 ppm)^[263] but in fairly good agreement with the anionic {PSi₃Tip₄} ring **D** (-93.9 ppm in toluene-*d*₈ and -56.6 ppm in tetrahydrofuran-*d*₈),^[252] although no similar solvent dependency was found for **7**. Accordingly, the second signal at +94.9 ppm originates from the CPSi^{Tbb} unit and lies well within the characteristic range of aryl-substituted phosphasilenes (δ _P = 66.2 – 105.4 ppm).^[264]

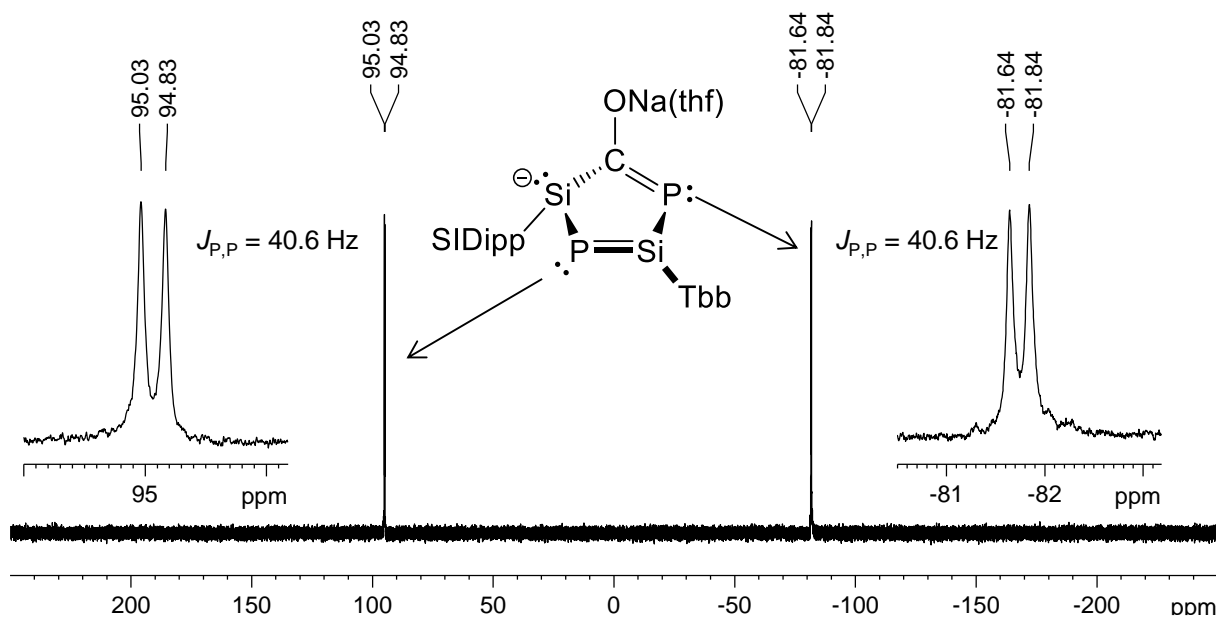


Figure 28. ³¹P{¹H} NMR (202.5 MHz) spectrum of **7** in tetrahydrofuran-*d*₈ at 298 K. Enlarged excerpt of both signals are depicted in the insets.

The ²⁹Si{¹H} NMR spectrum of **7** (Figure 29) features three signals, of which a singlet resonance at 1.5 ppm originates from the chemically equivalent SiMe₃ groups. The most characteristic signal appears at 176.7 ppm (¹J_{P,S} = 144.7 and 133.8 Hz) in shape of a doublet of a doublet and could be assigned to the Si^{Tbb} atom. This value lies in between the range of known

phosphasilenes (66.2 – 105.4 ppm, $^1J_{\text{P,Si}} \approx 150$ Hz)^[264] and an NHC-stabilized phosphasilene-ylidene (IDipp)Si=P(Mes*) ($\delta_{\text{Si}} = 267.3$ ppm, $^1J_{\text{P,Si}} = 170.4$ Hz)^[124] and considerably low field shifted in respect to **1** (86.0 ppm).^[134]

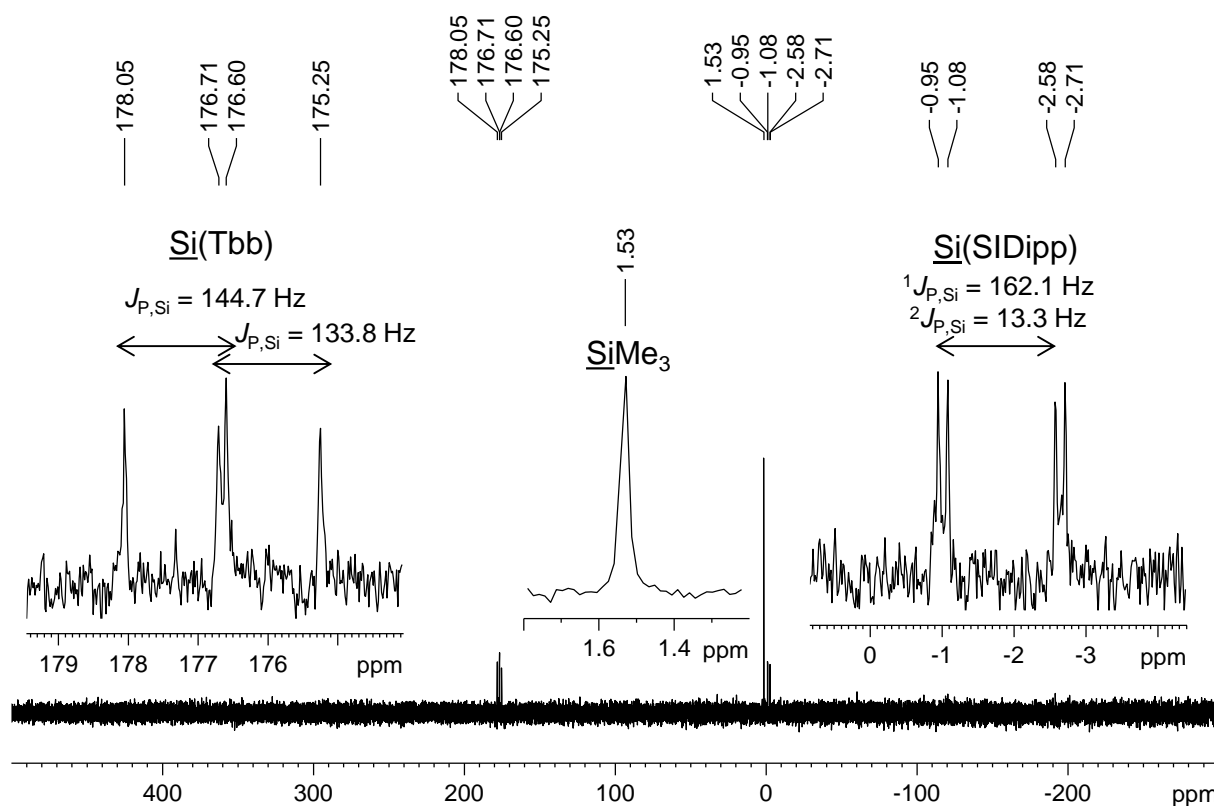


Figure 29. $^{29}\text{Si}\{^1\text{H}\}$ NMR (99.37 MHz) spectrum of **7** in tetrahydrofuran- d_8 solution at 298 K. Enlarged excerpt of all three signals are depicted in the insets.

An additional doublet of a doublet signal was found for the Si^{NHC} resonance at -1.8 ppm ($^1J_{\text{P,Si}} = 162.1$ Hz, $^2J_{\text{P,Si}} = 13.3$ Hz). Although this chemical shift is not very distinctive, it compares well with base-stabilized acyclic silylenes such as $\text{SiBr}_2(\text{SIDipp})$ (10.8 ppm),^[119] the silylsilylene $\text{SiBr}(\text{SiBr}_2\text{Tbb})(\text{SIDipp})$ (-1.9 ppm),^[134] the amino(phosphino)silylene $\text{Si}(\text{PPh}_2)\{\text{N}(\text{Dipp})\text{SiMe}_3\}$ (IiPr_2Me_2) (4.23 ppm, $^1J_{\text{P,Si}} = 78.37$ Hz)^[265] or compound **B-Ad** (-5.1 ppm).^[259] In contrast, base-stabilized silacyclopentenylidenes $(\text{NHC})\text{Si}\{\text{C}_4\text{Ph}_4\}$ have been reported to resonate at a higher field between -69.6 ppm and -43.6 ppm.^[266–268] Remarkably, neither of the chemical shifts matches those of the NHC-stabilized aryl(phosphino)silylene $\text{SiAr}^{\text{TriP}}(\text{PPh}_2)(\text{IME}_4)$ (-39.2 ppm),^[269] the PHSis **J** ($\text{R} = \text{Mes}^*$: $\delta_{\text{Si}} = 32.4$ ppm, $^1J_{\text{P,Si}} = 258.3$ Hz; $\text{R} = \text{Eind}$: $\delta_{\text{Si}} = 28.7$ ppm, $^1J_{\text{P,Si}} = 253.8$ Hz)^[133] or Wienkenhövers $\text{Si}(\text{Eind})(\text{PMe}_2)$ (246.2 ppm, $^1J_{\text{P,Si}} = 294$ Hz),^[40] the latter of which is best described with a $\text{Si}=\text{P}$ double bond.

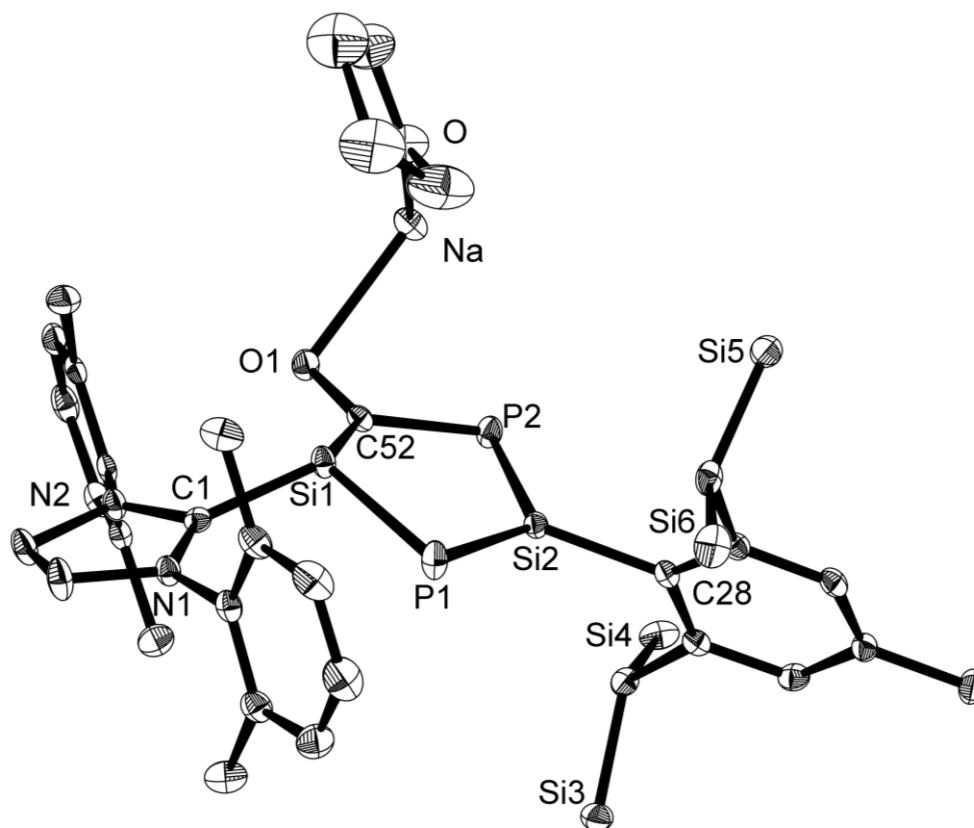


Figure 30. Molecular structure of the monomeric moiety $7 \cdot (\text{C}_6\text{H}_{14})_{0.5}$. Thermal ellipsoids are set to 50 % probability; methyl groups as well as hydrogen atoms are omitted for simplicity. Selected bond lengths (\AA) and angles ($^\circ$): Si1-P1 2.2195(9), Si1-C52 1.907(3), Si1-C1 1.875(2), P1-Si2 2.089(1), Si2-P2 2.1630(8), Si2-C28 1.882(2), P2-C52 1.807(3), C52-O1 1.280(3), O1-Na 2.377(2); C52-Si1-P1 113.92(8), C52-Si1-C1 117.3(1), C1-Si1-P1 108.39(7), Si1-P1-Si2 89.53(3), P1-Si2-P2 119.54(4), P1-Si2-C28 121.69(8), C28-Si2-P2 118.77(9), Si2-P2-C52 98.53(8), P2-C52-Si1 116.5(1), P2-C52-O1 117.4(2), O1-C52-Si1 124.7(2).

In the solid state, $7 \cdot (\text{C}_6\text{H}_{14})_{0.5}$ crystallizes as a sodium-bridged dimer with no close contact of the anionic moieties ($\text{O1} \cdots \text{O1}^\#$: 3.423(4) \AA). Most characteristic is the central five-membered ring, which consists of the atoms Si1^{NHC}, P1, Si2^{Tbb}, P2 and C52^{ONa} and is supported by the large Si-bonded SIDipp and Tbb groups (Figure 30). The Si1^{NHC}-P1 distance (2.2195(9) \AA) corresponds to a short single bond.^[264] It is fairly similar to the ones found in **E** (2.2655(7) – 2.2953(8) \AA)^[261] whilst considerably shorter than the respective bonds in the NHC-stabilized cyclic di(phosphino)silylene $\text{Si}\{\text{P}(\text{Mes}^*)\text{CH}\}_2(\text{IMe}_4)$ (**J**·**IMe**₄; 2.3094(6) \AA and 2.3410(6) \AA)^{[133], 14} or in acyclic NHC-stabilized aryl(phosphino)silylenes (2.346(1) \AA and 2.3748(7) \AA).^[265,269] Adjoining, the Si1^{NHC}-C52^{ONa} bond (1.907(3) \AA) also is in the range of a typical Si-C single bond and compares well to the Si-C^{sp2} bond in $\text{SiAr}^{\text{Trip}}(\text{PPh}_2)(\text{IMe}_4)$ (1.938(1) \AA).^[269]

¹⁴ The structure of $(\text{IMe}_4)\text{Si}\{\text{P}(\text{Mes}^*)\text{CH}\}_2$ features two P atoms with noticeable different coordination spheres. The Si-P distances (Si1-P2: 2.3094(6) \AA , Si-P2: 2.3410(6) \AA) as well as differences in the degree of pyramidalization (P1: $\Sigma = 324.8^\circ$, DP = 39 %; P2: $\Sigma = 300.8^\circ$, DP = 66 %) led the author to the conclusion, that “these findings are indicative of the presence of a marginal Si–P2 double bond with the more planarized P2, and a Si–P1 single bond.”^[133]

Together, these values corroborate the characterization of **7** as a base-stabilized alkenyl(phosphino)silylene, while also suggesting at least some electron delocalization around the Si1 atom. On the other hand, the P1-Si2^{Tbb} and P2-Si2^{Tbb} distances (2.089(1) Å and 2.1630(8) Å) lie in between a typical single- and a double bond. These values compare very well to the values found in the cationic ring **C** (2.169(2) Å and 2.175(5) Å)^[260] or NHC-stabilized ring **G** (2.0960(6) Å)^[263] and also span the one found in the NHC-stabilized phosphasilenylidene (IDipp)Si=P(Mes*) (Si=P: 2.1188(7) Å).^[124] Finally, the P-C52^{ONa} distance (1.807(3) Å) as well lies in between a single and a double bond (P-C: 1.86 Å, P=C: 1.70 Å).^[270] In the context of Si,P-rings, the distance is much longer than in **A** (1.686(6) Å),^[257] but much shorter than the stressed single-bond in Lips' NHC-stabilized housane (1.925(2) Å).^[263]

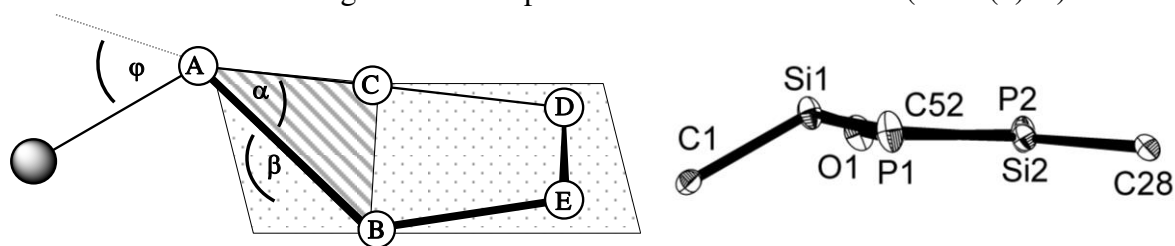


Figure 31. Specification of the diverging angles α , β and φ in the central ring system of compound **7**; the respective atoms are depicted as white circles (o) and a generic substituent is given as a grey sphere (\bullet) (left). Side view of the central ring of **7**-(C₄H₉)₂ and the angulation of the NHC. Substituents are omitted for simplicity (right).

As a whole, the ring system is slightly puckered (envelope conformation) with the Si1^{NHC} atom in the endo position by 0.261(1) Å (Figure 31, right). The deviation from an ideal pentagon can be described by the three angles α (interior angle in a respective vertex), β (angulation of the respective vertex in respect to the best plane defined by the remaining four ring atoms) and φ (angular deflection of a substituent in respect to the plane of the vertex). Expectedly, all interior angles α deviate from the 108° of an ideal pentagon (Table 5): Following Bents rule, the angles at the phosphorous atoms (P1: 89.53(3)°, P2: 98.53(8)°) are more narrow because of the free electron pairs with high s-character. Concurrently, the inner angles α at the other ring atoms are compensatively widened (Si1^{NHC}: 113.92(8)°, Si2^{Tbb}: 119.54(4)°, C52^{ONa}: 116.5(1)°), which is also observed for the reference compounds **A** – **J**.

Table 5. Geometrical distortion of the central ring in **7**. Calculated values are given in square brackets.^A

atom	Si1 ^{NHC}	Si2 ^{Tbb}	P1 ^{Si₂Si}	P2 ^{Si₂C}	C52 ^{ONa}
α /°	113.92(8) [111.9]	119.54(4) [121.9]	89.53(3) [90.2]	98.53(8) [97.0]	116.5(1) [117.8]
β /°	13.6(1) [10.8]	0.96(8) [2.5]	6.49(5) [6.2]	6.55(1) [3.9]	14.0(2) [10.6]
φ /°	45.7(3) [42.5]	0.8(1) [6.72]	-	-	11.2(3) [7.5]
d _{tc} /Å	1.6014(1) [1.673]	1.5767(8) [1.577]	1.9926(7) [2.021]	1.8159(8) [1.876]	1.617(2) [1.637]
Σ /°	339.6(1) [336.3]	360.0(1) [359.6]	-	-	358.6(2) [359.3]
Pyramid. /%	23 [27]	0 [0]	-	-	2 [0]

A: RI-B97-D3/def2-TZVP level of theory. α : interior angle at the respective atoms; β : angle between the respective vertex and the best plane of the remaining ring atoms; φ : angular deflection of the ipso-bonded peripheral substituent at the respective vertex; **d_{tc}**: distance of the respective atom to the center of the central plane; Σ : sum of angles at 3-coordinated atoms; Pyramid.: degree of pyramidalization of 3-coordinated atoms. For the definition of the angles α , β and φ see also Figure 31.

More interestingly, the ring system is not perfectly planar as evidenced by the angles β (0.96(8)° – 14.0(2)°). This means, that the atoms Si1^{NHC} and C52^{ONa} are out of the best plane defined by the remaining four atoms by perpendiculars of 0.261(3) Å and 0.239(3) Å, respectively, suggesting a disturbance of the delocalized electron system. Whereas the Si2^{Tbb} and the C52^{ONa} atoms have trigonal planar environments, the silylene atom Si1^{NHC} is slightly pyramidalized (Σ_{Si1} : 339.6(1)°, 23 % pyramid.). This can be addressed to the presence of a stereoactive electron pair at the Si1 atom, but the effect is less pronounced than the respective lone pairs found in Lapperts NHC/NHSi adduct ($\Sigma = 291.6^\circ$, 76 % pyramidalization)^[107] or {SiC₄Ph₄}(LiPr₂Me₂) (302.6°, 64 % pyramidalization).^[266]

Remarkably, this effect is also perceptible by the bending of the bonded NHC ligand in respect to the {Si1,P1,C52} vertex by 45.7(3)°, which is precisely in between 90° (as expected in an idealized base-stabilized silylene) and 0° (as substituent in an sp² hybridized system). This opposes the related NHC-supported di(phosphino)silylene Si{P(Mes*)CH}₂(IMe₄), where the NHC meets the expectations and is nearly perpendicular to the {Si,P,P} plane ($\varphi = 82.55(5)^\circ$), although this system shows an angulation of the respective vertex ($\beta = 24.59(5)^\circ$) as well.^[133] This intermediate behavior of the carbene is also observed in the decreasing Si1-C1^{NHC} bond length (1.875(2) Å) when compared to the starting material **1** (1.937(4) Å) or the silyl(bromo)silylene SiBr(SiBr₂Tbb)(SIDipp) (1.978(3) Å). The shorter distance can be evidence for a stronger backbonding of the Si atom to the NHC, which is also in agreement with the aforementioned shielding of the ¹³C{¹H} NMR signal ($\delta_c = 179.5$ ppm).

To shed further light on the electronic delocalization, quantum-chemical calculations were performed on the RI-B97-D3/def2-TZVP level of theory for the complete, free anion 7-calc. Overall, the structure is well represented (Table 6, for a depiction see Figure 120 on page 281 in the appendix), but since the $\text{Na}(\text{thf})^+$ counter cation was excluded due to the methods necessity, a greater C=O double bond character is represented in the calculated structural data, artificially elongating the innercyclic C52-Si1^{NHC} and C52-P2 bonds (marked with an asterisk in the table below). Experimentally, no intensive band corresponding to a C=O double bond was found in the ATR-IR spectrum of **7** between 1600 and 2800 cm^{-1} (Figure 32).

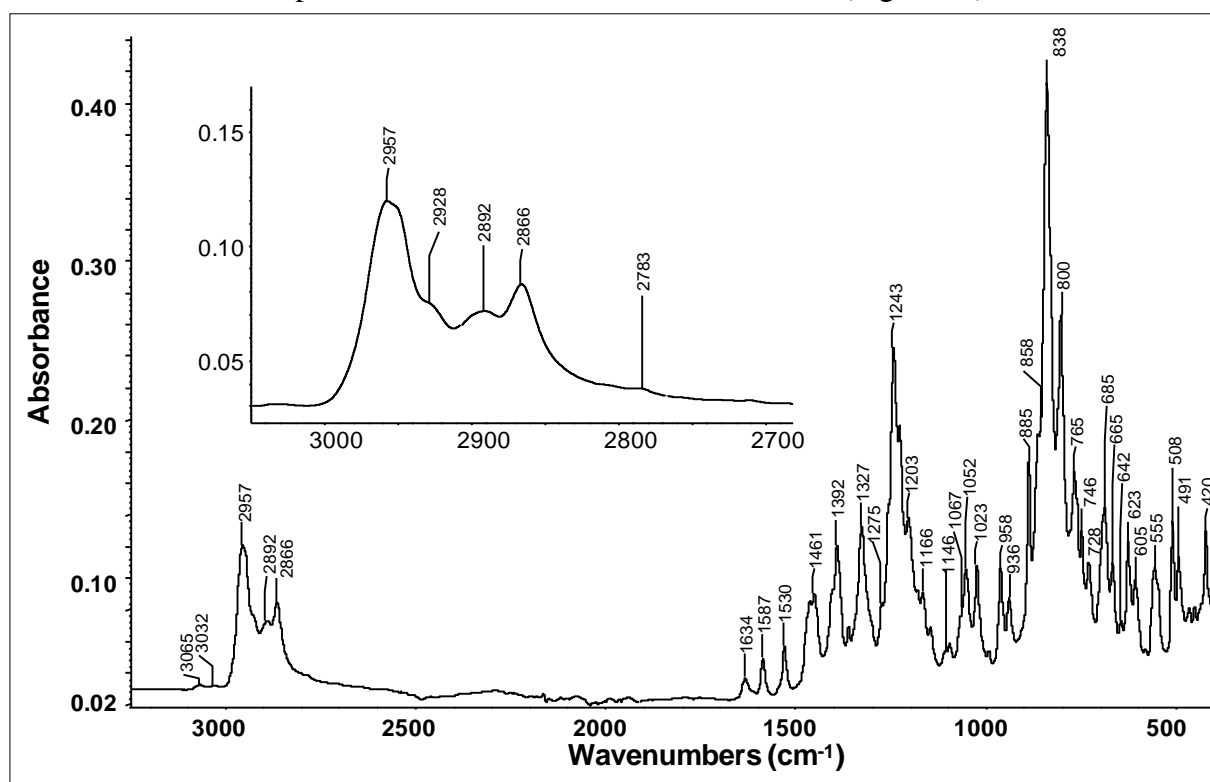


Figure 32. ATR-IR spectrum of **7** at ambient temperature. An enlarged excerpt of the region between 2650 and 3050 cm^{-1} is given in the inset.

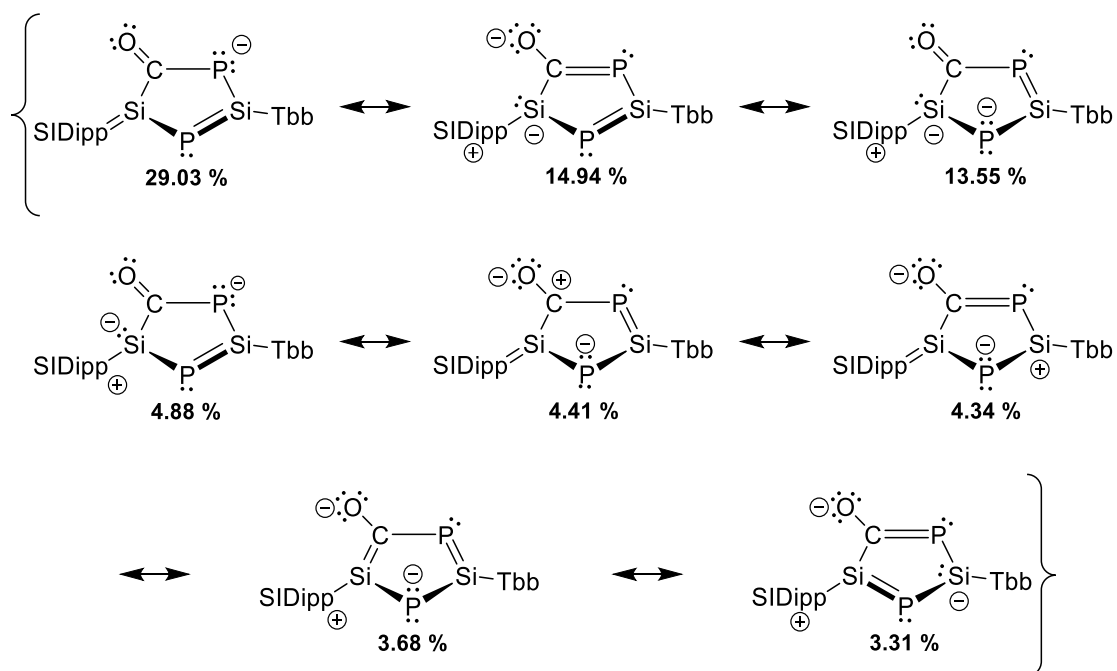
Table 6. Bond distances d , Wiberg Bond Indices and Bonding orders of **7** according to NRT.

	Si1-C25 ^{NHC}	Si1 ^{NHC} -P1	P1-Si2 ^{Tbb}	Si2 ^{Tbb} -P2	P2-C52 ^{Ring}	C52 ^{Ring} -Si1
Exp. $d / \text{Å}$	1.875(2)	2.2195(9)	2.089(1)	2.1630(8)	1.807(3)	1.907(3)
Calc. $d / \text{Å}$	[1.865]	[2.252]	[2.129]	[2.160]	[1.876]*	[1.983]*
WBI	1.05	1.00	1.45	1.26	1.19	0.90
B.O.	1.50	1.03	1.59	1.28	1.28	1.00

RI-B97-D3/def2-TZVP level of theory

The local NRT analysis (including all ring atoms, the ipso atoms of the substituents and both N atoms of the NHC) resulted in eight major resonance formulae that overall confirm the expectations (Scheme 20, for details see Table 51 on page 282 in the appendix). Hence,

extensive delocalization throughout the ring system and the CO moiety is suggested, with only the Si^{NHC} atom being less engaged: while the other innercyclic interactions show respective bonding orders and WBI as expected for a delocalized system (Table 6), the two bonds towards the Si^{NHC} atom are described as single bonds by this method. Instead, a significant Si=C^{NHC} double bond contribution was found, that is expressed by a bonding order of 1.50 by NRT but not represented in the related WBI (only 1.05, but potentially reduced by the polar nature of the bond, see also NPA charges in Table 8 below).



Scheme 20. Leading resonance formulae (contribution ≥ 2.5 %) of **7** as obtained from the NRT analysis.

Table 7. NICS values of **7** and related compounds.^[133,258,259,262]

Compound	7	B-P	B-CAd	F	J
NICS (0) /ppm	-5.0	-2.57	-4.17	-4.7	-14.1
NICS (± 1) /ppm	-6.2	-6.01	-12.42	-2.8	-9.7

For depictions of the reference compounds **B**, see Figure 27 on page 54.

The nucleus independent chemical shifts (NICS values) were calculated for the central {Si₂P₂C}-ring system.^[271] The negative values (NICS(0) = -5.0 ppm and NICS(± 1) = -6.2 ppm) are in agreement with the results of the NRT and MO analysis, hinting towards an aromatic 6-electron π -system with no sign of antiaromaticity. Those values compare reasonably well with data available in the literature, however, quantification of aromaticity has been proven to be problematic (Table 7).^[272] This is in consent with the NBO analysis (for details see Table 51 on page 282 in the appendix). The leading electronic structure is best represented as a congener of a cyclic butadiene with Si1=C1^{NHC} and Si2=P1 double bonds, as well as two free electron pairs at the P2 atom. Especially the for an NHC uncommonly large contribution of a Si1 \rightarrow C1 backbonding (the putative π -bond is polarized towards the Si1 atom by 58.57 %) is in good

agreement with the experimentally observed folding angle β (Table 5 on page 59). The Si atoms use hybrid orbitals with each about 35 % s character for the $\sigma(\text{P1-Si1})$ and $\sigma(\text{P1-Si2})$ bonds, which are polarized towards the P1 atom by 59 % and 56 %, respectively. This is caused by the difference in electronegativity (P: 2.19, Si: 1.90), which is also responsible for the polarization of the $\pi(\text{P1-Si2})$ bond (69.7 % towards P1, 99 % p character). As mentioned before, the negligence of the sodium counter cation artificially strengthens the C52-O1 interaction, which is therefore described as a distinct, polarized C=O double bond by NBO.

Table 8. NPA natural charges of selected atoms in compound 7.

atom	Si1 ^{NHC}	Si2 ^{Tbb}	P1 ^{Si, Si}	P2 ^{Si, C}	C52 ^{ONa}	O1	C1 ^{NHC}	C28 ^{Tbb}
Charge	+0.66	+0.74	-0.21	-0.73	-0.26	-0.65	+0.03	-0.51

To study the effect of the angular deflection of the NHC substituent, the angle ε between the Si1-C1^{NHC} axis and the Si1-Si2 axis was artificially deviated in a range of 90 – 180° in steps of about 5° each and the respective structures were allowed to relax (see Figure 33 and page 281 in the appendix). As expected, the minimum energy (for $\varepsilon = 135.96^\circ$) is in good agreement with the experimental structure ($\varepsilon = 138.89(9)^\circ$) while bending the NHC in either direction always resulted in less stable conformations.

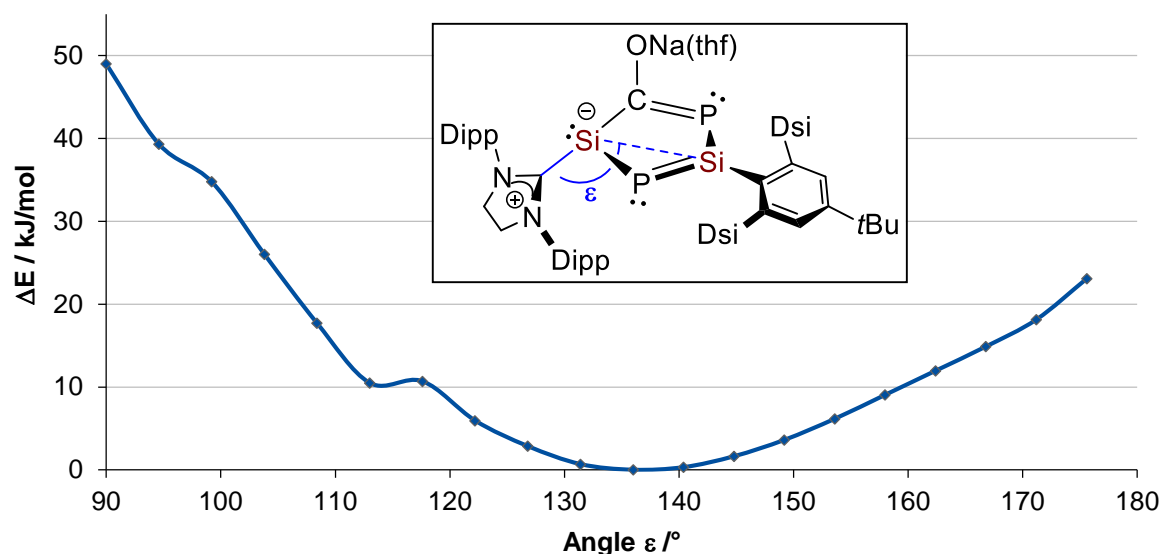


Figure 33. Changes of the absolute energy dependent on the angular deflection of the NHC.

Observing the structural parameters affected by the angular deflection (see Table 50 on page 282 in the appendix) revealed conspicuous correlations: Folding the NHC substituent in plane with the central $\{\text{Si}_2\text{P}_2\text{C}\}$ ring ($\varepsilon = 180^\circ$, 7-_{calc}^{max}) decreases the Si1-C1^{NHC} distance even further, whereas increasing the P1-Si1-C52^{ONa} angle was accompanied by elongation to a Si-C^{NHC} single bond as expected for a silene-type structure. In fact, the resulting calculated distance in the most

stable conformer (1.799 Å) lies in between the lengths of the double bonds reported for the cyclic silene cAAC^{c-hex}Si=SiR ($d_{\text{Si-C}} = 1.824(2)$ Å, R = C-H-activated cAAC^{c-hex} substituent)^[273] and a Tbt-substituted 2-Silanaphthalene (1.728 Å).^[274] On the other hand, artificial perpendicular orientation of the NHC in respect to the central ring seemingly reduces the orbitals overlap, resulting in a larger Si1-C1^{NHC} distance (1.927 Å, $\Sigma_{\text{Si}} = 298.7^\circ$, pyramid. = 68 %). That is now within the typical range of Si-NHC interactions and also the growing Si1-P1 and Si1-C52^{ONa} distances (2.309 Å and 2.051 Å) are indicating silylene character.

Additional insight is provided by the MO analysis. The Kohn-Sham frontier orbitals (Figure 34) are close in energy and again suggest a high delocalization of electron density over the molecules core unit, featuring multicentered composition of most MOs. Whereas the LUMO is mostly ligand-based, the HOMO is best described as a nonbonding combination of two P-centered lone pairs and the C=O p* bond. This proposes a nucleophilic P-centered reactivity with a relatively small $\Delta(\text{HOMO-LUMO})$ gap of 1.524 eV (Figure 34). Lower lying orbitals consist of combinations of multiple π -bonds as well as electron lone pairs of the phosphorous atoms, which makes correct interpretation very complicated. The Si1^{NHC} lone pair is involved in the HOMO-5, HOMO-3 and HOMO-2 orbitals.

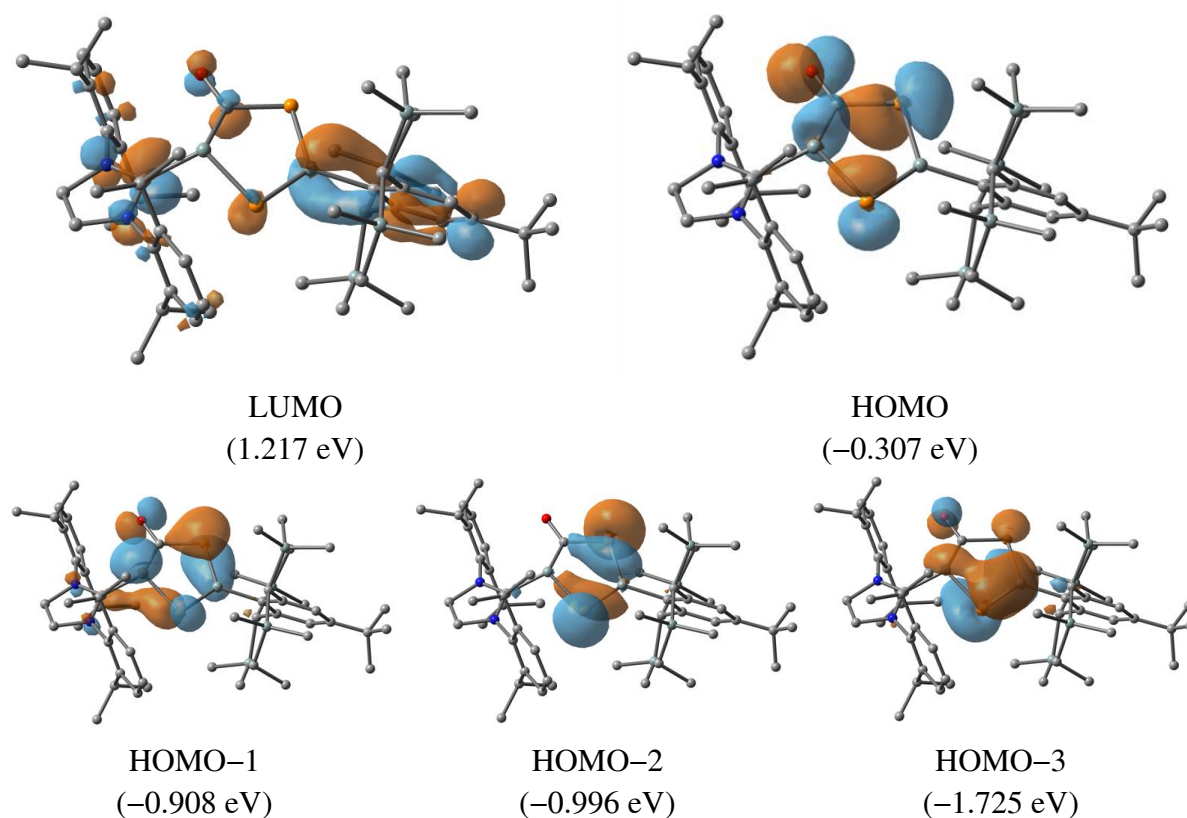


Figure 34. Selected Kohn-Sham orbitals of **7-oxa** and their energy eigenvalues; isosurface value: 0.04 e-bohr⁻³.

2.6 Coinage metal complexes

The use of Cu(I) NHC complexes in industry as well as academic research has been on the rise for years and is constantly highlighted in review papers due to the importance of copper in cross coupling reactions and dual dimetal catalysis.^[275–278] In comparison, only a handful of stable silylene complexes (**A** in Figure 35) has been reported so far,^[279–284] of which the groups of Stalke and Khan used tri- and mononuclear derivatives stabilized by (benzamidinato)silylenes (**D**) as promising catalysts for the synthesis of 1,2,3-triazoles in click chemistry.^[283,284] In 2016, Papazoglou obtained a copper(I)-bonded disilene dianion (**E**) upon reduction of $[(\text{Me}_3\text{P})_2\text{CuSiBr}_2\text{Tbb}]^{[41]}$ whereas Scheschkewitz obtained a lithium bis(disilylenyl)cuprate (**B**) from $\text{Li}(\text{Tip})\text{Si}=\text{SiTip}_2$ and CuI already in 2012.^[38] In contrast, addition of CuCl to the NHC-stabilized phosphasilylenylidene resulted in a straight end-on complex (**C**) and a similar compound was independently obtained from $\text{Si}_2(\text{IDipp})_2$ (**I**) by Arz and Robinson, who also investigated an equilibrium between the $^1\eta$ and $^2\eta$ complex in solution (**F**).^[285,286]

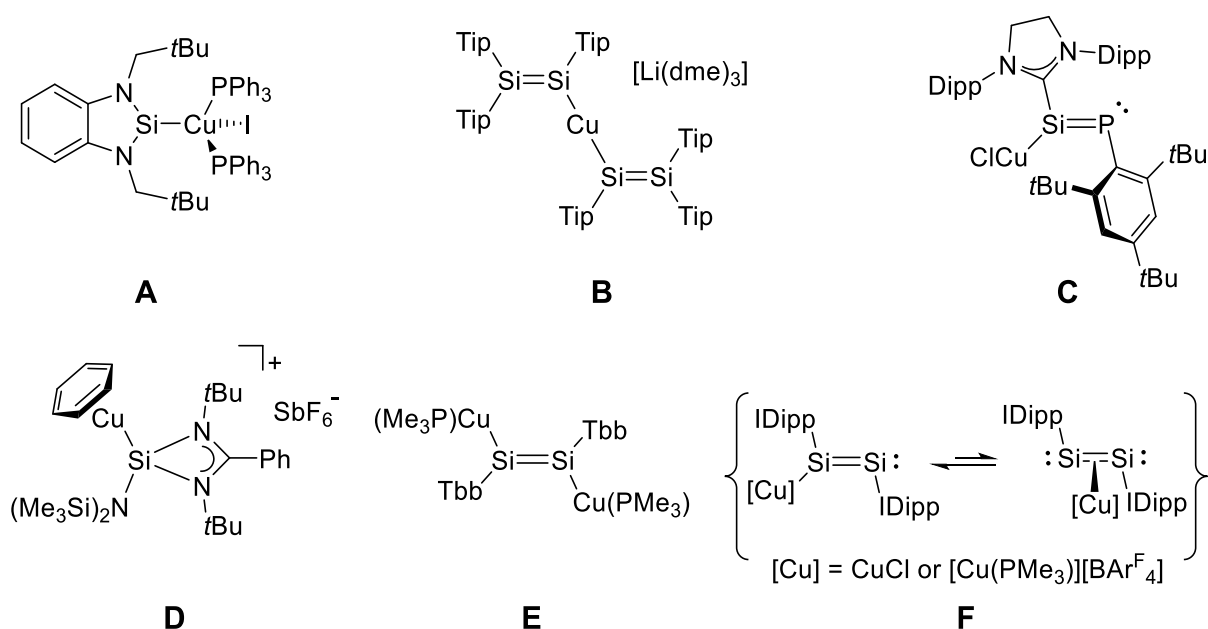


Figure 35. Selected Cu(I) complexes of silylenes, a phosphasilylenylidene and disilicon(0) (**I**). Formal charges are omitted for simplicity.^[279,38,280,287,284,285,41,286]

The first fully characterized Ag(I)-silyl complex has been reported by Lappert and coworkers as late as 2007,^[288] and until today isolable examples are scarce.^[289–291] The challenges in the syntheses of such compounds are mostly inherent due to particularly labile Si-Ag bonds that have been predicted to be significantly weaker than Si-Cu or Si-Au bonds by Frenking.^[182,292] When it comes to low-valent Si compounds, coinage metal silylene complexes have been described since 2014 with both three- and four coordinated Si atoms (Figure 36).^[182,280,293–295] Noteworthy, cationic $[\text{Ag}(\text{silylene})(\text{arene})][\text{BAR}^{\text{F}}_4]$ complexes have recently been used by Khan and coworkers as highly effective catalysts for A^3 coupling reactions outperforming known

NHC- and MOF catalysts under solvent-free conditions^[295] and silver silylidene complexes ($L_nAg=SiR_2$) have been identified as intermediates in transsilyranation reactions (“silylene transfers”) by Woerpel and Salvatella in 2004 and 2010.^[296,297] In this context it should be noted, that hydrosilylation reactions catalyzed by Cu(I) or Ag(I) probably don’t succeed via metal-silyl complexes but are believed to involve metal hydride species instead.^[298]

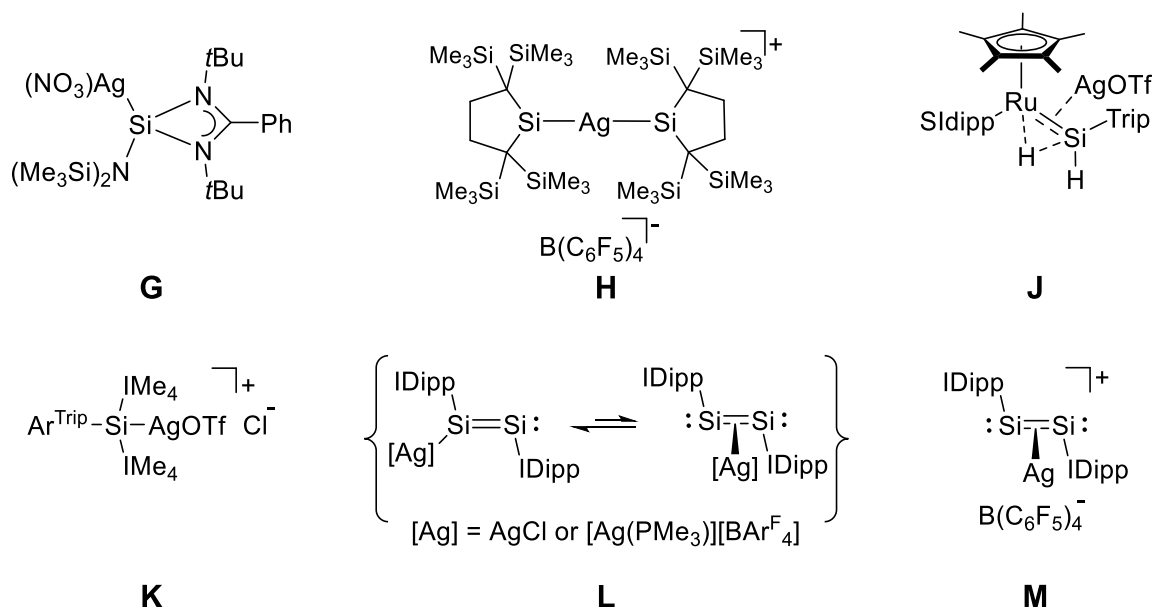
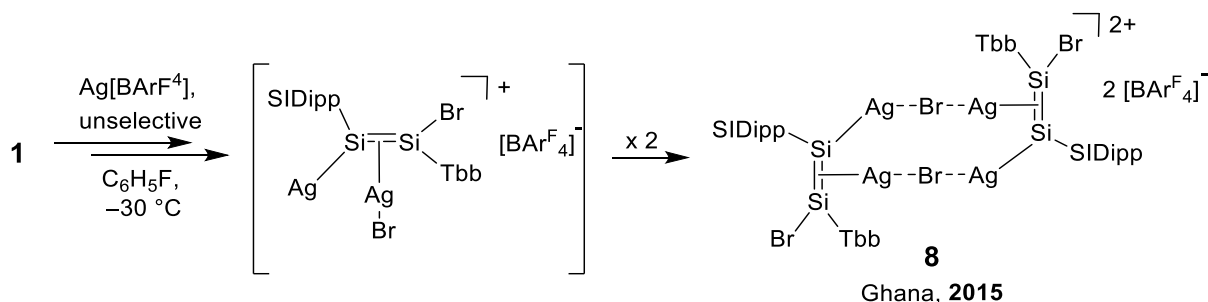


Figure 36. Ag(I) complexes of silylenes, a silylidene, a base-stabilized silyliumylidene ion and disilicon(0) (I). Formal charges are omitted for simplicity.^[280,286,295,299,300]

A well investigated example is the reaction of $Si_2(IDipp)_2$ (I) with $[AgCl(PMe_3)]$, that gave access to the respective η^1 -complexes $[AgCl\{\eta^1-I\}]$ as well as $[Ag(PMe_3)\{\eta^1-I\}][BArF_4]$ after chloride abstraction (Figure 36). Those complexes feature fluctional behavior with a change in hapticity from η^1 to η^2 in solution, whereas only the η^2 -complex was found in case of $[Ag\{\eta^2-I\}][B(C_6F_5)_4]$ due to additional stabilization from its Dipp groups.^[286]

As part of his preliminary reactivity study, Dr. P. Ghana from the Filippou group researched the reaction of **1** with $Ag[BArF_4]$ in an unsuccessful attempt to obtain “[$(SIDipp)Si\equiv SiTbb$][$BArF_4$]” ($BArF_4 = B\{C_6H_3-3,5-(CF_3)_2\}_4$) by AgBr elimination. Instead, several reaction products were formed of which only a dimeric cation could be identified by XRD analysis (**8**, Scheme 21).^[174] The product is best described as a Br-bridged cyclic dimer of a binuclear Ag(I) complex, where **1** is coordinated towards an Ag^+ ion via the lone pair of the Si^{NHC} atom and the $Si=Si$ π -bond is coordinated towards AgBr. Despite the low selectivity of the reaction and the incomplete bromine abstraction, the product poses valuable findings: the disilavinylidene **1** can act as a ligand and displays both η^1 - and η^2 -coordination modes.

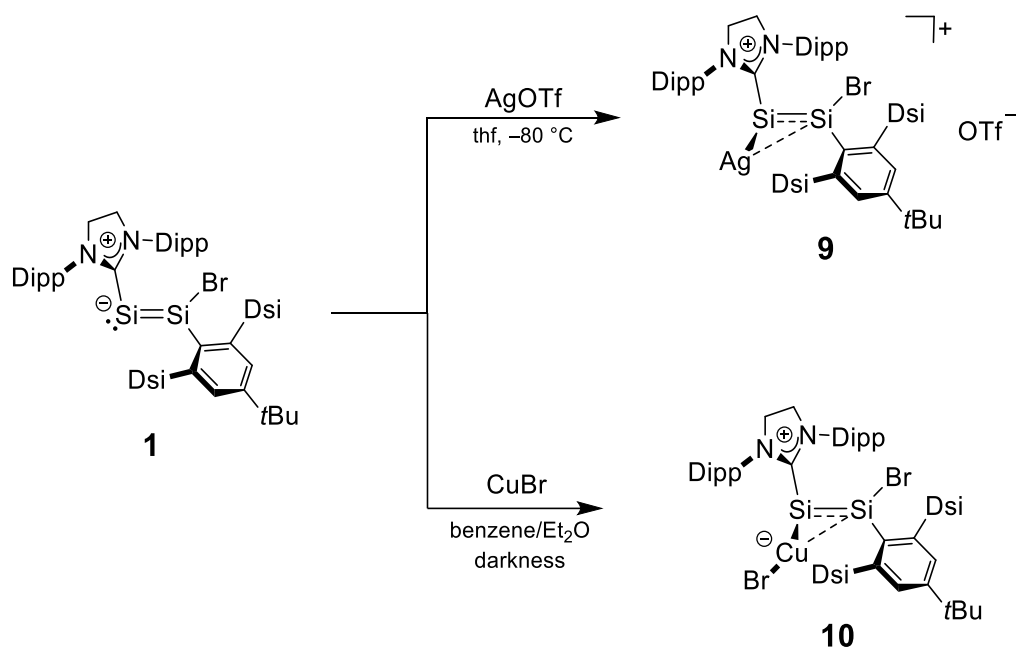


Scheme 21. Reaction of **1** with $\text{Ag}[\text{BAr}^{\text{F}_4}]$ to **8** reported by Dr. P. Ghana and a plausible monomeric intermediate.

2.6.1 Fluxional complexes of Cu(I) and Ag(I)

Silver triflate (OTf , F_3CSO_3^-) was chosen as a promising substrate because it has been reported to yield silylene complexes before and features an intermediate Lewis acidity when compared to AgBr and $\text{Ag}[\text{BAr}^{\text{F}_4}]$ or $\text{Ag}[\text{SbF}_6]$.^[293,294] A solid mixture of **1** and AgOTf was suspended in 6 ml of precooled thf at -80°C and warmed to ambient temperature, whereupon the color changed from dark red to greenish and finally yellow-brown. After extraction from a black byproduct (presumably some coarse elemental silver), $[\text{Ag}\{\eta^n\text{-(Z)-(SIDipp)Si=Si(Br)Tbb}\}][\text{OTf}]$ (**9**, $n = 1$ or 2) was obtained as an orange-yellow solid in 54 % yield (Scheme 22). Similarly, the reaction of **1** with CuBr afforded the complex $[\text{CuBr}\{\eta^n\text{-(Z)-(SIDipp)Si=Si(Br)Tbb}\}]$ (**10**, $n = 1$ or 2 ; Scheme 22). Compound **10** was isolated after stirring a mixture of **1** and CuBr in a mixture of benzene and diethyl ether (20:1) overnight in a vessel protected from light. Simple extraction afforded nearly quantitative yield in 90 – 95 % purity, while recrystallization from benzene/n-hexane at -30°C gave an analytically pure yellow powder (orange-brown when still wet) in a reduced yield of about 50 %. Compound **9** is very sensitive towards air- or moisture but can be stored as a solid. It is insoluble in aliphatic solvents or benzene, sparingly soluble in Et_2O , and well soluble in dme or thf although it polymerizes thf solutions within a couple of hours at ambient temperature. In comparison the copper derivative **10** has a much higher solubility in aromatic solvents and small amounts are even somewhat soluble in n-hexane. This can be an indication of $\text{Ag}\cdot\text{OTf}$ dissociation in solution while complex **10** is considered neutral. Both compounds are light sensitive in solution and gradually decompose at ambient temperature, but can be stored at -30°C in the dark for several weeks.¹⁵

¹⁵ Decomposition of compound **9** leads to a black, mostly insoluble mass that consists of multiple Tbb- and SIDipp- containing products according to ^1H NMR spectroscopy in thf- d_6 . Decomposition of **10** yields $[\text{CuBr}(\text{SIDipp})]$ among some unidentified products.



Scheme 22. Reactions of **1** with silver triflate and CuBr to the respective complexes **9** and **10**.

Surprisingly, compound **1** was found to undergo mostly unselective redox reactions with a variety of different Ag(I)- and Cu(I)-salts, leading to precipitation of black solids or metallic mirrors (Table 9). While the exact outcome of the reactions was highly dependent on the exact reaction conditions, their low selectivity complicates general statements. Also, copper and silver salts gave very different outcomes: for instance, the reaction with CuBr was very selective whereas AgBr only yielded oxidation products. Contrary, the reaction with AgOTf was successful whereas the [CuOTf·(toluene)] complex gave an unselective redox reaction that resulted in a beautiful copper mirror.

Table 9. Reactions of Ag(I) and Cu(I) compounds with **1** (overview).

Reagent	Conditions	Outcome
Ag[BAr ^F ₄]	C ₆ H ₆ F, -30 °C	Scheme 21, page 66 ⁽¹⁷⁴⁾
AgBr	Benzene, r.t.	Unselective ¹
AgBF ₄	C ₆ H ₆ F, r.t.	Unselective ¹
AgONC	Benzene, 80 °C	Unselective, very slow reaction
Ag[C(O)CF ₃]	Benzene, r.t.	Unselective, excess needed ¹
Ag[B ₁₂ Cl ₁₂]	Thf, -30 °C to r.t.	Unselective, slow reaction
AgOTf	Benzene, r.t.	See chapter 2.6.1, page 66
Cu[BAr ^F ₄]	Benzene, r.t.	Vide infra
CuBr	Benzene, r.t.	Vide infra
CuOtBu	Benzene, r.t.	Vide infra
CuOPh	Benzene, r.t.	Unselective ¹
CuC ₆ F ₅ ·(1,4-dioxane) _{0.5}	Benzene, r.t.	Unselective, slow reaction ¹
[CuOTf·(toluene)]	Benzene, r.t.	Unselective ¹
[Cu(MeCN) ₄]PF ₆	Benzene, r.t.	Fast decomposition
CuC≡C-C ₆ H ₄ -tBu	Benzene, 80 °C	Very slow decomposition

1: Deposition of elemental Ag/Cu was observed. All reactions were followed by ¹H NMR spectroscopy.

Yellow plates of **9** suitable for XRD were obtained upon cooling a concentrated dme solution to -30 °C for several weeks and orange needles of complex **10**·C₆H₁₄·C₅H₁₂ were obtained from a mixture of toluene, n-hexane and n-pentane at -30 °C (Figure 37). The solid state structures of **9** and **10** are closely related and each feature a side-on η²-complexation of the coinage metal via the Si=Si π-bond. As a result of the (Si₂)→Cu π-electron donation, the Si=Si double bonds (**9**: 2.234(2) Å, **10**: 2.254(3) Å) are elongated in respect to the starting material **1** (2.167(2) Å) by 6 and 9 pm respectively, which is likewise observed when comparing Si₂(IDipp)₂ **I** (Si=Si:2.229(1) Å) to its η²-[M][B(C₆F₅)₄] complexes (M = Cu: 2.281(2) Å, M = Ag : 2.292(3) Å).^(106,286) Yet the predominant sp² hybridization of the Si1^{Tbb} atom is still apparent by its almost planar environment in both **9** (Σ_{Si1}: 357.2(2)°, 3 % pyramidalization) and **10** (Σ_{Si1}: 356.1(2)°, 4 % pyramidalization).¹⁶ At the Si^{NHC} atom, the metal coordination only causes a negligible stretching of the Si-C25^{NHC} bond (**9**: 1.942(6) Å, **10**: 1.948(6) Å, **1**: 1.937(4) Å) and the carbene remains in an orthogonal orientation in respect to the central {C1,Br,Si1,Si2,C25} moiety (∠NHC **9**: 87.8(2)°, **10**: 89.8(2)°, **1**: 87.1(1)°).

¹⁶ Calculated for a three-coordinated Si1 atom without consideration of the coinage metal atom.

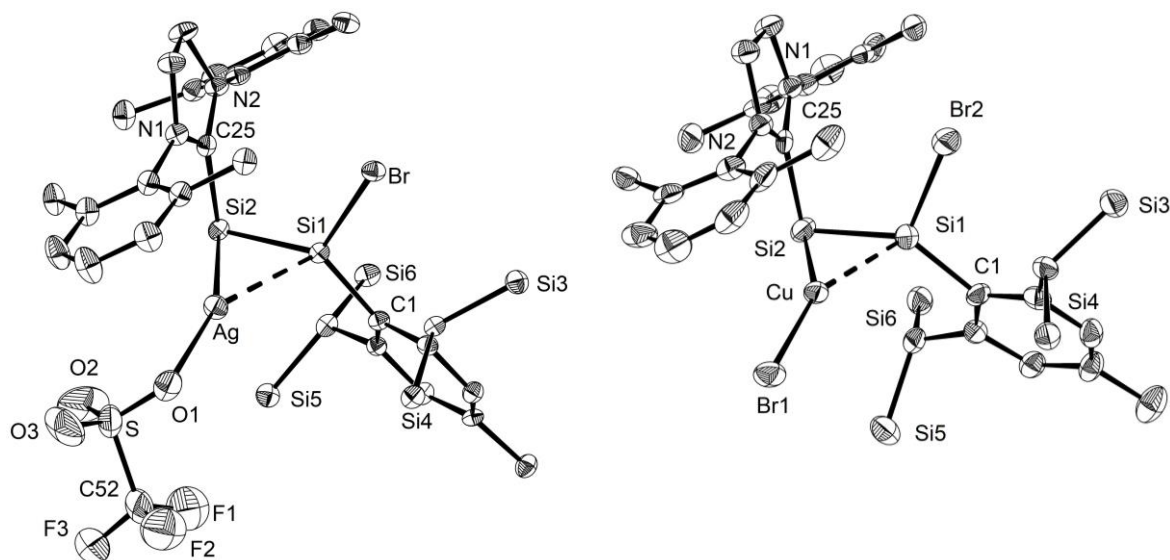


Figure 37. Molecular structure of **9**·(dme)_{2.5} (left) and **10**·C₆H₁₄·C₅H₁₂ (right). Thermal ellipsoids are set to 50 % probability; hydrogen atoms and peripheral methyl groups are omitted for simplicity. Selected bond lengths (Å), angles (°) and torsion angles (°): **9**: Si1–Si2 2.234(2), Si1··Ag 2.617(2), Si2··Ag 2.497(2), Ag–O 2.251(5), Si1–Br 2.261(2), Si1–C1 1.891(6), Si2–C25 1.942(6); Si1–Ag–Si2 51.75(5), Si1–Si2–C25 97.5(2), C25–Si1–Ag 100.6(2), Br–Si1–Si2 117.64(7), Br–Si1–C1 110.2(2), Br–Si1–Ag 119.04(8), C1–Si1–Ag 108.5(2), Si1–Ag–O1 152.0(1), Si2–Ag–O1 153.1(1); C1–Si1–Si2–C25 170.4(4), Br–Si1–Si2–C25 –11.4(2), O1–Ag–Si1–Br –93.2(3), O1–Ag–Si1–C1 33.9(4), O1–Ag–Si2–C25 107.8(4). **10**: Si1–Si2 2.254(3), Si1··Cu 2.411(2), Si2··Cu 2.318(2), Si1–C1 1.898(7), Si1–Br2 2.255(2), Si2–C25 1.948(6), Cu–Br 2.288(1); Si2–Cu–Si1 56.88(7), Si1–Cu–Br1 154.17(8), Si2–Cu–Br1 144.18(7), C1–Si1–Si2 132.1(2), C1–Si1–Br2 109.4(2), Si2–Si1–Br2 114.6(1), Si1–Si2–Cu 63.64(7), Si1–Si2–C25 96.2(2), C25–Si2–Cu 103.0(2); C25–Si2–Si1–C1 164.5(3), C25–Si2–Si1–Br2 9.7(2), Br2–Si1–Cu–Br1 106.4(2).

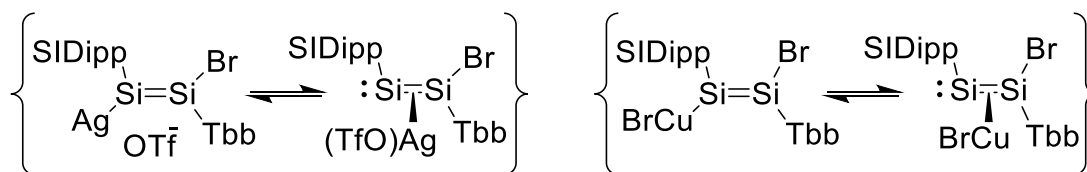
In both **9** and **10** the metal atom is closer to the Si^{NHC} (Si2–Cu: 2.318(2) Å, Si2–Ag: 2.497(2) Å) than to the Si^{Tbb} center (Si1–Cu: 2.411(2) Å, Si1–Ag: 2.617(2) Å), which can be explained by the higher nucleophilicity of the Si(0) atom. As expected, both Si–Cu distances in **10** (Si1–Cu: 2.411(2) Å, Si2–Cu: 2.318(2) Å) are much longer than the single bonds found in the bis(disilene)cuprate [Li(dme)₃][Cu(Si₂Tip₃)₂] (Si–Cu: 2.2412(8) Å and 2.2458(8) Å)^[38], the disilene {(Me₃P)Cu}TbbSi=SiTbb{Cu(PMe₃)} (2.248(1) Å)^[41] or in the end-on complex CuCl{η¹–I} (2.2081(9) Å).^[286] However, they compare well to the cationic η²-complex [Cu{η²–I}][B(C₆F₅)₄] with coordination via the Si=Si π-bond (∅Si–Cu: 2.4152(7) Å).^[286] The bonding can also be described by the distance of the metal atom to the Si=Si axis, which again is shorter in **10** (⊥: 2.077(2) Å) than those found in [Cu{η²–I}][B(C₆F₅)₄] (∅2.129(5) Å).^[286] This is probably caused by the lower coordination number of Cu. In the silver complex **10**, the Si^{NHC}–Ag distance of 2.497(2) Å lies in between those of [Ag{silylene}₂][anion] (2.33 to 2.42 Å)^[280,293,294] and Tilley's ruthenium silylidene complex of silver triflate η²–(OTf)Ag{Cp*(IDipp)Ru=Si(μ-H)(H)Tip} (2.562(1) Å). Meanwhile, the Si^{Tbb}–Ag distance (2.617(2) Å) is longer but compares well to those found in [Ag{η²–I}][B(C₆F₅)₄] (2.55(3) and 2.600(8) Å) which shows an almost identical Ag··Si₂ vector (⊥: 2.304(3) Å) as **9** (⊥: 2.297(2) Å).^[286]

Table 10. Selected structural and spectroscopic features of the metal complexes **9** and **10**.

Compound	Si=Si /Å	⊥Si ₂ ··M ^A /Å	∠NHC ^B /°	δ _{Si} (Si ^{Tbb}) /ppm	δ _{Si} (Si ^{NHC}) /ppm
9	2.234(2)	2.297(2)	87.8(2)	114.8 ^c	10.3 ^c
10	2.254(3)	2.077(2)	89.8(2)	105.1 ^D	35.6 ^D
1	2.167(2)	-	87.1(1)	86.0 ^D	34.6 ^D

A: distance between the metal atom and the Si-Si vector; **B:** angle between the imidazolium ring and the best plane of the {C,Si,Si,C,Br} moiety; **C:** measured in tetrahydrofuran-d₈; **D:** measured in benzene-d₆.

Multinuclear magnetic resonance spectroscopy of both **9** in tetrahydrofuran-d₈ and **10** in benzene-d₆ (Figure 38 and Figure 39 on page 72) revealed local C_{2v} symmetry for the SIDipp and the Tbb substituent. This requires rapid rotations around the respective Si-C bonds as well as an approximate mirror plane in the central {Si1,Si2,C1,C25} moiety which contradicts the side-on coordination mode found in the solid state. A plausible explanation would be a η¹/η²-equilibrium of the metal atoms in complexes **9** and **10** yielding disilenide-type isomers (Scheme 23) akin to the process described by Arz for [AgCl{η¹-I}] and [Ag(PMe₃){η¹-I}][BARF₄] (compare Figure 36 on page 65).^[286] Upon cooling a sample of **9** to -70 °C, some broadening of the aliphatic signals was observed, which could be caused by the aforementioned dynamic process or simply by slowed rotations of the bulky substituents. In either case, the very low coalescence temperature was not reached.

**Scheme 23.** Proposed η¹/η²-equilibrium of the metal atoms in complexes **9** and **10** in solution.

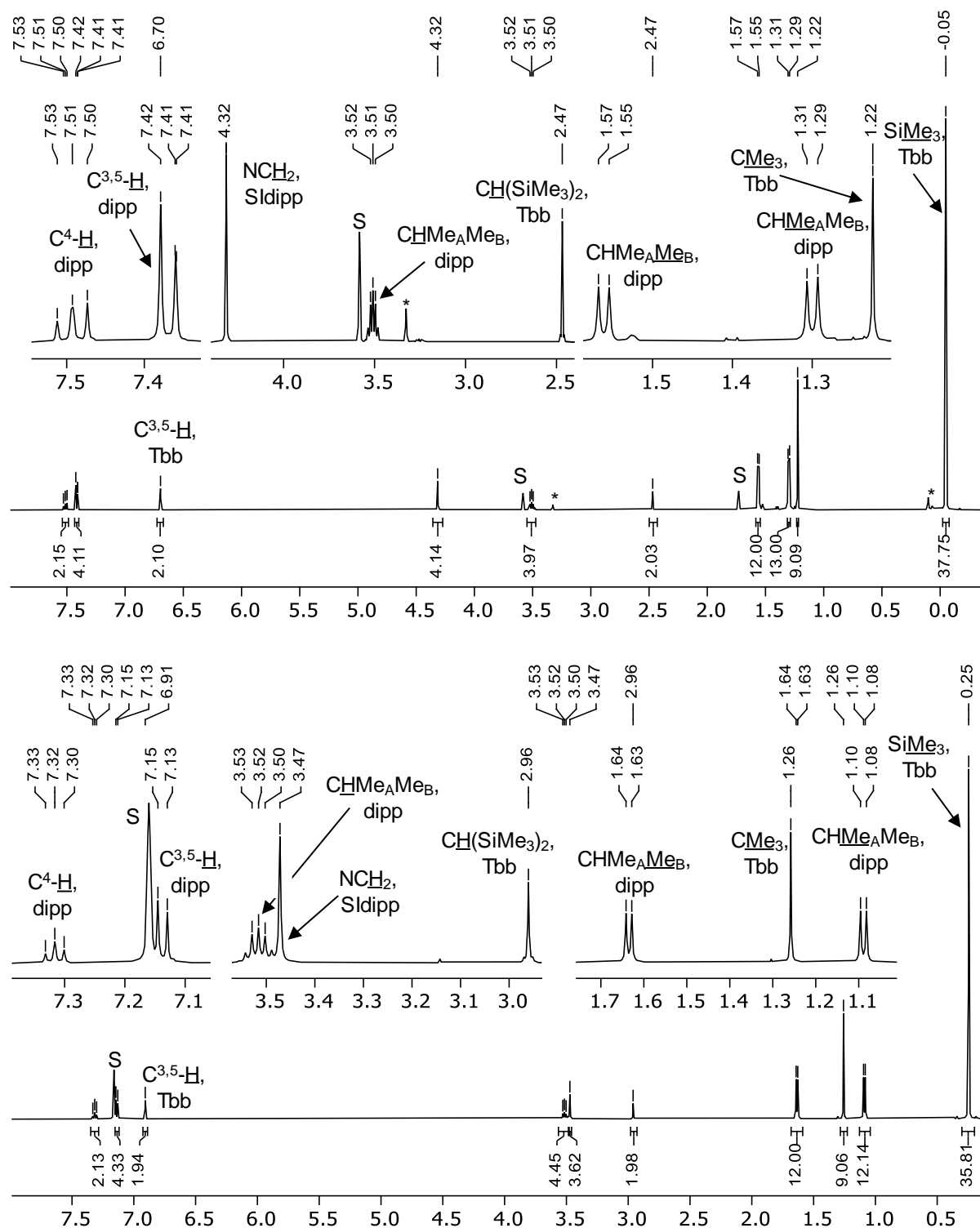


Figure 38. ^1H NMR (500.1 MHz) spectra of **9** in tetrahydrofuran- d_8 (top) and **10** in benzene- d_6 (below) at 298 K. As a result of decomposition in thf solution, the sample of **9** contains a small amount of an unknown impurity visible at $\delta_{\text{H}} = 3.33$ (s), 4.76 (s), 7.37 (d) and 8.81 ppm (s).

The ^{13}C NMR resonances of **9** and **10** barely deviate from those of **1** with the most indicative carbene signal appearing at $\delta_{\text{C}} = 196.8$ ppm and 199.2 ppm, respectively, which is only slightly highfield from the starting material (204.6 ppm).^[134] Strengthening of the Si-NHC bond is

expected since electron density is donated to the coinage metal atoms, however, these values are close to those of the NHC-stabilized zincosilylene **5-Br** with a Si^{NHC}-Zn bond (200.3 ppm) and thus not characteristic for either coordination mode. More pivotal, an unusual doublet signal at $\delta_c = 132.1$ ppm was found for the C¹ atom of the Tbb group of **9**, which is caused by a $^3J(\text{Ag},\text{C}) = 1.4$ Hz coupling.¹⁷ The simultaneous absence of a visible coupling of the NCN carbene resonance is an additional indication for an unsymmetrical coordination of the Ag in respect to the Si=Si bond in solution, since the $^2J(\text{Ag},\text{C})$ in a η^1 -complex would likely not be resolved. In this context it should also be mentioned, that no ^{15}N NMR signal could be detected for compound **9**, which would be in line with a decreased intensity due to a $^3J_{\text{Ag},\text{N}}$ coupling.

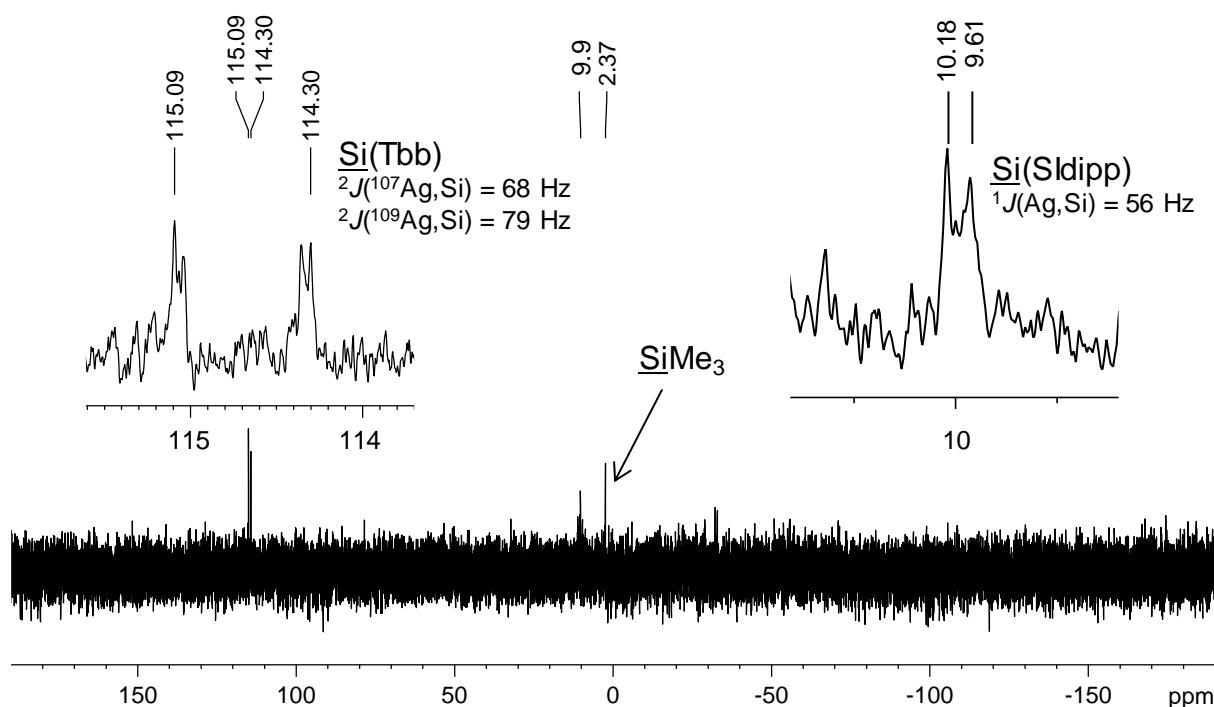


Figure 39. $^{29}\text{Si}\{^1\text{H}\}$ NMR (99.37 MHz) spectrum of **9** in tetrahydrofuran- d_8 solution at 298 K. As a result of decomposition in solution and the Ag,Si-coupling, only spectra with a low signal to noise ratios could be obtained. The $\underline{\text{SiMe}}_3$ signal at $\delta_{\text{Si}} = 2.4$ ppm has an artificially lowered intensity due to the inverse-gated measurement but can be observed as an intensive singlet signal in a dept20 NMR experiment, where the low-valent Si atoms are, in turn, not observed at all. Assignments and signal positions are backed up by 2D spectroscopy.

The $^{29}\{^1\text{H}\}$ Si NMR spectra of the AgOTf complex **9** and the CuBr complex **10** reveal new insights: the signal of the Si^{Tbb} atom (**9**: 114.8 ppm, **10**: 105.1 ppm) is shifted to a lower field in respect to the starting material (**1**: 86.0 ppm), which can be a sign of a higher anisotropy of the chemical shift tensor due to metal coordination. However, both values still appear within the span given by the metal-free disilavinylidenes **1-Me** (127.9 ppm) and **1-CHPh** (123.7 ppm). The Si^{NHC} resonance of **10** (35.6 ppm) is almost identical to that of **1** (34.6 ppm) but the signal

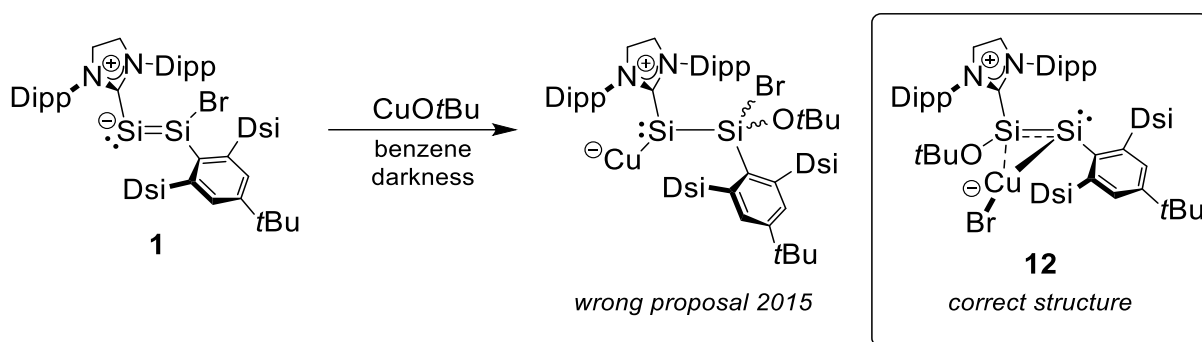
¹⁷ The ^{107}Ag and ^{109}Ag isotopes (natural abundance $\approx 52:48\%$, $I = 1/2$) are NMR active. Yet only one distinct coupling constant was resolved for both the ^{107}Ag - and the ^{109}Ag isotopomer, which is common for couplings below ca. 50 Hz. The strength of coupling constants follows the general trend $^1J > ^3J \gg ^2J > ^4J \approx ^5J$.

of **9** was found more shielded at $\delta_{\text{Si}} = 10.3$ ppm. While not too pronounced, this difference is likely caused by Ag \cdot OTf dissociation in solution and the accompanying strengthening of the Si \cdot Ag interaction. Whereas the signals of compound **10** appear as simple singlets, coupling to the Ag atom is observed for the low-valent Si atoms in complex **9** (Figure 39). The signal of the Si^{Tbb} atom is a superposition of two doublets caused by the ¹⁰⁷Ag/¹⁰⁹Ag isotopomers with distinguishable, Ag,Si coupling constants of 68 and 79 Hz. Surprisingly, only one weaker, averaged coupling constant of about 56 Hz is found for the Si^{NHC} signal which concurrently appears in the shape of a broad doublet.

These findings contradict a description of **9** (and presumably **10**) as defined η^1 complexes in solution, as much larger coupling constants are expected: Ag(silyl) compounds with a Si(sp³)-Ag bond show coupling constants in the range of 150 – 240 Hz^[288,289] and the silylene adduct (Ph₃P)_nAg{Si(tBu)₂(OTf)} (n = 1,2) that was characterized by in situ spectroscopy by Woerpel shows even stronger couplings (n = 1: 225 and 260 Hz; n = 2: 322 and 373 Hz).^[296] Especially Arz's end-on Ag complexes of the disilicon(0) AgCl{ η^1 -(**I**)} (¹J_{Ag,Si} = 384 Hz and 330 Hz) and [Ag(PMe₃)₃{ η^1 -(Si₂(IDipp)₂)}][BAr^F₄] (¹J_{Ag,Si} = 315 Hz and 273 Hz) clearly show coupling constants a magnitude larger when compared with the side-on complex [Ag{ η^2 -(Si₂(IDipp)₂)}][B(C₆F₅)₄] (¹J_{Ag,Si} = 35 Hz).^[286] Altogether the metal coordination has a surprisingly small impact on the ²⁹Si NMR shifts of **9** and **10**, suggesting mostly electrostatic interactions. The overall symmetry in solution is indicative for an end-on coordination via the Si^{NHC} electron lone pair while the small Ag,Si coupling constants detected for **9** are characteristic for a π -complexation that was also found in the solid state for both complexes. An equilibrium between the two isomers is likely, but ¹H NMR spectroscopy at -70 °C did not give any additional insights.

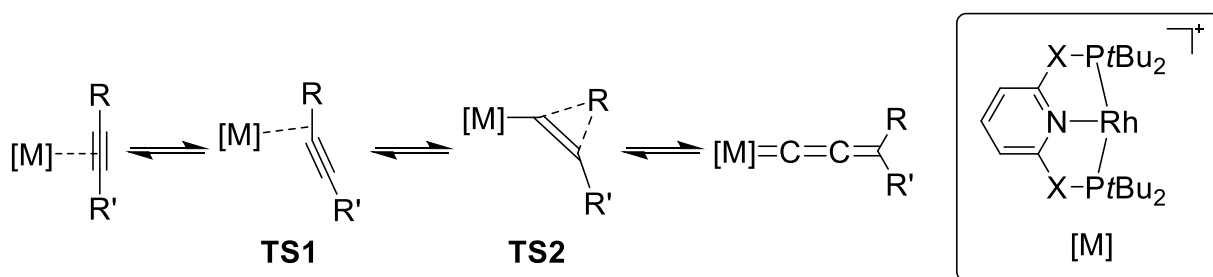
2.6.2 Push-pull complex of a disilyne

The reaction of **1** with CuOtBu was already described in the master thesis preceding to this work as preliminary results. Based on NMR-spectroscopy, the connectivity of the dark brown reaction product was wrongly assigned as “Cu{ η^1 -Si[SiBr(OtBu)Tbb](SIDipp)}”, the product of a hypothetical 1,2-addition of Cu⁺/OtBu⁻ across the Si=Si π -bond analogous to the ZnX₂ addition products **5-X** and **6** (page 46ff). As an alternative, a potential η^1 -complex of **1** was discussed as well.^[135] Now, after numerous experiments, the correct structure based on both XRD and multinuclear magnetic resonance spectroscopy could be determined: CuBr{ η^2 -(Z)-(SIDipp)(OtBu)Si=SiTbb} (**12**, Scheme 24).



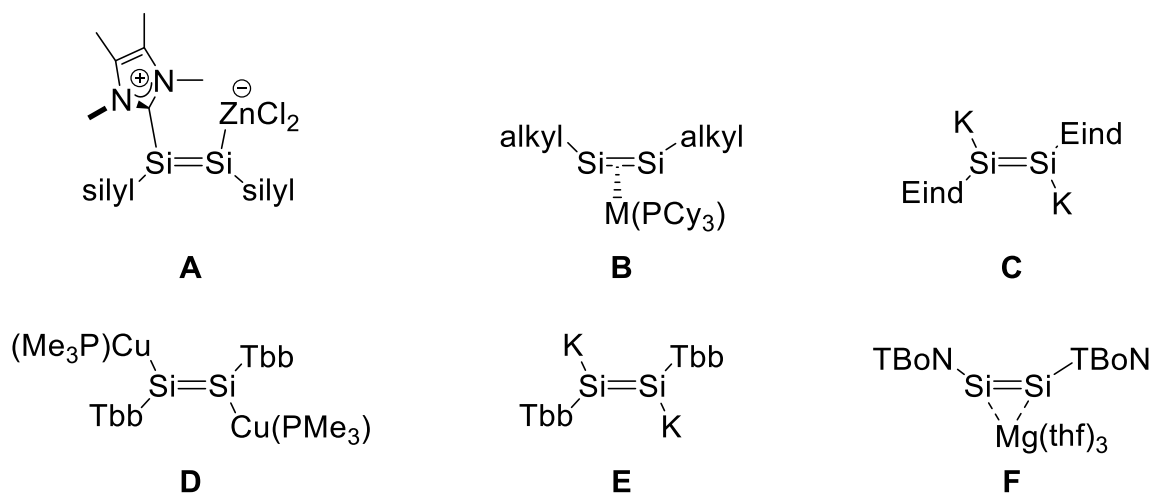
Scheme 24. Synthesis and structural assignment of compound **12**.

Compound **12** is a η^2 -complex of an NHC-stabilized oxy-disilyne and CuBr in which the OtBu group is bonded to the Si^{NHC} atom, while the formerly Si^{Tbb}-bonded bromide migrated to the Cu atom. The alkyne/vinylidene isomerization in the coordination sphere of transition metals is of great interest. Starting from side-on alkyne π -complexes, recent DFT studies by Rajabi and McMullin predict alkyne slippage to a σ (C-R) complex (**TS1** in Scheme 25) followed by migration of the substituent (**TS2**) to be key steps^[301] whereas the reverse reaction starting from Fe and Ru vinylidene complexes has been described experimentally by Mutoh et al. more than a decade ago.^[302]



Scheme 25. Mechanism of an alkyne/vinylidene complex isomerization calculated by Rajabi and McMullin.^[301]

Although a few examples of disilyne-metal complexes are known (Scheme 26), the isolation of compound **12** marks the first example of an isomerization of a disilavinylidene.



Scheme 26. Related disilyne complexes and disilene dianions.^[40–43,63,303] M = Pd, Pt; silyl = Si(iPr)(dsi)₂; alkyl = CCHtBu(SiMe₃)₂; TBoN = B{N(Dipp)CH}₂.

Experimentally, the best results were obtained when 1.4 equiv. CuOtBu were added to **1** in benzene at ambient temperature under strict exclusion of light. The dark brown product is purified by extraction with n-pentane and precipitated by cooling to about $-50\text{ }^{\circ}\text{C}$ and subsequent drying. Compound **12** is extremely air sensitive and slowly decomposes at ambient temperature within a few days even in a glove box but the solid can be stored in the dark at $-30\text{ }^{\circ}\text{C}$ for several weeks. The NMR spectra in benzene-*d*₆ solution suggest C₂ symmetric substituents with free rotations around the respective Si-C bonds, while the CuBr coordination renders the peripheral SiMe₃, isopropyl- and NCH₂H₆ groups diastereotopic. Noteworthy is the high field shift of the ¹³C{¹H} carbene resonance at $\delta_{\text{c}} = 185.1\text{ ppm}$, which is strongly shielded in respect to the starting material **1** (204.6 ppm) and the aforementioned complexes (**9**: 196.8 ppm; **10**: 199.2 ppm). This can be traced back to a more electron deficient Si^{NHC} atom in **12** due to the oxy-substituent and the change in formal oxidation state from 0 to +I (calculated charge +0.90 e). Similarly, the ¹³C resonances of the Tbb group in **12** appears at $\delta_{\text{c}} = 135.7\text{ ppm}$, which is in the same region as the disilyne TbbSi≡SiTbb (137.4 ppm)^[157] and low field from resonances of the Si(II)-bonded C¹ atoms in the disilene Tbb(Br)Si=Si(Br)Tbb (128.3 ppm)^{[48],18} or the disilavinylidene **1** (129.2 ppm).

In the ²⁹Si NMR spectrum of complex **12** (see Figure 48 on page 91), the signals of the unsaturated Si atoms are found at $\delta_{\text{si}} = 5.7\text{ ppm}$ and 25.9 ppm . The more highfield resonance at $\delta_{\text{si}} = 5.7\text{ ppm}$ was assigned to the Si^{Tbb} atom and is significantly shielded from the NHC-stabilized disilavinylidenes (86.0 – 127.9 ppm for **1** and derived products, 160.8 ppm for Iwamotos derivative **II**^[164]) and also upfield from typical disilenes (~ 60 to 150 ppm).^[16] The value

¹⁸ Note that the authors provide no assignment of ¹³C NMR data. However, the assignment given here is based on comparison to similar compounds and fairly conclusive due to the characteristic shifts of the C^{3,5}-H atoms (around 120 ppm) and the much stronger deshielding of the C^{2,6} and the C¹ resonances at around 150 ppm.

instead somewhat resembles the related disilyne $\text{TbbSi}=\text{SiTbb}$ ($\delta_{\text{Si}} = 16.2$ ppm),^{[157],19} but is far from the known η^1 -complex **A** (Si^{Zn} : 190.8 ppm)^[303] or the base-free η^2 -complexes **B** ($\text{M} = \text{Pd}$: $\delta_{\text{Si}} = 93.3$ ppm; $\text{M} = \text{Pt}$: $\delta_{\text{Si}} = 109.8$ ppm).^[63] The signal at $\delta_{\text{Si}} = 25.9$ ppm originates from the three-coordinated Si^{NHC} atom. It appears only slightly high field from **1** and derived DSV products (34.6 ppm to 65 ppm after alkyl substitution), which probably can be attributed to the oxygen atom. However, it should be pointed out that the increased coordination number does not have a large effect in this case.

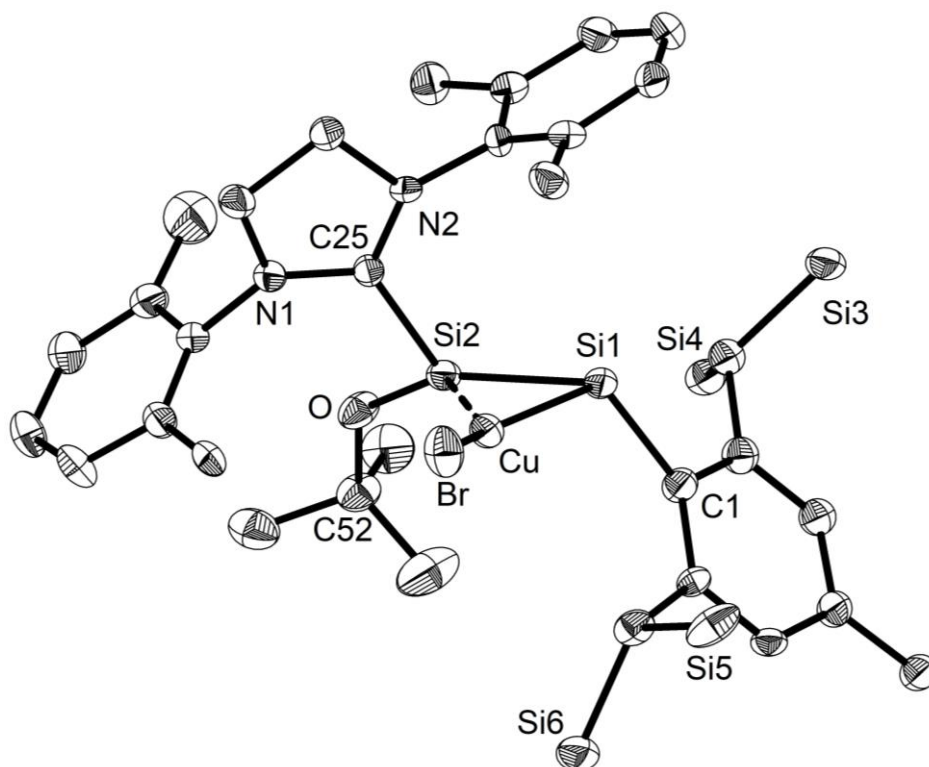


Figure 40. Molecular structure of **12**. Thermal ellipsoids are set to 30 % probability; hydrogen atoms and peripheral methyl groups are omitted for simplicity. Selected bond lengths (\AA), angles ($^\circ$) and torsion angles ($^\circ$): Si1-Si2 2.217(3), Si1-C1 1.930(9), Si1 \cdots Cu 2.309(2), Si2 \cdots Cu 2.453(2), Si2-C25 1.936(8), Si2-O 1.631(6), Cu-Br 2.286(1); Si2-Si1-C1 115.6(3), Si1-Si2-C25 113.5(2), Si1-Si2-O 148.1(3), C25-Si2-O 97.8(3), Si1-Cu-Si2 55.40(8), C25-Si2-Cu 86.3(2), O-Si2-Cu 132.6(3); C1-Si1-Si2-C25 $-179.4(4)$, C1-Si1-Si2-O $-11.2(6)$.

For the structural assignment, single crystals of complex **12** were grown by gas-phase diffusion of acetonitrile into a diethyl ether solution at -30 $^\circ\text{C}$ (Figure 40). The solid-state structure is best described as a CuBr η^2 -complex of an NHC-stabilized oxydisilyne. The bulky SiDipp - and Tbb -substituent are trans-oriented in respect to the central $\text{Si1}=\text{Si2}$ bond ($-179.4(4)^\circ$) and the OtBu substituent is cis relative to the Tbb ($-11.2(6)^\circ$). The $\text{Si1}=\text{Si2}$ double bond length (2.217(3) \AA) in **12** is a little longer than those of the disilavinylidenes (**1**: 2.167(2) \AA), **1-Me** (2.171(1) \AA), **1-CHPh** (2.190(2) \AA) or **II** (2.1787(8) \AA)^[164] and shorter

¹⁹ Known C-substituted disilynes resonate from 16.2 to 31.8 ppm, silyl-substituted disilynes at 62.6 – 106.3 ppm. See Table 19 on page 86.

than the one of the related CuBr-complex **10** (2.254(3) Å). Compared to the known disilyne complexes, the bond distance lies in between those of **A** (2.201(1) Å)^[303] and **B** (M = Pd: 2.170(1) Å, M = Pt: 2.167(3) Å).^[63] A large cavity as well as the narrow C1^{Tbb}-Si1-Si2 angle (115.6(3)°) confirm the presence of an electron lone pair at the Si1 atom which is now in the formal oxidation state of +I. Not accounting for the CuBr moiety, the Si2 atom is in a planar environment (Σ_{Si2} : 359.4(3)°), similar to the three-coordinated Si atom in **10** (356.1(2)°). Consequently, the Si2-O distance (1.631(6) Å) resembles a typical single bond. Interestingly, the angle between the central {Si1, Si2, C^{NHC}, C^{Tbb}, O} plane and the SIDipp ligand (\sphericalangle 29.4(5)°) is much smaller than the one found in **1** or Si₂(IDipp)₂ (each nearly orthogonal).^[106,134] It is plausible, that a parallel orientation of the planes as found in the alkylation products [Si^R(IDipp)₂][BAR^{F4}]₄ (R = H, Me)^[286] for the Si^R-bonded NHC ligand is aspired but prevented by steric bulk: the rigid CuBr unit is encapsulated by two iPr and a CH(SiMe₃)₂ group, locking the substituents in place.

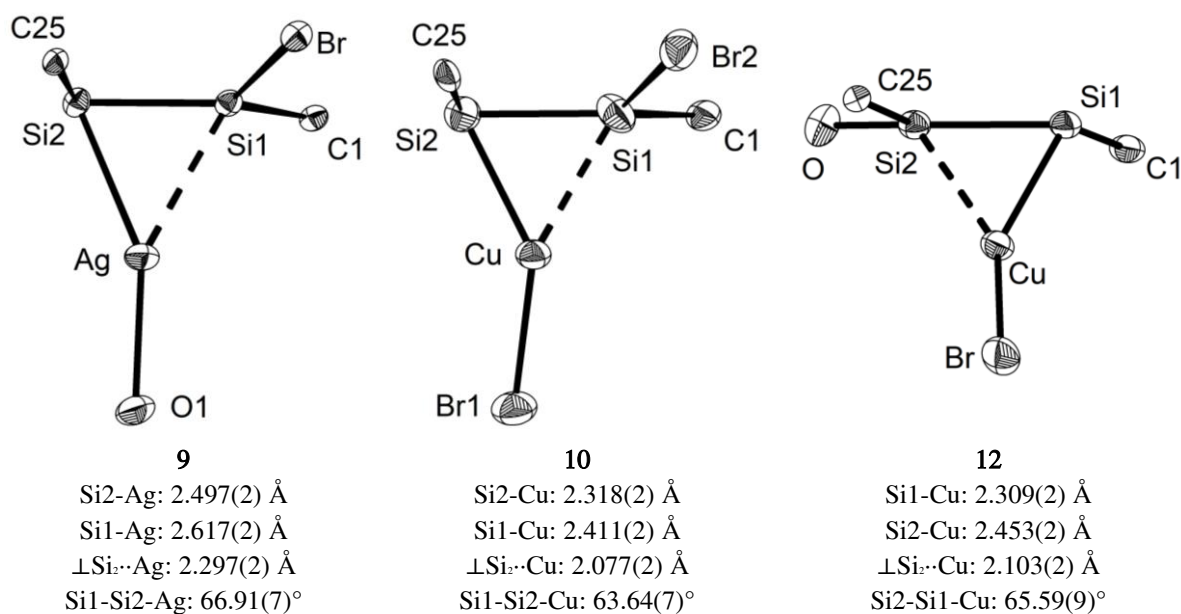


Figure 41. Coordination sphere of the metal atoms in the complexes **9**, **10** and **12**. Peripheral groups are omitted.

Akin to the complexes **9** and **10**, the copper atom in **12** occupies a slightly offcentered η^2 coordination at the Si=Si π -bond. The Si-Cu distances in **12** (Si1^{Tbb}: 2.309(2) Å and Si2^{NHC}: 2.453(2) Å) are noticeably different, which compares very well to those found in **10** (Si1^{Tbb}: 2.411(2) Å and Si2^{NHC}: 2.318(2) Å). In either case, the shorter Si-Cu distances are found for the Si atom with the lower coordination number. This is reminiscent to the alkyne/vinylidene complex isomerization mechanism via alkyne slippage depicted in Scheme 25 (page 74) and can be further explained by the smaller coordination sphere of a lower coordinated Si atom and its higher nucleophilicity. Overall, the CuBr unit is bound a little closer in **10**, as evidenced by the distance of the Cu atom to the Si=Si axis (\perp **10**: 2.077(2) Å; \perp **12**: 2.103(2) Å), but nearly identical dissociation energies were calculated for both complexes (Table 11).

Table 11. Calculated (B97-D3(BJ)/def2-TZVP) Cu-Si bond dissociation energies and Wiberg bond indices of the CuBr complexes **10** and **12**.

Cpd.	BDE / kJ·mol ⁻¹			NRT bond order ^A	
	gas phase	n-hexane	thf	Si ^{Tbb} -Cu	Si ^{NHC} -Cu
10	270.9	262.5	258.6	0.0/0.0/0.0	0.5/0.2/0.3
12	296.3	285.7	279.0	0.4/0.2/0.2	0.1/0.1/0.0

A: total / covalent / ionic contribution.

DFT calculation of the frontier orbitals of the CuBr complexes **10** and **12** revealed their complex electronic structures (Figure 42 and Figure 43). Type and energetic order of the Kohn-Sham orbitals of the disilavinylidene complex **10** are comparable with those of **1**: the HOMO represents the Si=Si π -bond while the electron lone pair at the two-coordinated Si^{NHC} atom and nonbonding p-orbitals at the CuBr bromide contribute to the nearly isoenergetic HOMO–1 and HOMO–2. With an energy gap of about 2.16 eV, (**1**: 2.00 eV), the LUMO of **10** is best described as an antibonding π^*_{out} orbital involving the out of plane p orbitals of the central atoms. Albeit close in energy, the inverse order of the occupied orbitals is found in case of the disilyne complex **12**. Here, the HOMO is best described as the lone pair at the two-coordinated Si^{Tbb} atom while the Si=Si π -bond manifests as HOMO–1. Interestingly, the HOMO–3 of **12** displays an antibonding $\pi^*(\text{Cu}-\text{Br})$ interaction involving a d-orbital at the Cu atom and a p-orbital at the Br atom. Finally, the LUMO of **12** ($\Delta_{\text{HOMO/LUMO}}$: 1.58 eV) is a nonbonding orbital involving the antibonding combination of the out-of-plane p-orbitals at N1, N2 and the carbene carbon atom as well as the out-of-plane p-orbital of the Si^{Tbb} atom.

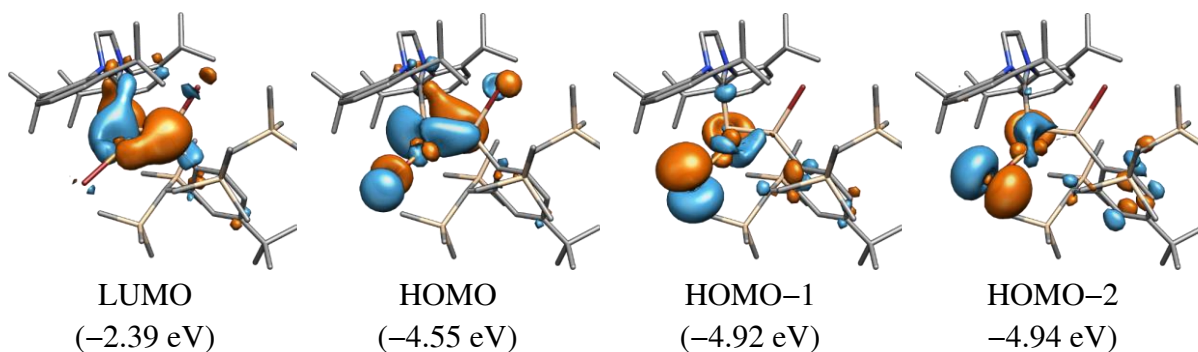


Figure 42. Selected Kohn-Sham orbitals of complex **10** on the B97-D3(BJ)/def2-TZVP level of theory. $\Delta(\text{HOMO-LUMO})$: 2.16 eV. Isosurface value = $0.04 \text{ e}^{1/2} \text{ Bohr}^{-3/2}$. For details see Table 47 on page 279.

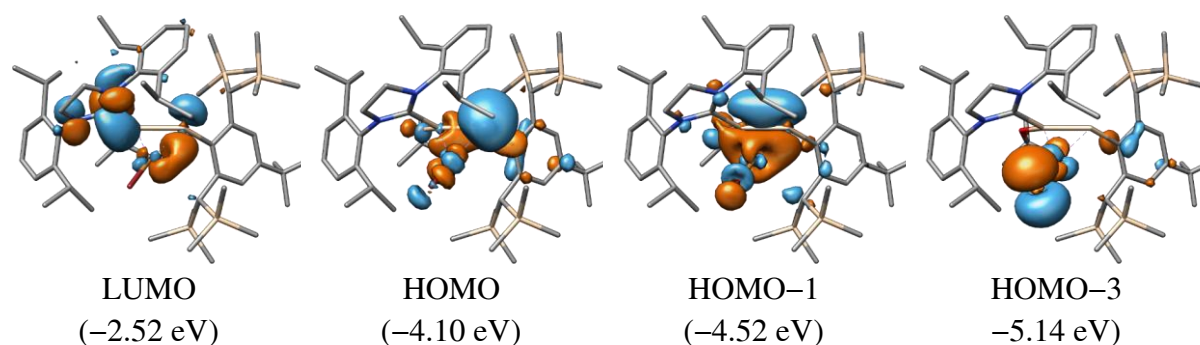


Figure 43. Selected Kohn-Sham orbitals of complex **12** on the B97-D3(BJ)/def2-TZVP level of theory. $\Delta(\text{HOMO-LUMO})$: 1.58 eV. Isosurface value = $0.04 \text{ e}^{1/2} \text{ Bohr}^{-3/2}$. For details see Table 47 on page 279.

Table 12. Combined resonance weight of NRT formulae featuring the given bond order of **10** and **12** (B97-D3(BJ)/def2-TZVP level of theory).

Bond	Si-Si	Si=Si	Si≡Si	LP(Si1)	LP(Si2)	Si-Br/O	Si=Br/O	Si1-Cu	Si1=Cu	Si2-Cu
10	32.4	54.7	4.8	16.9	69.6	63.5	19.0	0.0	0.0	52.4
12	30.4	38.7	24.6	59.9	19.2	73.4	2.5	28.1	13.9	4.7

No salient bonding interactions between the Cu and Si atoms are found in any frontier orbitals of either derivative, which is also reflected in the NRT-derived resonance structures and low bond orders ($\text{Si}^{\text{Tbb}}\text{Cu}$: 0.00 and $\text{Si}^{\text{NHC}}\text{Cu}$: 0.52), which are essentially the same as in **10** ($\text{Si}^{\text{Tbb}}\text{Cu}$: 0.56 and $\text{Si}^{\text{NHC}}\text{Cu}$: 0.05) (Table 12). The nature of the bonding is hence believed to be mostly electrostatic.

The absorption properties of the light sensitive complexes **10** and **12** were investigated by UV-vis spectroscopy (Figure 44 and Table 13). Broad absorptions with three not particularly distinct maxima ($\lambda_{\text{max}} = 401 \text{ nm}$) were observed for an orange-yellow solution of **10** in thf, which is reminiscent of the yellow disilene $\text{Tbb}(\text{Br})\text{Si}=\text{Si}(\text{Br})\text{Tbb}$ ($\lambda_{\text{max}} = 427 \text{ nm}$ in n-hexane). In comparison, a solution of **12** in n-hexane shows a noticeable red-shift with a distinct band at $\lambda = 466 \text{ nm}$ and a very diffuse absorption around $\lambda_{\text{max}} = 588 \text{ nm}$ that is responsible for the intense dark brown color. But again, no clear indication of a $\text{Si}\cdots\text{Cu}$ interaction could be identified.

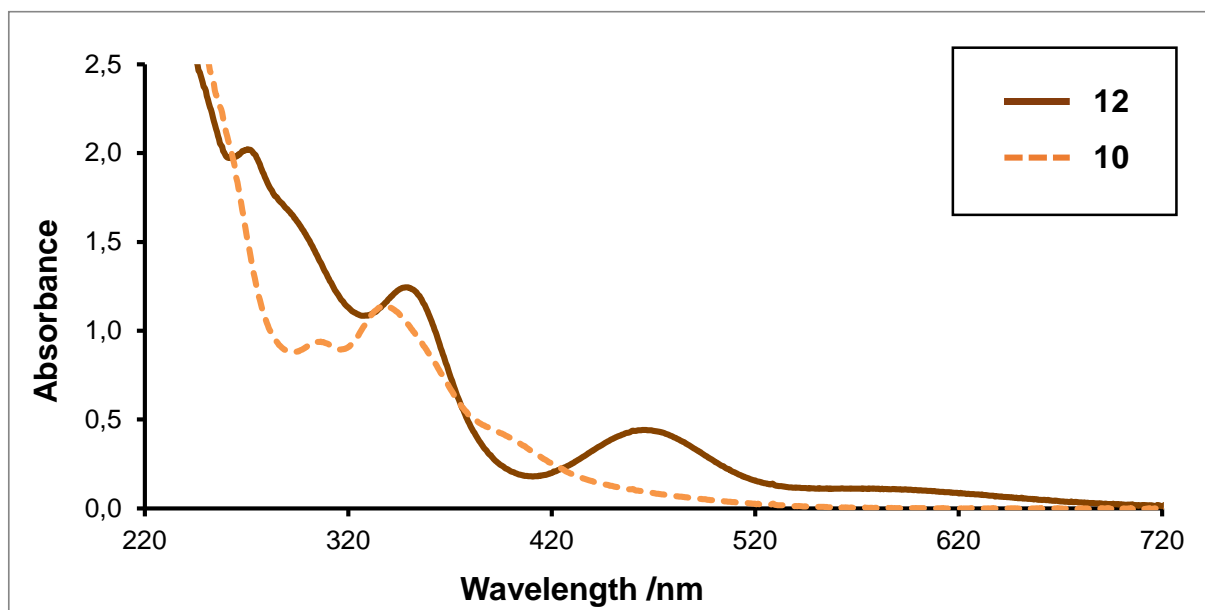


Figure 44. Comparison of the UV-vis/NIR spectra of the CuBr complexes **10** in thf (orange, dashed) and **12** in n-hexane (brown, solid). See also page 270 in the appendix for the deconvoluted spectra.

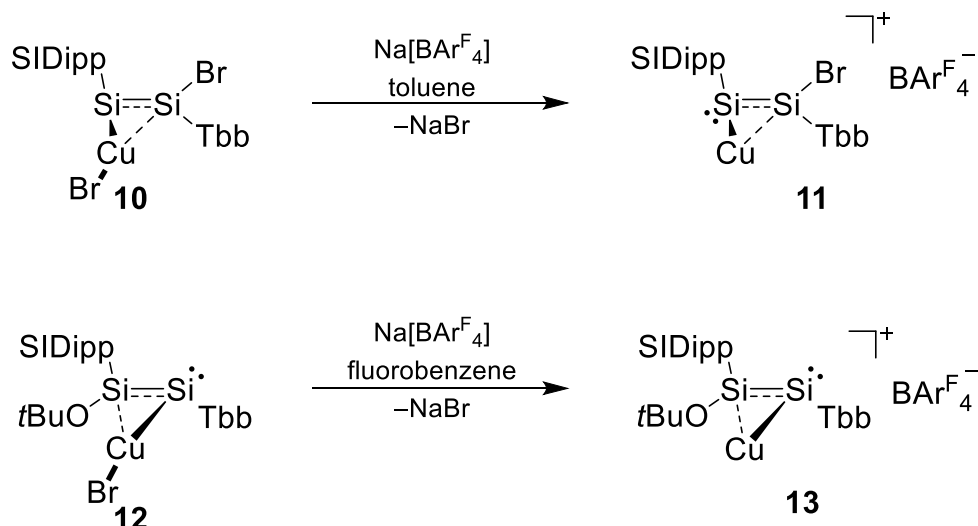
Table 13. Absorption maxima of **10** in thf and **12** in n-hexane and their molar extinction coefficients ϵ .

	color	λ_1	λ_2	λ_3	λ_4
12	Dark brown	271 nm	349 nm	466 nm	588 nm
		(20698 l·mol ⁻¹ ·cm ⁻¹)	(12566 l·mol ⁻¹ ·cm ⁻¹)	(4528 l·mol ⁻¹ ·cm ⁻¹)	(1126 l·mol ⁻¹ ·cm ⁻¹)
10	Orange-yellow	307 nm	339 nm	401 nm	-
		(13126 l·mol ⁻¹ ·cm ⁻¹)	(16067 l·mol ⁻¹ ·cm ⁻¹)	n. a.	

For more details see page 269 and 270 in the appendix.

2.6.3 Cationic Cu⁺ complexes

Addition of Na[BAr^F₄] to a toluene solution of the CuBr complexes **10** selectively afforded the cationic bromine abstraction product [Cu{(Z)-(SIDipp)Si=Si(Br)Tbb)}][BAr^F₄] (**11**), which is also directly available from **1** and [Cu(MeCN)₂][BAr^F₄] in fluorobenzene. Similarly, [Cu{(Z)-(SIDipp)(tBuO=Si=SiTbb)}][BAr^F₄] (**13**) can be made from **12** and Na[BAr^F₄] but the use of thf or fluorobenzene is needed in this case (Scheme 27).²⁰



Scheme 27. Bromide abstraction from the CuBr complexes **10** and **12**. Compound **13** is also available from **1** and [Cu(MeCN)₂][BAr^F₄] in fluorobenzene solution. Formal charges are omitted for simplicity.

Complexes **11** and **13** were obtained as orange and cherry red powders with a high tendency to form oils. Both compounds are extremely soluble in etheral or fluorinated solvents (decomposition in thf was observed within a few hours for **11** and much faster for **13**), while the formation of oils immiscible with aromatic or aliphatic solvents hampered typical workup procedures. Precipitation from a toluene/n-hexane mixture using an ultrasonic bath (**11**) and slow precipitation from layered fluorobenzene/n-pentane mixtures (**13**) gave almost pure powders in yields of about 60 % and 80 % but, small adhesions of solvents could not be removed and contamination with some NaBr cannot be excluded (Figure 45).

²⁰ Li[Al{OC(CF₃)₃}₄] can be used for both abstraction reactions as well, but the reaction product showed an even higher tendency to form oils.

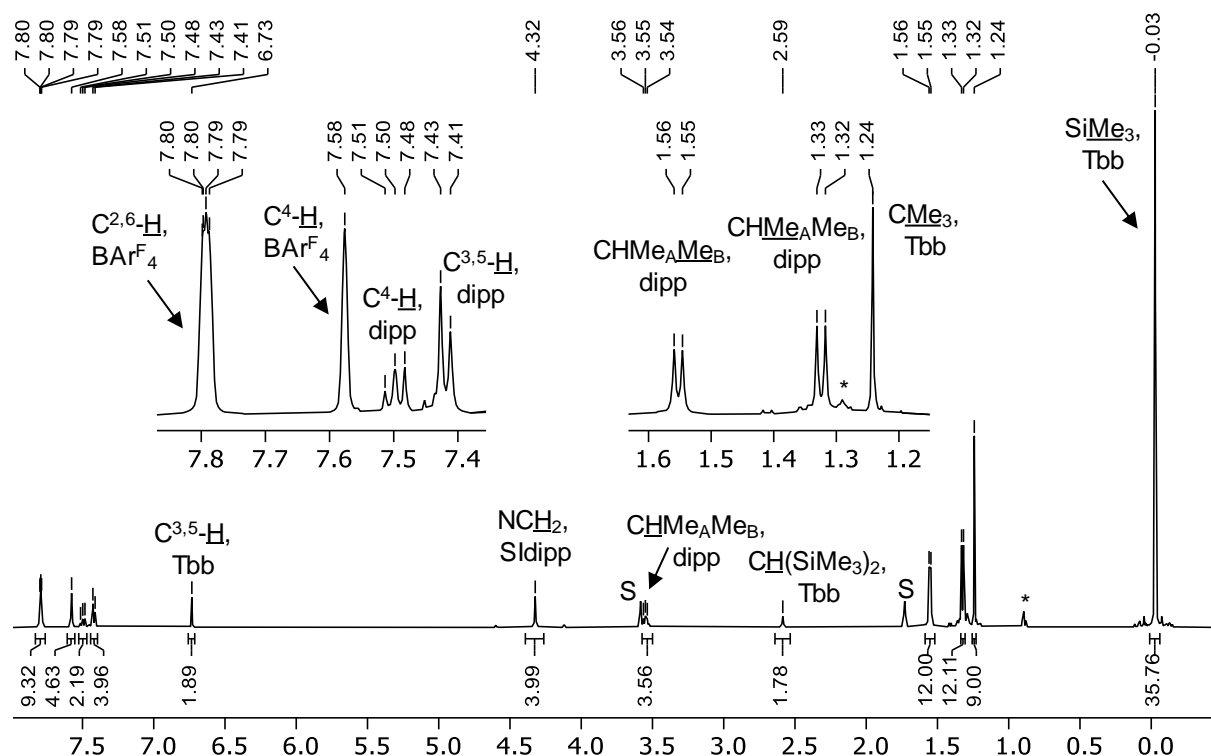


Figure 45. ^1H NMR (500.1 MHz) spectra of **11** in tetrahydrofuran- d_4 . The signals marked with an asterisk (*) originate from a small amount of n-hexane present in the sample.

Remarkably, the ^1H and ^{13}C NMR spectra of **11** and **13** revealed local C_{2v} symmetry of the SIDipp- and the Tbb groups, which is equal to **1** and **10** but higher than the local C_2 symmetry observed for **12**. The increased symmetry of **13** in respect to **12** can either be explained by the reduction of steric pressure allowing for easier rotations of the substituents or by a re-isomerization to a vinylidene motif (a 1,2-shift of the OtBu group) that would also explain the color change from brown to red. This hypothesis is rejected by the characteristic ^{13}C NMR resonance of the carbene atom: only minimal shifts are observed after bromide abstraction and the disilyne complexes **12** and **13** appear around 15 ppm highfield from the disilyvinylidene complexes **10** and **11** (Table 14). All aforementioned arguments regarding potential η^1/η^2 equilibrium of the Cu coordination remain true for the abstraction products as well.

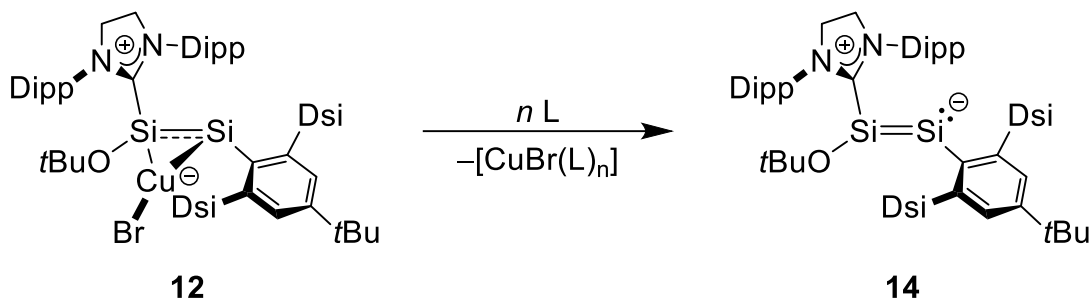
Table 14. $^{29}\text{Si}\{^1\text{H}\}$ NMR and $^{13}\text{C}\{^1\text{H}\}$ carbene resonances of the copper complexes **10** – **13** and **1**.

Cpd.	$\delta_{\text{Si}} (\text{Si}^{\text{NHC}})$ /ppm	$\delta_{\text{Si}} (\text{Si}^{\text{Tbb}})$ /ppm	$\delta_{\text{C}} (\text{C}^{\text{NHC}})$ /ppm	Solvent	color	Local symmetry
1	34.6	86.0	204.6	benzene- d_6	red	C_{2v}
10	35.6	105.1	199.2	benzene- d_6	orange	C_{2v}
11	-4.3	111.2	198.8	chlorobenzene- d_5	orange	C_{2v}
12	25.9	5.7	185.2	benzene- d_6	brown	C_2
13	39.6	20.1	185.7	chlorobenzene- d_5	red	C_{2v}

In the ^{29}Si NMR spectra, mild low-field shifts are observed for the 3-coordinated Si atoms of both **11** (111.2 ppm, $\Delta\delta = 6.1$ ppm) and **13** (39.6 ppm, $\Delta\delta = 13.7$ ppm). But whereas the pronounced highfield shift of the 2-coordinated Si^{NHC} atom in **11** (-4.3 ppm, $\Delta\delta = 39.9$ ppm) can be explained by the reduction of electron density due to a stronger binding of the Cu cation after bromide abstraction, the opposite is observed for the two-coordinated Si^{Tbb} atom of the disilyne complex **13** (20.1 ppm, $\Delta\delta = +14.4$ ppm).

2.6.4 Liberation of an NHC-stabilized disilyne

Addition of suitable small, neutral donor ligands to complex **12** was intended to cleave the $\text{Si} \rightarrow \text{CuBr}$ interaction, liberating an NHC-stabilized disilyne unit (*Z*)-TbbSi=Si(OtBu)(SIDipp) (**14**). In fact, addition of PMe_3 to a solution of **12** resulted in an immediate color change from brown to dark violet. The reaction is very fast and robust in respect to stoichiometry, temperature or solvent (toluene, diethyl ether, aliphatic hydrocarbons) and leads to the formation of $[\text{Cu}(\text{PMe}_3)_4]\text{Br}$ as a side product.²¹



Scheme 28. Synthesis of the NHC-stabilized (oxy)disilyne **14** by abstraction of CuBr. L = PMe_3 ($n = 4$), IMe_4 ($n = 2$) or LiPr_2Me_2 ($n = 2$).

Best abstraction results were obtained using an excess of PMe_3 (up to a ratio of 10:1, or “just one drop” of neat PMe_3 for smaller reaction scales). However, the presence of free PMe_3 considerably increased the solubility of the copper phosphane complex whereas subsequent evaporation of excess PMe_3 and/or solvent from the mixture induced a reverse reaction. Less

²¹ The formation of the known complexes $[\text{CuBr}(\text{PMe}_3)_n]$ ($n = 1, 2$) was not observed by ^1H or ^{31}P NMR spectroscopy even when working in stoichiometric ratios. These complexes are stable under fine vacuum.

volatile but sterically more demanding phosphanes or N-bases did not yield any conversion (Table 15), but the small NHCs IMe_4 and IiPr_2Me_2 were successfully used to abstract $[\text{CuBr}(\text{NHC})_2]$ from **12**. Here, IMe_4 gave less selective outcomes even at reduced temperatures, whereas IiPr_2Me_2 offered a suitable compromise of donor strength and steric protection as well as the needed lower solubility of the byproduct when compared to PMe_3 .

Table 15. Different ligands used for the abstraction of CuBr from **12**.

Reagent	Conditions	Reaction outcome (¹ H NMR)
PMe_3	Excess, various solvents, r.t.	Selective abstraction, inseparable
PMe_2Ph	Excess, benzene, Δ	Slow reaction, unclear outcome ^A
$\text{P}(\text{iPr})_3$	Excess, benzene, Δ	Very slow reaction ^A
PPh_3	1 equiv., benzene, Δ	No reaction
pyridine	Excess, benzene, Δ	Decomposes upon heating
TMEDA	Excess, benzene, Δ	No reaction
CD_2Cl_2	Excess, toluene, $-30\text{ }^\circ\text{C}$	Fast decomposition
IMe_4	2 equiv., toluene, $-30\text{ }^\circ\text{C}$	Less selective abstraction
IiPr_2Me_2	2 equiv., various solvents, r.t.	Best outcome

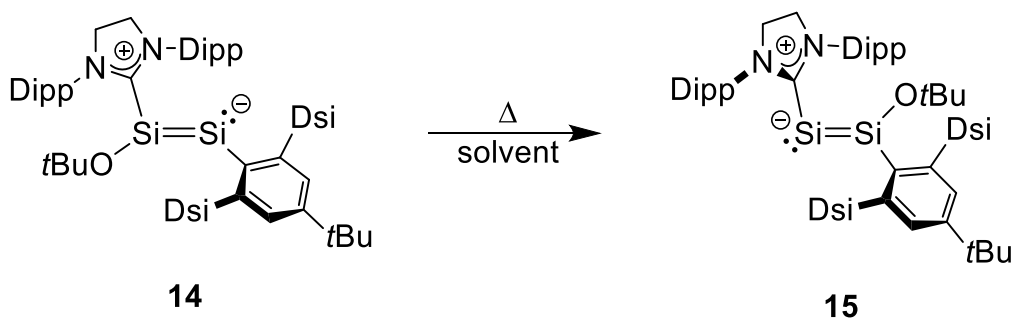
A: A color change to violet was observed after several days at ambient temperature but the reaction time was limited due to the instability of **12** in solution.

Although the reaction is very selective when using PMe_3 or IiPr_2Me_2 (>95 %), a major difficulty lied in the extreme solubility of **14** in common solvents: 200 mg of freeze-dried powder readily liquefy upon addition of 0.1 ml of aliphatic hydrocarbons, hexamethyl-disiloxane, benzene, diethyl ether or thf just to slowly decompose over the timespan of several days. Analytically pure samples of compound **14** were therefore isolated after repeated extractions with n-pentane from the $[\text{CuBr}(\text{IiPr}_2\text{Me}_2)_2]$ byproduct at $-80\text{ }^\circ\text{C}$ ²² and subsequent drying at ambient temperature in satisfactory yields of 60 – 80 %, highly depending on the purity of the starting materials. The intense dark violet solid slowly decomposes at ambient temperature but can be stored at $-30\text{ }^\circ\text{C}$ for several months.

²² $[\text{CuBr}(\text{IiPr}_2\text{Me}_2)_2]$ was synthesized independently from CuBr and 2 equiv. IiPr_2Me_2 in thf following the procedure described by Kuehn et al. for $[\text{CuCl}(\text{IiPr}_2\text{Me}_2)_2]$.^[304] Pure $[\text{CuBr}(\text{IiPr}_2\text{Me}_2)_2]$ is insoluble in aliphatic hydrocarbons, but a considerable increase in solubility was found under the reaction conditions described in the main text. This is interpreted as a sign for attractive interactions with compound **14** and **15** in solution (vide infra). Indeed, a cocrystal of isomer **15** and the related copper complex $[\text{CuBr}(\text{IiPr}_2\text{Me}_2)(\text{SIDipp})]$ was obtained later (see page 86ff).

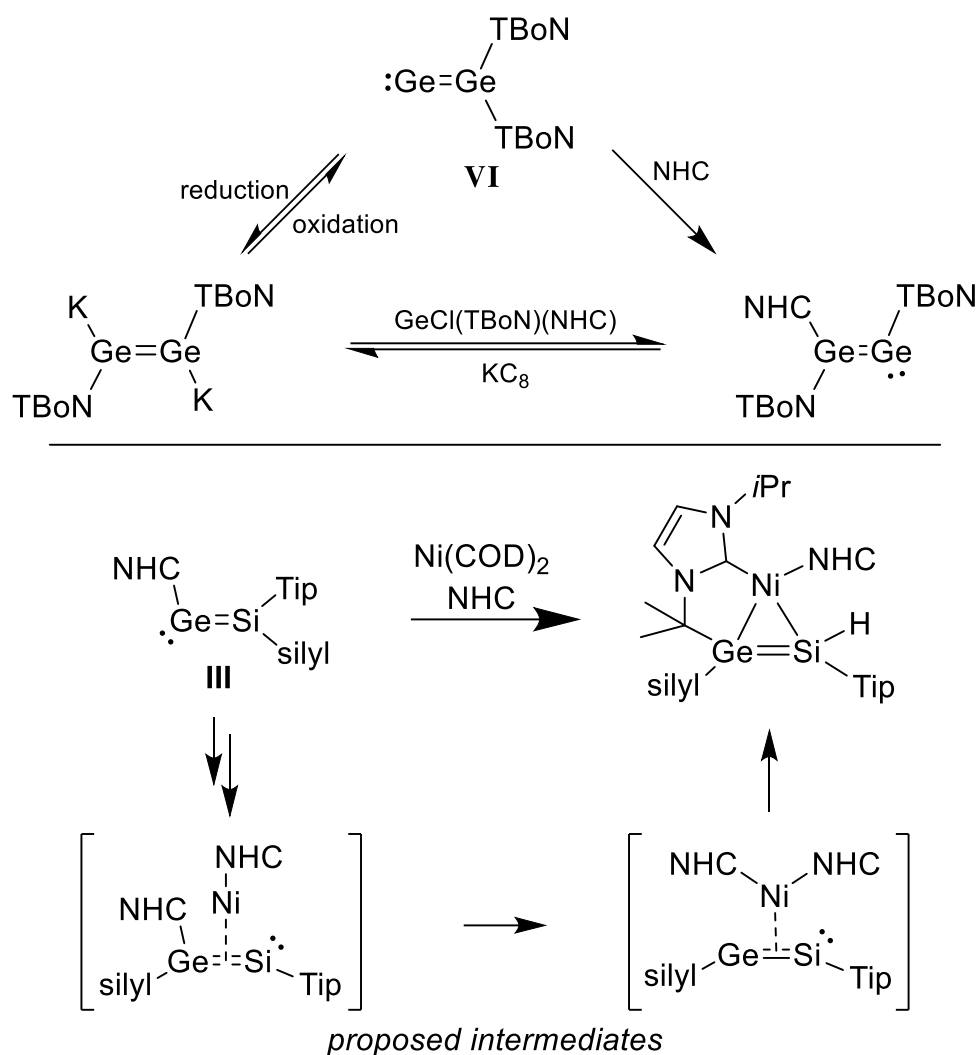
2.6.5 Disilyne-Disilavinylidene-Isomerization

Despite the instability at ambient temperature, heating a benzene- d_6 solution of **14** to 70 °C for about 3 hours circumvented the decomposition described above and instead led to a color change from dark violet to crimson red. This was caused by the unprecedented isomerization of the NHC-stabilized disilyne **14** to the NHC-stabilized disilavinylidene (Z)-Tbb(OtBu)Si=Si(SiDipp) (**15**, Scheme 29). This is the first time, an isomerization of a disilyne to a disilavinylidene or vice versa has been perceived.



Scheme 29. Unprecedented isomerization of the NHC-stabilized (oxy)disilyne **14** to the NHC-stabilized disilavinylidene **15** at elevated temperatures in solution.

As mentioned already in the introduction part, the relationship between disilynylidene and disilyne isomers has been a major interest for decades. In fact, when Wiberg and coworkers were unable to grow single crystals of their disilyne in 2002,^[45,59] theoretical calculations by Nagase predicted the respective disilavinylidene isomer to be higher in energy by 33.4 kcal/mol only because of the immense steric bulk of the employed $\text{SiMe}(\text{Si}t\text{Bu}_3)_2$ substituents.^[305] In 2016, the synthesis of Aldridges base free digermavinylidene **VI** included a 1,2-boryl shift from a trans-digermene and subsequent addition of an NHC induced a re-isomerization to a base-stabilized digermene (Scheme 30).^[161] And recently, Scheschkewitz obtained a side-on Ni(0) complex of a silagermene from his NHC-stabilized silagermenylidene **III-SiTip₂NMe₂** that is believed to form from a transient silagermyne nickel complex.^[160]



Scheme 30. Isomerizations of heavier vinylidene derivatives. Formal charges are omitted for simplicity.^[160,161]

On a synthetic scale, conversion of **14** into **15** could be conveniently achieved by simple heating of a toluene solution to 100 °C for 30 minutes. No concentration effects were observed, but the increased temperature was found to further inhibit the formation of unknown byproducts. Compound **15** could finally be isolated in 81 % yield as large, very dark red crystals after recrystallization from hot toluene or n-hexane. The analytically pure carmine-red powder decomposes upon heating at 177 °C.

To determine the reaction rate $k(T)$, the half life time $t_{1/2}(T)$, and the activation barrier ΔG^\ddagger , samples of identical concentration (9 mg/ml) were heated in toluene- d_8 and the reaction progress was diligently monitored by ^1H NMR spectroscopy at intervals of 15 minutes at temperatures of 60 and 70 °C (Figure 46). The progress was determined on basis of the integration of the signals of the $\text{C}^{3,5}\text{-H}$ and the $\text{CH}(\text{SiMe}_3)_2$ groups of the Tbb substituents and the integrations did not differ by more than 0.7 % at any time. Averaged values were used for

the determination of $k(T)$, allowing a precise tracing of the conversion (for the Arrhenius plot see Figure 118 on page 275 in the appendix).

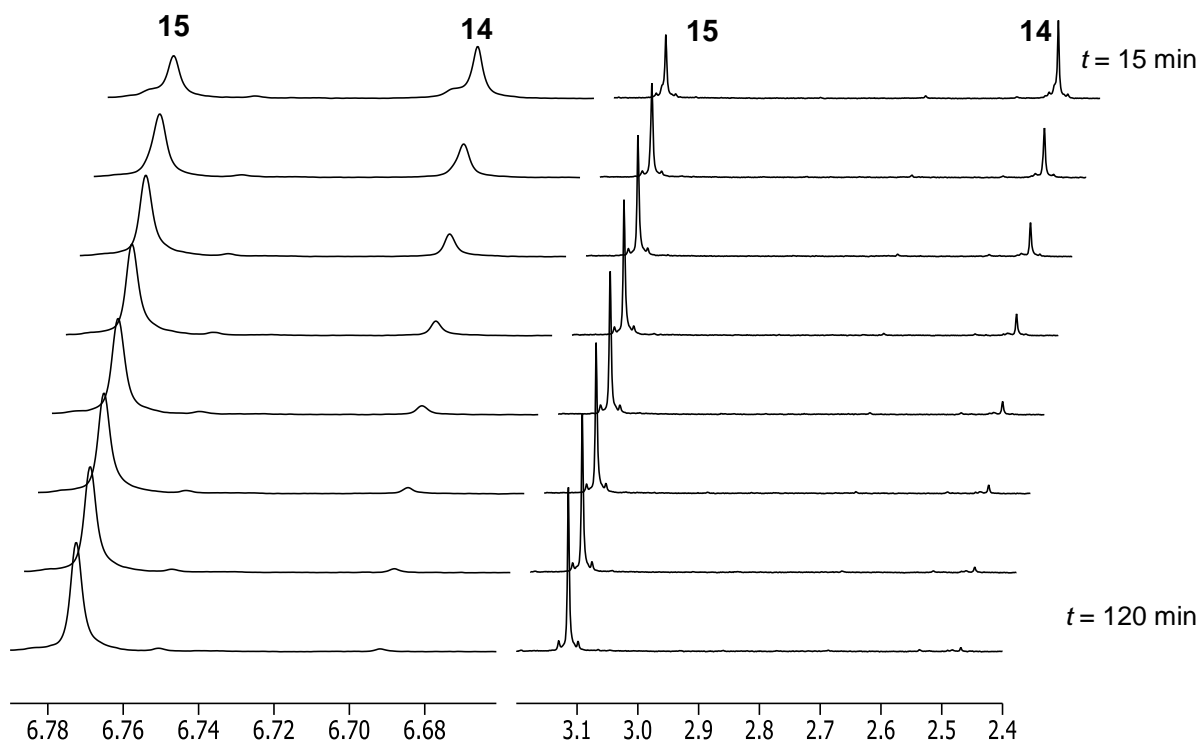


Figure 46. Conversion of **14** into **15** at $T = 60\text{ }^{\circ}\text{C}$ as observed for the signals of the $\text{C}^{3\text{s}}\text{-H}$ (left) and the $\text{CH}(\text{SiMe}_3)_2$ groups (right) of the Tbb substituent.

$$k(T) = A \times e^{-\frac{E_A}{R \times T}} / s \quad \text{Eq. 1}$$

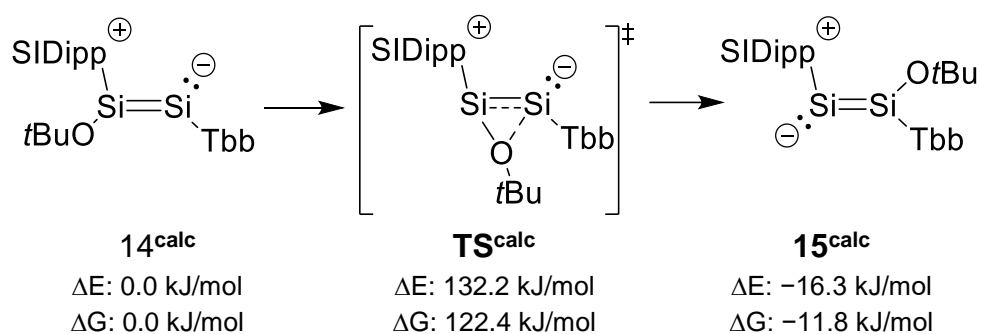
$$t_{1/2} = \frac{\ln(2)}{k} / s \quad \text{Eq. 2}$$

$$\Delta G = R \times \ln\left(\frac{k_2}{k_1}\right) \times \left(\frac{T_1 + T_2}{T_1 \times T_2}\right) / J \times \text{mol}^{-1} \quad \text{Eq. 3}$$

Using standard methods and equations Eq. 1 – Eq. 3 for a first-order reaction, half-life times $t_{1/2}$ of 66.0 min ($60\text{ }^{\circ}\text{C}$) and 20.9 min ($70\text{ }^{\circ}\text{C}$) were determined. The estimated ΔG value of 109.3 kJ/mol also validates the values predicted by theory (122 kJ/mol, B97-D3(BJ)/def2-TZVP, Scheme 31).

Table 16. Reaction rate constants $k(T)$ and half life times $t_{1/2}$ for the isomerization of **14** at $T = 60$ and 70 °C

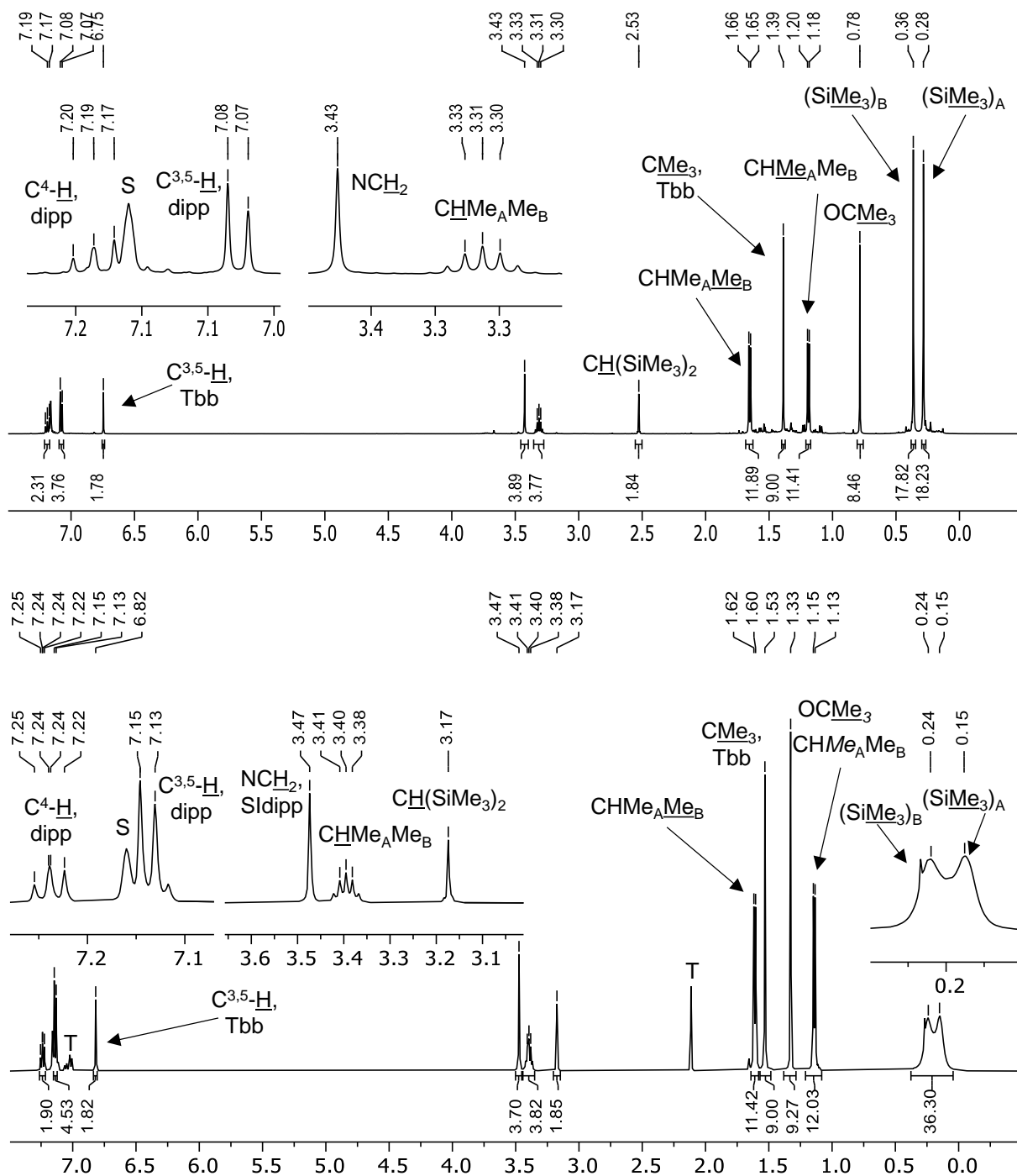
T	$k(T)$ /s ⁻¹	$t_{1/2}$ /min
60 °C	0.0105	66.0
70 °C	0.0332	20.9



Scheme 31. Calculated mechanism of the isomerization of **14** into **15** (B97-D3(BJ)/def2-TZVP).

According to DFT calculations, the reaction proceeds by migration of the OtBu group from the Si^{NHC} to the Si^{Tbb} atom via a $^2\mu\text{-O}$ transition state. This finding also vividly elucidates the conformational stability of the precursor complex **12**, where the CuBr unit “blocks” the Si=Si π -bond and therefore prevents an isomerization.

More general NMR spectroscopic studies revealed that the entire sets of ¹H and ¹³C resonances of both **14** and **15** appear within their expected regions. Local C_{2v} symmetry of the SIDipp- but only C_s symmetry of the Tbb groups was found for **14** and **15** (see Figure 47) as best illustrated by the splitting of the SiMe₃ signals in both isomers. This is presumably caused by collision with the OtBu group which hinders the rotation (in contrast, the SiMe₃ groups in the disilavinylidenes **1**, **1-CH₂Ph**, **1-CH₂SiMe₃** and **1-Me** are chemically and magnetically equivalent). The respective signals in **15** are further broadened at ambient temperature ($\nu_{1/2} = 38 \text{ Hz}$) but coalesce to a singlet signal when moderately warmed ($T_c \approx 30$ °C, $\Delta G^\ddagger = 63 \text{ kJ/mol}$ by ¹H NMR).



Remarkably, a low-field shift by about 20 ppm was observed when comparing the ^{13}C NMR resonances of the carbene atoms in the CuBr complex **12** and the NHC-stabilized disilyne **14** to the disilavinylidenes **15** and **1**. This is caused by the different oxidation states of the Si^{NHC} atom and correlates well with the calculated partial charges (Table 17). Similar trends can also be found when comparing the disilicon(0) compound $\text{Si}_2(\text{SIDipp})_2$ ($\delta_{\text{C}^{\text{NHC}}} = 217.0$ ppm)^[205] to the respective Si(I) and Si(II) oxidation products $\text{Si}_2\text{Br}_2(\text{SIDipp})_2$ (198.8 ppm)^[306] and $\text{SiBr}_2(\text{SIDipp})_2$ (188.7 ppm).^[205] These findings are not transferable to the C^{I} resonances of the Tbb substituent, where the well-defined $\text{Si}-\text{C}^{\text{Tbb}}$ single bonds don't reflect the different formal oxidation state and coordination number of the Si^{Tbb} atom. For example, the disilyne $\text{TbbSi}\equiv\text{SiTbb}$ ($\delta_{\text{C}^{\text{ipso}}} = 137.4$ ppm)^{[157], 23} features an almost identical ^{13}C NMR resonance as disilavinylidene **1** (137.9 ppm) but both are considerably shifted in respect to the disilene $\text{Tbb}(\text{Br})\text{Si}=\text{Si}(\text{Br})\text{Tbb}$ (128.3 ppm).^[48]

Table 17. Comparison of the ^{13}C NMR resonance of the ipso C atoms and the calculated charge of the corresponding Si atoms of compounds **12**, **14**, **15** and **1**.

	12	14	15	1
$\delta_{\text{C}^{\text{NHC}}}$ /ppm	185.1	189.1	205.0	204.6
NPA(Si^{NHC}) /e	0.82	0.92	-0.11	-0.02
$\delta_{\text{C}^{\text{Tbb}}}$ /ppm	135.7	146.2	141.1	137.9
NPA(Si^{Tbb}) /e	0.06	0.17	1.14	0.59

B97-D3(BJ)/def2-TZVP level of theory

In the $^{29}\text{Si}\{^1\text{H}\}$ NMR spectrum, significant shifts were observed for the unsaturated Si atoms while the less meaningful SiMe_3 signals of compounds **12** - **15** all appear in the standard region at about 2 ppm²⁴ (Figure 48).

²³ The authors provide no assignment of the ^{13}C NMR data, yet a confusion with one of the other quaternary carbon atoms ($\delta_{\text{C}} = 150.16$ and 151.35 ppm) is unlikely.

²⁴ The SiMe_3 signals of compound **15** could only be detected in a dept20 spectrum at elevated temperatures, presumably due to the same dynamic process that also caused the broadening observed in the respective ^1H and ^{13}C NMR spectra. See also Figure 47.

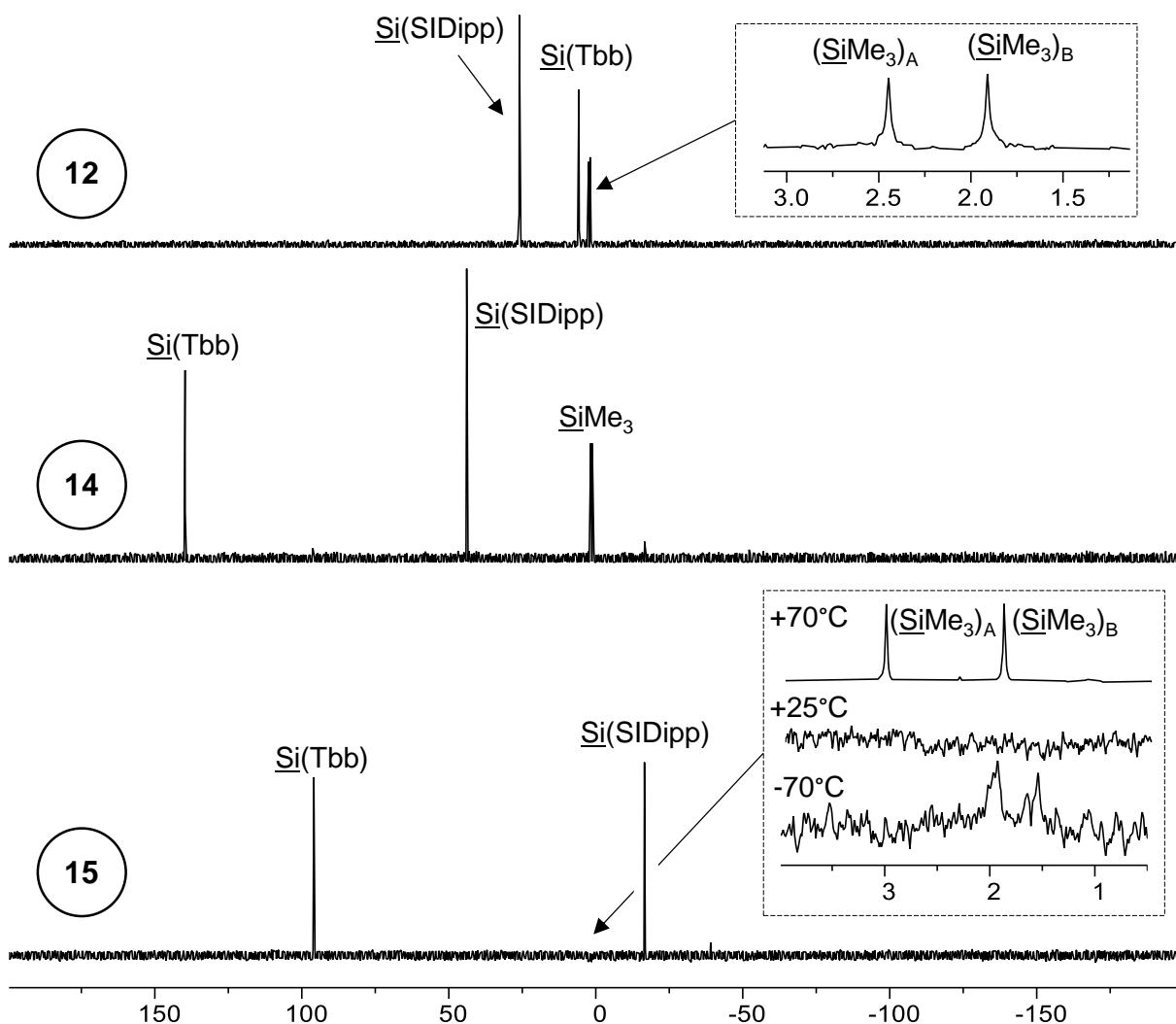


Figure 48. ^1H NMR (99.36 MHz) zgig spectra of **12** (top), **14** (middle) and **15** (bottom) in benzene- d_6 at 298 K. The insets show the enlarged TMS signals of **12** (top) as well as excerpts of dept20 spectra of **15** at temperatures of +70 °C, +25 °C and -70 °C in toluene- d_8 (bottom).

CuBr elimination from the disilyne complex **12** ($\delta_{\text{Si}^{\text{Tbb}}}$: 5.7 ppm, $\delta_{\text{Si}^{\text{NHC}}}$: 25.9 ppm), is accompanied with a low-field shift of both resonances in **14** ($\delta_{\text{Si}^{\text{Tbb}}}$: 139.2 ppm, $\delta_{\text{Si}^{\text{NHC}}}$: 43.7 ppm), which is more pronounced for the Si^{Tbb} atom with the free electron lone pair. A similar pattern with a strongly deshielded two-coordinated Si atom and a much more shielded Si^{NHC} atom was also observed for several disilyne-NHC-adducts $\text{Si}_2\text{Tbb}_2(\text{NHC})$ (NHC = IME_4 , IET_2Me_2 , IiPr_2Me_2 ; δ_{Si^2} = 200.5 – 200.2 ppm; $\delta_{\text{Si}^{\text{NHC}}}$ = 15.4 – 21.1 ppm)^[42] as well as Sekiguchi's $\text{Si}_2(\text{silyl})_2(\text{IME}_4)$ (δ_{Si^2} : 276.3 ppm; $\delta_{\text{Si}^{\text{NHC}}}$: 28.7 ppm; silyl = $\text{Si}(\text{dsi})_i\text{Pr}$),^[303] where the deshielding is further amplified by the silyl substituent.²⁵ Subsequent isomerization leads to a

²⁵ The large absolute difference in chemical shift between the disilyne-NHC-adducts discussed above ($\Delta\delta_{\text{Si}} \approx 75$ ppm) can presumably be traced back to the $\text{Si}(\text{dsi})_i\text{Pr}$ substituent. An identical difference is found when comparing the two NHC-free disilynes (R = Tbb: $\delta_{\text{Si}} = 16.2$ ppm; R = $\text{Si}(\text{dsi})_i\text{Pr}$: $\delta_{\text{Si}} = 89.9$ ppm, $\Delta\delta_{\text{Si}} = 73.7$ ppm).^[42,62,303]

distinct high-field shift of both resonances. The Si^{Tbb} signal is now found at $\delta_{\text{Si}} = 95.9$ ppm, which is within the range of the signals of the other disilavinylidene derivatives **1** (86.0 ppm), **1-CH₂Ph** (123.7 ppm) and **1-Me** (127.9 ppm). In contrast, the Si^{NHC} atom ($\delta_{\text{Si}} = -16.6$ ppm) is considerably more shielded than the derivatives **1** (34.6 ppm), **1-CH₂Ph** (65.6 ppm), **1-Me** (50.4 ppm) or Iwamotos **II** (65.0 ppm).^[164]

Table 18. Calculated ²⁹Si NMR shielding tensors (δ_{ii}), span of the chemical shielding tensors ($\Delta\delta$), anisotropy of the chemical shift (CSA) and the calculated and experimental isotropic chemical resonances (δ_{iso}) of **12** – **15**.

Cpd.	nucleus	δ_{11}	δ_{22}	δ_{33}	$\Delta\delta^A$	CSA ^B	δ_{iso}^C	$\delta_{\text{iso}}(\text{exp})^D$
12	Si1 ^{Tbb}	179	77	-92	272	194	55	5.7
	Si2 ^{NHC}	234	-3	-120	355	357	37	25.9
14	Si1 ^{Tbb}	329	172	-38	367	195	154	139.2
	Si2 ^{NHC}	178	10	-81	259	249	36	43.7
15	Si1 ^{Tbb}	302	27	-18	320	293	103	95.9
	Si2 ^{NHC}	89	-10	-51	140	150	9	-16.6
1	Si1 ^{Tbb}	358	81	-15	374	292	141	86.0
	Si2 ^{NHC}	312	-4	-98	410	414	70	34.6

All values are given in ppm. **A:** $\Delta\delta = \delta_{11} - \delta_{33}$; **B:** $\text{CSA} = \delta_{11} - (\delta_{22} + \delta_{33})$; **C:** $\delta_{\text{iso}} = (\delta_{11} + \delta_{22} + \delta_{33})/3$; **D:** measured in benzene-d₆.

Table 19. Structural and spectroscopic data of known disilynes. Calculated data are given in parentheses.

Substituents	Si-Si /Å	R-Si-Si /°	δ_{Si} /ppm	Color	Ref.
SiMe(SitBu ₃) ₂	[2.072] ^A	[148] ^A	91.5	yellow	[45]
Si(iPr)(dsi) ₂	2.0622(9)	137.44(4)	89.9	green	[62]
Bbt	2.108(5)	133.0(3)	18.7	orange	[46]
Si(iPr)(dsi) ₂ ,	2.057(1)	138.78(5),	62.6,	green	[156]
SiCH ₂ tBu(dsi) ₂		137.89(5)	106.3		
CCH ₂ tBu(SiMe ₃) ₂	2.086(1)	132.05(7)	31.8	green	[63]
Tbb	2.105(2)	131.42(9)	16.2	yellow	[157]

A: calculated on the B3LYP/3-21G* level of theory.^[305]

High-quality single crystals of **14** suitable for structural analysis could be obtained after dissolving 150 mg in 0.2 ml of diethyl ether, dropwise addition of about 0.1 ml of acetonitrile (incipient precipitation), dilution with a very small amount of diethyl ether followed by filtration and subsequent gas-phase diffusion of acetonitrile into that solution at -30 °C. For this procedure, precooled solvents, vessels and syringes had to be used inside a glove box to prevent decomposition that is caused by acetonitrile at ambient temperature. In contrast, crystals of the disilavinylidene-isomer **15** were readily obtained from n-hexane, diethyl ether or toluene at varied temperatures (see Figure 49 and Table 20). Noteworthy, medium-quality cocrystals of

15 and the mixed copper NHC complex [CuBr(iPr₂Me₂)(SIDipp)] were also obtained from n-hexane at -30 °C during the experiments.²⁶

Table 20. Selected structural data of **12** – **15** and **1**.

	Si-Si /Å	Si-O /Å	Si1-Si2-C ^{NHC} /°	Si2-Si1-C ^{Tbb} /°	C ^{Tbb} -Si-Si-C ^{NHC} /°	∠(NHC) ^A /°
12	2.217(3)	1.631(6)	113.5(2)	115.6(3)	-179.4(4)	29.4(3)
14	2.2243(7)	1.651(2)	115.68(8)	109.40(7)	178.35(9)	3.82(8)
15^B	2.1997(7)	1.662(1)	106.90(6)	119.45(6)	166.4(1)	71.92(6)
1 ^[134]	2.167(2)	-	97.6(1)	123.4(1)	177.3(2)	87.4(1)

A: angle between the best plane of the central ring of the SIDipp and the plane described by the {Si1,Si2,C^{NHC},C^{Tbb},O} core moiety.

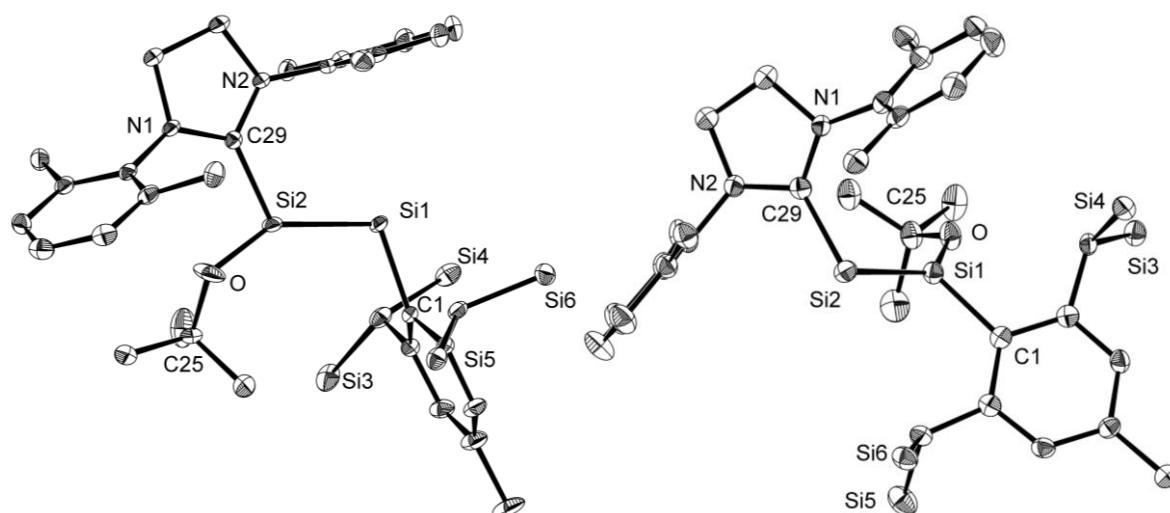


Figure 49. Molecular structures of **14**-C-H_s (left, 50 % probability) and **15** (right, 50 % probability). Methyl groups as well as hydrogen atoms are omitted for simplicity. Selected bond lengths (Å) and angles (°): **14**: Si1-Si2 2.2243(7), Si1-C1 1.940(2), Si2-O 1.651(2), Si2-C29 1.891(2), O-C52 1.435(2); Si2-Si1-C1 109.40(7), Si1-Si2-C29 115.68(8), Si1-Si2-O 143.91(5), C29-Si2-O 100.31(9), Si2-O-C25 128.3(2); C29-Si2-Si1-C1 1.65(9), C1-Si1-Si2-O 3.1(2), Si1-Si2-O-C25 -39.1(1). **15**: Si1-Si2 2.1997(7), Si1-C1 1.908(2), Si2-C25 1.930(2), Si1-O 1.662(1), O-C52 1.452(2); C1-Si1-Si2 119.45(6), C1-Si1-O 107.01(7), Si2-Si1-O 132.66(5), C29-Si2-Si1 106.90(6), Si1-O-C52 128.4(1); C1-Si1-Si2-C29 166.4(1), C1-Si1-O-C25 116.9(1).

The molecular structures of compound **14** and **15** are shaped by the inner coordination spheres of their Si=Si units. While both show the typical antiplanar orientation of Tbb and SIDipp, the difference is found in the position of the OtBu group at the Si2 atom (in **14**) or the Si1 atom (in **15**). In both structures, the O-bonded Si atom is trigonal planar (**14**: Σ_{Si2} : 359.90(8)^o

²⁶ The [CuBr(iPr₂Me₂)(SIDipp)] presumably originates from some residual [Cu(iPr₂Me₂)₂Br] that was not properly separated during the preceding work-up procedure and therefore present during the thermal isomerization of **14** to **15**. For a comparison reasons, [Cu(iPr₂Me₂)(SIDipp)]Br (found as a separated complex salt) was also isolated. See chapter 4.6.39 on page 246 for experimental data and Figure 96 on page 264 in the appendix for a structural comparison with [CuBr(iPr₂Me₂)(SIDipp)].

and **15**: 360.0(4)^o) whereas the di-coordinate Si1 atom exhibits a stereoactive electron lone pair with moderate Si-Si-C angles (**14**: 109.40(7)^o, **15**: 111.0(6)^o). The Si=Si double bond in **14** (2.2243(7) Å) compares well to the disilyne-NHC-adduct Si₂Tbb₂(iPr₂Me₂) (2.214(3) Å)^[42] and is only marginally shorter than the one found in the CuBr complex **12** (2.217(3) Å), again demonstrating how little the presence of CuBr affects the sterics. On the other hand, the Si=Si bond in **15** (2.1997(7) Å) is a little longer than the respective bonds in the disilavinylidenes **1** (2.167(2) Å), 1-Me (2.171(1) Å) or **II** (2.1787(7) Å) but almost identical to that in **1-CH₂Ph** (2.190(2) Å). Interestingly, the imidazolium ring of the NHC in the disilyne isomer **14** is almost in plane with the central moiety (∠3.82(8)^o), whereas the disilavinylidene isomer **15** (∠77.5(5)^o) approaches the perpendicular orientation that was found in the disilavinylidenes **1**, 1-Me and **II** or the related Si₂(IDipp)₂ and (IDipp)Si=PMes*.^[106,124,164] A coplanar alignment of the SiR-bonded NHCs similar to **14** was meanwhile found in the cationic [Si₂R(IDipp)₂][BAR^F₄] (R = H, Me²⁷),^[307] and potentially enables a stronger delocalization of electron density throughout the {C,Si,Si} unit. This matches the more pronounced high field shift of the corresponding ¹³C NMR resonances in respect to the free NHCs (Table 21) but only a marginal contraction is found for the Si-C^{NHC} bond distance (**14**: 1.891(2) Å, **1**: 1.937(4) Å). Altogether, no strong effect is expected since free rotation around the respective Si-C bonds was observed by NMR spectroscopy at ambient temperature. And indeed, rotation barriers of 27 kJ/mol (∠NHC: 63^o) for compound **14** and 46 kJ/mol (∠NHC: 37^o) for compound **15** were obtained by DFT calculations (see Figure 119 on page 281 in the appendix).

Table 21. High field shifts of the ¹³C NMR NCN carbene signals of **14** and related compounds.

Compound	δ _c / ppm	Compound	δ _c / ppm
SIDipp	244.0	IDipp	220.6
1	204.6 (Δδ: 39.4)	Si ₂ (IDipp) ₂	196.3 (Δ: 24.3)
14	189.1 (Δδ: 54.9)	[Si ₂ Me(IDipp) ₂][BAR ^F ₄]	162.9 (Δδ: 57.7)

Note that the disilicon(I) compound Si₂(Br₂(IDipp)₂) (177.1 ppm; Δδ: 43.5 ppm) resonates at a lower field and has significantly pyramidalized Si atoms (Σ_{Si} ≈ 303^o).^[106,111,176,286]

²⁷ The value of the ethyl-substituted [Si₂Et(IDipp)₂][BAR^F₄] lies in between (∠51.91(8)^o).

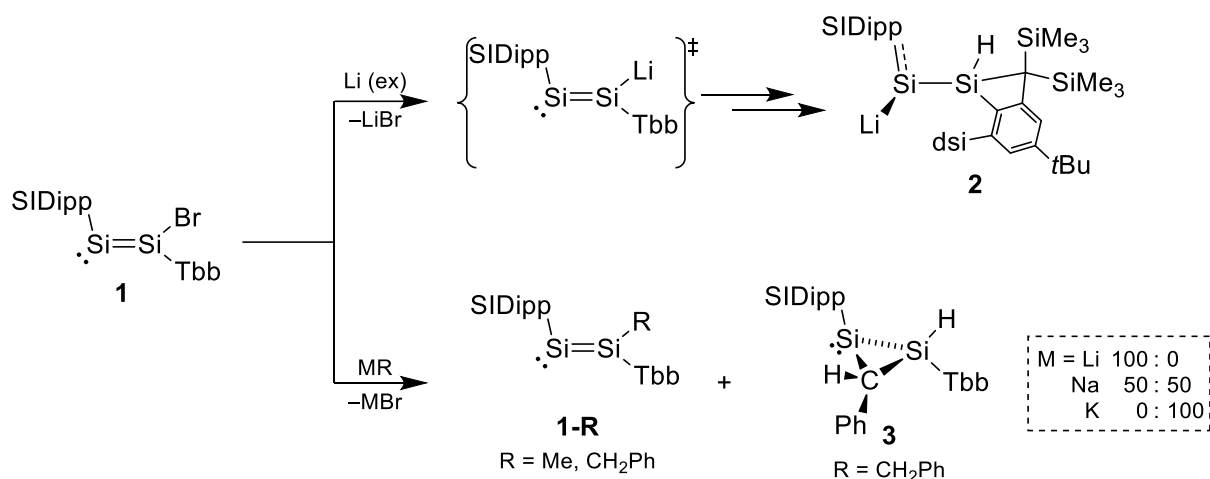
2.7 Summary & Outlook: Disilavinylidene Chemistry

2.7.1 Summary

Vinylidenes (:C=CR_2) are a transient subclass of carbenes and readily isomerize to the respective alkynes ($\text{R-C}\equiv\text{C-R}$). No isolable vinylidene is known in the literature, but their instability is utilized in the Fritsch-Buttenberg-Wiechell rearrangement^[136–139] which, in turn, is a key step in the Corey-Fuchs-reaction^[140] and the Seyferth–Gilbert homologation.^[141] Stabilization of vinylidenes by metal coordination has been established in the literature and the corresponding $[\text{L}_n\text{M=C=CR}_2]$ complexes containing an electrophilic α -carbon and nucleophilic β -carbon atom have some synthetic importance.^[142–145]

Within the last decade, several examples of heavier vinylidene analogues have been prepared by the groups of Scheschkewitz, Aldridge, Filippou, Wesemann and Iwamoto, which in most cases are supported by Lewis bases: silagermenylidenes ((base)Ge=SiR_2), a digermavinylidene Ge=GeR_2 , a gerasilenyliidene ($\text{(phosphane)Si=GeR}_2$) and two examples of disilavinylidenes (NHC)Si=SiR_2 .^[134,158–163,308] But despite the many-sided synthetic effort, relatively little is known about the reactivity of this class of compounds. Therefore, the objective of this work was to explore the synthetic potential of the first NHC-stabilized disilavinylidene, $\text{(SIDipp)Si=Si(Br)Tbb}$ (**1**), that was isolated by Dr. P. Ghana from the Filippou group in 2015.^[134,309] This compound can be seen as a hybrid of a 1,2-dibromodisilene and Robinsons NHC-stabilized disilicon(0) compound and is therefore expected to be a versatile, ambiphilic building block.^[46–48,106]

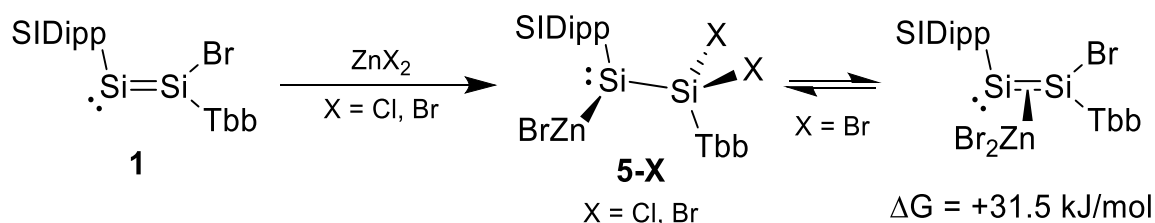
Attempts to metallate the Si-Br bond of **1** using lithium powder instead led to the respective C-H activation product (**2**, Scheme 32) already at low temperatures. Compound **2** is a very rare example of a metallasilylene and was characterized spectroscopically as well as by XRD, revealing some characteristics of a silenide with considerable silicon carbon double bond character towards the NHC. Reaction of **1** with tBuLi in cold toluene surprisingly led to the substitution product $\text{(SIDipp)Si=Si(CH}_2\text{Ph)Tbb}$ (**1-CH₂Ph**) instead of the anticipated lithiation product after incorporation of a benzyl group from the solvent. Compound **1-CH₂Ph** was fully characterized and has displayed similar properties and reactivity as the starting material although XRD and Raman spectroscopy suggest a weaker Si=Si double bond (Table 22 on page 99). This is explained by theory: substitution with a more electropositive group increases the s-electron density in that bond which inevitably both weakens the Si-Si σ -bond and reduces the occupancy of the π -bond.



Scheme 32. Reactivity of **1** towards lithium and alkyl(alkali) reagents. The outcome of the reaction with MCH_2Ph strongly depends on the employed alkali metal. The LiCH_2Ph needed for the synthesis of **1-CH₂Ph** was originally formed in situ from $t\text{BuLi}$ and toluene.^[309] Formal charges are omitted for simplicity.

The formation of **1-CH₂Ph** was proven to advance via deprotonation of toluene to LiCH_2Ph rather than initial lithiation of **1** and subsequent reaction with toluene. And while addition of methyl lithium in thf smoothly yielded the respective substitution product **1-Me**, changing the alkali metal instead had an influence on the reaction's chemoselectivity: When KCH_2Ph was used, an NHC-stabilized disilacyclopropylidene (**3**), which is the formal C-H activation product of **1-CH₂Ph**, was isolated instead and NaCH_2Ph gave a 50:50 mixture of the constitutional isomers. The reaction mechanism was researched by DFT calculations and is believed to proceed via an initial 1,2-addition of MCH_2Ph to the $\text{Si}=\text{Si}$ double bond followed by either salt elimination to form **1-CH₂Ph** or a cascade of rearrangements to compound **3**.

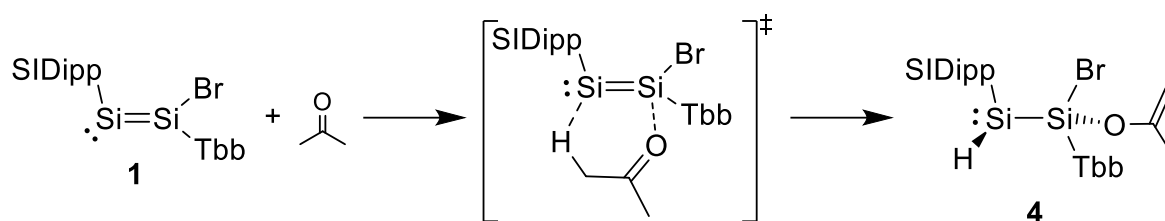
The formation of such unprecedented NHC-stabilized metalla(silyl)silylene intermediates $\text{MSi}\{\text{SiBr(R)Tbb}\}(\text{SIDipp})$ is further supported by the reaction of **1** or **1-CH₂Ph** with zinc halides and the full characterization of the first known zinco silylenes **5** and **6**. While XRD showed the structure depicted in Scheme 33, a combination of ^1H NMR spectroscopy at varied temperatures and DFT calculations revealed a dynamic equilibrium with the respective $\eta^2\text{-ZnBr}_2$ complexes in solution where **1** coordinates to the metal center via the $\text{Si}=\text{Si}$ π -bond rather than the free electron lone pair.



Scheme 33. Reaction of **1** with zinc halides. Formal charges are omitted for simplicity.

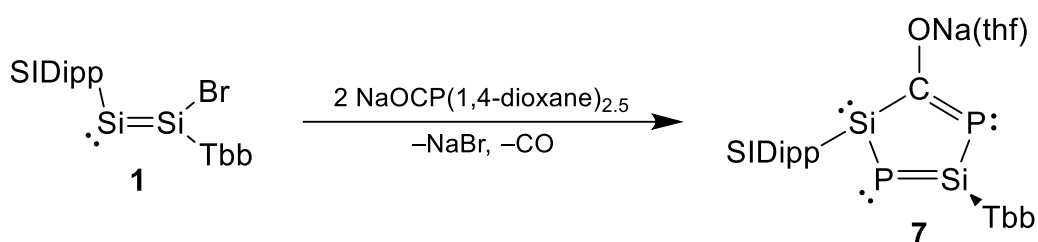
A different addition mechanism was identified for the reaction with acetone in refluxing *n*-hexane which gave the hydridosilylene $\text{SiH}[\text{SiBr}\{\text{OC}(\text{CH}_3)_2\text{Me}\}\text{Tbb}](\text{SIDipp})$ (**4**).

The reaction was initially believed to proceed via protonation by the enolic form (Scheme 34)^[135] and the same assumption exists in the literature for the reaction of disilenes with enolizable ketones.^[27] This hypothesis was disproven by a combination of experiments and DFT calculations, that instead suggest a coordination of the oxygen atom to the electrophilic Si(II) center followed by direct C-H activation and a subsequent thermal rearrangement to the more stable product of a formal anti addition. Interestingly, the last step was computed to traverse a transition state with a planarized three-coordinate silicon atom. Similar reaction mechanisms for the activation of acetone by a trisilaallene, a iminoborane and an NHC-stabilized diboryne have already been proposed by the groups of Kira and Braunschweig, respectively.^[234,235]



Scheme 34. Reaction of **1** with acetone via direct C-H activation. Formal charges are omitted for simplicity.

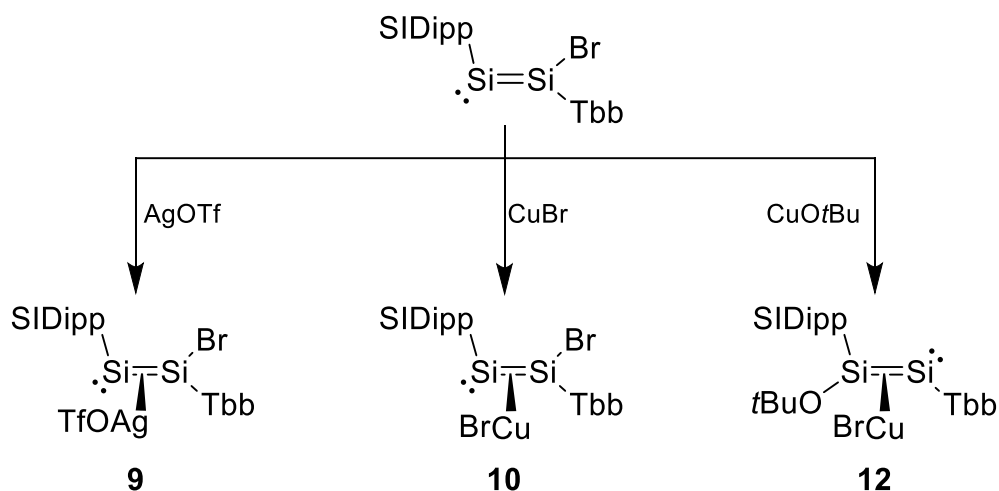
In contrast, a very slow reaction of **1** with the 2-phosphaethynolate anion ($\text{P}\equiv\text{C}-\text{O}^-$)^[244-247] cleaved the Si=Si bond. After formal incorporation of one NaOCP unit and the transfer of another P atom, the resulting 5-membered aromatic ring system **7** could be isolated and fully characterized. Based on XRD, spectroscopic data and DFT calculations, compound **7** is best described as a hybrid of an NHC-stabilized P-heterocyclic silylene with an unusually strong $\text{Si}\rightarrow\text{C}^{\text{NHC}}$ backbonding and a diphospha(disila)pentadiene with extensive electronic delocalization.



Scheme 35. Synthesis of compound **7** by an unknown mechanism. Formal charges are omitted for simplicity.

An unselective and incomplete bromide abstraction reaction using $\text{Ag}[\text{BARF}_4]$ leading to a mixed Ag^+/AgBr complex was investigated by Ghana as part of his pioneering studies as early as 2015.^[174] Now, the selective formations of light sensitive AgOTf and CuBr complexes **9** and **10** are reported (Scheme 36). Here, the molecular structures by XRD show coordination to the $\text{Si}=\text{Si}$ double bond, but clear spectroscopic evidence for an η^1/η^2 equilibrium in solution,

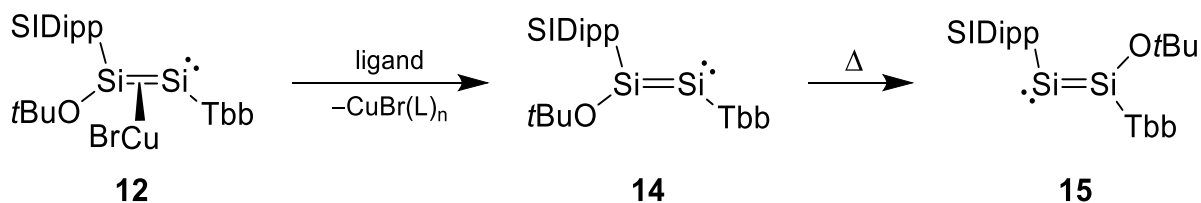
synonymous to a coordination via the free electron lone pair, was found. Unfortunately, the process could not be investigated in detail because no low temperature limits could be reached.



Scheme 36. Reaction of **1** with coinage metal salts. Formal charges are omitted for simplicity.

Interestingly, the addition of CuOtBu instead leads to a different product: cleavage of the Si-Br bond and addition of the alkoxy group to the Si(0) atom results in the formation of an unprecedented NHC-stabilized oxy-disilyne in the coordination sphere of the copper atom, which is once again bound to the Si=Si π -bond (**12**). Bromide abstraction from complexes **10** and **12** using Na[BAr⁺₄] gave the corresponding cations **11** and **13** that could only be characterized spectroscopically because of their poor crystallizability.

Focusing on complex **12**, addition of donor ligands such as PMe₃ or small NHCs allowed the liberation of (SIDipp)(tBuO)Si=SiTbb (**14**), a very rare example of an NHC-stabilized disilyne (Scheme 37). Although only metastable, compound **14** was isolated and fully characterized. Subsequent heating of a dark violet toluene solution resulted in a rearrangement to the disilavinylidene isomer (SIDipp)Si=Si(OtBu)Tbb (**15**) via 1,2-alkoxy shift. This is the first time that a disilyne/disilavinylidene isomerization was observed and the considerable energy barrier was determined by NMR spectroscopy ($\Delta G = 109.3$ kJ/mol).



Scheme 37. Liberation of a metastable NHC-stabilized oxy-disilyne **14** and its subsequent thermal isomerization to the disilavinylidene derivative **15**. Formal charges are omitted for simplicity.

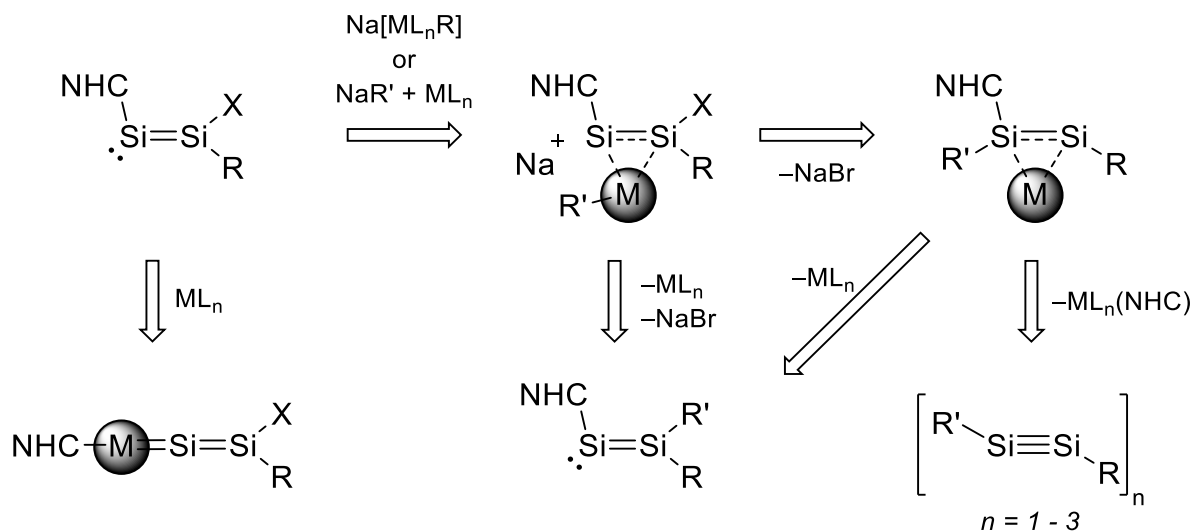
Table 22. Selected structural and spectroscopic parameters of substituted NHC-stabilized disilavinylidenes.

	1-Me	1-CH₂Ph	1-OtBu (15)	1-Br	II
d(Si=Si) / Å	2.171(1)	2.190(2)	2.175(5)	2.167(2)	2.1787(7)
d(Si1-R ^A) / Å	1.888(3)	1.924(4)	1.634(9)	2.286(1)	1.945(2) ^c
d(Si2-C ^{NHC}) / Å	1.932(3)	1.942(4)	1.92(1)	1.937(4)	1.962(2)
R-Si1-C1 / °	109.0(1)	108.6(2)	107.1(6)	109.5(1)	96.66(9)
C ^{NHC} -Si2-Si1-R / °	0.0(1)	-3.1(3)	168.9(5)	-4.0(2)	0.1(1) ^c
∠ _{NHC} B	90.0(0)	57.1(1)	77.5(5)	94.8(1)	90.45(8)
δ(SiNHC) / ppm	50.4	65.5	-16.6	34.6	65.0
δ(SiR) / ppm	127.9	123.7	95.9	86.0	160.8
color	dark red	dark red	dark red	dark red	yellow
λ _{max} / nm	521	524	n.a.	515	418
Reference	This work	This work	This work	[134]	[164]

A: R = Me, OtBu, Br, CH₂Ph or [C_{Ar}:CH₂]₂, respectively. Ar = 3,5-tBu₂-4-OMe-C₆H₃. **B:** angle between the central plane of the NHC and the {Si, Si, C^{NHC}} plane. **C:** The (Z)-oriented carbon atom was used.

2.7.2 Outlook

The isomerization behavior of **1** in the coordination sphere of copper is utterly exciting. Inverse to the aforementioned Fritsch-Buttenberg-Wiechell rearrangement,^[136-139] the concept could be utilized for the synthesis of different disilavinylidene- and disilyne derivatives {Si₂RR'} or their oligomerization products depending on the steric and electronic properties of R'. Coordination of the Si=Si bond towards the soft Cu atom was shown to encourage bromide substitution (no reaction occurred with alkali metal salts), making complexes **10** and **12** interesting synthons.



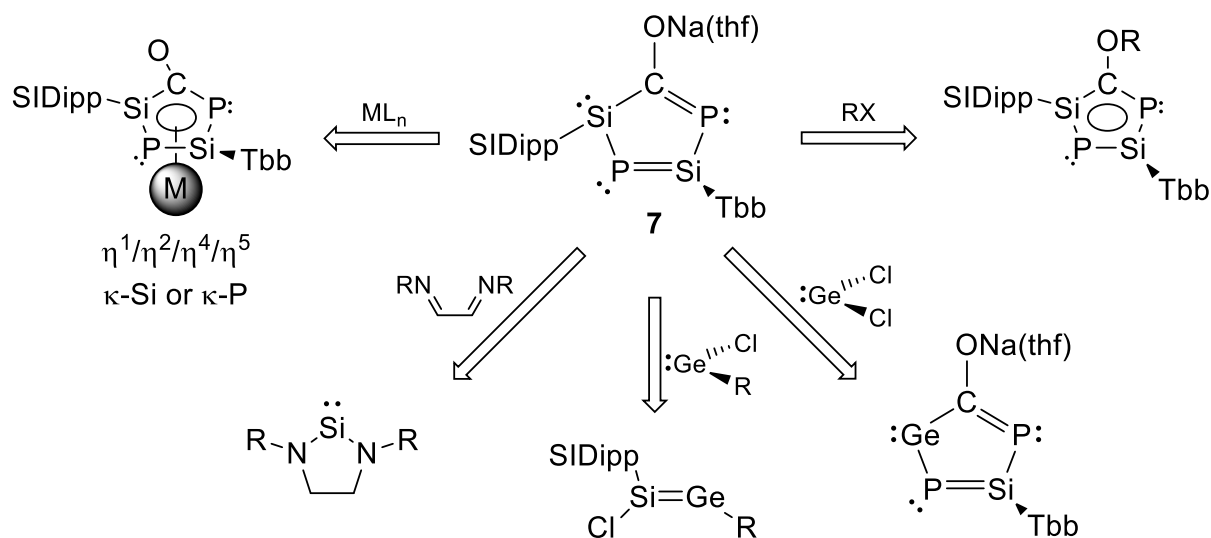
Scheme 38. Potential synthetic strategies to obtain disilavinylidene complexes, substituted disilavinylidenes or disilynes. M = late transition metal, R' = electronegative, medium-sized or large substituent. Formal charges are omitted for simplicity.

The possibility to also transfer the NHC to a suitable metal complex would allow for an elegant reaction cascade (Scheme 38). Three requirements have to be met:

1. Reasonable acceptor capabilities by a soft, electron rich metal center
2. Availability for a transfer of R' (oxy-, amino- or aryl-based)
3. Formation of a strong metal-NHC bond

The group 10 metals Ni, Pd and Pt seem to be a logical choice. Especially palladium is omnipresent in modern organometallic- and catalysis chemistry after taking its leading position from copper within the last decades: both metals are often used interchangeably or even hand in hand in the famous Sonogashira coupling.^{[310-312], [313]} Additionally, all group 10 metals form strong M-NHC bonds, whose energies mostly depend on the oxidation state and the ligand in trans position to the NHC.^[314] In fact, a test reaction between **1** and Ni(CO)₄ gave Ni(CO)₃(SIDipp) based on IR spectroscopy. Although no Si-containing products could be identified from the mixture, the abstraction of the carbene by such a simple metal complex is already promising. The synthesis of end-on bonded disilavinylidene complexes is another

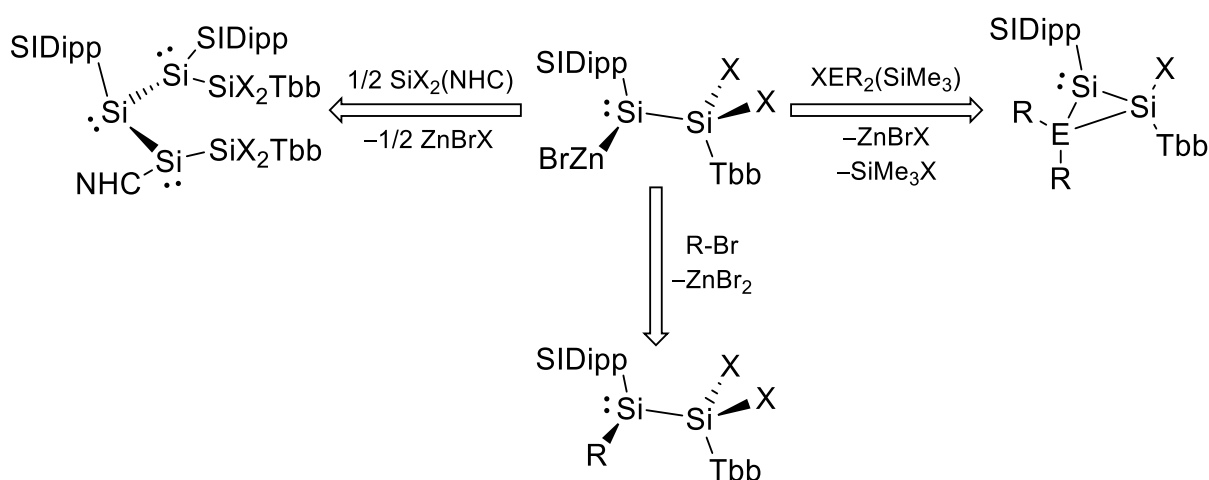
worthwhile target. This could possibly be achieved either by insertion of a metal complex into the Si-NHC bond or by NHC abstraction and subsequent trapping of the $\{\text{Si}=\text{SiR}_2\}$ unit with an electron deficient metal complex. To reduce the risk of redox side reactions, the substituted derivatives **1-CH₂Ph** and **1-Me** could be valuable starting materials in this case.



Scheme 39. Possible reactivity studies

Despite considerable efforts, the synthesis of **7** only gave low (but reproducible) yields and due to the scarcity, no follow-up chemistry of this multifaceted compound could be studied yet (Scheme 39). Potential modifications to the synthesis procedure also include the use of NaSCP^[315] or NaOCAs instead of NaOCP as well as the use of different alkali metals in the future.^[316] Compound **7** has several reactive sites: it may serve as a heavily substituted cyclopentadiene derivative in sandwich complexes with potentially flexible coordination modes between η^5 and η^1 or a coordination towards metals via the one of the electron lone pairs at the Si^{NHC} or one either P atom. As an NHC-stabilized P-heterocyclic silylene it is reminiscent of the di(phosphino)silylene $\text{Si}\{\text{P}(\text{Ar})\text{NCH}\}_2$ (Ar = Mes*, Eind) that was recently reported by Dr. M. Bogner.^[133] Especially reactions with electrophilic Ge(II) compounds have exciting potential: Bogner reported on a Si/Ge exchange reaction with $\text{GeCl}_2 \cdot \text{dioxane}$ with the “loss” of $\{\text{SiCl}_2\}$ in his case. Meanwhile, Filippous Si(0)-Isocyanide compound $(\text{SIDipp})\text{Si}=\text{C}=\text{NAr}^{\text{Mes}}$ and Wesemanns phosphano-stabilized germasilylenylidene $\text{cyclo}-(\text{R}_3\text{P})\text{Si}=\text{GeR}_2$ were effectively used for the transfer of a Si(NHC) unit or atomic Si in 2021.^[132,163] And, of course, the sodium salt **7** can presumably undergo nucleophilic substitutions. Concerning this matter, the addition of a small excess Me_3SiCl to an NMR sample was already found to result in a color change to blue but no product could be isolated from the mixture.

Finally, the formation of metallasilylenes **2**, **5** and **6** enabled access to a novel class of compounds. Whereas compound **2** can be seen as a lithium silenide, the isolation of acyclic metallasilylenes closes a synthetic gap between silanides (MSiR_3) and disilenides ($\text{R}_2\text{Si}=\text{Si}(\text{M})\text{R}$).^[34–38] Therefore, the use of NHC-stabilized zinco(silyl)silylenes as nucleophilic silylene transfer reagents in analogy to organometallic alkyl(zinc)- or Grignard reagents should be researched in the future (Scheme 40). Especially interesting coupling products could thereby emerge from silicon-based substrates such as halosilylenes or TMS-substituted halosilanes $\text{XSiR}_2(\text{SiMe}_3)$ that would allow for a subsequent elimination of SiMe_3Br . Potential improvements of the synthetic access include the use of labile ligands at the Zn centers to increase the solubility as well as the exchange of the Br atoms to reduce the overall sensibility of the metallasilylenes.

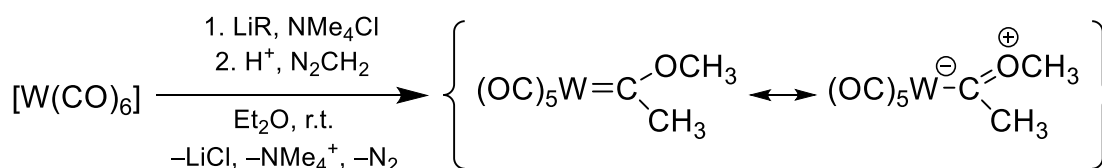


Scheme 40. Potential use of NHC-stabilized zinco(silyl)silylenes as silylene transfer reagents.

3 Part II: Oxysilylenes

3.1 Introduction

Transition metal (oxy)carbene complexes $[L_nM=C(OR)R']$ are the oldest known carbene complexes, dating back to the pioneering work of Fischer in the 1960s (Scheme 41).^[317] They are traditionally obtained upon addition of alkyl lithium to metal carbonyl complexes and subsequent alkylation of the resulting acyl metallate $Li[L_{n-1}M-C(O)R]$ using Meerwein salts ($[R_3O][BF_4]$) or diazomethanes.^[318]



Scheme 41. The first unambiguously identified carbene complexes featuring alkyl(oxy)carbenes.^[317]

These “Fischer carbenes” (where the OR moiety may be replaced by another electron withdrawing group) feature formal electronic singlet ground states and act as strong donors with electrophilic carbon centers.^[68,319] Fischer carbene complexes have been employed in a variety of C-C coupling reactions, most famously in the Dötz-reaction.^[68,319–321] Albeit no free oxy-carbenes are involved here, rare examples of stable amino(oxy)carbenes have been reported by the groups of Alder and Bertrand between 1998 and 2004 (Figure 50).^[322]

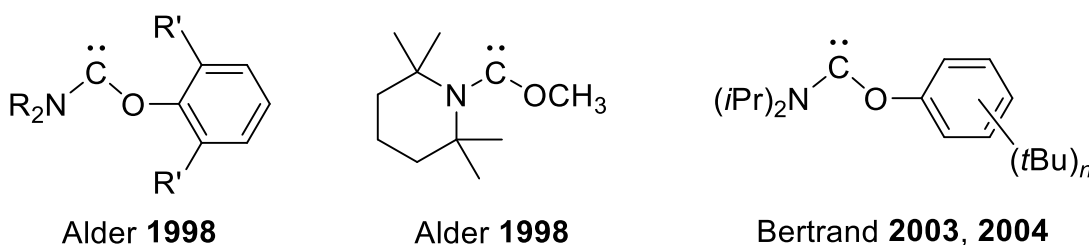


Figure 50. Known stable amino(oxy)carbenes; R/R' = Me/iPr, Me/tBu or iPr/tBu; n = 1 or 3.^[323–325]

Di(alkoxy)carbenes $C(OR)_2$ are transient species that readily rearrange to esters. The parent $C(OMe)_2$ can be generated by e.g. pyrolysis of norbornadiene precursors and has been studied after isolation in an argon matrix at 10 K since the 1960s.^[326,327] In contrast to Fischer carbenes, free di(alkoxy)carbenes react as strong nucleophiles because the +M-effects of the oxygens electron lone pairs suppresses the typical electrophilicity akin to the internal stabilization of NHCs.^[319]

3.1.1 Heavier di(oxy)tetrylenes E(OR)₂

Stable di(oxy)tetrylenes E(OR)₂ (E = Ge, Sn, Pb) have been introduced by Lappert and Atwood in 1980.^[328] In comparison to the development of di(amino)tetrylenes as versatile starting materials, the O-substituted congeners have drawn less attention. Mixed (oxy)tetrylenes with halo- or amino substituents are known and until today, di(oxy)tetrylenes are usually obtained by alcoholysis of E{N(SiMe₃)₂} or salt elimination from the tetryl(II)halides and alkali alkoxides.^[329,330] Dimerization of less crowded examples such as [Ge(OtBu)₂]₂ via μ²-bridging oxygen atoms is commonly observed (Figure 51),^[331,332] whereas chelating ligands can enforce more complicated clusters including octahedral geometries around the tetrel atoms.^[333,334] This renders the differentiation between “true” di(oxy)tetrylenes and the more general class of tetryl(II)alkoxides difficult. A list of isolable, monomeric di(oxy)tetrylenes is provided in Table 23, although in some cases a fluent transition depending on outer conditions can be observed and the reactivity doesn't exclusively depend on the most stable aggregation state.^[329,335]

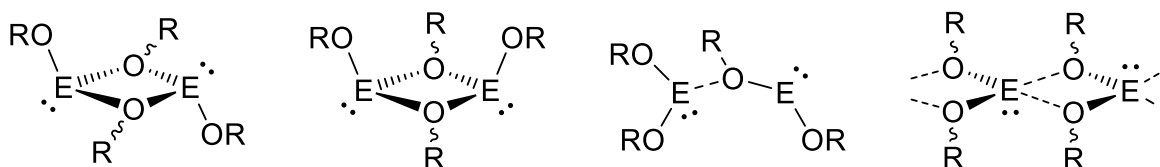


Figure 51. Different aggregation modi observed for di(oxy)tetrylenes with small substituents. Formal charges are omitted for simplicity.^[331,332,336]

When compared to more common tetrylenes, the chemistry of isolable di(oxy)tetrylenes has only been briefly studied. Expectedly, insertion into appropriate chemical bonds (e.g. in MeI, alcohols, thiols) takes place as well as scrambling (“transalkoxidization”) of the alkoxy substituents in {Sn(OR)₂}_n.^[335,337] Monomeric as well as dimeric units have been used as ligands in simple transition metal carbonyl complexes since the mid 1980s, whereas the alkali metal cage complexes [M(μ-OAr)₃Ge] (M = Li – Cs, Ar = meta-terphenyls) are directly accessible from MOAr and GeI₂.^[331,338–341] More recent results include the oxidation of Sn(OAr)₂ by PdCl₂(1,4-cyclooctadiene)^[334] or the transfer of an {GeOAr} unit to ketones.^[335] Apart from academic research, heavier di(oxy)tetrylenes have found some technical applications. For example, Sn(Oct)₂ (Oct = 2-ethylhexanoate) was proven by mass spectrometry to be an active (pro-)catalytic species in the polymerization of cyclic esters^[342] and Boyle described remarkably clean thermolysis reactions of Ge(OAr)₂ as a bulk material for crystalline germanium(0) nanowires whereby the morphology is influenced by the substituent.^[332,343] Likewise, tin- and tin oxide (SnO_x) nanowires obtained from [Sn(OAr)₂]_n (n = 1, 2, ∞) have been proposed as lithium ion battery anode materials,^[344] whereas thin Sn or SnO_x ceramic films can be made by aerosol-assisted chemical vapor deposition (AACVD) or metal-organic chemical vapor deposition (MOCVD).^[345–347]

Table 23. Monomeric, heavier di(oxy)tetrylenes E(OR)₂ (E = Ge – Pb).

E	Substituent R	color	$\alpha(\text{O-E-O}) / ^\circ$	Year	Ref.
Ge	2,6-tBu ₂ -4-Me-C ₆ H ₂	yellow	92.0(4)	1980	[328]
Ge	Mes*	colorless	n. a.	1985	[329]
Ge	Dipp	colorless	n. a.	1985	[329]
Ge	C ₆ Cl ₅	colorless	n. a.	1985	[329]
Ge	C ₆ F ₅	colorless	n. a.	1985	[329]
Ge	C(tBu) ₃	colorless	85.9(4)	1985	[348]
Ge	naphthoxide ^A	yellow	89.4(7)	2002	[349]
Ge	2,6-Ph ₂ -C ₆ H ₃	colorless	92.10(5)	2003	[332,335]
Ge	2,3,5,6-Ph ₄ -C ₆ H	colorless	91.09(7)	2003	[335]
Ge	2,6-tBu ₂ -C ₆ H ₃	yellow	92.2(1)	2006	[343]
Ge	Ar ^{Dipp}	colorless	92.54(6)	2006	[350]
Ge	Ar ^{Mes}	colorless	n. a.	2008	[351]
Ge	2-Me-6-tBu-C ₆ H ₃	colorless	90.83(9)	2009	[333]
Ge	2-(CH ₂ NMe ₂)-C ₆ H ₄	colorless	93.9(1) ^B	2013	[334]
Ge	B{N(Dipp)CH} ₂	orange	93.46(7)	2019	[102]
Sn	2,6-tBu ₂ -4-Me-C ₆ H ₂	yellow	88.8(1)	1980	[328]
Sn	Mes*	yellow	87.4(4)	1980	[328]
Sn	C(tBu) ₃	colorless	n. a.	1985	[348]
Sn	2,6-tBu ₂ -C ₆ H ₃	yellow	88.8(2)	1994	[344,352]
Sn	Ar ^{Dipp}	colorless	92.18(6)	2006	[350]
Sn	Ar ^{Mes}	colorless/yellow	87.3(1) ^B	2008	[351]
Sn	2-(CH ₂ NMe ₂)-C ₆ H ₄	colorless	n. a.	2013	[334]
Sn	B{N(Dipp)CH} ₂	orange	93.25(8) ^B	2019	[102]
Pb	2,6-tBu ₂ -4-Me-C ₆ H ₂	red	86.2(4)	1980	[328]
Pb	Ar ^{Dipp}	yellow	100.62(6)	2013	[353]
Pb	2-(CH ₂ NMe ₂)-C ₆ H ₄	colorless	n. a.	2013	[334]
Pb	B{N(Dipp)CH} ₂	yellow	92.66(6) ^B	2019	[102]

A: (R,R)-3-C₂₀H₁₀(OSiMe₃)-2-(SiMe₃)₂; **B:** intramolecular π -stabilization is observed.

3.1.2 Oxysilylenes

The oxophilicity of silicon is proverbial and examples of molecules, polymers and minerals containing Si(IV)-oxygen bonds can be found like sand at the ocean.^[1,354] Yet, when the experimental work of this thesis was started in 2016, not even a single molecule containing a two-coordinated, oxygen-bonded silicon center had been isolated.

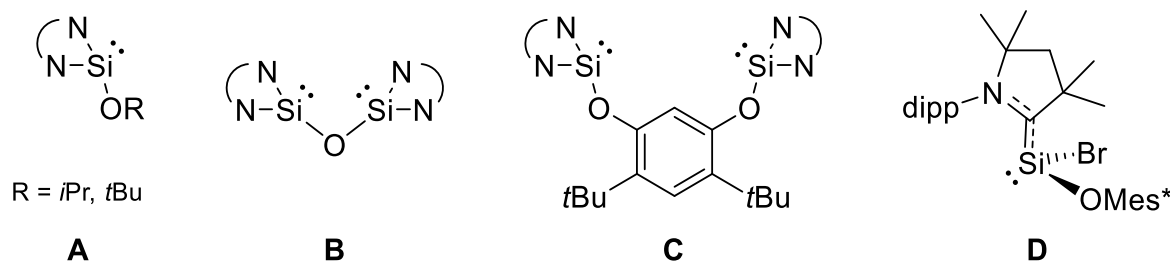
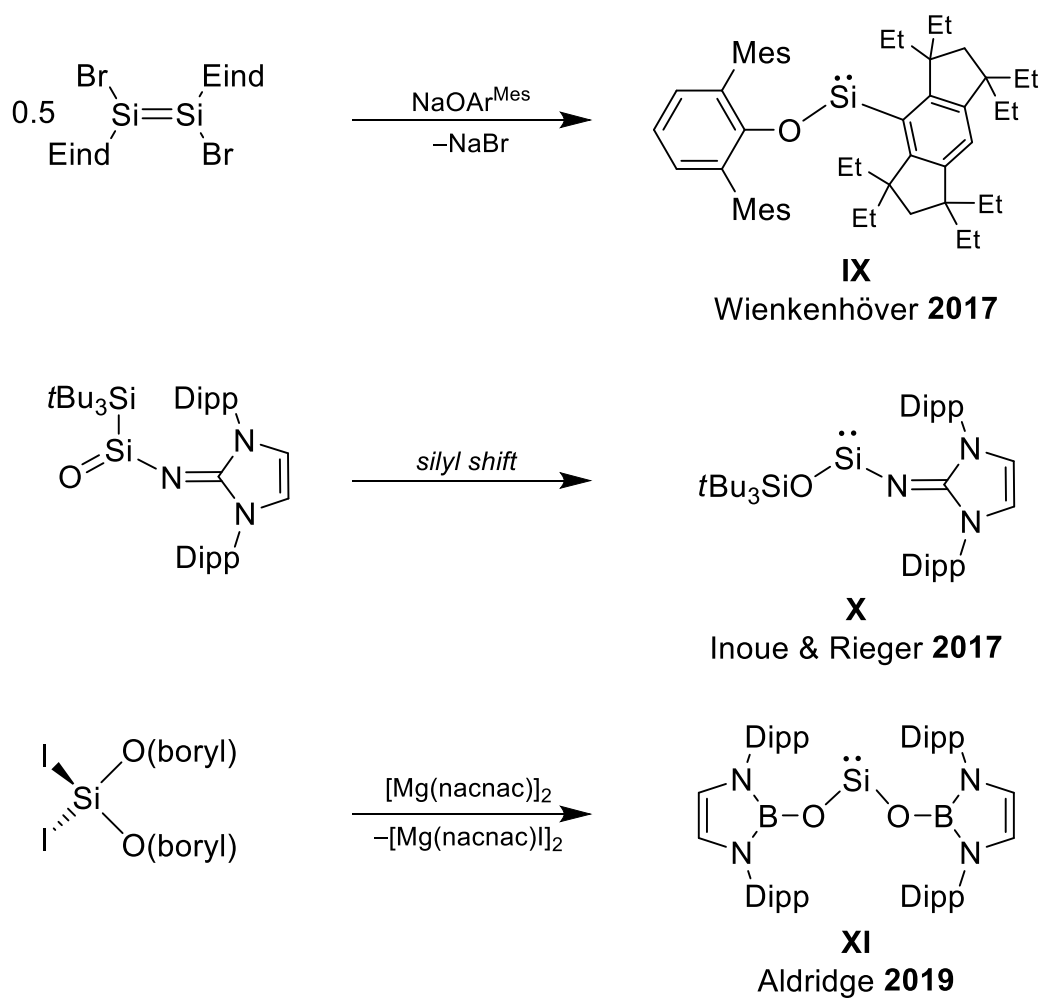


Figure 52. The first benzamidinato-stabilized oxosilylenes reported in the literature and a cAAC-stabilized aryloxy(bromo)silylene (right). Formal charges are omitted for simplicity; SiN₂ = cyclo-Si{N(*t*Bu)}₂CPh.^[355–358]

Base-stabilized examples are also extremely rare. In 2007, So and Roesky obtained the benzamidinato-stabilized oxosilylenes Si(OR){N₂(*t*Bu)₂CPh} (**A**, R = *t*Bu, *i*Pr) from hypervalent dichlorosiloxanes using potassium as a reducing agent.^[355] The same silylene (R = *t*Bu) was later also obtained upon substitution of the benzamidinato-stabilized chlorosilylene Si(Cl){N₂(*t*Bu)₂CPh} with KO*t*Bu in toluene, but no structural data are available.^[359] Starting from Si(IV), Driess and coworkers reported the synthesis of O[Si{N₂(*t*Bu)₂CPh}]₂ (**B**), a benzamidinato-stabilized “bis-silylene oxide” or bis(silylene)ether, obtained by dehydrochlorination of a siloxane in 2010 and demonstrated its usefulness as a pincer ligand.^[356] In the following years, the same group then introduced a larger backbone by salt elimination from 1,3-dilithium resorcinolate and two equiv. of Si(Cl){N₂(*t*Bu)₂CPh}₂ (**C**).^[85,357] Finally, SiBr(OMes*)(cAAC^{Me}) (**D**), which is a hybrid of a base-stabilized silylene and a silene, was isolated by F. Gstrein from the Filippou group parallel to this work (Figure 52).^[358]

However, in the meantime several publications have described exciting breakthroughs in this field of silicon chemistry (Scheme 42): In 2017, Dr. N. Wienkenhöver from the Filippou group succeeded in the isolation of the aryl(aryloxy)silylene Si(Eind)OAr^{Mes} (**IX**), starting from the di(bromo)disilene (E)-EindSi(Br)=Si(Br)Eind and NaOAr^{Mes}.^[40] By the end of the same year, Inoue and Rieger reported on the imino(siloxy)silylene Si(NR)(OSitBu₃) (**X**, NR: N=C{N(Dipp)CH}₂) resulting from a thermal silyl shift in the corresponding imino(silyl)silanone {RN}Si(O)SitBu₃.^[101] And finally in 2019, Aldridge et al. announced the successful isolation of the first di(boryloxy)silylene Si{O(TBoN)}₂ (**XI**) after classical reduction of the corresponding diiodosilane.^[102]

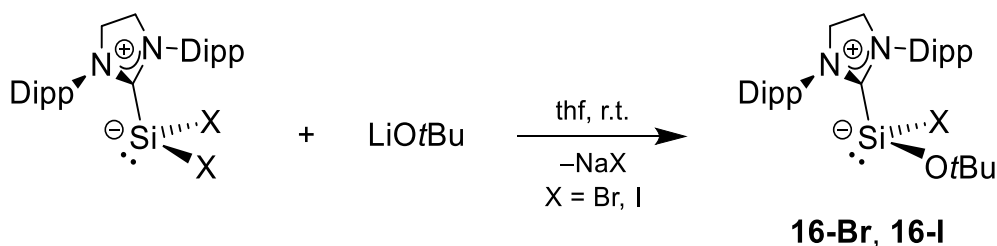


Scheme 42. Syntheses of **IX** – **XI** reported in the literature.^[40,101,102] Formal charges are omitted for simplicity.

3.2 Synthesis of Base-stabilized Oxysilylenes

With compounds **IX** – **XI** unknown at the beginning of this work, the synthesis of acyclic oxysilylenes with and without base stabilization was aspired. Two routes were considered: classical reduction of $\text{SiX}_2(\text{OR})_2$, hypervalent $\text{SiX}_3(\text{OR})(\text{NHC})$ or $[\text{SiX}_2(\text{OtBu})(\text{NHC})]\text{X}$ as well as substitution of the dihalosilylenes $\text{SiX}_2(\text{NHC})$. Encouragingly, Aldridge and coworkers reported on the successful substitution of $\text{SiCl}_2(\text{IDipp})$ with a bulky amide leading to the NHC-free di(amino)silylene $\text{Si}(\text{TBoN})_2$ in 2016.^[100]

Initial salt metathesis reactions of $\text{SiX}_2(\text{NHC})$ ($\text{X} = \text{Cl}, \text{Br}, \text{I}$; $\text{NHC} = \text{IDipp}, \text{SIDipp}$) with MOtBu ($\text{M} = \text{Li}, \text{Na}, \text{K}$) in toluene led to a gradual color change to yellow and formation of the desired mono-substituted NHC-stabilized oxy(halo)silylenes $\text{SiX}(\text{OtBu})(\text{NHC})$ (**16-X**) could be observed. Generally, the reactions were rather slow (8 – 10 h) and accompanied with the formation of some free NHC. Heavier halogens gave more selective reactions, while lighter alkali alcoholates reacted both faster and less selective. Best results were hence obtained in thf solutions starting from $\text{SiBr}_2(\text{SIDipp})$ or $\text{SiI}_2(\text{SIDipp})$ and LiOtBu with a reaction time of only about 2 h (Scheme 43).



Scheme 43. Synthesis of the NHC-stabilized alkoxy(halo)silylenes **16-Br** and **16-I**.

While the conversions were very selective (>90 % based on ^1H NMR spectroscopy), the isolation of **16-X** bulk material was prevented by parallel decomposition: throughout the workup procedures, re-formation of the $\text{SiX}_2(\text{NHC})$ starting material and free NHC was observed. This is presumably caused by X/OtBu scrambling in presence of excess MX or MOtBu and subsequent decomposition of the putative “ $\text{Si}(\text{OtBu})_2(\text{SIDipp})$ ”. It can be speculated, that the +M effect of the OtBu groups encourages this by weakening the Si-NHC and the Si-X bond, which is also reflected in their solid-state structures (vide infra).

After extraction from the salts with toluene/n-hexane mixtures and subsequent precipitation at $-30\text{ }^\circ\text{C}$, silylenes **16-Br** and **16-I** were obtained as yellow solids in 60 % yield that still contained ca. 20 mol% and 9 mol% of free SIDipp, respectively. Akin to their precursors, the substitution products are well soluble in thf, moderately soluble in Et_2O or aromatic solvents and barely soluble in aliphatic hydrocarbons. Despite the aforementioned decomposition of samples in solution, NMR spectra recorded from single crystalline samples of **16-I** showed no

signs of decomposition for several days (Figure 53), proving that the completely pure compound would be isolable under the right conditions.

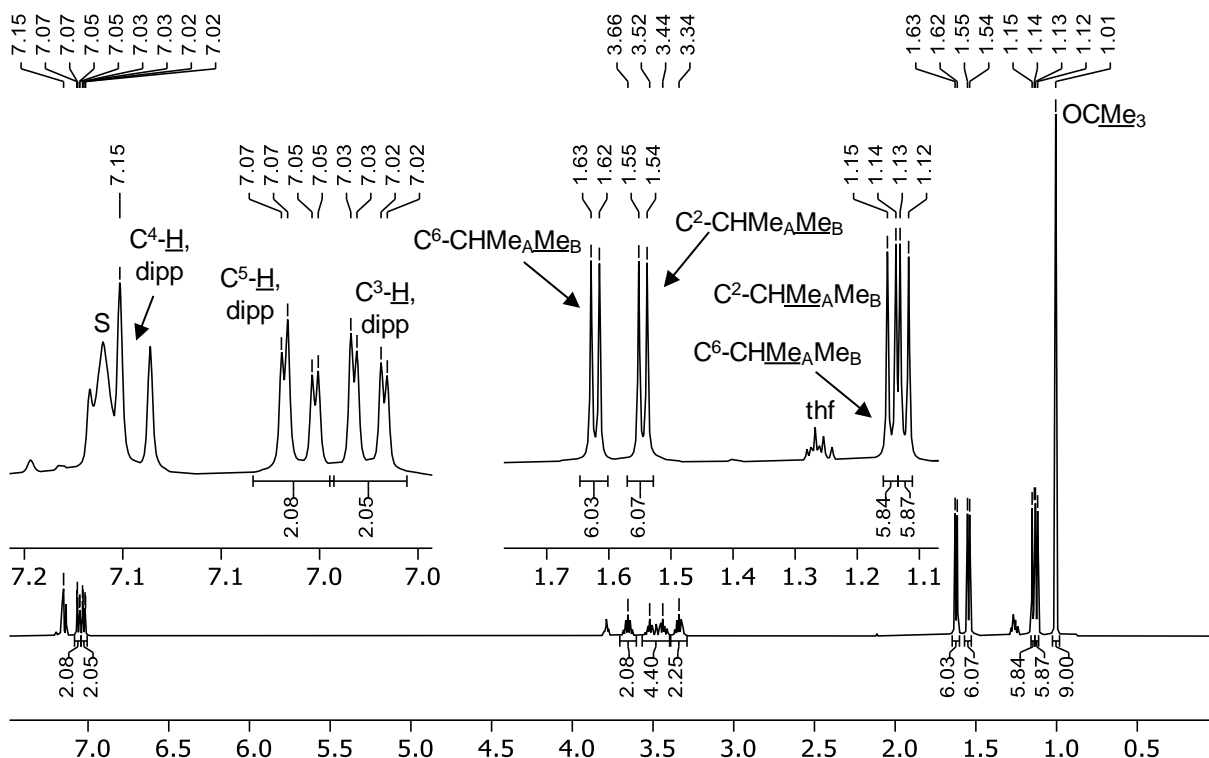


Figure 53. ^1H NMR spectrum (500.0 MHz) of **16-I** in benzene- d_6 . The spectrum contains a small amount of residual thf and the solvent signal is marked with the character S.

Spectroscopically, **16-Br** and **16-I** displayed local C_2 symmetry for the carbene ligand as evidenced by the four doublet signals in the aliphatic region and the inequivalence of the two ortho- and meta positions. A very complex multiplet signal was detected for the NCH_2 groups and could be somewhat reproduced by spectra simulation, but no unambiguous explanation could be found (Figure 54).^[360] The ^{29}Si NMR resonances appear within the typical region of NHC-supported silylenes at $\delta_{\text{Si}} = 18.0$ ppm (**16-Br**) and 13.2 ppm (**16-I**). Compared to the starting materials ($\text{SiBr}_2(\text{SIDipp})$: 10.8 ppm; $\text{SiI}_2(\text{SIDipp})$: -11.2 ppm)^[205] the alkoxy-substitution is accompanied with a shift to lower fields and the signals also appear at lower field when compared to the known benzamidinato-oxsilylenes **A** – **C** depicted in Figure 52 (-5.2 to -24.0 ppm, page 106).^[355–357]

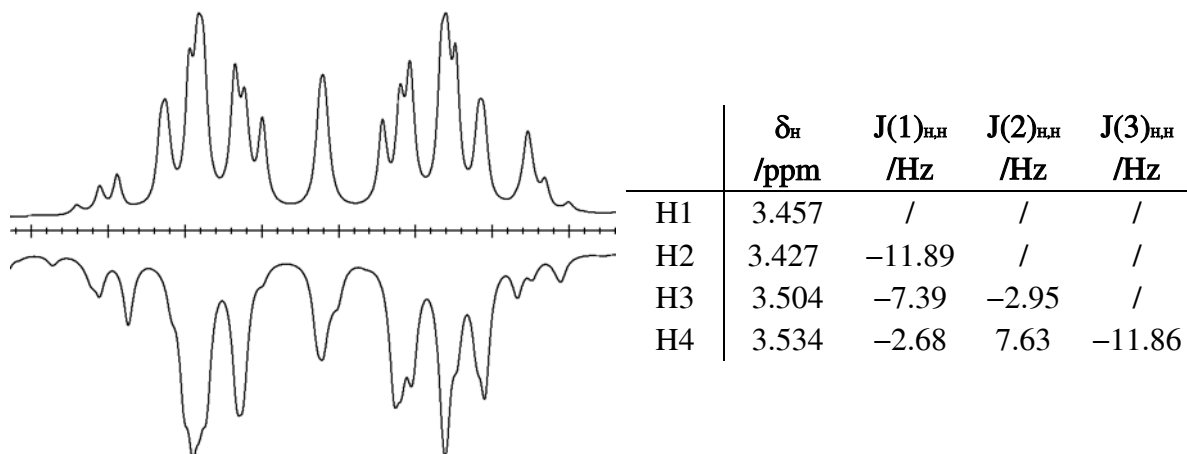


Figure 54. Excerpt of the experimental (top, benzene- d_6) and the simulated (bottom) ^1H NMR spectrum of **16-I** displaying the multiplet observed for the two NCH_2 groups of the SIDipp ($\delta \approx 3.576 - 3.375$ ppm). The respective chemical shifts and coupling constants simulated by gNMR are given in the table.^[360,361]

Single crystals suitable for XRD were obtained upon evaporation of solutions from benzene (**16-Br**) or toluene/*n*-hexane (**16-I**), respectively. The silylenes are essentially isostructural to the $\text{SiX}_2(\text{SIDipp})$ starting materials. For compound **16-I**, two independent molecules were found in the asymmetric unit but averaged values are discussed.

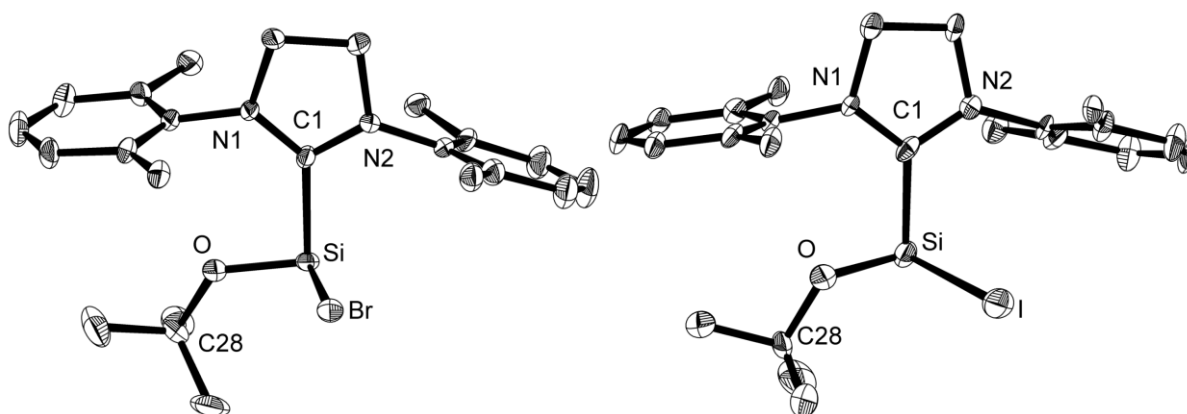


Figure 55. Molecular structures of **16-Br** and **16-I**. Thermal ellipsoids are set to 30 % probability; methyl groups as well as hydrogen atoms are omitted for simplicity. Two independent molecules of **16-I** were found in the asymmetric unit and values given in brackets correspond to the second molecule but averaged values are discussed in the text. Selected bond lengths (\AA) and angles ($^\circ$): **16-Br**: Si-Br 2.410(2), Si-C1 2.020(8), Si-O 1.677(6), O-C28 1.45(1); Br-Si-C1 90.5(3), Br-Si-O 98.7(3), O-Si-C1 94.8(3), Si-O-C28 124.0(5). **16-I**: Si-I: 2.682(2) [2.730(2)], Si-C1 2.000(7) [1.986(8)], Si-O 1.686(6) [1.663(6)], O-C28 1.437(9) [1.433(9)]; I-Si-C1 93.8(2) [87.4(2)], I-Si-O 99.7(8) [101.3(2)], O-Si-C1 96.3(3) [94.8(3)], Si-O-C28 126.2(5) [126.5(5)].

Both compounds feature pyramidalized 3-coordinated Si atoms (**16-Br**: 84%, **16-I**: \emptyset 81 %) with large O-Si-X angles of $98.7(3)^\circ$ and $\emptyset 100.5(5)^\circ$, which consists with the presence of a lone pair at the Si atoms (Figure 55). The Si-O bonds are nearly identical (**16-Br**: 1.677(6) \AA and **16-I**: $\emptyset 1.675(6)$ \AA) and a bit longer when compared to those found in Driess benzamidinato-stabilized bis-silylene **B** (1.641(2) \AA and 1.652(2) \AA), resembling typical Si-O single bonds. In contrast, the Si-X bonds are elongated by another 3 % and 5 % compared to

the already long Si-X bonds in their respective starting materials. In fact, the Si-Br bond in **16-Br** (2.410(2) Å) is the longest reported for a three-coordinated Si atom and compares well to the axial Si-Br bonds of the trigonal bipyramidal SiBr₄(IDipp) (axial: 2.3936(7) Å; equatorial: 2.2360(4) Å).^[362] Likewise, the Si-I distance in **16-I** (2.706(2) Å) is the longest reported for three- or four-coordinated silicon (typically 2.45 – 2.55 Å)²⁸ and only slightly shorter than the longest known Si-I bonds which were found in the five-coordinated Si(IV) complexes SiRI(SONC) (R = Ph: 2.7396(8) Å; R = Me: 2.8225(7) Å; SONC = tridentate dianionic S,N,O-ligand).^[364,365]

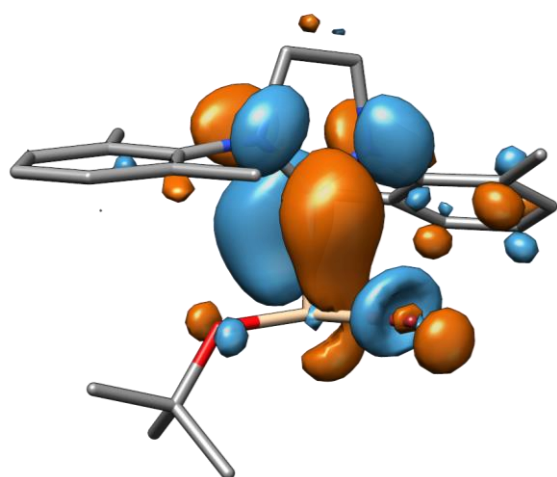
Table 24. Selected structural and spectroscopic data of **16-Br**, **16-I** and their precursors.

Cpd.	∅Si-C /Å	∅Si-O /Å	∅Si-X /Å	E-Si-X ^A /°	Pyr. ^B /%	δ _c (NCN) ^C /ppm	δ _{SiP} /ppm
16-Br	2.020(8)	1.677(6)	2.410(2)	98.7(2)	84	194.7	18.0
SiBr ₂ (SIDipp) ^[205]	2.007(5)	-	2.3354(7)	97.92(3)	78	188.7	10.8
16-I	1.993(7)	1.675(6)	2.706(2)	100.5(2)	81	195.9	13.2
SiI ₂ (SIDipp) ^[205]	2.022(5)	-	2.584(4)	96.60(5)	75	n.a.	-11.2

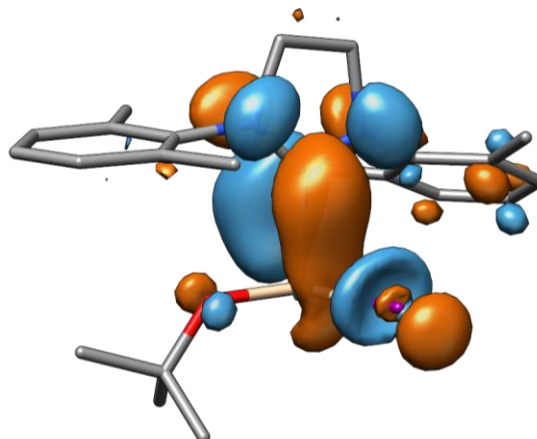
A: E = O or X; **B:** degree of pyramidalization; **C:** ¹³C{¹H} NMR resonance of the carbene atom in benzene-d₆; **D:** measured in benzene-d₆. Averaged values are given for SiBr₂(SIDipp) and SiI₂(SIDipp). Six independent molecules are found in the unit cell of SiI₂(SIDipp), four of which exhibiting nearly identical structural data with deviations usually within the 3σ range. But it should be pointed out, that the C-Si-Br₂ angle (the bromine atom perpendicular to the central plane of the NHC) considerably varied in the remaining two structures (89.1(2)° and 95.3(2)°), resulting in individual pyramidalizations of 79 and 68 %, respectively. However, data given in the table are averaged over all six molecules for easier comparison.

Those similarities extend to the electronic structures as well (Figure 56). The HOMOs of both silylenes are mostly defined by the electron lone pair at the Si atom with some smaller contributions of p-orbitals at the carbene carbon, the halogen and the oxygen atom. The LUMOs represent Si-NHC π-bonds and are higher in energy by only ΔE = 2.23 eV and 2.18 eV, which accounts for a relatively small gap similar to those of acyclic silylenes (about 2.0 – 2.5 eV, see Table 26 on page 121).

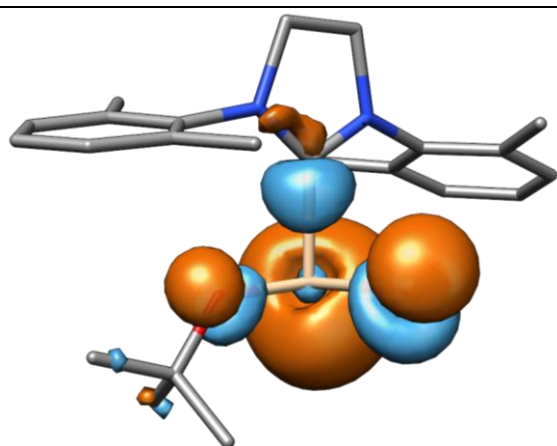
²⁸ On the basis of a CSD 5.4.1 search. For 3-coordinated Si atoms, a total of 13 examples with Si-Br distances between 2.2279(6) Å in (E)-Eind(Br)Si=Si(Br)Eind and 2.3922(9) Å in SiBr(Eind)(4-DMAP) was found.^[47] For the heavier Si-I congeners, 8 examples with distances between 2.4520(7) Å in Trip₂Si=Si(I)Trip and 2.6036(6) Å in the disilicon(I) Si₂I₂(IDipp)₂ were listed.^[111,363]



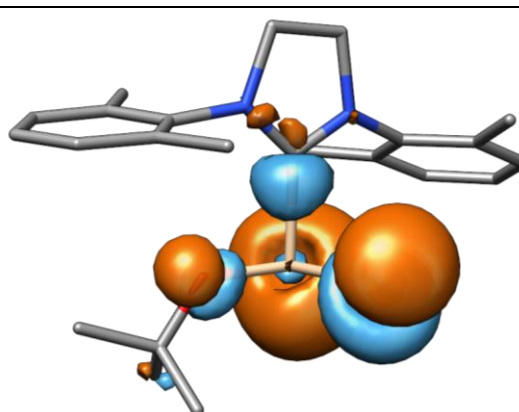
16-Br^{calc}: LUMO (-1.71 eV)



16-I^{calc}: LUMO (-1.83 eV)



16-Br^{calc}: HOMO (-3.94 eV)



16-I^{calc}: HOMO (-4.01 eV)

Figure 56. Selected Kohn-Sham-frontier orbitals of **16-Br** and **16-I** and their respective energies in eV (isosurface value 0.04 e-bohr⁻³) on the PW6B95-D3(BJ)^{ATM}/def2-QZVPP//B97-D3(BJ)^{ATM}/def2-TZVP level of theory.

3.3 Synthesis of Cp*Si(OAr^{Mes})

Another promising source for Si(II) is Jutzi's decamethylsilicocene SiCp*₂ (**A** in Figure 57) or rather the silyliumylidene cation [Cp*Si]⁺ (**B**⁺).^[70,366,367] Nucleophilic addition of amides was already reported to yield disilenes by the authors in 2004 (**C**),^[367] and in 2012 Inoue and Leszczyńska reported on the hyperconjugated zwitterionic silaimine (or imino-silylene) η²-Cp*SiN=C{N(Dipp)CH}₂ (**D**) from the lithium imide and [Cp*Si][B(C₆F₅)₄].^[97]

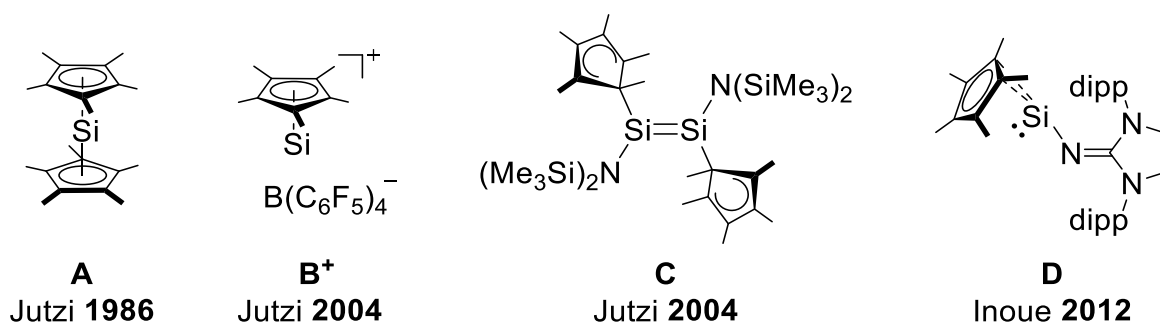
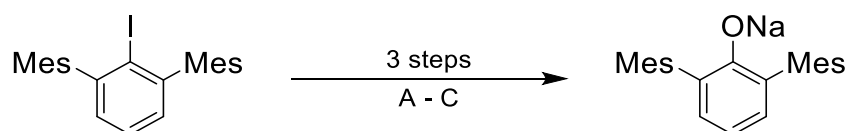


Figure 57. SiCp*₂, [Cp*Si][B(C₆F₅)₄] and products of nucleophilic addition. Formal charges are omitted for simplicity.

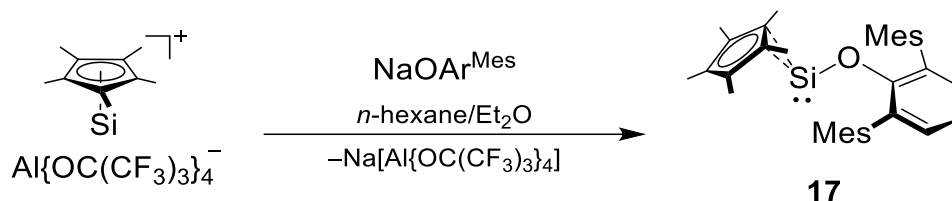
Here, different silyliumylidene salts were made from SiBr₂(SIDipp) and 2 equiv. of NaCp* and subsequent protonation with “Brookhart type” acids [H(OEt)₂][anion]^[368] (anion = [B(C₆F₅)₄]⁻, [B(3,5-(CF₃)₂-C₆H₃)₄]⁻ or [Al{OC(CF₃)₃}₄]⁻).^[127] For the synthesis of an oxy-substituted derivative, NaOAr^{Mes} was chosen as a promising starting material. The terphenyl oxide was thereby synthesized from Ar^{Mes}I on a 15 g scale in a yield of 62 % following an established literature procedure (Scheme 44).^[369,351]



Scheme 44. Synthesis of NaOAr^{Mes}. **A**: 2 equiv. nBuLi, Et₂O, -30 °C; **B**: 1.05 equiv. PhNO₂, Et₂O, -80 °C to r.t., then aq. HCl; **C**: 2.5 equiv. sodium sand, toluene, reflux.

Surprisingly, the outcome of the reaction between NaOAr^{Mes} and [Cp*Si][anion] was reproducibly dependent on the counter anion: whereas salts with the boronate anions [B(C₆F₅)₄]⁻ or [B(3,5-(CF₃)₂-C₆H₃)₄]⁻ led to decomposition, the aluminate salt reacted smoothly to the desired product Cp*SiOAr^{Mes} (**17**, Scheme 45). Although the reactions were initially carried out in CD₂Cl₂, thf or fluorobenzene, best outcomes were obtained when the starting materials were first suspended in n-hexane and the reaction was then started by addition of diethyl ether at ambient temperature. The mixture was then stirred overnight when no more NaOAr^{Mes} was detected by in situ ¹H NMR spectroscopy. Workup by repeated extractions with pure n-pentane and crystallization from n-pentane/diethyl ether gave **17** as a highly soluble, extremely air sensitive, colorless powder in 57 % yield. Unfortunately, a small amount of salt was visible by

^{19}F NMR spectroscopy (but not in the ^{13}C NMR spectrum) despite the low solubility of pure $\text{Na}[\text{Al}\{\text{OC}(\text{CF}_3)_3\}_4]$ and repeated extraction steps. Accordingly, the elemental analysis showed considerable deviations.



Scheme 45. Synthesis of $\text{Cp}^*\text{SiOAr}^{\text{Mes}}$ (**17**). Formal charges are omitted for simplicity.

High-quality single crystals were obtained by slow evaporation of a concentrated solution in diethyl ether at $-30\text{ }^\circ\text{C}$. Interestingly, they were extremely sensitive towards cooling and repeatedly cracked on the diffractometer head. Therefore, they had to be cooled to the measurement temperature of 100 K over a timespan of several hours to minimize physical stress.

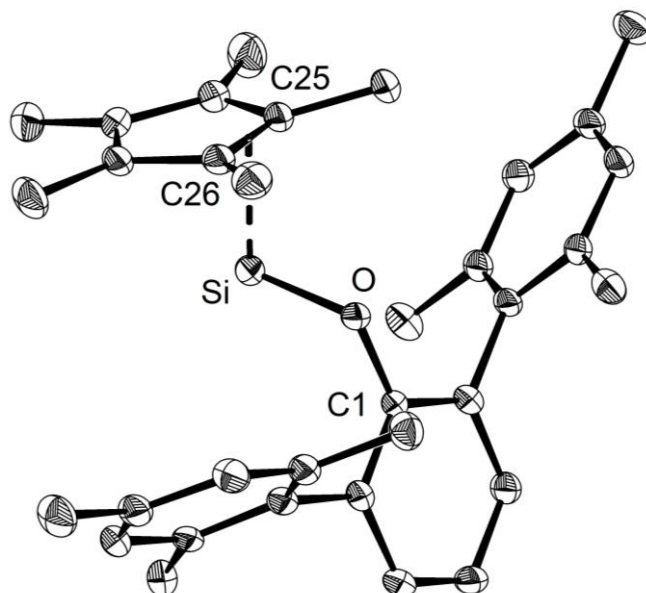


Figure 58. Molecular structure of **17**. Thermal ellipsoids are set to 50 % probability and hydrogen atoms are omitted for simplicity. Selected bond lengths (\AA) and angles ($^\circ$): Si-O 1.716(2), O-C1 1.379(3), Si-C25 2.116(3), Si-C26 2.132(3), $\perp\text{Si}\cdots(\text{C}25\text{-C}26)$ 1.997(2), $\text{Si}\cdots\text{centroid}$ 2.070(2); C1-Si-O 118.4(2); the angle between the Si-O bond and the dashed vector between the Si atom and the C25-C26 bond is 97.79(2) $^\circ$.

Compound **17** is monomeric in the solid state (Figure 58) and isostructural to Inoues silimine **D**.¹⁹⁷¹ The Cp^* substituent adopts a η^2 coordination mode with Si-C $_{\text{Cp}^*}$ distances of 2.116(3) and 2.132(3) \AA that are shorter when compared to **D** (2.124(6) and 2.218(6) \AA).¹⁹⁷¹ The angle between the Cp^* ring and the {Si,C25,C26} plane is 80.1(1) $^\circ$, synonymous to a light tilting towards the free electron lone pair at the Si center. A relatively narrow Si-O-C1 angle of only 118.4(2) $^\circ$ is found for compound **17**, which is smaller than those in typical

hexa(alkyl)siloxanes (130°–180°) or the known oxysilylenes (124.0(5) in **16-Br** to 153.2(1)° in **X**), but those angles are known to be strongly dependent on steric bulk. More characteristically, the Si-O bond distance (1.716(2) Å) is longer than those found in the oxysilylenes **IX** (1.6699(9) Å)^[40], **X** (1.643(1) Å)^[101] and **XI** (Ø1.606(1) Å)^[102] or those of the base-stabilized NHC-stabilized oxy(halo)silylenes **16-Br** and **16-I** (1.677(6) Å and Ø1.675(6) Å). This is a clear sign for an undisturbed Si-O single bond, which is remarkable since Inoue and coworkers found a strong +M effect of the nitrogen atom in **D**, which consequently has a shorter Si-N bond than aminosilylenes.^[97] A detailed overview is also provided in Table 27 on page 124.

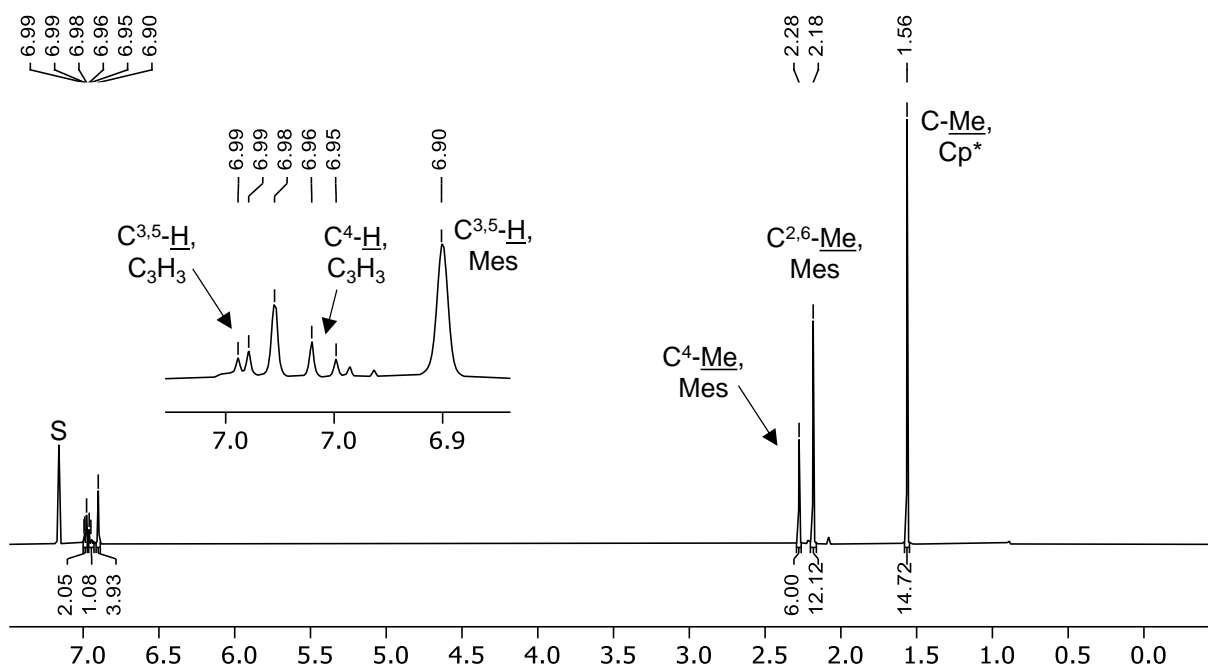


Figure 59. ¹H NMR spectrum (500.0 MHz) of **17** in benzene-d₆. The spectrum contains a small amount of residual thf and the solvent signal is marked with the character S.

The ¹H- and ¹³C NMR spectra of **17** in benzene-d₆ solution show local C_{2v} symmetry of the Ar^{Mes} substituent with clearly separated aliphatic methyl resonances but some second order coupling for the aromatic protons of the central ring (Figure 59). Averaged signals are observed for the Cp* substituent, which is typical for a rotation of the ring system in solution.^[70,97] The ²⁹Si NMR resonance is found at δ_{Si} = −138.2 ppm, which is far high field from the literature-known oxysilylenes **IX** (282.6 ppm)^[40], **X** (58.9 ppm)^[101] and **XI** (35.5 ppm).^[102] This immense discrepancy is a result of two effects and has to be seen in a greater context: First, the aryl group in **IX** has a dominating effect on the chemical shift, which appears within the “standard” region of acyclic silylenes in this case (Figure 60).²⁹

²⁹ Isolable acyclic silylenes typically resonate between 200 and 250 ppm, or up to 440 ppm depending on the donor strength of the substituents.^[95–104] The current low-field record (δ_{Si} = 826.6 ppm) is given by the cationic

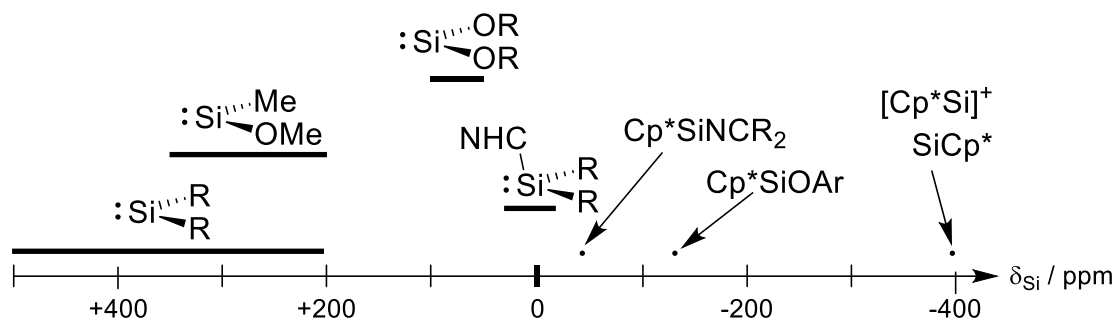


Figure 60. Approximate scale of ^{29}Si chemical shifts of acyclic silylenes and related compounds.²⁹

Incorporation of only one oxy group alone does not have a significant effect on the ^{29}Si NMR resonance of silylenes if the second substituent is sufficiently bulky. Addition of a second $-I/+M$ -substituent, however, results in an immense shift towards higher field by about 200 ppm. No concrete explanation can be given at this point, but it should be noted that calculations on such simple model compounds as SiMe_2 ($\delta_{\text{Si}} = 740$ ppm), $\text{SiMe}(\text{OMe})$ (377 ppm) and $\text{Si}(\text{OMe})_2$ (97 ppm) show a similar trend. In his theoretical work from 2003, Müller found a linear correlation between ^{29}Si NMR resonances and electronic excitation energies, which are dependent on the R-Si-R angle and were traced back to paramagnetic contributions of the electron lone pairs having a deshielding effect on the δ_{11} tensor. As the latter can be estimated by means of UV-vis spectroscopy, a rough linear correlation between the ^{29}Si NMR resonance and λ_{max} was found as well.^[370] Consequently, SiH_2 (purple)^[370] or SiMe_2 (orange)^[371] are vividly colored whereas known $\text{SiR}(\text{OR})$ are offwhite to yellow and di(alkoxy)silylenes $\text{Si}(\text{OR})_2$ appear colorless.^[370,373] The chemical shift of compound **17** is yet affected by another factor: hypercoordination by the Cp^* ring results in an additional strong highfield shift. Therefore, the chemical shift of **17** ($\delta_{\text{Si}} = -138.2$ ppm) appears in between those of comparable silylenes (≈ 200 ppm) and SiCp^* or $[\text{Cp}^*\text{Si}]^+$ (around -400 ppm)^[70,366,367] and compares reasonably well with the shift observed for Inoues silaimine **D** (-43.8 ppm).

chromiosilylene complex $[(\text{Cp}^*)(\text{CO})_3\text{Cr-Si}(\text{SIDipp})][\text{BAr}^{\text{F}_4}]$.^[120] ^{29}Si NMR shifts of small, transient silylenes in argon matrices have been recorded between 300 and 550 ppm.^[370-372]

3.4 Excursus: Synthesis of $\text{Si}\{\text{N}(\text{Me})\text{Ar}^{\text{Mes}}\}_2$

As mentioned already, the chemistry of heavier di(oxy)tetrylenes is connected to that of their di(amino) congeners. The heavier di(amino)tetrylenes $\text{E}(\text{NR}_2)_2$ ($\text{E} = \text{Ge}, \text{Sn}, \text{Pb}$; $\text{R} = \text{alkyl}, \text{aryl}, \text{silyl}$) have been established by the groups of Lappert and Harris in the 1970s,^[89–91] and the fairly stable E-N bonds can be further functionalized.^[328,374,375] N-heterocyclic silylenes (NHSis) are known since the pioneering work of Denk and West^[173] and their reactivity has been researched throughout the years.^[69,77–79,81,82] Finally, bulky amino groups have also consistently been used to protect acyclic silylenes such as the isolable examples that are listed in Figure 61 below.^{[40,96,98,100].}

30

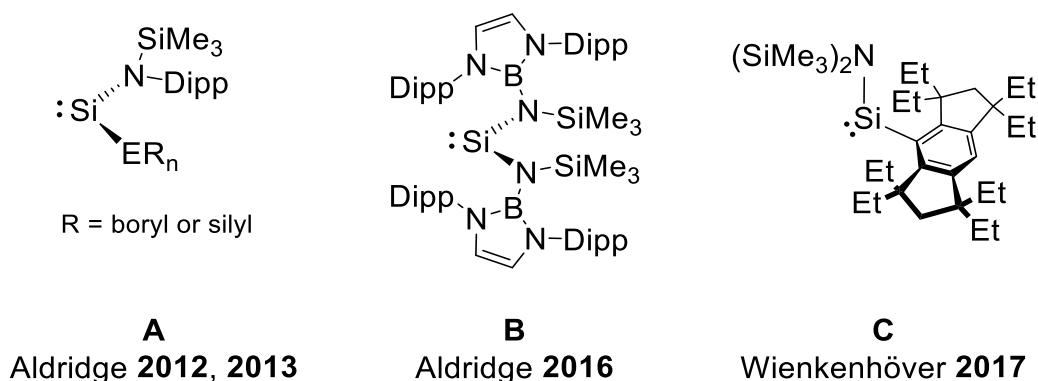


Figure 61. Known acyclic aminosilylenes **A**,^[96,98] **B**^[100] and **C**;^[40] silyl = $\text{Si}(\text{SiMe}_3)_3$; boryl = $\text{B}\{\text{N}(\text{Dipp})\text{CH}\}_2$.

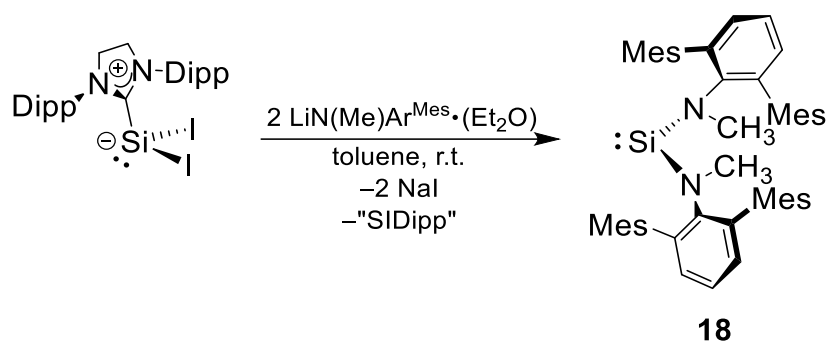
To obtain a homoleptic di(amino)silylene, the substitution approach starting from $\text{SiX}_2(\text{NHC})$ was once more favored over a reduction to minimize the risk of Si-N bond cleavage.^[100] $\text{LiN}(\text{Me})\text{Ar}^{\text{Mes}}$ was chosen as a promising bulky amide that was likewise used for the synthesis of the $\text{Ge}\{\text{N}(\text{Me})\text{Ar}^{\text{Mes}}\}_2$ from $\text{GeCl}_2(1,4\text{-dioxane})$ by Buchem in 2005.^[377]

Addition of 2.02 equiv. of solid $\text{LiN}(\text{Me})\text{Ar}^{\text{Mes}}\cdot\text{Et}_2\text{O}$ to a suspension of $\text{SiI}_2(\text{SIDipp})$ in benzene resulted in a color change from dark yellow to red and the reaction was completed within two hours. After workup, the di(amino)silylene $\text{Si}\{\text{N}(\text{Me})\text{Ar}^{\text{Mes}}\}_2$ (**18**) was isolated as an analytically pure solid in a satisfactory yield of 55 % (Scheme 46). The reaction was accompanied by the formation of about 15 % of $\text{HN}(\text{Me})\text{Ar}^{\text{Mes}}$ and an equimolar amount of a red, carbene-containing compound of unknown composition.³¹ Compound **18** is extremely sensitive towards air and moisture but thermally very robust and only melts at 259°C. It is well soluble in THF, moderately soluble in aromatic solvents and diethyl ether, and sparingly soluble

³⁰ Theoretical calculations at that time predicted the formation of a bridged dimer for $\text{Si}(\text{NH}_2)_2$,^[376] but $\text{Si}\{\text{N}(\text{iPr})_2\}_2$ lies in an equilibrium with its dimer and could be characterized spectroscopically in solution after photochemical generation by Kira about 20 years ago.^[93] Likewise, $\text{Si}\{\text{N}(\text{SiMe}_3)_2\}_2$ could be generated by reduction of the corresponding dibromosilane by West and Müller in 2003, but rapidly decomposes at 0 °C.^[94]

³¹ Attempts to isolate or crystallize the unknown side product failed. The compound displayed a set of signals expected for C_2 -symmetric SIDipp with no evidence of further ^1H or ^{29}Si NMR active groups (page 219 in the experimental part). Although the yield of **18** is only moderate, its initial formation is nearly quantitative.

in aliphatic solvents. The di(amino)silylene **18** is colorless in pure form, which differs from the intense yellow color of **A^{boryl}**, **B** and **C** or the purple **A^{silyl}**.^[40,96-98,100]



Scheme 46. Synthesis of the di(amino)silylene $\text{Si}\{\text{N}(\text{Me})\text{Ar}^{\text{Mes}}\}_2$ (**18**). A red byproduct could not be identified.

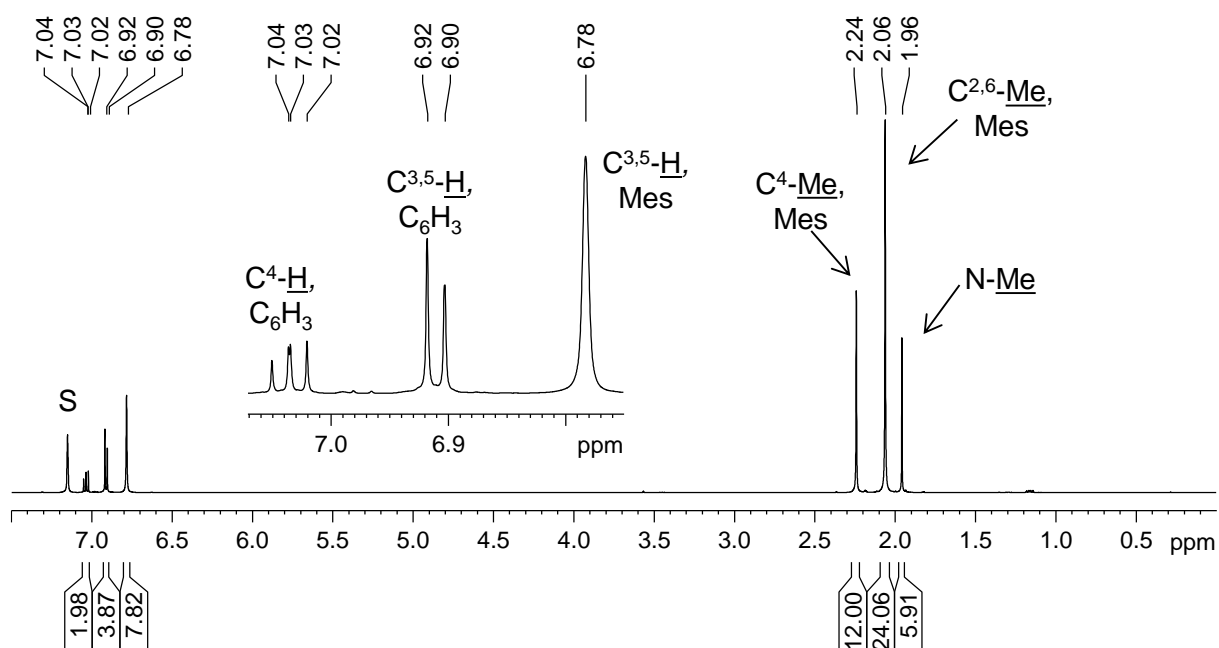


Figure 62. ¹H NMR spectrum (500.2 MHz) of **18** in benzene-d₆. The solvent signal is marked with the character S; an enlarged excerpt displays the aromatic signals.

Multinuclear magnetic resonance spectroscopy in benzene-d₆ solution revealed overall C_{2v} symmetry with all signals within in the expected ranges (Figure 62). Interestingly, a considerable low-field shift was observed for the ¹³C{¹H} resonances of the ortho and para carbon atoms when compared to the free amines (Table 25). A similar trend was also observed for Ge{N(Me)Ar^{Mes}}₂ and can be interpreted as an expression of the acceptor capabilities of the germylene and – even more – silylene.

Table 25. Selected $^{13}\text{C}\{^1\text{H}\}$ NMR data of **18** and related compounds.

Compound	C ¹	C ^{2,6}	C ^{3,5}	C ⁴	N-Me
$\text{Ar}^{\text{Mes}}\text{NH}_2$	141.2	126.1	128.9	118.6	-
$\text{Ar}^{\text{Mes}}\text{N}(\text{Me})\text{H}$	145.6	128.6	130.0	119.4	33.2
$\text{Si}\{\text{N}(\text{Me})\text{Ar}^{\text{Mes}}\}_2$ (18)	145.2	142.1	130.3	126.1	37.3
$\text{Ge}\{\text{N}(\text{Me})\text{Ar}^{\text{Mes}}\}_2$ [377]	148.9	140.4	130.9	125.0	39.7

Compound **18** and the amines were measured in benzene- d_6 solution; $\text{Ge}\{\text{N}(\text{Me})\text{Ar}^{\text{Mes}}\}_2$ in tetrahydrofuran- d_8 .

In the $^{29}\text{Si}\{^1\text{H}\}$ NMR spectrum of **18**, a singlet signal is found at $\delta_{\text{Si}} = 130.3$ ppm (computed: 137.3 ppm). This is more shielded than those of the di(amino)silylenes $\text{Si}\{\text{N}(\text{SiMe}_3)_2\}_2$ (223.9 ppm)^[94] and **B** (204.6 ppm),^[100] which can be rationalized by the more electron rich amino groups in **18** as well as the narrower N-Si-N angle.^[370] However, silaimines resonate at even higher fields from 89.9 ppm to -66.6 ppm (typically around 50 ppm).^[378–381] The ^{15}N resonance of **18** ($\delta_{\text{N}} = 113.7$ ppm) was deduced by ^1H - ^{15}N MNR correlation spectroscopy. This is shielded when compared to the (amidinato)silylene $\text{Si}(\text{NMe}_2)\{(\text{NDipp})_2\text{CPh}\}$ ($\delta_{\text{N}} = 155$ and 171 ppm for the SiN_2C unit)^[382],³² but high field from NHSis such as Denks $\text{Si}\{\text{N}(\text{tBu})\text{CH}\}_2$ ($\delta_{\text{N}} = 210.2$ ppm).^[73]

Single crystals were grown by slow evaporation of a benzene solution. Compound **18** is isostructural to the di(amino)silylene **B** with a V-shaped coordination of the Si atom by crystallographically equivalent amino groups and a stereochemically active lone electron pair (Figure 63). The Si–N distance (1.722(1) Å) corresponds to a single bond and matches those of the aminosilylenes **A** – **C** (1.720(1) to 1.743(1) Å).^[40,98,100] Compared to Inoues hyperconjugated $\eta^2\text{-Cp}^*\text{SiNC}\{\text{N}(\text{Dipp})\text{CH}\}_2$ (1.691(5) Å) and Jutzi's disilene $[\text{Cp}^*\text{Si}\{\text{N}(\text{SiMe}_3)_2\}]_2$ (1.748 Å), compound **18** enqueues in between,^[97,383] whereas a considerable difference is found when compared to the silaimines $\text{Mes}^*\text{N}=\text{Si}(\text{iPr})_2$ (1.568(3) Å) or $\text{Mes}^*\text{N}=\text{Si}\{\text{N}(\text{Dipp})\text{CH}\}_2$ (1.533(2) Å).^[379,384] Concurrently, the N-Si-N# angle of $103.38(9)^\circ$ is narrower than that of **B** ($110.94(5)^\circ$)^[100] which can be rationalized by the lower steric repulsion. Despite the planar environment of the nitrogen atoms of **2** (sum of angles at N, N# = $359.9(1)^\circ$), the molecules core consisting of the atoms N, C25, Si, N# and C25# is twisted by $32.79(5)^\circ$.

³² Values from the literature were converted and are given in respect to liquid ammonia. For further information see P. Bertani, J. Raya, B. Bechinger, *Solid State Nucl. Magn. Reson.* **2014**, 61-62, 15.

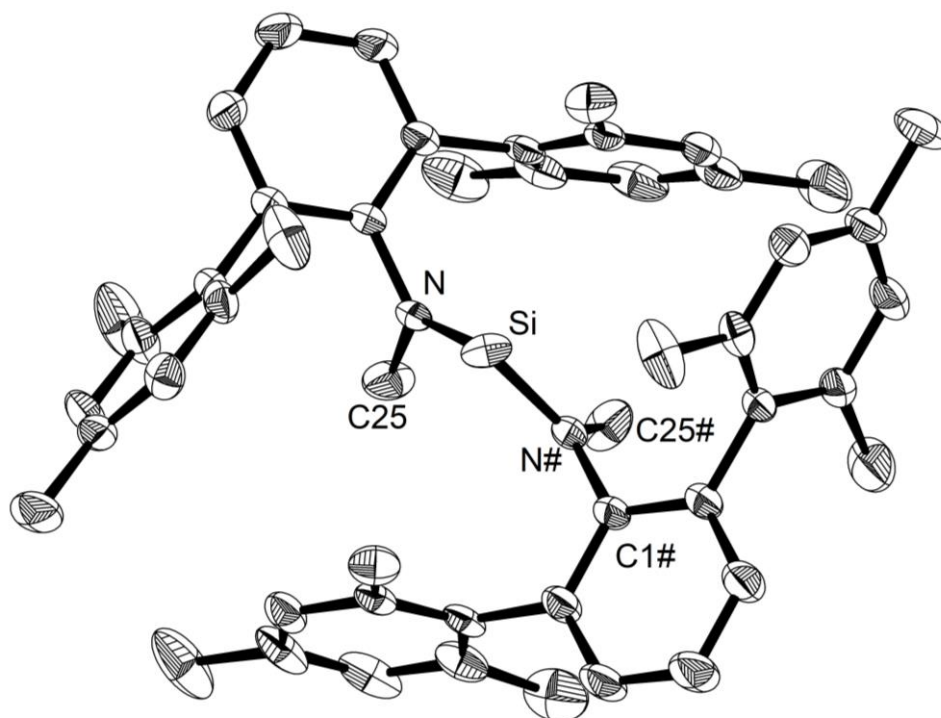


Figure 63. Molecular structure of **18**. Thermal ellipsoids are set to 50 % probability and hydrogen atoms are omitted for simplicity. Selected bond lengths (\AA), angles ($^\circ$) and torsion angles ($^\circ$): Si-N 1.722(1), N-C1 1.439(2), N-C25 1.461(2); N-Si-N# 103.38(9), C1-N-Si 121.6(1), C1-N-C25 114.0(1), C25-N-Si 124.3(1); N-Si-N#-C1# $-150.6(1)$, N1-Si-N#-C25 33.3(1).

The electronic structure of **18^{calc}** was calculated at the B97-D3(BJ)/def2-TZVP level of theory (see appendix, page 283f). Expectedly, an NBO analysis revealed an enormous polarization of the Si-N bonds (86.5% towards N, WBI = 0.62), caused by the high difference in electronegativity. Considerable π -stabilization is expressed by a single Si=N π -bond, that is again mostly located at the respective N atom (87.4 %). Furthermore, electron lone pairs are found at the Si atom (79.5 % s character) and the single-bonded N atom (99.5 % p). This is in agreement with the results of the NRT analysis where the +M effect of the N atoms is reflected by Si-N bonding orders of 1.49 as well as the atomic charges of +1.19 at Si and -0.93 at the N atoms.

Yet the Kohn–Sham orbitals of **18^{calc}** (Figure 64) reveal typical silylene character with an empty p orbital at the Si atom as LUMO and the electron lone pair at the Si atom dominating the HOMO. Here, minor antibonding contribution of the N atoms is found as well and additional combinations of the lone pairs at the Si and both N atoms are found in the HOMO–2. Overall, these findings can be interpreted as the predicted delocalization of 6 electrons over the {N,Si,N} moiety, whereby the character of the lone pair at the Si atom is largely preserved.

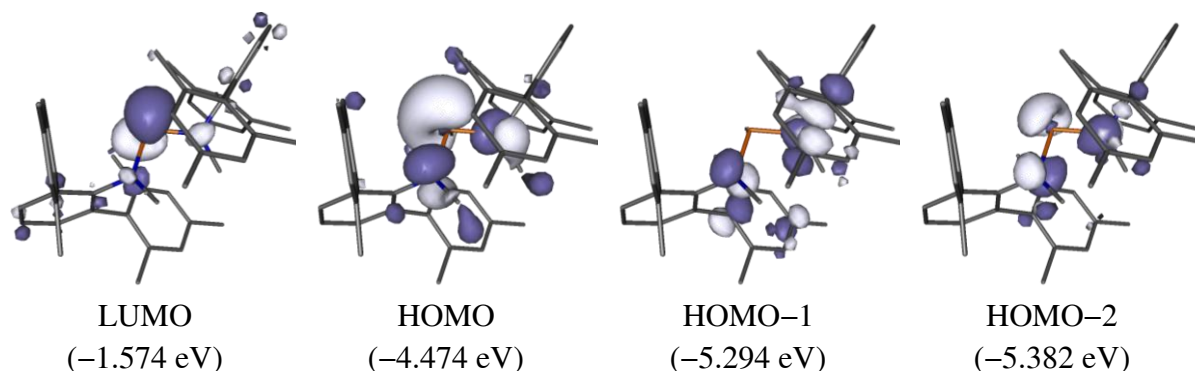


Figure 64. Selected Kohn–Sham orbitals of $\mathbf{18}^{\text{calc}}$ and their corresponding energy eigenvalues; isosurface value: $0.04 \text{ e}\cdot\text{bohr}^{-3}$. B97-D3(BJ)/def2-TZVP level of theory.

The computed HOMO/LUMO energy gap is 2.90 eV, which is larger when compared to other aminosilylenes (Table 26) but considerably smaller when compared to Powers bis(thiolato)silylene $\text{Si}(\text{SAr}^{\text{Mes}})_2$ (4.26 eV).^[95]

Table 26. Comparison of the $\Delta\text{HOMO-LUMO}$ -gaps (in eV) of aminosilylenes.^[40,96,98,100]

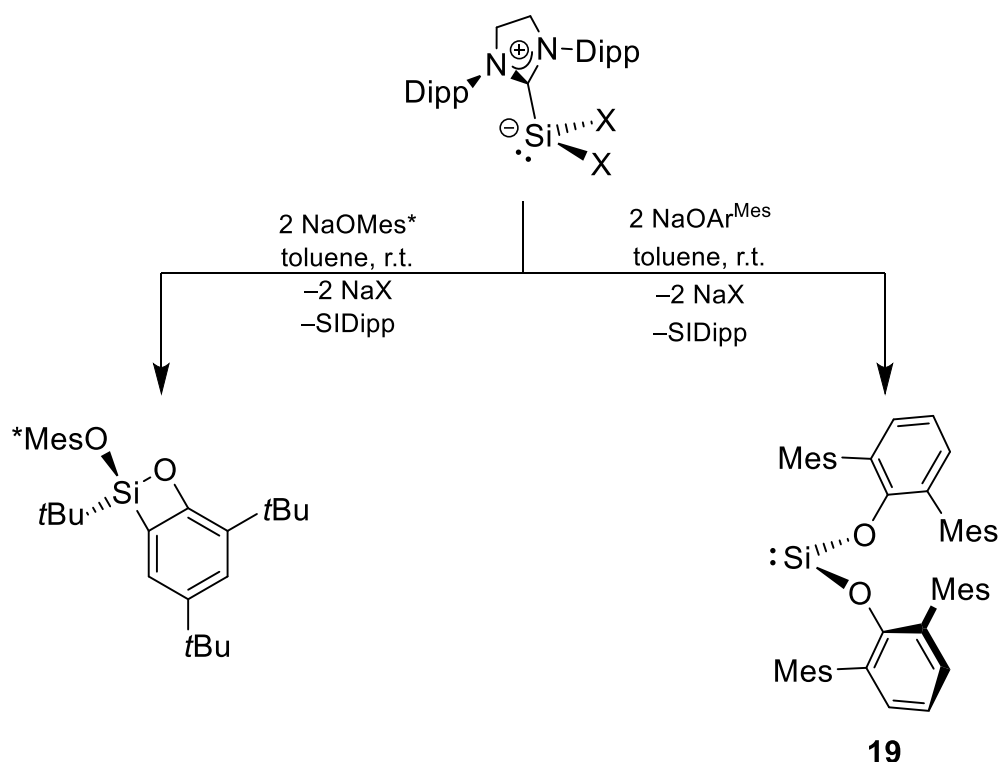
Cpd.	18	A ^{boryl}	A ^{allyl}	B	C
$\Delta\text{HOMO-LUMO}$	2.90	2.04	1.99	2.55	2.54
$\delta_{\text{Si}}/\text{ppm}$	130.3	439.7	438, 467	204.6	319.1

As more electronegative substituents are known to result in higher s character lone pairs (rule of Bent), the HOMO-LUMO gap is expected to grow. This also reasons the experimentally observed upfield shift in ^{29}Si NMR spectroscopy (vide supra).^[99]

3.5 The first di(aryloxy)silylene

Encouraged by the successful synthesis of **16**, **17** and **18**, the substitution approach was chosen for the synthesis of an acyclic di(aryloxy)silylene as well. Indeed, reactions of the silicon dihalides $\text{SiX}_2(\text{SIDipp})$ ($\text{X} = \text{Br}, \text{I}$) with 2.05 equiv. of $\text{NaOAr}^{\text{Mes}}$ in toluene proceeded smoothly at ambient temperature. Accompanied by gradual decolorization of the yellow suspensions within one hour, in situ $^1\text{H-NMR}$ spectroscopy revealed the formation of the first di(aryloxy)silylene $\text{Si}(\text{OAr}^{\text{Mes}})_2$ (**19**) and stoichiometric amounts of free SIDipp (Scheme 47). At that time, **19** was the first example of a base-free compound with a low-valent Si atom to contain a Si-O bond.

Attempts to synthesize analogous silylenes using a variety of alcoholates NaOR ($\text{R} = \text{Ar}^{\text{Trip}}$, Ar^{pTol} , 2,6-*t*Bu-4-Me- C_6H_2 , Mes^* , Mes , *p*Tol or CH_2Ph) were performed together with C. Lippmann in the year 2016 but failed for no obvious reasons.^[385] Only the reaction of $\text{SiI}_2(\text{SIDipp})$ with NaOMes^* ($\text{Mes}^* = 2,4,6\text{-}t\text{Bu}_3\text{-C}_6\text{H}_2$) under identical conditions resulted in the formation of a colorless oxosilacyclobutene, the formal C-C insertion product of the putative silylene, that was fully characterized as part of his bachelor thesis. No intermediates could be detected.^[385]



Scheme 47. Synthesis of the first di(aryloxy)silylene $\text{Si}(\text{OAr}^{\text{Mes}})_2$ (**19**, right, $\text{X} = \text{Br}$ or I). The synthesis of the oxosilacyclobutene (left, $\text{X} = \text{I}$) is described in the bachelor thesis of C. Lippmann.^[385]

After workup, compound **19** was isolated as a colorless, solid in yields of 50 – 70 %, strongly dependent on the quality of the employed precursors: while the reactions were very selective

(I: 98 %, Br: 95 % from in situ ¹H NMR spectroscopy), small amounts of impurities render the separation of **19** and free SIDipp very difficult due to an increased solubility in mixtures. If pure, **19** is sparingly soluble in aliphatic hydrocarbons, moderately soluble in aromatic solvents or diethyl ether and well soluble in thf or dme, but follow-up reactions in ethereal solvents were generally found to be much less selective. The silylene is extremely sensitive towards hydrolysis but thermally stable and only decomposes upon melting at 134 °C.

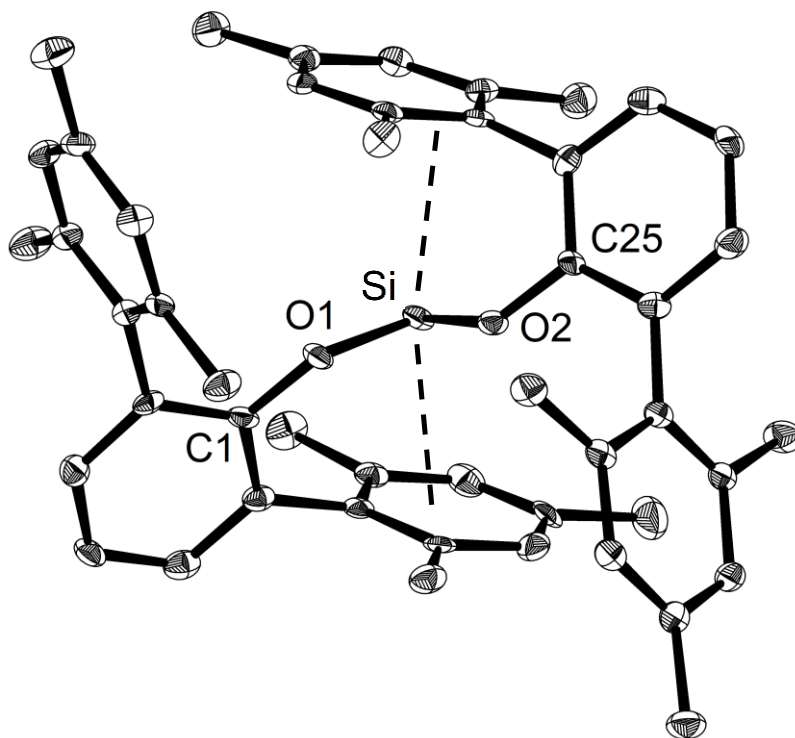


Figure 65. Molecular structure of **19**. Thermal ellipsoids are set to 50 % probability and hydrogen atoms are omitted for simplicity. Selected bond lengths (\AA), angles ($^\circ$) and torsion angles ($^\circ$): Si-O1 1.676(1), Si-O2 1.681(1), O1-C1 1.366(2), O2-C25 1.368(2); O1-Si-O2 93.07(6), C1-O1-Si 131.1(1), C25-O2-Si 128.0(1); C1-O1-Si-O2 142.0(1), C25-O2-Si-O1 147.2(1). A weak π -interaction between the Si atom and two mesityl groups is depicted as dashed lines.

Single crystals were grown by slow evaporation of a benzene solution (Figure 65). Compound **19** is isostructural to Powers famous Si(SAr^{Mes})₂ (**VII**) and the di(amino)silylene **18** and features a V-shaped coordination skeleton, caused by the presence of a stereochemically active lone electron pair at the Si atom. The central O-Si-O bond angle of 93.1(1) $^\circ$ is slightly wider when compared to **VII** (\angle S-Si-S: 90.52(2) $^\circ$) but considerably narrower when compared to Aldridges di(boryloxy)silylene **XI** (\angle O-Si-O: 100.02(8) $^\circ$), which presumably is reasoned by the bulky peripheral Dipp groups in **XI**.^[102] More general, it appears within the range observed for analogous di(aryloxy)tetrylenes E(OAr)₂ (E = Ge, Sn, Pb; \angle O-E-O: 85.9(4) $^\circ$ – 93.9(1) $^\circ$ with one bulky outlier at 100.62(6) $^\circ$; \emptyset 91.6 $^\circ$; see also Table 23 on page 105). A weak π -interaction between the formally vacant p-orbital of the Si atom and the π -electron systems of two of the mesityl groups is observed in the crystal lattice. This results in a sandwich-like arrangement

with nearly parallel mesityl groups ($\approx 5.09(6)^\circ$) with Si...centroid distances of only 3.0965(9) and 3.1151(9) Å below the sum of the van der Waals radii (3.80 Å).^[386] However, those distances are not even close to those in the sandwich complexes SiCp*₂ (about 2.11 Å)^[70] and [Cp*Si][B(C₆F₅)₄] (1.76 Å)^[367] and were not reproduced by gas-phase calculations of the full structure (see page 284 in the appendix), relativizing the strength of the π -interaction to the dimension of a packing effect. Notably, a similar effect was also reported by Clyburne for the analogous di(aryloxy)stannylene Sn(OAr^{Mes})₂ with an inter-plane angle of 2.0(1)° and even shorter Sn...centroid distances of 2.942(2) and 2.980(2) Å.^[351]

Table 27. Structural and ²⁹Si NMR spectroscopic data of **19** and related silylenes (averaged values).

Compound	Si-O /Å	\angle Si /°	\angle O /°	δ_{Si} /ppm	Color	Reference
Si(SAr ^{Mes}) ₂ (VII)	-	90.52(2)	-	285.5	Colorless	^[95]
Si(Eind)OAr ^{Mes} (IX)	1.6699(9)	101.38(5)	127.16(8)	282.6	Yellow	^[40]
Si(NR)(OSitBu ₃) (X)	1.643(1)	103.56(8)	153.2(1)	58.9	Colorless	^[101]
Si{O(TBoN)} ₂ (XI)	\emptyset 1.606(1)	100.02(8)	139.9	35.5	Offwhite	^[102]
SiBr(OtBu)(SIDipp) (16-Br)	1.677(6)	98.7(3) ^A	124.0(5)	18.0	Yellow	This work
SiI(OtBu)(SIDipp) (16-I)	1.675(6)	100.5(5) ^A	126.4(5)	13.2	Yellow	This work
Cp*SiOAr ^{Mes} (17)	1.716(2)	97.79(2) ^B	118.4(2)	-138.2	Colorless	This work
Si(OAr ^{Mes}) ₂ (19)	\emptyset 1.679(1)	93.07(6)	129.6(1)	31.9	Colorless	This work

A: SIDipp is not considered; **B:** the angle between the Si-O bond and the vector towards the C-C bond of the Cp* substituent is given (see Figure 58 on page 114). Mean values are given for compounds **X** and **16-I** with several molecules within the unit cell. All ²⁹Si NMR spectra were measured in benzene-d₆ solution. The molecular structure of compounds **16-Br**, **16-I**, **17** and **19** are depicted on pages 110, 114 and 123.

The averaged Si-O distance of **19** (1.688(3) Å) is nearly identical to that of Si(Eind)OAr^{Mes} (**IX**, 1.6699(9) Å)^[40] or the NHC-supported alkoxy(halo)silylenes **16-Br** and **16-I** (1.677(6) Å and \emptyset 1.675(6) Å). Compared to the bonds in Inoues imino(siloxy)silylene (**X**, 1.643(1) Å)^[101] and Aldridges di(boryloxy)silylene **XI** (1.606(1) Å) the Si-O distance of **19** is longer (Table 27). This finding refutes Aldridges hypothesis, who explained the shorter Si-O distances observed in **XI** by a dominance of the N(π)- over O(π)-donation in **X**.^[102] Compound **19** contradicts this trend (Table 27), yet it should be pointed out, that despite the inevitable electronic stabilization in the silylenes, true Si=O double bonds of three-coordinated silanones are even shorter (1.517 Å – 1.543 Å).^[101,120,387-389] Similar insights were gathered by both ATR-IR and Raman spectroscopy of solid samples (see page 285 in the appendix). Although relatively weak in intensity, bands of the symmetrical and asymmetrical stretching vibrations of the Si-O bonds were detected in the fingerprint region (IR: $\tilde{\nu}_{\text{sym}} = 727 \text{ cm}^{-1}$, $\tilde{\nu}_{\text{sym}} = 714 \text{ cm}^{-1}$; Raman: $\tilde{\nu}_{\text{sym}} = 724 \text{ cm}^{-1}$) and undoubtedly assigned with help of calculations. These bands are within the range given by the model compounds Si(OMe)₂ and Si(OPh)₂ ($\tilde{\nu} = 717 - 740 \text{ cm}^{-1}$) and significantly shifted to lower wavenumbers when compared to the characteristic stretching vibrations reported for Filippous metallasilanone ($\tilde{\nu} = 1157 \text{ cm}^{-1}$)^[120] or Inoues imino(silyl)silanone ($\tilde{\nu} = 1144 \text{ cm}^{-1}$) with distinct Si=O double bonds.^[101] Further investigation of the bonding

situation around the Si atom in **19** by NRT analysis revealed an enormous polarization of the Si-O bonds (93% towards O) as well as the expected +M effect of the adjacent O atoms. This is reflected in both the direct bonding order of 1.39 each (0.16 covalent, 1.23 ionic) and the corresponding Wiberg bond index of only 0.44. Combined with the atomic charges obtained from a natural population analysis (Si: +1.14, O: -0.93), these findings suggest strong Si-O single bonds with separated electron lone pairs at the two oxygen atoms (occupancy of the lone pair orbitals between 1.85 and 1.96 electrons) and thereby overall justify the description of compound **19** as a silylene.

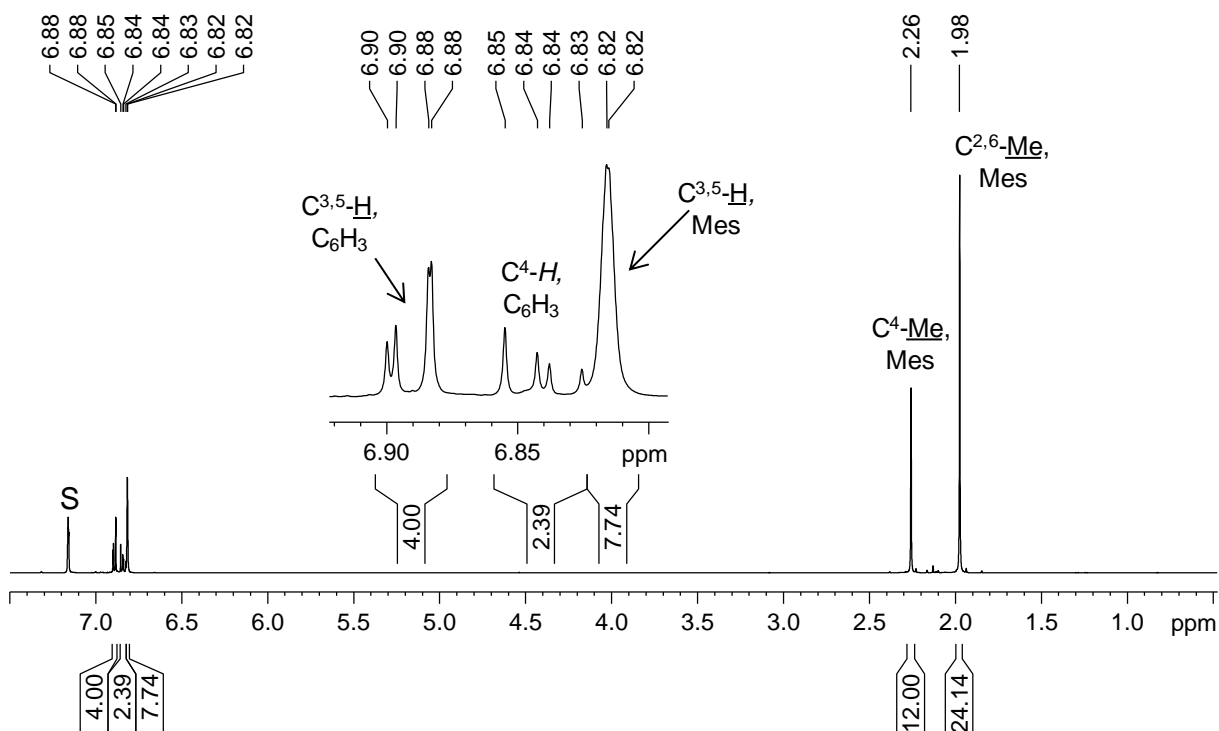


Figure 66. ¹H NMR spectrum (500.2 MHz) of **19** in benzene-d₆. The solvent signal is marked with the character S; an enlarged excerpt displays the aromatic signals.

The ¹H and ¹³C{¹H} NMR spectra of compound **19** in benzene-d₆ solution indicate C_{2v} symmetry with free rotations around the Si-O and/or the O-C bonds (Figure 66). All ¹H and ¹³C resonance signals appear within the expected ranges with the most characteristic signal being the ipso atom of the central ring at δ_c = 148.7 ppm, which is high field from Ar^{Mes}OH (150.2 ppm), LiOAr^{Mes} (160.1 ppm), NaOAr^{Mes} (163.4 ppm) and the heavier congener Sn(OAr^{Mes})₂ (157.8 ppm).^{[351], 33} In contrast to the observations on the +M-effect in **18** (compare Table 25 on page 119), no clear trend was found for the ortho and para positions of the oxy compounds. In the ²⁹Si NMR spectrum (Figure 67), a sharp singlet signal arises at δ_{si} = 31.9 ppm. This is

³³ Clyborne and coworkers also describe the synthesis of the germylene Ge(OAr^{Mes})₂, starting from 2 equiv. Ar^{Mes}OH and Ge{N(SiMe₃)₂}, but the respective NMR data from dichloromethane-d₂ solution appear to be incomplete, most likely due to low solubility: only seven signals of aromatic carbon atoms were detected, with a maximum chemical shift of δ_c = 138.1 ppm, and no assignment is given by the authors.^[351]

remarkably upfield from those of the bis(thiolato)silylene **VII** (285.5 ppm)^[95] or **IX** ($\delta_{\text{Si}} = 282.6$ ppm)^[40] but matches the chemical shifts of **X** ($\delta_{\text{Si}} = 58.9$ ppm) and especially Aldridges di(boryloxy)silylene **XI** ($\delta_{\text{Si}} = 35.5$ ppm; for an overview see also Figure 60 on page 116).

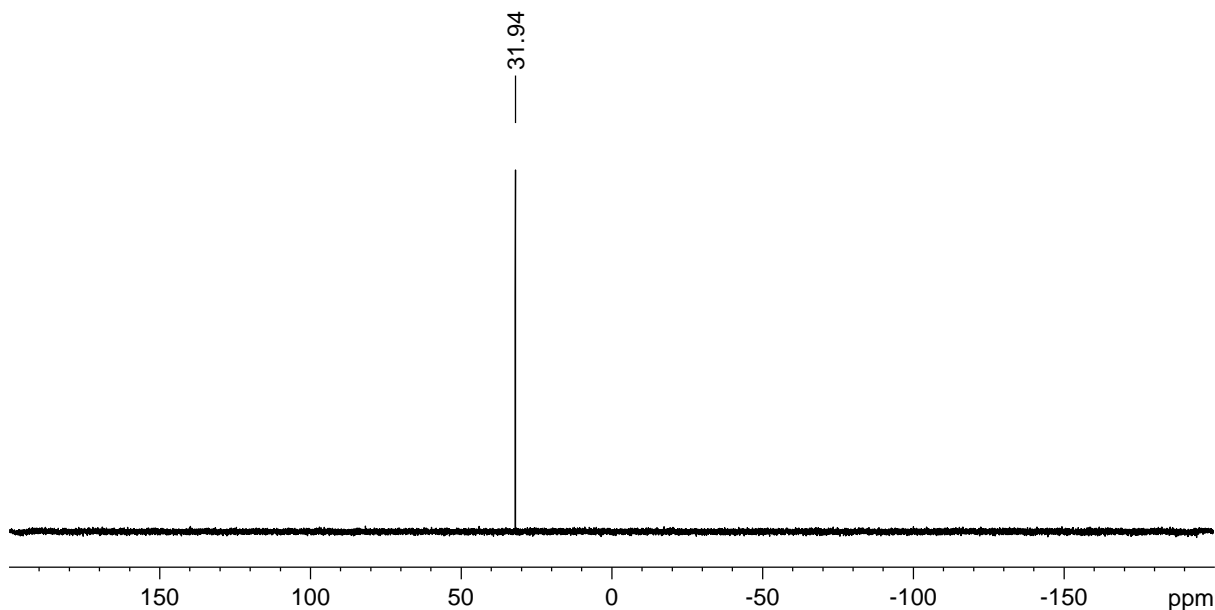


Figure 67. $^{29}\text{Si}\{^1\text{H}\}$ NMR spectrum (99.37 MHz) of **19** in benzene- d_6 .

The UV/Vis-NIR absorption spectrum of a colorless thf solution (Figure 113 on page 271 in the appendix) revealed its longest wavelength absorption at $\lambda_{\text{max}} = 284$ nm ($\epsilon = 7.68 \cdot 10^4$ L·mol $^{-1}$ ·cm $^{-1}$). The adsorption profile could also be quantitatively reproduced by TDDFT calculations on the optimized structure, although the computed bands are considerably shifted. Expectedly, the longest wavelength transition in **19**^{calc} is dominated by the HOMO/LUMO transition (86 %), which involves the n. lone pair and the vacant p orbital at the Si atom (Figure 115 on page 272). In fact, Maier et. al. already concluded, that “unexpectedly short-waved UV adsorptions of alkoxy-silylenes are inherent” to this class based on spectroscopic studies in argon matrices, which is illustrated on the magnitude of the hypsochromic shift in for the row SiMe $_2$, Si(OMe)Me and Si(OMe) $_2$ ($\lambda_{\text{max}} = 460$ nm, 377 nm and 243 nm, respectively).^[372,373]

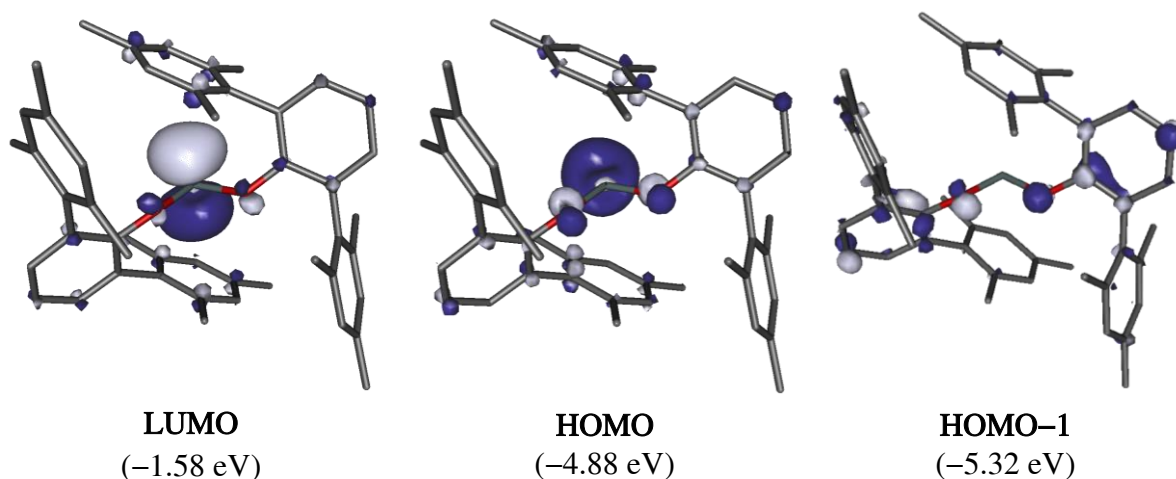


Figure 68. Selected Kohn-Sham orbitals (RI-B97-D3/def2-TZVP) of **19**^{calc} and their corresponding energy eigenvalues; isosurface value: 0.05 e bohr⁻³. Hydrogen atoms are omitted for simplicity.

The electronic structure of **19** was studied by DFT calculations at the RI-B97-D3/def2-TZVP level of theory and NBO analysis revealed the characteristics of a silylene (Figure 68). Expectedly, the HOMO mainly consists of a lone pair at the Si atom with a high *s* character of 86 % and is followed by a mostly O-centered HOMO–1 which is lower in energy by only 0.44 eV. The LUMO represents a lone vacancy at the Si atom (99% *p* character) with a relatively high HOMO/LUMO energy difference of 3.3 eV. This is higher than the gaps of the aminosilylenes (1.99 – 2.90 eV, see Table 26 on page 121), but appears to lie well within the range of reported oxysilylenes (2.55 – 5.45 eV, Table 28).^[40,95,101,102]

Table 28. Calculated energy differences between the highest occupied and the lowest unoccupied molecular orbital in **19** and related silylenes reported in the literature.^[40,95,101,102]

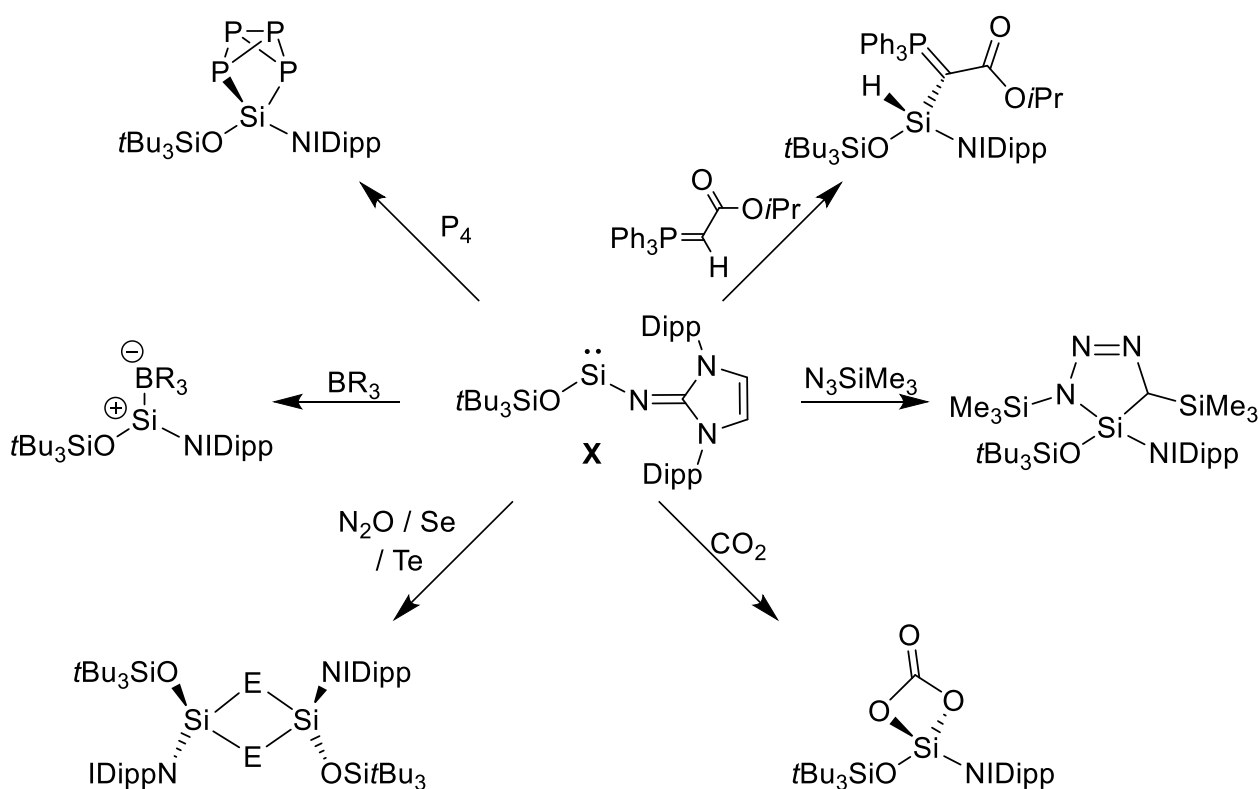
Compound	19	VII	IX	X	XI
$\Delta E_{\text{HOMO/LUMO}} / \text{eV}$	3.30	4.26	2.55	4.33	5.45

The tendency to a higher energy separation can be addressed to two factors: while π -donations destabilize the LUMO, the HOMOs absolute energy is lowered by the more electronegative oxygen atoms.^[68] In fact, the lower energy separation in the aryl(aryloxy)silylene **IX** (2.55 eV) appears to be an outlier due to its much less electronegative Eind substituent, while the boryloxy substituents in **XI** were even designed to achieve a maximum of π -stabilization and a HOMO/LUMO-gap as wide as possible to increase the stability.^[102] When comparing the excitation energies of **19** with those of the closely-related di(thiolato)silylene **VII** (4.26 eV) or the di(boryloxy)silylene **XI** (5.45 eV), compound **19** has the by far lowest gap and is thus potentially more reactive towards electron-rich substrates.

3.6 Reactivity of $\text{Si}(\text{OAr}^{\text{Mes}})_2$

Historically, the generation of silylenes as transient intermediates or at low temperatures has often been proven by trapping experiments with a large scope of substrates. These reactions utilize the pronounced electrophilicity of silylenes, which in case of **19** is tamed by the +M-effect and the steric bulk of the adjacent oxy substituents.

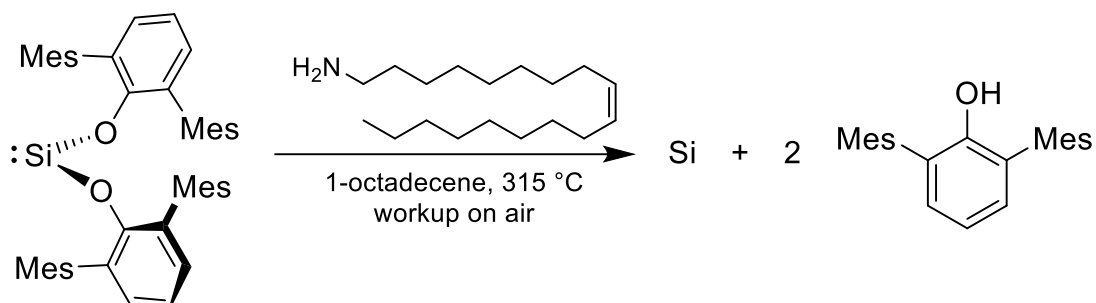
A preliminary reactivity study of **19** towards the very small and highly reactive substrates HCl, Br₂, I₂ and MeI as well as oxidation by SiBr₄ (vide infra) has already been outlined in the bachelor thesis of C. Lippmann in 2016.^[385] Also the group of Inoue reported on the rich chemistry of their imino(oxy)silylene **X** in 2019 and 2020. These reactions include insertion of the silylene center into polar hydrogen bonds, activation of small molecules such as P₄ and CO₂, oxidation with chalcogens and coordination towards boranes (Scheme 48). Additionally, the authors investigated reactions with different silyl azides as well as base-coordination reactions that led to complex product mixtures.^[390,391]



Scheme 48. Reactivity of Inoue's imino(oxy)silylene **X**.^[390,391] BR₃ = BPh₃ or B(C₆F₅)₃; E = O, Se, Te.

3.6.1 Thermolysis of Si(OAr^{Mes})₂

As mentioned before, Boyle and coworkers demonstrated the use of Ge(OAr)₂ as a bulk material for the production of crystalline germanium(0) nanowires by thermolysis in solution at ~300 °C some years ago.^[332,343] Thermolysis of a large sample of silylene **19** in an oleylamine/1-octadecene mixture (1:4) at 315 °C for 1 – 2 h resulted in the selective formation of Ar^{Mes}OH as only Ar^{Mes}-containing product according to GC/MS analysis (Scheme 49).³⁴ Unfortunately, the formation of a viscous gel made precipitation or enrichment of Si nanoparticles by standard methods impossible (the total Si content of **19** is only 4 mass%). The evaporated solution was thus analyzed by Dr. W. Assenmacher using a combination of Energy-dispersive X-ray spectroscopy (EDX) and transmission electron microscopy (TEM).



Scheme 49. The thermolysis of **19** yields Ar^{Mes}OH and Si “nanoparticles”.

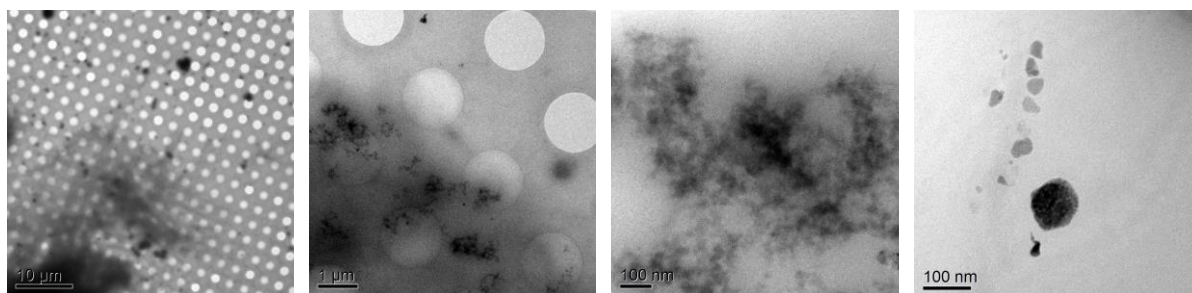


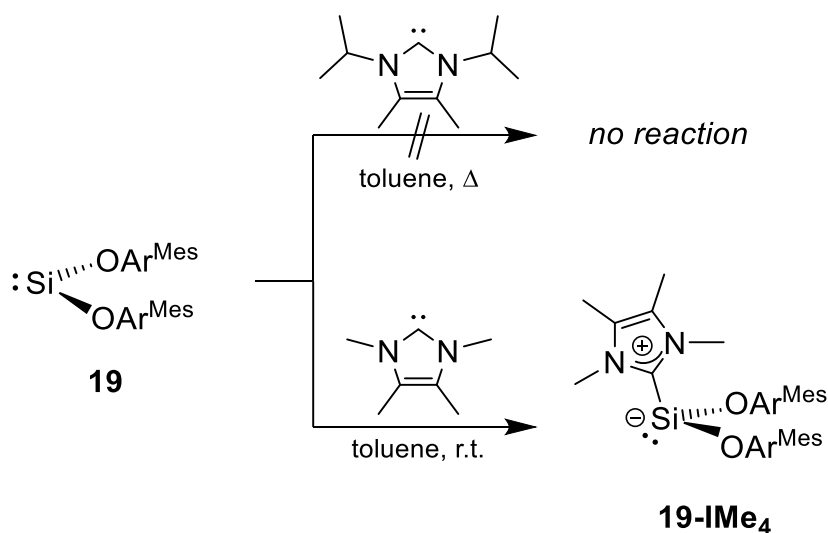
Figure 69. TEM recordings of the Si-particles obtained from the thermolysis of **19**. The particles are agglomerated and coated with a gel of Ar^{Mes}OH/oleylamine.

The formation of elemental silicon could be verified by these methods, but the Ar^{Mes}OH/oleylamine gel inhibited the recording of high-resolution images (Figure 69, for details see chapter 4.6.22 on page 216). Agglomeration of Si nanoparticles is not uncommon and was attributed to “the strong hydrophobic character of silicon hydride termination and their high surface energy” by Rütteli before.^[392]

³⁴ Silicon nanoparticles are usually obtained by the sol-gel method or chemical reduction of SiCl₄. For a recent paper on the synthesis of silicon nanoparticles see reference ^[392] and for a recent review on synthesis and applications of silica (SiO₂) nanoparticles see reference ^[393].

3.6.2 Base coordination

The synthesis of **19** is accompanied by the loss of SIDipp and despite numerous attempts, no intermediate could be observed under altered reaction conditions. For steric reasons, a potential intermediate “Si(OAr^{Mes})₂(SIDipp)” with three large substituents is not sustainable according to calculations. However, formation of a monosubstituted “SiX(OAr^{Mes})(SIDipp)” intermediate akin to the isolable oxy(halo)silylenes **16-X** could not be excluded. To test whether an NHC-supported di(aryloxy)silylene is electronically stable or if the +M-effect of the O atoms inevitably cleaves the carbene, compound **19** was reacted with IMe₄ and IiPr₂Me₂ (Scheme 50). Interestingly, the expected base-adduct **19-IMe₄** could be isolated as a lemon yellow powder in 68 % yield, whereas no reaction occurred with the larger carbene. **19-IMe₄** inhibits an increased solubility when compared to its precursor and was found to slowly decompose in solution as evidenced by the slow precipitation of an off-white material (*vide infra*). This matches the reports of Inoue, who later observed no reaction of his derivative with IiPr₂Me₂ or 4-DMAP whereas a complex mixture of products was obtained after warming a mixture of **X** and IMe₄ from -130 °C to ambient temperature. However, the formation of base-stabilized silylenes (L = IMe₄, IEt₂Me₂, 4-DMAP) was indirectly verified by subsequent oxidation to the NHC-stabilized silaesters IdippNSi(O)OSi(tBu)₃(L) at low temperatures.^[390]



Scheme 50. Reaction of **19** with IMe₄ to the base-adduct **19-IMe₄**; no reaction occurs with the larger IiPr₂Me₂.

Compound **19-IMe₄** was characterized spectroscopically as well as by XRD. Multinuclear magnetic resonance spectroscopy in benzene-d₆ revealed a C_s symmetric structure of **19-IMe₄** in solution with blocked rotations of the substituents as evidenced by the inequivalence of all four methyl groups of the IMe₄ substituent in combination with equivalent terphenyls. In the ¹³C{¹H} NMR spectrum, the indicative N_CN carbene resonance (δ_c = 164.1 ppm) is significantly shielded in respect to the free NHC (212.7 ppm)^[394] and compares very well to the NHC-stabilized aryl(chloro)silylene Ar^{Mes}SiCl(IMe₄) (165.2 ppm). The ²⁹Si{¹H} NMR resonance

at $\delta_{\text{Si}} = 7.5$ ppm matches those of **16-Br** and **16-I** (18.0 and 13.2 ppm) as well as other typical NHC-stabilized silylenes (usually around 10 ppm). Remarkably, two separate signals were detected by $^{15}\text{N}\{^1\text{H}\}$ NMR spectroscopy at $\delta_{\text{N}} = 174.8$ and 176.8 ppm, but the chemical shifts are uncharacteristic considering free IME_4 resonates at a nearly identical field ($\delta_{\text{N}} = 178.8$ ppm).^[395]

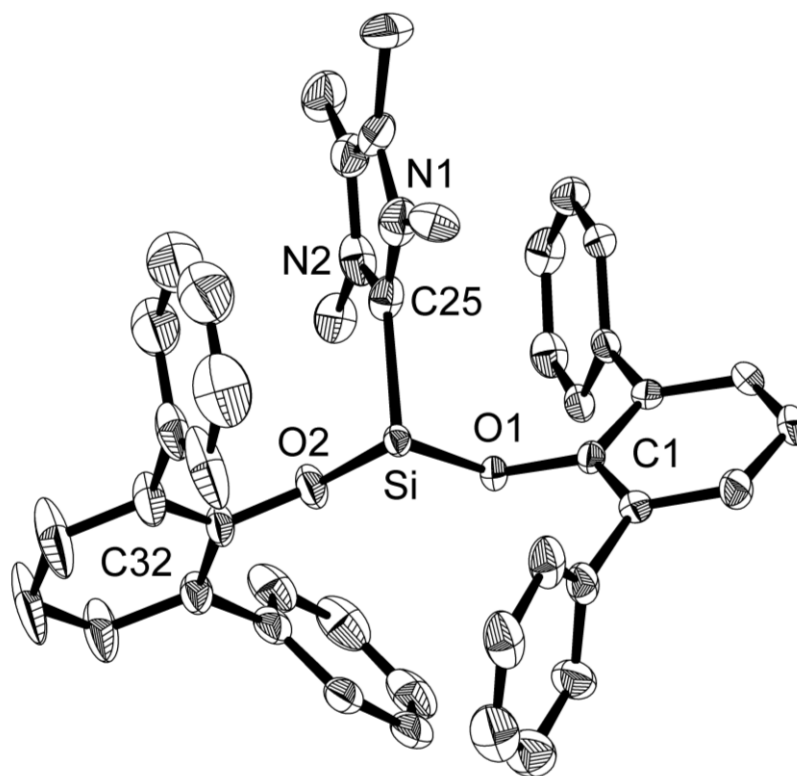


Figure 70. Molecular structure of **19-IME₄**. Thermal ellipsoids are set to 50 % probability; methyl groups of the mesityl substituents as well as hydrogen atoms are omitted for simplicity. The structural data contain a crystallographic side occupancy (ca. 19 % disorder at the {Si(IME₄)} moiety) which was solved independently. Selected bond lengths (Å) and angles (°): Si1-O1 1.715(2), Si1-O2 1.684(3), Si1-C25 2.013(5), O1-C1 1.358(3), O2-C32 1.336(4), O1-Si1-C25 97.3(2), O2-Si1-O1 92.8(1), O2-Si1-C25 96.5(2), C1-O1-Si1 123.8(2), C32-O2-Si1 140.1(3).

Crystals of **19-IME₄** suitable for X-ray structure analysis were obtained by evaporation of a solution in a mixture of benzene and n-pentane at ambient temperature (Figure 70). Expectedly, **19-IME₄** is best described as a classical NHC-stabilized silylene with a highly pyramidalized (82 %) Si center and a stereoactive electron lone pair. Obeying Bent's rule, a clear trend is found when comparing to the NHC-stabilized alkoxy(halo)silylenes **16-Br** (84%) and **16-I** (Ø81 %), the less electronegative dihalides $\text{SiX}_2(\text{IDipp})$ (X = Cl: 78 %, X = Br: 75 %, X = I: 70 %)^[112–114] or $\text{Ar}^{\text{Trip}}\text{SiCl}(\text{IME}_4)$ (67.6 %).^[396] The Si-O bonds (Ø1.700(3) Å) are slightly elongated when compared to the two-coordinated starting material **19** (Ø1.679(1) Å) or the NHC-stabilized alkoxy(halo)silylenes **16-Br** and **16-I** (1.677(6) and 1.675(6) Å), which might just be explained by the saturation of the lone vacancy with the stronger donor IME_4 and the concomitant reduction of $\text{O} \rightarrow \text{Si}$ π -donation. Likewise, the central O-Si-O angle of 92.8(1)° is

almost identical to that in the donor-free silylene **19** (93.07(6)°) and remains relatively narrow when compared to other base-stabilized silylenes (typically around 100°), allowing a more flexible orientation of the substituents when compared to direct Si-aryl bonds. Nevertheless, the steric overload becomes apparent at the IME_4 , that is encapsulated and locked from rotations between two of the mesityl groups ($\approx 1.2(3)^\circ$ and $2.7(2)^\circ$).

The aforementioned slow decomposition of **19-IME₄** leads to the precipitation of a sparingly soluble, offwhite solid of unknown composition. Interestingly, ^1H and ^{13}C NMR spectroscopy suggested a 1:1 ratio of Ar^{Mes} and IME_4 and a characteristic ^{29}Si NMR signal was found at $\delta_{\text{Si}} = -62.8$ ppm in benzene- d_6 . This is considerably high field from both **19-IME₄** (7.5 ppm) or $\text{Ar}^{\text{Mes}}\text{SiCl}(\text{IME}_4)$ (-1.3 ppm) and well within the range of reported base-stabilized silyliumylidene ions like $[\text{SiI}(\text{IME}_4)(\text{IDipp})]\text{I}$ (-55.3 ppm in dichloromethane- d_2)^[114] or $[\text{SiAr}^{\text{Mes}}(\text{IME}_4)_2]\text{Cl}$ (-78.9 ppm in acetonitrile- d_3)^[397] but is not as shielded as the dication $[\text{Si}(\text{IME}_4)_3]\text{I}_2$ (-89.9 ppm in dichloromethane- d_2). It can thus be speculated that the addition of IME_4 to **19** results in an electronic and steric overload that ultimately causes the delayed cleavage of a Si-O bond to “[$\text{Si}(\text{IME}_4)_2(\text{OAr}^{\text{Mes}})]$ ” $[\text{OAr}^{\text{Mes}}]$ and some unknown polymeric byproduct.

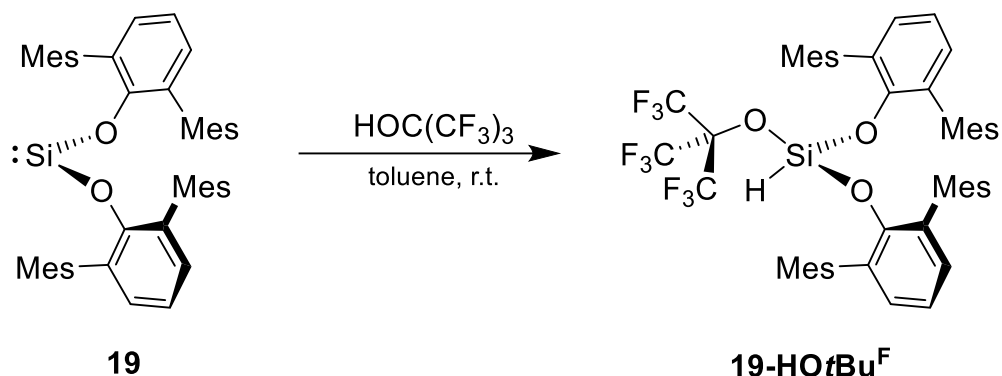
3.6.3 Protonation

Typical for a silylene, compound **19** is extremely sensitive towards hydrolysis. The reaction with stoichiometric amounts of water in cold thf led to the oxidative addition product $\text{SiH}(\text{OH})(\text{OAr}^{\text{Mes}})_2$ (**19-H₂O**),³⁵ but some $\text{Ar}^{\text{Mes}}\text{OH}$ was formed as well due to partial overreaction or intermolecular condensation. Subsequent addition of a small excess of water then gave $\text{Ar}^{\text{Mes}}\text{OH}$ as the only aryl containing component. Likewise, $\text{SiHCl}(\text{OAr}^{\text{Mes}})_2$ (**19-HCl**) was first obtained by C. Lippmann in 2016 upon protonation of **19** with a diluted solution of HCl in diethyl ether and described in his bachelor thesis.^[385] In this work, the same compound was instead obtained from SiHCl_3 and 2 equiv. of $\text{NaOAr}^{\text{Mes}}$.

Protonation of **19** was extended to nonafluoro-tert-butyl alcohol ($\text{HOC}(\text{CF}_3)_3$). The reaction was performed in toluene solution at ambient temperature and smoothly proceeded to the tri(oxy)silane $\text{SiH}(\text{OC}(\text{CF}_3)_3)(\text{OAr}^{\text{Mes}})_2$ (**19-HOtBu^F**), which was isolated as colorless, moderately

³⁵ $\text{SiH}(\text{OH})(\text{OAr}^{\text{Mes}})_2$ was characterized spectroscopically: $^1\text{H NMR}$ (500.2 MHz, benzene- d_6 , 298 K): δ /ppm = 0.82 (s, $^3J_{\text{H,H}} = 2$ Hz, 1H, O-H), 1.94 (s, 12H, 2 \times C²-Me, Mes), 1.97 (s, 12H, 2 \times C⁶-Me, Mes), 2.23 (s, 12H, 2 \times C⁴-Me, Mes), 3.08 (s, $^1J_{\text{Si,H}} = 314$ Hz, $^3J_{\text{H,H}} = 2$ Hz, 1H, Si-H), 6.84, 6.87 (each s, each 4H, 4 \times C³-H, and 4 \times C⁵-H, Mes), 6.90 (m, 6H, 2 \times C⁴-H and 2 \times C^{3,5}-H, C₆H₅). $^{29}\text{Si}\{^1\text{H}\}$ NMR (99.37 MHz, benzene- d_6 , 298 K): δ /ppm = -68.8 (s).

air-sensitive crystals in 76 % yield after recrystallization from diethyl ether (Scheme 51). Compound **19-HOtBu^F** is well soluble in aromatic or ethereal solvents, moderately soluble in aliphatic hydrocarbons and thermally very robust (decomposition upon melting at 202 °C).



Scheme 51. Synthesis of **19-HOtBu^F** by oxidative addition of HOC(CF₃)₃.

The oxidative addition reduces the overall symmetry from C_{2v} to C_s. Hindered rotations of the {OAr^{Mes}} groups cause an inequivalence of the ortho-methyl groups akin to the spectroscopic features of **19-HCl** and **19-IMe₄**. The Si-H proton resonates at δ_H = 3.67 ppm in form of a characteristic decet signal (resolved as an octet due to technical limitations, see Figure 71) and is flanked by nicely resolved ²⁹Si satellites (¹J_{Si,H} = 359 Hz). This signal lies in a somewhat common field for silanes and appears slightly high field compared to SiH(OMe)₃ (δ_H = 4.18 ppm in chloroform-d₁) or SiH(OPh)₃ (δ_H = 5.02 ppm in chloroform-d₁). Consequently, a weak band corresponding to the Si-H stretching vibration was found in the ATR-IR spectrum at $\tilde{\nu}$ = 2297 cm⁻¹, which is at higher wavenumbers than typical tri(oxy)silanes such as SiH(OPh)₃ ($\tilde{\nu}$ = 2200 cm⁻¹)^[398] due to the electron withdrawing CF₃ groups.

The ²⁹Si NMR resonance was found as an intensive doublet signal at δ_{Si} = -84.4 ppm (¹J_{Si,H} = 359 Hz). This is heavily shielded in respect to the precursor **19** (31.9 ppm) and primarily an effect of the higher coordination number. The chemical shift compares very well to related aryloxy(halo)silanes SiX_nR_{2-n}(OAr)₂ and fairly well to all other silanes SiRR'(OAr^{Mes})₂ obtained from **19** that have at least one additional electronegative substituent (vide infra). When it comes to ²⁹Si NMR spectroscopy, the exact number of oxy substituents hence appears to only play a subordinate role.

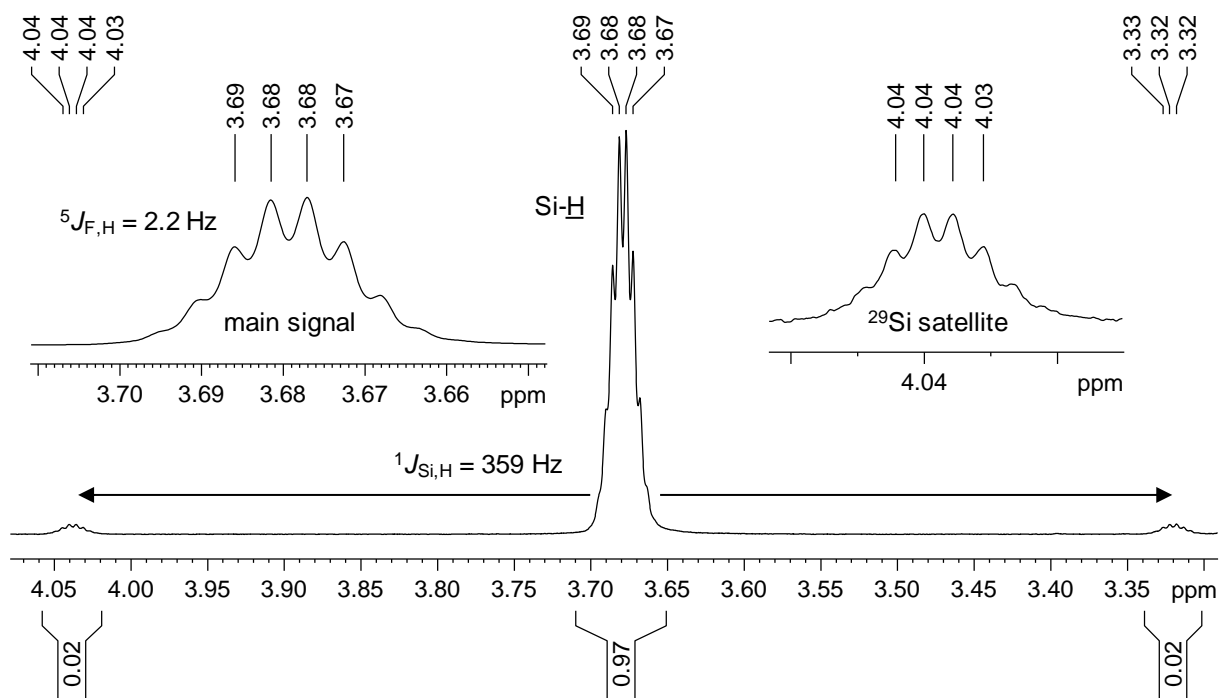


Figure 71. Excerpt of the ^1H NMR (500.2 MHz) spectrum of **19-HOtBu^F** in benzene- d_6 at 298 K; further enlarged excerpts displaying the Si-H main signal (left) and one of the ^{29}Si satellites (right) are depicted in the insets.

Colorless plates of **19-HOtBu^F** suitable for XRD analysis were obtained by cooling a concentrated solution in diethyl ether to $-30\text{ }^\circ\text{C}$ for 4 days. Solid-state structures of mixed oxysilanes are generally extremely rare and surprisingly, no x-ray diffraction structures of any four-coordinated trioxy(hydrido)silane has been reported yet.³⁶ Thus, **19-HOtBu^F** appears to be the first example of a four-coordinated tri(oxy)silane $\text{Si}(\text{OR})_3\text{X}$ (R = any carbon-based substituent, X = hydrogen or halogen) with no additional hypercoordination to be structurally characterized by X-ray diffraction. Expectedly, the central Si atom in **19-HOtBu^F** is adopts a distorted tetrahedral geometry. Due to the increased coordination number, the nearly equal Si-O distances (1.611(4) to 1.650(4) Å, O 1.625(4) Å) are a bit shorter when compared to the bonds found in silylene **19** (O 1.679(1) Å). This is noteworthy since greater individual $\text{O}(\pi)\rightarrow\text{Si}(\pi^*)$ contributions are expected for **19**. Oxidative addition not only leads to a decrease of the Si-O bond lengths but also an increase of the O-Si-O angles ($104.2(2)^\circ$ to $111.0(2)^\circ$; Σ_{Si} : 319.8°) that are widened in respect to the starting material (**19**: $93.07(6)^\circ$). This observation is in agreement with Bent's rule which explains O-Si-O angles below 109.5° (which is expected for an ideal tetrahedron) with an high p-electron density in the corresponding hybrid orbitals that results in narrower angles.^[399] While the core $\{\text{SiHO}_3\}$ moiety of **19-HOtBu^F** is relatively undisturbed by the steric pressure of the substituents, those impact can be seen in the proximate Si-O-C angles,

³⁶ On the basis of a CSD 5.4.1 search for molecular compounds $\text{SiH}(\text{OR})$ (R = any carbon-based substituent) with four-coordinated Si atoms, no result was found. However, two five-coordinated trigonal bipyramidal silatranes $\text{SiH}\{(\text{alkoxy})_3\text{N}\}$ containing N-chelating derivatives of the triethanolamine substituent, one five-coordinated salt $[\text{K}(18\text{-crown-6})][\text{SiH}_2(\text{OiPr})_3]$ and four structures of hydrosilasesquioxane clusters $[\text{RH}_{n-1}\text{Si}_n\text{O}_{1.5n}]$ ($n = 8$ or 10) have been reported.

which are significantly bend open ($\angle\text{Si-O-C}$: $139.4(4)^\circ$). All three angles are much larger when compared to the one found in the less crowded silylene **19** ($129.6(1)^\circ$).

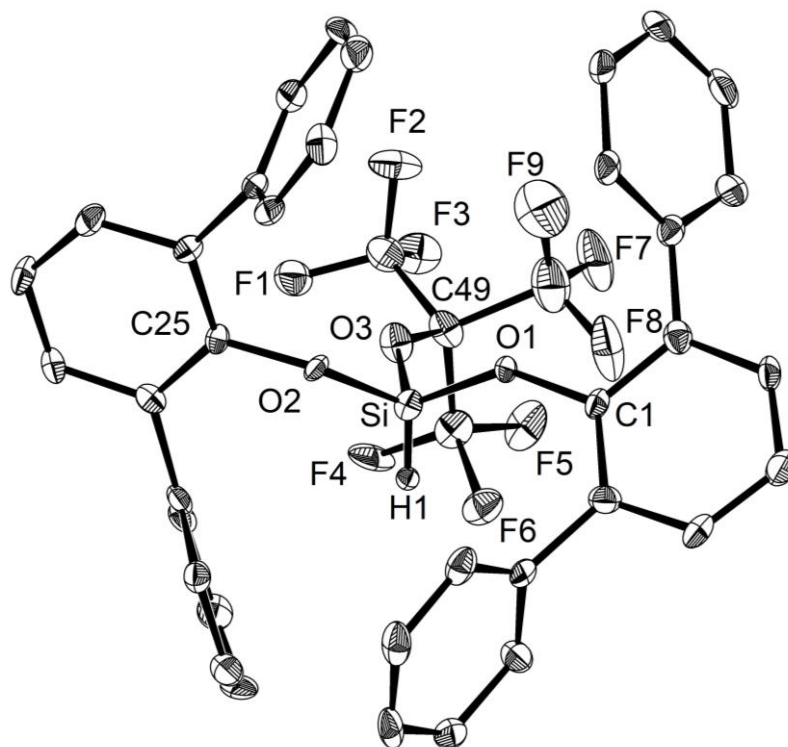
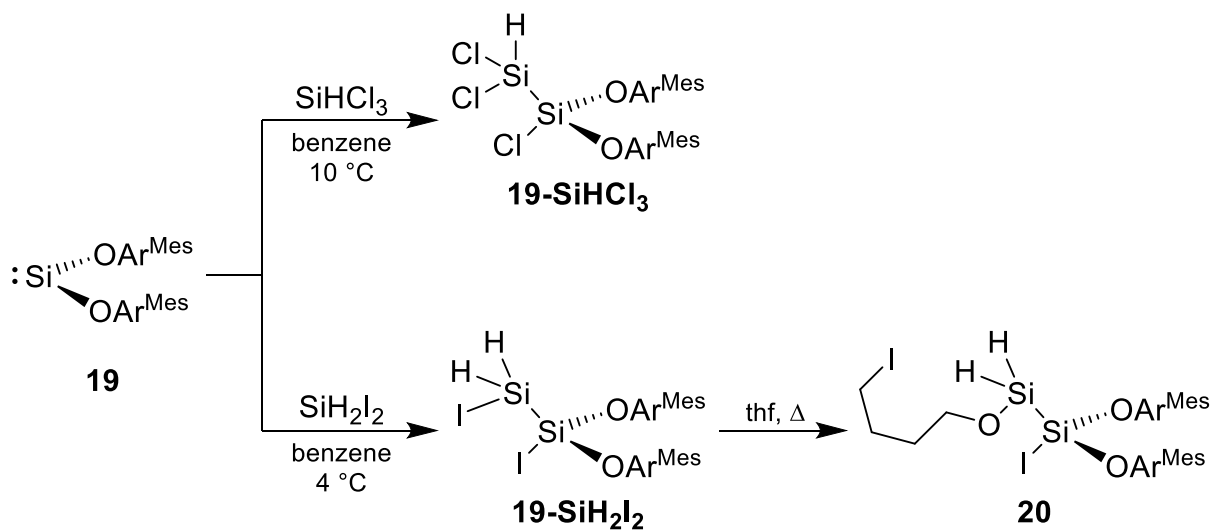


Figure 72. Molecular structure of **19-HOtBu**. Thermal ellipsoids are set to 50 % probability; peripheral methyl groups as well as hydrogen atoms except for the Si-H atom are omitted for simplicity. The structural data contain a small crystallographic site occupancy (ca. 7 % disorder) which was solved independently. Selected bond lengths (\AA) and angles ($^\circ$): Si-O1 1.615(4), Si-O2 1.611(4), Si-O3 1.650(4), O1-C1 1.391(7), O2-C25 1.402(7), O3-C49 1.390(7); O1-Si-O2 104.6(2), O1-Si-O3 111.0(2), O2-Si-O3 104.2(2), C1-O1-Si 141.7(4), C25-O2-Si 137.1(4), C49-O3-Si 139.5(4).

3.6.4 Silane activation

After protonation, the reactivity of **19** towards molecules with formally hydridic hydrogen atoms appeared to be an interesting subject. Because **19** was found to be inert towards an excess of SiHEt_3 , the halosilanes SiHCl_3 and SiH_2I_2 with stronger $-I$ -substituents were chosen as substrates instead. Contrary to intuition, the reactions led to the very selective formations of the disilanes $\text{SiCl}(\text{SiHCl}_2)(\text{OAr}^{\text{Mes}})_2$ (**19-SiHCl₃**) and $\text{SiI}(\text{SiH}_2\text{I})(\text{OAr}^{\text{Mes}})_2$ (**19-SiH₂I₂**) as a result of insertion into the respective Si-halogen bonds instead of the anticipated Si-H insertion products (Scheme 52).



Scheme 52. Synthesis of the disilanes **19-SiHCl₃** and **19-SiH₂I₂** and its subsequent reaction with thf to **20**.

The activation of the strong Si-Cl bond is surprising (Table 29), but since equally strong bonds are formed in either case, no simple thermodynamic prediction can be made. It is likely, that the reactions are kinetically controlled by the more easily accessible Si-halogen bonds.

Table 29. Experimental bond energies (BE) and bond dissociation energies (BDE) from $\text{Me}_3\text{Si-X}$ ($\text{X} = \text{H}, \text{Cl}, \text{I}$).

	Si-H	Si-Cl	Si-I
BE / $\text{kJ}\cdot\text{mol}^{-1}$	295 ^[400]	359 ^[400]	213 ^[400]
BDE / $\text{kJ}\cdot\text{mol}^{-1}$	378 ^[401]	473 ^[401]	322 ^[401]

Compound **19-SiHCl₃** could be isolated as a colorless solid in quantitative yield and analytically pure form by simple evaporation of all volatiles. While still somewhat sensitive towards hydrolysis, the solid is thermally extremely robust and melts at $229\text{ }^\circ\text{C}$ with no sign of decomposition. The congener **19-SiH₂I₂** was isolated as a colorless solid in 92 % yield after washing with cold n-hexane at $-30\text{ }^\circ\text{C}$ and is extremely sensitive towards air/moisture. Whereas **19-SiHCl₃** shows the typical solubility trend of similar compounds (very soluble in thf, well soluble in aromatics or diethyl ether and a little less soluble in aliphatic hydrocarbons), **19-SiH₂I₂** displays an anomaly: it is again well soluble in aromatic solvents and not so soluble in aliphatic

hydrocarbons but nearly insoluble in diethyl ether for unknown reasons. Compound **19-SiHL** is also highly soluble in thf but slowly undergoes a ring opening insertion reaction at the SiH₂ atom yielding SiI{SiH₂(OC₄H₈I)}(OAr^{Mes})₂ (**20**, Scheme 52). On a synthetic scale the conversion into **20** was achieved by heating a thf solution of **19-SiHL** to 65°C overnight and subsequent crystallization of the crude product from Et₂O and Et₂O/n-hexane (1:4). Compound **20** is highly soluble in all common solvents.

The ¹H and ¹³C{¹H} NMR spectra of **19-SiHCl** and **19-SiHL** display C_s symmetry in solution as evidenced by the inequality of the two ortho and meta positions of the mesityl rings. Noteworthy, the aromatic ¹H NMR signals of the central ring system of **19-SiHCl** in benzene-d₆ coincide to only one intensive singlet signal (Figure 73, left) but show the regular pattern of a separated doublet and a triplet signal in chloroform-d₁ (Figure 73, right). While this phenomenon could be explained by a coincidental isochrony as demonstrated by spectral simulation (Figure 74), the same effect in benzene-d₆ solution was as well observed for the derivatives **19-BI**, **19-PCl** and **21-Cl** (vide infra).

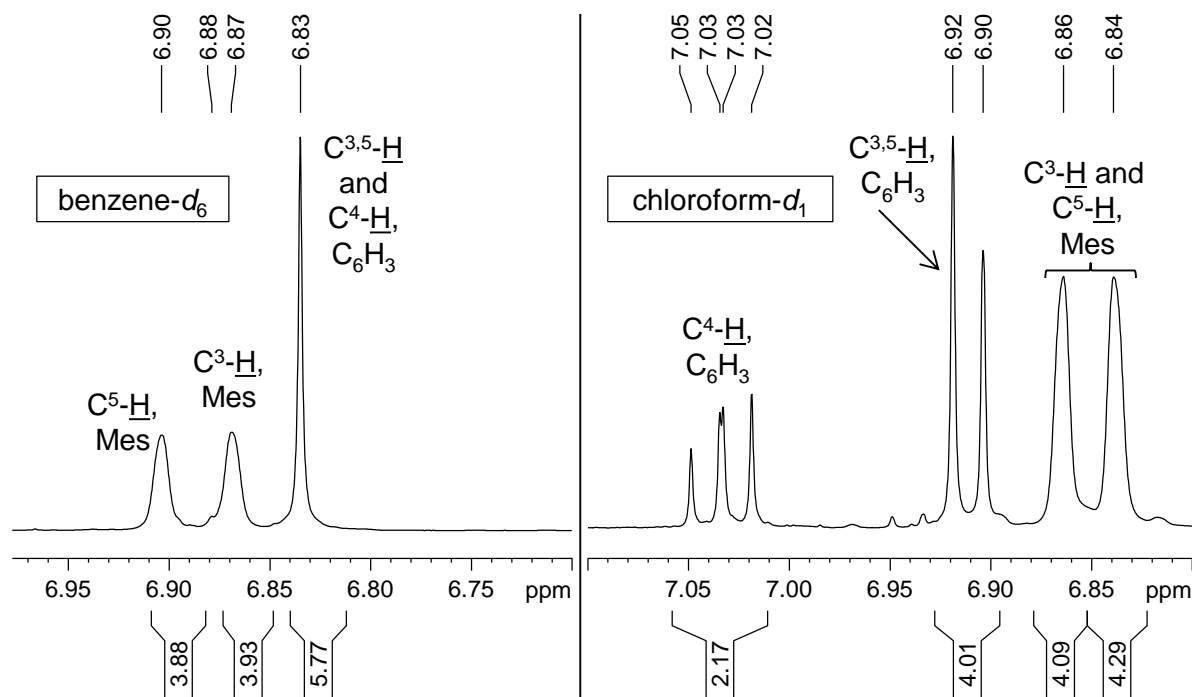


Figure 73. Aromatic region of the ¹H NMR spectra of compound **19-SiHCl** in benzene-d₆ (left) and chloroform-d₁ (right). The C^{3,5}-H and C⁴-H signals are isochronous in benzene-d₆ solution for unknown reasons.

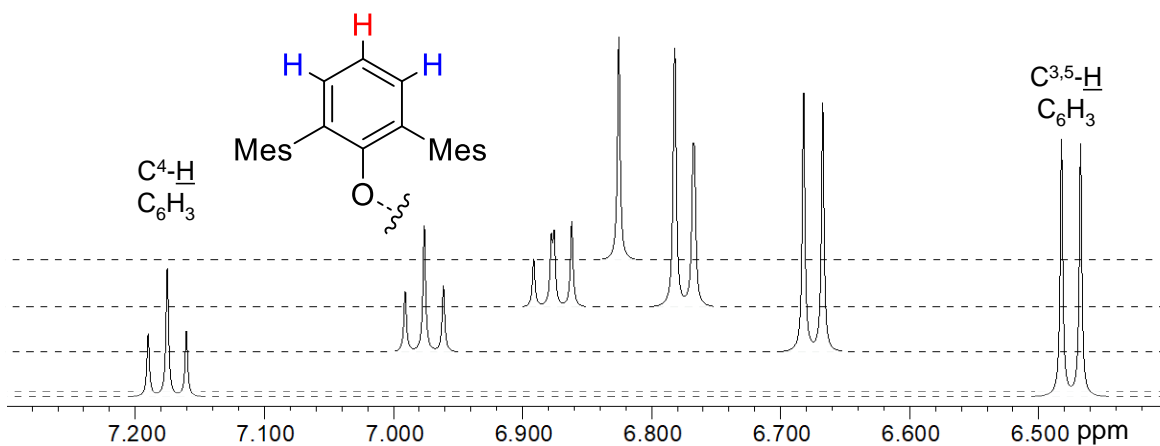


Figure 74. Simulated signals for the C^{3,5}-H and C⁴-H protons of **19-SiHCl₃** assuming different separations $\Delta\delta_{\text{H}} = 0.7, 0.3, 0.1$ and 0 ppm (from bottom to top). The coupling constant ${}^3J_{\text{H,H}} = 7.5$ Hz was taken from the ${}^1\text{H}$ NMR spectrum in chloroform-*d*₁, the linewidth $\Delta\nu_{1/2} = 1.1$ Hz was estimated from the $\Delta\nu_{1/2}$ value of the aliphatic proton signals.

The SiH₂ signal of **19-SiH₂L₂** could not be detected at 298 K but after cooling to 193 K, the atoms are diastereotopic and resonate at $\delta_{\text{H}} = 1.32$ and 3.23 ppm (${}^1J_{\text{Si,H}} = 250$ Hz). In contrast, the Si-H resonance is found at $\delta_{\text{H}} = 4.01$ ppm with two nicely resolved coupling constants to the different Si atoms (${}^1J_{\text{Si,H}} = 283$ Hz, ${}^1J_{\text{Si,H}} = 40$ Hz) at room temperature. The corresponding Si-H stretching vibration appears at $\tilde{\nu} = 2210$ cm⁻¹ in the ATR-IR spectrum. This band is thereby shifted to lower wavenumbers by almost 90 cm⁻¹ when compared to **19-HOtBu^F** (2297 cm⁻¹) due to the less electronegative substituents and the consequentially weaker Si-H bond. Expectedly, the band compares much better with the ones reported for SiH(OPh)₃ ($\tilde{\nu} = 2200$ cm⁻¹),^[398] Ar^{Mes}SiHCl₂ ($\tilde{\nu} = 2240$ cm⁻¹)^[402] or **19-HCl** ($\tilde{\nu} = 2254$ cm⁻¹).^[385] In the ²⁹Si NMR spectra, **19-SiHCl₃** shows doublet signals at $\delta_{\text{Si}} = -61.5$ ppm (${}^2J_{\text{Si,H}} = 40$ Hz) and -7.5 ppm (${}^2J_{\text{Si,H}} = 283$ Hz) that were assigned to the SiCl(OAr^{Mes})₂ and the SiHCl₂ silicon atom, respectively. In comparison, the Si(OAr^{Mes})₂ resonance in **19-SiH₂L₂** (-76.7 ppm, ${}^1J_{\text{Si,H}} = 39$ Hz) appears in a similar field, while the iodine is responsible for a strong shielding of the SiH₂ resonance towards -70.0 ppm (${}^1J_{\text{Si,H}} = 240$ Hz). Both Si(OAr^{Mes})₂ resonances are again high-field shifted in respect to the silylene **19** (31.9 ppm) and compare reasonably well with those of other derivatives described in the following (see Table 31 on page 168). Likewise, the chemical shifts of the SiH and SiH₂ atoms resemble those found in the starting materials SiHCl₃ (-9.6 ppm) and SiH₂L₂ (-101.2 ppm) fairly well. Consequently, the thf activation product **20** with no iodine at the SiH₂ atom displays a nearly unchanged Si(OAr^{Mes})₂ resonance at $\delta_{\text{Si}} = -70.5$ ppm, whereas the SiH₂ signal is low-field shifted to -28.8 ppm (${}^1J_{\text{Si,H}} = 210$ Hz).

The molecular structures of **19-SiHCl₃** and **20** were confirmed by XRD (Figure 75). Both are isostructural to the other known derivatives **19-AB** with a distorted tetrahedral geometry around the Si1 atom. The Si1-Si2 distances of 2.343(3) Å and 2.345(2) Å are nearly identical and compare very well with those of the single bonds found in chlorosilanes such as MesSiCl₂-SiCl₂Mes (2.349(3) Å)^[403] or the more recently reported R^NSiH(Cl)-SiCl₂R^N

(2.3680(8) Å; R^N = N(SiMe₃)Dipp).^[404] The Si-O^{aryl} distances in **19-SiHCl** (1.605(5) and 1.624(4) Å, Ø1.615(5) Å) and **20** (1.629(4) Å and 1.626(4) Å, Ø1.628(4) Å) are shorter when compared to the single bonds found in silylene **19** (Ø1.679(1) Å), confirming the trend observed already in **19-HOtBu^F** (ØSi-O: 1.625(4) Å).

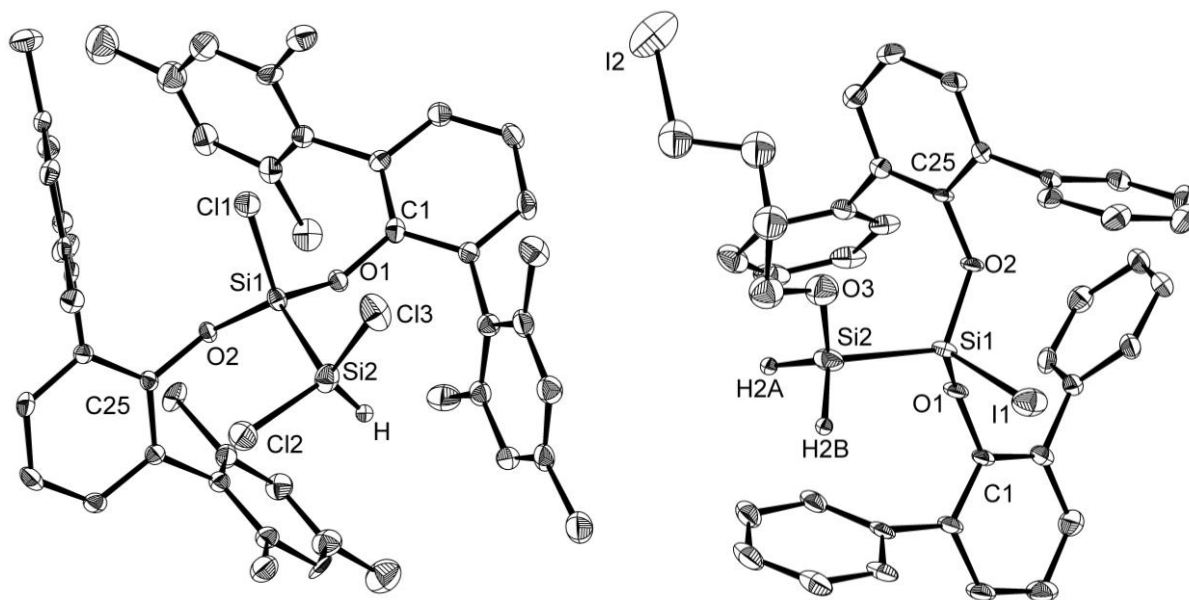
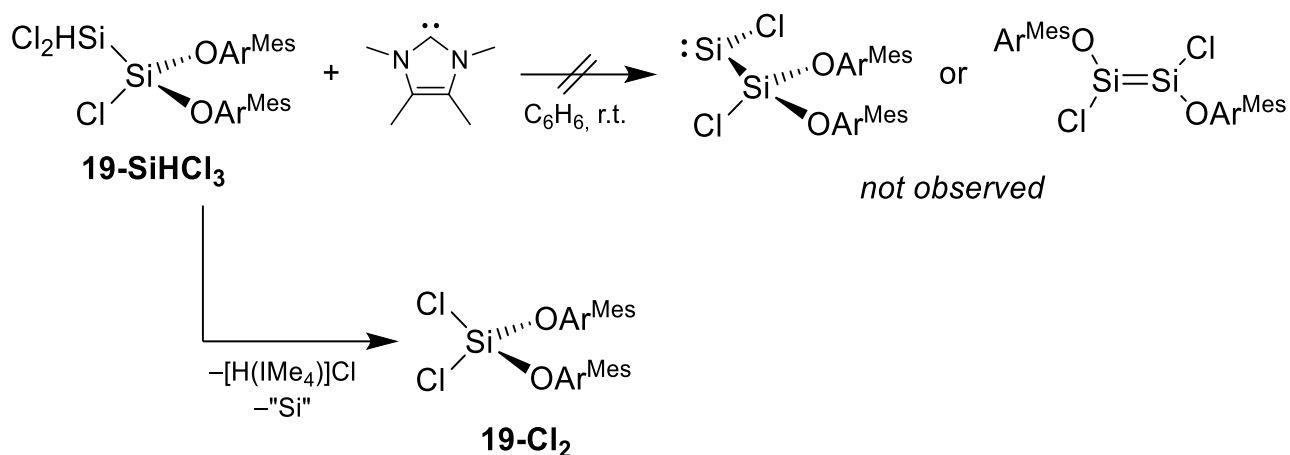


Figure 75. Molecular structures of **19-SiHCl** (left) and **20-Et.O** (right). Thermal ellipsoids are set to 50 % probability; hydrogen atoms except for the Si-H atoms are omitted for simplicity. Selected bond lengths (Å) and angles (°): **19-SiHCl**: Si1-Si2 2.343(3), Si1-O1 1.605(5), Si1-O2 1.624(4), Cl1-Si1 2.046(3), Cl2-Si2 2.050(3), Cl3-Si2 2.055(3), O1-C1 1.380(8), O2-C25 1.389(7); Cl1-Si1-Si2 105.0(1), O1-Si1-Cl1 110.6(2), O1-Si1-Si2 110.7(2), O1-Si1-O2 102.8(2), O2-Si1-Cl1 111.5(2), O2-Si1-Si2 116.3(2), Cl2-Si2-Cl3 106.2(1), Cl2-Si2-Si1 109.9(1), Cl3-Si2-Si1 107.5(1), C1-O1-Si1 138.7(4), C25-O2-Si1 135.6(4); Cl1-Si1-Si2-Cl3 -30.8(1), Cl1-Si1-Si2-Cl2 84.5(1). **20-Et.O**: Si1-Si2 2.345(2), Si1-I1 2.474(2), Si1-O1 1.629(4), Si1-O2 1.626(4), Si2-O3 1.684(6), O1-C1 1.382(6), O1-C25 1.381(6), C25-I2 2.16(1); Si2-Si1-I1 101.61(7), O1-Si1-O2 103.8(2), O1-Si1-I1 101.7(2), O2-Si1-I1 106.6(2); O1-Si1-Si2-O3 159.8(3).

Featuring both a 1,1- and a 1,2-arrangement of H and Cl at the Si-Si bond, compound **19-SiHCl** is a potential target for dehydrohalogenation to the silylsilylene SiCl{(SiCl(OAr^{Mes})₂)} or the disilene Cl₂Si=Si(OAr^{Mes})₂. Presumably, either species would rearrange to the less crowded 1,2-dichlorodisilene (E)-Ar^{Mes}O(Cl)Si=Si(Cl)OAr^{Mes}. Although the group of West reported on the observation of Mes(RO)Si=Si(OR)Mes (R = Ph, Mes, Dipp) by dimerization of photochemically generated oxysilylenes upon warming up a frozen hydrocarbon matrix from 77 K as early as 1988,^[405,406] isolable oxy-substituted disilenes are elusive to date.



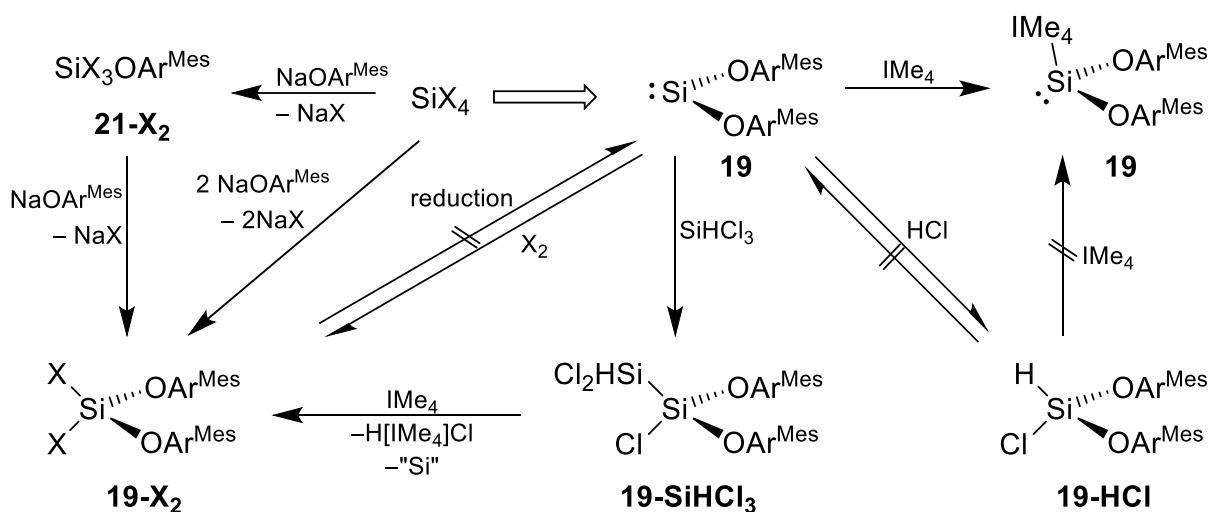
Scheme 53. The attempted dehydrohalogenation of **19-SiHCl₃** leads to **19-Cl₂**.

In practice, the reaction of **19-SiHCl₃** with IMe_4 led to the formal exclusion of “SiHCl”, resulting in the formation of the dichlorosilane **19-Cl₂** (Scheme 53) that was isolated as an analytically pure, colorless solid in 91 % yield. This compound is more easily accessible starting from 2 equiv. $\text{NaOAr}^{\text{Mes}}$ and SiCl_4 (94 % in only one step). **19-Cl₂** is less sensitive towards hydrolysis and thermally very robust (m.p. 264 °C with no sign of decomposition); it is well soluble in aromatic or ethereal solvents and less soluble in aliphatic hydrocarbons.

Halosilanes have significant industrial importance as precursors in the synthesis of orthosilicic acid ($\text{Si}(\text{OH})_4$) and its esters, for example throughout the Sol-gel process or for the synthesis of silanols and silicones generated therefrom.^[1,68,407] Depending on the substituents, these reactions are often accompanied by scrambling and oligo- or polycondensations induced by residual HX, hampering the isolation of pure $[\text{SiX}_{4-n}(\text{OR})_n]$ ($n = 1 - 3$).^[1,408,409] Direct laboratory-scale syntheses therefore utilize salt metathesis reactions, bypassing the formation of HX and as well increasing the nucleophilicity of sterically crowded alcohols.^[409] Alternatively, halogenation of alkoxy(hydrido)silanes is possible.^[410,411] But given the immense industrial importance of halosilanes and silicones, surprisingly little academic research has been done regarding mixed alkoxy(halo)- or aryloxy(halo)silanes.

The unexpected isolation of compound **19-Cl₂** completes the series of the diaryloxy(dihalo)silanes **19-X₂** ($X = \text{Cl}, \text{Br}, \text{I}$), of which **19-Br₂** and **19-I** were obtained by C. Lippmann in his bachelor thesis 2016 by reaction of **19** with SiBr_4 and **I**, respectively.^[385] In this work, compounds **19-Br₂** and **19-I** have been synthesized from **19** and X_2 for comparison reason in yields of 54 % and 60 %, respectively. Additionally, the aryloxy(trihalo)silanes $\text{SiX}_3\text{OAr}^{\text{Mes}}$ (**21-Cl**, **21-Br** and **21-I**) have been synthesized as colorless, moderately moisture sensitive solids from SiX_4 and $\text{NaOAr}^{\text{Mes}}$ in diethyl ether at -60 °C (Scheme 54). The silanes are highly soluble in aromatic or ethereal solvents, with **21-Cl** being also very soluble in aliphatic hydrocarbons. This exception is also reflected in the isolated yields after crystallization from n-hexane or $\text{Et}_2\text{O}/\text{n-hexane}$ mixtures in yields of 32 %, 82 % and 67 %, respectively: the low

yield of **21-Cl** is caused by the much higher solubility and may be enhanced by increasing the reaction scale or crystallization of additional crops. Notably, reductions of **19-Br₂** or **19-I₂** to obtain silylene **19** using [Mg(nacnac)]₂, KC₈ or sodium sand were not successful. In this context it should also be noted, that the attempted dehydrohalogenation of **19-HCl** with varying amounts of IMe₄ also did not lead to **19** or **19-IMe₄**, although IMe₄ has been used for the generation of NHC-stabilized silylenes before.^[396,412] Instead, the reactions resulted in the formation of the yellow imidazolium salt [H(IMe₄)] [OAr^{Mes}] with the “loss” of the Si atom as evidenced by the ¹H NMR spectroscopy and XRD (see Figure 97 on page 257 in the appendix). These results highlight the superiority of the chosen Si(II) precursor for the synthesis of di(aryloxy)silylenes.



Scheme 54. Synthesis of compounds **19-X₂** and **21-X** (X = Cl, Br, I). Reduction of **19-X₂** (X = Br, I) was attempted using KC₈ in benzene, sodium sand in thf (X = I) and Mg₂(nacnac)₂ in toluene (X = Br).

¹H and ¹³C NMR spectroscopy of **19-X₂** and **21-X** revealed local C_{2v} symmetry of the terphenyl substituents with all signals within the expected ranges. The ²⁹Si NMR resonances are given in Table 30 on page 143 and compare well with those of the oxidative addition products **19-AB** presented so far. Only the I-substituted derivatives experience a significant shift to higher fields, which is characteristic for heavier halogens^[385] and appear in between those of MesSiI₃ (−175.3 ppm) and SiI₄ (−350 ppm).^[202,413] The relatively small effect on the ²⁹Si NMR resonance when formally substituting a Br for a {OAr^{Mes}} unit suggests similar shielding capabilities, whereas the more diffuse iodine cannot be matched.

Surprisingly, solid-state structures of mixed aryloxy(halo)silanes without additional hypercoordination of the silicon atom are extremely rare³⁷ and {Cl₃SiO-C(Ph)=(Ph)C-

³⁷ On the basis of a CSD 5.4.1 search. For [SiX_{4-n}(OR)_n] (n = 1 – 3) with four-coordinated Si atoms only one compound with n = 1, two cyclic compounds with n = 2 and not even a single compound for n = 3 have been published so far. Higher coordination numbers usually result from intramolecular stabilization by chelating N-

OSiCl₃·(Si₂Cl₆), which was obtained by insertion of the diketone PhC(O)C(O)Ph in the Si-Si bond of hexachlorodisilane, is the only known structure of a base-free alkoxy(trihalo)silane.^[414] Even more surprising considering their importance silicon chemistry, structural data of heavier aryl(trihalo)silanes are very scarce as well: whereas several structures of aryl(trichloro)silanes have been reported, the structures of EindSiBr₃ and MesSiI₃ are the only heavier derivatives that have been published so far.^[40,413]

Conveniently, the crystalline bulk materials of **21-Cl** and **21-Br** were suitable for X-ray structural analysis and large blocks of **21-I** and **19-Cl₂** were readily available upon evaporation of benzene solutions at ambient temperature. All derivatives are closely related with Si atoms in distorted tetrahedral coordination spheres but show no signs of additional intermolecular Si··O- or Si··X interactions (see Figure 76 as well as Figure 94 on page 253 in the appendix). All bond distances and angles are within the expected ranges and the individual Si-O distances (ca. 1.60 Å) are nearly identical and about 5 % shorter than those in silylene **19** (Table 30). Whereas the Si-Cl and Si-I distances in **19-X₂** and **21-X** match, the respective bond in **21-Br** is shortened by about 3.5 % for no obvious reason. It is also noticeable that the Si-O-C angle in both Br-substituted derivatives is larger, which can be a sign of a lower Si-X hyperconjugation. Interestingly, **21-Br** not only features the largest C-Si-O angle but also a relatively short distance between the mesityl groups and the large Br atoms. In fact, exclusion of “SiBr₂” upon crystallization of the related silane Ar^{Mes}SiBr₃ has been reported by Weidemann^[413] and was also observed during this work in the failed syntheses of the slightly smaller congener Ar^{Tol}SiBr₃ (see page 258 and 258 in the appendix). Meanwhile, Simons et al. reported on the successful synthesis of the less crowded Ar^{Mes}SiCl₃ as early as 1998.^[402] It is thus plausible, that **21-Br** and **21-I** are only stable due to the “placeholder effect” of the additional oxygen atom.

or O- donors. If five- or six-coordinated silicon compounds are to be included, an additional 6 (n = 1), 34 (n = 2) and 18 (n = 3) structures were found. However, twelve of the latter are ionic and are arguably best described as salt-like adducts of fluoride to tetraalkoxysilanes instead.

Another search for structures of halosilanes A(B)Si(OR)X (with A, B = any, R = carbon-based, X = halogen) with four-coordinated silicon atoms gave a total of 35 hits, including the structures listed above.

Table 30. Structural and ²⁹Si{1H} NMR (298 K, benzene-d₆) data of 19-X₂ and 21-X.

Compound	δ_{Si} /ppm	O-Si-O /Å	O-Si-X /Å	O-Si-O /°	O-Si-O-C /°	Reference
19	31.9	1.679(1)	-	93.07(6)	129.6(1)	This work
19-Cl₂	-69.9	1.605(1)	2.0191(8)	105.87(5)	131.66(9)	This work
19-Br₂	-86.1	1.611(2)	2.2623(7)	105.35(9)	136.0(2)	[385]
19-I	-152.0	1.615(2)	2.4234(6)	104.4(1)	132.0(2)	[385]
21-Cl	-47.5	1.598(1)	2.0112(5)	-	135.31(9)	This work
21-Br	-87.2	1.599(2)	2.1849(9)	-	138.5(2)	This work
21-I	-238.1	1.609(2)	2.4238(7)	-	135.93(2)	This work

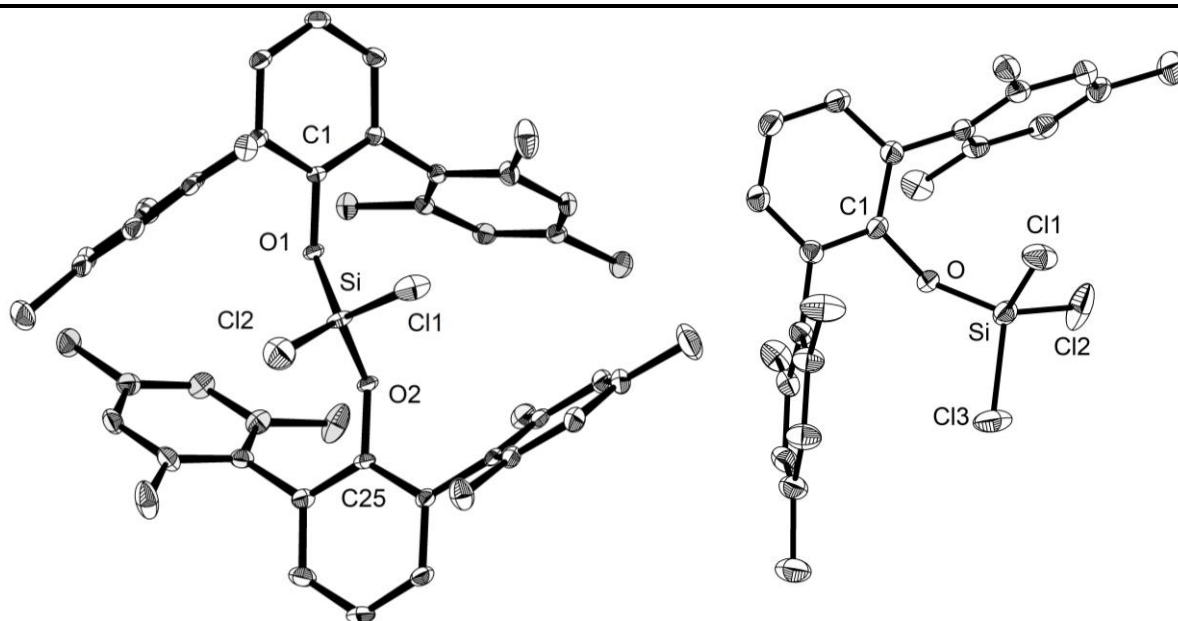
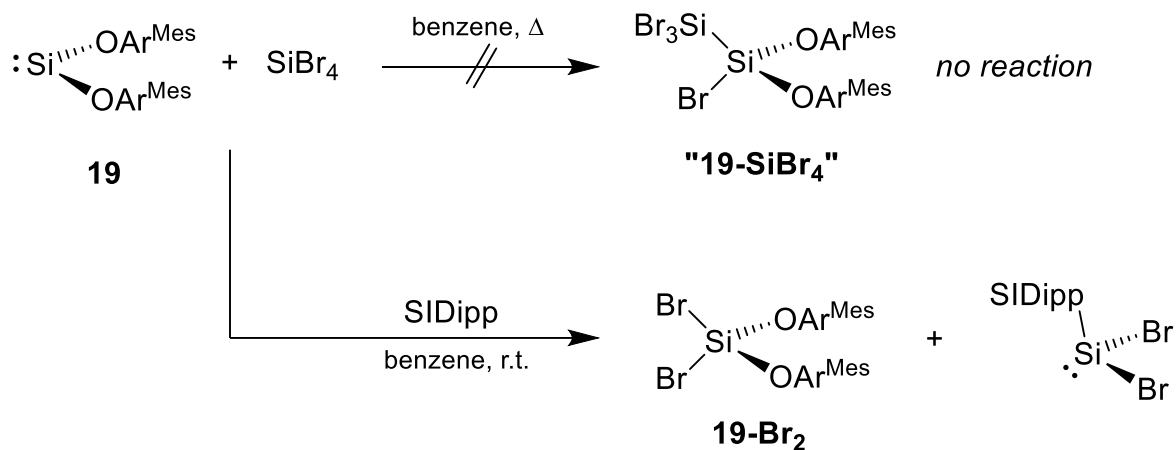


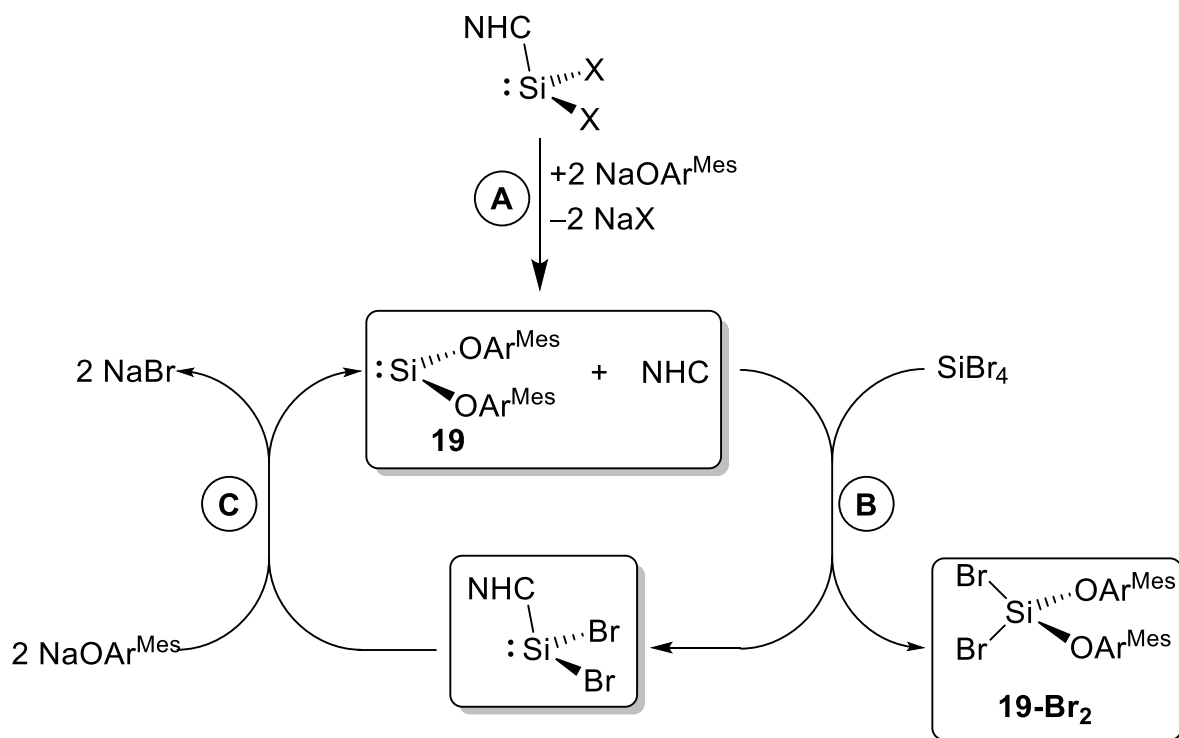
Figure 76. Molecular structures of **19-Cl₂** (left) and **21-Cl** (right). Thermal ellipsoids are set to 50 % probability and hydrogen atoms are omitted for simplicity. The structural data of **19-Cl₂** contain a crystallographic site occupancy (ca. 10 % disorder at the Cl atoms) which was solved independently. Selected bond lengths (Å) and angles (°): **19-Cl₂**: Si-O1 1.605(1), Si-O2 1.605(1), Cl1-Si 2.0175(7), Cl2-Si 2.0207(9), O1-C1 1.392(2), O2-C25 1.388(2); Cl1-Si-Cl2 82.6(2), O1-Si-Cl1 113.01(7), O1-Si-Cl2 122.1(2), O1-Si-O2 105.87(5), O2-Si-Cl1 116.27(7), O2-Si-Cl2 116.1(2), C1-O1-Si 132.98(9), C25-O2-Si 130.33(9). **21-Cl**: Si-O 1.598(1), Si-Cl1 2.0130(5), Si-Cl2 2.0157(5), Si-Cl3 2.0049(6), O-C1 1.392(2); Si-O-C1 135.31(9), Cl1-Si-Cl2 107.72(3), Cl2-Si-Cl3 108.61(3), Cl3-Si-Cl1 111.55(3), O-Si-Cl1 112.03(4), O-Si-Cl2 109.69(4), O-Si-Cl3 107.19(4); C1-O-Si-Cl1 -4.9(1). **21-Br**: Si-O 1.599(2), Si-Br1 2.1886(9), Si-Br2 2.1751(9), Si-Br3 2.1911(9), O-C1 1.389(3); Si-O-C1 138.5(2), Br1-Si-Br3 109.12(4), Br2-Si-Br1 110.61(4), Br2-Si-Br3 108.37(4), O-Si-Br1 111.34(9), O-Si-Br2 108.42(9), O-Si-Br3 108.91(8); C1-O-Si-Br1 3.1(3). **21-I**: Si-O 1.609(2), I1-Si 2.4180(7), I2-Si 2.4245(7), I3-Si 2.4290(8), O-C1 1.399(3); Si-O-C1 135.9(2), I1-Si-I2 110.47(3), I1-Si-I3 110.40(3), I2-Si-I3 107.92(3), O-Si-I2 108.14(7), O-Si-I3 108.05(7), O-Si-I1 111.74(7); C1-O-Si-I1 4.0(3). For a depiction of the isostructural compounds **21-Br** and **21-I**, see Figure 94 on page 253 in the appendix.

Compound **19-Br₂** was obtained from the reaction of in situ generated **19** with SiBr₄ by C. Lippmann in his bachelor thesis with the fate of the missing SiBr₂ unknown at that time.^[385] This simple oxidation instead of the anticipated insertion reaction to SiBr(SiBr₃)(OAr^{Mes})₂ ("**19-SiBr₄**") lies in contrast to the formation of **19-SiHCl₃** and **19-SiHL₂** from **19** and halosilanes. Lippmann's approach was originally intended to improve the workup procedure of the freshly generated **19**, which has to be separated from the arising free carbene: reaction of SIDipp with SiBr₄ would result in the mostly insoluble adduct SiBr₄(NHC) or [SiBr₃(NHC)]Br. In the course of this work, carbene-free **19** was found to be inert towards SiBr₄ even at 80 °C, suggesting an involvement of the free NHC (Scheme 55).



Scheme 55. The reaction of **19** with SiBr₄ only proceeds in presence of free SIDipp.

Indeed, addition of free SIDipp to a solution of **19** and SiBr₄ in benzene led to a color change from colorless to yellow and the mostly selective formation of **19-Br₂** as well as an equimolar amount of SiBr₂(SIDipp), which was unquestionably identified by NMR spectroscopy. While no attempts were undertaken to isolate any of the known compounds from that mixture, addition of 2 equiv. of NaOAr^{Mes} led to the selective consumption of the generated SiBr₂(SIDipp) and the re-formation of **19** and SIDipp (Scheme 56). The generation of **19-Br₂** and SiBr₂(NHC) by addition of SiBr₄ presumably involves either SiBr₂(NHC) or colloidal [SiBr₃(NHC)]Br as an intermediate. However, in an independent reaction, pure **19** did not react with the isolated SiBr₄(NHC) under identical conditions.



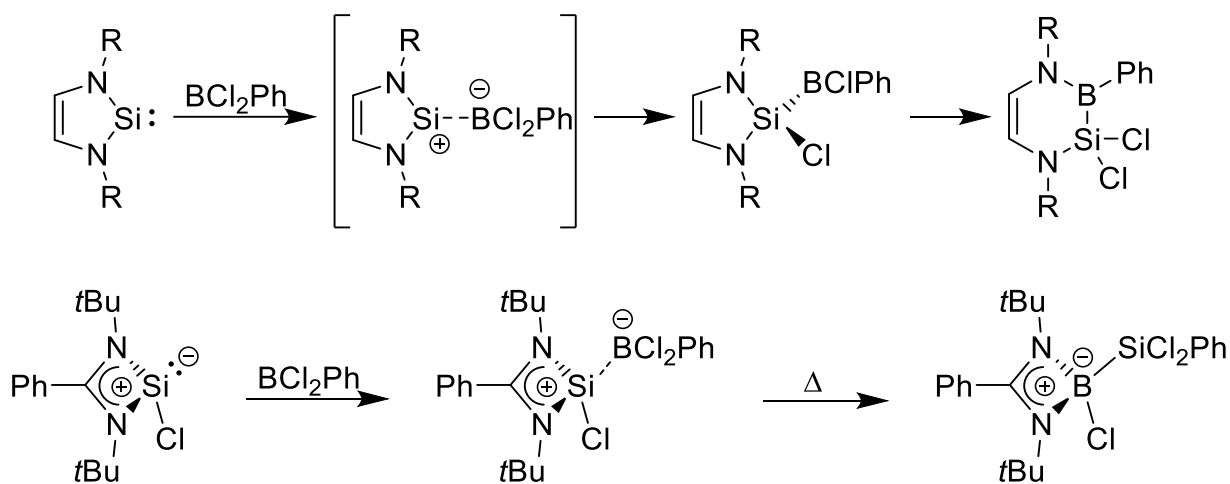
Scheme 56. Generation of silylene **19** by salt metathesis starting from SiX₂(NHC) (**A**), oxidation to **19-Br₂** with re-formation of SiBr₂(NHC) (**B**) and repeated generation of **19** (**C**). X = Br or I; NHC = IDipp or SIDipp.

In praxis, this procedure is not quantitative: whilst the stoichiometry and purity of all extremely air-sensitive reactants is absolutely crucial, inevitable precipitation of smaller amounts of SiBr₄(NHC) hampers the quantitative re-formation of SiBr₂(NHC). Also, enrichment of **19-Br₂** and NaBr in the reaction suspension as well as repeated taking of analytical samples to follow the reaction progress noticeably disturbed the process.

As presented beforehand, every species that was observed in this reaction cascade can be prepared and isolated independently and more efficiently. But the overall cascade might serve as a blueprint for the synthesis of future silylenes SiXX'(NHC) that are not accessible by classical reduction of Si(IV) precursors. Practically, the reaction cycle has already been demonstrated to be adaptable to the employed carbene and the formal synthesis of SiBr₂(NHC) from SiI₂(NHC) was not accompanied with any halogen scrambling as judged from NMR spectroscopy. Hence, addition of small, substituted silanes SiBr₃R in step **B** might give access to silylenes SiBr(R)(NHC) and **19-Br₂**.

3.6.5 Reactions with BX_3 and PCl_3

Lewis basic silylenes are known to form donor-acceptor-complexes ($R_2Si \cdot BR_3$) with Lewis acidic boranes that can then undergo subsequent rearrangement reactions.^[415,416,121,417–425] While oxidative addition to silylboranes is most common, examples of ring expansion are known and Si,B ligand exchange has been reported by the groups of Stalke and Roesky as well (Scheme 57).^[415] Generally, frustrated Lewis acid/base pairs (FLPs) of silylenes and boranes can activate small molecules such as H_2 , O_2 , CO_2 or N_2O and have been used for the dehydrogenation of water under controlled conditions.^{[426], [427–429]} The reaction of silylene **19** with haloboranes is particularly interesting, since scrambling of halogens and alkoxy substituents cannot be ruled out due to the oxophilicity of boron and the steric pressure at the silicon fragment. Interestingly, Inoue and coworkers recently reported on the formation of thermally stable borane adducts ($R = Ph$ or C_6F_5) for their imino(oxy)silylene **X** (see Scheme 48 on page 128).^[390]



Scheme 57. Exemplary reactions between an NHSi and an amidinato-supported silylene with BCl_2Ph reported in the literature.^[415,416]

Stabilization of low-valent Si(II) compounds with Lewis basic phosphano groups was among the first synthetic strategies and successfully applied by Karsch as early as 1990 (**A** in Figure 77). Adduct formation with external phosphanes is known as well. For example, Bornemann and Sander described the barrier-free formation of $[Me(Ph)Si \cdot PH_3]$ (**B**) and its subsequent 1,2-hydrogen migration under matrix conditions,^[430] while the very first report addressing the reactivity of $SiCl_2$ by Timms depicted its reaction with PCl_3 to $Cl_3Si \cdot PCl_2$ as early as 1967.^[431] Likewise, oxidative addition of PH_3 with no observable intermediate was also reported by Driess for their nacnac-type silylene in 2010.^[432] More recently, intermolecular stabilization of silylene centers by chelating phosphane groups has been utilized by the groups of Bacciero and Kato for the synthesis of Si(II) hydrides and chlorides (**C**)^[433–435] and by Nikonov for his bis-silylene (**D**).^[436] The same strategy was also effective for the stabilization of Wesemanns digermavinylidene (**V**) and germasilylenylidene (**IV**) derivatives mentioned in the introduction.^[162,163] Isolable dihalo(silyl)phosphanes are relatively rare. They are accessible by

different approaches such as oxidative cleavage of disilanes with neat PCl₃, salt elimination from alkali silanides and silyl(zinc) reagents or by thermal elimination of Me₃SiX from (Me₃Si)₃Si-P(SiMe₃)₂.^[437–440] Notably, the use of PCl₂(SiMe₃) is described in a series of patents regarding a “Method of producing doped polycrystalline semiconductor layers” by EVONIK DEGUSSA.^[441]

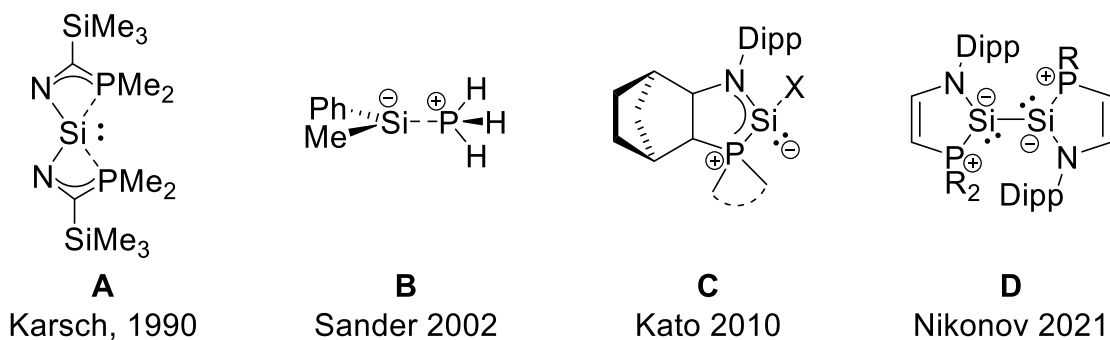
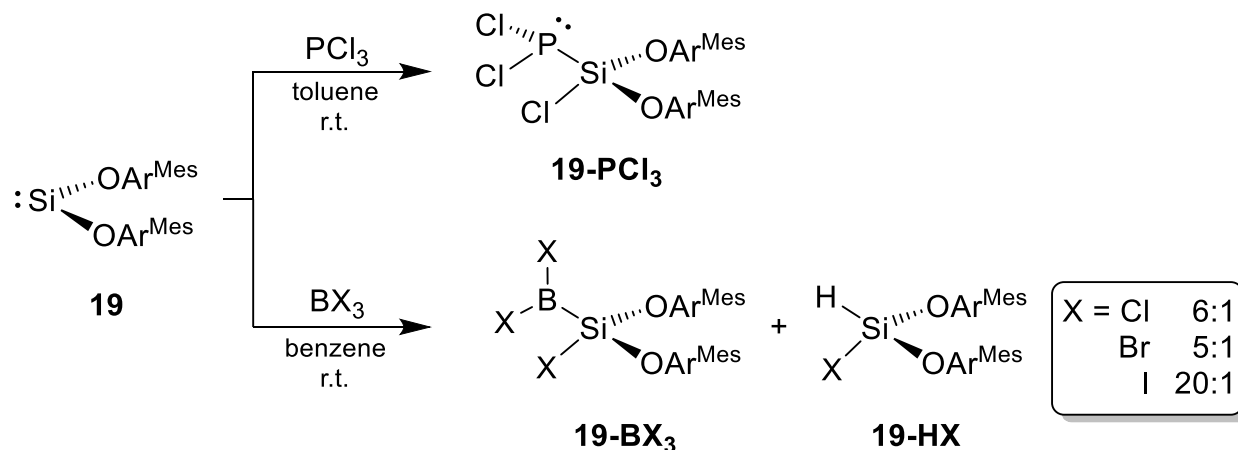


Figure 77. Examples of silylene/phosphane adducts or silylenes stabilized by P-bases; X = H, Cl; R = *i*Pr.^[71,430,433,434,436,442]

The reaction of silylene **19** with an excess PCl₃ proceeds smoothly to the insertion product SiCl(PCl₂)(OAr^{Mes})₂ (**19-PCl₃**) that was isolated as a colorless, analytically pure solid in a combined yield of 87 % after washing with Et₂O. A substantial second crop of crystals suitable for X-ray diffraction analysis was thereby obtained by cooling the filtrate to –30 °C. Compound **19-PCl₃** shows a similar solubility as **19-SiHCl** in common solvents but is thermally less stable (decomposition at 112 °C with gas evolution).



Scheme 58. Reactions of **19** with PCl₃ (top) and boron trihalides (below). In the latter case, inseparable mixtures of the insertion products **19-BX₃** and their decomposition products **19-HX** were obtained.

By contrast, stoichiometric reactions of **19** with BX₃ (X = Cl, Br, I) in benzene or *n*-hexane at ambient temperature or about –10 °C always led to neon yellow mixtures of SiX(BX₂)(OAr^{Mes})₂ (**19-BX₃**) and the colorless diaryloxy(halo)silanes SiHX(OAr^{Mes})₂ (**19-HX**) with their content depending on the employed BX₃ (Cl: ~15 %, Br: ~17 %, I: < 5%, see Scheme 58). Unfortunately, attempts to purify the borylsilanes **19-BX₃** by washing or recrystallization

at lower temperatures were unsuccessful and additional purification of the boron halides had no visible effect. Even handling the compounds exclusively in a glove box with <0.1 ppm of water or oxygen resulted in the slow decomposition at ambient temperature and crystals obtained in the glove box at about $-25\text{ }^{\circ}\text{C}$ repeatedly consisted of **19-HX**; the solid-state structures of **19-HI** and **19-HBr** are depicted in Figure 93 on page 252 in the appendix. Structural assignment of **19-BX₃** as oxidative addition products rather than hypothetical Lewis acid/base adducts $\text{Si}(\text{BX}_3)(\text{OAr}^{\text{Mes}})_2$ (“**19-BX₃**”) was therefore guided by DFT calculations on the B97-D3(BJ)^{ATM}/def2-TZVP level of theory. The insertion product **19-BI^{calc}** was thereby found to be lower in energy by $81.1\text{ kJ}\cdot\text{mol}^{-1}$ (for details, see page 286 in the appendix).

Compound **19-PCl₃** is the first dihalo(silyl)phosphane and, after Marschners $\text{PBr}(\text{NEt}_2)\{\text{Si}(\text{SiMe}_3)_3\}$, only the second example of a halo(silyl)phosphane to be structurally characterized (Figure 78). Expectedly, **19-PCl₃** is isostructural to the derivatives **19-AB** already discussed before (for an overview, see Table 31 on page 168). The Si atom lies in a distorted tetrahedral environment, which is dominated by the bulky $\{\text{OAr}^{\text{Mes}}\}$ units and the three-coordinated P atom is pyramidalized ($\Sigma_{\text{P}} = 293.69(5)^{\circ}$). The average Si-O distance ($1.612(2)\text{ \AA}$) is slightly decreased when compared to the silylene **19**, the O-Si-O angle ($103.3(1)^{\circ}$) is widened by about 10° upon oxidation and the Si-Cl distance of $2.027(1)\text{ \AA}$ lies well within the range observed for **19-Cl₂** ($1.956(3)\text{ \AA}$), **19-SiHCl₂** ($2.046(3)\text{ \AA}$) and **19-HCl** ($2.086(2)\text{ \AA}$).^[385] The Si-P bond distance ($2.294(1)\text{ \AA}$) is close to that of $\text{PBr}(\text{NEt}_2)\{\text{Si}(\text{SiMe}_3)_3\}$ ($2.2792(8)\text{ \AA}$) but at the upper end of the range given by the single bonds observed for (halosilyl)phosphanes $\text{R}_2\text{P-SiR}_2\text{X}$.³⁸ The $\{\text{PCl}_2\}$ moiety occupies no exact conformation as evidenced by the Cl1-Si-P-Cl2/Cl3 torsion angles ($-25.94(6)$ and $74.34(7)^{\circ}$, respectively) but the electron lone pair at the P atom is approximately anti in respect to the Si-bonded Cl1 atom. Finally, the P-Cl distances of $2.062(1)$ and $2.072(1)\text{ \AA}$ compare very well with those of simple dichlorophosphanes such as $\text{Ar}^{\text{Mes}}\text{PCl}_2$ ($2.061(1)\text{ \AA}$) or MesPCl_2 ($2.081(6)\text{ \AA}$).^[443]

³⁸ On the basis of a CSD 5.4.1 search for neutral, metal-free molecular compounds $\text{R}_2\text{P-SiR}_2\text{X}$ (R = any substituent, X = any halogen) with acyclic, three-coordinated P- as well as acyclic, four-coordinated Si atoms. A total of 19 structures with Si-P distances between 2.185 and 2.284 \AA (2.247 \AA) was found.

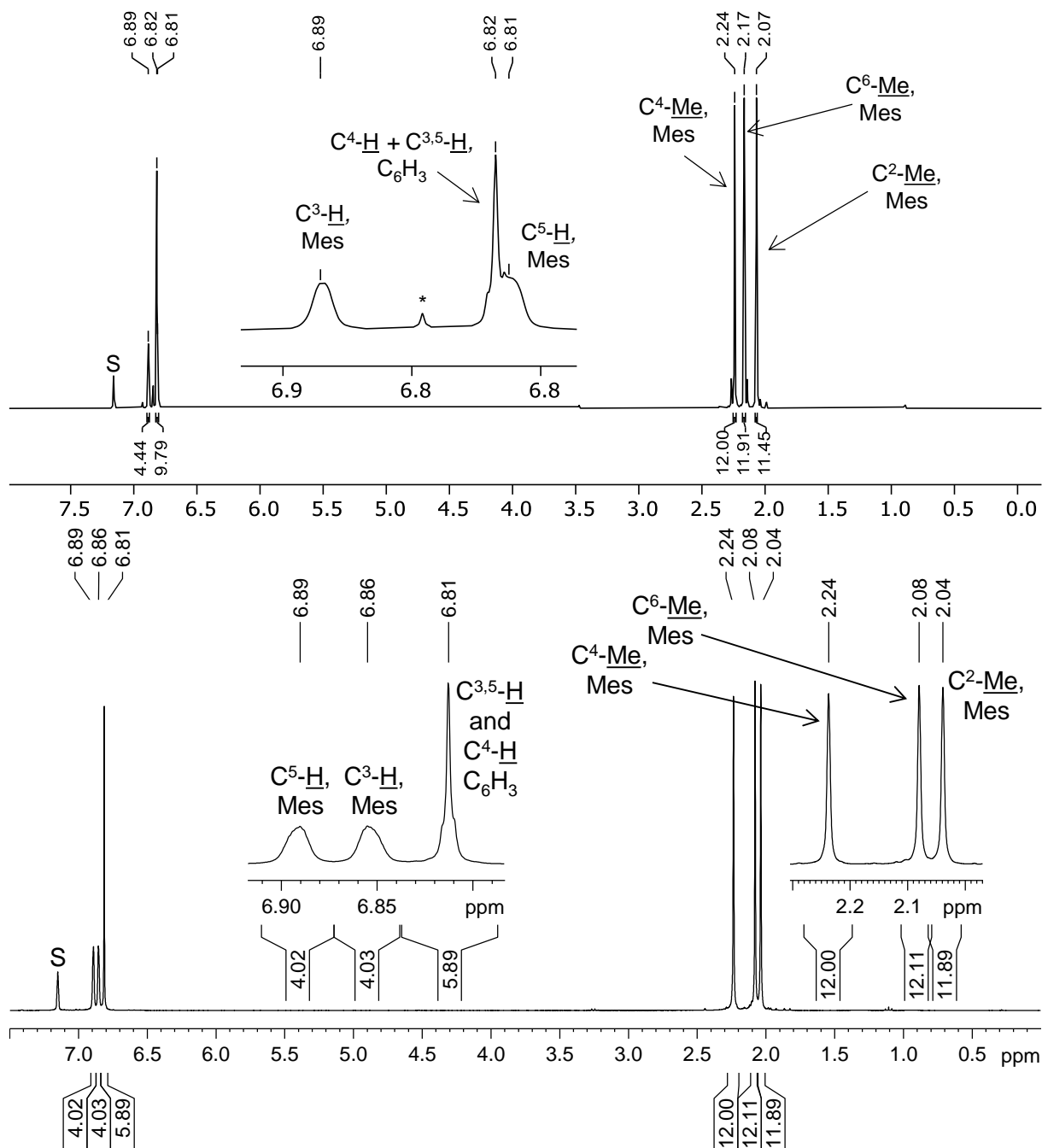


Figure 79. ^1H NMR (500.1 MHz) spectra of **19-BI** (top) and **19-PCI** (below) in benzene- d_6 at 298 K. The signal marked with an asterisk (*) originates from a small amount of **19-HI** present in the sample of **19-BI** and the character S marks the solvent residual signals.

Three singlet signals were detected in the $^{31}\text{P}\{^1\text{H}\}$ NMR spectrum of **19-PCI** (Figure 80) which do not alter upon changing the temperature (up to 80 $^\circ\text{C}$) or the magnetic field of the spectrometer. The intensity ratio of the three signals (57 : 36 : 8) compares well with the calculated ratio of the three isotopologues $\text{SiCl}(\text{P}^{35}\text{Cl}_2)(\text{OAr}^{\text{Mes}})_2$, $\text{SiCl}(\text{P}^{35}\text{Cl}^{37}\text{Cl})(\text{OAr}^{\text{Mes}})_2$ and $\text{SiCl}(\text{P}^{37}\text{Cl}_2)(\text{OAr}^{\text{Mes}})_2$ of 57.4 : 36.7 : 5.9 obtained from the natural abundance of the ^{35}Cl and ^{37}Cl isotopes (75.77 and 24.23 %, respectively). As expected for a chemical shift isotope effect,

replacement of a ³⁵Cl atom by the heavier isotope ³⁷Cl causes a slight high-field shift of the ³¹P signal. The overall chemical shift of **19-PCl₃** ($\delta_P = 131.2$ ppm, $^1J_{P,Si} = 80$ Hz) is thereby notably high field from the other known dichloro(silyl)phosphanes *t*Bu₃Si-PCl₂ ($\delta_P = 211.9$ ppm, $^1J_{P,Si} = 91.8$ Hz),^[438] (Me₃Si)₃Si-PCl₂ (236.2 ppm),^[439] and Ar^{Dipp}(*dsi*)₂Si-PCl₂ (217.7 ppm, $^1J_{P,Si} = 102$ Hz),^[440] which all appear in a similar field as PCl₃ ($\delta_P = 220$ ppm). This trend is counterintuitive to the expected β -deshielding caused by the oxygen atoms and there is no apparent reason for a high field shift of about 100 ppm. However, the observed resonance of **19-PCl₃** is only slightly highfield from carbon-based dichlorophosphanes RPCl₂ (204 – 166 ppm),^[445] which may be explained by lower paramagnetic contributions (σ_{para}) in a Si-P bond when compared to Si-C bonds (α -effect).^[445]

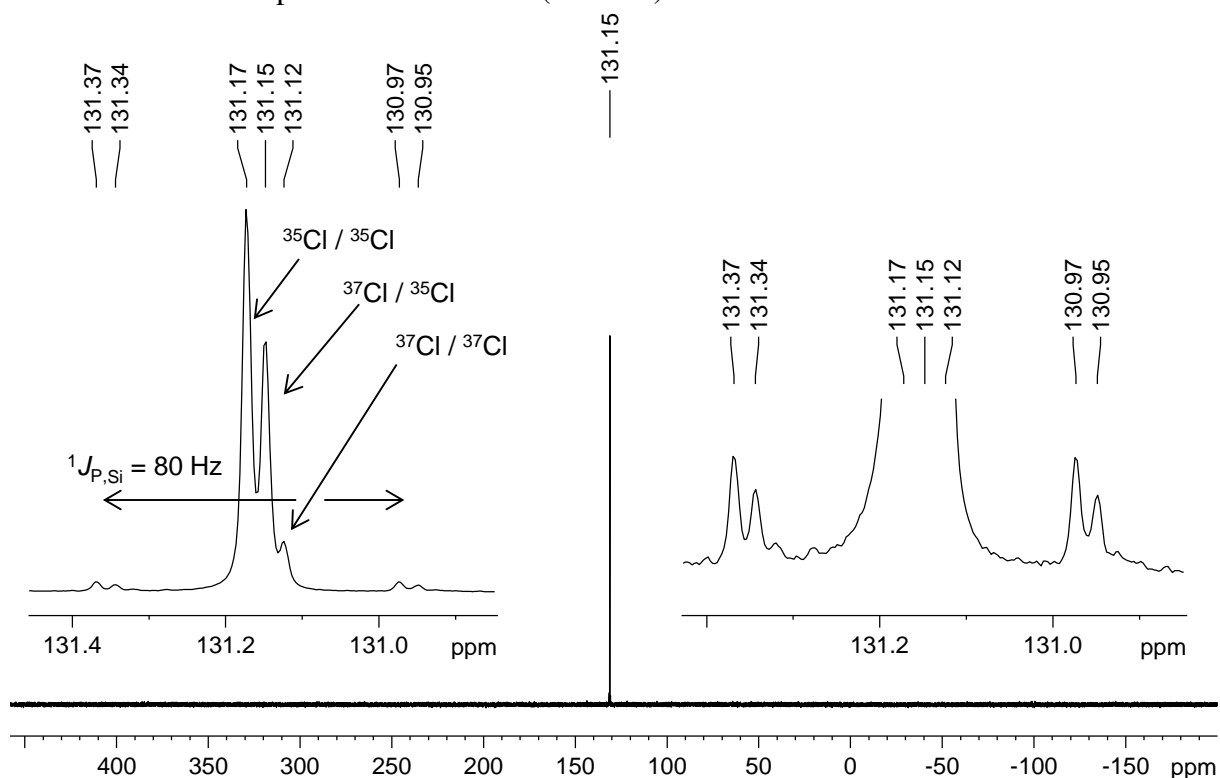


Figure 80. ³¹P{¹H} NMR (99.36 MHz) spectrum of **19-PCl₃** in benzene-*d*₆ at 298 K. Enlarged excerpts showing the three different ³¹P signals as well as the ²⁹Si satellites are shown in the insets. The signals presumably arise from the three isotopologues SiCl(P³⁵Cl₂)(OAr^{Mes})₂, SiCl(P³⁵Cl³⁷Cl)(OAr^{Mes})₂ and SiCl(P³⁷Cl₂)(OAr^{Mes})₂.

As mentioned above, distinction between oxidative addition products **19-BX₃** and hypothetical Lewis acid/base adducts “**19·BX₃**” was guided by calculations. An experimental confirmation was obtained by ¹¹B NMR spectroscopy, which is very sensitive towards the coordination number of boron. Here, very broad signals were detected at $\delta_B = 63.3$ ppm and $\delta_B = 58.0$ ppm for compounds **19-BBr₃** and **19-BI₃**, respectively, which is characteristic for three-coordinated boron atoms with uneven substituents. The shifts compare reasonably well

with the RBX_2 type (about 50 – 65 ppm; R = aryl or alkyl, X = Br, Cl)³⁹ whereas higher coordinated silylene-borane adducts like Inoues $(\text{C}_6\text{F}_5)_3\text{B}\cdot\text{Si}(\text{NIDipp})\text{Si}t\text{Bu}_3$ ($\delta_{\text{B}}: -20.3$ ppm),^[390] $(\text{C}_6\text{F}_5)_3\text{B}\cdot\text{Si}\{\text{N}(\text{tBu})_2\text{CH}\}_2$ (-14.3 ppm)^[417] or $\text{H}_3\text{B}\cdot\text{SiH}(\text{Si}t\text{Bu}_3)(\text{NHC})$ (-40.31 ppm; $\text{NHC} = \text{C}\{\text{N}(\text{Et})\text{CH}\}_2$)^[421] instead experience a shift to higher fields. Notably, a broad and weak signal with an intensity matching the molar amount of $\{\text{BL}_2\}$ elimination product visible in the ^1H NMR spectrum was detected for a sample of **19-BL** at $\delta_{\text{B}} = 28.5$ ppm ($\nu_{1/2} = 825$ Hz). The identity of this impurity remains unknown; it does not contain any H atoms and resonates high field from B_2I_4 ($\delta_{\text{B}} = 70$ ppm).^[447]

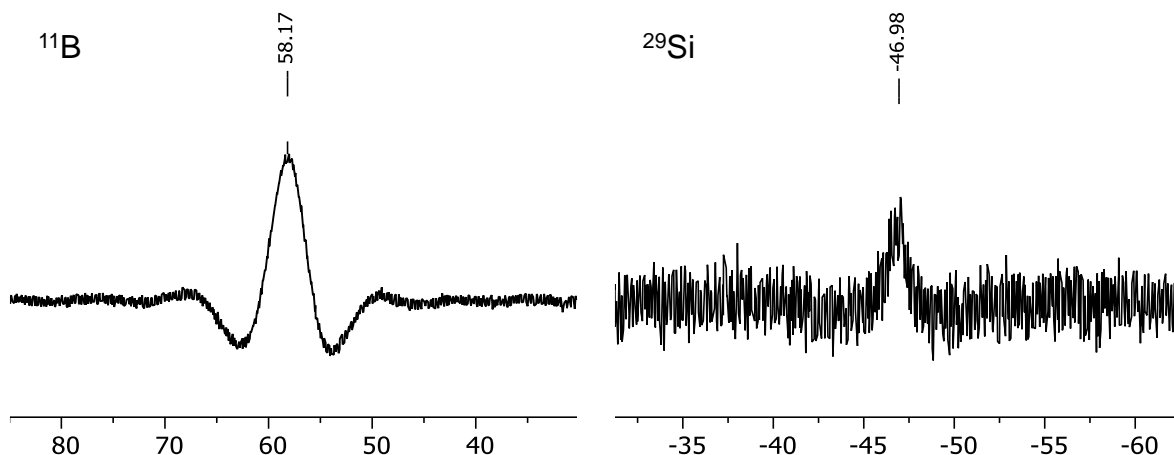


Figure 81. $^{11}\text{B}\{^1\text{H}\}$ NMR (99.36 MHz) spectrum (left) and $^{29}\text{Si}\{^1\text{H}\}$ NMR (160.46 MHz) spectrum (right) of **19-BL** in benzene- d_6 at 298 K.

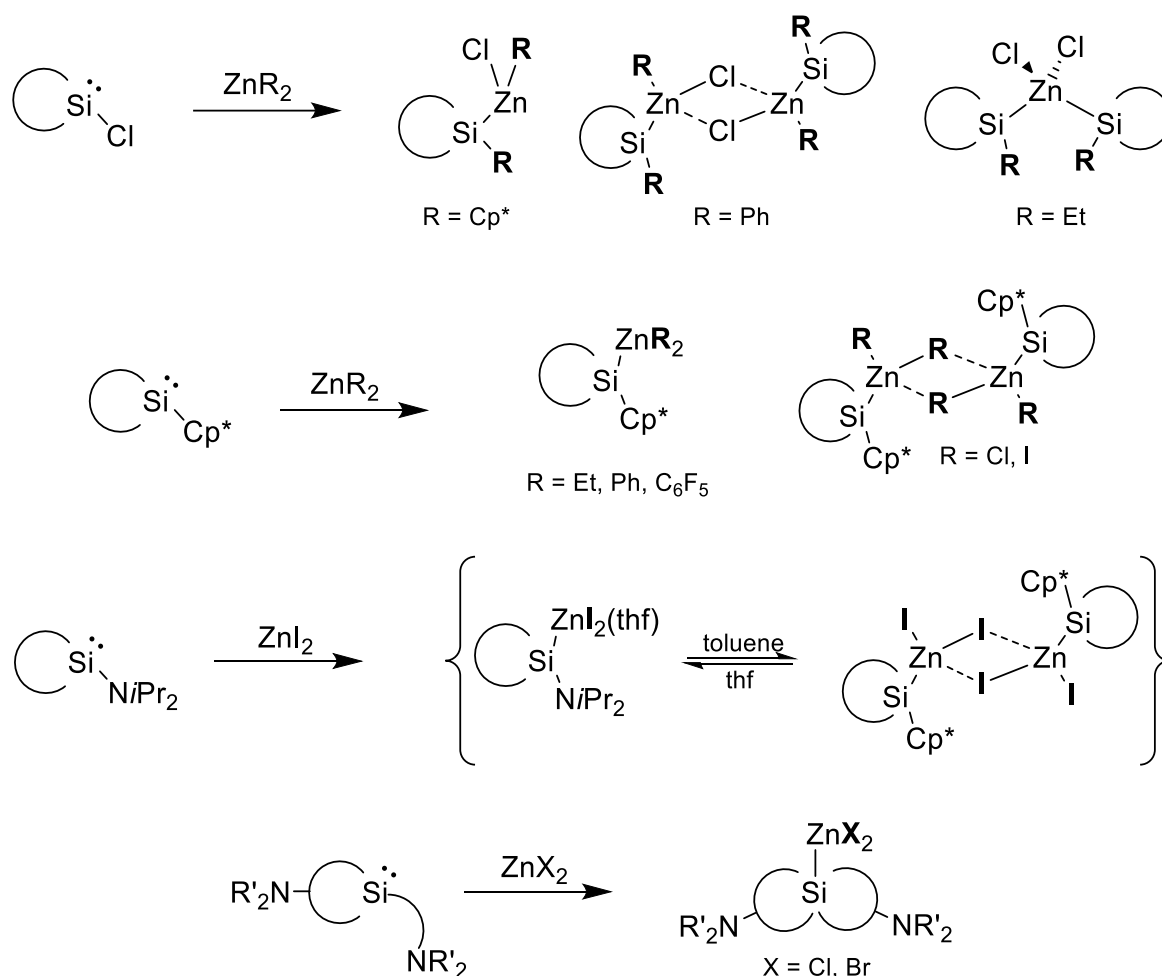
Finally, the $^{29}\text{Si}\{^1\text{H}\}$ NMR spectrum of **19-PCl₃** exhibits a sharp, intensive doublet signal at $\delta_{\text{Si}} = -68.6$ ppm ($^1J_{\text{P,Si}} = 80$ Hz) which is almost identical to that of **19-Cl₂** ($\delta_{\text{Si}} = -69.9$ ppm). In contrast, recording of ^{29}Si NMR spectra of **19-BX₃** was hampered presumably because of unresolved scalar couplings to the ^{10}B and ^{11}B nuclei and fast quadrupolar-induced relaxation of the silicon center as already reported by Metzler and Denk.^[417] Thus only a very broad signal could be observed for **19-BL** at $\delta_{\text{Si}} = -47.0$ ppm, which compares well to **19-MeI** (-54.3). But in respect to **19-L** (-152.0 ppm), the electropositive boron atom is responsible for a respectable low field shift.^[385]

3.6.6 Addition of ZnMe_2

From 2014 to 2017, Roesky and coworkers researched the reactivity of multiple amidinato-silylenes towards zinc(II) compounds (Scheme 59). In a series of papers, the authors provided systematic investigations supported by quantum chemical calculations that led to

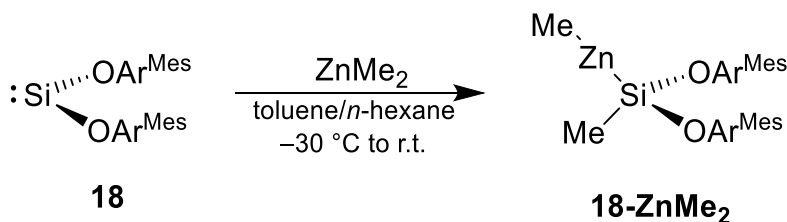
³⁹ For general interpretation of $^{11}\text{B}\{^1\text{H}\}$ NMR spectroscopy see reference ^[446] as well as the extensive database $\langle^{11}\text{B}$ NMR Chemical Shifts \rangle of the Cole Research Group, SDSU Department of Chemistry & Biochemistry, San Diego State University, available on the internet at <https://www.chemistry.sdsu.edu/research/BNMR/>

differentiation between two types of Zn(II)-Si(II) bonds: relatively strong polar single bonds (~200 kJ/mol) of classical Zn(silyl)₂ ion pairs as well as weaker donor-acceptor bonds (~115 kJ/mol), which were described as silylene-zinc adducts.^[237,238,240,448]



Scheme 59. Reactivity studies of benzamidinato-stabilized silylenes towards various Zn(II) compounds presented by the group of Roesky in 2014 - 2017. The circular segments are used as an abbreviation for the benzamidinate ligands $\eta^2\text{-}\{\text{N}_2(\text{tBu})_2\text{CPh}\}$ (row 1-3) or $\{\text{N}_2(\text{tBu})_2\text{CN}(\text{iPr})_2\}$ (last row) and formal charges are omitted for simplicity.^[237,238,240,448]

Reactions with benzamidinato-silylenes thereby led to coordination of the Zn atom via the Si electron lone pair, resulting in monomeric or dimeric complexes with four- or five-coordinated Si atoms and three- or four-coordinated Zn atoms.^[238,240,448] By contrast, the groups of Power and Nikonov reported on the insertion of germynes and stannyls into a Zn-C bond of ZnMe₂ to give the oxidative addition products ZnMe(EMeR₂) as classical zinc organyles.^[449,80] After the successful syntheses of NHC-stabilized zinco(silyl)silylenes from disilavinylidenes **1** and **1-CH₂Ph** and ZnX₂ or ZnEt₂^[135] and the discovery of the respective ZnX₂ complexes of higher energy by NMR spectroscopy and DFT calculations (see page 46ff), we were also interested in the reactivity of the donor-free silylene **19** towards Zn(II).



Scheme 60. Synthesis of compound **19-ZnMe₂**.

Addition of a slight excess ZnMe_2 solution in *n*-hexane to a cold suspension of **19** in toluene quickly led to the selective formation of the zinco-silane $\text{SiMe}(\text{ZnMe})(\text{OAr}^{\text{Mes}})_2$ (**19-ZnMe₂**, Scheme 60). **19-ZnMe₂** was isolated as a colorless solid in analytically pure form in quantitative yield after evaporation of all volatiles. Similar to the derivatives presented earlier, **19-ZnMe₂** is well soluble in typical solvents. Although very sensitive towards hydrolysis, the solid is thermally robust and only decomposes to a grey mass when heated to 227 °C (gas evolution was observed). This is the first example of a simple silylene insertion into a zinc organyl. Presumably, this deviation from the results described in Scheme 59 is caused by the additional base coordination in the amidinato-stabilized silylenes used by Roesky, which amplify the η^1 -donor capabilities but tame their electrophilicity. In contrast, electrophilicity must be considered the major characteristic of **19** which, in turn, behaves like the germylene and stannylene reported by Power and Nikonov.^[449,80] The reaction pathway of **19** with ZnMe_2 can therefore be considered a blueprint for the reaction of base-free silylenes with ZnR_2 .

Once again, the ^1H and $^{13}\text{C}\{^1\text{H}\}$ NMR spectra suggest local C_s symmetry with locked rotations of the terphenyl substituents in benzene-*d*₆ solution. All resonances appear within the expected ranges, although not all positions of the mesityl groups could be undoubtedly assigned by 2D NMR spectroscopy due to poor separation of the aromatic signals. Most characteristically, the signals of the Si-Me and the Zn-Me group are found at $\delta_{\text{H}} = -0.84$ ppm ($^2J_{\text{Si,H}} = 5.0$ Hz) and -0.64 ppm, respectively. The Si-Me signal is surprisingly shielded, considering that the methyl groups in $[\text{Zn}(\text{SiMe}_3)_2]$ still resonate at a standard field (0.20 ppm).^[450] This can be interpreted as a sign for a more polar nature of the Si-Me bond, but no anomalies were found by X-ray diffraction (vide infra). The ^{29}Si NMR spectrum of **19-ZnMe₂** displays a sharp singlet signal at $\delta_{\text{Si}} = 5.4$ ppm, which is significantly low-field from the other derivatives **19-AB** (about -80 ppm). This difference is rationalized by the much lower electronegativity of Zn and the formal oxidation state of +II of the Si atom. Only in comparison to zinc silanides such as $[\text{Zn}\{\text{Si}(\text{tBu})_3\}_2]$ ($\delta_{\text{Si}} = 25.9$ ppm), $[\text{ZnCl}\{\text{Si}(\text{tBu})_3\}]_4$ (37.6 ppm) or $[\text{ZnCl}\{\text{Si}(\text{tBu})_3\}\cdot\text{thf}]_2$ (34.1 ppm) the shielding effect of the oxy substituents is still visible.^[241] By contrast, zinc-coordination had only negligible effects on the NMR shifts of Roesky's amidinato-silylenes which resonate around 50 to 60 ppm.^[238]

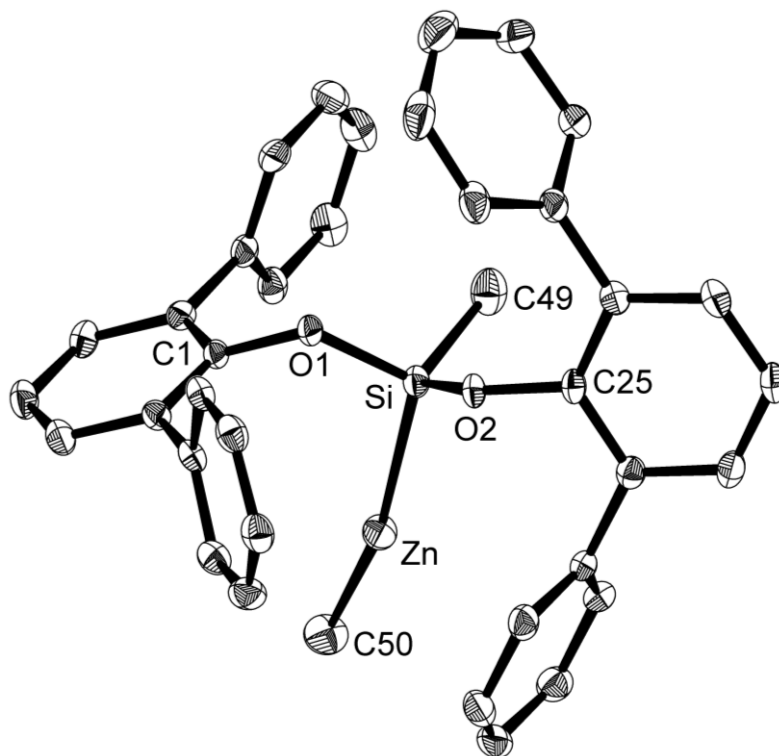


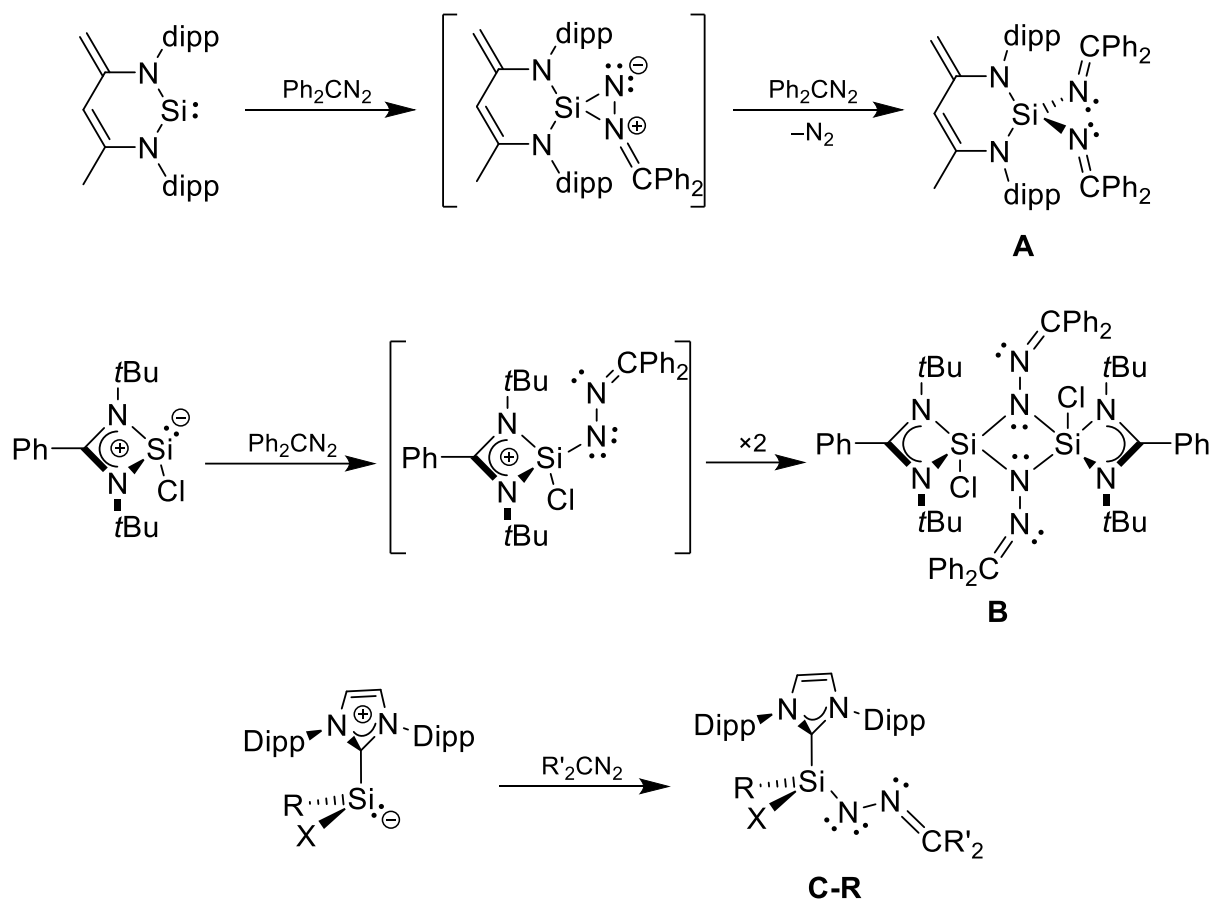
Figure 82. Molecular structure of **19-ZnMe₂**. Thermal ellipsoids are set to 50 % probability and peripheral methyl groups as well as hydrogen atoms are omitted for simplicity. The structural data contain a crystallographic site occupancy (ca. 10 % disorder) which was solved independently. Selected bond lengths (Å), angles (°) and torsion angles (°): Si-Zn 2.3755(7), Si-C49 1.837(4), Zn-C50 1.954(3), Si-O1 1.662(2), Si-O2 1.663(2), O1-C1 1.375(3), O2-C25 1.376(3); O1-Si-O2 99.82(8), C50-Zn-Si 165.38(9), O1-Si-Zn 108.47(6), O1-Si-C49 109.8(2), O2-Si-Zn 117.01(6), O2-Si-C49 105.8(1), C49-Si-Zn 114.8(1), C1-O1-Si 127.0(1), C25-O2-Si 129.5(1); C1-O1-Si-O2 -138.0(2), C25-O2-Si-O1 -148.9(2).

Colorless plates of **19-ZnMe₂** were obtained by slow evaporation of a saturated solution in benzene (Figure 82). Once again, the Si atom lies in a distorted tetrahedral environment but the trends observed for the derivatives **19-AB** -although evident- are less pronounced in this case. The Si-Zn distance (2.3755(7) Å) is longer than those in the NHC-stabilized zinco(silyl)silylenes **5-X** and **6** (Ø3.329(2) Å) and compares well with those in bulky di(silyl)zinc compounds like Zn{Si(SiMe₃)₃}₂ (2.355 Å)^[242] or Zn{Si(tBu)₃}₂ (2.384 Å).^[241] Following Roeskys investigations, the Si···Zn interaction in **19-ZnMe₂** is therefore best described as a strong, polar single bond (about 2.39 Å and 200 kJ/mol) rather than a weak donor-acceptor interaction (about 2.49 Å and 115 kJ/mol).^[238] The Si-O distances can be considered identical (1.662(2) and 1.663(2) Å) and are nearly as long as in the silylene precursor **19** (1.679(1) Å) although the silanes typically experience a shortage to about 1.62 Å. Likewise, the O1-Si-O2 angle of 99.82(8)° is the smallest observed for any **19-AB**, albeit still significantly widened when compared to **19** (93.07(6)°, see also Table 31 on page 168). Meanwhile, the C49^{Me}-Si-Zn angle (114.8(1)°) is the largest measured for any compound **19-AB** presented in this work, presumably obeying the lower oxidation state. As mentioned above, the Si-C49^{Me} bond of 1.837(4) Å is not out of the ordinary and precisely matches those in the di(aryloxy)silane Me₂Si(OC₆H₄-4-NO₂)₂ (Ø1.837(3) Å).^[451] Since the long Zn···C49^{Me} (3.561(4) Å) distance

excludes any further interactions with the metal atom, the solid-state structure doesn't provide additional information about the unusual high field shift observed in the ^1H NMR spectrum ($\delta_{\text{H}} = -0.84$ ppm).

3.6.7 Ambiphilic reaction with a diazoalkane

The ability of **19** to react with electron donors or to insert into electron rich bonds demonstrates its powerful electrophilicity. To further explore its synthetic potential as an ambiphilic building unit, the reaction of **19** towards ambiphilic molecules with several conceivable outcomes was fascinating. Since 2009, only a few research papers addressing the reactivity of electron-rich silylenes with diazoalkanes (R_2CN_2) have been published, but the existing data already show a fundamental difference between electron rich cyclic- and base-stabilized acyclic silylenes (Scheme 61). Surprisingly, the conceivable formation of silenes $\text{R}_2\text{Si}=\text{CR}'_2$ as a result of N_2 elimination and formal carbene-addition has not been observed. Instead Si-N bond formations are favored: whilst Driess's NHSi gave access to diiminylsilane **A** after reaction with 2 equiv. of Ph_2CN_2 accompanied by the loss of only 2 nitrogen atoms,^[452] base-stabilized Si(II)halides yield silazines as a result of end-on coordination of the electrophilic N^α atom towards the electron lone pair at the silicon atom without nitrogen elimination (**B** and **C**).^[453] Meanwhile, reactions with base-free acyclic silylenes such as **19** have not yet been investigated to the best of our knowledge.

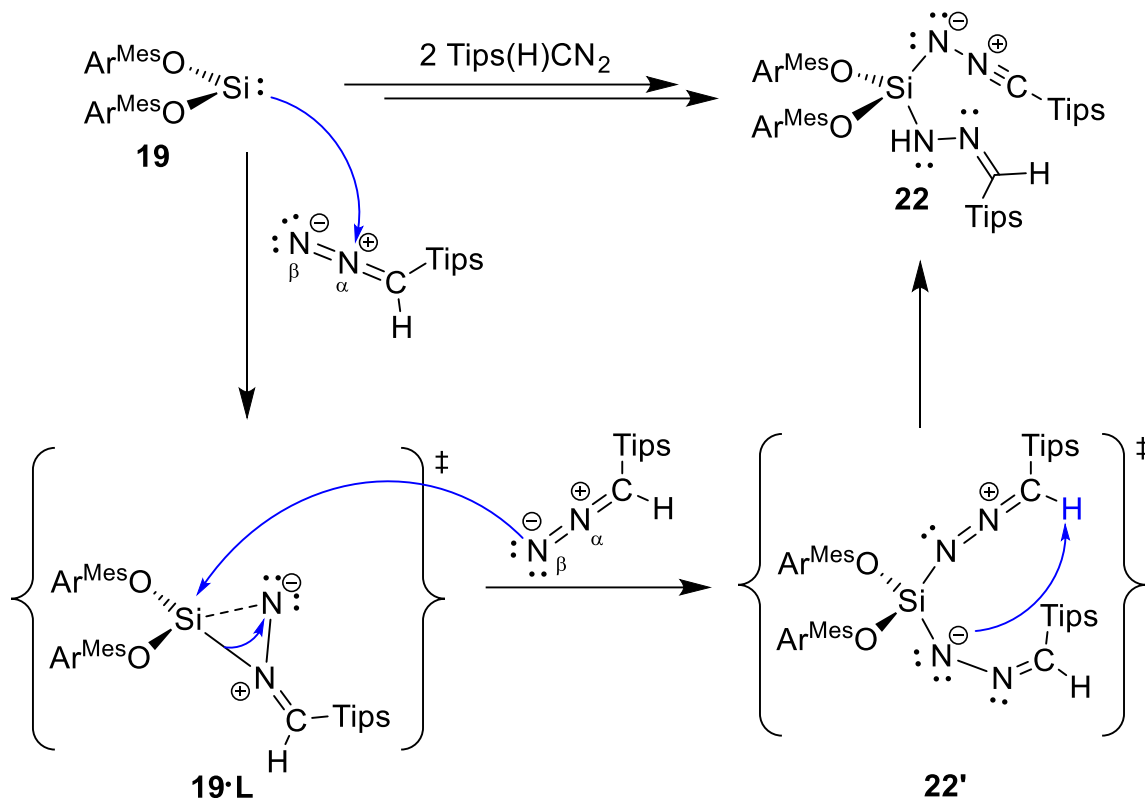


Scheme 61. Known reactions of silylenes with diazoalkanes; proposed intermediates could not be observed experimentally. Formal charges are omitted for simplicity. **C:** R = X = I, R' = pTol; R = Ar^{Mes} or Ar^{Trip}, X = Cl, R'₂CN₂ = Ar^{Mes}(H)CN₂.^[116,452,453]

Interestingly, the reaction of **19** with 2 equiv. of (T_{ips})CHN₂ (T_{ips} = Si(iPr)₃) in a toluene/Et₂O mixture at ambient temperature led to the selective formation of Si{HN=NC(H)T_{ips}}{N≡NCT_{ips}}(OAr^{Mes})₂ (**22**), which formally contains a nitrilimine and a hydrazonyl substituent at the now four-coordinated silicon center (Scheme 62). Compound **22** was isolated after recrystallization from an n-hexane/Et₂O mixture as an air sensitive, colorless solid in 77 % yield. It is well soluble in ethereal or aromatic solvents and melts upon heating to 277 °C.

Akin to the postulated mechanism leading to **A** (Scheme 61), an initial nucleophilic attack of the Si at the N^α atom of the diazoalkane is suggested (**19-L** in Scheme 62). Subsequent addition of a second diazoalkane via the N^β atom could then induce a rearrangement of the first ligand to a terminal Si-N^β bond to reduce steric pressure in intermediate **22'**. Finally, an intramolecular proton shift from the second diazoalkane unit to the N^α atom of the first ligand leads to the final isomer **22**. Involvement of free carbenes in the second step as proposed for the reaction leading to diiminylsilane **A**^[452] can be excluded in this case, since no dinitrogen gas is formed. Instead, the proposed mechanism underlines the ambiphilicity of silylene **19**.

Unfortunately, no experimental evidence can be provided. Despite the relatively long reaction time at ambient temperature, no intermediates could be detected by in situ NMR or IR spectroscopy. This proves the initial step to be rate-determining and consequently altering the reaction stoichiometry only led to an incomplete conversion.



Scheme 62. Formation of compound **22** via two plausible intermediates **19-L** and **22'**.

Although analytically pure, spectroscopic characterization of compound **22** was hampered by slow rotations of the substituents that resulted in severely broadened signals in the ^1H and ^{13}C NMR spectra in different solvents and at varied temperatures (see Figure 86 on page 162). Additionally, the XRD structure of compound **22** was affected by a significant crystallographic site occupancy that superimposed substructures with interchanged substituents N(H)-N=C(H)Tips and $\text{N-N}\equiv\text{C-Tips}$ (Figure 83).

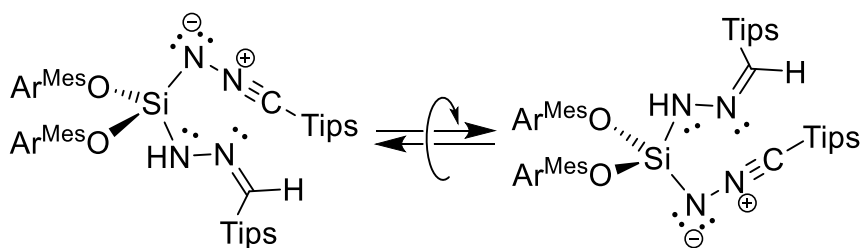


Figure 83. Two different orientations of compound **22** are superimposed in the solid-state structure.

Normally this phenomenon can be addressed by the crystallographer, however, in this case it was found to be very difficult due to the light weight of the affected atoms, the similarity of both groups and the lack of a reliable structural proposal based on NMR spectroscopy. Luckily, the ATR-IR spectrum gave pivotal insights (Figure 84). A very strong absorption band was found at $\tilde{\nu} = 2143 \text{ cm}^{-1}$, which is characteristic for organic isocyanides ($\tilde{\nu} = 2165$ to 2110 cm^{-1})^[361] but very different from the Si-N-N=C(pTol)₂ unit in **C**, which shows no characteristic bands.^[116] Another characteristic band was detected at $\tilde{\nu} = 3264 \text{ cm}^{-1}$, confirming the presence of a (secondary) amino group.^[361] These crucial information finally led to the correct solid-state structure (Figure 85).

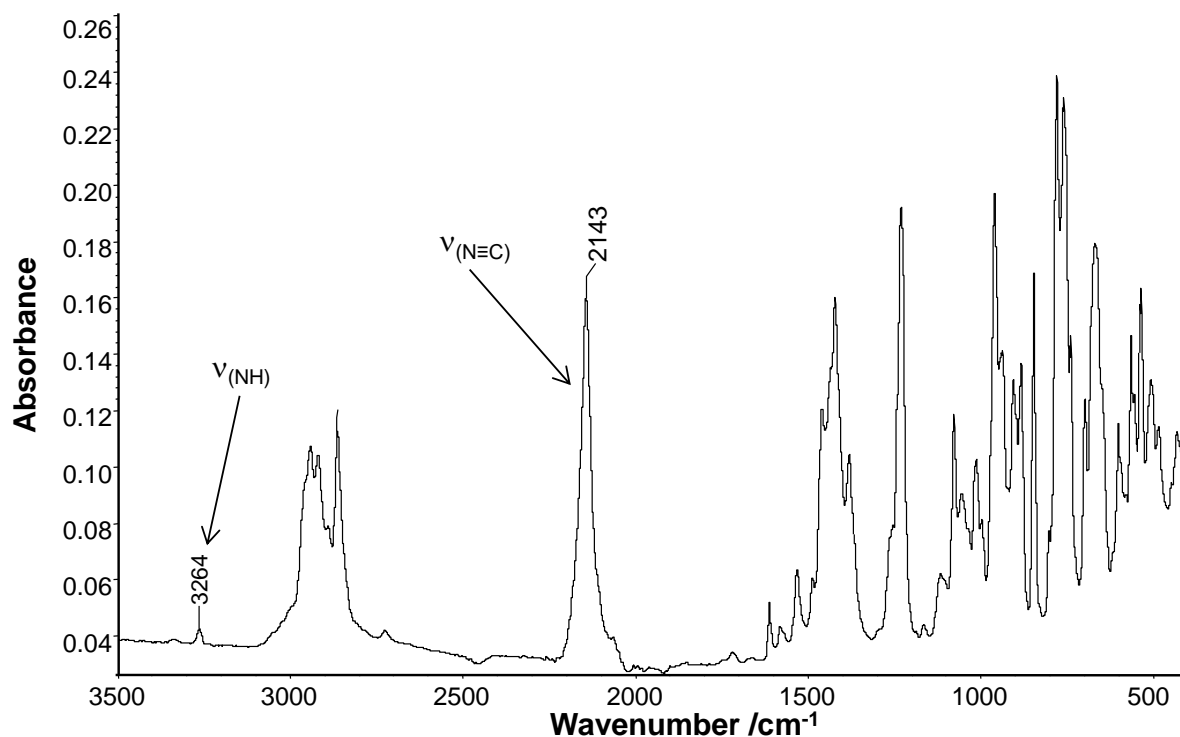


Figure 84. ATR-IR spectrum of a solid sample of **22** at ambient temperature.

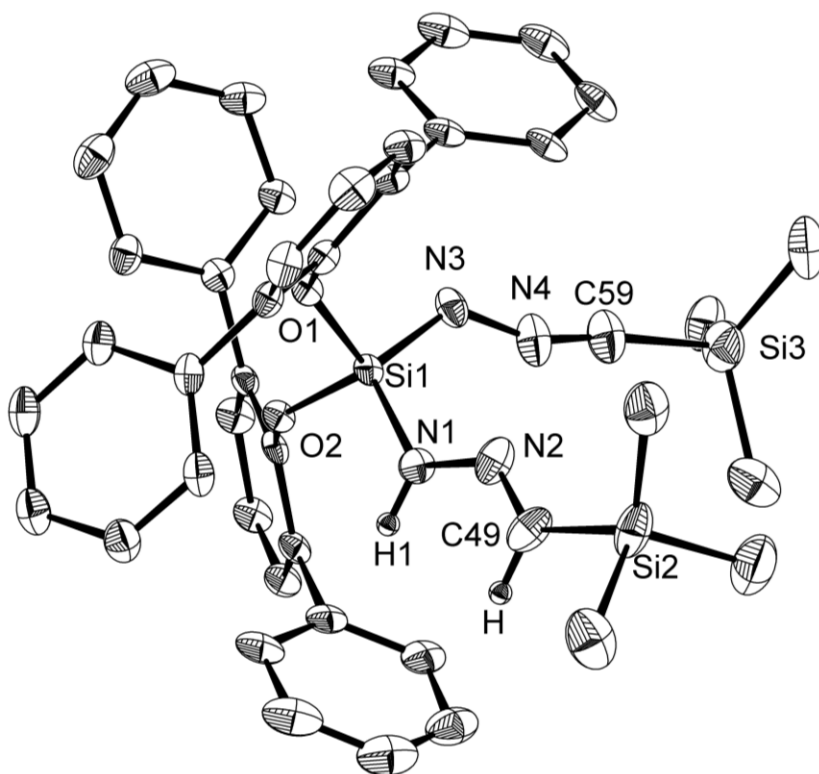


Figure 85. Molecular structure of compound **22** with thermal ellipsoids set to 30 % probability. All methyl groups as well as hydrogen atoms except for H1 and H49 are omitted for simplicity. Selected bond lengths (\AA), angles ($^\circ$) and torsion angles ($^\circ$): Si1-O1 1.630(2), Si1-O2 1.619 (2), Si1-N1 1.702(3), Si1-N3 1.681(3), O1-C1 1.378(3), O2-C25 1.377(3), N1-N2 1.331(4), N2-C49 1.223(6), N3-N4 1.299(4), N4-C59 1.124(6); O2-Si1-O1 100.4(1), N3-Si1-N1 114.2(1), O1-Si1-N1 114.2(1), O1-Si1-N3 108.1(1), O2-Si1-N1 105.9(1), O2-Si1-N3 113.3(1), N2-N1-Si1 125.8(2), C49-N2-N1 126.0(4), N4-N3-Si1 128.6(2), C59-N4-N3 157.5(5); Si1-N1-N2-C49 179.5(4), Si1-N3-N4-C59 $-175.9(10)$, N1-N2-C49-Si2 $-174.5(3)$, N3-N4-C59-Si3 $-177.6(7)$.

The correct solid-state structure of **22** is in agreement with the aforementioned spectroscopic data and of overall good quality. Expectedly, the $\text{Si}(\text{OAr}^{\text{Mes}})_2$ unit it is closely related to those of the other di(aryloxy)silanes **19-AB** with an average Si1-O bond length (1.625(2) \AA) and a O1-Si1-O2 angle of 100.4(1) $^\circ$ (see Table 31 on page 168 for an overview). The N1-Si1-N3 angle of 114.2(1) $^\circ$ is more widened and even larger when compared to the its counterpart in **A** (110.01(8) $^\circ$).^[452] The Si-N distances are fairly similar (Si1-N1: 1.702(3) \AA , Si1-N3: 1.681(3) \AA) and match typical Si(IV)-N single bonds of hydrazido silanes such as $\text{Ph}_2\text{Si}\{\text{N}(\text{H})\text{NMe}_2\}_2$ (1.704(3) \AA) or $\text{Si}\{\text{N}(\text{H})\text{NMe}_2\}_4$ (1.703(2) \AA).^[454] Comparison to the five-coordinated Si(IV) hydrosila hydrazone dimer $[\text{HSi}\{\text{N}_2(\text{Dipp})_2\text{CPh}\}\{\mu^2\text{-N-N=CPh}_2\}]_2$ (1.752(1) \AA)^[455] or the divalent di(amino)silylene **18** (1.722(1) \AA) shows no significant effect of the coordination number of the Si atom. The “upper” nitrilimine substituent is as nearly linear as evidenced by the torsion angles Si1-N3-N4-C59 ($-176(1)$ $^\circ$) and N3-N4-C59-Si3 ($-177.6(7)$ $^\circ$). The N3-N4 distance of 1.299(4) \AA is in between the ranges of a short single- and a double bond and thus considerably shorter than the N-N single bond found in **C-Mes** (1.398(3) \AA),^[116] while the N4-C59 distance of 1.124(6) \AA clearly corresponds to a $\text{C}\equiv\text{N}$ triple bond. These structural parameters also compare well with those of the N-bridged dimeric gallane

[μ^2 -{(Me₃Si)C \equiv N-N}₂Ga(dsi)₂]₂ (O-N-N : 1.251(5) Å, $\text{O-N}\equiv\text{C}$: 1.168(5); $\text{O-N-N}\equiv\text{C}$ 178.9(4)° bridged by the N^β atom).^[456] The “lower” hydrazone substituent adopts a nearly planar core structure as evidenced by the C49-N2-N1 angle of 126.0(4)° as well as the torsion angles Si1-N1-N2-C49 and N1-N2-C49-Si2 of 179.5(4) and -174.5(3)°, respectively. The N1-N2 distance (1.331(4) Å) is again surprisingly short for a single bond and lies in between the N-N single bond found in **C-Mes** (1.398(3) Å)^[116] and the N=N double bond found in the dimeric compound [Ga(dsi)₂{C(SiMe₃)N=N}]₂ (1.200(6) Å; an isomer of the gallane mentioned above and bridged by the terminal N atom).^[456] Consequently, the adjacent N2=C49 bond distance (1.223(6) Å) appears in between a triple and a double bond and is noticeable shorter when compared to the C=N bond in **C-Mes** (1.280(4) Å).^[116]

As briefly mentioned above, detailed NMR-spectroscopic studies were hampered by the severe broadening and overlapping of several signal groups at all accessible temperatures in benzene-d₆, toluene-d₈ and thf-d₆. Compound **22** also slowly decomposes in chloroform-d₁ solutions. Best overall results were obtained at 243 K in toluene-d₈ (Figure 86, bottom), but nevertheless a complete and undoubtful assignment could not be realized even with the help of sliced correlation spectra with enhanced resolution. At this temperature, compound **22** showed an overall C₁ symmetric structure as evidenced by the total number of 10 independent signals for the methyl groups of the Ar^{Mes} substituents in the ¹H NMR spectrum (with two signals of double intensity due to coincidental superposition). While the Tips groups resonate as complex multiplet signals in the aliphatic region around 1 ppm, the chemical shifts observed for the NH moiety at $\delta_{\text{H}} = 3.91$ ppm and the proton of the C(H)Tips group at $\delta_{\text{H}} = 6.28$ ppm are characteristic. In the ¹³C{¹H} NMR spectrum, all signals of the Ar^{Mes} and Tips substituents appear within the expected regions.

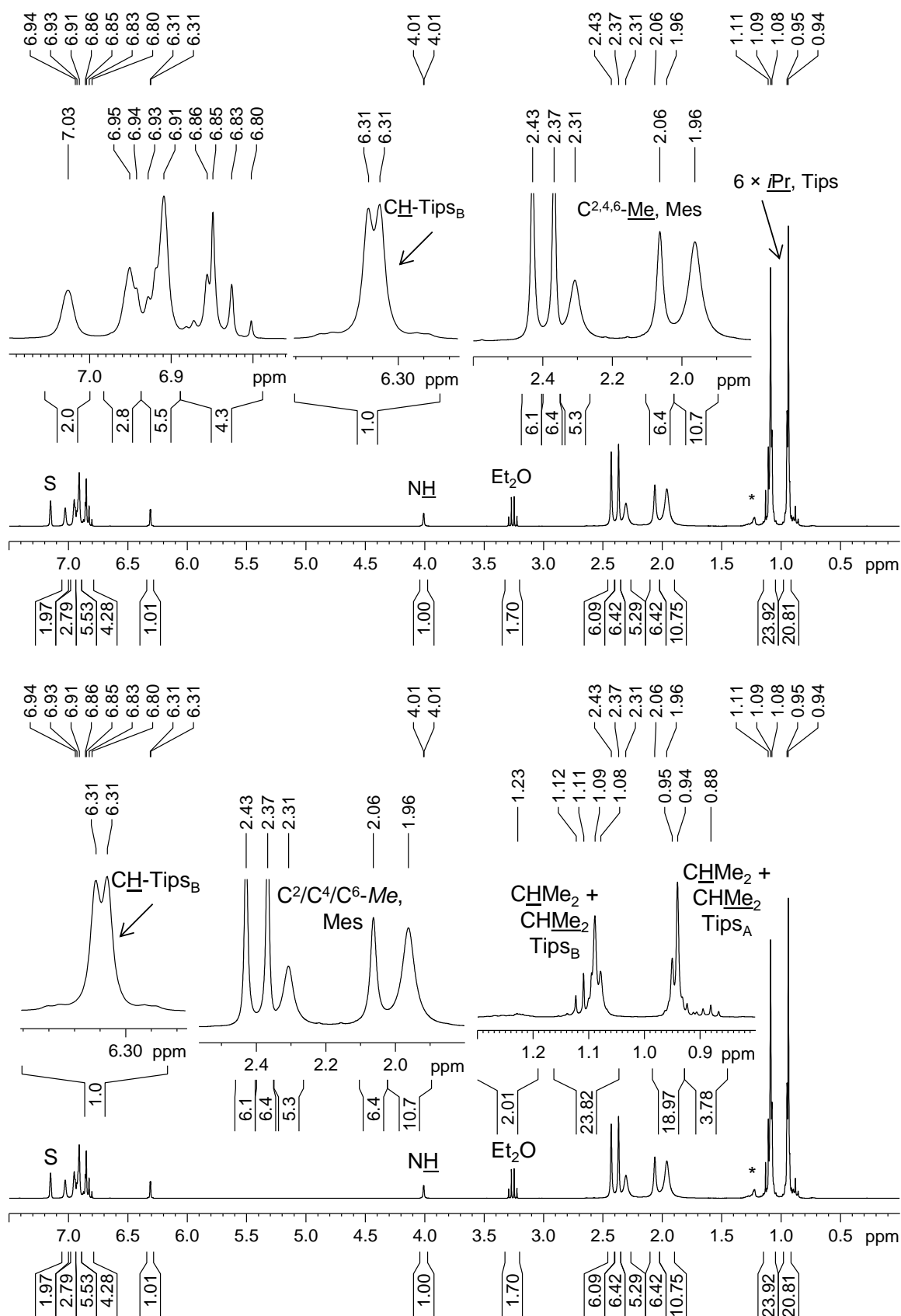


Figure 86. ^1H NMR spectra (500.1 MHz) of **22** in benzene- d_6 at 298 K (top) and in toluene- d_6 at 243 K (below). The spectrum measured in benzene- d_6 still contains a small amount of residual diethyl ether (marked as Et₂O).

Extensive $^{15}\text{N}\{^1\text{H}\}/^1\text{H}$ correlation spectroscopy with a saturated sample at 243 K revealed two signals at $\delta_{\text{N}} = 144.3$ and 372.2 ppm, which were assigned to the Si-bonded NH and the adjacent $\text{N}=\text{C}(\text{H})\text{Tips}$ group of the hydrazoneyl substituent (Figure 87).

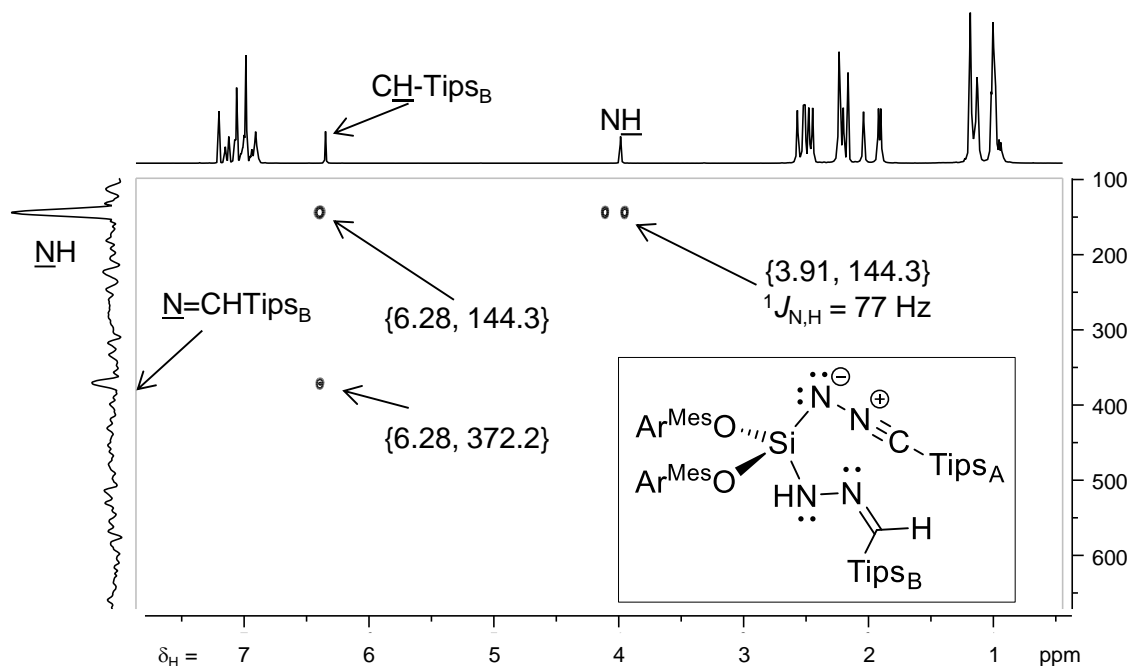


Figure 87. $^1\text{H}/^{15}\text{N}$ HMBC spectrum of **22** in toluene- d_6 at 243 K. The Si- $\text{N}=\text{N}=\text{C}$ -Tips_A signals were not detected.

Unfortunately, no ^{15}N NMR data of compounds **B** and **C-R** with related Si-N-N=C moieties are available for comparison. But in 2015, Tacke and coworkers reported on the five-coordinated benzamidinato-stabilized silimine (SiMe_3) $\text{N}=\text{Si}(\text{NMe}_2)\{\text{N}_2(\text{Dipp})_2\text{CPh}\}$, that was studied by solid-state ^{15}N NMR spectroscopy.^[382] Here, the signal of the imino group is shifted high field up to $\delta_{\text{N}} = 152.0$ ppm, probably as a result of the higher conjugation of the Si atom and the consequential weakening of the Si=N bond. Compared to typical shifts of organic compounds, the resonance of the amino group ($\delta_{\text{N}} = 144.3$) is low field from typical secondary amines R_2NH ($\delta_{\text{N}} = 0$ to 90 ppm) but within the range of secondary amides (110 to 160 ppm), which can be reasoned by the large difference in electronegativity. Meanwhile, the adjacent imino group (372.2 ppm) lies at the upper range expected for organic imines (300 to 375 ppm).^[457]

Finally, in the $^{29}\text{Si}\{^1\text{H}\}$ NMR spectrum of **22**, three singlet signals were, of which the resonances at $\delta_{\text{Si}} = 1.3$ and -3.5 ppm could easily be assigned to the $\text{N}\equiv\text{C}$ -Tips and the $\text{N}=\text{C}(\text{H})$ -Tips group by correlation spectroscopy. The central Si atom resonates at a higher field at $\delta_{\text{Si}} = -88.1$ ppm, which is very close to the resonances of the comparable di(oxy)silanes like **19-Br₂** (-86.1 ppm) or **19-HOtBu^F** (-84.4 ppm).

3.7 Summary & Outlook: Oxysilylene chemistry

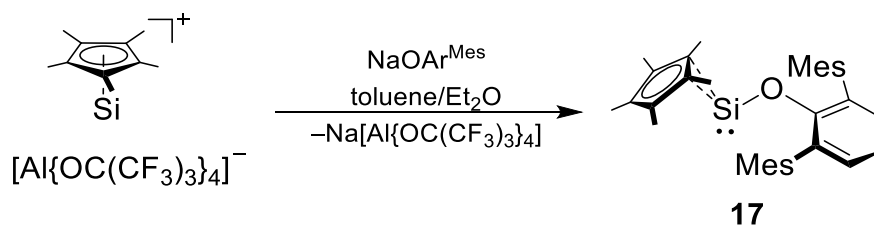
3.7.1 Summary

Transition metal complexes of (oxy)carbenes are the oldest known carbene complexes.^[317,321] Whereas these “Fischer carbenes” have drawn significant attention and found applications in C-C coupling reactions,^[68,319–321] free oxy-carbenes typically rearrange to esters and isolable amino-substituted derivatives remain a very rare academic curiosity.^[323–325]

Heavier di(oxy)tetrrels $E(OR)_2$ ($E = Ge, Sn, Pb$) are known since the 1980s and are typically obtained from EX_2 by salt elimination or by alcoholysis of $E\{N(SiMe_3)_2\}_2$.^[328–330] Depending on the tetrel, substituents and the reaction conditions, a smooth transition between molecular tetrylenes and ionic tetrel(II) alcoxides is observed, which hampers general statements.^[331,332,336] Altogether, the chemistry of $E(OR)_2$ has only been studied briefly but they found limited application as precursor for E or EO_n materials.^[332,342–347]

Given the proverbial oxophilicity of silicon and the recent accomplishments of silicon chemistry, surprisingly little research has been performed on oxy-substituted Si compounds. Whereas the race to the first silanone ($O=SiR_2$, “Kippings dream”) has been decided by Filippou in 2014,^[120] their low-valent derivatives $Si(OR)_2$ were nearly unheard of: when this thesis was started in 2016, no isolable example of a two-coordinated, oxygen-bonded silicon compound was known and only a handful of base-stabilized amidinato-silylenes $Si(OR)\{N_2(tBu)_2CPh\}$ had been published by the groups of Roesky and Driess.^[85,355–357,359] However, in the meantime, considerable progress has been made in the literature: Dr. N. Wienkenhöver obtained an acyclic aryl(aryloxy)silylene **IX** after substitution and monomerization of a dibromodisilene,^[40] Inoue isolated an imino(siloxy)silylene **X** after unprecedented silyl shift of the corresponding silanone isomer^[101] and the group of Aldridge reported on the isolation of a di(boryloxy)silylene **XI** after reduction of the corresponding diiodosilane.^[102]

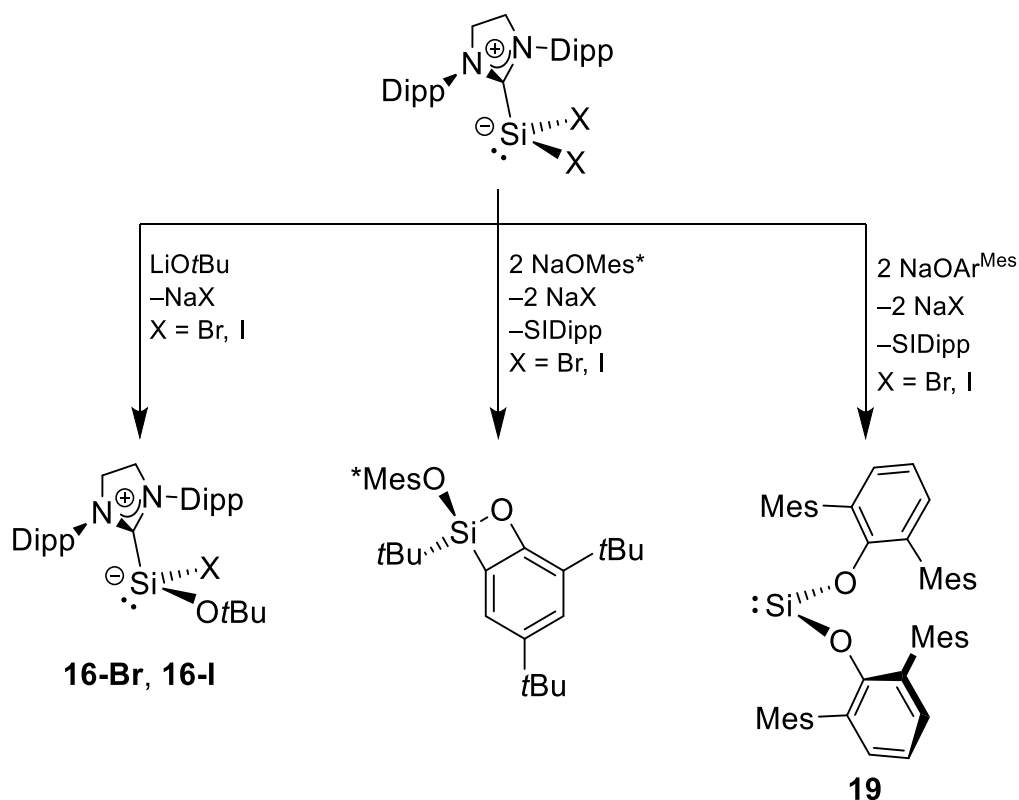
Different synthetic pathways to oxysilylenes were tested in this work: classical reduction of Si(IV) halides, dehydrohalogenation of hydrido(halo)silanes and substitution of Si(II) precursors. Whereas the first approaches were found to be not expedient, the latter were successful. Jutzi’s silyliumylidene cation^[70,366,367] was chosen as a promising starting material, since successful substitution with N-based nucleophiles had already been reported.^[97,367] Indeed, the reaction between $[Cp^*Si][Al\{OC(CF_3)_3\}_4]$ and the bulky terphenyl oxide $NaOAr^{Mes}$ gave the desired hyperconjugated substitution product Cp^*SiOAr^{Mes} (**17**) as a colorless solid in 57 % yield (Scheme 63). Surprisingly, the substitution is dependent on the counter anion and only proceeds with the aluminate salt, whereas the classical boranate anions $[B(C_6F_5)_4]^-$ or $[B(3,5-(CF_3)_2-C_6H_3)_4]^-$ interfere. Unfortunately, similar physical properties hampered the complete separation of the salt from **17**.



Scheme 63. Synthesis of compound **17** from $[\text{Cp}^*\text{Si}][\text{Al}\{\text{OC}(\text{CF}_3)_3\}_4]$ and $\text{NaOAr}^{\text{Mes}}$.

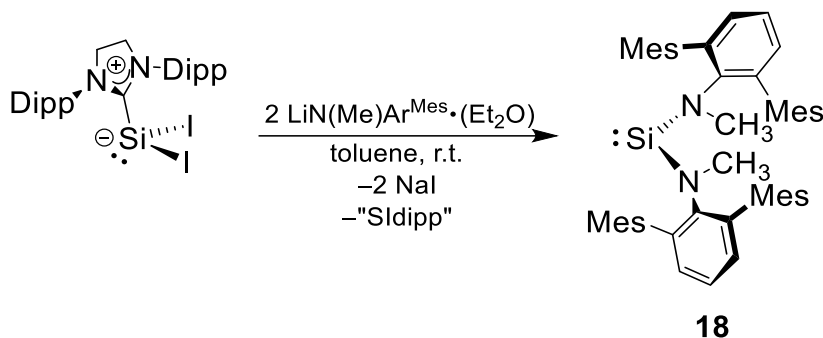
Spectroscopically, a typical fast rotation of the Cp^* substituent in solution was found. The ^{29}Si NMR resonance of compound **17** ($\delta_{\text{Si}} = -138.2$ ppm) compares reasonably well to Inoues silaimine $\eta^2\text{-Cp}^*\text{SiN}=\text{C}\{\text{N}(\text{Dipp})\text{CH}\}_2$ but the aryloxy substituent is responsible for a characteristic shift to higher fields. The monomeric structure was also confirmed by XRD, which revealed a typical η^2 coordination mode of the Cp^* ligand in the solid state as well as an undisturbed Si-O single bond.

Roeskys and Filippous base-stabilized silicon dihalides $\text{SiX}_2(\text{NHC})$ ^[112–114] are among the most versatile building units in modern silicon chemistry and have been used for the synthesis of numerous exciting compounds, including the recent synthesis of cyclic di(phosphano)silylenes $\text{Si}\{\text{P}(\text{Ar})\text{CH}\}_2$ ($\text{Ar} = \text{Mes}^*, \text{Eind}$) by nucleophilic substitution with lithium bisphosphanides.^[133] Here, the reaction of $\text{SiX}_2(\text{SIDipp})$ with LiOtBu in thf resulted in the formation of the first NHC-stabilized oxy(halo)silylenes $\text{SiX}(\text{OtBu})(\text{NHC})$ (**16-X**, $\text{X} = \text{Br}, \text{I}$) which were characterized by NMR spectroscopy, XRD and DFT calculations. Increasing the steric bulk of the alcoholate led to a cleavage of the Si-C^{NHC} bond and twofold substitution: the first di(aryloxy)silylene $\text{Si}(\text{OAr}^{\text{Mes}})_2$ (**19**) was isolated as a colorless solid in 70 % yield on a gram scale (Scheme 64).



Scheme 64. Reaction of $\text{SiX}_2(\text{SIDipp})$ with different alcoholates. The oxosilacyclobutene (middle) is described in detail in the bachelor thesis of C. Lippmann.^[385]

Compound **19** was fully characterized including XRD, Raman spectroscopy and DFT calculations. It features a monomeric structure with long Si-O single bonds, a HOMO/LUMO energy gap of 3.30 eV and a characteristic high field shift to $\delta_{\text{Si}} = 31.9$ ppm was observed by NMR spectroscopy. Silylene **19** is extremely sensitive towards air/moisture but thermally stable; akin to the decomposition of related di(oxy)germylenes,^[332,343] thermolysis under controlled conditions led to the formation of very disperse silicon nanoparticles as evidenced by EDX and TEM. Surprisingly, the synthesis of **19** is very much dependent on the employed alcoholate as no stable derivatives $\text{Si}(\text{OR})_2$ could be obtained by this procedure and reactions with $\text{LiP}(\text{Me})\text{Ar}^{\text{Mes}}$ and $\text{LiB}\{\text{N}(\text{Dipp})\text{CH}\}_2$ only gave $\text{HP}(\text{Me})\text{Ar}^{\text{Mes}}$ and $\text{BrB}\{\text{N}(\text{Dipp})\text{CH}\}_2$, respectively.^[411] Only the reaction with NaOMes^* led to the isolation of an oxosilacyclobutene as result of C-C activation of the putative silylene intermediate, which was isolated and described in the bachelor thesis of C. Lippmann.^[385]



Scheme 65. Synthesis of silylene **18** from $\text{SiI}_2(\text{SIDipp})$ and $\text{LiN}(\text{Me})\text{Ar}^{\text{Mes}}$.

In an excursus, twofold substitution of $\text{SiI}_2(\text{SIDipp})$ using the terphenyl amide $\text{LiN}(\text{Me})\text{Ar}^{\text{Mes}}$ led to the mostly selective formation of the acyclic di(amino)silylene $\text{Si}\{\text{N}(\text{Me})\text{Ar}^{\text{Mes}}\}_2$ (**18**) that was isolated in 55 % yield as a colorless solid and fully characterized. Remarkably, Aldridge and coworkers simultaneously reported on the discovery of $\text{Si}\{\text{N}(\text{SiMe}_3)\text{TBoN}\}_2$ by a similar approach.^[100] Compared to known acyclic aminosilylenes, compound **18** has the highest HOMO-LUMO gap (2.90 eV).^[40,96,98,100] The electronegative amino groups thereby increase the s character of the electron lone pair, which is in agreement with the enormous high field shift of the ^{29}Si NMR resonance.

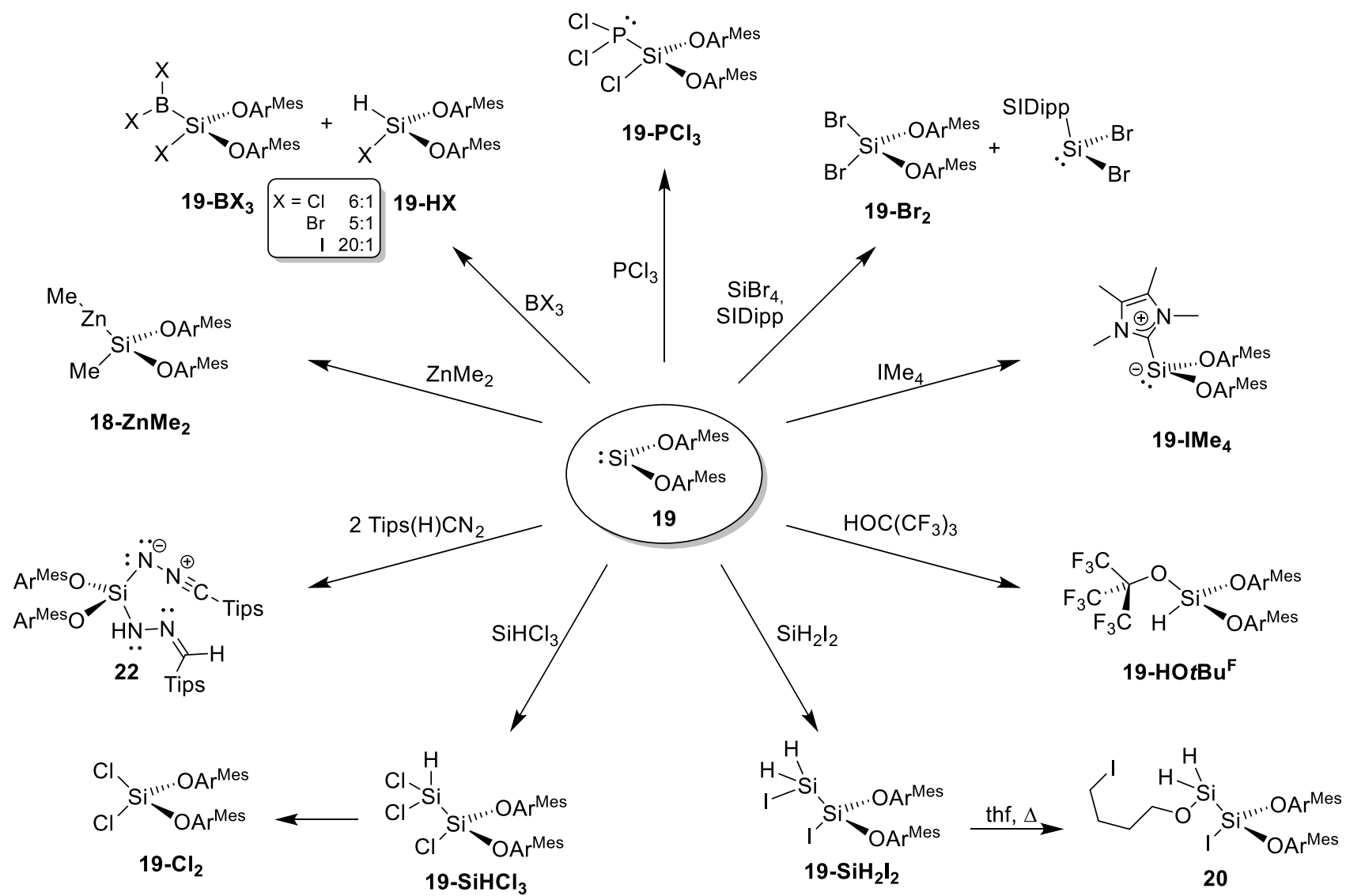
From here, the reactivity of $\text{Si}(\text{OAr}^{\text{Mes}})_2$ (**19**) towards numerous substrates was investigated (Scheme 66 on page 169). Although the free electron lone pair and a vacant p orbital at the Si center make silylene **19** ambiphilic, its reactivity is dominated by its strong electrophilicity. NHC coordination as well as multiple examples of insertions into (or oxidative additions at) electron rich bonds R-R' were found, yielding the respective di(aryloxy)silanes $\text{SiRR}'(\text{OAr}^{\text{Mes}})_2$. While both alkoxysilanes and halosilanes have considerable industrial importance,^[1,68,407] surprisingly little academic research has been done. Compound **19** is a versatile synthon in the synthesis of heavily substituted compounds allowing for the introduction of H, BX_2 , OR, alkyl, SiR_3 , PCl_2 , Cl, Br, I and ZnR groups. With exception of compounds **19-BX₂** which slowly decompose under formal exclusion of $\{\text{BX}_2\}$, all reaction products were isolated and comprehensively characterized (Table 31).

Table 31. Selected structural and spectroscopic data of **19** and its oxidative addition products **19-RR'**.

Compound	O-Si-O /Å	$\text{Si-R/R}'^1$ /Å	O-Si-O /°	$\text{R-Si-R}'$ /°	δ_{Si} (NMR) ² /ppm
19	1.679(1)	-	93.07(6)	-	+31.9
19-IMe₄	1.700(3)	2.013(5) (Si-C)	92.8(1)	-	+7.5
19-HCl ^[385]	1.626(2)	2.086(2) (Si-Cl)	101.5(1)	n.a.	-56.5
19-HBr	1.628(2)	2.213(1) (Si-Br)	101.9(1)	n.a.	n.a.
19-HI	1.629(4)	2.415(2) (Si-I)	102.6(2)	n.a.	n.a.
19-SiHCl₃	1.615(5)	2.343(3) (Si-Si) 2.046(3) (Si-Cl)	102.8(2)	105.0(1)	-61.5
20	1.628(4)	2.345(2) (Si-Si) 2.474(2) (Si-I)	103.8(2)	101.61(7)	-70.5
19-Cl₂	1.6047(9)	Ø1.956(3) (Si-Cl)	105.85(4)	94.3(4)	-69.9
19-Br₂ ^[385]	1.611(2)	Ø2.2623(7) (Si-Br)	105.35(9)	107.49(3)	-86.1
19-I₂ ^[385]	1.615(2)	Ø2.4234(6) (Si-I)	104.4(1)	106.92(4)	-152.0
19-MeI ^[385]	1.644(6)	2.345(3) (Si-I) 1.91(2)(Si-C)	104.2(3)	108.4(5)	-54.3
19-PCl₃	1.612(2)	2.294(1) (Si-P) 2.027(1) (Si-Cl)	103.3(1)	110.93(5)	-68.6
19-ZnMe₂	1.663(2)	2.3755(7) (Si-Zn) 1.837(4) (Si-C)	99.82(8)	114.8(1)	+5.4
19-HOtBu^F	1.613(4)	1.650(4) (Si-O)	104.6(2)	n.a.	-84.4
19-BL₃	[1.653] ³	[2.025 (Si-B)] ³ [2.470 (Si-I)] ³	[101.99] ³	[108.26] ³	-47.0
22	1.625(2)	1.702(3) (Si-N1) 1.681(3) (Si-N3)	100.4(1)	114.2(1),	-88.1

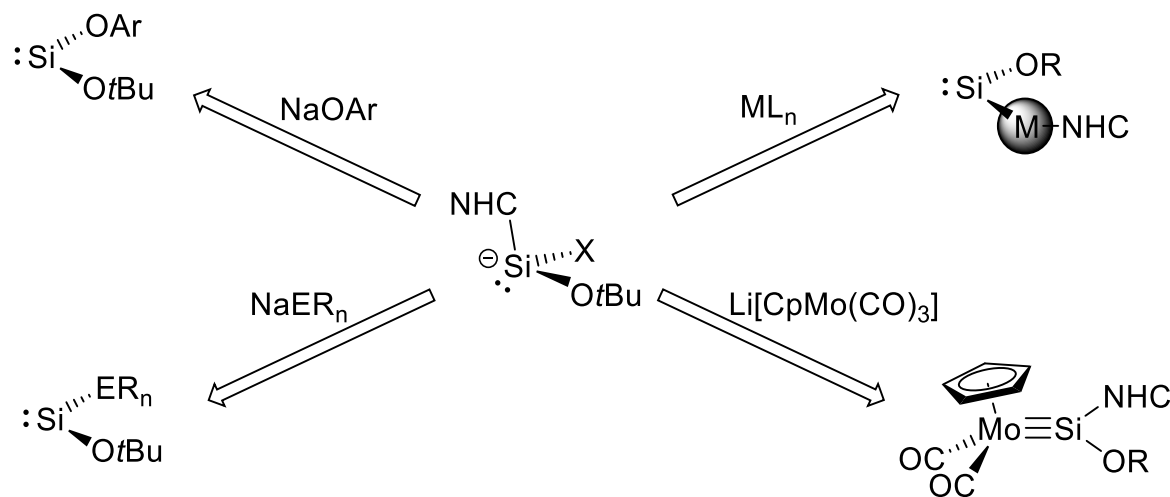
1: R,R' = peripheral substituent; no structural data are given for R,R' = hydrogen and average data are given for R = R'; 2: Resonance of the central alkoxy-substituted Si atom in benzene-d₆; 3: calculated data (B97-D3(BJ)^{ATM}/def2-TZVP level of theory, see page 286 in the appendix).

A noteworthy evidence for the nucleophilicity of **19** was found in reaction with the diazoalkane N₂CHTips. Here its ambiphilicity allowed for a complex reaction cascade, leading to Si{HN=NC(H)Tips}{N≡NCTips}(OAr^{Mes})₂ (**22**), which formally contains a nitrilimine and a hydrazonyl substituent at the now four-coordinated silicon center.

Scheme 66. Reactivity study of the first di(aryloxy)silylene **19**.

3.7.2 Outlook

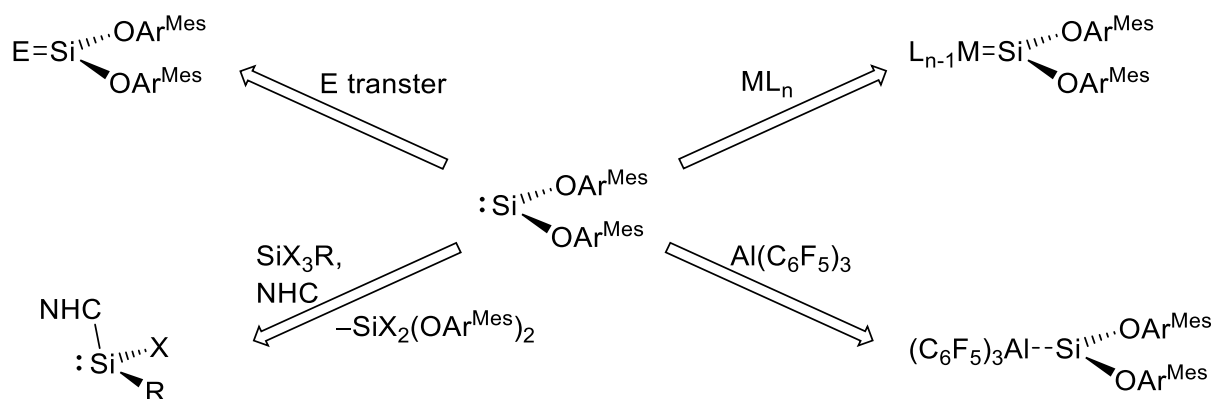
After the successful isolation of base stabilized alkoxy(halo)silylenes $\text{SiX}(\text{OtBu})(\text{NHC})$ (**16-X**), a hyperconjugated oxysilylene $\text{Cp}^*\text{SiOAr}^{\text{Mes}}$ (**17**) and the first acyclic di(aryloxy)silylene $\text{Si}(\text{OAr}^{\text{Mes}})_2$ (**19**) in this work, the field of oxysilylenes has been significantly expanded. Future synthetic targets include mixed di(oxy)silylenes $\text{Si}(\text{OR})(\text{OR}')$ as well as elusive metalla(oxy)silylenes $\text{Si}(\text{ML}_n)(\text{OR})$ or oxy-substituted silylidene and silylidyne complexes $\text{L}_n\text{M}=\text{Si}(\text{OR})(\text{NHC})$ and $\text{L}_n\text{M}\equiv\text{SiR}$. Hereby, compounds **16-X** could be valuable starting points for further functionalization (Scheme 67).



Scheme 67. Potential access to heteroleptic di(oxy)silylenes and metalla(oxy)silylenes. E = B, C, Si, N, P. ML_n = $[\text{Ni}(\text{CDT})]$, $[\text{Pd}(\text{dba})_3]$, $[\text{Pt}(\text{C}_6\text{H}_5)_3]$ or similar unsaturated complexes.

Although nucleophilic substitution of $\text{SiX}_2(\text{NHC})$ were found to be very susceptible to specific reaction conditions and the employed nucleophile as demonstrated by the failed substitutions using a variety of alcoholates, $\text{LiP}(\text{Me})\text{Ar}^{\text{Mes}}$ and $\text{LiB}\{\text{N}(\text{Dipp})\text{CH}\}_2$, further substitution of **16-X** should be possible under the right conditions. For example, $\text{Li}[\text{CpMo}(\text{CO})_3]$ has famously been used for the synthesis of $\text{Si}=\text{Mo}$ and $\text{Si}\equiv\text{Mo}$ bonds starting from $\text{SiClAr}^{\text{Trip}}(\text{IME}_4)$ – a related NHC-stabilized halosilylenes with one bulky substituent.^[458] Potential NHC abstraction from a silylidene complex might be easier in this case because of the +M-effect of the oxygen atom and the weaker $\text{Si}-\text{SiDipp}$ bond.

Driess's benzamidinato-stabilized “bis-silylene oxide” $\text{O}[\text{Si}\{\text{N}_2(\text{tBu})_2\text{CPh}\}]_2$ has successfully been used as a pincer ligand in metal silylene complexes,^[79,81,356] so coordination of **19** towards small metal fragments could be tested as well. The silylene was proven to be ambiphilic, but the steric bulk of the terphenyl substituents limits the selection of suitable substrates (Scheme 68).



Scheme 68. Potential reactions of **19** to be researched. E = chalcogen, X = halogen.

Oxidation with elemental chalcogens (S, Se, Te) or chalcogen transfer reagents (N₂O, peroxides, E=PMe₃) would lead to elusive heavier carbonate derivatives E=Si(OAr^{Mes})₂ whereas coordination of MR₃ (M = B, Al) could yield frustrated Lewis acid/base pairs (FLPs). In fact, test reactions between **19** and Al(C₆F₅)₃ already showed dynamic interactions in the ¹H and ²⁷Al NMR spectra, but no stable adduct could be isolated as workup only afforded the separation of the starting materials. FLPs have recently drawn attention due to their capabilities of metal-free small molecule activation and applications in catalysis,^[427–429] but examples containing silylenes are still rare.^[459–462,428,426,463]

Last but not least, **19** was found to selectively reduce SiBr₄ in presence of free SIDipp, resulting in the clean formation of SiBr₂(OAr^{Mes})₂ and SiBr₂(SIDipp). This concept of a dehalogenation reaction could be applied to a wider variety of small halosilanes, potentially giving access to hitherto unknown derivatives SiX(R)(NHC).

4 Experimental Part

4.1 General Part

Unless specified otherwise, all experiments were carried out under strict exclusion of water and oxygen using Schlenk- or glove box techniques.

Argon was used as a protecting gas. It was commercially received with a purity of $\geq 99.998\%$ and passed through a gas purification system composed of three consecutive columns to remove traces of oxygen and water. The first column was filled with active charcoal, the second column was filled with the BTS catalyst PURISTAR®R3–11G operating at ca. 80 °C and the third was filled with 4 Å molecular sieves. Both molecular sieves and active charcoal were regenerated in an MBRAUN copper catalyst vessel with an integrated heating unit. Regeneration of the catalyst was achieved by heating under commercial hydrogenation gas (NOXAL 4P by AIR LIQUIDE) and subsequent draining of released water.

All glassware was cleaned using standard KOH/isopropanol and dilute HCl baths and subsequent washing with tap water and distilled water. The glassware was then dried in the oven at approximately 110 °C overnight and flame-dried with a heatgun (electric torch) in fine vacuum (10^{-2} mbar) prior to use. Transfer of liquids was facilitated either by ROTH laboratory syringes (0.5 – 25 ml) or using stainless steel transfer- and filter-cannula ($\varnothing = 1$ mm and 2 mm) by applying argon pressure in the originating flask relative to the receiving vessel. For filtrations, WHATMAN™ glass microfiber filters (GF/B 25) were fixed to cannulas with a filterhead on one end and fixed with Teflon tape. Ground glass joints and stopcocks were greased using either PTFE paste (for sensitive compounds) or GLISSEAL® high vacuum lubricating grease (for less sensitive compounds or when the joints were cooled to below -30 °C in a fridge). In some cases, flasks with J. YOUNG valves were used as well.

Protection from light could be achieved by three methods: 1) for reactions at ambient temperature, small vessels usually were covered with a metal can inside a glovebox excluding any light source; 2) for some reactions, brown glassed Schlenk tubes (protection up to $\lambda \approx 500$ nm) were available; 3) in all other cases, regular Schlenk tubes were wrapped with paper towels and aluminum foil. All NMR samples of light sensitive compounds were measured in brown-glassed NMR tubes with J. YOUNG valves and transported in a dark box.

Reduced pressure was generated by mobile diaphragm pumps (up to about 20 mbar) or a diaphragm pump (up to about 5×10^{-3} mbar) that was integrated into the schlenk line. Additionally, air stable compounds could be filtered using water jet pumps and Buchner funnels.

Solids were weighed either inside the glove box using an EXTORIUS EXTEND ED153 electronic scale or in evacuated Schlenk tubes outside the glovebox. The technical weighing error was each about ± 1 mg, but in practice significantly higher due to the constant argon stream inside the gloveboxes. For higher accuracy, stock solutions of less expensive compounds were used in some cases.

Solvents were usually refluxed over a suitable drying agent for 3 – 6 days, purged several times with argon during reflux, distilled under argon and degassed by two freeze-pump-thaw cycles prior to use. Alternatively, an automated MBRAUN solvent purification system (SPS-5) was used and the respective solvents were dispensed directly inside a glove box by a piping system. Fluorobenzene was purged with argon, dried by stirring over CaH_2 for several days, followed by LiAlH_4 overnight and trap-to-trap condensed. Chloroform and dichloromethane were stored in schlenk flasks over 4 Å molecular sieves, acetonitrile was stored in a regular schlenk flask and all other solvents were stored in a glove box in 500 ml SCHOTT DURAN® laboratory glass bottles. For the syntheses of air stable compounds, commercial solvents of technical grade were used without further purification. For drying of deuterated solvents, see Table 32.

Table 32. Drying agents for laboratory solvents.

Solvent	Predrying	Final Drying
Acetonitrile	Sodium wire	CaH_2
Benzene	Sodium wire	Sodium wire
Dichloromethane	SICAPENT®	Na/Pb alloy
Diethyl ether (Et_2O)	Sodium wire	Sodium wire ^A
Dimethoxyethane (DME)	Sodium wire	Sodium wire ^A
Fluorobenzene	CaH_2	LiAlH_4
n-Hexane	-	SPS-5 ^B
Petrol ether (40/60)	-	SPS-5
n-Pentane	-	SPS-5
Tetrahydrofuran (thf)	Sodium wire	Sodium wire
Toluene	-	SPS-5

A: Small amounts of benzophenone were added as an indicator. **B:** for some reactions, commercial n-hexane was first treated with a mixture of conc. H_2SO_4 and 65 % HNO_3 , washed with water and subsequently dried over MgSO_4 and sodium wire to destroy any unsaturated impurities.

Reaction temperatures were usually adjusted by immersing the reaction vessel into a heating/cooling bath. Warming was carried out in silicone oil baths with adjustable mercury contact thermometers; cooling was performed in Dewar vessels containing mixtures of isopropanol or acetone and dry ice or liquid nitrogen. For some reactions, JULABO FPW50-HL cryostats (-50 °C to about 80 °C; fluxes: ethanol for low temperatures, silicon oil for high temperatures) were attached to schlenk tubes with integrated cooling mantles and run for up to

3 days consecutively. For long-time cooling, deep freezers (4 °C, -25 °C, -30 °C and -60 °C) were used.

4.2 Analytical Methods

All nuclear magnetic resonance (NMR) spectra were recorded on either a BRUKER AV I-300 (Oxford Magnet), a BRUKER AV I-400 or a BRUKER AV III HD PRODEGY-500 NMR spectrometer in the NMR department of the University of Bonn. The exact measurement frequencies were changed thorough the years and are given for each respective compound. Samples were prepared by dissolving an appropriate amount (usually 5 – 10 mg for ^1H , ^{19}F or ^{31}P NMR spectra, 30 mg for ^{13}C NMR spectra and up to 100 mg for ^{15}N or ^{29}Si NMR spectra) in 0.4 ml of solvent and transferred into NMR tubes (\varnothing : 5 mm). For air sensitive compounds, tubes with J. YOUNG valves were used. The deuterated solvents were degassed, dried over an appropriate drying agent (see Table 33) and stored under strict exclusion of air and moisture: dimethylsulfoxide- d_6 was stored in a tight vial over molecular sieves (4 Å), acetonitrile- d_3 was stored in a regular J. YOUNG flask and all other solvents were stored in J. YOUNG flasks over molecular sieves (4 Å).

The ^1H and $^{13}\text{C}\{^1\text{H}\}$ NMR spectra were calibrated against the residual proton and natural abundance ^{13}C resonances of the deuterated solvent relative to tetramethylsilane (see Table 33). Heteronuclear spectra were calibrated using the ^2H frequency of the deuterated solvent (lock frequency) as recommended by IUPAC.^[464] The values obtained by this method are identical to a calibration against traditional external reference compounds (see Table 34).

Table 33. Deuterated solvents for NMR spectroscopy.

Solvent	δ_{H}	δ_{C}	Drying Agent
Acetonitrile- d_3	1.94	118.3	CaH_2
Benzene- d_6	7.16	128.0	Na/K alloy
Chlorobenzene- d_5	7.14	134.2	CaH_2
Chloroform- d_1	7.26	77.2	CaH_2
Dichloromethane- d_2	5.32	53.8	CaH_2
Dimethylsulfoxide- d_6	2.05	39.5	Molecular sieves (4 Å)
Tetrahydrofuran- d_5	1.72	25.3	Na/K alloy
Toluene- d_8	2.08	20.4	Na/K alloy

For solvents with several signals, the respective signal used for the calibration is given.

Table 34. Referencing of NMR spectra.^[66]

Nucleus	Ξ /%	Traditional Reference
⁷ Li	38.863797	LiCl, 9.7 mol/kg in D ₂ O
¹¹ B	32.083 97	BF ₃ ·Et ₂ O, φ = 15 % in CDCl ₃
¹⁵ N	10.132912	neat NH ₃ (liquid)
¹⁹ F	94.094 011	neat CCl ₃ F
²⁷ Al	26.056 859	Al(NO ₃) ₃ , 1.1 mol/kg in D ₂ O
²⁹ Si	19.867 187	SiMe ₄ , φ = 15 % in CDCl ₃
³¹ P	40.480 742	external H ₃ PO ₄

The following abbreviations were used for the multiplicities and forms of the individual NMR signals: s = singlet, d = doublet, t = triplet, sept = septet, dec = decet, m = multiplet, br = broad. The full width at half maximum of broad signals was designated as $\Delta\nu_{1/2}$.

For several compounds, more complex aromatic signals (particularly the C^{3,5}-H and C⁴-H proton signals of C₆H₃ groups) were observed. This could be lead back to the ratio of the difference in chemical shift $\Delta\nu$ and the coupling constant ${}^3J_{\text{H,H}}$: whereas for $\Delta\nu \gg J_{\text{H,H}}$ regular doublet and singlet signals are expected for a first order spectrum (AX₂ spin system), for $\Delta\nu \approx J_{\text{H,H}}$ additional second-order splitting is observed (AB₂ spin system).^[361] In the transitional area between “clean” doublet or triplet signals and classic multiplet signals, the respective signals are marked as d* or t* and their ${}^3J_{\text{H,H}}$ coupling constants were obtained by standard methods or, in case of hardship, simulated using the NMR simulation program gNMR.^[360] Likewise, some compounds created pseudo-triplet or pseudo-singlet signals for isochronous C^{3,5}-H and C⁴-H groups of the Ar^{Mes} substituent and affected signals were described as s* or multiplet signals.

The ¹H, ¹³C, ¹⁵N, ¹⁹F, ²⁹Si and ³¹P NMR signals were assigned by a combination of Heteronuclear Multiple-Quantum Correlation (HMQC), Heteronuclear Multiple Bond Correlation (HMBC), Distortionless Enhancement by Polarization Transfer (DEPT) and one- or two-dimensional Nuclear Overhauser Effect Spectroscopy (NOESY) experiments using the program TOPSPINTM 3.0 developed by BRUKER. This allowed an unequivocal assignment of all proton, carbon and heteronuclear resonances of almost all compounds. Signals of diastereotopic groups were labeled with the subscript letters A and B, respectively, whereas the label A was used for the group with the lower ¹H NMR chemical shift. For the determination of apparent point groups in solution see appendix 5.1 on page 237.

ATR-IR spectra were recorded at ambient temperature in the spectral range of 4000 – 400 cm⁻¹ on a BRUKER ALPHA FT-IR spectrometer with a PLATINUM single reflection diamond ATR module inside a glove box. For film spectra (common for in situ reaction controls), a few drops of a solution were evaporated directly on the sample holder. For isolated solids, a few

milligrams were placed on the sample holder and pressed down. The Raman spectra of solids were recorded by Dr. Jürgen Tirr e on a BRUKER MULTIRAM Raman spectrometer ($\tilde{\nu} = 1064$ nm, 1000 mW; Nd:YAG laser, Germanium detector) in the spectral range of $4000 - 100$ cm^{-1} . The measurements were typically performed at ambient temperature, but samples could be cooled manually to reduce fluorescence effects. All samples were filled in glass capillaries ($\text{Ø} = 2$ mm) and sealed off under vacuum. All IR and Raman spectra were analyzed using the program OMNIC 7.3 from the THERMO ELECTRON CORPORATION. The following abbreviations were used for the intensities and shape of the IR or Raman bands: vs = very strong, s = strong, m = medium, w = weak, vw = very weak, sh = shoulder. Assignment of some of the observed bands was performed by comparison with calculated spectra.

UV-vis spectra of solutions were measured by Dr. Andreas L lsdorf, Marcel Krumholz or Leonard Maurer using a THERMO FISHER SCIENTIFIC EVOLUTION 300 spectrophotometer. Samples of analytically pure compounds were dissolved in an exactly weighed amount of an extremely dry solvent, which was prior dried over $\text{K}_2\text{S}_2\text{O}_8$ or LiAlH_4 for several days and then trap-to-trap condensed. The spectra were recorded at 298 K, using a specially designed quartz cell with variable optical path lengths ($d = 10$ mm, 5 mm and 1 mm). Several concentrations were measured and the extinction coefficient ϵ was determined by plotting absorbance versus concentration of the appropriate band. The absorption bands were determined by means of band deconvolution assuming a Gaussian line profile.

All C, H, N elemental analyses were carried out in quadruplicate on an ELEMENTAR VARIO MICRO elemental analyser by the central analytic department of the University of Bonn. The individual results did not differ by more than ± 0.4 % and mean values are given for each compound.

The melting points of all products were studied in quadruplicate for each compound in vacuum sealed glass capillaries using a B CHI M 560 melting point apparatus. The first sample of each compound was heated once with a gradient of 10 $^\circ\text{C}/\text{min}$ for a rough determination of the temperature of melting or starting decomposition. Heating of the other three samples of each compound was then repeated with a gradient of 3 $^\circ\text{C}/\text{min}$, starting ca. 20 $^\circ\text{C}$ below the temperature of melting or starting decomposition of the first sample. The individual temperatures of melting or starting decomposition determined in these three experiments differed by less than 2 $^\circ\text{C}$, and the average of these temperature values is given for each compound. Decomposition of the compounds was verified by recording the ^1H NMR or ATR/IR spectra of the heated samples. Generally, only melting points of analytically pure compounds that are stable at ambient temperature for several days were measured.

The cyclic voltammetric studies were performed by Dr. Burhanshah Lewall or Jens Rump using an AUTOLAB ECO electrochemical workstation (AUTOLAB PGSTAT 20 potentiostat/galvanostat). The results were analyzed with the AUTOLAB software version 4.9. Experiments at ambient temperature were carried out in a glove box using a specially designed, tight full-glass three-electrode cell. 0.1 M [NBu]₄[PF₆] was added to the substrate as a conductivity salt. A glass-carbon disk electrode ($\varnothing = 2$ mm) was used as working electrode and a platinum wire ($\varnothing = 1$ mm) as counter electrode. A 4 mM [Cp*₂Fe]^{0/+} solution in thf was used as a reference electrode and separated from the substrate/electrolyte solution with a VYCOR frit (4 mm). The electrolyte was recrystallized twice from ethanol and carefully dried for 24 h at 80 °C. iR-drop compensation was applied for the experiment. All potentials are given relative to the reference electrode.

For crystal structure determinations, suitable single crystals were isolated from the mother liquor, dried and covered in argon-saturated FOMBLIN®Y inside a glovebox. The crystals were then individually selected using a polarization microscope, transferred to a glass filament attached to a goniometer head and measured by Dr. Gregor Schnakenburg or Charlotte Rödde at the Single crystal X-ray diffraction service of the department of chemistry. Temperature sensitive crystals instead were isolated at lower temperatures at the Schlenk line, FOMBLIN®YH (with lower viscosity) was added by syringe and the selection process was performed in a constant stream of cool gas rising from a dewar filled with liquid nitrogen. The data collections were performed by Dr. Gregor Schnakenburg or Charlotte Rödde on any of the devices listed below (Table 35).

Table 35. Equipment of the Single crystal X-ray diffraction service.

Diffractometer	Radiation ^A , Monochromating	Temperature Device	T ^B /K
STOE IPDS-2T	Mo-K _α , Graphite	CRYOSTREAM 700	123
BRUKER X8-KAPPA APEX II	Mo-K _α Graphite	BRUKER KRYOFLEX	100
NONIUS KAPPACCD	Mo-K _α Graphite	OXFORD CRYOSYSTEMS 600	123
BRUKER D8 VENTRUE	Cu-K _α and Mo-K _α INCOATEC HELIOS	OXFORD CRYOSYSTEMS 800	100

A: Radiation wavelengths: Mo-K_α = 0.71073 Å, Cu-K_α = 1.5418 Å. **B:** The default measurement temperature is given for each device; individual measurement temperatures might differ for technical reasons and are listed in the appendices 5.2 and 5.4.

The respective intensities were measured by fine-slicing φ - and ω -scans and corrected for background, polarization and Lorentz effects. Numerical, empirical or semi-empirical

absorption correction was applied and the structures were solved by direct methods and refined anisotropically by the least-squares procedure implemented in the SHELX program system.^[465] All hydrogen atoms were included isotropically using the riding model on the bound carbon atoms unless specifically stated otherwise.

Some structures contained crystallographic side occupancies (usually percentages of 5 – 10 %, but in exceptions up to about 50 %): Whereas the framework built by the sterically directing substituents was always unambiguous, the respective molecular core moieties could show different, superimposed orientations as a whole. In these cases, substructures were solved independently by standard methods to increase the overall data quality but only the major structure is discussed in the text. This well-known phenomenon is especially common for the silanes obtained from compound **19** (Figure 88) but also for the “rotating” tBu group of the Tbb substituent.

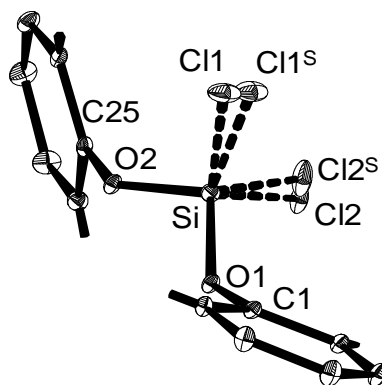


Figure 88. Exemplary side occupancy (48 %) as observed in **19-Cl**. Mesityl groups and H atoms are omitted.

All crystallographic information (distances, angles, torsion angles) were either directly provided by the Single crystal X-ray diffraction service or taken from the respective .res or .cif files using the program OLEX2.^[466] Plane-to-plane angles or special geometric information were generated using functions of OLEX2, but all depictions of molecular structures were generated using the program DIAMOND 2.1C or DIAMOND 4.6.1.^[467,468]

For the crystallographic data files of novel and supporting compounds, see chapter 5.2 and 5.4 in the appendix on pages 239ff and 262ff, respectively.

4.3 Commercially available starting materials

Table 36. Commercially available starting materials.

Compound	Supplier	Purification
Acetone	SIGMA ALDRICH	distillation from molecular sieves (3 Å) under argon
Sodium metal	ACROS ORGANICS	washed with petrol ether, freshly cut under argon
Potassium metal	MERCK	washed with petrol ether, freshly cut under argon
nBuLi	CHEMMETALL	None; stored in a J. Young flask at 4 °C
tBuLi	ALDRICH	None; stored in a J. Young flask at 4 °C
Naphthalene	ACROS ORGANICS	sublimation at 60 °C
Magnesium turnings	ROTH	washing with dil. hydrochloric acid, deionized water, ethanol and diethyl ether; dried in vacuo
Na ₂ CO ₃	SOLVAY CHEMICALS	dried at 110 °C
BCl ₃	ABCR	distillation from Na ₂ CO ₃ under argon
BBr ₃ , 99%	ALDRICH	distillation from Na ₂ CO ₃ under argon
BI ₃ , 98%	ALDRICH	distillation from copper powder
PCl ₅	N.A.	distillation from Na ₂ CO ₃ under argon
Bromine (Br ₂)	ACROS	distillation from Na ₂ CO ₃ under argon
Iodine (I ₂)	VWR	twofold sublimation at 100 °C
LiAlH ₄	ACROS ORGANICS	extraction with Et ₂ O at 40 °C
KOtBu	N.A.	sublimation at 140 °C
SiHCl ₃	ACROS	distillation from K ₂ CO ₃ under argon
SiCl ₄ , 99%	ALDRICH	distillation from K ₂ CO ₃ under argon
Iodomethane	MERCK	distillation from K ₂ CO ₃ under argon
ZnMe ₂ , 98 %	PARKES	None; stored in a glovebox
HOC(CF ₃) ₃ , 97%	FLUOROCHEM	distillation under argon
ZnBr ₂	N.A.	dried at 200 °C
AgOTf	ABCR	used as received
SiH ₃ I	SIGMA ALDRICH	recondensed from Cu powder
SO ₃ , solid	Pure SO ₃ was obtained by the group of Prof. M. Wickleder (cologne university)	

4.4 Literature-known starting materials

Table 37. Starting materials, that were generated following established procedures.

Compound	Experimentator ^A	Reference ^B
[Cp*Si][Al{OC(CF ₃) ₃ } ₄]	S. Schwarzwald, Dr. M. Arz	[127]
[Cp*Si][B(Ar ^{Ar} -CF ₃) ₄]	S. Schwarzwald, Dr. P. Ghana	[127]
[Cp*Si][B(C ₆ F ₅) ₄]	Dr. P. Ghana	[127]
[CuMes] _n	S. Schwarzwald	[469]
[H(OEt) ₂][Al{OC(CF ₃) ₃ } ₄]	S. Schwarzwald, J. Tewes	[368]
[H(OEt) ₂][B(Ar ^{Ar} -CF ₃) ₄] ²	S. Schwarzwald	[368]
{Mg ^{Ar} (nacnac ^{Mes}) ₂ }	S. Schwarzwald, Dr. B. Peerless	[470]
Ag[B(Ar ^{Ar} -CF ₃) ₄]	G. Hofer	[471]
Ar ^{Mes} I	AK Filippou	[472]
Ar ^{Mes} Li	S. Schwarzwald, C. Lippmann	[473]
Ar ^{Mes} OH	S. Schwarzwald, K. Puffler, J. Tewes	[351,369]
NaOAr ^{Mes}	S. Schwarzwald, K. Puffler, J. Tewes	[351]
B(C ₆ F ₅) ₃	G. Hofer, J. Tewes	[474]
SiCp* ₂	S. Schwarzwald	[127]
CuBr	K. Puffler	[475]
CuOtBu	S. Schwarzwald, J. Tewes	[476,477]
IDipp	AK Filippou	[478]
IPr ₂ Me ₂	Dr. D. Geiß	[394]
IMe ₄	S. Schwarzwald	[394]
KC ₈	AK Filippou	[479,480]
KCH ₂ Ph	S. Schwarzwald, Y. Bermes	[481,482]
KCH ₃	S. Schwarzwald	[483]
Li[B(C ₆ F ₅) ₄](Et ₂ O) _{2,5}	K. Puffler	[484]
LiB{N(Dipp)CH} ₂	S. Schwarzwald	[411,485,486]
LiCH ₂ Ph·(thf) _{1,25}	S. Schwarzwald	[487]
Lithium sand	Dr. D. Hoffmann	
Na[B(Ar ^{Ar} -CF ₃) ₄]	K. Puffler, J. Tewes	
NaCH ₂ Ph	S. Schwarzwald	[481]
NaOCAs·(1,4-dioxane) _{2,5}	S. Schwarzwald	[316]
NaOCP·(1,4-dioxane) _{2,25} ¹	Dr. M. Bogner, K. Puffler	[246,247]
PMe ₃	S. Schwarzwald	[488]
SiBr ₂ (SIDipp)	S. Schwarzwald, K. Puffler, J. Tewes	[119]
SiBr ₄	F. Gstrein, D. Kühlmorgen	[175]
SiCl ₂ (IDipp)	J. Tewes	[112]
SIDipp	AK Filippou	[176]
SiI ₂ (SIDipp)	S. Schwarzwald, C. Lippmann	[205]
SiI ₄	K. Puffler, J. Tewes	[175]
Sodium sand	K. Kühnel-Lysek	
Tbb(Br)Si=Si(SIDipp)	S. Schwarzwald, K. Puffler, J. Tewes	[134]
Ar ^{Mes} NH ₂	K. Puffler	[489]
Ar ^{Mes} N(H)Li·(Et ₂ O) _n	S. Schwarzwald, K. Puffler	[377,489]

$\text{Ar}^{\text{Mes}}\text{N}(\text{Me})\text{H}$ ⁴⁰	S. Schwarzwald, K. Puffler	[377]
$\text{Ar}^{\text{Mes}}\text{N}(\text{Me})\text{Li}\cdot(\text{Et}_2\text{O})$	S. Schwarzwald	[377]
$\text{ZnCl}_2\cdot(1,4\text{-dioxane})$	Dr. D. Geiß	n.a.

A: Extremely common starting materials were made by numerous members of the AK Filippou including undergraduate students throughout the years and have been freely available within the group. In this case, no individual experimentators are declared. **B:** For several compounds, group-internal synthetic protocols based on published procedures were available or optimized during this work. In all cases the original scientific publications are cited. **1:** The amount of residual 1,4-dioxane was determined by quantitative $^{31}\text{P}\{^1\text{H}\}$ NMR spectroscopy vs. an internal standard of PPh_3 and further confirmed by elemental analysis. **2:** The reaction was performed in a mixture of fluorobenzene and n-hexane instead of diethyl ether.

⁴⁰ The amine has first been published by the group of Power in 2006 (addition of MeI to a solution of $\text{Ar}^{\text{Mes}}\text{NH}_2$ followed by reflux in MeCN) but no assignment of the provided $^{13}\text{C}\{^1\text{H}\}$ NMR data was given.^[489] It was thus synthesized and characterized following the procedure described in the diploma thesis of Ingo Buchem in 2005 (addition of MeLi to a solution of $\text{Ar}^{\text{Mes}}\text{NH}_2$ in Et_2O at 0 °C).^[377]

4.5 Additional spectroscopic data and improved syntheses of known compounds

Some of the beforehand mentioned compounds were characterized by additional spectroscopic methods or in different solvents, that had not been used by the original authors. These data and/or improved syntheses procedures of known compounds are listed below.

4.5.1 (E)-(SIDipp)Si=Si(Br)Tbb (1)

(E)-(SIDipp)Si=Si(Br)Tbb was prepared in two steps from TbbLi and SiBr₂(SIDipp) by a modified procedure following the one described in the literature.^[134,135]

Two portions of TbbLi are generated from TbbBr (2.05 g, 3.87 mmol, 1.0 equiv.) and tBuLi (2.5 M in n-pentane, 4.17 ml, 7.93 mmol, 2.05 equiv.) by stirring in each 200 ml Et₂O at a temperature between -50 and -55 °C for 5 h. During the last hour the clear, light yellow solutions is exposed to fine vacuum (2×10^{-2} mbar) to evaporate any isobutene from the solutions.⁴¹ The cold solutions are then slowly added to two yellow-orange suspensions of SiBr₂(SIDipp) (4.25 g, 7.35 mmol, 1.9 equiv.) in each 350 ml of toluene at -78 °C under vigorous stirring. The colors immediately change to dark orange-brown and the suspensions are allowed to warm to ambient temperature overnight. The reaction outcomes are investigated by ¹H NMR to determine the amount of free SIDipp present in the mixtures (usually about 0.95 equiv.) and the suspensions are evaporated to dryness. The residues are each suspended in 300 ml toluene and neat SiBr₄ is added (about 5 mol% less than the absolute amount of free SIDipp present in the respective mixture, typically around 1.3 g, 0.45 ml, 3.74 mmol).⁴² The suspensions are again evaporated to dryness and the brown residues are extracted with each 100 ml of warm (50 °C) n-hexane into one joint schlenk tube. Cooling the dark orange to brown filtrate to -30 °C gives a small amount of a pale solid that is filtered off and discarded. The filtrates are then evaporated until incipient precipitation of a yellow solid and cooled to -30 °C at least overnight. The resulting bright yellow precipitate is isolated by filtration at low temperatures and pulverized by a freeze-pump-thaw cycle. The purity is checked by ¹H NMR spectroscopy: if the compound is not pure by at least 95 %, recrystallization from n-hexane is necessary. In a glovebox, small amounts of n-hexane are added which are adsorbed to form a thick, oily, orange suspension (about 3 – 5 ml). During the addition the schlenk is shaken and abruptly stopped, until a large amount of a bright yellow solid crashed out. Another 5 – 10 ml

⁴¹ Isobutene is formed nearly stoichiometric by the side reaction of tBuLi and tBuBr. If it is not removed completely, some of the formed silylene intermediate is trapped by the alkene and the yield of the desired SiBr(SiBr₂Tbb)(SIDipp) drops drastically due to an immensely increased solubility in aliphatic hydrocarbons.

⁴² The resulting [SiBr₂(SIDipp)]Br can be collected, purified and used for the synthesis of SiBr₂(SIDipp). Alternatively, solid FeBr₃ can also be used. In this case, the reaction time is much longer and sonification of the mixture might be needed. An influence of leftover thf in the mixture cannot be ruled out.

of n-hexane is added and the suspension is cooled to $-30\text{ }^{\circ}\text{C}$ overnight to afford $\text{SiBr}(\text{SiBr}_2\text{Tbb})(\text{SIDipp})$ as a pure, bright yellow solid (orange if containing solvent, brown in solution) in yields between 50 and 65 % (ca. 4 to 5.5 g).

Subsequent reduction of the isolated $\text{SiBr}(\text{SiBr}_2\text{Tbb})(\text{SIDipp})$ closely followed the procedure described in the literature.^[134,135] However it was found, that after washing the crude product with a minimal amount of n-hexane and recrystallization from warm ($60\text{ }^{\circ}\text{C}$) toluene at $-30\text{ }^{\circ}\text{C}$, (E)- $(\text{SIDipp})\text{Si}=\text{Si}(\text{Br})\text{Tbb}$ (**1**) can be reproducibly obtained as dark red single crystals with one equivalent of co-crystallized toluene in yields of about 75 %. The crystalline $1\cdot\text{C}_7\text{H}_8$ obtained by this procedure was used for most syntheses, but the toluene can be removed by completely dissolving the solvate in n-hexane or Et_2O and subsequent drying at ambient temperature.

UV-vis (n-hexane, 298 K, dark red solution): λ /nm = 339 ($\epsilon = 10.2\cdot 10^3\text{ L}\cdot\text{mol}^{-1}\cdot\text{cm}^{-1}$), 383 ($\epsilon = 10.2\cdot 10^3\text{ L}\cdot\text{mol}^{-1}\cdot\text{cm}^{-1}$), 524 ($\epsilon = 2.98\cdot 10^3\text{ L}\cdot\text{mol}^{-1}\cdot\text{cm}^{-1}$).

ATR-IR (solid state, RT): $\tilde{\nu}/\text{cm}^{-1} = 3065$ (vw), 3029 (vw), 2958 (s), 2926 (m), 2898 (m), 2867 (m), 2803 (vw), 1587 (w), 1528 (w), 1473 (m), 1451 (m), 1426 (m), 1404 (m), 1395 (m), 1387 (sh), 1362 (w), 1323 (w), 1280 (m), 1271 (m), 1258 (s), 1244 (s), 1177 (w), 1157 (w), 1106 (vw), 1049 (w), 1033 (w), 1013 (w), 989 (vw), 954 (m), 938 (w), 886 (m), 856 (sh), 836 (vs), 800 (s), 772 (sh), 761 (sh), 754 (s), 746 (sh), 724 (w), 685 (s), 664 (m), 619 (m), 611 (sh), 569 (w), 544 (w), 457 (w), 433 (m), 422 (m).

Raman (solid state, RT, 25 mW) : $\tilde{\nu}/\text{cm}^{-1} = 3058$ (m), 3035 (w), 2955 (s), 2930 (s), 2899 (vs), 2868 (m), 2795 (s), 1605 (w), 1589 (s), 1459 (m), 1443 (w), 1406 (s), 1283 (s), 1212 (w), 1176 (m), 1141 (w), 1106 (w), 1038 (w), 1031 (w), 1020 (w), 1004 (s), 955 (vw), 926 (m), 887 (w), 843 (vw), 807 (w), 787 (m), 761 (vw), 755 (vw), 732 (vw), 687 (m), 639 (m), 622 (w), 612 (w), 573 (vs, $\nu_{\text{Si-Si}}$), 546 (w), 522 (vw), 460 (vw), 439 (vw).

^1H NMR (500.1 MHz, tetrahydrofuran- d_8 , 298 K): δ /ppm = -0.13 (s, 36H, $4 \times \text{SiMe}_3$, Tbb), 1.19 (s, 9H, CMe_3 , Tbb), 1.28 (d, 12H, $^3J_{\text{H,H}} = 6.8\text{ Hz}$, $\text{C}^{2,6}\text{-CHMe}_A\text{Me}_B$, Dipp), 1.51 (d, 12H, $^3J_{\text{H,H}} = 6.8\text{ Hz}$, $\text{C}^{2,6}\text{-CHMe}_A\text{Me}_B$, Dipp), 2.90 (s, 2H, $^2J_{\text{Si,H}} = 9.2\text{ Hz}$, $\text{C}^{2,6}\text{-CH}(\text{SiMe}_3)_2$, Tbb), 3.44 (sept, 4H, $^3J_{\text{H,H}} = 6.8\text{ Hz}$, $\text{C}^{2,6}\text{-CHMe}_A\text{Me}_B$, Dipp), 4.16 (s, 4H, $2 \times \text{NCH}_2$, SIDipp), 6.61 (s, 2H, $\text{C}^{3,5}\text{-H}$, Tbb), 7.26 (d, 4H, $^3J_{\text{H,H}} = 7.8\text{ Hz}$, $2 \times \text{C}^{3,5}\text{-H}$, Dipp), 7.32 (t, $^3J_{\text{H,H}} = 7.8\text{ Hz}$, 2H, $2 \times \text{C}^4\text{-H}$, Dipp).

^1H NMR (500.1 MHz, toluene- d_8 , 298 K): δ /ppm = 0.11 (s, 36H, $4 \times \text{SiMe}_3$, Tbb), 1.12 (d, 12H, $^3J_{\text{H,H}} = 6.9\text{ Hz}$, $\text{C}^{2,6}\text{-CHMe}_A\text{Me}_B$, Dipp), 1.27 (s, 9H, CMe_3 , Tbb), 1.57 (d, 12H, $^3J_{\text{H,H}} = 6.9\text{ Hz}$, $\text{C}^{2,6}\text{-CHMe}_A\text{Me}_B$, Dipp), 3.06 (s, 2H, $^2J_{\text{Si,H}} = 9.2\text{ Hz}$, $\text{C}^{2,6}\text{-CH}(\text{SiMe}_3)_2$, Tbb), 3.38 (sept, 4H, $^3J_{\text{H,H}} = 6.9\text{ Hz}$, $\text{C}^{2,6}\text{-CHMe}_A\text{Me}_B$, Dipp), 3.55 (s, 4H, $2 \times \text{NCH}_2$, SIDipp), 6.85 (s, 2H, $\text{C}^{3,5}\text{-H}$, Tbb), 7.07 (d, 4H, $^3J_{\text{H,H}} = 7.7\text{ Hz}$, $2 \times \text{C}^{3,5}\text{-H}$, Dipp), 7.18 (t, $^3J_{\text{H,H}} = 7.7\text{ Hz}$, 2H, $2 \times \text{C}^4\text{-H}$, Dipp).

$^{13}\text{C}\{^1\text{H}\}$ NMR (125.8 MHz, tetrahydrofuran- d_8 , 298 K): δ /ppm = 1.4 (s, 12C, $4 \times \text{SiMe}_3$, Tbb), 25.2 (s, 4C, $2 \times \text{C}^{2,6}\text{-CHMe}_A\text{Me}_B$, Dipp), 26.2 (s, 4C, $2 \times \text{C}^{2,6}\text{-CHMe}_A\text{Me}_B$, Dipp), 29.1 (s, 4C,

$2 \times \text{C}^{2,6}\text{-CHMe}_A\text{Me}_B$, Dipp), 31.3 (s, 3C, CMe_3 , Tbb), 32.9 (s, 2C, $\text{C}^{2,6}\text{-CH}(\text{SiMe}_3)_2$, Tbb), 34.4 (s, 1C, $\text{C}^4\text{-CMe}_3$, Tbb), 53.8 (s, 2C, $2 \times \text{NCH}_2$, SIDipp), 120.5 (s, 2C, $\text{C}^{3,5}\text{-H}$, Tbb), 125.3 (s, 4C, $2 \times \text{C}^{3,5}\text{-H}$, Dipp), 130.0 (s, 2C, $2 \times \text{C}^4\text{-H}$, Dipp), 136.0 (s, 2C, $2 \times \text{C}^1$, Dipp), 137.9 (s, 1C, C^1 , Tbb), 146.7 (s, 4C, $2 \times \text{C}^{2,6}\text{-CHMe}_A\text{Me}_B$, Dipp), 150.9 (s, 2C, $\text{C}^{2,6}\text{-CH}(\text{SiMe}_3)_2$, Tbb), 151.0 (s, 1C, $\text{C}^4\text{-CMe}_3$, Tbb), 204.6 (s, 1C, NCN , SIDipp).

$^{13}\text{C}\{^1\text{H}\}$ NMR (125.8 MHz, toluene- d_8 , 298 K): δ /ppm = 1.4 (s, 12C, $4 \times \text{SiMe}_3$, Tbb), 25.2 (s, 4C, $2 \times \text{C}^{2,6}\text{-CHMe}_A\text{Me}_B$, Dipp), 26.2 (s, 4C, $2 \times \text{C}^{2,6}\text{-CHMe}_A\text{Me}_B$, Dipp), 29.1 (s, 4C, $2 \times \text{C}^{2,6}\text{-CHMe}_A\text{Me}_B$, Dipp), 31.3 (s, 3C, CMe_3 , Tbb), 32.8 (s, 2C, $\text{C}^{2,6}\text{-CH}(\text{SiMe}_3)_2$, Tbb), 34.6 (s, 1C, $\text{C}^4\text{-CMe}_3$, Tbb), 53.8 (s, 2C, $2 \times \text{NCH}_2$, SIDipp), 120.5 (s, 2C, $\text{C}^{3,5}\text{-H}$, Tbb), 125.2 (s, 4C, $2 \times \text{C}^{3,5}\text{-H}$, Dipp), 130.0 (s, 2C, $2 \times \text{C}^4\text{-H}$, Dipp), 136.0 (s, 2C, $2 \times \text{C}^1$, Dipp), 137.9 (s, 1C, C^1 , Tbb), 146.7 (s, 4C, $2 \times \text{C}^{2,6}\text{-CHMe}_A\text{Me}_B$, Dipp), 150.88 (s, 2C, $\text{C}^{2,6}\text{-CH}(\text{SiMe}_3)_2$, Tbb), 150.91 (s, 1C, $\text{C}^4\text{-CMe}_3$, Tbb), 204.7 (s, 1C, NCN , SIDipp).

^{15}N NMR (125.8 MHz, tetrahydrofuran- d_8 , 298 K): δ /ppm = 133.6 (s). This signal could not be detected via 1D NMR spectroscopy, but its position was deduced from a wide-ranged $^1\text{H}\text{-}^{15}\text{N}\{^1\text{H}\}$ HMBC spectrum instead.

4.5.2 Cp^*SiBr_3

Cp^*SiBr_3 was first prepared by Jutzi et al. in 1988 upon nucleophilic substitution of SiBr_4 with LiCp^* in thf.⁴⁹⁰¹ The compound was isolated after distillation in a yield of 30 % and described as a pale yellow liquid. The following procedure is derived from the published one, yielding the compound in a slightly lower yield (26 %) but as a colorless solid instead.

An offwhite suspension of LiCp^* (5.60 g, 39.4 mmol, 1.0 equiv.) in 200 ml of thf was cooled to -80 °C and treated dropwise with neat SiBr_4 (4.94 ml, $\rho = 2.79$ g/ml, ca. 13.83 g, 39.8 mmol, 1.0 equiv.) using a syringe. The reaction mixture was stirred at that temperature for another 15 minutes and then allowed to warm to ambient temperature, whereupon the beige suspension was transformed into a yellow solution.⁴³ ^1H NMR spectroscopy in CDCl_3 revealed a single, broad singlet signal ($\delta_{\text{H}} = 1.786$ ppm, $\nu_{1/2} = 16$ Hz; literature: $\delta_{\text{H}} = 1.80$ ppm) as well as some residual thf. The mixture was reduced to a volume of 20 ml and diluted with a total of 50 ml of n-hexane in portions, resulting in the precipitation of a colorless solid (LiBr). The solid was separated by filtration and extracted with another 15 ml of n-hexane (residue: 3.8 g of a pale violet solid). The combined, bright yellow filtrates were carefully distilled at fine vacuum (about 5×10^{-2} mbar) resulting in four fractions of which the middle fractions at head temperature of ~ 100 °C (colorless, 4.6 g) and $100 - 110$ °C (light yellow, incipient crystallization, 5.9 g) were found to contain Cp^*SiBr_3 by NMR spectroscopy. Both were combined, diluted with 5 ml of n-hexane and re-distilled to obtain about 4.8 g of a colorless,

⁴³ In contrast to the report of Jutzi et al., no precipitation of LiBr was observed yet.

oily liquid at a head temperature of 65 °C. This was dissolved in 5 ml of n-hexane and cooled to -30 °C to obtain large, colorless crystals. Grinding and drying at ambient temperature for 2 h afforded Cp*SiBr₃ as a colorless solid. Yield: 4.10 g (10.2 mmol, 26 % from LiCp*). No melting point could be measured because the sticky Cp*SiBr₃ would clog the glass capillary and liquefy when pressured with a steel wire. Elemental analysis calcd. (%) for C₁₀H₁₅Br₃Si (597.25): C 29.80, H 3.75; found: C 30.18, H 3.68 %.

¹H NMR (300.1 MHz, chloroform-d₁, 298 K): δ/ppm = 1.82 (s, 15H, C₅Me₅).

¹³C{¹H} NMR (125.8 MHz, chloroform-d₁, 298 K): δ /ppm = 12.3 (s, 5H, C₅Me₅), 135 – 145 (very broad, 5C, C₅Me₅).

²⁹Si{¹H} NMR (99.36 MHz, chloroform-d₁, 298 K): δ /ppm = -15.6 (s).

4.5.3 Benzyl lithium (LiCH₂Ph·(thf)_{1.25})

Benzyl lithium was prepared upon metalation of toluene with n-BuLi in the presence of excess thf.^[487] The isolated yellow solid was identified as the solvate LiCH₂Ph·(THF)_{1.25} by NMR spectroscopy. Yield: 6.11 g (32.5 mmol, 87% from n-butyllithium).

¹H NMR (300.1 MHz, benzene-d₆, 298 K): δ/ppm = 1.32 (m, 5H, C^{3,4}H₂, THF), 1.68 (s, 2H, CH₂Li), 3.44 (m, 5H, C^{2,5}H₂, THF), 6.54 (tt, ³J_{H,H} = 7.2 Hz, ⁴J_{H,H} = 1.1 Hz, 1H, C⁴-H, phenyl), 6.73 (m, 2H, C^{2,6}-H, phenyl), 7.09 (m, 2H, C^{3,5}-H, phenyl).

⁷Li{¹H} NMR (116.6 MHz, benzene-d₆, 298 K): δ/ppm = 1.16 (s).

¹³C{¹H} NMR (125.8 MHz, benzene-d₆, 298 K): δ/ppm = 25.5 (s, C^{3,4}H₂, THF), 28.0 (s, 1C, CH₂Li), 68.3 (s, C^{2,5}H₂, THF), 114.0 (s, 1C, C⁴-H, phenyl), 120.3 (s, 2C, C^{2,6}-H, phenyl), 129.9 (s, 2C, C^{3,5}-H, phenyl), 156.0 (s, 1C, C¹, phenyl).

4.5.4 Benzyl sodium (NaCH₂Ph)

Benzyl sodium was synthesized following the procedure described for KCH₂Ph.^[481] Metalation of toluene with nBuLi using NaOtBu instead of KOtBu afforded the compound as a dark yellow to orange solid. It was shown to be pure by NMR spectroscopy but decomposes in thf solution within a few hours to give toluene and (presumably) an thf oligomer. Yield: 2.10 g (18.4 mmol, 92% from NaOtBu).

¹H NMR (300.1 MHz, tetrahydrofuran-d₈, 298 K): δ/ppm = 1.92 (s, 2H, CH₂Na), 5.03 (tt, ³J_{H,H} = 6.8 Hz, ⁴J_{H,H} = 1.2 Hz, 1H, C⁴-H, phenyl), 5.83 (m, 2H, C^{2,6}-H, phenyl), 6.15 (m, 2H, C^{3,5}-H, phenyl).

¹³C{¹H} NMR (75.47 MHz, tetrahydrofuran-d₈, 298 K): δ/ppm = 0.7 (s, 1C, CH₂Na), 100.1 (s, 1C, C⁴-H, phenyl), 113.1 (s, 2C, C^{2,6}-H, phenyl), 129.5 (s, 2C, C^{3,5}-H, phenyl), 157.2 (s, 1C, C¹, phenyl).

4.6 Syntheses of novel Compounds

4.6.1 [(SIDipp)Si(Li·dme)Si(H){C(SiMe₃)₂-C₆H₂-4-*t*Bu,6-(CH)(SiMe₃)₂] (2)

A solid mixture of **1** (570 mg, 0.584 mmol, 1.0 equiv.) and lithium sand (10 mg, 1.46 mmol, 2.5 equiv.) was suspended in precooled dme at about $-60\text{ }^{\circ}\text{C}$ (just above freezing temperature). The suspension was warmed to ambient temperature over a period of 3 h whereby the color darkened from orange-brown to a deep red-brown. The mixture was stirred for another hour when the solvent was evaporated. The dark, sticky residue was digested in a small amount of *n*-pentane, dried again and then extracted with 2×5 ml of *n*-pentane. The volume was reduced to about 3 ml and the solution was cooled to $-30\text{ }^{\circ}\text{C}$ for 5 days when dark red crystals had grown. The solid was isolated by filtration at $-30\text{ }^{\circ}\text{C}$, recrystallized from a small amount of *n*-pentane following the same procedure. The resulting crystals were then collected at low temperature, dried by a freeze-pump-thaw cycle and for another 30 minutes at ambient temperature. Yield: 273 mg (0.30 mmol, 52 %). Compound **2** gradually turns to a very dark red tone above $160\text{ }^{\circ}\text{C}$ and melts under decomposition at $171\text{ }^{\circ}\text{C}$. Elemental analysis calcd. (%) for C₅₁H₈₇LiN₂Si₆C₄H₁₀O₂ (975.81): C 66.47, H 9.84, N 2.82; found: C 64.90, H 9.25, N 2.67 %. The elemental analysis revealed too low C and H contents which might be explained by contamination with LiBr or decomposition material due to the extreme sensitivity of **2**.

ATR-IR (solid state, RT): $\tilde{\nu}/\text{cm}^{-1} = 3056$ (vw), 2951 (m), 2898 (w), 2866 (w), 2073 (w, $\nu_{\text{Si-H}}$), 1574 (vw), 1545 (vw), 1459 (w), 1441 (w), 1382 (vw), 1316 (vw), 1345 (vw), 1325 (vw), 1272 (sh), 1244 (m), 1236 (sh), 1218 (m), 1183 (m), 1158 (w), 1115 (w), 1078 (m), 1050 (w), 1072 (vw), 1018 (vw), 991 (w), 919 (m), 891 (m), 870 (sh), 856 (sh), 834 (vs), 801 (m), 781 (w), 763 (s), 732 (m), 723 (m), 686 (m), 668 (m), 637 (w), 606 (w), 591 (w), 560 (m), 523 (vw), 502 (m), 473 (w), 460 (vw), 440 (vw), 429 (m).

¹H NMR (500.2 MHz, benzene-*d*₆, 298 K):⁴⁴ $\delta/\text{ppm} = 0.294$ (s, 9H, C²-C(SiMe₃)_A(SiMe₃)_B, Tbb^{act}), 0.295 (s, 9H, C²-C(SiMe₃)_A(SiMe₃)_B, Tbb^{act}), 0.30 (s, 9H, C⁶-CH(SiMe₃)_A(SiMe₃)_B, Tbb^{act}), 0.35 (s, 9H, C⁶-CH(SiMe₃)_A(SiMe₃)_B, Tbb^{act}), 1.22 (d, $^3J_{\text{H,H}} = 6.7$ Hz, 3H, C²-CHMe_AMe_B, Dipp_A), 1.26 (d, $^3J_{\text{H,H}} = 6.7$ Hz, 3H, C²-CHMe_AMe_B, Dipp_B), 1.36 (d, $^3J_{\text{H,H}} = 6.7$ Hz, 3H, C²-CHMe_AMe_B, Dipp_B), 1.37 (s, 9H, CMe₃, Tbb^{act}), 1.40 (d, $^3J_{\text{H,H}} = 6.7$ Hz, 3H, C⁶-CHMe_AMe_B, Dipp_A), 1.51 (d, $^3J_{\text{H,H}} = 6.7$ Hz, 3H, C⁶-CHMe_AMe_B, Dipp_A), 1.53 (d, $^3J_{\text{H,H}} = 6.7$ Hz, 3H, C²-CHMe_AMe_B, Dipp_A), 1.71 (d, $^3J_{\text{H,H}} = 6.7$ Hz, 3H, C⁶-CHMe_AMe_B, Dipp_B), 1.78 (s, 1H, C⁶-CH(SiMe₃)_A(SiMe₃)_B, Tbb^{act}), 1.84 (d, $^3J_{\text{H,H}} = 6.7$ Hz, 3H, C⁶-CHMe_AMe_B, Dipp_B), 2.58 (br, 4H, $2 \times \text{CH}_2$, DME), 2.89 (br s, $\nu_{1/2}$

⁴⁴ Despite considerable efforts, full assignment of all ¹H and ¹³C NMR data was found to be very difficult due to the low symmetry of compound **2**, small amounts of unknown impurities and the limitation of the spectral resolution. It is possible, that the C⁶-bonded isopropyl group of Dipp_A was confused with one of the isopropyl groups of Dipp_B. Similarly, distinction of the C¹ atoms of the Dipp groups and the C² atom of Dipp_B is not unambiguous.

= 7 Hz, 6H, 2 × OMe, DME), 3.28 (sept, $^3J_{\text{H,H}} = 6.8$ Hz, 1H, C⁶-CHMe_AMe_B, Dipp_A), 3.45 (m, 1H, N¹C⁵H_AH_B, SIDipp), 3.51 (m, 1H, N³C⁴H_AH_B, SIDipp), 3.60 (m, 1H, C²-CHMe_AMe_B, Dipp_A), 3.65 (m, 1H, N¹C⁵H_AH_B, SIDipp), 3.84 (m, 1H, N³C⁴H_AH_B, SIDipp), 3.86 (m, 1H, C²-CHMe_AMe_B, Dipp_B), 3.96 (sept, $^3J_{\text{H,H}} = 6.8$ Hz, 1H, C⁶-CHMe_AMe_B, Dipp_B), 5.09 (s, $^1J_{\text{Si,H}} = 172$ Hz, 1H, Si-H), 6.82 (d, $^4J_{\text{H,H}} = 1.5$ Hz, 1H, C³-H, Tbb^{act}), 6.86 (d, $^4J_{\text{H,H}} = 1.5$ Hz, 1H, C⁵-H, Tbb^{act}), 6.92 (m, 1H, C⁴-H, Dipp_A), 6.95 (dd, $^3J_{\text{H,H}} = 7.4$ Hz, $^4J_{\text{H,H}} = 1.8$ Hz, 1H, C³-H, Dipp_A), 6.99 (dd, $^3J_{\text{H,H}} = 7.4$ Hz, $^4J_{\text{H,H}} = 1.8$ Hz, 1H, C³-H, Dipp_A), 7.26 (dd, $^3J_{\text{H,H}} = 6.8$ Hz, $^4J_{\text{H,H}} = 2.8$ Hz, 1H, C³-H, Dipp_B), 7.31 (m, 1H, C⁵-H, Dipp_B), 7.32 (m, 1H, C⁴-H, Dipp_B).

¹³C{¹H} NMR (125.8 MHz, benzene-d₆, 298 K):⁴⁴ δ /ppm = 1.4 (s, 3C, C²-C(SiMe₃)_A(SiMe₃)_B, Tbb^{act}), 1.6 (s, 3C, C²-C(SiMe₃)_A(SiMe₃)_B, Tbb^{act}), 2.1 (s, 3C, C⁶-CH(SiMe₃)_A(SiMe₃)_B, Tbb^{act}), 3.3 (s, 3C, C⁶-CH(SiMe₃)_A(SiMe₃)_B, Tbb^{act}), 23.8 (s, 1C, C²-C(SiMe₃)_A(SiMe₃)_B, Tbb^{act}), 24.68, 24.72 (C²-CHMe_AMe_B and C⁶-CHMe_AMe_B, each Dipp_A), 24.9 (s, 1C, C⁶-CHMe_AMe_B, Dipp_B), 25.2 (s, 1C, C²-CHMe_AMe_B, Dipp_A), 25.5 (s, 1C, C⁶-CHMe_AMe_B, Dipp_A), 25.79, 25.81 (each s, each 1C, C²-CHMe_AMe_B, and C⁶-CHMe_AMe_B, each Dipp_B), 26.4 (s, 1C, C²-CHMe_AMe_B, Dipp_B), 27.1 (s, 1C, C⁶-CH(SiMe₃)_A(SiMe₃)_B, Tbb^{act}), 28.64 (s, 1C, C²-CHMe_AMe_B, Dipp_B), 28.8 (s, 1C, C²-CHMe_AMe_B, Dipp_B), 28.9 (s, 1C, C⁶-CHMe_AMe_B, Dipp_A), 29.0 (s, 1C, C⁶-CHMe_AMe_B, Dipp_B), 31.8 (s, 3C, CMe₃, Tbb^{act}), 34.5 (s, 1C, CMe₃, Tbb^{act}), 51.7 (s, 1C, N¹C⁵H_AH_B, SIDipp), 55.0 (s, 1C, N³C⁴H_AH_B, SIDipp), 60.1 (br, $\nu_{1/2} = 41$ Hz, 2C, 2 × OMe, DME), 69.6 (br, $\nu_{1/2} = 20$ Hz, 2C, 2 × CH₂, DME), 117.3 (s, 1C, C³-H, Tbb^{act}), 120.7 (s, 1C, C⁵-H, Tbb^{act}), 123.9 (s, 1C, C³-H, Dipp_A), 124.7 (s, 1C, C³-H, Dipp_A), 125.1 (s, 1C, C⁴-H, Dipp_A), 125.4 (s, 1C, C⁴-H, Dipp_B), 127.1 (s, 1C, C³-H, Dipp_B), 127.7 (s, 1C, C⁵-H, Dipp_B), 141.8 (s, 1C, C¹, Dipp_A), 144.0 (s, 1C, C¹, Tbb), 144.2 (s, 1C, C¹, Dipp_B), 145.1 (s, 1C, C⁶, Tbb^{act}), 147.4 (s, 1C, C⁶, Dipp_A), 147.9 (s, 1C, C⁶, Dipp_B), 149.6 (s, 1C, C², Dipp_A), 150.0 (C², Dipp_B), 150.3 (s, 1C, C⁴-CMe₃, Tbb^{act}), 157.5 (s, 1C, C², Tbb^{act}), 197.9 (s, 1C, NCN, SIDipp).

⁷Li{¹H} NMR (194.3 MHz, benzene-d₆, 298 K): δ /ppm = -0.57 (s, $^1J_{\text{Si,Li}} = 72$ Hz, $\nu_{1/2} = 12$ Hz), (br, $\nu_{1/2} = 228$ Hz). The signal ratio is about 2:1, presumably caused by the formation of different clusters or solvates in solution.

²⁹Si{¹H} NMR (59.63 MHz, benzene-d₆, 298 K): δ /ppm = -62.3 (s, $^1J_{\text{Si,Li}} = 70$ Hz, 1Si, LiSi(SIDipp), -14.7 (s, $^1J_{\text{Si,H}} = 173$ Hz, 1Si, SiH), -1.1, -0.5, 0.5, 1.6 (each s, each 1Si, 4 × SiMe₃). See also Figure 14 on page 25.

4.6.2 (E)-(SIDipp)Si=Si(CH₂Ph)Tbb (1-Me)

A dark red solution of 1·C₇H₈ (770 mg, 0.72 mmol, 1.0 equiv.) in 20 ml thf was treated with a solution of MeLi in diethyl ether (0.47 ml, 1.7 M, 0.79 mmol, 1.1 equiv.) at -50 °C and the reaction mixture was warmed to ambient temperature overnight. The reaction progress was

investigated by ^1H NMR spectroscopy (ca 50 % conversion). The mixture was then cooled to $-60\text{ }^\circ\text{C}$ and treated with another portion of MeLi in diethyl ether (0.51 ml, 1.7 M, 0.87 mmol, 1.2 equiv.) and slowly warmed to ambient temperature over 8 h. Full conversion was verified by ^1H NMR spectroscopy and the solvent was evaporated in vacuo. The red, sticky residue was suspended in 5 ml on n-hexane, again evaporated and the residue was extracted with about 20 ml of n-hexane in 3 portions. The colorless residue (LiBr) was discarded and the red filtrate was reduced to incipient precipitation. Cooling to $-30\text{ }^\circ\text{C}$ overnight afforded ca. 600 mg crude product as a red powder, which was recrystallized from hot diethyl ether at $-30\text{ }^\circ\text{C}$ for three days. During this time, large blocks of the hemisolvate **1-Me**·0.5 Et₂O had formed. Yield: 495 mg (0.52 mmol, 72 %). Compound **1-Me** melts at $233\text{ }^\circ\text{C}$ to a dark red, nearly black liquid. Elemental analysis calcd (%) for (C₅₂H₉₀N₂Si₆)·0.5(C₄H₁₀O) (948.86): C 68.35, H 10.09, N 2.95; found: C 68.43, H 10.29, N 2.93 %.

^1H NMR (500.2 MHz, benzene-d₆, 298 K): δ /ppm = 0.15 (s, 36H, $^2J_{\text{Si,H}} = 119\text{ Hz}$, 4 × SiMe₃, Tbb), 1.15 (d, 12H, $^3J_{\text{H,H}} = 6.8\text{ Hz}$, C^{2,6}-CHMe_AMe_B, Dipp), 1.33 (s, 3H, Si=SiMe), 1.34 (s, 9H, CMe₃, Tbb, this signal partially overlaps with the signal at $\delta = 1.33\text{ ppm}$), 1.56 (d, 12H, $^3J_{\text{H,H}} = 6.8\text{ Hz}$, C^{2,6}-CHMe_AMe_B, Dipp), 3.04 (s, 2H, $^2J_{\text{Si,H}} = 9.3\text{ Hz}$, C^{2,6}-CH(SiMe₃)₂, Tbb), 3.32 (sept, 4H, $^3J_{\text{H,H}} = 6.8\text{ Hz}$, 2 × C^{2,6}-CHMe_AMe_B, Dipp), 3.51 (s, 4H, 2 × NCH₂, SIDipp), 6.91 (s, 2H, C^{3,5}-H, Tbb), 7.09 (d, 4H, $^3J_{\text{H,H}} = 7.8\text{ Hz}$, 2 × C^{3,5}-H, Dipp), 7.22 (t, $^3J_{\text{H,H}} = 7.8\text{ Hz}$, 2H, 2 × C⁴-H, Dipp).

$^{13}\text{C}\{^1\text{H}\}$ NMR (75.47 MHz, benzene-d₆, 298 K): δ /ppm = 1.4 (s, 12C, $^1J_{\text{Si,C}} = 51.0\text{ Hz}$, 4 × SiMe₃, Tbb), 10.1 (s, 1C, Si=SiMe), 24.7 (s, 4C, 2 × C^{2,6}-CHMe_AMe_B, Dipp), 26.0 (s, 4C, 2 × C^{2,6}-CHMe_AMe_B, Dipp), 29.1 (s, 4C, 2 × C^{2,6}-CHMe_AMe_B, Dipp), 31.4 (s, 3C, CMe₃, Tbb), 32.4 (s, 2C, C^{2,6}-CH(SiMe₃)₂, Tbb), 34.3 (s, 1C, C⁴-CMe₃, Tbb), 53.4 (s, 2C, 2 × NCH₂, SIDipp), 120.3 (s, 2C, C^{3,5}-H, Tbb), 125.1 (s, 4C, 2 × C^{3,5}-H, Dipp), 129.8 (s, 2C, 2 × C⁴-H, Dipp), 136.5 (s, 2C, 2 × C¹, Dipp), 139.5 (s, 1C, C¹, Tbb), 146.5 (s, 4C, 2 × C^{2,6}-CHMe_AMe_B, Dipp), 149.4 (s, 1C, C⁴-CMe₃, Tbb), 149.8 (s, 2C, C^{2,6}-CH(SiMe₃)₂, Tbb), 208.7 (s, 1C, NCN, SIDipp).

^{29}Si NMR (99.37 MHz, benzene-d₆, 298 K): δ /ppm = 1.5 (s, 4Si, 4 × SiMe₃), 50.4 (s, 1Si, (SIDipp)Si=Si), 127.9 (s, 1Si, Si=Si(Me)Tbb).

4.6.3 (*E*)-(SIDipp)Si=Si(CH₃)Tbb (1-CH₂Ph)

This compound was originally described in the preceding master thesis by reacting **1** with tBuLi in toluene at low temperatures.^[135] In this work, the full characterization as well as an additional synthetic access are described.

Method A: A solution of tBuLi (0.44 mL, 1.9 M, 0.84 mmol, 2.05 equiv.) in n-pentane was added dropwise within 3 minutes to an orange-red solution of **1** (400 mg, 0.41 mmol, 1.0 equiv.) in 4 mL of toluene at $-40\text{ }^{\circ}\text{C}$. The reaction mixture was stirred at $-30\text{ }^{\circ}\text{C}$ for 1.5 h and then slowly warmed to ambient temperature overnight (ca. 12 h), whereupon an orange-red solution containing a small amount of a colorless precipitate (LiBr) was obtained. The solution was filtered, and the red filtrate was evaporated to dryness under vacuum. The resulting dark red residue was dissolved in approximately 5 mL of n-pentane, and the red solution was concentrated under vacuum to ca. 3 mL (incipient crystallization) and stored at $-30\text{ }^{\circ}\text{C}$ for 16 h. The dark red, microcrystalline solid was collected by filtration at $-30\text{ }^{\circ}\text{C}$ and dried under vacuum for 3 h at ambient temperature. Yield: 282 mg (0.29 mmol, 70 %). Compound **1-CH₂Ph** decomposes to a dark brown oil upon melting at $206\text{ }^{\circ}\text{C}$. Elemental analysis calcd. (%) for C₅₈H₉₄N₂Si₆ (987.89): C 70.52, H 9.59, N 2.84; found: C 70.18, H 9.47, N 2.77 %.

Method B: A yellow solution of LiCH₂Ph·(THF)_{1.25} (92 mg, 0.49 mmol, 0.96 equiv.) in 4 mL of toluene was added to a dark red solution of **1** (500 mg, 0.51 mmol, 1.0 equiv.) in 7 mL of toluene at ambient temperature over a period of 5 minutes. The dark red reaction mixture was stirred at ambient temperature for 2 h. A ¹H NMR spectrum of an aliquot of the reaction mixture in benzene-d₆ showed ca. 70 % conversion of **1** to **1-CH₂Ph**. The reaction mixture was treated again with a solution of LiCH₂Ph·1.25(THF) (28 mg, 0.149 mmol, 0.29 equiv.) in 1 mL of toluene and stirred at ambient temperature for 16 h. 2 mL of n-hexane were added and a small amount of an off-white solid precipitated out (LiBr). The suspension was filtered and the dark red filtrate was evaporated to dryness under vacuum. The residue was dissolved in 3 mL of toluene and the solution stored at $-30\text{ }^{\circ}\text{C}$ for 4 days. The dark red, microcrystalline precipitate was separated from the mother liquor by filtration at $-30\text{ }^{\circ}\text{C}$, dried by three consecutive freeze-pump-thaw cycles and finally dried under vacuum for 2 h at ambient temperature. The dark red mother liquor was evaporated to dryness under vacuum, and a second crop of the product was isolated upon crystallization of the residue from 2 mL of benzene at $6\text{ }^{\circ}\text{C}$ for 3 days. The purity of the product was confirmed by ¹H NMR spectroscopy. Combined yield: 350 mg (0.35 mmol, 69 %).

UV-vis (n-hexane, 298 K, dark red solution) : λ /nm = 327 ($\epsilon = 19.2 \cdot 10^3\text{ L}\cdot\text{mol}^{-1}\cdot\text{cm}^{-1}$), 388 ($\epsilon = 5.96 \cdot 10^3\text{ L}\cdot\text{mol}^{-1}\cdot\text{cm}^{-1}$), 460 ($\epsilon = 2.84 \cdot 10^3\text{ L}\cdot\text{mol}^{-1}\cdot\text{cm}^{-1}$), 515 ($\epsilon = 2.36 \cdot 10^3\text{ L}\cdot\text{mol}^{-1}\cdot\text{cm}^{-1}$).

ATR-IR (solid state, RT): $\tilde{\nu}$ /cm⁻¹ = 3059 (vw), 3026 (vw), 2959 (m), 2928 (sh), 2897 (w), 2866 (w), 2802 (vw), 1597 (sh), 1587 (w), 1524 (w), 1491 (w), 1474 (sh), 1459 (sh), 1452 (w), 1439 (sh), 1409 (m), 1389 (m), 1362 (w), 1320 (vw), 1302 (vw), 1259 (sh), 1244 (s), 1201 (w), 1179 (w), 1152 (w), 1108 (vw), 1093 (vw), 1081 (vw), 1056 (w), 1045 (w), 1031 (vw), 1016 (w), 989 (vw), 947 (m), 939 (w), 885 (m), 857 (m), 836 (vs), 800 (s), 770 (sh), 753 (s),

730 (s), 697 (s), 682 (m), 666 (m), 643 (w), 621 (m), 609 (sh), 585 (vw), 562 (w), 546 (m), 497 (vw), 483 (vw), 463 (m), 422 (m), 408 (w).

Raman (solid, 25 mW): $\tilde{\nu}$ /cm⁻¹ = 3061 (m), 2951 (s), 2900 (vs), 2868 (m), 2804 (m), 1588 (s), 1454 (w), 1445 (w), 1418 (vw), 1390 (m), 1342 (vw), 1267 (s), 1252 (m), 1202 (w), 1179 (w), 1151 (w), 1138 (w), 1118 (vw), 1104 (vw), 1038 (w), 1020 (w), 1004 (m), 956 (vw), 920 (w), 886 (w), 840 (vw), 808 (w), 788 (w), 754 (w), 732 (m), 700 (vw), 683 (w), 632 (m), 603 (w), 589 (vw), 564 (s), 548 (w), 525 (vs, $\nu_{\text{Si=Si}}$), 464 (m), 427 (w), 408 (vw), 294 (w), 234 (w), 184 (s).

¹H NMR (500.2 MHz, benzene-d₆, 298 K): δ /ppm = 0.14 (s, 36H, 4 × SiMe₃, Tbb), 1.12 (d, 12H, ³J_{H,H} = 6.8 Hz, C^{2,6}-CHMe_AMe_B, Dipp), 1.342 (s, 9H, CMe₃, Tbb), 1.345 (d, 12H, ³J_{H,H} = 6.8 Hz, C^{2,6}-CHMe_AMe_B, Dipp), 3.01 (s, 2H, ²J_{Si,H} = 9.3 Hz, C^{2,6}-CH(SiMe₃)₂, Tbb), 3.18 (s, 2H, CH₂Ph), 3.35 (sept, 4H, ³J_{H,H} = 6.8 Hz, C^{2,6}-CHMe_AMe_B, Dipp), 3.57 (s, 4H, 2 × NCH₂, SIDipp), 6.91 (s, 2H, C^{3,5}-H, Tbb), 7.07 (t, 1H, C⁴-H, Ph; this signal overlaps with the doublet signal at δ = 7.08 ppm), 7.08 (d, 4H, ³J_{H,H} = 7.8 Hz, 2 × C^{3,5}-H, Dipp), 7.15 – 7.18 (m, 2H, C^{3,5}-H, Ph; this signal overlaps partly with the residual proton signal of the deuterated solvent at δ = 7.15 ppm), 7.21 (t, ³J_{H,H} = 7.8 Hz, 2H, 2 × C⁴-H, Dipp) 7.40 (d, 2H, ³J_{H,H} = 7.2 Hz, C^{2,6}-H, Ph).

¹³C{¹H} NMR (75.47 MHz, benzene-d₆, 298 K): δ /ppm = 1.7 (s, 12C, 4 × SiMe₃, Tbb), 24.1 (s, 4C, 2 × C^{2,6}-CHMe_AMe_B, Dipp), 26.2 (s, 4C, 2 × C^{2,6}-CHMe_AMe_B, Dipp), 29.2 (s, 4C, 2 × C^{2,6}-CHMe_AMe_B, Dipp), 31.4 (s, 3C, CMe₃, Tbb), 32.2 (s, 2C, C^{2,6}-CH(SiMe₃)₂, Tbb), 34.3 (s, 1C, C⁴-CMe₃, Tbb), 35.2 (s, 1C, CH₂Ph), 53.8 (s, 2C, 2 × NCH₂, SIDipp), 120.8 (s, 2C, C^{3,5}-H, Tbb), 124.5 (s, 1C, C⁴-H, Ph), 125.2 (s, 4C, 2 × C^{3,5}-H, Dipp), 128.1 (s, 2C, C^{3,5}-H, Ph), 129.8 (s, 2C, 2 × C⁴-H, Dipp), 130.3 (s, 2C, C^{2,6}-H, Ph), 136.5 (s, 2C, 2 × C¹, Dipp), 139.1 (s, 1C, C¹, Tbb), 142.0 (s, 1C, C¹, Ph), 146.9 (s, 4C, 2 × C^{2,6}-CHMe_AMe_B, Dipp), 149.1 (s, 1C, C⁴-CMe₃, Tbb), 149.8 (s, 2C, C^{2,6}-CH(SiMe₃)₂, Tbb), 208.8 (s, 1C, N₂CN, SIDipp).

²⁹Si NMR (99.37 MHz, benzene-d₆, 298 K): δ /ppm = 1.8 (br, 4Si, 4 × SiMe₃), 65.5 (s, 1Si, Si(SIDipp)), 123.7 (t, ²J_{Si,H} = 10.3 Hz, 1Si, Si(Tbb)CH₂Ph).

4.6.4 *cyclo*-{Si(SIDipp)(SiHTbb)(CHPh)} (3)

The formation of this compound was first observed in the preceding master thesis, however, only a single crystal could be isolated at that time.^[135] In this work, the full characterization as well as some calculations are described.

A mixture of **1** (302 mg, 0.31 mmol, 1.0 equiv.) and benzyl potassium (45 mg, 0.35 mmol, 1.1 equiv.) was treated with 5 mL of benzene at ambient temperature. The resulting dark red suspension was immersed in an ultrasonic bath for 2 minutes and then stirred for 48 h at ambient

temperature, whereupon the color of the suspension slowly turned reddish-yellow. Complete conversion of the starting materials was confirmed by a ^1H NMR spectrum of an aliquot of the reaction mixture in benzene- d_6 . Then the reddish-yellow suspension was evaporated to dryness under vacuum, and the red residue extracted with n-pentane (3×2 mL). The reddish-yellow extract was separated from a small amount of an off-white solid (KBr) by filtration and stored at -30 °C for 5 days. The yellow precipitate formed was isolated by filtration of the light orange supernatant at -30 °C and dried by three consecutive freeze-pump-thaw cycles followed by drying under vacuum for ca. 5 h at ambient temperature. Yield: 80 mg (0.08 mmol, 26 %). Compound **3** decomposes upon melting at 194 °C (evolution of gas) to give an orange slurry, which fully melts at 221 °C to an orange liquid. Elemental analysis calcd. (%) for $\text{C}_{58}\text{H}_{94}\text{N}_2\text{Si}_6$ (987.89): C 70.52, H 9.59, N 2.84; found: C 70.82, H 9.82, N 2.66 %.

ATR-IR (solid state, RT): $\tilde{\nu}/\text{cm}^{-1} = 3066$ (vw), 3048 (vw), 3021 (vw), 2960 (m), 2927 (w), 2900 (w), 2868 (w), 2837 (vw), 2101 (w, $\nu_{\text{Si-H}}$), 1590 (w), 1530 (w), 1485 (w), 1473 (w), 1461 (sh), 1448 (w), 1423 (w), 1395 (w), 1384 (sh), 1363 (vw), 1324 (w), 1304 (vw), 1271 (m), 1257 (m), 1243 (s), 1178 (w), 1161 (w), 1105 (vw), 1056 (w), 1037 (w), 1020 (w), 996 (vw), 954 (w), 941 (w), 886 (w), 858 (sh), 836 (vs), 801 (s), 781 (m), 762 (sh), 755 (s), 741 (w), 729 (w), 711 (w), 692 (m), 666 (w), 644 (m), 630 (w), 621 (w), 611 (sh), 557 (w), 546 (w), 536 (w), 498 (w), 469 (vw), 445 (w), 430 (w), 420 (w).

^1H NMR (500.2 MHz, benzene- d_6 , 298 K): δ /ppm = -0.03 (br, $\Delta\nu_{1/2} = 107$ Hz, 18H, $\text{C}^{2,6}\text{-CH}(\text{SiMe}_3)_A(\text{SiMe}_3)_B$, Tbb), 0.35 (s, 18H, $\text{C}^{2,6}\text{-CH}(\text{SiMe}_3)_A(\text{SiMe}_3)_B$, Tbb), 1.10 (d, $^3J_{\text{H,H}} = 6.8$ Hz, 6H, $2 \times \text{C}^2\text{-CHMe}_A\text{Me}_B$, Dipp), 1.18 (d, $^3J_{\text{H,H}} = 6.8$ Hz, 6H, $2 \times \text{C}^6\text{-CHMe}_A\text{Me}_B$, Dipp), 1.29 (s, 9H, CMe_3 , Tbb), 1.31 (d, $^3J_{\text{H,H}} = 6.8$ Hz, 6H, $2 \times \text{C}^2\text{-CHMe}_A\text{Me}_B$, Dipp), 1.76 (d, $^3J_{\text{H,H}} = 6.8$ Hz, 6H, $2 \times \text{C}^6\text{-CHMe}_A\text{Me}_B$, Dipp), 1.84 (d, $^3J_{\text{H,H}} = 6.4$ Hz, 1H, CHPh), $3.23 - 3.44$ (m, 10H, $2 \times \text{C}^{2,6}\text{-CHMe}_A\text{Me}_B$ (Dipp) + $2 \times \text{NCH}_A\text{H}_B$ (Dipp), + $\text{C}^{2,6}\text{-CH}(\text{SiMe}_3)_A(\text{SiMe}_3)_B$ (Tbb)), 4.62 (d, $^1J_{\text{Si,H}} = 202$ Hz, $^3J_{\text{H,H}} = 6.4$ Hz, 1H, SiH), 6.20 (d, $^3J_{\text{H,H}} = 7.4$ Hz, 2H, $\text{C}^{2,6}\text{-H}$, Ph), 6.76 (t, $^3J_{\text{H,H}} = 7.4$ Hz, 1H, $\text{C}^4\text{-H}$, Ph; this signal partially overlaps with the singlet signal at $\delta = 6.78$ ppm), 6.78 (s, 2H, $\text{C}^{3,5}\text{-H}$, Tbb), 6.94 (pseudo-t, $^3J_{\text{H,H}} = 7.4$ Hz, 2H, $\text{C}^{3,5}\text{-H}$, Ph), 7.07 (dd, $^3J_{\text{H,H}} = 7.6$ Hz, $^4J_{\text{H,H}} = 1.2$ Hz, 2H, $2 \times \text{C}^5\text{-H}$, Dipp), 7.18 (dd, $^3J_{\text{H,H}} = 7.6$ Hz, $^4J_{\text{H,H}} = 1.2$ Hz, 2H, $2 \times \text{C}^3\text{-H}$, Dipp; this signal partially overlaps with the residual proton signal of the deuterated solvent at $\delta = 7.16$ ppm), 7.23 (t, $^3J_{\text{H,H}} = 7.6$ Hz, 2H, $2 \times \text{C}^4\text{-H}$, Dipp). See Figure 19 on page 35.

^1H NMR (300.1 MHz, toluene- d_8 , 298 K): δ /ppm = -0.13 (br, $\Delta\nu_{1/2} = 18$ Hz, 18H, $\text{C}^{2,6}\text{-CH}(\text{SiMe}_3)_A(\text{SiMe}_3)_B$, Tbb), 0.28 (s, 18H, $\text{C}^{2,6}\text{-CH}(\text{SiMe}_3)_A(\text{SiMe}_3)_B$, Tbb), 1.10 (d, $^3J_{\text{H,H}} = 6.7$ Hz, 6H, $2 \times \text{C}^2\text{-CHMe}_A\text{Me}_B$, Dipp), 1.18 (d, $^3J_{\text{H,H}} = 6.7$ Hz, 6H, $2 \times \text{C}^6\text{-CHMe}_A\text{Me}_B$, Dipp), 1.25 (d, $^3J_{\text{H,H}} = 6.7$ Hz, 6H, $2 \times \text{C}^2\text{-CHMe}_A\text{Me}_B$, Dipp), 1.26 (s, 9H, CMe_3 , Tbb), 1.76 (d, $^3J_{\text{H,H}} = 6.7$ Hz, 6H, $2 \times \text{C}^6\text{-CHMe}_A\text{Me}_B$, Dipp), 1.84 (d, $^3J_{\text{H,H}} = 6.4$ Hz, 1H, CHPh), $3.18 - 3.52$ (m, 10H, $2 \times \text{C}^{2,6}\text{-CHMe}_A\text{Me}_B$ (Dipp) + $2 \times \text{NCH}_A\text{H}_B$ (Dipp), + $\text{C}^{2,6}\text{-CH}(\text{SiMe}_3)_A(\text{SiMe}_3)_B$ (Tbb)),

4.55 (d, $^1J_{\text{Si,H}} = 203$ Hz, $^3J_{\text{H,H}} = 6.4$ Hz, 1H, SiH), 6.20 (d, $^3J_{\text{H,H}} = 7.4$ Hz, 2H, C^{2,6}-H, Ph), 6.65 (tt, $^3J_{\text{H,H}} = 7.3$ Hz, $^4J_{\text{H,H}} = 1.2$ Hz, 1H, C⁴-H, Ph; this signal partially overlaps with the singlet signal at $\delta_{\text{H}} = 6.71$ ppm), 6.71 (s, 2H, C^{3,5}-H, Tbb), 6.82 (m, $^3J_{\text{H,H}} = 7.7$ Hz, 2H, C^{3,5}-H, Ph), 7.10 – 7.23 (m, $2 \times$ C³-H, Dipp + $2 \times$ C⁵-H, Dipp + $2 \times$ C⁴-H, Dipp; ; this signal partially overlaps with the singlet signal at $\delta_{\text{H}} = 7.09$ ppm).

¹³C{¹H} NMR (125.8 MHz, benzene-d₆, 298 K): δ /ppm = 1.0 (s, 6C, C^{2,6}-CH(SiMe₃)_A(SiMe₃)_B, Tbb), 1.9 (br, 6C, C^{2,6}-CH(SiMe₃)_A(SiMe₃)_B, Tbb), 17.1 (s, 1C, CHPh), 24.2 (s, 2C, $2 \times$ C²-CHMe_AMe_B, Dipp), 24.6 (s, 2C, $2 \times$ C⁶-CHMe_AMe_B, Dipp), 25.9 (s, 2C, $2 \times$ C²-CHMe_AMe_B, Dipp), 26.0 (s, 2C, $2 \times$ C⁶-CHMe_AMe_B, Dipp), 29.1 (s, 4C, $2 \times$ C^{2,6}-CHMe_AMe_B, Dipp), 29.9 (s, 2C, C^{2,6}-CH(SiMe₃)_A(SiMe₃)_B, Tbb), 31.2 (s, 3C, CMe₃, Tbb), 34.2 (s, 1C, CMe₃, Tbb), 53.8 (s, 2C, $2 \times$ NCH₂, SIDipp), 120.4 (s, 1C, C⁴-H, Ph), 121.9 (br, $\Delta\nu_{1/2} = 78$ Hz, 2C, C^{3,5}-H, Tbb), 125.1 (s, 2C, $2 \times$ C³-H, Dipp), 126.2 (s, 2C, $2 \times$ C⁵-H, Dipp), 126.7 (s, 1C, C¹, Tbb), 127.1 (s, 2C, C^{3,5}-H, Ph), 127.4 (s, 2C, C^{2,6}-H, Ph), 129.8 (s, 2C, $2 \times$ C⁴-H, Dipp), 135.3 (s, 2C, $2 \times$ C¹, Dipp), 146.4 (s, 2C, $2 \times$ C⁶-CHMe_AMe_B, Dipp), 146.7 (s, 2C, $2 \times$ C²-CHMe_AMe_B, Dipp), 149.5 (s, 1C, C⁴-CMe₃, Tbb), 150.8 (s, 1C, C¹, Ph), 152.5 (br, 2C, C^{2,6}-CH(SiMe₃)_A(SiMe₃)_B, Tbb), 200.6 (s, 1C, NCN, SIDipp).

¹³C{¹H} NMR (75.47 MHz, toluene-d₈, 298 K): δ /ppm = 1.1 (s, 6C, C^{2,6}-CH(SiMe₃)_A(SiMe₃)_B, Tbb), 1.7 (br, 6C, C^{2,6}-CH(SiMe₃)_A(SiMe₃)_B, Tbb), 17.1 (s, 1C, CHPh), 24.1 (s, 2C, $2 \times$ C²-CHMe_AMe_B, Dipp), 24.6 (s, 2C, $2 \times$ C⁶-CHMe_AMe_B, Dipp), 25.9 (s, 2C, $2 \times$ C²-CHMe_AMe_B, Dipp), 26.0 (s, 2C, $2 \times$ C⁶-CHMe_AMe_B, Dipp), 29.2 (s, 4C, $2 \times$ C^{2,6}-CHMe_AMe_B, Dipp), 29.9 (s, 2C, C^{2,6}-CH(SiMe₃)_A(SiMe₃)_B, Tbb), 31.3 (s, 3C, CMe₃, Tbb), 34.3 (s, 1C, CMe₃, Tbb), 53.9 (s, 2C, $2 \times$ NCH₂, SIDipp), 120.5 (s, 1C, C⁴-H, Ph), 121.9 (br, $\Delta\nu_{1/2} = 78$ Hz, 2C, C^{3,5}-H, Tbb), 125.1 (s, 2C, $2 \times$ C³-H, Dipp; this signal is hidden by the solvent signal at $\delta_{\text{C}} = 125.1$ ppm), 126.2 (s, 2C, $2 \times$ C⁵-H, Dipp), 126.8 (s, 1C, C¹, Tbb), 127.1 (s, 2C, C^{3,5}-H, Ph), 127.5 (s, 2C, C^{2,6}-H, Ph), 129.9 (s, 2C, $2 \times$ C⁴-H, Dipp), 135.4 (s, 2C, $2 \times$ C¹, Dipp), 146.4 (s, 2C, $2 \times$ C⁶-CHMe_AMe_B, Dipp), 146.7 (s, 2C, $2 \times$ C²-CHMe_AMe_B, Dipp), 149.5 (s, 1C, C⁴-CMe₃, Tbb), 150.8 (s, 1C, C¹, Ph), 152.4 (br, 2C, C^{2,6}-CH(SiMe₃)_A(SiMe₃)_B, Tbb), 200.8 (s, 1C, NCN, SIDipp).

²⁹Si{¹H} NMR (99.37 MHz, benzene-d₆, 298 K): δ [ppm] = -116.4 (s, 1Si, Si(SIDipp)), -75.6 (s, $^1J_{\text{Si,H}} = 201.6$ Hz, 1Si, Si-H; coupling constant was determined from a ¹H-²⁹Si{¹H} HMBC spectrum), 1.4 (br, 4Si, $4 \times$ SiMe₃, Tbb). The SiMe₃ signal was not detected in the ²⁹Si{¹H} NMR spectrum, but was obtained from a ¹H-²⁹Si{¹H} HMBC spectrum instead.

4.6.5 SiH[SiBr{OC(CH₂)Me}Tbb](SIDipp) (4)

This synthesis was originally described in the preceding master thesis, but the compound could not be isolated in pure form.^[135] In this work, the full characterization of **4** is given.

In a 10 mL Schlenk tube, an orange-red solution of **1** (200 mg, 0.205 mmol, 1.0 equiv.) in 5 mL of benzene was treated with a solution of acetone (0.1 mL, $\rho = 0.791$ g/mL, 1.36 mmol, 6.6 equiv.) in 5 mL of benzene.⁴⁵ The mixture was heated to 60 °C for 18 h, whereupon the color of the solution gradually changed to bright yellow. The resulting solution was filtered off, evaporated to dryness and the yellow residue was recrystallized from ca. 3 mL of n-hexane at -30 °C. The resulting yellow powder was collected by filtration at -30 °C and dried under vacuum at 60 °C for 6 h. Yield: 118 mg (0.11 mmol, 55 %). Compound **4** gradually turns brown between 147 – 153 °C and melts under decomposition and gas evolution above 240 °C to give a yellow liquid as well as a colorless solid. Elemental analysis calcd. (%) for C₅₄H₉₃BrN₂OSi₆ (1034.75): C 62.68, H 9.06, N 2.71; found: C 62.30, H 9.09, N 2.62 %.⁴⁶

ATR-IR (solid state, RT): $\tilde{\nu}$ /cm⁻¹ = 3062 (vw), 2960 (m), 2950 (m), 2927 (w), 2899 (w), 2867 (w), 2049 (w, $\nu_{\text{Si-H}}$), 1642 (sh), 1619 (w), 1589 (w), 1527 (w), 1472 (sh), 1462 (w), 1444 (w), 1417 (w), 1393 (m), 1367 (w), 1323 (vw), 1267 (sh), 1256 (s), 1245 (s), 1179 (w), 1153 (vw), 1132 (vw), 1098 (vw), 1057 (sh), 1030 (m), 984 (w), 948 (w), 941 (w), 885 (m), 855 (sh), 837 (vs), 802 (s), 757 (s), 722 (w), 682 (s), 666 (sh), 645 (vw), 630 (w), 621 (w), 611 (w), 587 (vw), 561 (w), 547 (w), 495 (s), 462 (w), 439 (s).

¹H NMR (500.2 MHz, benzene-d₆, 298 K):⁴⁶ δ /ppm = 0.17 (s, 18H, C^{2,6}-CH(SiMe₃)_A(SiMe₃)_B, Tbb), 0.32 (s, 18H, C^{2,6}-CH(SiMe₃)_A(SiMe₃)_B, Tbb), 1.10 (d, ³J_{H,H} = 6.8 Hz, 6H, 2 × C²-CHMe_AMe_B, Dipp), 1.14 (d, ³J_{H,H} = 6.8 Hz, 6H, 2 × C⁶-CHMe_AMe_B, Dipp), 1.30 (s, 9H, C⁴-CMe₃, Tbb), 1.52 (s, 3H, OC(CH₂H^E)Me), 1.59 (d, ³J_{H,H} = 6.7 Hz, 6H, 2 × C²-CHMe_AMe_B, Dipp), 1.70 (d, ³J_{H,H} = 6.8 Hz, 6H, 2 × C⁶-CHMe_AMe_B, Dipp), 2.71 (s, 2H, C^{2,6}-CH(SiMe₃)_A(SiMe₃)_B, Tbb), 2.90 (s, 1H, ¹J_{Si,H} = 117 Hz, SiH), 3.30 – 3.38 (m, 2H, 2 × NCH_AH_B), 3.43 (br, $\Delta\nu_{1/2}$ = 27 Hz, 2H, 2 × C⁶-CHMe_AMe_B, Dipp), 3.51 – 3.61 (m, 2H, 2 × NCH_AH_B), 3.67 (sept, ³J_{H,H} = 6.8 Hz, 2H, 2 × C²-CHMe_AMe_B, Dipp), 3.73⁴⁷ (s, 1H, OC(CH₂H^E)Me), 4.44⁴⁷ (s, 1H, OC(CH₂H^E)Me), 6.82 (s, 2H, C^{3,5}-H, Tbb), 7.09 (dd, ³J_{H,H} = 7.4 Hz, ⁴J_{H,H} = 1.6 Hz, 2H, 2 × C³-H, Dipp; this signal partially overlaps with that at δ_{H} = 7.11 ppm), 7.11 (dd, ³J_{H,H} = 7.5 Hz, ⁴J_{H,H} = 1.6 Hz, 2H, 2 × C³-H, Dipp), 7.18 (t, ³J_{H,H} = 7.7 Hz,

⁴⁵ The size of the reaction vessel has a strong influence on the reaction time. Thus, no conversion of the starting materials was observed even after 3 days, when the reaction was carried out under identical conditions in a 50 mL Schlenk tube. It is assumed, that in this case the acetone evaporated to the gas phase as well as a condensate in the Schlenk tubes cap.

⁴⁶ Despite the satisfactory elemental analysis results, the ¹H NMR spectrum of the isolated material in benzene-d₆ at 298 K showed a small amount of an unknown impurity at δ_{H} = 0.24 ppm. Recrystallization from hot n-hexane afforded crystals of the hemisolvate **4**·0.5(n-C₅H₁₂), which were used for the ¹H, ¹³C and ²⁹Si NMR spectroscopy.

⁴⁷ The assignment of these signals was further confirmed by ¹H NOESY spectroscopy.

2H, 2 × C⁴-H; Dipp, this signal partially overlaps with the residual proton signal of the deuterated solvent at $\delta_{\text{H}} = 7.16$ ppm).

¹³C{¹H} NMR (125.8 MHz, benzene-d₆, 298 K): δ /ppm = 1.7 (s, 6C, 2 × CH(SiMe₃)_A(SiMe₃)_B, Tbb), 2.0 (s, 6C, 2 × CH(SiMe₃)_A(SiMe₃)_B, Tbb), 23.8 (s, 2C, 2 × C²-CHMe_AMe_B, Dipp), 24.0 (s, 1C, OC(CH₂)Me), 24.6 (s, 2C, 2 × C⁶-CHMe_AMe_B, Dipp), 26.5 (s, 2C, 2 × C²-CHMe_AMe_B, Dipp), 26.6 (s, 2C, 2 × C⁶-CHMe_AMe_B, Dipp), 29.0 (s, 2C, 2 × C²-CHMe_AMe_B, Dipp), 29.1 (s, 2C, 2 × C⁶-CHMe_AMe_B, Dipp), 29.5 (s, ¹J_{Si,C} = 43 Hz, 2C, 2 × CH(SiMe₃)_A(SiMe₃)_B, Tbb), 31.2 (s, 3C, CMe₃, Tbb), 34.2 (s, 1C, CMe₃, Tbb), 53.9 (s, 2C, 2 × NCH₂, SIDipp), 93.7 (s, 1C, OC(CH₂)Me), 122.6 (s, 2C, C^{3,5}-H, Tbb), 125.4 (s, 2C, 2 × C³-H, Dipp), 125.7 (s, 2C, 2 × C⁵-H, Dipp), 129.7 (s, 2C, 2 × C⁴-H, Dipp), 131.8 (s, 1C, C¹, Tbb), 136.3 (s, 2C, 2 × C¹, Dipp), 146.8 (s, 2C, 2 × C²-CHMe_AMe_B, Dipp), 147.0 (s, 2C, 2 × C⁶-CHMe_AMe_B, Dipp), 150.4 (s, 1C, C⁴-CMe₃, Tbb), 151.5 (s, 2C, C^{2,6}-CH(SiMe₃)_A(SiMe₃)_B, Tbb), 154.7 (s, 1C, OC(CH₂)Me), 199.5 (s, 1C, NCN, SIDipp).

²⁹Si{¹H} NMR (59.63 MHz, benzene-d₆, 298 K): δ /ppm = -94.2 (s, 1Si, SiH(SIDipp)), 2.2 (s, 2Si, C^{2,6}-CH(SiMe₃)_A(SiMe₃)_B), 2.4 (s, 2Si, C^{2,6}-CH(SiMe₃)_A(SiMe₃)_B), 9.8 (s, 1Si, Si(Br)Tbb).

4.6.6 Si(ZnBr)(SiCl₂Tbb)(SIDipp) (5-Cl)

A mixture of crystalline 1·(C₆H₆) (250 mg, 0.23 mmol, 1.0 equiv.) and ZnCl₂·(1,4-dioxane)₂ (131 mg, 0.42 mmol, 1.8 equiv.) was treated with 10 mL of benzene at ambient temperature. The reaction mixture was immersed in an ultrasonic bath for 30 minutes whereupon the color of the suspension changed from dark red to yellow. The suspension was stirred at ambient temperature for additional 1.5 h. Complete conversion of 1 to 5-Cl was confirmed by a ¹H NMR spectrum of an aliquot of the reaction mixture in benzene-d₆. The yellow suspension was filtered, and the off-white insoluble part was extracted with 2 mL of benzene. The combined yellow filtrates were evaporated to dryness under vacuum and the resulting light yellow residue was dried by a freeze-pump-thaw cycle. The obtained yellow powder was dried under vacuum at 40 °C for 3 h. Yield: 255 mg (0.23 mmol, 98 %). Compound 5-Cl decomposes to a dark brown mass at 219 °C. Elemental analysis calcd. (%) for C₅₁H₈₇BrCl₂N₃Si₆Zn (1112.98): C 55.04, H 7.88, N 2.52; found: C 54.99, H 7.86, N 2.42 %.

¹H NMR (500.1 MHz, benzene-d₆, 298 K): δ /ppm = 0.28 (s, 36H, 4 × SiMe₃, Tbb), 1.06 (d, ³J_{H,H} = 6.8 Hz, 12H, 2 × C^{2,6}-CHMe_AMe_B, Dipp), 1.25 (s, 9H, CMe₃, Tbb), 1.64 (d, ³J_{H,H} = 6.8 Hz, 12H, 2 × C^{2,6}-CHMe_AMe_B, Dipp), 3.29 (s, ²J_{Si,H} = 9.4 Hz, 2H, C^{2,6}-CH(SiMe₃)₂, Tbb), 3.35 (sept, ³J_{H,H} = 6.7 Hz, 4H, 2 × C^{2,6}-CHMe_AMe_B, Dipp), 3.44 (s, 4H, 2 × NCH₂, SIDipp), 6.81 (s, 2H, C^{3,5}-H, Tbb), 7.17 (d, ³J_{H,H} = 7.8 Hz, 4H, 2 × C^{3,5}-H, Dipp), 7.33 (d, ³J_{H,H} = 7.8 Hz, 2H, 2 × C⁴-H, Dipp).

$^{13}\text{C}\{^1\text{H}\}$ NMR (125.8 MHz, benzene- d_6 , 298 K): δ/ppm = 2.2 (s, 12C, 4 \times SiMe_3 , Tbb), 24.3 (s, 4C, 2 \times $\text{C}^{2,6}\text{-CHMe}_A\text{Me}_B$, Dipp), 26.2 (s, 4C, 2 \times $\text{C}^{2,6}\text{-CHMe}_A\text{Me}_B$, Dipp), 29.1 (s, 2C, $\text{C}^{2,6}\text{-CH}(\text{SiMe}_3)_2$, Tbb), 29.3 (s, 4C, 2 \times $\text{C}^{2,6}\text{-CHMe}_A\text{Me}_B$, Dipp), 31.0 (s, 3C, CMe_3 , Tbb), 34.2 (s, 1C, CMe_3 , Tbb), 53.8 (s, 2C, 2 \times NCH_2 , SIDipp), 123.4 (s, 2C, $\text{C}^{3,5}\text{-H}$, Tbb), 126.9 (s, 4C, 2 \times $\text{C}^{3,5}\text{-H}$, Dipp), 130.9 (s, 1C, C^1 , Tbb), 131.6 (s, 2C, 2 \times $\text{C}^4\text{-H}$, Dipp), 135.9 (s, 2C, 2 \times C^1 , Dipp), 146.7 (s, 4C, 2 \times $\text{C}^{2,6}$, Dipp), 150.9 (s, 1C, C^4 , Tbb), 151.3 (s, 2C, $\text{C}^{2,6}$, Tbb), 201.0 (s, 1C, NCN , SIDipp).

$^{29}\text{Si}\{^1\text{H}\}$ NMR (99.36 MHz, benzene- d_6 , 298 K): δ/ppm = -81.8 (s, 1Si, $\text{Si}(\text{SIDipp})$), 2.6 (s, 4Si, 4 \times SiMe_3 , Tbb), 29.4 (s, 1Si, SiCl_2Tbb).

4.6.7 **Si(ZnBr)(SiBr₂Tbb)(SIDipp) (5-Br)**

The formation of this compound was first observed in the preceding master thesis, however, it could not be isolated or characterized by spectroscopy other than ^1H NMR at that time.^[135] In this work, the full characterization is given.

A mixture of crystalline **1**·(C_7H_8) (320 mg, 0.30 mmol, 1.0 equiv.) and ZnBr_2 (169 mg, 0.75 mmol, 2.5 equiv.) was treated with a solvent mixture of 10 mL of toluene and 0.5 mL of diethyl ether at ambient temperature. The reaction mixture was stirred at ambient temperature for 20 h, whereupon the color of the suspension gradually changed to dark yellow and most of the solid dissolved. The complete conversion of **1** into **5-Br** was confirmed by ^1H NMR. The suspension was concentrated to ca. 6 mL under vacuum to evaporate the diethyl ether and filtered. The off-white insoluble part (excess ZnBr_2) was extracted with 3 \times 2 mL of toluene and the combined yellow extracts were evaporated to dryness under vacuum. The resulting orange residue was dried by two consecutive freeze-pump-thaw cycles, washed with 2 \times 3 mL of precooled n-hexane⁴⁸ at -30 °C and dried under vacuum at ambient temperature for 5 h. Yield: 337 mg (0.28 mmol, 94 %). The product was shown by ^1H NMR spectroscopy to be ca. 90 – 95 % pure. Numerous attempts to purify the compound either by washing with n-hexane and diethyl ether at ambient temperature or by recrystallization from benzene or toluene/n-hexane mixtures at low temperature failed and led only to further decomposition of the highly sensitive product.

^1H NMR (500.2 MHz, benzene- d_6 , 298 K):⁴⁹ δ/ppm = 0.31 (s, 36H, 4 \times SiMe_3 , Tbb), 1.07 (d, 12H, $^3\text{J}_{\text{H,H}} = 6.8$ Hz, 4 \times CHMe_AMe_B , Dipp), 1.26 (s, 9H, CMe_3 , Tbb), 1.66 (d, 12H, $^3\text{J}_{\text{H,H}} =$

⁴⁸ The n-hexane used for this procedure has to be absolutely free from any unsaturated impurities. This can be achieved by shaking commercial solvent over $\text{H}_2\text{SO}_4/\text{HNO}_3$ (1:1), washing with water and subsequent drying by standard procedure.

⁴⁹ For a detailed analysis of the isomerization mechanism see page 51ff.

6.8 Hz, 4 × CHMe_AMe_B, Dipp), 3.41 (br m, 4H, 4 × CHMe_AMe_B, SIDipp), 3.47 (br, 6H, 2 × NCH₂ (SIDipp) + 2 × CH(SiMe₃)₂ (Tbb)), 6.82 (s, 2H, C^{3,5}-H, Tbb), 7.18 (d, ³J_{H,H} = 7.7 Hz, 4H, 2 × C^{3,5}-H, Dipp; this signal overlaps partly with the residual proton signal of the deuterated solvent at δ_H = 7.16 ppm), 7.32 (t, ³J_{H,H} = 7.7 Hz, 2H, 2 × C⁴-H, Dipp).

¹³C{¹H} NMR (125.8 MHz, benzene-d₆, 298 K): δ/ppm = 2.5 (s, 12C, 4 × SiMe₃, Tbb), 24.3 (s, 4C, 4 × CHMe_AMe_B, Dipp), 26.4 (s, 4C, 4 × CHMe_AMe_B, Dipp), 29.3 (br, 2C, 2 × CH(SiMe₃)₂, Tbb; this signal overlaps with the signal at δ_C = 29.4 ppm), 29.4 (s, 4C, 4 × CHMe_AMe_B, Dipp), 31.1 (s, 3C, CMe₃, Tbb), 34.2 (s, CMe₃, Tbb), 54.0 (s, 2C, 2 × NCH₂, SIDipp), 123.6 (s, 2C, C^{3,5}-H, Tbb), 127.0 (s, 4C, 2 × C^{3,5}-H, Dipp), 129.3 (s, 1C, C¹, Tbb), 131.6 (s, 2C, 2 × C⁴-H, Dipp), 136.0 (s, 2C, 2 × C¹, Dipp), 146.7 (s, 4C, 2 × C^{2,6}-CHMe_AMe_B, Dipp), 151.0 (s, 1C, C⁴-CMe₃, Tbb), 151.4 (s, 2C, C^{2,6}-CH(SiMe₃)₂, Tbb), 200.3 (s, 1C, NCN, SIDipp).

²⁹Si{¹H} NMR (59.63 MHz, benzene-d₆, 298 K): δ/ppm = -63.9 (s, 1Si, Si(SIDipp)), 2.7 (s, 4Si, 4 × SiMe₃, Tbb), 6.6 (s, 1Si, Si(Tbb)).

4.6.8 Si(ZnBr)(SiBrCH₂PhTbb)(SIDipp) (6)

A mixture of **1-CH₂Ph** (210 mg, 0.21 mmol, 1.0 equiv.) and ZnBr₂ (105 mg, 0.47 mmol, 2.2 equiv.) was suspended in 5 mL of benzene and stirred for 3 days at ambient temperature and the color of the suspension gradually changed from bright red to yellow. Completion of the reaction was confirmed by ¹H NMR spectroscopy and the reaction mixture was filtered from excess ZnBr₂. The yellow filtrate was evaporated to dryness and the resulting yellow residue was extracted with benzene (2 × 1 mL). The combined yellow extracts were evaporated to dryness and the yellow residue was re-crystallized from 1 mL of a toluene/n-hexane mixture (1:1) at -30 °C. The microcrystalline yellow solid obtained by this method was isolated by filtration at -30 °C and dried under vacuum at ambient temperature for 3 h. Yield: 135 mg (0.11 mmol, 52 % from **1-CH₂Ph**). Compound **6** gradually turns dark red between 130 – 150 °C and melts under decomposition at 158 °C. Elemental analysis calcd. (%) for C₅₈H₉₄Br₂N₃Si₆Zn (1213.11): C 57.42, H 7.81, N 2.31; found: C 56.87, H 8.06, N 2.12 %.

¹H NMR (300.1 MHz, benzene-d₆, 298 K): ⁵⁰ δ /ppm = 0.24 (s, 36H, 2 × CH(SiMe₃)_A(SiMe₃)_B and 2 × CH(SiMe₃)_A(SiMe₃)_B, Tbb), 1.08 (d, 12H, ³J_{H,H} = 6.7 Hz, 2 × C²-CHMe_AMe_B and 2 × C⁶-CHMe_AMe_B, Dipp), 1.319 (s, 9H, CMe₃, Tbb), 1.321 (m, 1H, CH_AH_BPh; this signal is mostly hidden by the signal at δ_H = 1.319 ppm), 1.56 (d, 6H, ³J_{H,H} = 6.7 Hz, 2 × C²-CHMe_AMe_B, Dipp), 1.72 (d, 6H, ³J_{H,H} = 6.7 Hz, 2 × C⁶-CHMe_AMe_B, Dipp), 2.61 (d, 1H, ²J_{H,H} = 15.7 Hz, CH_AH_BPh), 3.13 (s, 2H, C^{2,6}-CH(SiMe₃)₂, Tbb), 3.25 (br, 4H, Δ_{V₂} = 21 Hz, 2 × NCH_AH_B and 2

⁵⁰ For a detailed analysis of the isomerization mechanism see page 51ff.

\times C²-CHMe_AMe_B, SIDipp), 3.58 (br, $\Delta\nu_{1/2} = 27$ Hz, 4H, 2 \times NCH_AH_B and 2 \times C⁶-CHMe_AMe_B, SIDipp), 6.80 (d, $^3J_{\text{H,H}} = 7.6$ Hz, 2H, C^{2,6}-H, Ph), 6.83 (s, 2H, C^{3,5}-H, Tbb), 6.98 (m, 1H, C⁴-H, Ph), 7.03 – 7.10 (m, 2H, C^{3,5}-H, Ph), 7.09 – 7.16 (m, 2H, 2 \times C³-H, Dipp; the signals partially overlap with the residual proton signal of the deuterated solvent at $\delta_{\text{H}} = 7.16$ ppm), 7.18 – 7.25 (m, 2H, 2 \times C⁵-H, Dipp) 7.25 – 7.36 (br m, 2H, 2 \times C⁴-H, Dipp).

¹³C{¹H} NMR (75.47 MHz, benzene-d₆, 298 K):⁵⁰ δ /ppm = 2.9, 3.2 (s each, 6C each, 2 \times CH(SiMe₃)_A(SiMe₃)_B and 2 \times CH(SiMe₃)_A(SiMe₃)_B, Tbb), 24.7 (s, 4C, 2 \times C²-CHMe_AMe_B and 2 \times C⁶-CHMe_AMe_B, Dipp), 25.8 (br, 2C, 2 \times C⁶-CHMe_AMe_B, Dipp), 26.2 (br, 2C, 2 \times C²-CHMe_AMe_B, Dipp), 29.2 (s, 2C, 2 \times C²-CHMe_AMe_B, Dipp), 29.3 (br, 2C, 2 \times C⁶-CHMe_AMe_B, Dipp) 30.4 (s, 2C, C^{2,6}-CH(SiMe₃)₂, Tbb), 31.2 (s, 3C, CMe₃, Tbb), 31.8 (s, 1C, CH₂Ph), 34.2 (s, 1C, C⁴-CMe₃, Tbb), 53.8 (s, 2C, 2 \times NCH₂, SIDipp), 124.0 (s, 2C, C^{3,5}-H, Tbb), 124.8 (s, 1C, C⁴-H, Ph), 127.1 (br, 4C, 2 \times C³-H and 2 \times C⁵-H, Dipp), 127.9 (s, 2C, C^{3,5}-H, Ph), 129.2 (s, 1C, C¹, Tbb), 131.4 (s, 2C, C^{2,6}-H, Ph), 131.6 (br, 2C, 2 \times C⁴-H, Dipp), 136.6 (br, 2C, 2 \times C¹, Dipp), 139.9 (s, 1C, C¹-CH₂, Ph), 146.5 (br, 2C, 2 \times C⁶-CHMe_AMe_B, Dipp), 147.6 (s, 2C, 2 \times C²-CHMe_AMe_B, Dipp), 150.2 (s, 1C, C⁴-CMe₃, Tbb), 151.8 (s, 2C, C^{2,6}-CH(SiMe₃)₂, Tbb), 201.6 (s, 1C, NCN, SIDipp).

²⁹Si{¹H} NMR (99.37 MHz, benzene-d₆, 298 K):⁵⁰ δ /ppm = -67.0 (s, $^2J_{\text{Si,H}} = 15.6$ Hz, 1Si, Si(SIDipp); the $^2J_{\text{Si,H}}$ coupling constant was determined from a ¹H-²⁹Si{¹H} HMBC correlation spectrum), 2.1, 2.5 (s each, 2Si each, 2 \times CH(SiMe₃)_A(SiMe₃)_B and 2 \times CH(SiMe₃)_A(SiMe₃)_B, Tbb), 15.0 (s, 1Si, SiCH₂Ph).

4.6.9 *cyclo*-Si[C{ONa(thf)}PSi(Tbb)P](SIDipp) (7)

Caution: in several cases, the black-discolored filters used for the filtration spontaneously ignited when exposed to air. This was accompanied by a very unpleasant smell. Isolated 7 is not pyrophoric but decolorizes when exposed to air.

A suspension of 1·C₇H₈ (202 mg, 0.189 mmol, 1.0 equiv.) and NaOCP·(1,4-dioxane)_{2.6} (124 mg, 0.397 mmol, 2.1 equiv.) was stirred in 30 ml of thf for 3 days, using a glass-coated stirring bar. While the color of the reaction mixture gradually changed from dark red to brown, the conversion was followed by ¹H NMR spectroscopy.⁵¹ Another portion of NaOCP·(1,4-dioxane)_{2.6} (ca. 30 mg, 0.096 mmol, 0.51 equiv.) was added and the suspension was stirred for another 20 hours at ambient temperature when nearly complete conversion of 1

⁵¹ During these days, the slow conversion of 1 into 7 accompanied by simultaneous decomposition of 7 into an unknown product was observed. The workup was usually started when only a very small amount of 1 was left. The unknown decomposition product displays very broad signals in the aliphatic region which may translocate depending on the relative ratio of the components in the crude mixture.

was confirmed by ^1H NMR spectroscopy. The mixture was evaporated to dryness and the residue was washed with 25 ml of n-hexane in small portions and the brown filtrate was discarded. The residue was then extracted with 6 ml of a mixture of toluene and thf (5:1) and the dark green filtrate was cooled to $-30\text{ }^\circ\text{C}$ for ca. 2 weeks. During this time, a small crop of dark green to black crystals was obtained. These were isolated by filtration at $-30\text{ }^\circ\text{C}$ and dried under vacuum for 30 minutes at ambient temperature. Compound 7 was obtained as a dichroic reddish-dark green to black, extremely air-sensitive, microcrystalline solid. Yield: 51 mg (0.05 mmol, 25 %). At $-30\text{ }^\circ\text{C}$ the solid can be stored for 2 months without any sign of decomposition. Elemental analysis calcd. (%) for $\text{C}_{56}\text{H}_{95}\text{N}_2\text{NaO}_2\text{P}_2\text{Si}_6$ (1081.82): C 62.17, H 8.85, N 2.59; found: C 62.14, H 8.74, N 2.45 %. Compound 7 slowly decomposes in solution to give the same unidentified compound that was also present during the synthesis. Changing the reaction solvent to Et_2O , fluorobenzene, dme, or mixtures of benzene and the aforesaid ethereal solvents only led to lower yields or no conversion (fluorobenzene or benzene/ Et_2O) as judged by ^1H NMR.

UV-vis (tetrahydrofuran, 298 K, dark green-blue solution): λ /nm = 247 ($\epsilon = 7.82 \cdot 10^3\text{ L}\cdot\text{mol}^{-1}\cdot\text{cm}^{-1}$), 421 ($\epsilon = 6.21 \cdot 10^3\text{ L}\cdot\text{mol}^{-1}\cdot\text{cm}^{-1}$), 593 ($\epsilon = 16.44 \cdot 10^3\text{ L}\cdot\text{mol}^{-1}\cdot\text{cm}^{-1}$). See Figure 107 on page 268 in the appendix.

ATR-IR (solid state, RT): $\tilde{\nu}$ / cm^{-1} = 3065 (vw), 3032 (vw), 2957 (w), 2892 (vw), 2866 (vw), 1634 (vw), 1587 (vw), 1530 (vw), 1461 (vw), 1452 (vw), 1402 (sh), 1392 (w), 1361 (vw), 1327 (w), 1275 (sh), 1255 (sh), 1243 (s), 1226 (m), 1203 (w), 1179 (vw), 1166 (vw), 1146 (vw), 1106 (vw), 1094 (vw), 1067 (sh), 1052 (w), 1023 (w), 990 (vw), 958 (w), 936 (vw), 885 (m), 858 (sh), 838 (vs), 800 (vs), 765 (m), 746 (w), 728 (w), 685 (w), 665 (w), 642 (vw), 623 (w), 605 (vw), 555 (w), 508 (w), 491 (w), 464 (vw), 449 (vw), 420 (w).⁵²

^1H NMR (500.1 MHz, tetrahydrofuran- d_6 , 298 K): δ /ppm = -0.04 (s, 36H, 4 \times SiMe_3 , Tbb), 1.24 (s, 9H, CMe_3 , Tbb), 1.23 (d, 12H, $^3J_{\text{HH}} = 6.8\text{ Hz}$, 4 \times CHMe_AMe_B , Dipp), 1.39 (d, 12H, $^3J_{\text{HH}} = 6.8\text{ Hz}$, 4 \times CHMe_AMe_B , Dipp), 3.10 (s, 2H, $^2J_{\text{Si,H}} = 9.2\text{ Hz}$, $\text{C}^{2,6}\text{-CH}(\text{SiMe}_3)_2$, Tbb), 3.40 (sept, 4H, $^3J_{\text{HH}} = 6.8\text{ Hz}$, 4 \times CHMe_AMe_B , Dipp), 3.85 (s, 4H, 2 \times NCH_2 , SIDipp), 6.63 (s, 2H, $\text{C}^{3,5}\text{-H}$, Tbb), 7.06 (d, 4H, $^3J_{\text{HH}} = 7.8\text{ Hz}$, 2 \times $\text{C}^{3,5}\text{-H}$, Dipp), 7.15 (t, $^3J_{\text{HH}} = 7.8\text{ Hz}$, 2H, 2 \times $\text{C}^4\text{-H}$, Dipp).

$^{13}\text{C}\{^1\text{H}\}$ NMR (125.8 MHz, tetrahydrofuran- d_6 , 298 K): δ /ppm = 1.2 (s, 12C, 4 \times SiMe_3 , Tbb), 24.8 (s, 4C, 4 \times CHMe_AMe_B , Dipp), 25.8 (s, 4C, 4 \times CHMe_AMe_B , Dipp), 29.6 (s, 4C, 4 \times CHMe_AMe_B , Dipp), 31.7 (s, 3C, CMe_3 , Tbb), 32.6 (s, 2C, 2 \times $\text{CH}(\text{SiMe}_3)_2$, Tbb), 34.8 (s, 1C, CMe_3 , Tbb), 55.0 (s, 2C, 2 \times NCH_2 , SIDipp), 120.2 (s, 2C, $\text{C}^{3,5}\text{-H}$, Tbb), 124.6 (s, 4C, 2 \times $\text{C}^{3,5}\text{-H}$, Dipp), 128.2 (s, 2C, 2 \times $\text{C}^4\text{-H}$, Dipp), 139.3 (s, 2C, 2 \times C^1 , Dipp), 140.2 (s, 1C, C^1 , Tbb),

⁵² Due to immediate decomposition of 7 upon contact with a liquid IR cell (NaCl window) in a glovebox, no IR spectra in solution could be measured.

148.7 (s, 4C, $2 \times \underline{C}^{2,6}\text{-CHMe}_A\text{Me}_B$, Dipp), 149.6 (s, 2C, $\underline{C}^{2,6}\text{-CH}(\text{SiMe}_3)_2$, Tbb), 150.3 (s, 1C, $\underline{C}^4\text{-CMe}_3$, Tbb), 179.5 (s, 1C, $\underline{N}\underline{C}\underline{N}$, SIDipp).

$^{15}\text{N}\{^1\text{H}\}$ NMR (50.68 MHz, tetrahydrofuran- d_8 , 298 K): δ /ppm = 105.2 (s). This signal was not observed via 1D NMR spectroscopy but its position was deduced from a $^1\text{H}\text{-}^{15}\text{N}\{^1\text{H}\}$ HMBC spectrum.

$^{29}\text{Si}\{^1\text{H}\}$ NMR (59.63 MHz, tetrahydrofuran- d_8 , 298 K): δ /ppm = -1.8 (dd, 1Si, $^1\text{J}(^{31}\text{P},^{29}\text{Si}) = 162.1$ Hz, $^2\text{J}(^{31}\text{P},^{29}\text{Si}) = 13.3$ Hz, $\underline{\text{Si}}(\text{SIDipp})$), 1.5 (s, 4Si, $4 \times \underline{\text{Si}}\text{Me}_3$, Tbb), 176.7 (dd, 1Si, $^1\text{J}(^{31}\text{P},^{29}\text{Si}) = 144.7$ Hz, $^1\text{J}(^{31}\text{P},^{29}\text{Si}) = 133.8$ Hz, $\underline{\text{Si}}(\text{Tbb})$). See Figure 29 on page 56.

$^{31}\text{P}\{^1\text{H}\}$ NMR (282.4 MHz, THF- d_6 , 298 K): δ /ppm = -81.7 (d, 1P, $^2\text{J}(^{31}\text{P},^{31}\text{P}) = 40.6$ Hz, $\underline{\text{Si}}\underline{\text{P}}\underline{\text{C}}$), 94.9 (d, 1P, $^2\text{J}(^{31}\text{P},^{31}\text{P}) = 40.6$ Hz, $\underline{\text{Si}}\underline{\text{P}}\underline{\text{Si}}$). Due to proportionate coupling to signals of either substituent, the assignment was verified by calculations (see Figure 28 on page 55).

4.6.10 $[\text{Ag}\{\eta^1\text{-}(\underline{Z})\text{-}(\text{SIDipp})\text{Si}=\text{Si}(\text{Br})\text{Tbb}\}][\text{OTf}]$ (9)

A solid mixture of $1\cdot\text{C}_7\text{H}_8$ (200 mg, 0.19 mmol, 1.0 equiv.) and AgOTf (48 mg, 0.19 mmol, 1.0 equiv.) was suspended in 6 ml of precooled thf at -80 °C and the dark reaction mixture was allowed to warm to ambient temperature within 30 minutes. During this time, the color changed from initial dark red to green-brown and finally yellow-brown, while small amounts of a voluminous black solid precipitated. The suspension was evaporated to dryness and the black residue washed with 1 ml of benzene and 1 ml of a 1 : 1 mixture of benzene and n-hexane. While the washings were discarded, the residue was extracted with 5 ml of thf and the filtrate was dried at ambient temperature for 3 h to obtain **9** as a dark yellow powder. Yield: 105 mg (0.10 mmol, 54 % from **1**). Compound **9** slowly polymerizes thf at ambient temperature but solutions are stable for a few hours; the solid slowly decomposes at ambient temperature but can be stored at -30 °C for several weeks. Although the compound was spectroscopically pure, the elemental analysis showed considerable deviations: calcd. (%) for $\text{C}_{52}\text{H}_{87}\text{AgBrF}_3\text{N}_2\text{O}_3\text{SSi}_6$ (1233.6): C 50.63, H 7.11, N 2.27; found: C 51.97, H 7.60, N 2.16 %.

^1H NMR (500.1 MHz, tetrahydrofuran- d_8 , 298 K):⁵³ δ /ppm = -0.05 (s, 36H, $4 \times \underline{\text{Si}}\underline{\text{Me}}_3$, Tbb), 1.22 (s, 9H, $\underline{\text{C}}\underline{\text{Me}}_3$, Tbb), 1.30 (d, 12H, $^3\text{J}_{\text{H,H}} = 6.8$ Hz, $\underline{\text{C}}^{2,6}\text{-CHMe}_A\text{Me}_B$, Dipp), 1.56 (d, 12H, $^3\text{J}_{\text{H,H}} = 6.8$ Hz, $\underline{\text{C}}^{2,6}\text{-CHMe}_A\text{Me}_B$, Dipp), 2.47 (s, 2H, $^2\text{J}_{\text{Si,H}} = 9.2$ Hz, $\underline{\text{C}}^{2,6}\text{-CH}(\text{SiMe}_3)_2$, Tbb), 3.51 (sept, 4H, $^3\text{J}_{\text{H,H}} = 6.9$ Hz, $\underline{\text{C}}^{2,6}\text{-CHMe}_A\text{Me}_B$, Dipp), 4.32 (s, 4H, $2 \times \underline{\text{NCH}}_2$, SIDipp), 6.70 (s, 2H,

⁵³ As a result of decomposition in thf solution, the ^1H NMR signal displayed a small amount of an unknown impurity at $\delta_i = 3.33$ (s), 4.76 (s), 7.37 (d) and 8.81 ppm (s).

$C^{3.5}\text{-H}$, Tbb), 7.42 (d, 4H, ${}^3J_{\text{H,H}} = 7.7$ Hz, $2 \times C^{3.5}\text{-H}$, Dipp), 7.51 (t, ${}^3J_{\text{H,H}} = 7.7$ Hz, 2H, $2 \times C^4\text{-H}$, Dipp). See Figure 38 on page 71.

${}^{13}\text{C}\{\text{H}\}$ NMR (125.8 MHz, tetrahydrofuran- d_8 , 298 K): δ /ppm = 1.5 (s, 12C, $4 \times \text{SiMe}_3$, Tbb), 25.7 (s, 4C, $2 \times C^{2.6}\text{-CHMe}_A\text{Me}_B$, Dipp), 26.7 (s, 4C, $2 \times C^{2.6}\text{-CHMe}_A\text{Me}_B$, Dipp), 30.0 (s, 4C, $2 \times C^{2.6}\text{-CHMe}_A\text{Me}_B$, Dipp), 31.2 (s, 3C, CMe_3 , Tbb), 34.0 (s, 2C, $\text{CH}(\text{SiMe}_3)_2$, Tbb), 34.9 (s, 1C, CMe_3 , Tbb), 55.6 (s, 2C, $2 \times \text{NCH}_2$, SIDipp), 122.7 (s, 2C, $C^{3.5}\text{-H}$, Tbb), 127.3 (s, 4C, $2 \times C^{3.5}\text{-H}$, Dipp), 128.4 (pt, ${}^1J_{\text{F,C}} = 24$ Hz, 1C, CF_3 , OTf), 132.1 (d, ${}^2J(\text{Ag,Si}) = 56.4$ Hz, 1C, C^1 , Tbb), 132.5 (s, 2C, $2 \times C^4\text{-H}$, Dipp), 135.0 (s, 2C, $2 \times \text{C}^1$, Dipp), 147.0 (s, 4C, $2 \times C^{2.6}\text{-CHMe}_A\text{Me}_B$, Dipp), 151.7 (s, 2C, $C^{2.6}\text{-CH}(\text{SiMe}_3)_2$, Tbb), 152.7 (s, 1C, $\text{C}^4\text{-CMe}_3$, Tbb), 196.8 (s, 1C, NCN , SIDipp).

${}^{19}\text{F}\{\text{H}\}$ NMR (470.6 MHz, tetrahydrofuran- d_8 , 298 K): δ /ppm = -78.20 (s).

${}^{29}\text{Si}\{\text{H}\}$ NMR (99.37 MHz, tetrahydrofuran- d_8 , 298 K): δ /ppm = 2.4 (br, 4Si, $4 \times \text{CH}(\text{SiMe}_3)_2$, Tbb), 10.3 (br, ${}^1J(\text{Ag,Si}) = 56.4$ Hz, 1Si, $\text{Si}(\text{SIDipp})$), 114.8 (br dd, ${}^2J({}^{109}\text{Ag,Si}) = 79$ Hz and ${}^3J({}^{107}\text{Ag,Si}) = 68$ Hz, 1Si, $\text{Si}(\text{Tbb})$). See Figure 39 on page 72.

4.6.11 **CuBr{ $\eta^2\text{-}(Z)\text{-}(\text{SIDipp})\text{Si}=\text{Si}(\text{Br})\text{Tbb}$ }** (10)

The reaction and workup have to be performed under strict exclusion of light.

A mixture of dark red $1\text{-C}_7\text{H}_8$ (400 mg, 0.37 mmol, 1.0 equiv.) and offwhite CuBr (59 mg, 0.41 mmol, 1.1 equiv.) was suspended in a mixture of 10 ml of benzene and 0.5 ml of diethyl ether and stirred overnight, whereupon most of the solid dissolved and the color changed to dark yellow. The suspension was treated with 1 ml of n-hexane and filtered off. The filtrate was evaporated and the yellow residue was dried at ambient temperature for 3 – 4 h to obtain **10** as a yellow solid in nearly quantitative yields and purities of 90 – 95 % that could be used for further reactions. Analytically pure samples could be obtained upon recrystallization from benzene/n-hexane mixtures at -30 °C, lowering the yield to 40 – 60 % (from **1**). Compound **10** is light sensitive in solution and gradually decomposes at ambient temperature to give $[\text{CuBr}(\text{SIDipp})]$ among some unidentified products, but can be stored at -30 °C in the dark for several weeks. Elemental analysis calcd. (%) for $\text{C}_{51}\text{H}_{87}\text{Br}_2\text{CuN}_2\text{Si}_6$ (1120.12): C 54.69, H 7.83, N 2.50; found: C 54.59, H 7.73, N 2.39 %.

${}^1\text{H}$ NMR (500.1 MHz, benzene- d_6 , 298 K): δ /ppm = 0.25 (s, 36H, $4 \times \text{SiMe}_3$, Tbb), 1.09 (d, 12H, ${}^3J_{\text{H,H}} = 6.7$ Hz, $C^{2.6}\text{-CHMe}_A\text{Me}_B$, Dipp), 1.26 (s, 9H, CMe_3 , Tbb), 1.63 (d, 12H, ${}^3J_{\text{H,H}} = 6.7$ Hz, $C^{2.6}\text{-CHMe}_A\text{Me}_B$, Dipp), 2.96 (s, 2H, ${}^2J_{\text{Si,H}} = 9.4$ Hz, $C^{2.6}\text{-CH}(\text{SiMe}_3)_2$, Tbb), 3.47 (s, 4H, $2 \times \text{NCH}_2$, SIDipp), 3.52 (sept, 4H, ${}^3J_{\text{H,H}} = 6.9$ Hz, $C^{2.6}\text{-CHMe}_A\text{Me}_B$, Dipp), 6.91 (s, 2H, $C^{3.5}\text{-H}$,

Tbb), 7.14 (d, 4H, $^3J_{\text{H,H}} = 7.7$ Hz, $2 \times \text{C}^{3,5}\text{-H}$, Dipp), 7.32 (t, $^3J_{\text{H,H}} = 7.7$ Hz, 2H, $2 \times \text{C}^4\text{-H}$, Dipp). See Figure 38 on page 71.

^1H NMR (300.1 MHz, toluene- d_6 , 298 K): δ /ppm = 0.19 (s, 36H, $4 \times \text{SiMe}_3$, Tbb), 1.09 (d, 12H, $^3J_{\text{H,H}} = 6.7$ Hz, $\text{C}^{2,6}\text{-CHMe}_A\text{Me}_B$, Dipp), 1.25 (s, 9H, CMe_3 , Tbb), 1.58 (d, 12H, $^3J_{\text{H,H}} = 6.7$ Hz, $\text{C}^{2,6}\text{-CHMe}_A\text{Me}_B$, Dipp), 2.90 (s, 2H, $^2J_{\text{Si,H}} = 9.4$ Hz, $\text{C}^{2,6}\text{-CH}(\text{SiMe}_3)_2$, Tbb), 3.51 (s, 4H, $2 \times \text{NCH}_2$, SIDipp), 3.48 (sept, 4H, $^3J_{\text{H,H}} = 6.9$ Hz, $\text{C}^{2,6}\text{-CHMe}_A\text{Me}_B$, Dipp; this signal overlaps with the neighbouring signal), 6.86 (s, 2H, $\text{C}^{3,5}\text{-H}$, Tbb), 7.08 (d, 4H, $^3J_{\text{H,H}} = 7.7$ Hz, $2 \times \text{C}^{3,5}\text{-H}$, Dipp; this signal overlaps with the solvent residual signal), 7.26 (t, $^3J_{\text{H,H}} = 7.7$ Hz, 2H, $2 \times \text{C}^4\text{-H}$, Dipp).

$^{13}\text{C}\{^1\text{H}\}$ NMR (125.8 MHz, benzene- d_6 , 298 K): δ /ppm = 1.9 (s, 12C, $4 \times \text{SiMe}_3$, Tbb), 24.8 (s, 4C, $2 \times \text{C}^{2,6}\text{-CHMe}_A\text{Me}_B$, Dipp), 26.4 (s, 4C, $2 \times \text{C}^{2,6}\text{-CHMe}_A\text{Me}_B$, Dipp), 29.3 (s, 4C, $2 \times \text{C}^{2,6}\text{-CHMe}_A\text{Me}_B$, Dipp), 31.1 (s, 3C, CMe_3 , Tbb), 33.3 (s, 2C, $\text{C}^{2,6}\text{-CH}(\text{SiMe}_3)_2$, Tbb), 34.4 (s, 1C, CMe_3 , Tbb), 54.6 (s, 2C, $2 \times \text{NCH}_2$, SIDipp), 122.1 (s, 2C, $\text{C}^{3,5}\text{-H}$, Tbb), 126.6 (s, 4C, $2 \times \text{C}^{3,5}\text{-H}$, Dipp), 131.4 (s, 2C, $2 \times \text{C}^4\text{-H}$, Dipp), 132.4 (s, 1C, C^1 , Tbb), 134.7 (s, 2C, $2 \times \text{C}^1$, Dipp), 146.5 (s, 4C, $2 \times \text{C}^{2,6}\text{-CHMe}_A\text{Me}_B$, Dipp), 151.9 (s, 2C, $\text{C}^{2,6}\text{-CH}(\text{SiMe}_3)_2$, Tbb), 152.0 (s, 1C, $\text{C}^4\text{-CMe}_3$, Tbb), 199.2 (s, 1C, NCN , SIDipp).

$^{29}\text{Si}\{^1\text{H}\}$ NMR (99.37 MHz, benzene- d_6 , 298 K): δ /ppm = 2.7 (s, 4Si, $4 \times \text{CH}(\text{SiMe}_3)_2$, Tbb), 35.6 (s, 1Si, Si (SIDipp), 105.1 (s, 1Si, Si (Tbb)).

4.6.12 $[\text{Cu}\{\text{(Z)}\text{-(SIDipp)Si=Si(Br)Tbb}\}][\text{B}(\text{Ar}^{\text{F}}\text{-CF}_3)_4]$ (11)

Method A: A red solution of $1\text{-C}_7\text{H}_8$ (200 mg, 0.19 mmol, 1.0 equiv.) in 3 ml fluorobenzene was slowly treated with a colorless solution of $[\text{Cu}(\text{MeCN})_2][\text{BAr}^{\text{F}}_4]$ (189 mg, 0.19 mmol, 1.0 equiv.) in 3 ml fluorobenzene, whereupon the reaction mixture quickly turned orange. Completeness of the reaction was verified by ^1H NMR spectroscopy in tetrahydrofuran- d_8 and the reaction mixture was evaporated to dryness. The following attempts to purify the crude product (ca. 15 % unknown impurities) were unsuccessful, partly due to the high sensitivity of compound 11:

1. addition of n-pentane to a solution in 1 ml of fluorobenzene (gives oil)
2. crystallization from mixtures of fluorobenzene, diethyl ether and n-pentane at -30 °C
3. phase separation and washing of the oily phase with more n-pentane
4. crystallization from pure diethyl ether by evaporation and/or cooling (4 °C, -30 °C)

Method B: A suspension of $1\text{-C}_7\text{H}_8$ (100 mg, 0.09 mmol, 1.0 equiv.) and CuBr (15 mg, 0.10 mmol, 1.1 equiv.) in 3 ml of toluene was stirred overnight in the dark to afford the

CuBr-complex **10**. The now dark yellow to brown solution was filtered from the excess CuBr and treated with a suspension of Na[BAr^F₄] (83 mg, 0.09 mmol, 1.0 equiv.) in 1 ml of toluene. The reaction mixture was stirred for 2 h at ambient temperature whereupon the color changed to orange-yellow and in situ ¹H NMR spectroscopy in tetrahydrofuran-d₈ revealed the selective formation of **11**. The solution was filtered from a small, colorless precipitate (NaBr) and carefully treated with 2 ml of n-hexane under vigorous stirring, whereupon a very sticky waxy to oily solid formed. The mixture was digested in an ultrasonic bath for some minutes, whereupon the sticky precipitate transformed into a fine, orange powder with a yellow supernatant. The suspension was cooled to -30 °C and filtered off to give 108 mg (0.59 mmol, 63 % in respect to **1**) of a yellow-orange solid. This solid contained some n-hexane (ca. 50 mol%) that could not be removed in vacuo or by several freeze-pump-thaw cycles.

¹H NMR (500.1 MHz, tetrahydrofuran-d₈, 298 K): δ /ppm = -0.03 (s, 36H, 4 × SiMe₃, Tbb), 1.24 (s, 9H, CMe₃, Tbb), 1.32 (d, 12H, ³J_{H,H} = 6.7 Hz, C^{2,6}-CHMe_AMe_B, Dipp), 1.55 (d, 12H, ³J_{H,H} = 6.7 Hz, C^{2,6}-CHMe_AMe_B, Dipp), 2.59 (s, 2H, ²J_{Si,H} = 9.4 Hz, C^{2,6}-CH(SiMe₃)₂, Tbb), 3.55 (sept, 4H, ³J_{H,H} = 6.9 Hz, C^{2,6}-CHMe_AMe_B, Dipp), 4.32 (s, 4H, 2 × NCH₂, SIDipp), 6.73 (s, 2H, C^{3,5}-H, Tbb), 7.42 (d, 4H, ³J_{H,H} = 7.7 Hz, 2 × C^{3,5}-H, Dipp), 7.50 (t, ³J_{H,H} = 7.7 Hz, 2H, 2 × C⁴-H, Dipp), 7.58 (s, 4H, 4 × C⁴-H, BAr^F₄), 7.58 (s, 8H, 4 × C^{2,6}-H, BAr^F₄). See Figure 45 on page 82.

¹H NMR (500.1 MHz, chlorobenzene-d₃, 298 K): δ /ppm = -0.06 (s, 36H, 4 × SiMe₃, Tbb), 1.11 (d, 12H, ³J_{H,H} = 6.7 Hz, C^{2,6}-CHMe_AMe_B, Dipp), 1.17 (s, 9H, CMe₃, Tbb), 1.36 (d, 12H, ³J_{H,H} = 6.7 Hz, C^{2,6}-CHMe_AMe_B, Dipp), 2.08 (s, 2H, ²J_{Si,H} = 9.4 Hz, C^{2,6}-CH(SiMe₃)₂, Tbb), 3.12 (br, 4H, $\nu_{1/2}$ = 24 Hz, C^{2,6}-CHMe_AMe_B, Dipp), 4.00 (br, 4H, $\nu_{1/2}$ = 24 Hz, 4H, 2 × NCH₂, SIDipp), 6.67 (s, 2H, C^{3,5}-H, Tbb), 7.15 (d, 4H, ³J_{H,H} = 7.7 Hz, 2 × C^{3,5}-H, Dipp), 7.28 (t, ³J_{H,H} = 7.7 Hz, 2H, 2 × C⁴-H, Dipp), 7.60 (s, 4H, 4 × C⁴-H, BAr^F₄), 8.23 (s, 8H, 4 × C^{2,6}-H, BAr^F₄).

¹³C{¹H} NMR (125.8 MHz, tetrahydrofuran-d₈, 298 K): δ /ppm = 1.60, 1.62 (each s, ¹J_{Si,C} = 50 Hz, each 6C, 4 × SiMe₃, Tbb), 25.2 (s, 4C, 2 × C^{2,6}-CHMe_AMe_B, Dipp, this signal overlaps with the solvent signal at δ_c = 25.3 ppm), 26.4 (s, 4C, 2 × C^{2,6}-CHMe_AMe_B, Dipp), 30.0 (s, 4C, 2 × C^{2,6}-CHMe_AMe_B, Dipp), 31.2 (s, 3C, CMe₃, Tbb), 34.3 (s, 2C, C^{2,6}-CH(SiMe₃)₂, Tbb), 35.1 (s, 1C, CMe₃, Tbb), 56.0 (s, 2C, 2 × NCH₂, SIDipp), 118.2 (br, $\nu_{1/2}$ = 16 Hz, 4C, 4 × C⁴-H, BAr^F₄), 122.8 (s, 2C, C^{3,5}-H, Tbb), 125.5 (q, ¹J_{F,C} = 272 Hz, 8C, 4 × C^{3,5}-CF₃, BAr^F₄), 127.3 (s, 4C, 2 × C^{3,5}-H, Dipp), 130.0 (qq, 8C, ²J_{F,C} = 32 Hz, ³J_{C,B} = 2.7 Hz, 4 × C^{3,5}-CF₃, BAr^F₄), 132.0 (s, 2C, 2 × C⁴-H, Dipp), 132.3 (s, 1C, C¹, Tbb), 135.4 (s, 2C, 2 × C¹, Dipp), 135.6 (br, $\nu_{1/2}$ = 11 Hz, 8C, 4 × C^{2,6}-H, BAr^F₄), 147.7 (s, 4C, 2 × C^{2,6}-CHMe_AMe_B, Dipp), 152.3 (s, 2C, C^{2,6}-CH(SiMe₃)₂, Tbb), 153.4 (s, 1C, C¹-CMe₃, Tbb; this signal has a very low intensity), 162.8 (q, 4C, ¹J_{C,B} = 49.4 Hz, 4 × C¹, BAr^F₄), 196.7 (s, 1C, NCN, SIDipp).

¹³C{¹H} NMR (125.8 MHz, chlorobenzene-d₃, 298 K): δ /ppm = 0.4 (s, 12C, ¹J_{Si,C} = 50 Hz 4 × SiMe₃, Tbb), 24.7 (br, 4C, $\nu_{1/2}$ ≈ 80 Hz, 2 × C^{2,6}-CHMe_AMe_B, Dipp), 25.7 (s, 4C, 2 × C^{2,6}-

CHMe_AMe_B, Dipp), 29.5 (s, 4C, 2 × C^{2,6}-CHMe_AMe_B, Dipp), 30.7 (s, 3C, CMe₃, Tbb), 34.0 (s, 2C, C^{2,6}-CH(SiMe₃)₂, Tbb), 34.5 (s, 1C, CMe₃, Tbb), 54.1 (s, 2C, 2 × NCH₂, SIDipp), 117.8 (sept, 4C, ⁴J_{F,C} = 4 Hz, 4 × C⁴-H, BAr^F₄), 122.0 (s, 2C, C^{3,5}-H, Tbb), 125.0 (q, ¹J_{F,C} = 272 Hz, 8C, 4 × C^{3,5}-CF₃, BAr^F₄), 127.3 (s, 4C, 2 × C^{3,5}-H, Dipp), 129.6 (qq, 8C, ²J_{F,C} = 32 Hz, ³J_{C,B} = 2.7 Hz, 4 × C^{3,5}-CF₃, BAr^F₄, this signal overlaps with the solvent signal at δ_c = 129.3 ppm), 131.1 (s, 1C, C¹, Tbb), 132.1 (s, 2C, 2 × C⁴-H, Dipp), 132.6 (s, 2C, 2 × C¹, Dipp), 135.2 (br, ν_{1/2} = 11 Hz, 8C, 4 × C^{2,6}-H, BAr^F₄), 146.7 (s, 4C, 2 × C^{2,6}-CHMe_AMe_B, Dipp), 149.8 (s, 2C, C^{2,6}-CH(SiMe₃)₂, Tbb), 154.0 (br, 1C, ν_{1/2} ≈ 80 Hz, C⁴-CMe₃, Tbb), 162.5 (q, 4C, ¹J_{C,B} = 49.4 Hz, 4 × C¹, BAr^F₄), 198.8 (s, 1C, NCN, SIDipp).

¹¹B{¹H} NMR (160.5 MHz, tetrahydrofuran-d₈, 298 K): δ/ppm = -6.54 (s).

¹¹B{¹H} NMR (160.5 MHz, chlorobenzene-d₅, 298 K): δ/ppm = -6.08 (s).

¹⁹F NMR (470.6 MHz, tetrahydrofuran-d₈, 298 K): δ/ppm = -63.44 (s).

¹⁹F NMR (470.6 MHz, chlorobenzene-d₅, 298 K): δ/ppm = -62.09 (s).

²⁹Si{¹H} NMR (99.37 MHz, tetrahydrofuran-d₈, 298 K): δ/ppm = 2.3 (s, 4Si, 4 × CH(SiMe₃)₂, Tbb). Due to slow decomposition of 11 in tetrahydrofuran-d₈, the resonances of the low-valent Si atoms could not be detected. See below for data in chlorobenzene-d₅.

²⁹Si{¹H} NMR (99.37 MHz, chlorobenzene-d₅, 298 K): δ/ppm = -4.3 (br, 1Si, ν_{1/2} ≈ 40 Hz, Si(SIDipp), 3.2 (s, 4Si, 4 × CH(SiMe₃)₂, Tbb), 111.2 (s, 1Si, Si(Tbb)).

4.6.13 $\text{CuBr}\{\eta^2\text{-(Z)-(SIDipp)(OtBu)Si=SiTbb}\}$ (**12**)

The reaction and workup have to be performed under strict exclusion of light.

A dark red solution of **1**-C₇H₈ (1.50 g, 1.40 mmol, 1.0 equiv.) in 30 ml of benzene was treated with a colorless to light yellowish solution of CuOtBu (259 mg, 1.90 mmol, 1.35 equiv.) in 15 ml of benzene at ambient temperature. The solution was stirred overnight whereupon the color changed to dark brown and the reaction progress was monitored by ¹H NMR spectroscopy.⁵⁴ When the reaction was completed, the solution was evaporated at 40 °C and the dark brown residue was finely dispersed in 45 ml of n-pentane. The mixture was cooled to -50 °C for 1.5 h and the dark brown precipitate was isolated by filtration at -50 °C. Drying at ambient temperature for 2 h gave **12** as a very dark brown powder. Yield: 1.175 g (1.06 mmol, 75 % from **1**). Compound **12** slowly decomposes at ambient temperature (thermal decomposition to a black mass at 236 °C) but can be stored in the dark at -30 °C for several months. Elemental analysis calcd. (%) for C₅₅H₉₆BrCuN₂OSi₆ (1113.33): C 59.33, H 8.69, N 2.52; found: C 59.02, H 8.71, N 2.33 %.

¹H NMR (500.1 MHz, benzene-d₆, 298 K): δ /ppm = 0.28 (s, 18H, 2 × CH(SiMe₃)_A(SiMe₃)_B, Tbb), 0.38 (s, 18H, 2 × CH(SiMe₃)_A(SiMe₃)_B, Tbb), 0.84 (s, 9H, OCM₃), 1.05 (d, 6H, ³J_{H,H} = 6.9 Hz, C²-CHMe_AMe_B, Dipp), 1.33 (s, 9H, CM₃, Tbb), 1.35 (d, 6H, ³J_{H,H} = 6.9 Hz, C⁶-CHMe_AMe_B, Dipp), 1.47 (d, 6H, ³J_{H,H} = 6.9 Hz, C²-CHMe_AMe_B, Dipp), 1.90 (d, 6H, ³J_{H,H} = 6.9 Hz, C²-CHMe_AMe_B, Dipp), 2.74 (s, 2H, ²J_{Si,H} = 9.2 Hz, CH(SiMe₃)₂(SiMe₃)_B, Tbb), 2.95 (s, 4H, 2 × NCH_AH_B, SIDipp), 3.03 (sept, 2H, ³J_{H,H} = 6.9 Hz, C²-CHMe_AMe_B, Dipp), 3.81 (s, 4H, 2 × NCH_AH_B, SIDipp), 4.35 (sept, 2H, ³J_{H,H} = 6.9 Hz, C⁶-CHMe_AMe_B, Dipp), 6.82 (s, 2H, C^{3,5}-H, Tbb), 6.98 (t, ³J_{H,H} = 7.7 Hz, 2H, 2 × C⁴-H, Dipp), 7.14 (d*, 4H, ³J_{H,H} = 7.7 Hz, 2 × C^{3,5}-H, Dipp),

¹H NMR (500.1 MHz, tetrahydrofuran-d₈, 298 K): δ /ppm = -0.04 (s, 18H, 2 × CH(SiMe₃)_A(SiMe₃)_B, Tbb), 0.10 (s, 18H, 2 × CH(SiMe₃)_A(SiMe₃)_B, Tbb), 0.77 (s, 9H, OCM₃, Tbb), 1.19 (s, 9H, CM₃, Tbb), 1.24 (d, 6H, ³J_{H,H} = 6.5 Hz, C²-CHMe_AMe_B, Dipp), 1.33 (d, 6H, ³J_{H,H} = 6.5 Hz, C⁶-CHMe_AMe_B, Dipp), 1.58 (d, 6H, ³J_{H,H} = 6.7 Hz, C⁶-CHMe_AMe_B, Dipp, this signal overlaps with the signal at δ_H = 1.16 ppm), 1.61 (d, 6H, ³J_{H,H} = 6.7 Hz, C²-CHMe_AMe_B, Dipp), 2.51 (s, 2H, ²J_{Si,H} = 9.0 Hz, ³J_{C,H} = 109 Hz, CH(SiMe₃)₂(SiMe₃)_B, Tbb), 3.26 (br sept, 2H, ³J_{H,H} = 6.9 Hz, C²-CHMe_AMe_B, Dipp), 3.86 (br t, 4H, 2 × NCH_AH_B, SIDipp), 4.12 (br sept, 2H, ³J_{H,H} = 6.9 Hz, C⁶-CHMe_AMe_B, Dipp), 4.33 (br pt 4H, 2 × NCH_AH_B, SIDipp), 6.53 (s, 2H, C^{3,5}-H, Tbb), 7.27 (d, 4H, ³J_{H,H} = 7.7 Hz, 2 × C^{3,5}-H, Dipp), 7.33 (t, ³J_{H,H} = 7.7 Hz, 2H, 2 × C⁴-H, Dipp).

⁵⁴ Sometimes another 5 – 10 mol% of CuOtBu had to be added for unknown reason, but the excess of about 0.35 equiv. was always consumed. However, adding too much of an excess from the beginning of the reaction should be avoided due to the high solubility of CuOtBu and **12** in common unpolar solvents, which significantly hamper the workup.

$^{13}\text{C}\{^1\text{H}\}$ NMR (125.8 MHz, benzene- d_6 , 298 K): δ /ppm = 1.7 (s, 6C, $2 \times \text{CH}(\text{SiMe}_3)_A(\text{SiMe}_3)_B$, Tbb), 2.9 (s, 6C, $2 \times \text{CH}(\text{SiMe}_3)_A(\text{SiMe}_3)_B$, Tbb), 24.9 (s, 2C, $2 \times \text{C}^2\text{-CHMe}_A\text{Me}_B$, Dipp), 25.7 (s, 2C, $2 \times \text{C}^2\text{-CHMe}_A\text{Me}_B$, Dipp), 25.8 (s, 2C, $2 \times \text{C}^6\text{-CHMe}_A\text{Me}_B$, Dipp), 26.5 (s, 2C, $2 \times \text{C}^6\text{-CHMe}_A\text{Me}_B$, Dipp), 29.1 (s, 2C, $2 \times \text{C}^2\text{-CHMe}_A\text{Me}_B$, Dipp), 29.5 (s, 2C, $2 \times \text{C}^6\text{-CHMe}_A\text{Me}_B$, Dipp), 31.4 (s, 3C, CMe_3 , Tbb), 32.7 (s, 3C, OCMe_3), 34.0 (s, 2C, $\text{C}^{2,6}\text{-CH}(\text{SiMe}_3)_2$, Tbb), 34.2 (s, 1C, $\text{C}^4\text{-CMe}_3$, Tbb), 54.9 (s, 2C, $2 \times \text{NCH}_2$, SIDipp), 74.6 (s, 1C, OCMe_3), 122.4 (s, 2C, $\text{C}^{3,5}\text{-H}$, Tbb), 124.6 (s, 2C, $2 \times \text{C}^3\text{-H}$, Dipp), 126.4 (s, 2C, $2 \times \text{C}^5\text{-H}$, Dipp), 130.1 (s, 2C, $2 \times \text{C}^4\text{-H}$, Dipp), 135.7 (s, 1C, C^1 , Tbb), 137.6 (s, 2C, $2 \times \text{C}^1$, Dipp), 143.8 (s, 2C, $2 \times \text{C}^2\text{-CHMe}_A\text{Me}_B$, Dipp), 147.6 (s, 1C, $\text{C}^4\text{-CMe}_3$, Tbb), 148.2 (s, 4C, $2 \times \text{C}^6\text{-CHMe}_A\text{Me}_B$, Dipp), 149.7 (s, 2C, $\text{C}^{2,6}\text{-CH}(\text{SiMe}_3)_2$, Tbb), 185.1 (s, 1C, NCN , SIDipp).

$^{13}\text{C}\{^1\text{H}\}$ NMR (125.8 MHz, tetrahydrofuran- d_8 , 298 K): δ /ppm = 1.8 (s, 6C, $2 \times \text{CH}(\text{SiMe}_3)_A(\text{SiMe}_3)_B$, Tbb), 2.9 (s, 6C, $2 \times \text{CH}(\text{SiMe}_3)_A(\text{SiMe}_3)_B$, Tbb), 25.8 (br s, 4C, $2 \times \text{C}^6\text{-CHMe}_A\text{Me}_B$ and $2 \times \text{C}^6\text{-CHMe}_A\text{Me}_B$, Dipp), 26.0 (s, 2C, $2 \times \text{C}^2\text{-CHMe}_A\text{Me}_B$, Dipp), 26.5 (s, 2C, $2 \times \text{C}^2\text{-CHMe}_A\text{Me}_B$, Dipp), 30.0 (s, 4C, $2 \times \text{C}^2\text{-CHMe}_A\text{Me}_B$ and $2 \times \text{C}^6\text{-CHMe}_A\text{Me}_B$, Dipp), 31.5 (s, 3C, CMe_3 , Tbb), 33.1 (s, 3C, OCMe_3), 34.2 (s, 2C, $\text{C}^{2,6}\text{-CH}(\text{SiMe}_3)_2$, Tbb), 34.6 (s, 1C, $\text{C}^4\text{-CMe}_3$, Tbb), 56.3 (s, 2C, $2 \times \text{NCH}_2$, SIDipp), 75.2 (s, 1C, OCMe_3), 122.9 (s, 2C, $\text{C}^{3,5}\text{-H}$, Tbb), 125.5, 126.6 (each s, each 2C, $2 \times \text{C}^3\text{-H}$ and $2 \times \text{C}^5\text{-H}$, Dipp), 130.6 (s, 2C, $2 \times \text{C}^4\text{-H}$, Dipp), 137.0 (s, 1C, C^1 , Tbb), 138.4 (s, 2C, $2 \times \text{C}^1$, Dipp), 144.9 (s, 2C, $2 \times \text{C}^6\text{-CHMe}_A\text{Me}_B$, Dipp), 147.5 (s, 1C, $\text{C}^4\text{-CMe}_3$, Tbb), 148.5 (s, 2C, $2 \times \text{C}^2\text{-CHMe}_A\text{Me}_B$, Dipp), 150.1 (s, 2C, $\text{C}^{2,6}\text{-CH}(\text{SiMe}_3)_2$, Tbb), 185.2 (s, 1C, NCN , SIDipp).

$^{15}\text{N}\{^1\text{H}\}$ NMR (50.68 MHz, benzene- d_6 , 298 K): δ /ppm = 279.0 (s). This signal was not observed via 1D NMR spectroscopy but its position was deduced from a $^1\text{H}\text{-}^{15}\text{N}\{^1\text{H}\}$ HMBC spectrum.

$^{29}\text{Si}\{^1\text{H}\}$ NMR (99.37 MHz, benzene- d_6 , 298 K): δ /ppm = 1.9 (s, 2Si, $2 \times \text{CH}(\text{SiMe}_3)_A(\text{SiMe}_3)_B$, Tbb), 2.5 (s, 2Si, $2 \times \text{CH}(\text{SiMe}_3)_A(\text{SiMe}_3)_B$, Tbb), 5.7 (s, 1Si, Si (Tbb)), 25.9 (s, 1Si, Si (SIDipp)). Figure 48 on page 91.

4.6.14 **[Cu $\{\eta^2\text{-}(\text{Z})\text{-}(\text{SIDipp})(\text{OtBu})\text{Si}=\text{SiTbb}\}][\text{BAR}^{\text{F}_4}]$ (13)**

A dark brown solution of 12 (104 g, 0.094 mmol, 1.0 equiv.) in 3 ml of fluorobenzene was dropwise treated with a colorless solution of $\text{Na}[\text{BAR}^{\text{F}_4}]$ (83 mg, 0.094 mmol, 1.00 equiv.) in 3 ml of fluorobenzene at ambient temperature. The color of the reaction mixture quickly changed to an intense cherry red and the solution was stirred for 1 h. The mixture was diluted with the same volume of n-pentane (no visible precipitation of NaBr), filtered off and reduced to a total volume of about 1 – 2 ml. The oily mixture was diluted with 1 ml of fluorobenzene and carefully layered with 5 ml of n-pentane. After cooling to -30°C for 3 days, a colorless residue had formed and the red supernatant was filtered off. The filtrate was dried, dissolved in benzene (formation of a thick oil), and dried again in vacuo by a freeze-pump-thaw cycle. The resulting red powder was washed with a minimum amount of n-pentane and dried in vacuo at

60 °C for 6h. Approximately 150 mg (84 % from 12) were collected, that still contained about 60 mol% of benzene as well as traces of n-hexane. A ^1H NMR spectrum that was measured as quickly as possible showed less than 5 % of unknown impurities, but to ongoing decomposition in chlorobenzene- d_5 solution no final evaluation was possible (**13** quickly decomposes in thf, while addition of benzene- d_6 led to the formation of a finely dispersed oil that gave broad NMR signals).

^1H NMR (500.1 MHz, chlorobenzene- d_5 , 298 K): δ /ppm = 0.22 (s, 36H, 4 \times SiMe_3 , Tbb), 0.86 (s, 9H, OCMe_3), 1.25 (d, 12H, $^3J_{\text{H,H}} = 6.8$ Hz, 4 \times CHMe_AMe_B , Dipp), 1.36 (s, 9H, CMe_3 , Tbb), 1.64 (d, 12H, $^3J_{\text{H,H}} = 6.8$ Hz, 4 \times CHMe_AMe_B , Dipp), 2.30 (s, 2H, $^2J_{\text{Si,H}} = 8.9$ Hz, $\text{CH}(\text{SiMe}_3)_2$, Tbb), 3.12 (sept, 4H, $^3J_{\text{H,H}} = 6.8$ Hz, CHMe_AMe_B , Dipp), 4.08 (s, 4H, 2 \times NCH_2 , SIDipp), 6.76 (s, 2H, $\text{C}^{3,5}\text{-H}$, Tbb), 7.25 (d, 4H, $^3J_{\text{H,H}} = 7.8$ Hz, 2 \times $\text{C}^{3,5}\text{-H}$, Dipp), 7.43 (t, $^3J_{\text{H,H}} = 7.8$ Hz, 2H, 2 \times $\text{C}^4\text{-H}$, Dipp), 7.76 (br s, $\nu_{1/2} = 4.8$ Hz, 4H, 4 \times $\text{C}^4\text{-H}$, Ar^F), 8.38 (m, 8H, 4 \times $\text{C}^{2,6}\text{-H}$, Ar^F).

$^{13}\text{C}\{^1\text{H}\}$ NMR (125.8 MHz, chlorobenzene- d_5 , 298 K): δ /ppm = 1.9 (br, $\nu_{1/2} = 87$ Hz, 12C, 4 \times SiMe_3 , Tbb), 24.4 (s, 4C, 2 \times $\text{C}^{2,6}\text{-CHMe}_A\text{Me}_B$, Dipp), 25.4 (s, 4C, 2 \times $\text{C}^{2,6}\text{-CHMe}_A\text{Me}_B$, Dipp), 29.7 (s, 4C, 2 \times $\text{C}^{2,6}\text{-CHMe}_A\text{Me}_B$, Dipp), 31.0 (s, 3C, CMe_3 , Tbb), 32.2 (s, 3C, OCMe_3), 34.1 (s, 1C, CMe_3 , Tbb), 35.4 (s, 2C, 2 \times $\text{CH}(\text{SiMe}_3)_2$, Tbb), 54.4 (br, $\nu_{1/2} = 26$ Hz, 2C, 2 \times NCH_2 , SIDipp), 77.2 (s, 1C, OCMe_3), 117.8 (sept, $^3J_{\text{F,C}} = 3.8$ Hz, 4C, 4 \times $\text{C}^4\text{-H}$, BAr^F ; this signal was not fully resolved), 122.8 (s, 2C, $\text{C}^{3,5}\text{-H}$, Tbb), 124.5 (br, $\nu_{1/2} = 10$ Hz, 4C, 2 \times $\text{C}^{3,5}\text{-H}$, Dipp), 125.0 (q, $^1J_{\text{F,C}} = 272$ Hz, 8C, 4 \times $\text{C}^{3,5}\text{-CF}_3$, BAr^F), 129.3 (qq, 8C, $^2J_{\text{F,C}} = 32$ Hz, $^3J_{\text{C,B}} = 3.0$ Hz, 4 \times $\text{C}^{3,5}\text{-CF}_3$, BAr^F ; this signal is partially obscured by the solvent signal), 130.3 (br, $\nu_{1/2} = 11$ Hz, 2C, 2 \times $\text{C}^4\text{-H}$, Dipp), 135.3 (br, $\nu_{1/2} = 11$ Hz, 8C, 4 \times $\text{C}^{2,6}\text{-H}$, BAr^F), 144.6 (s, 4C, 2 \times $\text{C}^{2,6}\text{-CHMe}_A\text{Me}_B$, Dipp), 149.3 (s, 2C, $\text{C}^{2,6}\text{-CH}(\text{SiMe}_3)_2$, Tbb), 149.8 (s, 1C, $\text{C}^4\text{-CMe}_3$, Tbb), 162.5 (q, 4C, $^1J_{\text{C,B}} = 49.4$ Hz, 4 \times C^1 , BAr^F), 185.7 (s, 1C, NCN , SIDipp). The C1 carbon atoms of both the Dipp groups and the Tbb substituents were not detected, presumably due to broadening.

$^{11}\text{B}\{^1\text{H}\}$ NMR (160.5 MHz, chlorobenzene- d_5 , 298 K): δ /ppm = -5.95 (s).

^{19}F NMR (470.6 MHz, chlorobenzene- d_5 , 298 K): δ /ppm = -61.96 (s).

$^{15}\text{N}\{^1\text{H}\}$ NMR (50.68 MHz, chlorobenzene- d_5 , 298 K): δ /ppm = 142.9 (s). This signal was not observed via 1D NMR spectroscopy but its position was deduced from a $^1\text{H}\text{-}^{15}\text{N}\{^1\text{H}\}$ HMBC spectrum.

$^{29}\text{Si}\{^1\text{H}\}$ NMR (99.36 MHz, chlorobenzene- d_5 , 298 K): δ /ppm = 2.3 (br, $\nu_{1/2} = 23$ Hz, 4Si, 4 \times SiMe_3), 20.1 (br, $\nu_{1/2} = 23$ Hz, 1Si, SiTbb), 39.6 (s, 1Si, $\text{Si}(\text{SIDipp})$).

4.6.15 (Z)-TbbSi=Si(OtBu)(SIDipp) (14)

The reaction has to be performed under exclusion of light and all steps at ambient temperature have to be performed as quick as possible.

A dark brown solution of **12** (1140 mg, 1.02 mmol, 1.0 equiv.) in 25 ml of toluene was treated with a colorless to light yellowish solution of LiPr_2Me_2 (369 mg, 2.05 mmol, 2.0 equiv.) in 5 ml of toluene at ambient temperature over a duration of ca. 3 min. During the addition, the dark color of the reaction mixture gradually turned to dark violet. The solution was stirred for another 15 min and evaporated to dryness at ambient temperature. The dark violet, nearly black residue was treated with 10 ml of n-pentane, stirred for a short time and again evaporated to dryness to eliminate any residual toluene. The residue was extracted from a colorless solid (the $[\text{CuBr}(\text{LiPr}_2\text{Me}_2)_2]$ byproduct) with a total of 60 ml of n-pentane at $-80\text{ }^\circ\text{C}$ in several portions. The combined dark violet filtrates were evaporated and the residue was dried by two freeze-pump-thaw cycles to afford an intensely violet powder. Yield: 610 mg (0.63 mmol, 61 % from **12**). Compound **14** slowly decomposes at ambient temperature but can be stored at $-30\text{ }^\circ\text{C}$ for several months. Elemental analysis calcd. (%) for $\text{C}_{35}\text{H}_{96}\text{N}_2\text{OSi}_6$ (969.88): C 68.11, H 9.98, N 2.89; found: C 66.56, H 10.06, N 2.92 %.

$^1\text{H NMR}$ (500.1 MHz, benzene- d_6 , 298 K): δ /ppm = 0.28 (s, 18H, $2 \times \text{CH}(\text{SiMe}_3)_A(\text{SiMe}_3)_B$, Tbb), 0.36 (s, 18H, $2 \times \text{CH}(\text{SiMe}_3)_A(\text{SiMe}_3)_B$, Tbb), 0.78 (s, 9H, OCMe_3), 1.19 (d, 12H, $^3J_{\text{H,H}} = 6.8$ Hz, $\text{C}^{2,6}\text{-CHMe}_A\text{Me}_B$, Dipp), 1.39 (s, 9H, CMe_3 , Tbb), 1.65 (d, 6H, $^3J_{\text{H,H}} = 6.8$ Hz, $\text{C}^{2,6}\text{-CHMe}_A\text{Me}_B$, Dipp), 2.53 (s, 2H, $^2J_{\text{Si,H}} = 9.5$ Hz, $\text{CH}(\text{SiMe}_3)_A(\text{SiMe}_3)_B$, Tbb), 3.31 (sept, 4H, $^3J_{\text{H,H}} = 6.9$ Hz, $4 \times \text{CHMe}_A\text{Me}_B$, Dipp), 3.43 (s, 4H, $2 \times \text{NCH}_2$, SIDipp), 6.75 (s, 2H, $\text{C}^{3,5}\text{-H}$, Tbb), 7.08 (d, 4H, $^3J_{\text{H,H}} = 7.7$ Hz, $2 \times \text{C}^{3,5}\text{-H}$, Dipp), 7.19 (t*, $^3J_{\text{H,H}} = 7.7$ Hz, 2H, $2 \times \text{C}^4\text{-H}$, Dipp).

$^{13}\text{C}\{^1\text{H}\}$ NMR (125.8 MHz, benzene- d_6 , 298 K): δ /ppm = 1.9 (s, 6C, $2 \times \text{CH}(\text{SiMe}_3)_A(\text{SiMe}_3)_B$, Tbb), 3.0 (s, 6C, $2 \times \text{CH}(\text{SiMe}_3)_A(\text{SiMe}_3)_B$, Tbb), 25.1 (s, 4C, $2 \times \text{C}^{2,6}\text{-CHMe}_A\text{Me}_B$, Dipp), 25.8 (s, 4C, $2 \times \text{C}^{2,6}\text{-CHMe}_A\text{Me}_B$, Dipp), 29.2 (s, 4C, $2 \times \text{C}^{2,6}\text{-CHMe}_A\text{Me}_B$, Dipp), 30.8 (s, 2C, $\text{C}^{2,6}\text{-CH}(\text{SiMe}_3)_2$, Tbb), 31.6 (s, 3C, CMe_3 , Tbb), 32.6 (s, 3C, OCMe_3), 34.1 (s, 1C, $\text{C}^4\text{-CMe}_3$, Tbb), 54.2 (s, 2C, $2 \times \text{NCH}_2$, SIDipp), 72.7 (s, 1C, OCMe_3), 122.0 (s, 2C, $\text{C}^{3,5}\text{-H}$, Tbb), 125.3 (s, 4C, $2 \times \text{C}^{3,5}\text{-H}$, Dipp), 129.4 (s, 2C, $2 \times \text{C}^4\text{-H}$, Dipp), 138.3 (s, 2C, $2 \times \text{C}^1$, Dipp), 146.1 (s, 4C, $2 \times \text{C}^{2,6}\text{-CHMe}_A\text{Me}_B$, Dipp), 146.2 (s, 1C, C^1 , Tbb), 146.3 (s, 2C, $\text{C}^{2,6}\text{-CH}(\text{SiMe}_3)_2$, Tbb), 146.8 (s, 1C, $\text{C}^4\text{-CMe}_3$, Tbb), 189.1 (s, 1C, NCN , SIDipp).

$^{29}\text{Si}\{^1\text{H}\}$ NMR (99.37 MHz, benzene- d_6 , 298 K): δ /ppm = 1.2 (s, 2Si, $2 \times \text{CH}(\text{SiMe}_3)_A(\text{SiMe}_3)_B$, Tbb), 1.7 (s, 2Si, $2 \times \text{CH}(\text{SiMe}_3)_A(\text{SiMe}_3)_B$, Tbb), 43.7 (s, 1Si, $\text{Si}(\text{SIDipp})$), 139.2 (s, 1Si, $\text{Si}(\text{Tbb})$). See Figure 48 on page 91.

4.6.16 (Z)-SiDippSi=Si(OtBu)Tbb (15)

A dark violet solution of compound **14** (610 mg, 0.63 mmol) in toluene was heated to 100 °C for about 30 minutes, whereupon the color changed to dark red.⁵⁵ The solution was evaporated to dryness and the dark carmine red residue was dissolved in about 5 ml on n-hexane. Heating to 60 °C, careful evaporation to incipient crystallization and slow cooling in a water bath overnight afforded large, very dark red crystalline needles of **15**·C₇H₈, which were suitable for X-ray analysis. Grinding, a freeze-pump-thaw cycle and final drying at 60 °C for 1 h afforded **15** as a carmine red powder. Yield: 495 mg (0.51 mmol, 81 % from **14**). Upon heating, compound **15** decomposes to a grey-black mass at 177 °C that melts to a dark liquid at 180 °C. Elemental analysis calcd. (%) for C₅₃H₉₆N₂OSi₆ (969.88): C 68.11, H 9.98, N 2.89; found: C 68.01, H 10.21, N 2.89 %.

¹H NMR (500.1 MHz, benzene-d₆, 298 K): δ /ppm = 0.15 (br, $\nu_{1/2}$ = 38 Hz, 18H, 2 × CH(SiMe₃)_A(SiMe₃)_B, Tbb), 0.24 (br, $\nu_{1/2}$ = 38 Hz, 18H, 2 × CH(SiMe₃)_A(SiMe₃)_B, Tbb), 1.14 (d, 12H, ³J_{H,H} = 6.7 Hz, C^{2,6}-CHMe_AMe_B, Dipp), 1.33 (s, 9H, CMe₃, Tbb), 1.61 (d, 12H, ³J_{H,H} = 6.7 Hz, C^{2,6}-CHMe_AMe_B, Dipp), 3.17 (s, 2H, ²J_{Si,H} = 9.4 Hz, C^{2,6}-CH(SiMe₃)₂, Tbb), 3.40 (sept, 4H, ³J_{H,H} = 6.9 Hz, C^{2,6}-CHMe_AMe_B, Dipp), 3.47 (s, 4H, 2 × NCH₂, SiDipp), 6.82 (s, 2H, C^{3,5}-H, Tbb), 7.13 (d, 4H, ³J_{H,H} = 7.7 Hz, 2 × C^{3,5}-H, Dipp), 7.24 (t, ³J_{H,H} = 7.7 Hz, 2H, 2 × C⁴-H, Dipp).

¹³C{¹H} NMR (125.8 MHz, benzene-d₆, 298 K): δ /ppm = 1.9 (br, $\nu_{1/2}$ = 52 Hz, 12C, 4 × SiMe₃, Tbb), 24.7 (s, 4C, 2 × C^{2,6}-CHMe_AMe_B, Dipp), 26.4 (s, 4C, 2 × C^{2,6}-CHMe_AMe_B, Dipp), 29.0 (s, 4C, 2 × C^{2,6}-CHMe_AMe_B, Dipp), 31.4 (s, 3C, CMe₃, Tbb), 31.8 (s, 2C, C^{2,6}-CH(SiMe₃)₂, Tbb), 34.4 (s, 1C, CMe₃, Tbb), 53.7 (s, 2C, 2 × NCH₂, SiDipp), 74.4 (s, 1C, OCMe₃), 120.7 (s, 2C, C^{3,5}-H, Tbb), 125.3 (s, 4C, 2 × C^{3,5}-H, Dipp), 129.6 (s, 2C, 2 × C⁴-H, Dipp), 137.3 (s, 2C, 2 × C¹, Dipp), 141.1 (s, 1C, C¹, Tbb), 146.6 (s, 4C, 2 × C^{2,6}-CHMe_AMe_B, Dipp), 148.8 (s, 1C, C⁴-CMe₃, Tbb), 149.9 (s, 2C, C^{2,6}-CH(SiMe₃)₂, Tbb), 205.0 (s, 1C, NCN, SiDipp).

²⁹Si{¹H} NMR (99.37 MHz, benzene-d₆, 298 K): δ /ppm = -16.6 (s, 1Si, Si(SiDipp), 1.6 (very broad, 4Si, 4 × CH(SiMe₃)₂, Tbb), 95.9 (s, 1Si, Si(Tbb)). Figure 48 on page 91

4.6.17 SiBr(OtBu)(SiDipp) (16-Br)

The reaction followed the procedure for compound **16-I** described below starting from SiBr₂(SiDipp) (500 mg, 0.864 mmol, 1 equiv.) and LiOtBu (69 mg, 0.862 mmol, 1.0 equiv.) in 12 ml thf. While a selective conversion was found by ¹H NMR spectroscopy, decomposition of

⁵⁵ The isomerization is nearly selective (¹H NMR) and yields **15** in at least 95 % yield if the starting material was pure. Due to difficulties during the purification of **14**, the yield of **15** may drop significantly.

both $\text{SiBr}_2(\text{IDipp})$ and **16-Br** in thf solution as well as the later reformation of $\text{SiBr}_2(\text{SIDipp})$ and free SIDipp throughout multiple workup steps was observed. This was interpreted as the result of OtBu/Br scrambling, preventing the isolation of pure samples. The following ^1H NMR data were therefore taken from a sample that contained about 20 mol% of free SIDipp .

^1H NMR (500.1 MHz, benzene- d_6 , 298 K): $\delta/\text{ppm} = 1.04$ (s, 9H, OCMe_3), 1.15 (d, 6H, $^3J_{\text{H,H}} = 6.8$ Hz, $\text{C}^2\text{-CHMe}_A\text{Me}_B$, Dipp), 1.16 (d, 6H, $^3J_{\text{H,H}} = 6.8$ Hz, $\text{C}^6\text{-CHMe}_A\text{Me}_B$, Dipp; this signal overlaps with the signal at $\delta_{\text{H}} = 1.15$ ppm), 1.53 (d, 6H, $^3J_{\text{H,H}} = 6.8$ Hz, $\text{C}^2\text{-CHMe}_A\text{Me}_B$), 1.62 (d, 6H, $^3J_{\text{H,H}} = 6.8$ Hz, $\text{C}^6\text{-CHMe}_A\text{Me}_B$), 3.33 (sept, $^3J_{\text{H,H}} = 6.8$ Hz, 2H, $2 \times \text{C}^2\text{-CHMe}_A\text{Me}_B$, Dipp), 3.39 – 3.50 (m, 4H, $2 \times \text{CH}_A\text{H}_B$ and $2 \times \text{CH}_A\text{H}_B$, SIDipp ; this signal overlaps with both neighboring signals), 3.54 (sept, $^3J_{\text{H,H}} = 6.8$ Hz, 2H, $2 \times \text{C}^6\text{-CHMe}_A\text{Me}_B$, Dipp), 7.04 (d*, 2H, $2 \times \text{C}^3\text{-H}$, Dipp), 7.07 (d*, 2H, $2 \times \text{C}^5\text{-H}$, Dipp), 7.18 (t, 2H, $2 \times \text{C}^4\text{-H}$, Dipp).

$^{13}\text{C}\{^1\text{H}\}$ NMR (125.8 MHz, benzene- d_6 , 298 K): $\delta/\text{ppm} = 24.0$ (s, 2C, $2 \times \text{C}^6\text{-CHMe}_A\text{Me}_B$, Dipp), 24.3 (s, 2C, $2 \times \text{C}^2\text{-CHMe}_A\text{Me}_B$, Dipp), 25.8, 26.2 (each s, each 2C, $2 \times \text{C}^2\text{-CHMe}_A\text{Me}_B$ and $2 \times \text{C}^6\text{-CHMe}_A\text{Me}_B$, Dipp), 29.2 (s, 2C, $2 \times \text{C}^6\text{-CHMe}_A\text{Me}_B$, Dipp), 29.3 (s, 2C, $2 \times \text{C}^2\text{-CHMe}_A\text{Me}_B$, Dipp), 31.7 (s, 3C, OCMe_3), 54.0 (s, 2C, $2 \times \text{NCH}_A\text{H}_B$, SIDipp), 71.9 (s, 1C, OCMe_3), 124.0 (s, 2C, $2 \times \text{C}^4\text{-H}$, Dipp), 124.5 (s, 2C, $2 \times \text{C}^3\text{-H}$, Dipp), 124.7 (s, 2C, $2 \times \text{C}^5\text{-H}$, Dipp), 134.8 (s, 2C, $2 \times \text{C}^1$, Dipp), 146.1 (s, 2C, $2 \times \text{C}^2\text{-CHMe}_A\text{Me}_B$, Dipp), 146.7 (s, 2C, $2 \times \text{C}^6\text{-CHMe}_A\text{Me}_B$, Dipp), 194.7 (s, 1C, NCN , SIDipp).

$^{29}\text{Si}\{^1\text{H}\}$ NMR (99.36 MHz, benzene- d_6 , 298 K): $\delta/\text{ppm} = 18.0$ (s).

4.6.18 $\text{Si}(\text{OtBu})(\text{IDipp})$ (**16-I**)

A solution of $\text{SiI}_2(\text{SIDipp})$ (500 mg, 0.297 mmol, 1 equiv.) in 10 ml thf was treated with a stock solution of LiOtBu (23.8 mg, 0.297 mmol, 1.0 equiv.) in 2 ml thf and the resulting dark yellow solution was stirred at ambient temperature. The reaction was monitored by ^1H NMR spectroscopy and completed in about 3 h. The mixture was evaporated to dryness, the yellow wax-like residue digested in 5 ml of n-hexane and again dried. The residue was then extracted with 3 portions of a 1:1-mixture of n-hexane and toluene amounting to a total of 20 ml. The solvent was reduced to about 2 ml and 4 ml of n-hexane were added dropwise. Cooling to -30 °C gave ca. 150 mg (61 %) of crude **16-I** that contained about 9 % free SIDipp . Slow evaporation of a toluene/n-hexane solution at ambient temperature afforded a crop of single crystals (ca. 25 mg) that were used for NMR-spectroscopic characterization.

^1H NMR (500.0 MHz, benzene- d_6 , 298 K): $\delta/\text{ppm} = 1.01$ (s, 9H, OCMe_3), 1.12 (d, $^3J_{\text{H,H}} = 6.9$ Hz, 6H, $2 \times \text{C}^2\text{-CHMe}_A\text{Me}_B$, Dipp), 1.14 (d, $^3J_{\text{H,H}} = 6.9$ Hz, 6H, $2 \times \text{C}^6\text{-CHMe}_A\text{Me}_B$, Dipp), 1.55 (d, $^3J_{\text{H,H}} = 6.8$ Hz, 6H, $2 \times \text{C}^2\text{-CHMe}_A\text{Me}_B$, Dipp), 1.62 (d, $^3J_{\text{H,H}} = 6.8$ Hz, 6H, $2 \times \text{C}^6\text{-CHMe}_A\text{Me}_B$, Dipp), 3.34 (sept, $^3J_{\text{H,H}} = 6.8$ Hz, 2H, $2 \times \text{C}^2\text{-CHMe}_A\text{Me}_B$, Dipp), 3.40 – 3.47 and 3.49 – 3.57

(each m, each 2H, $2 \times \text{NCH}_A\text{H}_B$ and $2 \times \text{NCH}_A\text{H}_B$, SIDipp), 3.66 (sept, $^3J_{\text{H,H}} = 6.8$ Hz, 2H, $2 \times \text{C}^6\text{-CHMe}_A\text{Me}_B$, Dipp), 7.02 (d*, $^3J_{\text{H,H}} = 7.6$ Hz, 2H, $2 \times \text{C}^3\text{-H}$, Dipp), 7.06 (d*, $^3J_{\text{H,H}} = 7.8$ Hz, 2H, $2 \times \text{C}^5\text{-H}$, Dipp), 7.15 (t, $^3J_{\text{H,H}} = 7.8$ Hz, 2H, $2 \times \text{C}^4\text{-H}$, Dipp; this signal overlaps with the solvent residual signal). The compound contained a small amount of thf visible at $\delta_{\text{H}} = 1.27$ and 3.79 ppm. See Figure 53 on page 109.

$^{13}\text{C}\{^1\text{H}\}$ NMR (125.7 MHz, benzene- d_6 , 298 K): $\delta/\text{ppm} = 24.0$ (s, 2C, $2 \times \text{C}^6\text{-CHMe}_A\text{Me}_B$, Dipp), 24.7 (s, 2C, $2 \times \text{C}^2\text{-CHMe}_A\text{Me}_B$, Dipp), 26.0 (s, 2C, $2 \times \text{C}^2\text{-CHMe}_A\text{Me}_B$, Dipp), 26.5 (s, 2C, $2 \times \text{C}^6\text{-CHMe}_A\text{Me}_B$, Dipp), 29.1 (s, 2C, $2 \times \text{C}^2\text{-CHMe}_A\text{Me}_B$, Dipp), 29.2 (s, 2C, $2 \times \text{C}^6\text{-CHMe}_A\text{Me}_B$, Dipp), 31.0 (s, 3C, OCMe_3), 54.2 (s, 2C, $2 \times \text{NCH}_A\text{H}_B$, SIDipp), 72.6 (s, 1C, OCMe_3), 124.7 (s, 2C, $2 \times \text{C}^3\text{-H}$, Dipp), 124.9 (s, 2C, $2 \times \text{C}^5\text{-H}$, Dipp), 129.8 (s, 2C, $2 \times \text{C}^4\text{-H}$, Dipp), 134.7 (s, 2C, $2 \times \text{C}^1$, Dipp), 146.0 (s, 2C, $2 \times \text{C}^2\text{-CHMe}_A\text{Me}_B$, Dipp), 146.6 (s, 2C, $2 \times \text{C}^6\text{-CHMe}_A\text{Me}_B$, Dipp), 195.9 (s, 1C, NCN , SIDipp). Tiny impurities were detected at $\delta_{\text{C}} = 25.2$ and 25.4 ppm but no thf was visible in the spectra.

$^{29}\text{Si}\{^1\text{H}\}$ NMR (99.36 MHz, benzene- d_6 , 298 K): $\delta/\text{ppm} = 13.2$ (s).

4.6.19 $\text{Cp}^*\text{SiOAr}^{\text{Mes}}$ (17)

18 ml of n-hexane were added to a solid mixture of slightly brownish $[\text{Cp}^*\text{Si}][\text{Al}\{\text{OC}(\text{CF}_3)_3\}_4]$ (2.42 g, 1.89 mmol, 1.0 equiv.) and colorless $\text{NaOAr}^{\text{Mes}}$ (634 mg, 1.80 mmol, 0.95 equiv.), whereupon a suspension of a light brown solid in a medium brown supernatant was formed. Slow addition of 10 ml of diethyl ether caused a fast decolorization to light brown and a part of the solid dissolved. The reaction mixture was stirred overnight, when an almost colorless suspension of a voluminous solid had formed. Complete conversion of $\text{NaOAr}^{\text{Mes}}$ was confirmed by in situ NMR spectroscopy.⁵⁶ The solvent was evaporated, the residue was digested in 20 ml of n-hexane and dried again. The colorless residue was then extracted with 20 + 5 ml of n-pentane and the slightly yellow filtrate was evaporated and dried by a freeze-pump-thaw cycle to give 775 mg of the colorless crude product. This powder was extracted with 10 + 2 ml of n-pentane from a small colorless residue and the filtrate was cooled to -30 °C for 3 days, when a colorless powder had formed. Yield: 530 mg (1.08 mmol, 57 %

⁵⁶ An aliquot of the supernatant was taken, dried and dissolved in benzene- d_6 . The ^1H NMR spectrum of the clear solution showed the complete and almost selective formation of **17** as well as 8 % of an unknown side product with signals at $\delta_{\text{H}} = 2.00$ (6H), 2.12 ppm (12H) and 4.53 ppm (1H, additional aromatic signals are presumably obscured). The spectrum showed no additional Cp^* signals and only trace amounts of diethyl ether. No $\text{NaOAr}^{\text{Mes}}$, $\text{LiOAr}^{\text{Mes}}$, HOAr^{Mes} or **19** was detected; excess $[\text{Cp}^*\text{Si}][\text{Al}\{\text{OC}(\text{CF}_3)_3\}_4]$ is insoluble in benzene. Despite the low solubility of the $[\text{Al}\{\text{OC}(\text{CF}_3)_3\}_4]$ salts, the ^{27}Al NMR spectrum revealed the presence of an unknown amount of the $[\text{Al}\{\text{OC}(\text{CF}_3)_3\}_4]$ anion in solution.

from [Cp*Si][Al{OC(CF₃)₃}₄]. Compound **17** decomposes upon melting at 138 °C under vigorous gas evolution. No satisfactory elemental analysis for C₃₄H₄₀OSi (492.28) could be obtained for unknown reasons.

¹H NMR (500.2 MHz, benzene-d₆, 298 K): δ/ppm = 1.56 (s, 15H, 5 × C-Me, Cp*), 2.18 (s, 12H, 2 × C^{2,6}-Me, Mes), 2.28 (s, 6H, 2 × C⁴-Me, Mes), 6.90 (s, 4H, 2 × C^{3,5}-H, Mes), 6.95 (t*, ³J_{H,H} = 7.3 Hz, 1H, C⁴-H, C₃H₃), 6.95 (d*, ³J_{H,H} = 7.3 Hz, 2H, C^{3,5}-H, C₃H₃).

¹³C{¹H} NMR (125.8 MHz, benzene-d₆, 298 K): δ/ppm = 9.5 (s, 5C, 5 × C-Me, Cp*), 21.1 (s, 2C, 2 × C⁴-Me, Mes), 21.4 (s, 4C, 2 × C^{2,6}-Me, Mes), 119.0 (s, 5C, 5 × C-Me, Cp*), 122.3 (s, 1C, C⁴-H, C₆H₃), 128.3 (s, 4C, 2 × C^{3,5}-H, Mes), 129.4 (s, 2C, C^{3,5}-H, C₆H₃), 133.3 (s, 2C, C^{2,6}, C₆H₃), 136.5 (s, 2C, 2 × C⁴-Me, Mes), 136.9 (s, 2C, 2 × C¹, Mes), 137.1 (s, 4C, 2 × C^{2,6}-Me, Mes), 149.1 (s, 1C, C¹, C₆H₃).

²⁹Si{¹H} NMR (59.63 MHz, benzene-d₆, 298 K): δ/ppm = -138.2 (s).

4.6.20 Si{N(Me)Ar^{Mes}}₂ (**18**)

A slightly turbid, dark yellow solution of SiI₂(SIDipp) (400 mg, 0.59 mmol, 1.0 equiv.) in 15 mL of benzene was slowly treated with solid LiN(Me)Ar^{Mes}·Et₂O (465 mg, 1.20 mmol, 2.02 equiv.). Upon addition, the lithium amide quickly dissolved and the color of the suspension changed from dark yellow to red. The suspension was stirred for 2 hours at ambient temperature and the complete conversion of the starting materials was confirmed by ¹H NMR spectroscopy.⁵⁷ 3 mL of n-hexane were added and the suspension was filtered from an off-white solid (LiI). The filtrate was evaporated and the red residue was digested in 3 mL of diethyl ether. Upon stirring the resulting red suspension for 2.5 hours, a colorless solid precipitated. The solid was isolated after filtration of the mother liquor and washing with 3 × 2.5 mL of diethyl ether at ambient temperature as an almost colorless (light pink) solid. Yield: 225 mg (0.33 mmol, 55 %). Compound **18** melts at 259 °C to a colorless liquid. Elemental analysis calcd. (%) for C₅₀H₅₆N₂Si (713.08): C 84.21, H 7.92, N 3.93; found: C 83.87, H 7.98, N 3.90.

⁵⁷ The ¹H NMR spectrum in benzene-d₆ revealed a quantitative conversion of the starting materials leading to **18** and HN(Me)Ar^{Mes} in a molar ratio of 6:1. In addition, an unknown SIDipp containing, presumably dark red byproduct was formed. ¹H NMR (300.1 MHz, benzene-d₆, 298 K): δ/ppm = 1.18 (d, ³J_{H,H} = 6.5 Hz, 12H, 4 × CHMe_ΔMe_β, Dipp), 1.43 (d, ³J_{H,H} = 6.5 Hz, 12H, 4 × CHMe_ΔMe_β, Dipp), 3.13 (sept, ³J_{H,H} = 6.5 Hz, 4H, 4 × CHMe_ΔMe_β, Dipp), 3.30 (s, 4H, 2 × NCH₃, SIDipp), 6.92 (d, ³J_{H,H} = 7.5 Hz, 4H, 2 × C^{3,5}-H, C₆H₃), 7.05 (t, ³J_{H,H} = 7.5 Hz, 2H, 2 × C⁴-H, C₆H₃). The byproduct is well soluble in aromatic solvents or diethyl ether and moderately soluble in aliphatic hydrocarbons. The NMR resonances did not alter throughout the workup process as it would be expected for an equilibrium of free SIDipp and a {Si(SIDipp)}-containing impurity.

$^1\text{H NMR}$ (500.2 MHz, benzene- d_6 , 298 K): δ /ppm = 1.97 (s, 6H, 2 \times N-Me), 2.07 (s, 24H, 4 \times C^{2.6}-Me, Mes), 2.25 (s, 12H, 4 \times C⁴-Me, Mes), 6.79 (s, 8H, 4 \times C^{3.5}-H, Mes), 6.92 (d, $^3J_{\text{H,H}} = 7.5$ Hz, 2H, 2 \times C^{3.5}-H, C₆H₃), 7.05 (t, $^3J_{\text{H,H}} = 7.5$ Hz, 4H, 2 \times C⁴-H, C₆H₃).

$^{13}\text{C}\{^1\text{H}\}$ NMR (125.8 MHz, benzene- d_6 , 298 K): δ /ppm = 21.1 (s, 4C, 4 \times C⁴-Me, Mes), 21.8 (s, 8C, 4 \times C^{2.6}-Me, Mes), 37.3 (s, 2C, 2 \times N-Me), 126.1 (s, 2C, 2 \times C⁴-H, C₆H₃), 128.6 (s, 8C, 4 \times C^{3.5}-H, Mes), 130.3 (s, 4C, 2 \times C^{3.5}-H, C₆H₃), 136.1 (s, 4C, 4 \times C⁴-Me, Mes), 136.3 (br, $\nu_{1/2} = 11$ Hz, 8C, 4 \times C^{2.6}-Me, Mes), 138.4 (s, 4C, 4 \times C¹, Mes), 142.1 (s, 4C, 2 \times C^{2.6}, C₆H₃), 145.2 (s, 2C, 2 \times C¹, C₆H₃).

$^{15}\text{N}\{^1\text{H}\}$ NMR (50.68 MHz, benzene- d_6 , 298 K): δ /ppm = 113.7 (s). This signal was not observed via 1D NMR spectroscopy but its position was deduced from a ^1H - $^{15}\text{N}\{^1\text{H}\}$ HMBC spectrum.

$^{29}\text{Si}\{^1\text{H}\}$ NMR (99.37 MHz, benzene- d_6 , 298 K): δ /ppm = 130.3 (s).

4.6.21 **Si(OAr^{Mes})₂ (19)**

NaOAr^{Mes} (1.25 g, 3.55 mol, 2.05 equiv.) was slowly added to a suspension of SiBr₂(SIDipp) (1.00 g, 1.73 mmol, 1.0 equiv.) in ca. 50 mL of toluene over 10 minutes at ambient temperature. Upon addition the color of the yellow suspension first intensified, and then slowly faded to light brownish-yellow. The reaction mixture was stirred for 45 minutes at ambient temperature. Complete conversion of the starting materials was confirmed by ^1H -NMR spectroscopy. 5 mL of n-hexane were added to the reaction mixture and the suspension was filtered using a filter syringe in a glove box. The volume of the yellowish filtrate was concentrated under vacuum to ca. 35 mL and the resulting suspension was cooled to -30 °C for 16 hrs. The colorless precipitate was isolated by filtration of the yellow supernatant at -35 °C and dried under vacuum at ambient temperature for 3 hours to give **19** as a colorless solid. Yield: 730 mg (1.06 mmol, 61 % from SiBr₂(SIDipp)). Addition of 25 mL of n-hexane to the yellow mother liquor and cooling to 0 °C for 90 minutes led to the isolation of a second crop of compound **19** (329 mg, 0.48 mmol) that contained ca. 10 mol% of free SIDipp. No attempts were undertaken to isolate pure **19** from this crop. Compound **19** decomposes upon melting at 134 °C under gas evolution to give a yellow liquid. Elemental analysis calcd. (%) for C₄₈H₅₀O₂Si (686.99): C 83.92, H 7.34; found: C 83.82, H 7.41 %.

ATR-IR (solid state, RT): $\tilde{\nu}$ /cm⁻¹ = 3048 (vw), 3026 (sh), 3009 (sh), 2995 (sh), 2975 (w), 2916 (m), 2853 (w), 2731 (vw), 1612 (w), 1588 (vw), 1569 (vw), 1488 (w), 1458 (sh), 1432 (sh), 1415 (s), 1375 (m), 1338 (vw), 1257 (w), 1221 (vs), 1164 (vw), 1102 (vw), 1071 (m), 1032 (w), 1007 (w), 947 (vw), 904 (w), 875 (vs), 847 (vs), 798 (m), 787 (m), 754 (s), 740 (vw),

727 (sh, $\nu_{\text{sym}}(\text{Si-O})$), 714 (vs, $\nu_{\text{asym}}(\text{Si-O})$), 650 (vw), 617 (sh), 610 (w), 595 (vw), 574 (vw), 561 (w), 551 (w), 528 (w), 517 (w), 491 (vw), 476 (w).

Raman (solid state, RT, 25 mW) : $\tilde{\nu}/\text{cm}^{-1}$ = 3053 (m), 3010 (s), 2918 (vs), 2857 (m), 2733 (w), 1613 (vs), 1586 (m), 1484 (w), 1446 (w), 1381 (m), 1308 (vs), 1288 (vw), 1256 (w), 1188 (w), 1166 (w), 1075 (m), 1009 (m), 949 (w), 724 (w, $\nu_{\text{sym}}(\text{Si-O})$), 620 (m), 580 (vs), 565 (m), 553 (w), 523 (m), 512 (w), 407 (w), 394 (w), 367 (vw), 336 (w).

^1H NMR (500.2 MHz, benzene- d_6 , 298 K): δ/ppm = 1.98 (s, 12H, $2 \times \text{C}^4\text{-Me}$, Mes), 2.26 (s, 24H, $2 \times \text{C}^{2,6}\text{-Me}$, Mes), 6.82 (br s, 8H, $4 \times \text{C}^{3,5}\text{-H}$, Mes), 6.84 (t*, $J_{\text{H,H}} = 7.3$ Hz, 2H, $2 \times \text{C}^4\text{-H}$, C_6H_3), 6.89 (d*, $J_{\text{H,H}} = 7.3$ Hz, 4H, $2 \times \text{C}^{3,5}\text{-H}$, C_6H_3).

$^{13}\text{C}\{^1\text{H}\}$ NMR (125.8 MHz, benzene- d_6 , 298 K): δ/ppm = 20.5 (s, 8C, $4 \times \text{C}^{2,6}\text{-Me}$, Mes), 21.2 (s, 4C, $4 \times \text{C}^4\text{-Me}$, Mes), 122.2 (s, 2C, $2 \times \text{C}^4\text{-H}$, C_6H_3), 128.9 (s, 8C, $4 \times \text{C}^{3,5}\text{-H}$, Mes), 129.8 (s, 4C, $2 \times \text{C}^{3,5}\text{-H}$, C_6H_3), 131.2 (s, 4C, $2 \times \text{C}^{2,6}$, C_6H_3), 135.8 (s, 4C, $4 \times \text{C}^1$, Mes), 136.9 (s, 4C, $4 \times \text{C}^4\text{-Me}$, Mes), 137.3 (s, 8C, $4 \times \text{C}^{2,6}\text{-Me}$, Mes), 148.7 (s, 2C, $2 \times \text{C}^1$, C_6H_3).

$^{29}\text{Si}\{^1\text{H}\}$ NMR (99.37 MHz, benzene- d_6 , 298 K): δ/ppm = 31.9 (s).

4.6.22 Attempted synthesis of Si nanoparticles from 19

Method A - Steady heating: In a 100 ml three-necked Schlenk flask, 1.05 g 19 (1.53 mmol, containing 43 mg Si) were dissolved in 3 ml oleylamine (about 2.43 g, 9.1 mmol) at ambient temperature and the light yellow, viscous solution was added to 10 ml of 1-octadecene under vigorous stirring. The resulting nearly colorless solution was then warmed to 315 °C over a timespan of two hours (36 to 315 °C, 2.3°C/min) using an external custom-made temperature device; a heating mantle and some Al₂O₃ wool for isolation. The controlling device was constructed by the electromechanical workshop of the university and used a glassy temperature sensor (accuracy ±2 K) that could be inserted to the solution using a quickfit. The solution was held at 315 °C for 2 h and cooled to ambient temperature under argon, whereupon the color changed to light pink.

Method B - Hot injection: In a 100 ml 450 mg 19 (0.65 mmol) were dissolved in 3 ml oleylamine (about 2.44 g, 9.1 mmol) at ambient temperature and the light yellow solution was added to 10 ml of preheated 1-octadecene at 315 °C under vigorous stirring (at this point, the argon supply has to be reduced to prevent hot vapors from bursting out of the reaction vessel). The solution was held at that temperature for 1 hour.

Workup: Ca. 50 ml of a 2:3 mixture⁵⁸ of CHCl₃ and methanol were added and the now blue solution. After phase separation, the heavier CHCl₃/methanol phase was reduced to about 8 ml and the same volume of acetone was added. Centrifugation (2 × 5 minutes at 2600 r/min) afforded a tiny amount of a colorless, cloudy precipitate. When the experiment was repeated, multiple alternative work-up steps were tested to separate the Ar^{Mes}OH from the desired particles. Yet, no success was achieved using mixtures of MeOH, CHCl₃, CH₂Cl₂, acetone, MeCN, Et₂O and n-hexane alongside multiple centrifugation- and evaporation steps.

Analytcs: Coupled GC/MS analysis of the reaction mixture revealed the formation of Ar^{Mes}OH as the only Ar^{Mes} containing product (99 % confidence after comparison with a pure sample). No Ar^{Mes}H or any Si containing product could be detected. An additional fraction presumably consisted of oxidation products of the solvents that could not be identified individually.

Analysis by transmission electron microscopy (TEM) was performed by Dr. W. Assenmacher from university of Bonn. The final solution containing the Si nanoparticles was concentrated by evaporation for three days. Two drops were added to a Cu-network coated with a perforated carbon film and the sample was analyzed by TEM and energy-dispersive X-ray

⁵⁸ Boyle and coworkers use a 1:1 mixture, yet no phase separation from the 1-octadecene was observed when using less methanol. Even using the 2:3 mixture, the phase separation took well over 30 minutes and a second extraction had to be discarded due to remaining clouds of 1-octadecene as well as partial crystallization of Ar^{Mes}OH after reducing the overall volume.

spectroscopy (EDX). This way, the formation of small Si particles could be verified, but no high-resolution images could be obtained. See also Figure 69 on page 129.

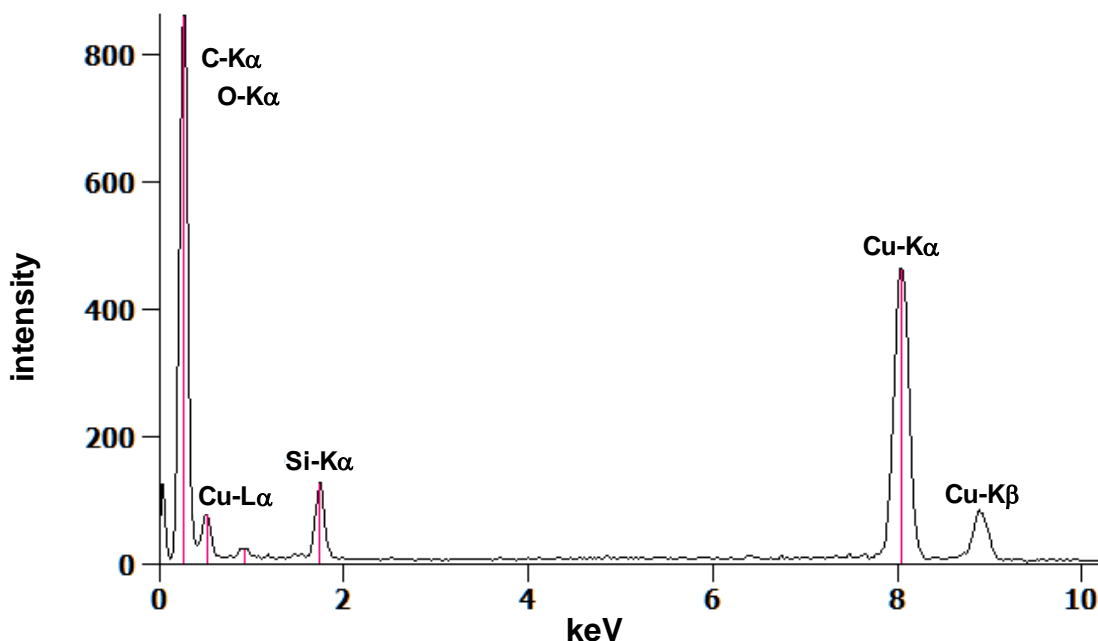


Figure 89. EDX spectrum of the Si particles obtained by the thermolysis of **19**. The Si particles were coated in a viscous mixture of oleylamine and Ar^{Mes}-OH (see also Figure 69 on page 129).

4.6.23 Si(OAr^{Mes})₂(IMe₄) (**19-IMe₄**)

A turbid solution of **19** (150 mg, 0.22 mmol, 1.0 equiv.) in 10 ml of toluene was treated dropwise with a slightly brownish solution of IMe₄ in toluene (27 mg, 0.22 mmol, 1.0 equiv.) over a period of 2 minutes at 0 °C. The reaction mixture was stirred for 1 h at ambient temperature, whereupon the color changed to yellow and most of the solid dissolved. The mixture was filtered from a small amount of solid and the filtrate was evaporated. The yellow residue was washed with a minimal amount of Et₂O and 2 ml of n-hexane and dried for 2 h at ambient temperature (ca. 80 % crude yield). ¹H NMR spectroscopy revealed the presence of small amounts of a decomposition material that could not be fully separated by a combination of washing, extraction and recrystallizations using mixtures of n-hexane, Et₂O and toluene. Instead, **19-IMe₄** was found to slowly decompose in solution.

¹H NMR (500.2 MHz, benzene-d₆, 298 K): δ /ppm = 1.34 (s, 3H, C⁴-Me, IMe₄), 1.36 (s, 3H, C⁵-Me, IMe₄), 1.97 (s, 12H, 2 × C²-Me, Mes), 2.05 (s, 12H, 2 × C⁶-Me, Mes), 2.25 (s, 12H, 2 × C⁴-Me, Mes), 2.44 (s, 3H, N¹-Me, IMe₄), 2.82 (s, 3H, N³-Me, IMe₄), 6.87 (br s, 8H, 4 × C^{3,5}-H, Mes), 6.82 (t*, J_{H,H} = 7.3 Hz, 2H, 2 × C⁴-H, C₆H₃), 6.88 (d*, J_{H,H} = 7.3 Hz, 4H, 2 × C^{3,5}-H, C₆H₃).

$^{13}\text{C}\{^1\text{H}\}$ NMR (125.8 MHz, benzene- d_6 , 298 K): δ /ppm = 7.4 (s, 1C, C⁵-Me, IMe₄), 7.5 (s, 1C, C⁴-Me, IMe₄), 21.27 (s, 4C, 4 × C⁴-Me, Mes), 21.35 (s, 4C, 4 × C⁶-Me, Mes), 21.37 (s, 4C, 4 × C²-Me, Mes), 31.1 (s, 1C, N¹-Me, IMe₄), 32.0 (s, 1C, N³-Me, IMe₄), 119.5 (s, 2C, 2 × C⁴-H, C₆H₃), 122.9 (s, 1C, C⁴-Me, IMe₄), 123.9 (s, 1C, C⁵-Me, IMe₄), 127.66, 127.70 (each s, each 4C, 4 × C³-H, and 4 × C⁵-H, Mes), 130.4 (s, 4C, 2 × C^{3,5}-H, C₆H₃), 133.3 (s, 4C, 2 × C^{2,6}, C₆H₃), 134.9 (s, 4C, 4 × C¹, Mes), 137.1 (s, 4C, 4 × C⁴-Me, Mes), 137.6 (s, 4C, 4 × C⁶-Me, Mes), 138.8 (s, 4C, 4 × C⁶-Me, Mes), 153.5 (s, 2C, 2 × C¹, C₆H₃), 164.1 (s, 1C, N $\overline{\text{CN}}$, IMe₄).

$^{15}\text{N}\{^1\text{H}\}$ NMR (50.68 MHz, benzene- d_6 , 298 K): δ /ppm = 174.8, 176.8 (each s, each 1N, N¹ and N²). Unequivocal assignment of the signals by correlation spectroscopy was not possible due to the small difference in chemical shift.

$^{29}\text{Si}\{^1\text{H}\}$ NMR (99.37 MHz, benzene- d_6 , 298 K): δ /ppm = 7.5 (s).

4.6.24 SiHCl(OAr^{Mes})₂ (19-HCl)

Compound 19-HCl was first obtained by C. Lippmann in 43 % yield starting from **19** and HCl.^[385] In this work, an alternative synthetic access is given. For the course of a clear arrangement, the synthesis is not listed in chapter 4.5.

A colorless solution of NaOAr^{Mes} (222 mg, 0.630 mmol, 2.0 equiv.) in 5 mL of toluene was dropwise treated with a colorless solution of SiHCl₃ (0.39 M in toluene, 0.8 mL, 0.31 mmol, 1.0 equiv.) at -30 °C over a period of 3 minutes. While the reaction mixture was stirred at -30 °C for another 15 minutes, a voluminous, off-white solid (NaCl) precipitated. The suspension was warmed to ambient temperature, stirred for 1 hour and evaporated. The colorless residue was extracted with 3 × 4 mL of toluene and the combined extracts were evaporated under vacuum. The colorless residue was washed with 5 mL of n-hexane at 0 °C and dried at 50 °C for 3 hours. Yield: 120 mg (0.17 mmol, 54% from NaOAr^{Mes}). The product was shown to be pure by NMR spectroscopy.^[385]

ATR-IR (solid state, RT): $\tilde{\nu}$ /cm⁻¹ = 3000 (sh), 2954 (w), 2918 (w), 2855 (vw), 2731 (vw), 2254 (w, \parallel Si-H), 1611 (w), 1571 (vw), 1487 (vw), 1459 (sh), 1433 (sh), 1421 (s), 1376 (w), 1259 (w), 1242 (vw), 1223 (vs), 1165 (w), 1076 (s), 1031 (w), 1009 (m), 973 (vs), 955 (s), 943 (m), 891 (vw), 877 (vw), 844 (vs), 814 (s), 801 (s), 781 (m), 760 (s), 736 (m), 675 (w), 649 (vw), 610 (sh), 601 (m), 577 (vw), 563 (m), 536 (s), 514 (s), 491 (m), 433 (m).

^1H NMR (500.2 MHz, chloroform- d_1 , 298 K): δ /ppm = 1.76 (s, $^1J_{\text{C,H}}$ = 127 Hz, 12H, 4 × C²-Me, Mes), 1.84 (s, $^1J_{\text{C,H}}$ = 127 Hz, 12H, 4 × C⁶-Me, Mes), 2.33 (s, $^1J_{\text{C,H}}$ = 126 Hz, 12H, 4 × C⁴-Me, Mes), 3.21 (s, $^1J_{\text{Si,H}}$ = 345 Hz, 1H, Si-H), 6.84 (s, 4H, 4 × C³-H, Mes), 6.87 (s, 4H, 4 × C⁵-H,

Mes), 6.96 (m, $^3J_{\text{H,H}} = 7.5$ Hz, 4H, $2 \times \text{C}^{3,5}\text{-H}$, C_6H_3), 7.05 (m, $^3J_{\text{H,H}} = 7.5$ Hz, 2H, $2 \times \text{C}^4\text{-H}$, C_6H_3).

^1H NMR (300.1 MHz, benzene- d_6 , 298 K): δ /ppm = 1.92 (s, $^1J_{\text{C,H}} = 126$ Hz, 12H, $4 \times \text{C}^2\text{-Me}$, Mes), 1.99 (s, $^1J_{\text{C,H}} = 127$ Hz, 12H, $4 \times \text{C}^6\text{-Me}$, Mes), 2.25 (s, $^1J_{\text{C,H}} = 126$ Hz, 12H, $4 \times \text{C}^4\text{-Me}$, Mes), 3.58 (s, $^1J_{\text{Si,H}} = 344$ Hz, 1H, Si-H), 6.82 – 6.90 (m, 14H, $4 \times \text{C}^{3,5}\text{-H}$ (Mes), $+ 2 \times \text{C}^{3,5}\text{-H}$ (C_6H_3)) $+ 2 \times \text{C}^4\text{-H}$ (C_6H_3)).

$^{13}\text{C}\{^1\text{H}\}$ NMR (125.8 MHz, chloroform- d_1 , 298 K): δ /ppm = 20.2 (s, 4C, $4 \times \text{C}^2\text{-Me}$, Mes), 20.4 (s, 4C, $4 \times \text{C}^6\text{-Me}$, Mes), 21.2 (s, 4C, $\text{C}^4\text{-Me}$, Mes), 122.9 (s, 2C, $2 \times \text{C}^4\text{-H}$, C_6H_3), 127.98 (s, 4C, $4 \times \text{C}^5\text{-H}$, Mes), 128.01 (s, 4C, $4 \times \text{C}^3\text{-H}$, Mes), 130.0 (s, 4C, $2 \times \text{C}^{3,5}\text{-H}$, C_6H_3), 132.6 (s, 4C, $2 \times \text{C}^{2,6}$, C_6H_3), 134.1 (s, 4C, $4 \times \text{C}^1$, Mes), 136.5 (s, 4C, $4 \times \text{C}^4\text{-Me}$, Mes), 136.7 (s, 4C, $4 \times \text{C}^6\text{-Me}$, Mes), 136.9 (s, 4C, $4 \times \text{C}^2\text{-Me}$, Mes), 146.8 (s, $2 \times \text{C}^1$, C_6H_3).

$^{13}\text{C}\{^1\text{H}\}$ NMR (benzene- d_6 , 75.47 MHz, 298 K): δ /ppm = 20.6 (s, 4C, $4 \times \text{C}^2\text{-Me}$, Mes), 20.8 (s, 4C, $4 \times \text{C}^6\text{-Me}$, Mes), 21.3 (s, 4C, $\text{C}^4\text{-Me}$, Mes), 123.5 (s, 2C, $2 \times \text{C}^4\text{-H}$, C_6H_3), 128.57, 128.62 (s each, 4C each, $4 \times \text{C}^3\text{-H}$ and $4 \times \text{C}^5\text{-H}$, Mes), 130.4 (s, 4C, $2 \times \text{C}^{3,5}\text{-H}$, C_6H_3), 133.3* (s, 4C, $2 \times \text{C}^{2,6}$, C_6H_3), 134.6* (s, 4C, $4 \times \text{C}^1$, Mes), 136.7*, 136.8* and 137.2* (s each, 4C each, $\text{C}^2\text{-Me}$, $\text{C}^4\text{-Me}$ and $\text{C}^6\text{-Me}$, Mes), 147.5* (s, 2C, $2 \times \text{C}^1$, C_6H_3). Due to extensive overlapping of the aromatic proton signals in the ^1H NMR spectrum, only a partial assignment could be achieved. Signals marked with an asterisk (*) were identified as quaternary carbon atoms by DEPT experiments and assigned by comparison with the corresponding signals in chloroform- d_1 solution, where an unambiguous assignment of all signals was possible.

^{29}Si NMR (99.37 MHz, chloroform- d_1 , 298 K): δ /ppm = -56.5 (d, $^1J_{\text{Si,H}} = 345$ Hz).

$^{29}\text{Si}\{^1\text{H}\}$ NMR (99.37 MHz, benzene- d_6 , 298 K): δ /ppm = -56.5 (s).

4.6.25 $\text{SiH}(\text{OC}(\text{CF}_3)_3)(\text{OAr}^{\text{Mes}})_2$ (**19-HOtBu^F**)

A colorless suspension of **19** (154 mg, 0.22 mmol, 1.0 equiv.) in 7 mL of toluene was treated dropwise with a colorless solution of $\text{HOC}(\text{CF}_3)_3$ in toluene (0.52 M, 0.45 mL, 0.23 mmol, 1.1 equiv.) over a period of 2 minutes. The reaction mixture was stirred for 18 h at ambient temperature, whereupon the solid dissolved within the first 2.5 hours to form a clear, colorless solution. ^1H NMR spectroscopy revealed a complete and selective conversion of the starting materials to **19-HOtBu^F** and the solution was evaporated. The colorless residue was dried for 1.5 hours at 30 °C and recrystallized from 2 mL of diethyl ether at -30 °C. The resulting colorless crystals were isolated at -30 °C, grinded and dried at 30 °C for 2 hours. Yield: 158 mg (0.17 mmol, 76 % from **19**). Compound **19-HOtBu^F** decomposes upon melting at 202 °C to a

colorless liquid under gas evolution. Elemental analysis calcd. (%) for $C_{52}H_{51}F_9O_3Si$ (923.03) C 67.66, H 5.57, found: C 67.67, H 5.92 %.

ATR-IR (solid state, RT): $\tilde{\nu}/cm^{-1}$ = 2996 (w), 2969 (w), 2919 (w), 2856 (vw), 2297 (vw, ν_{Si-H}), 1612 (w), 1582 (vw), 1572 (vw), 1487 (vw), 1452 (sh), 1434 (sh), 1420 (m), 1378 (w), 1332 (vw), 1302 (w), 1270 (vs), 1250 (vs), 1235 (sh), 1214 (vs), 1183 (vs), 1103 (sh), 1085 (m), 1032 (w), 1009 (m), 979 (vs), 971 (vs), 959 (sh), 944 (m), 861 (s), 846 (vs), 801 (m), 774 (m), 756 (s), 728 (s), 649 (vw), 607 (m), 577 (w), 562 (w), 539 (w), 519 (m), 489 (w), 469 (m), 411 (w).

Raman (solid state, RT, 25 mW): $\tilde{\nu}/cm^{-1}$ = 3208 (vw), 3192 (vw), 3051 (w), 3010 (m), 2972 (sh), 2943 (sh), 2920 (vs), 2855 (m), 2800 (vw), 2736 (w), 1614 (vs), 1591(m), 1584 (m), 1486 (w), 1446 (w), 1384 (m), 1377 (m), 1308 (vs), 1287 (w), 1275 (vw), 1191 (vw), 1094 (vw), 1009 (w), 940 (vw), 763 (vw), 580 (s), 564 (m), 526 (w), 240 (w).

1H NMR (500.2 MHz, benzene- d_6 , 298 K): δ /ppm = 1.98 (s, 12H, 4 \times C²-Me, Mes), 2.05 (s, 12H, 4 \times C⁶-Me, Mes), 2.35 (s, 12H, 4 \times C⁴-Me, Mes), 3.68 (dec, $^1J_{Si-H}$ = 359 Hz, $^5J_{F-H}$ = 2.2 Hz, 1H, Si-H), 6.76 (d*, $^3J_{H-H}$ = 7.4 Hz, 4H, 2 \times C^{3,5}-H, C₆H₃), 6.80 (t*, $^3J_{H-H}$ = 7.4 Hz, 2H, 2 \times C⁴-H, C₆H₃), 6.85 (s, 8H, 4 \times C³-H and 4 \times C⁵-H, Mes). See Figure 71 on page 134.

$^{13}C\{^1H\}$ NMR (125.8 MHz, benzene- d_6 , 298 K): δ /ppm = 20.6 (s, 4C, 4 \times C²-Me, Mes), 20.8 (s, 4C, 4 \times C⁶-Me, Mes), 21.3 (s, 4C, 4 \times C⁴-Me, Mes), 78.6 (dec, 1C, $^2J_{F-C}$ = 31.6 Hz, OC(CF₃)₃), 119.9 (q, $^1J_{F-C}$ = 292 Hz, 3C, OC(CF₃)₃), 123.2 (s, 4C, 2 \times C⁴-H, C₆H₃), 128.7 (s, 4C, 4 \times C³-H, Mes), 129.0 (s, 4C, 4 \times C⁵-H, Mes), 132.0 (s, 2C, 2 \times C^{3,5}-H, C₆H₃), 132.5 (s, 4C, 2 \times C^{2,6}, C₆H₃), 136.0 (s, 4C, 4 \times C¹, Mes), 136.3 (s, 4C, 4 \times C⁶-Me, Mes), 136.4 (s, 4C, 4 \times C⁴-Me, Mes), 136.8 (s, 4C, 4 \times C²-Me, Mes), 148.6 (s, 2C, 2 \times C¹, C₆H₃).

$^{19}F\{^1H\}$ NMR (469.7 MHz, benzene- d_6 , 298 K): δ /ppm = -72.4 (s).

^{29}Si NMR (99.37 MHz, benzene- d_6 , 99.37 MHz, 298 K): δ /ppm = -84.4 (d, $^1J_{Si-H}$ = 359 Hz).

4.6.26 **SiI(SiH₂I)(OAr^{Mes})₂ (19-SiH₂I₂)**

A colorless suspension of 1.5 g **19** (2.18 mmol, 1.0 equiv) in 50 ml of benzene was treated with neat SiH₂I₂ (0.23 ml, $r = 2.79$ g/cm³, 640 mg, 1.04 equiv.) under vigorous stirring at about 4 °C. Upon addition, the suspension turned slightly yellow and most of the solid dissolved within 10 minutes stirring at ambient temperature. Completeness of the reaction was verified by 1H NMR spectroscopy and the slightly turbid suspension was filtered off. The light yellow filtrate was evaporated to dryness and the colorless residue was homogenized by a freeze-pump-thaw cycle. The fine powder was then quickly washed with precooled (-30 °C) n-hexane in two portions of approx. 5 ml and dried at ambient temperature. Yield: 1.95 g

(2.01 mmol, 92 % from **19**). If necessary, the compound can be recrystallized from mixtures of n-hexane and diethyl ether.

¹H NMR (499.1 MHz, tetrahydrofuran-d₆, 298 K): δ /ppm = 1.97 (br, $\nu_{1/2}$ = 21 Hz, 24H, 4 × C^{2,6}-Me, Mes), 2.28 (s, 12H, 4 × C⁴-Me, Mes), 6.86 (br s, 4H, 4 × C³-H, Mes), 6.88 (br s, 4H, 4 × C⁵-H, Mes), 6.91 (d, $^3J_{\text{H,H}}$ = 7.1 Hz, 4H, 2 × C^{3,5}-H, C₆H₃), 7.06 (t, $^3J_{\text{H,H}}$ = 7.1 Hz, 2H, 2 × C⁴-H, C₆H₃). The SiH₂ signal was not detected, presumably due to a combination of broadening and overlapping with the methyl signals.

¹H NMR (499.1 MHz, tetrahydrofuran-d₆, 193 K): δ /ppm = 1.01 (s, $^1J_{\text{Si,H}}$ = 250 Hz, 1H, SiH_AH_B), 1.32 (s, 3H, Me^A), 1.65 (s, 3H, Me^B), 1.85 (s, 3H, Me^C), 2.06 (s, 3H, Me^D), 2.14 (s, 3H, Me^E), 2.15 (s, 3H, Me^F), 2.20 (s, 3H, Me^G), 2.21 (s, 3H, Me^H), 2.25 (s, 3H, Me^I), 2.33 (s, 3H, Me^J), 2.34 (s, 3H, Me^K), 2.36 (s, 3H, Me^L), 3.23 (s, $^1J_{\text{Si,H}}$ = 250 Hz, 1H, SiH_AH_B), 6.71 (s, 1H, C³-H or C⁵-H, Mes), 6.77 (s, 1H, C³-H or C⁵-H, Mes), 6.84 – 6.94 (m), 6.85 (s, 1H, C³-H or C⁵-H, Mes), 6.99 (s, 1H), 6.97 (s, 1H, C³-H or C⁵-H, Mes), 7.03 – 7.07 (m), 7.07 – 7.15 (m, 2H, 2 × C⁴-H, C₆H₃), 7.17 (s, 1H). Some of the aromatic signals could not be unquestionably integrated or assigned due to overlapping. For a partial assignment, the methyl groups were numbered and matched with their corresponding carbon atoms based on their HMQC crosspeaks without differentiation of the ring systems.

¹³C{¹H} NMR (125.5 MHz, tetrahydrofuran-d₆, 298 K): δ /ppm = 21.2 (2, 4C, 4 × C⁴-Me, Mes), 22.1 (br, $\nu_{1/2}$ = 21 Hz, 8C, 4 × C^{2,6}-Me, Mes), 123.8 (s, 2C, 2 × C⁴-H, C₆H₃), 129.6 (br, $\nu_{1/2}$ = 10 Hz, 4C, 4 × C⁵-H, Mes), 129.7 (s, 4C, 4 × C³-H, Mes), 132.2 (s, 4C, 2 × C^{3,5}-H, C₆H₃), 133.8 (br, $\nu_{1/2}$ = 8 Hz, 4C, 2 × C^{2,6}, C₆H₃), 135.8 (br, $\nu_{1/2}$ = 7 Hz, 4C, 4 × C¹, Mes), 137.7 (br, $\nu_{1/2}$ = 8 Hz, 4C, 4 × C² or C⁶, Mes), 137.9 (s, 4C, 4 × C² or C⁶, Mes), 149.9 (s, 2C, 2 × C¹, C₆H₃).

¹³C{¹H} NMR (125.5 MHz, tetrahydrofuran-d₆, 193 K): δ /ppm = 19.8 (s, 1C, Me^B), 21.0 (s, 1C, Me^A and Me^C), 21.3 (s, 1C, Me^I), 21.4 (s, 1C, Me^J), 21.5 (s, 1C, Me^F), 22.0 (s, 1C, Me^D), 22.6 (s, 1C, Me^E), 22.7 (s, 1C, Me^F), 22.9 (s, 2C, Me^F and Me^H), 23.2 (s, 1C, Me^K) 123.5, 124.3 (each s, each 1C, each C⁴-H, 2 × C₆H₃), 128.8 (s), 128.9 (s, C³ or C⁵, Mes), 129.0 (s), 129.2 (s, 1C C³ or C⁵, Mes), 130.2 (s, 1C C³ or C⁵, Mes), 130.4 (s, 1C, C³ or C⁵, Mes), 131.2 (s), 131.8 (s), 131.9 (s), 132.2 (s), 132.9 (s), 133.1 (s), 133.8 (s), 134.8 (s), 135.8 (s), 136.1 (s), 136.3 (s), 137.0 (s), 137.2 (s), 137.7 (s), 137.8 (s), 137.9 (s), 138.1 (s), 138.7 (s), 138.9 (s), 139.4 (s), 149.4, 149.8 (each s, each 1C, C¹, 2 × C₆H₃). A total of 31 distinguishable aromatic and 10 aliphatic signals was detected for 36 aromatic C atoms and 12 methyl groups.

²⁹Si{¹H} NMR (99.16 MHz, tetrahydrofuran-d₆, 298 K): δ /ppm = -70.0 (s, SiH₂, $^1J_{\text{Si,H}}$ = 240 Hz, $^2J_{\text{Si,H}}$ = 39 Hz), -76.7 (s, $^2J_{\text{Si,H}}$ = 39 Hz, Si(OAr^{Mes})₂). Due to opposite phases of the individual branches, the middle peaks of the signal at δ_{Si} = -70.0 ppm have an artificially lowered intensity; the resulting signal thus appears as a doublet signal with a fake coupling constant

of 480 Hz in lower resolution spectra. This also affects inverse-gated spectra, where the averaged signal is nearly canceled out completely.

4.6.27 **SiI{SiH₂(OC₄H₈I)}(OAr^{Mes})₂ (20)**

A colorless solution of **19-SiH₂** (1.0 g, 1.03 mmol) in 20 ml of thf was heated to 65 °C overnight.⁵⁹ Complete conversion was confirmed by ¹H NMR spectroscopy and the solution was filtered from a small residue. The filtrate was evaporated to dryness and the oily residue was dissolved in a small amount of n-hexane, from which a colorless solid precipitated. The suspension was briefly sonicated, again dried and the residue was recrystallized from 6 ml diethyl ether at -30 °C and again recrystallized from a minimal amount of a mixture of diethyl ether and n-hexane (1:4) at -30 °C. The obtained bulk material was a mixture of 20 and crystalline 20·Et₂O with very small amounts of unknown impurities that displayed broad signals in the aliphatic region of the ¹H NMR spectrum. No elemental analysis of this mixture was performed.

¹H NMR (499.1 MHz, tetrahydrofuran-d₆, 298 K): δ/ppm = 1.39 and 1.60 (each m, each 2H, CH₂CH₂), 1.91 (s, 12H, 4 × C²-Me, Mes), 1.94 (s, 12H, 4 × C⁶-Me, Mes), 2.28 (s, 12H, 4 × C⁴-Me, Mes), 3.11 (m, 2H, CH₂OSi), 3.26 (m, 2H, CH₂I), 3.50 (br, *v*_{1/2} = 8 Hz, 2H, SiH₂), 6.84 (br s, 4H, 4 × C³-H, Mes), 6.85 (br s, 4H, 4 × C⁵-H, Mes), 6.88 (d*, ³J_{H,H} = 7.1 Hz, 4H, 2 × C^{3,5}-H, C₆H₃), 7.04 (t*, ³J_{H,H} = 7.1 Hz, 2H, 2 × C⁴-H, C₆H₃).

¹H NMR (499.1 MHz, tetrahydrofuran-d₆, 333 K): δ/ppm = 1.75 – 1.95 (m, 6H, 2 × CH₂ and CH₂O), 1.98 (s, 12H, 4 × C^{2,6}-Me, Mes), 2.28 (s, 12H, 4 × C⁴-Me, Mes), 2.30 (m, 2H, CH₂I), 2.43 (br s, *v*_{1/2} = 4 Hz, ¹J_{Si,H} = 240 Hz,⁶⁰ 2H, SiH₂), 6.87 (br s, 8H, 4 × C^{3,5}-H, Mes), 6.90 (d*, ³J_{H,H} = 7.1 Hz, 4H, 2 × C^{3,5}-H, C₆H₃), 7.06 (t*, ³J_{H,H} = 7.1 Hz, 2H, 2 × C⁴-H, C₆H₃).

¹³C{¹H} NMR (125.5 MHz, tetrahydrofuran-d₈, 333 K): δ/ppm = 6.7 (s, 1C, CH₂I), 21.2 (2, 4C, 4 × C⁴-Me, Mes), 21.8 (br, *v*_{1/2} = 21 Hz, 8C, 4 × C^{2,6}-Me, Mes), 30.8, 33.4 (each s, each 1C, CH₂CH₂), 123.5 (s, 2C, 2 × C⁴-H, C₆H₃), 128.8 – 129.6 (br, 4C, 4 × C⁵-H and 4 × C³-H, Mes), 131.5 (s, 2C), 131.8 (s, 2C), 134.1 (s, 2C), 135.8 (s, 1C), 137.3 (s, 2C), 137.6 (s, 2C), 137.8 (s, 2C), 149.7 (s, 2C, 2 × C¹, C₆H₃). The CH₂O signal is presumably obscured by the solvent signal. No complete assignment of the aromatic signals can be given due to inconclusive couplings in the ¹H/¹³C{¹H} 2D NMR spectra.

⁵⁹ Test reactions on an NMR scale were most selective at a bath temperature of only 50 °C (completion within 2 h), however, in a Schlenk vessel higher temperatures were needed to yield any conversion. No internal temperature was measured.

⁶⁰ The ¹J_{Si,H} coupling constant was estimated to be 240 Hz from the ¹H NMR spectrum but approx. 210 Hz from the coupled, 2-dimensional ¹H/²⁹Si HMQC spectrum.

$^{29}\text{Si}\{\text{H}\}$ NMR (99.16 MHz, tetrahydrofuran- d_5 , 333 K): $\delta/\text{ppm} = -28.8$ (s, $^1J_{\text{Si,H}} = 210$ Hz, $^{60}\text{SiH}_2$), -70.5 (s, $\underline{\text{Si}}(\text{OAr}^{\text{Mes}})_2$). No ^{29}Si NMR signals could be detected at 298 K.

4.6.28 $\text{SiCl}(\text{SiHCl}_2)(\text{OAr}^{\text{Mes}})_2$ (**19-SiHCl₃**)

A turbid solution of **19** (250 mg, 0.36 mmol, 1.0 equiv.) in 15 mL of benzene was treated dropwise with HSiCl_3 (ca. 0.05 mL, 0.49 mmol, 1.4 equiv) at 10 °C under vigorous stirring. The reaction mixture was warmed to ambient temperature and stirred for 2 hours, whereupon the colorless solid slowly dissolved. The complete conversion of **19** into **19-SiHCl₃** was confirmed by ^1H NMR spectroscopy. The solvent was evaporated and the colorless residue dried by two freeze-pump thaw cycles under vacuum at ca. 40 °C for two hours. Yield: 290 mg (0.35 mmol, 97 % from **19**). Compound **19-SiHCl₃** melts to a colorless liquid at 229 °C. Elemental analysis calcd. (%) for $\text{C}_{48}\text{H}_{51}\text{Cl}_3\text{O}_2\text{Si}_2$ (822.45): C 70.10, H 6.25; found: C 70.48, H 6.25 %.

ATR-IR (solid state, RT): $\tilde{\nu}/\text{cm}^{-1} = 2992$ (sh), 2963 (vw), 2920 (w), 2854 (vw), 2732 (vw), 2210 (w, $\nu_{\text{Si-H}}$), 1722 (vw), 1611 (w), 1571 (vw), 1485 (w), 1441 (sh), 1416 (m), 1378 (w), 1249 (m), 1213 (vs), 1188 (sh), 1164 (w), 1081 (m), 1032 (vw), 1009 (w), 972 (s), 957 (m), 945 (m), 846 (s), 802 (m), 774 (m), 758 (s), 737 (w), 724 (m), 676 (w), 609 (sh), 601 (w), 583 (s), 553 (vs), 533 (m), 503 (w), 480 (vs), 409 (w).

^1H NMR (500.2 MHz, chloroform- d_1 , 298 K): $\delta/\text{ppm} = 1.87$ (s, 12H, 4 × $\text{C}^2\text{-Me}$, Mes), 1.91 (s, 12H, 4 × $\text{C}^6\text{-Me}$, Mes), 2.30 (s, 12H, 4 × $\text{C}^4\text{-Me}$, Mes), 3.65 (s, $^1J_{\text{Si,H}} = 283$ Hz, $^2J_{\text{Si,H}} = 40$ Hz, 1H, Si-H), 6.84, 6.86 (s each, 4H each, 4 × $\text{C}^3\text{-H}$ and 4 × $\text{C}^5\text{-H}$, Mes), 6.91 (d, $^3J_{\text{H,H}} = 7.5$ Hz, 4H, 2 × $\text{C}^{3,5}\text{-H}$, C_6H_3), 7.05 (t, $^3J_{\text{H,H}} = 7.5$ Hz, 2H, 2 × $\text{C}^4\text{-H}$, C_6H_3).

^1H NMR (300.1 MHz, benzene- d_6 , 298 K): $\delta/\text{ppm} = 2.03$ (s, 12H, 4 × $\text{C}^2\text{-Me}$, Mes), 2.09 (s, 12H, 4 × $\text{C}^6\text{-Me}$, Mes), 2.24 (s, 12H, 4 × $\text{C}^4\text{-Me}$, Mes), 4.01 (s, $^1J_{\text{Si,H}} = 282$ Hz, $^2J_{\text{Si,H}} = 40$ Hz, 1H, Si-H), 6.84 (s*, 6H, 2 × $\text{C}^{3,5}\text{-H}$ and $\text{C}^4\text{-H}$, C_6H_3), 6.88 (s, 4H, 4 × $\text{C}^3\text{-H}$, Mes), 6.90 (s, 4H, 4 × $\text{C}^5\text{-H}$, Mes). See Figure 73 on page 137.

$^{13}\text{C}\{\text{H}\}$ NMR (125.8 MHz, chloroform- d_1 , 298 K): $\delta/\text{ppm} = 20.8$ (s, 4C, 4 × $\text{C}^6\text{-Me}$, Mes), 21.1 (s, 4C, $\text{C}^4\text{-Me}$, Mes), 21.2 (s, 4C, 4 × $\text{C}^2\text{-Me}$, Mes), 123.2 (s, 2C, 2 × $\text{C}^4\text{-H}$, C_6H_3), 128.58, 128.64 (s each, 4C each, 4 × $\text{C}^3\text{-H}$ and 4 × $\text{C}^5\text{-H}$, Mes), 131.1 (s, 4C, 2 × $\text{C}^{3,5}\text{-H}$, C_6H_3), 132.8 (s, 4C, 2 × $\text{C}^{2,6}$, C_6H_3), 134.5 (s, 4C, 4 × C^1 , Mes), 136.8 (s, 4C, 4 × $\text{C}^4\text{-Me}$, Mes), 136.9 (s, 4C, 4 × $\text{C}^2\text{-Me}$, Mes), 137.2 (s, 4C, 4 × $\text{C}^6\text{-Me}$, Mes), 146.8 (s, 2 × C^1 , C_6H_3).

$^{13}\text{C}\{\text{H}\}$ NMR (75.47 MHz, benzene- d_6 , 298 K): $\delta/\text{ppm} = 21.1$ (s, 4C, 4 × $\text{C}^4\text{-Me}$, Mes), 21.2 (s, 4C, 4 × $\text{C}^6\text{-Me}$, Mes), 21.5 (s, 4C, 4 × $\text{C}^2\text{-Me}$, Mes), 123.7 (s, 2C, 2 × $\text{C}^4\text{-H}$, C_6H_3), 129.1 (s, 4C, 4 × $\text{C}^3\text{-H}$, Mes), 129.2 (s, 4C, 4 × $\text{C}^5\text{-H}$, Mes), 131.5 (s, 4C, 2 × $\text{C}^{3,5}\text{-H}$, C_6H_3), 133.4 (s,

4C, $2 \times \underline{C}^{2,6}$, C_6H_3), 135.0 (s, 4C, $4 \times \underline{C}^1$, Mes), 137.0 (s, 4C, $4 \times \underline{C}^4$ -Me, Mes), 137.1 (s, 4C, $4 \times \underline{C}^2$ -Me, Mes), 137.4 (s, 4C, $4 \times \underline{C}^6$ -Me, Mes), 148.5 (s, $2 \times \underline{C}^1$, C_6H_3).

^{29}Si NMR (99.37 MHz, chloroform- d_1 , 298 K): δ /ppm = -61.3 (d, $^2J_{\text{Si,H}} = 40$ Hz, $\underline{\text{SiCl}}(\text{OAr}^{\text{Mes}})_2$), -7.8 (d, $^1J_{\text{Si,H}} = 283$ Hz, $\underline{\text{SiHCl}}_2$).

^{29}Si NMR (99.37 MHz, benzene- d_6 , 298 K): δ /ppm = -61.5 (d, $^2J_{\text{Si,H}} = 40$ Hz, $\underline{\text{SiCl}}(\text{OAr}^{\text{Mes}})_2$), -7.5 (d, $^1J_{\text{Si,H}} = 283$ Hz, $\underline{\text{SiHCl}}_2$).

4.6.29 $\text{SiCl}_2(\text{OAr}^{\text{Mes}})_2$ (**19-Cl₂**)

Method A: A vigorously stirred, slightly turbid solution of **19-SiHCl₃** (171 mg, 0.21 mmol, 1.0 equiv.) in 6 mL of benzene was treated dropwise with a solution of IMe_4 in 0.5 mL of benzene (26 mg, 0.21 mmol, 1.0 equiv.) at ambient temperature, whereupon a pale yellow solid (mostly $[\text{H}(\text{IMe}_4)]\text{Cl}$)⁶¹ precipitated. The suspension was stirred for another 1.5 h at ambient temperature and filtered from the residue through a double-filter syringe. The filtrate was evaporated and the colorless residue was dried under vacuum for 1 hour at ambient temperature to give spectroscopically pure **19-Cl₂**. Yield: 144 mg (0.19 mmol, 91 % from **19-SiHCl₃**).

Method B: A vigorously stirred, pale yellow solution of $\text{NaOAr}^{\text{Mes}}$ (763 mg, 2.16 mmol, 2.0 equiv.) in 10 mL of toluene was treated dropwise with a solution of SiCl_4 (ca. 0.124 mL, $\rho = 1.483$ g/mL, 184 mg, 1.085 mmol, 1.0 equiv.) in 5 mL of toluene at -30 °C. Upon addition, the color of the solution immediately changed to yellow and the reaction mixture was slowly allowed to warm to ambient temperature overnight, whereby a colorless solid precipitated (NaCl). ^1H NMR spectroscopy revealed the formation of about 70 % of **19-Cl₂** and another portion of a solution of SiCl_4 (4.2 mL, 0.073 M in toluene, 0.31 mmol, 0.29 equiv.) was added dropwise at ambient temperature. The reaction mixture was stirred for additional 1.5 hours and the complete consumption of $\text{NaOAr}^{\text{Mes}}$ was confirmed by ^1H NMR spectroscopy. The suspension was treated with 2 mL of n-hexane and filtered off. The yellow residue was extracted with about 5 mL of n-hexane and the combined yellow filtrates were evaporated. The yellow residue was suspended in ca. 10 mL of hot n-hexane (60 °C) for 5 minutes and cooled to 6 °C for 18 hours. The resulting colorless precipitate was isolated by filtration from the yellow supernatant at -30 °C and dried under vacuum for 3 hours at ambient temperature. Yield: 770 mg (1.02 mmol, 94 % from $\text{NaOAr}^{\text{Mes}}$). Compound **19-Cl₂** melts to a colourless liquid

⁶¹ A saturated solution of the yellow residue in 1,2- $\text{C}_2\text{H}_2\text{F}_2$ was extensively studied by $^{29}\text{Si}\{^1\text{H}\}$ or ^{29}Si NMR spectroscopy (zgig, dept20, dept90, HMBC, HMQC) from +300 to -200 ppm, but no signal could be detected. The remaining of the second silicon atom as well as the origin of the hydrogen atom remain hence unknown.

at 264°C. Elemental analysis calcd. (%) for C₄₈H₅₀Cl₂O₂Si (757.90): C 76.07 H 6.65; found: C 76.21, H 7.07 %.

¹H-NMR (500.2 MHz, chloroform-d₁, 298 K): δ /ppm = 1.84 (s, 24H, 4 × C^{2,6}-Me, Mes), 2.29 (s, 12H, 4 × C⁴-Me, Mes), 6.85 (s, 8H, 4 × C^{3,5}-H, Mes), 6.96 (d, ³J_{H,H} = 7.5 Hz, 4H, 2 × C^{3,5}-H, C₆H₃), 7.07 (t, ³J_{H,H} = 7.5 Hz, 2H, 2 × C⁴-H, C₆H₃).

¹H-NMR (500.2 MHz, benzene-d₆, 298 K): δ /ppm = 1.99 (s, 24H, 4 × C^{2,6}-Me, Mes), 2.25 (s, 12H, 4 × C⁴-Me, Mes), 6.86 (m, 6H, 2 × C^{3,5}-H and 2 × C⁴-H, C₆H₃), 6.89 (s, 8H, 4 × C^{3,5}-H, Mes).

¹³C{¹H} NMR (125.8 MHz, chloroform-d₁, 298 K): δ /ppm = 20.5 (s, 8C, 4 × C^{2,6}-Me, Mes), 21.1 (s, 4C, 4 × C⁴-Me, Mes), 123.5 (s, 2C, 2 × C⁴-H, C₆H₃), 128.1 (s, 8C, 4 × C^{3,5}-H, Mes), 130.4 (s, 4C, 2 × C^{3,5}-H, C₆H₃), 132.9 (s, 4C, 2 × C^{2,6}, C₆H₃), 134.2 (s, 4C, 4 × C¹, Mes), 136.7 (s, 4C, 4 × C⁴-Me, Mes), 136.9 (s, 8C, 2 × C^{2,6}-Me, Mes), 147.4 (s, 2C, 2 × C¹, C₆H₃).

¹³C{¹H} NMR (125.8 MHz, benzene-d₆, 298 K): δ /ppm = 20.8 (s, 8C, 4 × C^{2,6}-Me, Mes), 21.2 (s, 4C, 4 × C⁴-Me, Mes), 123.9 (s, 2C, 2 × C⁴-H, C₆H₃), 128.6 (s, 8C, 4 × C^{3,5}-H, Mes), 130.8 (s, 4C, 2 × C^{3,5}-H, C₆H₃), 133.6 (s, 4C, 2 × C^{2,6}, C₆H₃), 134.7 (s, 4C, 4 × C¹, Mes), 136.8 (s, 4C, 4 × C⁴-Me, Mes), 137.1 (s, 8C, 2 × C^{2,6}-Me, Mes), 147.9 (s, 2C, 2 × C¹, C₆H₃).

²⁹Si{¹H} NMR (99.37 MHz, chloroform-d₁, 298 K): δ /ppm = -70.0 (s).

²⁹Si{¹H} NMR (99.37 MHz, benzene-d₆, 298 K): δ /ppm = -69.9 (s).

4.6.30 SiBr₂(OAr^{Mes})₂ (19-Br₂)

Compound **19-Br₂** was first described in the bachelor thesis of C. Lippmann after trying to trap free SIDipp from in situ generated **19** with an excess of SiBr₄.^[385] In this work, a synthesis from isolated **19** and Br₂ is described. It should further be noted, that **19** does not react with SiBr₄ in absence of free SIDipp in toluene at ambient temperature, as reported earlier.

A vigorously stirred, colorless solution of **19** (272 mg, 0.40 mmol, 1.0 equiv.) in 15 mL of benzene was treated dropwise with a brown solution of Br₂ in benzene (0.83 M, 0.48 mL, 0.40 mmol, 1.0 equiv.) at ambient temperature over a period of ca. 5 minutes. During the addition, the color of the Br₂ solution immediately disappeared leading finally to a slight yellow reaction solution. ¹H NMR spectroscopy revealed a complete and selective conversion of **19** to **19-Br₂**. The solution was evaporated and the almost colorless residue was recrystallized from a 1:2 n-hexane/toluene mixture at -30 °C (5 days). The resulting colorless crystals were isolated by filtration of the light yellow supernatant at -30 °C, grinded and finally dried at ambient temperature for 3 hours. Yield: 180 mg (0.21 mmol, 54% from **19**). Compound **19-Br₂** melts at

253°C to a colorless liquid. Elemental analysis calcd. (%) for C₄₈H₅₀Br₂O₂Si (846.80): C 68.08, H 5.95; found: C 67.39, H 5.91 %.

¹H NMR (500.2 MHz, chloroform-d₁, 298 K): δ /ppm = 1.86 (s, ¹J_{C,H} = 127 Hz, 24H, 4 × C^{2,6}-Me, Mes), 2.28 (s, ¹J_{C,H} = 126 Hz, 12H, 4 × C⁴-Me, Mes), 6.84 (s, 8H, 4 × C^{3,5}-H, Mes), 6.95 (d, ³J_{H,H} = 7.5 Hz, 4H, 2 × C^{3,5}-H, C₆H₃), 7.07 (t, ³J_{H,H} = 7.5 Hz, 2H, 2 × C⁴-H, C₆H₃).

¹H NMR (500.2 MHz, benzene-d₆, 298 K): δ /ppm = 2.03 (s, 24H, 4 × C^{2,6}-Me, Mes), 2.24 (s, 12H, 4 × C⁴-Me, Mes), 6.87 (m, 6H, 2 × C^{3,5}-H and 2 × C⁴-H, C₆H₃), 6.89 (s, *v*_{1/2} = 3.4 Hz, 8H, 2 × C^{3,5}-H, Mes).

¹³C{¹H} NMR (125.8 MHz, chloroform-d₁, 298 K): δ /ppm = 20.8 (s, 8C, 4 × C^{2,6}-Me, Mes), 21.1 (s, 4C, 4 × C⁴-Me, Mes), 123.5 (s, 2C, 2 × C⁴-H, C₆H₃), 128.2 (s, 8C, 4 × C^{3,5}-H, Mes), 130.7 (s, 4C, 2 × C^{3,5}-H, C₆H₃), 133.1 (s, 4C, 4 × C^{2,6}, C₆H₃), 134.5 (s, 4C, 4 × C¹, Mes), 136.8 (s, 4C, 4 × C⁴-Me, Mes), 137.0 (s, 8C, 4 × C^{2,6}-Me, Mes), 147.8 (s, 2 × C¹, C₆H₃).

¹³C{¹H} NMR (125.8 MHz, benzene-d₆, 298 K): δ /ppm = 21.1 (s, 8C, 4 × C^{2,6}-Me, Mes), 21.2 (s, 4C, 4 × C⁴-Me, Mes), 123.9 (s, 2C, 2 × C⁴-H, C₆H₃), 128.8 (s, 8C, 4 × C^{3,5}-H, Mes), 131.1 (s, 4C, 2 × C^{3,5}-H, C₆H₃), 133.8 (s, 4C, 2 × C^{2,6}, C₆H₃), 135.0 (s, 2C, 2 × C¹, Mes), 136.8 (s, 4C, 4 × C⁴-Me), 137.2 (s, 8C, 4 × C^{2,6}-Me), 148.3 (s, 2C, C¹, C₆H₃).

²⁹Si{¹H} NMR (99.34 MHz, chloroform-d₁, 298 K): δ /ppm = -86.2 (s).

²⁹Si{¹H} NMR (99.34 MHz, benzene-d₆, 298 K): δ /ppm = -86.1 (s).

4.6.31 SiI₂(OAr^{Mes})₂ (19-I₂)

Compound **19-I** was first described in the bachelor thesis of C. Lippmann but could not be obtained in pure form after crystallization from n-pentane at -60 °C.^[385] In this work, the full characterization is given.

A vigorously stirred, colorless suspension of **19** (200 mg, 0.29 mmol, 1.0 equiv.) in 5 mL of benzene was added dropwise with a violet solution of I₂ in benzene (0.061 M, 4.7 mL, 0.29 mmol, 1.0 equiv.). During the slow addition, the violet color of the added I₂ immediately disappeared, leading finally to a pale yellow solution. The reaction mixture was evaporated and the pale yellow residue was washed with 2.5 ml of a 4:1 n-hexane/benzene mixture. The colorless powder obtained was dried under vacuum for 3 hours at ambient temperature. Yield: 165 mg (0.18 mmol, 60 %). Compound **19-I** decomposes upon melting at 254°C to a yellowish

oil.⁶² Elemental analysis calc. (%) for C₄₈H₅₀L₂O₂Si (940.80): C 61.28, H 5.36; found: C 61.45, H 5.36 %.

¹H NMR (500.2 MHz, chloroform-d₁, 298 K): δ /ppm = 1.91 (s, 24H, 4 × C^{2,6}-Me, Mes), 2.27 (s, 12H, 4 × C⁴-Me, Mes), 6.84 (s, 8H, 4 × C^{3,5}-H, Mes), 6.94 (d, ³J_{H,H} = 7.5 Hz, 4H, 2 × C^{3,5}-H, C₆H₃), 7.08 (t, ³J_{H,H} = 7.5 Hz, 2H, 2 × C⁴-H, C₆H₃).

¹H NMR (benzene-d₆, 500.2 MHz, 298 K): δ /ppm = 2.10 (s, 24H, 4 × C^{2,6}-Me, Mes), 2.24 (s, 12H, 4 × C⁴-Me, Mes), 6.85 – 6.89 (m, 6H, 2 × C^{3,5}-H and 2 × C⁴-H, C₆H₃), 6.90 (s, 8H, 4 × C^{3,5}-H, Mes).

¹³C{¹H} NMR (125.8 MHz, chloroform-d₁, 298 K): δ /ppm = 21.1 (s, 4C, 4 × C⁴-Me, Mes), 21.5 (s, 8C, 4 × C^{2,6}-Me, Mes), 123.3 (s, 2C, 2 × C⁴-H, C₆H₃), 128.6 (s, 8C, 4 × C^{3,5}-H, Mes), 131.2 (s, 4C, 2 × C^{3,5}-H, C₆H₃), 133.4 (s, 4C, 2 × C^{2,6}, C₆H₃), 135.0 (s, 4C, 4 × C¹, Mes), 136.9 (s, 4C, 4 × C⁴-Me, Mes), 137.2 (s, 8C, 4 × C^{2,6}-Me, Mes), 148.6 (s, 2 × C¹, C₆H₃).

¹³C{¹H} NMR (125.8 MHz, benzene-d₆, 298 K): δ /ppm = 21.2 (s, 4C, 4 × C⁴-Me, Mes), 21.8 (s, 8C, 4 × C^{2,6}-Me, Mes), 123.8 (s, 4C, 2 × C⁴-H, C₆H₃), 129.1 (s, 8C, 4 × C^{3,5}-H, Mes), 131.6 (s, 2C, 2 × C^{3,5}-H, C₆H₃), 134.1 (s, 4C, 2 × C^{2,6}, C₆H₃), 135.6 (s, 2C, 2 × C¹, Mes), 137.0 (s, 4C, 4 × C⁴-Me, Mes), 137.4 (s, 8C, 4 × C^{2,6}-Me, Mes), 149.1 (s, 2C, 2 × C¹, C₆H₃).

²⁹Si{¹H} NMR (99.37 MHz, chloroform-d₁, 298 K): δ /ppm = -152.2 (s).

²⁹Si{¹H} NMR (99.37 MHz, benzene-d₆, 298 K): δ /ppm = -152.0 (s).

4.6.32 SiCl₃(OAr^{Mes}) (21-Cl)

A colorless solution of SiCl₄ (0.24 ml, ρ = 1.48 g/ml, 347 mg, 2.04 mmol, 1.10 equiv.) in 3 ml of diethyl ether was treated dropwise with a precooled, light brownish, very fine suspension of NaOAr^{Mes} (654 mg, 1.86 mmol, 1.0 equiv.) in 80 ml of diethyl ether at -60 °C under vigorous stirring. The reaction mixture was allowed to warm to ambient temperature overnight, when the color had changed to light olive-grey and filtered from a voluminous, colorless precipitate (NaCl). The filtrate was evaporated to dryness and the grey residue was recrystallized from about 7 ml of n-hexane at -30 °C. The resulting colorless crystals were isolated at low temperature, grinded with a spatula and dried at ambient temperature for 2 h. Yield: 277 mg (0.56 mmol, 32 % from NaOAr^{Mes}, but another batch can be obtained from the

⁶² ¹H NMR spectroscopy of the molten sample revealed a partial decomposition of **19-L** to form a compound of lower symmetry that was also present to a small extent in the mixture obtained after oxidation of **19** with I. ¹H NMR (benzene-d₆, 300.1 MHz, 298 K): δ /ppm = 2.03 (s, CH₃), 2.07 (s, CH₃), 2.22 (s, CH₃), 6.85 (s, C^{3,5}-H); the other aromatic signals overlap with those of **19-L**.

mother liquor). Elemental analysis calcd. (%) for $C_{24}H_{25}Cl_3OSi$ (463.90): C 62.14, H 5.43; found: C 62.14, H 5.49 %.

1H NMR (500.1 MHz, benzene- d_6 , 298 K): δ /ppm = 2.16 (s, 12H, $2 \times C^{2,6}$ -Me, Mes), 2.18 (s, 6H, $2 \times C^4$ -Me, Mes), 6.87 (br s, 4H, $2 \times C^{3,5}$ -H, Mes), 6.96 (s*, J = 1.9 Hz, 3H, $C^{3,5}$ -H, C_6H_3 and C^4 -H, C_6H_3).

1H NMR (500.1 MHz, chloroform- d_1 , 298 K): δ /ppm = 2.09 (s, 12H, $2 \times C^{2,6}$ -Me, Mes), 2.32 (s, 6H, $2 \times C^4$ -Me, Mes), 6.93 (br s, 4H, $2 \times C^{3,5}$ -H, Mes), 7.16 (t, $^3J_{H,H} = 7.4$ Hz, 2H, $C^{3,5}$ -H, C_6H_3), 7.26 (t, $^3J_{H,H} = 7.4$ Hz, 1H, C^4 -H, C_6H_3 , this signal overlaps with the solvent signal).

$^{13}C\{^1H\}$ NMR (125.8 MHz, benzene- d_6 , 298 K): δ /ppm = 20.7 (s, 4C, $2 \times C^{2,6}$ -Me, Mes), 21.1 (s, 2C, $2 \times C^4$ -Me, Mes), 124.8 (s, 1C, C^4 -H, C_6H_3), 128.8 (s, 4C, $2 \times C^{3,5}$ -H, Mes), 130.7 (s, 2C, $C^{3,5}$ -H, C_6H_3), 133.3 (s, 2C, $C^{2,6}$, C_6H_3), 134.2 (s, 2C, $2 \times C^4$ -Me, Mes), 136.7 (s, 4C, $2 \times C^{2,6}$ -Me, Mes), 137.5 (s, 2C, $2 \times C^1$, Mes), 148.0 (s, 1C, C^1 , C_6H_3).

$^{13}C\{^1H\}$ NMR (125.8 MHz, chloroform- d_1 , 298 K): δ /ppm = 20.7 (s, 4C, $2 \times C^{2,6}$ -Me, Mes), 21.2 (s, 2C, $2 \times C^4$ -Me, Mes), 124.6 (s, 1C, C^4 -H, C_6H_3), 128.4 (s, 4C, $2 \times C^{3,5}$ -H, Mes), 130.7 (s, 2C, $C^{3,5}$ -H, C_6H_3), 132.9 (s, 2C, $C^{2,6}$, C_6H_3), 134.0 (s, 2C, $2 \times C^4$ -Me, Mes), 136.9 (s, 4C, $2 \times C^{2,6}$ -Me, Mes), 137.5 (s, 2C, $2 \times C^1$, Mes), 147.7 (s, 1C, C^1 , C_6H_3).

$^{29}Si\{^1H\}$ NMR (99.37 MHz, benzene- d_6 , 298 K): δ /ppm = -47.5 (s).

$^{29}Si\{^1H\}$ NMR (99.37 MHz, chloroform- d_1 , 298 K): δ /ppm = -47.8 (s).

4.6.33 $SiBr_3OAr^{Mes}$ (21-Br)

A colorless solution of $SiBr_4$ (0.4 ml, $\rho = 2.79$ g/ml, 1.13 g, 3.24 mmol, 1.05 equiv.) in 10 ml of diethyl ether was treated dropwise with a precooled, light brownish, very fine suspension of $NaOAr^{Mes}$ (1.088 g, 3.09 mmol, 1.0 equiv.) in 80 ml of diethyl ether at -60 °C under vigorous stirring. The reaction mixture was allowed to warm to ambient temperature overnight, when the color had changed to light yellow and filtered from a voluminous, colorless precipitate (NaBr). The filtrate was evaporated to dryness and the grey residue was recrystallized from about 10 ml of a 1:1 mixture of diethyl ether and n-hexane at -30 °C. The resulting colorless crystals were isolated at low temperature, grinded with a spatula and dried at ambient temperature for 6 h. Yield: 1.51 g (2.53 mmol, 82 % from $NaOAr^{Mes}$). Upon heating, compound **21-Br** slowly turns green and gradually melts at 113 °C (decomposition). Green discoloration is also observed upon oxidation on air. Elemental analysis calcd. (%) for $C_{24}H_{25}Br_3OSi$ (597.25): C 49.26, H 4.22; found: C 48.93, H 4.40 %.

^1H NMR (500.1 MHz, benzene- d_6 , 298 K): δ /ppm = 2.18 (s, 6H, $2 \times \text{C}^4\text{-Me}$, Mes), 2.19 (s, 12H, $2 \times \text{C}^{2,6}\text{-Me}$, Mes), 6.87 (br s, 4H, $2 \times \text{C}^{3,5}\text{-H}$, Mes), 6.96 (m, 3H, $\text{C}^{3,5}\text{-H}$, C_6H_3 and $\text{C}^4\text{-H}$, C_6H_3).

$^{13}\text{C}\{^1\text{H}\}$ NMR (125.8 MHz, benzene- d_6 , 298 K): δ /ppm = 20.9 (s, 4C, $2 \times \text{C}^{2,6}\text{-Me}$, Mes), 21.1 (s, 2C, $2 \times \text{C}^4\text{-Me}$, Mes), 124.8 (s, 1C, $\text{C}^4\text{-H}$, C_6H_3), 128.9 (s, 4C, $2 \times \text{C}^{3,5}\text{-H}$, Mes), 130.9 (s, 2C, $\text{C}^{3,5}\text{-H}$, C_6H_3), 133.4 (s, 2C, $\text{C}^{2,6}$, C_6H_3), 134.5 (s, 2C, $2 \times \text{C}^4\text{-Me}$, Mes), 136.8 (s, 4C, $2 \times \text{C}^{2,6}\text{-Me}$, Mes), 137.5 (s, 2C, $2 \times \text{C}^1$, Mes), 148.8 (s, 1C, C^1 , C_6H_3).

$^{29}\text{Si}\{^1\text{H}\}$ NMR (99.37 MHz, benzene- d_6 , 298 K): δ /ppm = -87.2 (s).

4.6.34 $\text{SiI}_3\text{OAr}^{\text{Mes}}$ (21-I)

A colorless solution of SiI_4 (1.976 g, 3.69 mmol, 1.0 equiv.) in 20 ml of diethyl ether was treated slowly with a precooled, colorless, very fine suspension of $\text{NaOAr}^{\text{Mes}}$ (1.300 g, 3.69 mmol, 1.0 equiv.) in 80 ml of diethyl ether at -60 °C under vigorous stirring. The reaction mixture was allowed to warm to ambient temperature overnight, when the color had changed to light yellow and a voluminous, colorless precipitate (NaI) had formed. The suspension was evaporated to dryness whereupon its color changed to brownish yellow. Extraction of the brown residue with ~40 ml of toluene in two portions and subsequent recrystallization from about 30 ml of a 1:1 mixture of diethyl ether and toluene at -30 °C afforded a light brown powder. The crude product was isolated at -20 °C, washed with 2×10 ml of cold n-hexane and dried at ambient temperature for 2 h. Yield: 1.82 g (2.47 mmol, 67 % from $\text{NaOAr}^{\text{Mes}}$).⁶³ Upon heating, compound 21-I melts to a colorless liquid at 172.6 °C. Elemental analysis calcd. (%) for $\text{C}_{24}\text{H}_{25}\text{I}_3\text{OSi}$ (738.25): C 39.05, H 3.41; found: C 39.34, H 3.47 %.

^1H NMR (500.1 MHz, benzene- d_6 , 298 K): δ /ppm = 2.19 (s, 6H, $2 \times \text{C}^4\text{-Me}$, Mes), 2.25 (s, 12H, $2 \times \text{C}^{2,6}\text{-Me}$, Mes), 6.87 (br s, 4H, $2 \times \text{C}^{3,5}\text{-H}$, Mes), 6.93 – 6.96 (m, 3H, $\text{C}^{3,5}\text{-H}$, C_6H_3 and $\text{C}^4\text{-H}$, C_6H_3).

$^{13}\text{C}\{^1\text{H}\}$ NMR (125.8 MHz, benzene- d_6 , 298 K): δ /ppm = 21.1 (s, 2C, $2 \times \text{C}^4\text{-Me}$, Mes), 21.5 (s, 4C, $2 \times \text{C}^{2,6}\text{-Me}$, Mes), 124.5 (s, 1C, $\text{C}^4\text{-H}$, C_6H_3), 129.4 (s, 4C, $2 \times \text{C}^{3,5}\text{-H}$, Mes), 131.2 (s, 2C, $\text{C}^{3,5}\text{-H}$, C_6H_3), 133.6 (s, 2C, $\text{C}^{2,6}$, C_6H_3), 135.2 (s, 2C, $2 \times \text{C}^4\text{-Me}$, Mes), 136.8 (s, 4C, $2 \times \text{C}^{2,6}\text{-Me}$, Mes), 137.5 (s, 2C, $2 \times \text{C}^1$, Mes), 150.2 (s, 1C, C^1 , C_6H_3).

$^{29}\text{Si}\{^1\text{H}\}$ NMR (99.37 MHz, benzene- d_6 , 298 K): δ /ppm = -238.1 (s).

⁶³ No attempts were undertaken to increase the yield by crystallization of a second crop from the mother liquor.

4.6.35 Attempted syntheses of $\text{SiX}(\text{BX}_2)(\text{OAr}^{\text{Mes}})$ (**19-BX₃**)

Reactions between **19** and freshly purified BX_3 were performed either in benzene solution at ambient temperature or in toluene solution at $-65\text{ }^\circ\text{C}$. No significant influence of the reaction conditions was observed, but the content of the side product **19-HX** was dependent on the halogen (Cl: $\sim 15\%$, Br: $\sim 17\%$, I: $< 5\%$). No pure samples could be isolated but an exemplary procedure is given for **19-BI₃**:

A colorless suspension of **19** (200 mg, 0.29 mmol, 1.0 equiv.) in 5 mL of benzene was dropwise treated with a colorless solution of BI_3 (114 mg, 0.29 mmol, 1.0 equiv.) in 3 ml of benzene at ambient temperature over a period of 2 minutes. The mixture was stirred for 30 minutes when the color had turned to neon yellow. Complete conversion was verified by ^1H NMR spectroscopy and the solvent was evaporated. The yellow residue was recrystallized from 2 ml of n-hexane at $-30\text{ }^\circ\text{C}$ overnight, filtered cold and dried at ambient temperature for 4 h to afford 242 mg (0.22 mmol, 77% from **19**) of **19-BI₃** as a bright yellow solid that was contaminated with about 5 mol% of **19-HI**.

NMR data of **19-BCl₃**:

^1H -NMR (500.1 MHz, benzene- d_6 , 298 K): δ /ppm = 2.00, 2.06, 2.23 (each s, each 12H, $4 \times \text{C}^2\text{-Me}$ and $4 \times \text{C}^4\text{-Me}$ and $4 \times \text{C}^6\text{-Me}$, Mes), 6.83 (s^* , 6H, $2 \times \text{C}^4\text{-H}$ and $2 \times \text{C}^{3,5}\text{-H}$, C_6H_3), 6.84 (br, $\Delta\nu_{1/2} = 4.5$ Hz, 4H, $2 \times \text{C}^3\text{-H}$, Mes), 6.89 (br, $\Delta\nu_{1/2} = 4.5$ Hz, 4H, $2 \times \text{C}^5\text{-H}$, Mes).

NMR data of **19-BBr₃**:

^1H -NMR (500.1 MHz, benzene- d_6 , 298 K): δ /ppm = 2.03 (s, 12H, $4 \times \text{C}^2\text{-Me}$, Mes), 2.10 (s, 12H, $4 \times \text{C}^6\text{-Me}$, Mes), 2.24 (s, 12H, $4 \times \text{C}^4\text{-Me}$, Mes), 6.82 (s^* , 6H, $2 \times \text{C}^4\text{-H}$ and $2 \times \text{C}^{3,5}\text{-H}$, C_6H_3), 6.86 (br, $\Delta\nu_{1/2} = 4.2$ Hz, 4H, $2 \times \text{C}^5\text{-H}$, Mes), 6.90 (br, $\Delta\nu_{1/2} = 4.2$ Hz, 4H, $2 \times \text{C}^3\text{-H}$, Mes).

$^{13}\text{C}\{^1\text{H}\}$ -NMR (75.47 MHz, benzene- d_6 , 298 K): δ /ppm = 21.1 (s, 4C, $4 \times \text{C}^6\text{-Me}$, Mes), 21.59 (s, 4C, $4 \times \text{C}^6\text{-Me}$, Mes), 21.64 (s, 4C, $4 \times \text{C}^4\text{-Me}$, Mes), 123.3 (s, 2C, $2 \times \text{C}^4\text{-H}$, C_6H_3), 129.19 (s, 2C, $4 \times \text{C}^3\text{-H}$, Mes), 129.24 (s, 4C, $4 \times \text{C}^5\text{-H}$, Mes), 131.5 (s, 4C, $2 \times \text{C}^{3,5}\text{-H}$, C_6H_3), 133.3 (s, 4C, $2 \times \text{C}^{2,6}$, C_6H_3), 135.4 (s, 2C, $2 \times \text{C}^1$, Mes), 137.2 (s, 4C, $4 \times \text{C}^4\text{-Me}$, Mes), 137.25 (s, 4C, $4 \times \text{C}^2\text{-Me}$, Mes), 137.33 (s, 4C, $4 \times \text{C}^6\text{-Me}$, Mes), 148.6 (s, 2C, $2 \times \text{C}^1$, C_6H_3).

$^{11}\text{B}\{^1\text{H}\}$ -NMR (96.29 MHz, benzene- d_6 , 298 K): δ /ppm = 63.3 (br, $\nu_{1/2} = 1090$ Hz).

No signal was detected in the ^{29}Si NMR spectrum, presumably due to severe broadening and coupling to the ^{11}B nucleus.

NMR data of **19-BI₃**:

^1H -NMR (500.1 MHz, benzene- d_6 , 298 K): δ /ppm = 2.06 (s, 12H, $4 \times \text{C}^2\text{-Me}$, Mes), 2.17 (s, 12H, $4 \times \text{C}^6\text{-Me}$, Mes), 2.24 (s, 12H, $4 \times \text{C}^4\text{-Me}$, Mes), 6.81 (br, $\Delta\nu_{1/2} = 4.2$ Hz, 4H, $2 \times \text{C}^5\text{-H}$,

Mes), 6.82 (s*, 6H, 2 × C⁴-H and 2 × C^{3,5}-H, C₆H₃), 6.89 (br, Δv_{1/2} = 4.2 Hz, 4H, 2 × C³-H, Mes). See also Figure 79 on page 150.

¹³C{¹H}-NMR (75.47 MHz, benzene-d₆, 298 K): δ /ppm = 21.2 (s, 4C, 4 × C⁶-Me, Mes), 22.37 (s, 4C, 4 × C⁶-Me, Mes), 22.42 (s, 4C, 4 × C⁴-Me, Mes), 123.2 (s, 2C, 2 × C⁴-H, C₆H₃), 129.6 (s, 2C, 4 × C³-H, Mes), 129.7 (s, 4C, 4 × C⁵-H, Mes), 131.9 (s, 4C, 2 × C^{3,5}-H, C₆H₃), 133.6 (s, 4C, 2 × C^{2,6}, C₆H₃), 136.1 (s, 2C, 2 × C¹, Mes), 137.3 (s, 4C, 4 × C⁴-Me, Mes), 137.4 (s, 4C, 4 × C²-Me, Mes), 137.5 (s, 4C, 4 × C⁶-Me, Mes), 149.5 (s, 2C, 2 × C¹, C₆H₃).

¹¹B{¹H}-NMR (96.29 MHz, benzene-d₆, 298 K): δ /ppm = 58.0 (br, v_{1/2} = 640 Hz). See also Figure 81 on page 152.

²⁹Si{¹H}-NMR (99.37 MHz, benzene-d₆, 298 K): δ /ppm = -47.0 (br, v_{1/2} = 120 Hz). See also Figure 81 on page 152.

4.6.36 SiCl(PCI₂)(OAr^{Mes})₂ (19-PCI₃)

A vigorously stirred, colorless suspension of **19** (300 mg, 0.44 mmol, 1.0 equiv.) in 10 mL of toluene was dropwise treated with a colorless solution of PCI₃ (120 mg, 0.87 mmol, 2.0 equiv.) in 1 ml of toluene at ambient temperature over a period of 1 minute. During the addition, the colorless solid (**19**) quickly dissolved and the reaction mixture was stirred for 1 hour at ambient temperature. The solution was evaporated and the residue was washed with 1 × 3 mL and 1 × 1 mL of diethyl ether and dried under vacuum at 40 °C to afford 220 mg of **19-PCI₃** as a colorless, analytically pure solid. Cooling of the filtrate to -30 °C afforded a second crop (95 mg) of **19-PCI₃** which was pure according to ¹H NMR spectroscopy. Combined yield: 315 mg (0.38 mmol, 87 % from **19**). Compound **19-PCI₃** decomposes at 112 °C into a grey mass with gas evolution. Elemental analysis calcd. (%) for C₄₈H₅₀Cl₃O₂PSi (824.33): C 69.34, H 6.11; found: C 69.65, H 6.25 %.

¹H-NMR (500.1 MHz, benzene-d₆, 298 K): δ /ppm = 2.05 (s, 12H, 4 × C²-Me, Mes), 2.09 (s, 12H, 4 × C⁶-Me, Mes), 2.25 (s, 12H, 4 × C⁴-Me, Mes), 6.82 (s*, 6H, 2 × C⁴-H and 2 × C^{3,5}-H, C₆H₃), 6.86 (br, Δv_{1/2} = 4.5 Hz, 4H, 2 × C³-H, Mes), 6.90 (br, Δv_{1/2} = 4.5 Hz, 4H, 2 × C⁵-H, Mes).

¹³C{¹H}-NMR (75.47 MHz, benzene-d₆, 298 K): δ /ppm = 21.2 (s, 4C, 4 × C⁴-Me, Mes), 21.3 (s, 4C, 4 × C⁶-Me, Mes), 21.52, 21.53 (s each, 2C each, 2 × C²-Me each, Mes), 123.6 (s, 2C, 2 × C⁴-H, C₆H₃), 129.2 (s, 2C, 4 × C⁵-H, Mes), 129.3 (s, 4C, 4 × C³-H, Mes), 131.8 (s, 4C, 2 × C^{3,5}-H, C₆H₃), 133.1 (s, 4C, 2 × C^{2,6}, C₆H₃), 135.3* (d, J_{p,c} = 1.3 Hz, 2C each, 2 × C¹ each, Mes), 137.0 (s, 4C, 4 × C⁴-Me, Mes), 137.3* (d, J_{p,c} = 1.1 Hz, 2 × C²-Me each, Mes), 137.5

(s, 4C, 4 × $\underline{\text{C}}^6\text{-Me}$, Mes), 149.2 (s, 2C, 2 × $\underline{\text{C}}^1$, C_6H_3). Signals marked with an asterisk (*) show a weak through-space coupling to the ^{31}P nucleus.^[444,491]

$^{29}\text{Si}\{^1\text{H}\}\text{-NMR}$ (99.37 MHz, benzene- d_6 , 298 K): δ /ppm = -68.6 (d, $^1J_{\text{P,Si}} = 80$ Hz).

$^{31}\text{P}\{^1\text{H}\}\text{-NMR}$ (202.5 MHz, benzene- d_6 , 298 K): δ /ppm = 131.17 (s, $^1J_{\text{P,Si}} = 80$ Hz, $\underline{\text{P}}^{35}\text{Cl}_2$), 131.15 (s, $^1J_{\text{P,Si}} = 80$ Hz, $\underline{\text{P}}^{35}\text{Cl}^{37}\text{Cl}$), 131.12 (s, $\underline{\text{P}}^{37}\text{Cl}_2$). See also Figure 80 on page 151.

4.6.37 **SiMe(ZnMe)(OAr^{Mes})₂ (19-ZnMe₂)**

A vigorously stirred, colorless suspension of **19** (300 mg, 0.44 mmol, 1.0 equiv.) in 20 mL of toluene was dropwise treated with a precooled, colorless solution of ZnMe_2 (0.062 M, 7.5 mL, 0.46 mmol, 1.06 equiv.) in n-hexane at -30 °C over a period of 5 minutes. The reaction mixture was allowed to warm to ambient temperature over a period of 2.5 hours, whereupon the suspension turned into a colorless solution. ^1H NMR spectroscopy revealed a selective, but incomplete conversion (ca. 92 %) of **19** into **19-ZnMe₂**, so the solution was again treated with another portion of the ZnMe_2 solution (0.062 M, 1.0 mL, 0.062 mmol, 0.14 equiv.) in n-hexane at -30 °C. The mixture was stirred at that temperature for 3 hours, and then allowed to warm to ambient temperature. Completion of the reaction was confirmed by ^1H NMR spectroscopy, and the solution was evaporated to afford **19-ZnMe₂** as a colorless, analytically pure solid. Yield: 335 mg (0.43 mmol, 98 % from **19**). Compound **19-ZnMe₂** decomposes at 227 °C into a grey mass with gas evolution. Elemental analysis calcd. (%) for $\text{C}_{50}\text{H}_{56}\text{O}_2\text{SiZn}$ (782.47): C 76.75, H 7.21; found: C 76.43, H 7.42 %.

^1H NMR (500.2 MHz, benzene- d_6 , 298 K): δ /ppm = -0.84 (s, $^2J_{\text{Si,H}} = 5.0$ Hz, 3H, $\underline{\text{SiMe}}$), -0.64 (s, 3H, $\underline{\text{ZnMe}}$), 2.02, 2.03 and 2.25 (s each, 12H each, 4 × $\underline{\text{C}}^2\text{-Me}$, 4 × $\underline{\text{C}}^4\text{-Me}$ and 4 × $\underline{\text{C}}^6\text{-Me}$, Mes), 6.83 (t*, $^3J_{\text{H,H}} = 7.3$ Hz, 2H, 2 × $\underline{\text{C}}^4\text{-H}$, C_6H_3), 6.87 (s, 8H, 4 × $\underline{\text{C}}^3\text{-H}$ and 4 × $\underline{\text{C}}^5\text{-H}$, Mes), 6.87 (d*, $^3J_{\text{H,H}} = 7.3$ Hz, 4H, 2 × $\underline{\text{C}}^{3,5}\text{-H}$, C_6H_3 , the aromatic signals overlap).

$^{13}\text{C}\{^1\text{H}\}$ NMR (125.78 MHz, benzene- d_6 , 298 K): δ /ppm = -0.6 (s, 1C, $\underline{\text{ZnMe}}$), 4.8 (s, 1C, $\underline{\text{SiMe}}$), 21.1 (s, 4C, 4 × $\underline{\text{C}}^4\text{-Me}$, Mes), 21.3 (s, 4C, 4 × $\underline{\text{C}}^6\text{-Me}$, Mes), 21.4 (s, 4C, 4 × $\underline{\text{C}}^2\text{-Me}$, Mes), 121.8 (s, 2C, 2 × $\underline{\text{C}}^4\text{-H}$, C_6H_3), 128.6, 128.7 (each s, each 4C, 4 × $\underline{\text{C}}^3\text{-H}$ and 4 × $\underline{\text{C}}^5\text{-H}$, Mes), 130.5 (s, 4C, 2 × $\underline{\text{C}}^{3,5}\text{-H}$, C_6H_3), 133.4 (s, 4C, 2 × $\underline{\text{C}}^{2,6}$, C_6H_3), 136.3, 136.6, 136.7 and 137.1 (each s, each 4C, 4 × $\underline{\text{C}}^2\text{-Me}$, 4 × $\underline{\text{C}}^4\text{-Me}$, 4 × $\underline{\text{C}}^6\text{-Me}$ and 4 × $\underline{\text{C}}^1$, Mes), 150.9 (s, 2C, 2 × $\underline{\text{C}}^1$, C_6H_3).

$^{29}\text{Si}\{^1\text{H}\}$ NMR (99.37 MHz, benzene- d_6 , 298 K): δ /ppm = 5.4 (s).

4.6.38 **Si(HN=NC(H)Tips)(NN≡CTips)(OAr^{Mes})₂ (22)**

A vigorously stirred, colorless suspension of **19** (200 mg, 0.29 mmol, 1.0 equiv.) in 10 mL of toluene was dropwise treated with a yellow solution of Tips(H)CN₂ (116 mg, 0.58 mmol, 2.0 equiv.) in 2 mL of toluene over a period of 3 minutes. While the reaction mixture was stirred for 3 hours at ambient temperature, the color faded within the first hour and the colorless solid (**19**) dissolved. ¹H-NMR-spectroscopy revealed the complete conversion of the starting materials and the reaction mixture was filtered from a tiny amount of a colorless solid. The light yellow filtrate was evaporated and the residue was recrystallized from 12 mL of a 1:5 n-hexane/diethyl ether mixture at -30 °C. The resulting colorless crystals (ca 100 mg of analytically pure **22**·Et₂O) were isolated by filtration of the yellow mother liquor at -30 °C, thoroughly grinded and dried for 2 hours at ambient temperature. The mother liquor was evaporated and the yellow residue was washed with 2 mL of n-hexane at ambient temperature to give a second crop of the product that was found to be pure by ¹H NMR spectroscopy. Combined yield: 244 mg (0.23 mmol, 77 %). Compound **22** melts at 277 °C to a colorless liquid. Elemental analysis calcd. (%) for C₆₈H₉₄N₄O₂Si₃ (1083.76): C 75.36, H 8.74, N 5.17; found: C 75.13, H 8.69, N 5.14 %.

IR: (solid state, RT): $\tilde{\nu}$ (cm⁻¹) = 3264 (vw, ν_{NH}), 2958 (sh), 2943 (m), 2920 (m), 2891 (w), 2863 (m), 2726 (vw), 2143 (s, $\nu_{\text{N=C}}$), 2063 (vw), 1611 (w), 1580 (vw), 1531 (w), 1485 (w), 1459 (m), 1433 (sh), 1421 (s), 1380 (m), 1293 (vw), 1252 (sh), 1229 (vs), 1185 (vw), 1164 (vw), 1115 (w), 1102 (sh), 1077 (m), 1054 (m), 1033 (sh), 1010 (m), 995 (w), 958 (vs), 937 (m), 904 (m), 882 (m), 845 (s), 799 (w), 778 (vs), 759 (vs), 738 (m), 696 (m), 669 (s), 600 (m), 563 (m), 551 (m), 535 (s), 505 (m), 483 (m), 446 (sh), 430 (m), 407 (m).

An assignment of the ¹H and ¹³C NMR signals was not possible for spectra recorded at 298 K due to extensive broadening and overlapping of numerous signals. Broadening of the signals was also observed in toluene-d₆, thf-d₈ or chloroform-d₁ at 298 K (note: compound **22** was found to decompose slowly in chloroform-d₁ solution at 298 K). Cooling of a sample of **22** in toluene-d₆ stepwise to 238 K resulted in hindered rotations around the Si-O or O-C bonds, lowering both Ar^{Mes} substituents to C₁ symmetry, thus leading to a large number of sharpened, independent signals. The temperature of 243 K was chosen to give the best overall result, nevertheless a complete and undoubtful assignment could not be realised even with the help of sliced correlation spectra to enhance the spectral resolution. However, a partial assignment is given below:

¹H NMR (500.1 MHz, benzene-d₆, 298 K): δ /ppm = 0.95 (m, 21H, CHMe₂ + CHMe₂ Tips_A), 1.09 (m, 21H, CHMe₂ + CHMe₂ Tips_B), 1.97 (br, $\nu_{1/2}$ = 16 Hz, 12H, 4 × CH₃, Mes), 2.07 (s, 6H, 2 × CH₃, Mes), 2.32 (br, $\nu_{1/2}$ = 12 Hz, 6H, 2 × CH₃, Mes), 2.38 (s, 6H, 2 × CH₃, Mes), 2.44 (s, 6H, 2 × CH₃, Mes), 4.02 (d, ⁴J_{H,H} = 1.1 Hz, NH), 6.32 (d, ⁴J_{H,H} = 1.1 Hz, ²J_{Si,H} = 11.3 Hz, 1H, CH-Tips_B), 6.83 (t, ³J_{H,H} = 7.1 Hz, 2H, 2 × C⁴-H, C₆H₃), 6.86 (m, 2H, this signal overlaps

with the neighbouring signal), 6.92 (s, 4H, $2 \times \text{C}^{3,5}\text{-H}$, Mes), 6.95 (m, 2H, this signal overlaps with the neighbouring signal), 6.96, 7.04 (s each, 2H each, $4 \times \text{C}^{3,5}\text{-H}$, Mes).

^1H NMR (500.2 MHz, toluene- d_8 , 243 K): δ /ppm = 0.88 (m, 3H, $3 \times \text{CHMe}_2$, Tips_A), 0.93 (m, 18H, $3 \times \text{CHMe}_2$, Tips_A), 1.06 (br s, 9H, CHMe_AMe_B , Tips_B), 1.11 (s, 12H, CHMe_AMe_B , Tips_A + CHMe_2 , Tips_B), 1.83, 1.85, 1.97, 2.13 (s each, 3H each, $4 \times \text{C}^2/\text{C}^4/\text{C}^6\text{-Me}$), 2.15 (s, 9H, $3 \times \text{C}^2/\text{C}^4/\text{C}^6\text{-Me}$), 2.37, 2.40, 2.43, 2.45, 2.50 (s each, 3H each, $5 \times \text{C}^2/\text{C}^4/\text{C}^6\text{-Me}$), 3.91 (s, 1H, NH), 6.27 (s, 1H, CH-Tips_B), 6.80 – 6.89 (m, 4H, $\text{C}^4\text{-H}$, C_6H_3 + unidentified aromatic protons), 6.91 – 6.97 (s, 5H, $\text{C}^{3,5}\text{-H}$, Mes_A, Ar^{Mes_A} + $\text{C}^4\text{-H}$, C_6H_3 + unidentified aromatic protons), 7.00 (s, 2H, unidentified aromatic protons), 7.08 (s, 1H, unidentified aromatic proton).

$^{13}\text{C}\{^1\text{H}\}$ NMR (125.8 MHz, toluene- d_8 , 243 K): δ /ppm = 10.9 (s, 3C, $3 \times \text{CHMe}_A\text{Me}_B$, Tips_B), 11.5 (s, 3C, $3 \times \text{CHMe}_2$, Tips_A), 18.4 (s, 6C, $3 \times \text{CHMe}_2$, Tips_A), 18.9 (s, 3C, $3 \times \text{CHMe}_A\text{Me}_B$, Tips_B), 19.0 (s, 3C, $3 \times \text{CHMe}_A\text{Me}_B$, Tips_B), 19.8, 20.0, 20.9, 21.0, 21.2, 21.3 (each s, each 1C, $6 \times \text{C}^2/\text{C}^4/\text{C}^6\text{-Me}$, Mes), 21.65 (s, 2C, $2 \times \text{C}^2/\text{C}^4/\text{C}^6\text{-Me}$, Mes), 21.71 (s, 1C, $\text{C}^2/\text{C}^4/\text{C}^6\text{-Me}$, Mes), 22.3 (s, 2C, $2 \times \text{C}^2/\text{C}^4/\text{C}^6\text{-Me}$, Mes), 22.5 (s, 1C, $\text{C}^2/\text{C}^4/\text{C}^6\text{-Me}$, Mes), 48.2 (s, 1C, $\text{N}\equiv\text{CTips}_B$), 122.3, 122.6 (each s, each 1C, $\text{C}^4\text{-H}$, C_6H_3 , Ar^{Mes_A} + $\text{C}^4\text{-H}$, C_6H_3 , Ar^{Mes_B}), 127.2 (s, 1C), 127.7, 127.9, 128.3, 128.8, (each s, this signals overlap with the solvent signals), 129.4 (s, 1C), 130.0 (s, 2C), 130.9 (s, 1C), 132.5*, 133.0*, 134.3*, 134.7*, 134.8*, 135.1*, 135.5*, 135.7*, 135.8*, 135.9*, 136.0*, 136.4*, 136.5*, 136.9*, 137.0*, 137.2*, 138.4* (each s, each 1C), 143.8 (s, 1C, $\text{N}=\text{CH-Tips}_B$), 148.7* (s, 2C, C^1 , C_6H_3 , Ar^{Mes_A} and C^1 , C_6H_3 , Ar^{Mes_B}). Signals marked with an asterisk (*) were identified as quarternary carbon atoms by $^{135}\text{DEPT}$ spectroscopy.

^{15}N NMR (50.68 MHz, toluene- d_8 , 243 K): δ /ppm = 144.3 (dd, $^1\text{J}_{\text{N,H}} = 77$ Hz, NH), 372.2 (s, $\text{N}=\text{CHTips}_B$). The signals positions were determined from a $^1\text{H}\text{-}^{15}\text{N}\{^1\text{H}\}$ HMBC correlation spectrum, but no signals of the Si-N-N \equiv C-Tips_A moiety were detected.

$^{29}\text{Si}\{^1\text{H}\}$ NMR (99.36 MHz, benzene- d_6 , 298 K): δ /ppm = 1.3 (s, 1Si, $\text{N}\equiv\text{C-Tips}$), -3.5 (s, 1Si, $\text{N}=\text{CHTips}$), -88.1 (s, 1Si, $\text{Si}(\text{OAr}^{\text{Mes}})_2$).

4.6.39 [Cu(IiPr₂Me₂)(SIDipp)]Br

A small crop (~25 mg) of colorless crystals was obtained as a decomposition product of the NHC-stabilized disilavinylidene **15** and subsequent crystallization from n-hexane at ambient temperature. The formation can presumably be traced back to the presence of some [CuBr(IiPr₂Me₂)] or incomplete separation of [CuBr(IiPr₂Me₂)₂], which is formed during the synthesis of **14/15**. The crystals were soluble in thf and sparingly soluble in benzene.

^1H NMR (500.2 MHz, tetrahydrofuran- d_8 , 298 K): δ /ppm = 1.00 (d, $^3J_{\text{H,H}} = 7.0$ Hz, 12H, $2 \times \text{CHMe}_2$, IiPr_2Me_2), 1.26 (d, $^3J_{\text{H,H}} = 7.0$ Hz, 12H, $4 \times \text{CHMe}_A\text{Me}_B$, Dipp), 1.39 (d, $^3J_{\text{H,H}} = 7.0$ Hz, 12H, $4 \times \text{CHMe}_A\text{Me}_B$, Dipp), 1.94 (s, 6H, $2 \times \text{NCMe}$, IiPr_2Me_2), 3.62 (sept, $^3J_{\text{H,H}} = 7.0$ Hz, 4H, $4 \times \text{CHMe}_A\text{Me}_B$, Dipp), 3.69 (sept, $^3J_{\text{H,H}} = 7.0$ Hz, 2H, $2 \times \text{CHMe}_2$, IiPr_2Me_2), 4.08 (s, 4H, $2 \times \text{NCH}_2$, SIDipp), 7.26 (d*, $^3J_{\text{H,H}} = 7.0$ Hz, 4H, $2 \times \text{C}^{3,5}\text{-H}$, Dipp), 7.26 (d*, $^3J_{\text{H,H}} = 7.0$ Hz, 2H, $2 \times \text{C}^4\text{-H}$, Dipp).

$^{13}\text{C}\{^1\text{H}\}$ NMR (125.8 MHz, tetrahydrofuran- d_8 , 298 K): δ /ppm = 9.9 (s, 2C, $2 \times \text{NCMe}$, IiPr_2Me_2), 22.9 (s, 4C, $2 \times \text{CHMe}_2$, IiPr_2Me_2), 25.8 (s, 4C, $4 \times \text{CHMe}_A\text{Me}_B$, Dipp), 26.2 (s, 4C, $4 \times \text{CHMe}_A\text{Me}_B$, Dipp), 29.2 (s, 4C, $4 \times \text{CHMe}_A\text{Me}_B$, Dipp), 53.1 (s, 2C, $2 \times \text{CMe}_2$, IiPr_2Me_2), 54.6 (s, 2C, $2 \times \text{NCH}_2$, SIDipp), 124.0 (s, 2C, $2 \times \text{NCH}_2$, IiPr_2Me_2), 125.0 (s, 4C, $2 \times \text{C}^{3,5}\text{-H}$, Dipp), 129.2 (s, 2C, $2 \times \text{C}^4\text{-H}$, Dipp), 138.1 (s, 2C, $2 \times \text{C}^1$, Dipp), 149.0 (s, 4C, $2 \times \text{C}^{2,6}$, Dipp), 184.5 (s, 1C, NCN , IiPr_2Me_2), 213.5 (s, 1C, NCN , SIDipp).

4.6.40 [Cu(IiPr₂Me₂)₂Br]

The synthesis follows the procedure reported for [Cu(IiPr₂Me₂)₂Cl] described by Kuehn et al. using CuBr instead of CuCl.^[304]

A solid mixture of colorless CuBr (150 mg, 1.05 mmol, 1.0 equiv.) and IiPr₂Me₂ (360 mg, 2.14 mmol, 2.05 equiv.) was treated with 5 ml of thf. Initially, a precipitate of CuBr was observed, which dissolved within 5 minutes of vigorous stirring. The schlenk tube was wrapped in aluminium foil and the reaction mixture was stirred over night, when a small amount of a colorless solid had formed.⁶⁴ The suspension was constricted to dryness, 5 ml of n-hexane were added and the suspension was sonicated for 15 min. The crude product was isolated by filtration, washed with a total of 50 ml of n-hexane in three portions and dried in vacuo to obtain a colorless solid. Yield: 440 mg (917 μmol , 88 % from CuBr). Elemental analysis calcd. (%) for C₂₂H₄₀BrCuN₂ (504.03): C 52.42, H 7.99, N 11.12; found: C 51.51, H 8.02, N 10.74.33 %.

^1H NMR (300.1 MHz, benzene- d_6 , 298 K): δ /ppm = 1.50 (d, 12H, $^3J_{\text{H,H}} = 7.0$ Hz, $2 \times \text{CHMe}_2$), 1.69 (s, 6H, $2 \times \text{C}^{4,5}\text{-Me}$), 5.18 (br, 2H, $\nu_{1/2} = 40$ Hz, $2 \times \text{CHMe}_2$). No reliable ^{13}C NMR data could be obtained due to the low solubility in benzene- d_6 .

^1H NMR (500.2 MHz, tetrahydrofuran- d_8 , 298 K): δ /ppm = 1.54 (d, 12H, $^3J_{\text{H,H}} = 7.1$ Hz, $2 \times \text{CHMe}_2$), 2.15 (s, 6H, $2 \times \text{C}^{4,5}\text{-Me}$), 5.18 (br sept., 2H, $\nu_{1/2} = 28$ Hz, $2 \times \text{CHMe}_2$).

⁶⁴ Kuehn et al. described the formation of a brownish suspension during the synthesis of [Cu(IiPr₂Me₂)₂Cl],^[304] which was not observed in this case. This may be traced back to the very high quality of the employed CuBr and/or the additional protection from light.

$^{13}\text{C}\{^1\text{H}\}$ NMR (75.47 MHz, tetrahydrofuran- d_8 , 298 K): δ /ppm = 9.6 (s, 2C, $2 \times \text{C}^{4,5}\text{-Me}$), 23.0 (s, 4C, $2 \times \text{CHMe}_2$), 52.3 (s, 2C, $2 \times \text{C}^{4,5}\text{-Me}$), 123.6 (s, 1C, NCN).

4.6.41 $[\text{iPrO}(\text{H})\text{C}\{\text{N}(\text{Dipp})\text{CH}\}_2$

A solution of SIDipp (270 mg, 0.366 mmol, 1.0 equiv.) in 5 ml benzene was treated with a solution of isopropanol (22 mg, 366 mmol, 1.0 equiv.) in another 3 ml of benzene. The reaction mixture was stirred for 1 h at ambient temperature and the solvent was evaporated. The colorless residue was well soluble in benzene and moderately soluble in n-hexane; it was analyzed without any further purification (about 95 % pure). See also page 42ff.

^1H NMR (500.2 MHz, benzene- d_6 , 298 K): δ /ppm = 0.64 (d, 6H, $^3J_{\text{H,H}} = 8.1$ Hz, OCHMe_2), 1.22 (d, 6H, $^3J_{\text{H,H}} = 6.8$ Hz, $\text{C}^2\text{-CHMe}_A\text{Me}_B$, Dipp), 1.28 (d, 6H, $^3J_{\text{H,H}} = 6.8$ Hz, $\text{C}^6\text{-CHMe}_A\text{Me}_B$, Dipp), 1.34 (d, 6H, $^3J_{\text{H,H}} = 6.8$ Hz, $\text{C}^6\text{-CHMe}_A\text{Me}_B$, Dipp), 1.36 (d, 6H, $^3J_{\text{H,H}} = 6.8$ Hz, $\text{C}^2\text{-CHMe}_A\text{Me}_B$, Dipp), 3.13 (sept, 2H, $^3J_{\text{H,H}} = 6.8$ Hz, $2 \times \text{C}^6\text{-CHMe}_A\text{Me}_B$, Dipp), 3.30 – 3.37 (m, 2H, NCH_AH_B), 3.32 (sept, 2H, $^3J_{\text{H,H}} = 6.8$ Hz, $2 \times \text{C}^2\text{-CHMe}_A\text{Me}_B$, Dipp), 3.76 – 3.84 (m, 2H, NCH_AH_B), 4.12 (sept, 2H, $^3J_{\text{H,H}} = 6.8$ Hz, $2 \times \text{C}^2\text{-CHMe}_A\text{Me}_B$, Dipp), 3.51 (s, 4H, $2 \times \text{NCH}_2$, SIDipp), 5.65 (N_2CH), 7.08 – 7.13 (m, 4H, $2 \times \text{C}^3\text{-H}$, and $2 \times \text{C}^5\text{-H}$, Dipp), 7.17 (m, 2H, $2 \times \text{C}^4\text{-H}$, Dipp).

$^{13}\text{C}\{^1\text{H}\}$ NMR (75.47 MHz, benzene- d_6 , 298 K): δ /ppm = 23.0 (s, 2C, OCHMe_2), 23.9 (s, 2C, $2 \times \text{C}^2\text{-CHMe}_A\text{Me}_B$, Dipp), 24.2 (s, 2C, $2 \times \text{C}^6\text{-CHMe}_A\text{Me}_B$, Dipp), 25.6 (s, 2C, $2 \times \text{C}^2\text{-CHMe}_A\text{Me}_B$, Dipp), 26.0 (s, 2C, $2 \times \text{C}^6\text{-CHMe}_A\text{Me}_B$, Dipp), 28.3 (s, 2C, $2 \times \text{C}^2\text{-CHMe}_A\text{Me}_B$, Dipp), 28.55, 28.57 (2C, $2 \times \text{C}^6\text{-CHMe}_A\text{Me}_B$, Dipp), 52.0 (s, 2C, $2 \times \text{NCH}_2$, SIDipp), 68.9 (s, 1C, OCHMe_2), 104.1 (s, 1C, N_2CH , SIDipp), 123.9, 124.5 (each s, each 2C, $2 \times \text{C}^3\text{-H}$, and $2 \times \text{C}^5\text{-H}$, Dipp), 127.7 (s, 2C, $2 \times \text{C}^4\text{-H}$, Dipp), 139.2 (s, 2C, $2 \times \text{C}^1$, Dipp), 149.0 (s, 2C, $2 \times \text{C}^6\text{-CHMe}_A\text{Me}_B$, Dipp), 151.7 (s, 2C, $2 \times \text{C}^2\text{-CHMe}_A\text{Me}_B$, Dipp).

5 Appendices

5.1 Determination of symmetry from ^1H NMR spectra

The characterization by ^1H NMR provides a unique, cost-effective and fast recognition factor much like a finger print.^[361] But since individual chemical shifts are dependent on too many factors, only limited information regarding the structural connectivity of organometallic compounds can be obtained. In this work, the local symmetry of substituents was determined from ^1H and/or ^{13}C NMR spectra. This “observed symmetry” of a ligand is often higher than the overall point group of the molecule due to fast rotations around the Si-substituent axes.^[492] Inequivalence of substituents can be caused by either substitution with a chiral group (removing a mirror plane) or simply by a hindered rotation around a chemical bond by steric pressure. On the other hand, factors that should dispel a mirror plane e. g. in chiral compounds can be simply too far away to affect peripheral substituents – thus allowing for highly symmetric NMR spectra of individual subunits in an overall less symmetric compound.^[361]

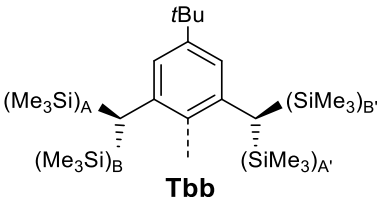
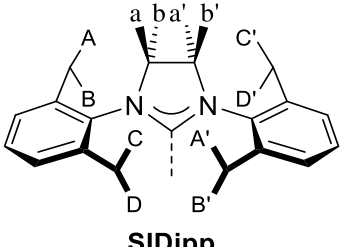
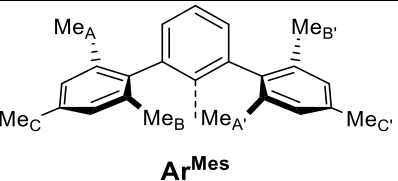
Substituent	Local point group / observed symmetry			
	C_{2v} (c_2 and σ_v)	C_2 (c_2)	C_s (σ_v)	C_1 (none)
 <p>Tbb</p>	$A = B'$ (σ_v) $A = A'$ (c_2) 1 <u>SiMe₃</u> signal	$A \neq B'$ $A = A'$ (c_2) 2 <u>SiMe₃</u> signals	$A = B'$ (σ_v) $A \neq A'$ s <u>SiMe₃</u> signals	$A \neq B'$ $A \neq A'$ 4 <u>SiMe₃</u> signals
 <p>SIDipp</p>	$A = C'$ (σ_v) $A = A'$ (c_2) $a = b'$ (σ_v) $a = a'$ (c_2) 2 <u>Me</u> signals 1 <u>NHH'</u> signal	$A \neq C'$ $A = A'$ (c_2) $a \neq b'$ $a = a'$ (c_2) 4 <u>Me</u> signals 2 <u>NHH'</u> signals	$A = C'$ (σ_v) $A \neq A'$ $a = b'$ (σ_v) $a \neq a'$ 4 <u>Me</u> signals 2 <u>NHH'</u> signals	$A \neq C'$ $A \neq A'$ $a \neq b'$ $a \neq a'$ 8 <u>Me</u> signals 4 <u>NHH'</u> signals
 <p>Ar^{Mes}</p>	$A = B'$ (σ_v) $A = A'$ (c_2) $C = C'$ (σ_v, c_2) 2 <u>Me</u> signals	$A \neq B'$ $A = A'$ (c_2) $C = C'$ (c_2) 3 <u>Me</u> signals	$A = B'$ (σ_v) $A \neq A'$ $C = C'$ (σ_v) 3 <u>Me</u> signals	$A \neq B'$ $A \neq A'$ $C \neq C'$ 6 <u>Me</u> signals

Figure 90. The effect of the elimination of different symmetry operations (σ_v , c_2) on characteristic non-aromatic ^1H NMR signals of Tbb, SIDipp and Ar^{Mes}. For highly symmetric groups (Br, SiX₃...) an additional mirror plane σ_v can be present within the paper plane. Note, that no rotation around the C-N bond in SIDipp is observed for steric reasons.

In practice, the bulky Tbb, SIDipp and Ar^{Mes} groups that were predominantly used in this work allow for a relatively easy differentiation of “highly symmetric” (C_{2v}), “less symmetric”

(C₂, C_s) and “unsymmetric” (C₁) subunits based on the number of aliphatic signals (one, two and four, respectively, doubled for the inherently diastereotopic methyl groups of SIDipp). Distinction between C₂ and C_s symmetry is more difficult. It can be performed with the help of XRD analysis or, for SIDipp, based on the coupling patterns of the NCH₂CH₂N backbone protons if a sufficient resolution was achieved. For Ar^{Mes} and Tbb, the two intermediate stages usually can not be distinguished without further data, since both result in identical spectra with pairs of equivalent positions (mirrored or “crosswise”).

5.2 Crystallographic data files of novel compounds

Compound	1-Me	1-CH ₂ Ph·C ₆ H ₆	2·C ₃ H ₁₂
Crystal Habitus	red prism	dark red plate	red plank
Device Type	Bruker D8-Venture	STOE IPDS-2T	Bruker D8-Venture
Empirical formula	C ₅₃ H ₉₀ N ₃ Si ₆	C ₆₄ H ₁₀₀ N ₃ Si ₆	C ₆₀ H ₁₀₉ LiN ₃ O ₂ Si ₆
Moiety formula	C ₅₃ H ₉₀ N ₃ Si ₆	C ₅₈ H ₈₁ N ₃ Si ₆ , C ₆ H ₆	C ₅₅ H ₉₇ LiN ₃ O ₂ Si ₆ , C ₃ H ₁₂
Formula weight	911.79	1065.99	1065.97
Temperature/K	165.02	123(2)	150.0
Crystal system	monoclinic	monoclinic	monoclinic
Space group	P2 ₁ /m	P2 ₁	P2 ₁ /n
a/Å	11.9785(4)	12.2965(5)	13.0422(3)
b/Å	20.2080(8)	20.0606(9)	21.5990(6)
c/Å	13.7564(5)	14.3048(8)	24.1942(6)
α/°	90	90	90
β/°	105.584(2)	110.252(4)	92.6810(9)
γ/°	90	90	90
Volume/Å ³	3207.5(2)	3310.5(3)	6808.0(3)
Z	2	2	4
ρ _{calc} /g/cm ³	0.944	1.069	1.040
μ/mm ¹	1.428	0.163	1.425
F(000)	1000.0	1164.0	2344.0
Crystal size/mm ³	0.24 × 0.22 × 0.16	0.21 × 0.15 × 0.06	0.5 × 0.16 × 0.1
Absorption correction	empirical	integration	empirical
Tmin; Tmax	0.3563; 0.7535	0.9681; 0.9881	0.5509; 0.7535
Radiation	CuKα (λ = 1.54178)	MoKα (λ = 0.71073)	CuKα (λ = 1.54178)
2θ range /°	6.67 to 135.498°	5.382 to 56°	7.556 to 135.496°
Completeness to theta	0.983	0.958	0.996
Index ranges	-14 ≤ h ≤ 14, -24 ≤ k ≤ 24, -16 ≤ l ≤ 16	-16 ≤ h ≤ 16, -23 ≤ k ≤ 26, -16 ≤ l ≤ 18	-13 ≤ h ≤ 15, -25 ≤ k ≤ 25, -29 ≤ l ≤ 29
Reflections collected	46193	15018	119679
Independent reflections	5903 R _{int} = 0.0522, R _{sigma} = 0.0341	11878 R _{int} = 0.0468, R _{sigma} = 0.0867	12290 R _{int} = 0.0346, R _{sigma} = 0.0166
Data/restraints/parameters	5903/19/295	11878/39/700	12290/68/703
Goodness-of-fit on F ²	1.081	0.907	1.027
Final R indexes [I ≥ 2σ (I)]	R ₁ = 0.0468, wR ₂ = 0.1215	R ₁ = 0.0498, wR ₂ = 0.1045	R ₁ = 0.0449, wR ₂ = 0.1147
Final R indexes [all data]	R ₁ = 0.0521, wR ₂ = 0.1253	R ₁ = 0.0723, wR ₂ = 0.1108	R ₁ = 0.0476, wR ₂ = 0.1169
Largest diff. peak/hole / e Å ⁻³	0.39/-0.34	0.89/-0.40	0.65/-0.77

Compound	3·C₆H₆	4·(C₆H₁₄)_{0.5}	5-Cl
Crystal Habitus	yellow block	yellow plank	yellow block
Device Type	Bruker D8-Venture	Bruker X8-KappaApex-II	Bruker D8-Venture
Empirical formula	C ₆₀ H ₁₀₀ N ₂ Si ₆	C ₅₇ H ₁₀₀ BrN ₂ OSi ₆	C ₅₁ H ₆₅ N ₂ Si ₆ Cl ₂ ZnBr
Moiety formula	C ₃₈ H ₅₄ N ₂ Si ₆ , C ₆ H ₆	C ₅₄ H ₉₃ BrN ₂ OSi ₆ , 0.5(C ₆ H ₁₄)	C ₅₁ H ₆₅ N ₂ Si ₆ Cl ₂ ZnBr
Formula weight	1065.99	1077.83	1112.94
Temperature/K	123	100	100.02
Crystal system	monoclinic	monoclinic	monoclinic
Space group	P2 ₁ /n	C2/c	P2 ₁
a/Å	13.0663(8)	44.332(4)	12.7947(9)
b/Å	30.2958(16)	13.0678(12)	15.6428(11)
c/Å	17.0458(10)	23.633(2)	15.6732(11)
α/°	90	90	90
β/°	100.382(2)	113.322(5)	100.183(2)
γ/°	90	90	90
Volume/Å ³	6637.2(7)	12573(2)	3087.5(4)
Z	4	8	2
ρ _{calc} /g/cm ³	1.067	1.139	1.197
μ/mm ⁻¹	0.163	0.805	1.280
F(000)	2328.0	4664.0	1180.0
Crystal size/mm ³	0.4 × 0.35 × 0.25	0.16 × 0.08 × 0.06	0.16 × 0.14 × 0.12
Absorption correction	empirical	empirical	empirical
Tmin; Tmax	0.6279; 0.7459	0.5877; 0.7459	0.6665; 0.7460
Radiation	MoKα (λ = 0.71073)	MoKα (λ = 0.71073)	MoKα (λ = 0.71073)
2θ range /°	4.53 to 56°	4.268 to 51.996°	4.522 to 55.994°
Completeness to theta	0.999	0.997	0.999
Index ranges	-17 ≤ h ≤ 17, -40 ≤ k ≤ 40, -22 ≤ l ≤ 22	-54 ≤ h ≤ 54, -16 ≤ k ≤ 16, -29 ≤ l ≤ 29	-16 ≤ h ≤ 16, -20 ≤ k ≤ 20, -20 ≤ l ≤ 20
Reflections collected	236450	144811	85009
Independent reflections	16024 R _{int} = 0.0788, R _{sigma} = 0.0295	12333 R _{int} = 0.0803, R _{sigma} = 0.0410	14912 R _{int} = 0.1080, R _{sigma} = 0.0827
Data/restraints/parameters	16024/54/666	12333/281/662	14912/85/592
Goodness-of-fit on F ²	1.035	1.249	1.038
Final R indexes [I >= 2σ (I)]	R ₁ = 0.0476, wR ₂ = 0.1154	R ₁ = 0.0843, wR ₂ = 0.1656	R ₁ = 0.0438, wR ₂ = 0.0878
Final R indexes [all data]	R ₁ = 0.0646, wR ₂ = 0.1262	R ₁ = 0.0971, wR ₂ = 0.1704	R ₁ = 0.0753, wR ₂ = 0.0993
Largest diff. peak/hole / e Å ⁻³	1.72/-1.06	1.59/-0.73	0.47/-1.06

Compound	5-Br·(C₆H₆)·(C₅H₁₂)	6·(C₆H₁₄)_{0.5}	7·(C₆H₁₄)_{0.5}
Crystal Habitus	yellow plate	yellow block	reddish green plate
Device Type	Bruker D8-Ventron	Bruker D8-Venture	Bruker D8-Venture
Empirical formula	C ₆₂ H ₁₀₀ Br ₁ N ₃ Si ₆ Zn	C ₆₁ H ₁₀₂ Br ₁ N ₃ Si ₆ Zn	C ₁₁₈ H ₂₀₀ N ₄ Na ₂ O ₄ P ₄ Si ₁₂
Moiety formula	C ₅₁ H ₈₇ Br ₁ N ₃ Si ₆ Zn, C ₆ H ₆ , C ₅ H ₁₂	C ₅₈ H ₉₈ Br ₁ N ₃ Si ₆ Zn, C ₃ H ₇	C ₁₁₂ H ₁₉₀ N ₄ Na ₂ O ₄ P ₄ Si ₁₂ , C ₆ H ₁₄
Formula weight	1352.11	1257.17	2249.78
Temperature/K	100.01	150	99.99
Crystal system	monoclinic	triclinic	triclinic
Space group	P2 ₁ /n	P-1	P-1
a/Å	18.7703(11)	13.2913(5)	12.7316(6)
b/Å	15.4637(9)	13.6363(5)	15.7784(8)
c/Å	24.8689(15)	19.2205(7)	19.5916(9)
α/°	90	89.524(2)	71.5555(14)
β/°	93.719(3)	88.737(2)	77.3544(15)
γ/°	90	75.942(2)	70.5045(15)
Volume/Å ³	7203.2(7)	3378.4(2)	3491.0(3)
Z	4	2	1
ρ _{calc} /g/cm ³	1.247	1.197	1.070
μ/mm ⁻¹	3.637	1.280	0.209
F(000)	2840.0	1180.0	1222.0
Crystal size/mm ³	0.2 × 0.08 × 0.03	0.16 × 0.14 × 0.12	0.16 × 0.12 × 0.05
Absorption correction	empirical	empirical	empirical
Tmin; Tmax	0.3268; 0.7533	0.6665; 0.7460	0.6867; 0.7459
Radiation	CuKα (λ = 1.54178)	MoKα (λ = 0.71073)	MoKα (λ = 0.71073)
2θ range /°	5.724 to 129.994°	4.522 to 55.994°	4.302 to 55.998°
Completeness to theta	0.949	0.999	0.999
Index ranges	-22 ≤ h ≤ 21, -18 ≤ k ≤ 18, -29 ≤ l ≤ 29	-16 ≤ h ≤ 16, -20 ≤ k ≤ 20, -20 ≤ l ≤ 20	-16 ≤ h ≤ 16, -20 ≤ k ≤ 20, -25 ≤ l ≤ 25
Reflections collected	84517	85009	103999
Independent reflections	11634 R _{int} = 0.0884, R _{sigma} = 0.0495	14912 R _{int} = 0.1080, R _{sigma} = 0.0827	16839 R _{int} = 0.0808, R _{sigma} = 0.0693
Data/restraints/parameters	11634/36/723	14912/85/592	16839/54/683
Goodness-of-fit on F ²	1.161	1.038	1.039
Final R indexes [I >= 2σ (I)]	R ₁ = 0.0854, wR ₂ = 0.1773	R ₁ = 0.0438, wR ₂ = 0.0878	R ₁ = 0.0587, wR ₂ = 0.1163
Final R indexes [all data]	R ₁ = 0.1011, wR ₂ = 0.1851	R ₁ = 0.0753, wR ₂ = 0.0993	R ₁ = 0.1004, wR ₂ = 0.1293
Largest diff. peak/hole / e Å ⁻³	1.16/-0.80	0.47/-1.06	0.89/-1.57

Compound	9 ·(Et ₂ O) _{2.5}	10 ·(C ₅ H ₁₂) _{0.5}	12
Crystal Habitus	orangish yellow plate	orange needle	brown plate
Device Type	Bruker APEX-II CCD	Bruker D8 Venture	Bruker X8-KappaApexII
Empirical formula	C ₆₂ H ₁₁₂ AgBrF ₃ N ₂ O ₅ SSi ₆	C ₁₁₅ H ₂₀₆ Br ₂ Cu ₂ N ₄ Si ₁₂	C ₅₅ H ₉₆ BrCuN ₂ OSi ₆
Moiety formula	C ₅₂ H ₈₇ AgBrF ₃ N ₂ O ₅ SS ₆ · 2.5(C ₅ H ₁₀ O)	2(C ₅₅ H ₈₇ Br ₂ CuN ₄ Si ₆), C ₅ H ₁₄ , C ₅ H ₁₂	C ₅₅ H ₉₆ BrCuN ₂ OSi ₆
Formula weight	1458.91	2398.56	1113.32
Temperature/K	100	99.99	100
Crystal system	triclinic	trigonal	monoclinic
Space group	P-1	R-3	C2/c
a/Å	12.567(5)	39.6914(11)	21.390(4)
b/Å	14.903(6)	39.6914(11)	13.563(3)
c/Å	22.154(8)	26.4389(9)	46.114(8)
α/°	87.365(16)	90	90
β/°	78.904(15)	90	98.216(4)
γ/°	68.285(15)	120	90
Volume/Å ³	3781(2)	36072(2)	13241(4)
Z	2	9	8
ρ _{calc} /cm ³	1.281	0.994	1.117
μ/mm ⁻¹	0.973	2.614	1.076
F(000)	1542.0	11448.0	4768.0
Crystal size/mm ³	0.3 × 0.3 × 0.12	0.11 × 0.03 × 0.02	0.22 × 0.12 × 0.05
Absorption correction	none	empirical	empirical
Tmin; Tmax	0.5798; 0.7460	0.4132; 0.7533	0.5935; 0.7461
Radiation	MoKα (λ = 0.71073)	CuKα (λ = 1.54178)	MoKα (λ = 0.71073)
2θ range /°	3.69 to 55.998°	4.216 to 135.496°	1.784 to 56°
Completeness to theta	0.997	0.988	0.998
Index ranges	-16 ≤ h ≤ 16, -19 ≤ k ≤ 19, -29 ≤ l ≤ 29	-45 ≤ h ≤ 48, -48 ≤ k ≤ 48, -32 ≤ l ≤ 31	-28 ≤ h ≤ 24, -17 ≤ k ≤ 17, -60 ≤ l ≤ 60
Reflections collected	145409	79539	127859
Independent reflections	18190 [R _{int} = 0.0610, R _{sigma} = 0.0348]	14372 R _{int} = 0.1620, R _{sigma} = 0.1162	15970 R _{int} = 0.2016, R _{sigma} = 0.1460
Data/restraints/parameters	18190/16/785	14372/113/695	15970/126/713
Goodness-of-fit on F ²	1.175	1.059	1.072
Final R indexes [I ≥ 2σ (I)]	R ₁ = 0.0847, wR ₂ = 0.2032	R ₁ = 0.0893, wR ₂ = 0.2532	R ₁ = 0.1135, wR ₂ = 0.3079
Final R indexes [all data]	R ₁ = 0.0940, wR ₂ = 0.2085	R ₁ = 0.1312, wR ₂ = 0.2721	R ₁ = 0.2045, wR ₂ = 0.3799
Largest diff. peak/hole / e Å ⁻³	2.009/-1.79	1.45/-1.06	0.89/-1.57

Compound	14·C ₇ H ₈	15	15-[CuBr(LiPr ₂ Me ₂)(SIDipp)]
Crystal Habitus	dark violet block	clear dark red block	clear dark red plate
Device Type	Bruker D8 Venture	Bruker D8-Venture	Bruker D8-Venture
Empirical formula	C ₆₂ H ₁₀₀ N ₂ OSi ₆	C ₃₅ H ₅₆ N ₂ OSi ₆	C ₆₃ H ₁₀₀ BrCuN ₂ OSi ₆
Moiety formula	C ₃₅ H ₅₆ N ₂ OSi ₆ , C ₇ H ₈	C ₃₅ H ₅₆ N ₂ OSi ₆	C ₃₈ H ₅₈ BrCuN ₂ , C ₃₅ H ₅₆ N ₂ OSi ₆
Formula weight	1062.01	969.87	1684.20
Temperature/K	100.0	123.0	100
Crystal system	triclinic	monoclinic	triclinic
Space group	P-1	P2 ₁ /n	P-1
a/Å	13.0862(14)	13.3150(5)	12.5125(7)
b/Å	14.5312(16)	25.0297(6)	20.5204(11)
c/Å	20.003(2)	19.1829(8)	21.6485(12)
α/°	98.068(4)	90	70.848(4)
β/°	106.095(4)	96.040(3)	78.146(4)
γ/°	112.256(3)	90	73.350(4)
Volume/Å ³	3251.0(6)	6357.6(4)	4992.4(5)
Z	2	4	2
ρ _{calc} /g/cm ³	1.085	1.013	1.120
μ/mm ⁻¹	1.483	0.165	1.798
F(000)	1164.0	2128.0	1820.0
Crystal size/mm ³	0.6 × 0.5 × 0.48	0.29 × 0.28 × 0.12	0.10 × 0.09 × 0.03
Absorption correction	multi-scan	integration	empirical
Tmin; Tmax	0.4795; 0.7535	0.8206; 0.9493	0.5165; 0.7536
Radiation	CuKα (λ = 1.54178)	MoKα (λ = 0.71073)	CuKα (λ = 1.54178)
2θ range /°	4.784 to 135.496°	5.252 to 56°	4.354 to 135.5°
Completeness to theta	0.996	0.995	0.969
Index ranges	-15 ≤ h ≤ 14, -17 ≤ k ≤ 17, -24 ≤ l ≤ 24	-13 ≤ h ≤ 17, -33 ≤ k ≤ 30, -21 ≤ l ≤ 25	-14 ≤ h ≤ 15, -24 ≤ k ≤ 24, -25 ≤ l ≤ 25
Reflections collected	117367	38029	90704
Independent reflections	11753 R _{int} = 0.0549, R _{sigma} = 0.0262	15098 R _{int} = 0.0545, R _{sigma} = 0.1331	17517 R _{int} = 0.1165, R _{sigma} = 0.1180
Data/restraints/parameters	11753/208/667	115098/8/603	17517/772/1177
Goodness-of-fit on F ²	1.042	0.782	1.221
Final R indexes [I ≥ 2σ (I)]	R ₁ = 0.0486, wR ₂ = 0.1201	R ₁ = 0.0462, wR ₂ = 0.0813	R ₁ = 0.2059, wR ₂ = 0.4001
Final R indexes [all data]	R ₁ = 0.0498, wR ₂ = 0.1210	R ₁ = 0.0990, wR ₂ = 0.0897	R ₁ = 0.2460, wR ₂ = 0.4174
Largest diff. peak/hole / e Å ⁻³	0.99/-0.54	0.37/-0.35	1.20/-1.48

Compound	16-Br	16-I	17
Crystal Habitus	yellow plate	yellow needle	colourless block
Device Type	Bruker D8-Venture	Bruker D8-Venture	STOE IPDS-2T
Empirical formula	C ₃₁ H ₄₇ BrN:OSi	C ₃₁ H ₄₇ IN:OSi	C ₃₄ H ₄₀ OSi
Moiety formula	C ₃₁ H ₄₇ BrN:OSi	C ₃₁ H ₄₇ IN:OSi	C ₃₄ H ₄₀ OSi
Formula weight	571.70	618.69	492.75
Temperature/K	100	100.01	100
Crystal system	monoclinic	monoclinic	monoclinic
Space group	P2 ₁ /c	P2 ₁ /n	P2 ₁ /n
a/Å	17.6725(13)	12.670(2)	12.1504(7)
b/Å	11.8242(8)	19.269(3)	14.4088(9)
c/Å	15.9463(11)	26.436(5)	16.4867(10)
α/°	90	90	90
β/°	112.707(4)	99.295(5)	97.315(2)
γ/°	90	90	90
Volume/Å ³	3073.9(4)	6369.4(19)	2862.9(3)
Z	4	8	4
ρ _{calc} /g/cm ³	1.235	1.290	1.143
μ/mm ⁻¹	2.373	1.067	0.888
F(000)	1216.0	2576.0	1064.0
Crystal size/mm ³	0.22 × 0.14 × 0.04	0.12 × 0.08 × 0.04	0.25 × 0.18 × 0.12
Absorption correction	empirical	empirical	empirical
Tmin; Tmax	0.4849; 0.7536	0.3966; 0.7459	0.491661; 0.753578
Radiation	CuKα (λ = 1.54178)	MoKα (λ = 0.71073)	CuKα (λ = 1.54178)
2θ range /°	5.42 to 135.496°	4.642 to 55.998°	8.178 to 139.972°
Completeness to theta	1.000	0.999	0.992
Index ranges	-21 ≤ h ≤ 20, -14 ≤ k ≤ 14, -19 ≤ l ≤ 19	-15 ≤ h ≤ 16, -25 ≤ k ≤ 25, -34 ≤ l ≤ 34	-14 ≤ h ≤ 14, 0 ≤ k ≤ 17, 0 ≤ l ≤ 20
Reflections collected	77518	92616	14762
Independent reflections	5560 R _{int} = 0.0854, R _{sigma} = 0.0318	15365 R _{int} = 0.2253, R _{sigma} = 0.1940	14762 R _{int} = 0.1018, R _{sigma} = 0.0541
Data/restraints/parameters	5560/6/335	15365/12/671	14762/0/337
Goodness-of-fit on F ²	1.115	1.051	1.032
Final R indexes [I ≥ 2σ (I)]	R ₁ = 0.0975, wR ₂ = 0.2917	R ₁ = 0.0958, wR ₂ = 0.2081	R ₁ = 0.0857, wR ₂ = 0.2360
Final R indexes [all data]	R ₁ = 0.1048, wR ₂ = 0.3043	R ₁ = 0.1982, wR ₂ = 0.2481	R ₁ = 0.1021, wR ₂ = 0.2556
Largest diff. peak/hole / e Å ⁻³	2.16/-0.77	1.97/-1.79	0.39/-0.80

Compound	18	19	19- IMe ₄ ·(C ₄ H ₁₀ O) _{0.5}
Crystal Habitus	colourless block	colourless plank	yellow block
Device Type	Bruker D8-Venture	Bruker D8-Venture	Bruker D8-Venture
Empirical formula	C ₃₀ H ₃₆ N ₂ Si	C ₃₀ H ₃₆ O ₂ Si	C ₁₁₄ H ₁₃₄ N ₂ O ₂ Si ₂
Moiety formula	C ₃₀ H ₃₆ N ₂ Si	C ₃₀ H ₃₆ O ₂ Si	2(C ₅₅ H ₆₂ N ₂ O ₂ Si), C ₄ H ₁₀ O
Formula weight	713.05	686.97	1696.42
Temperature/K	100	100	100
Crystal system	monoclinic	triclinic	triclinic
Space group	C2/c	P-1	P-1
a/Å	29.7548(15)	9.8183(5)	11.3396(8)
b/Å	8.3388(4)	11.4267(6)	11.5524(8)
c/Å	22.2124(12)	17.9678(10)	22.1091(16)
α/°	90	71.491(2)	97.923(2)
β/°	130.4416(14)	89.464(2)	94.997(3)
γ/°	90	89.154(2)	119.042(2)
Volume/Å ³	4194.5(4)	1911.32(18)	2467.9(3)
Z	4	2	1
ρ _{calc} /g/cm ³	1.129	1.194	1.141
μ/mm ⁻¹	0.091	0.100	0.091
F(000)	1536.0	736.0	914.0
Crystal size/mm ³	0.26 × 0.14 × 0.13	0.26 × 0.1 × 0.09	0.35 × 0.34 × 0.26
Absorption correction	empirical	empirical	empirical
Tmin; Tmax	0.6991; 0.7460	0.6752; 0.7459	0.7137; 0.7459
Radiation	MoKα (λ = 0.71073)	MoKα (λ = 0.71073)	MoKα (λ = 0.71073)
2θ range /°	4.82 to 55.996°	4.778 to 55.996°	4.498 to 56°
Completeness to theta	0.999	0.999	0.998
Index ranges	-39 ≤ h ≤ 39, -11 ≤ k ≤ 11, -29 ≤ l ≤ 29	-12 ≤ h ≤ 12, -15 ≤ k ≤ 15, -23 ≤ l ≤ 23	-14 ≤ h ≤ 14, -15 ≤ k ≤ 15, -29 ≤ l ≤ 29
Reflections collected	73662	86378	125497
Independent reflections	5058 R _{int} = 0.0476, R _{sigma} = 0.0173	9192 R _{int} = 0.1034, R _{sigma} = 0.0499	11892 R _{int} = 0.0662, R _{sigma} = 0.0332
Data/restraints/parameters	5058/0/247	9192/0/472	11892/231/672
Goodness-of-fit on F ²	1.034	1.059	1.057
Final R indexes [I >= 2σ (I)]	R ₁ = 0.0531, wR ₂ = 0.1408	R ₁ = 0.0508, wR ₂ = 0.1059	R ₁ = 0.1134, wR ₂ = 0.2781
Final R indexes [all data]	R ₁ = 0.0663, wR ₂ = 0.1499	R ₁ = 0.0819, wR ₂ = 0.1172	R ₁ = 0.1359, wR ₂ = 0.2934
Largest diff. peak/hole / e Å ⁻³	0.32/-0.44	0.32/-0.37	1.66/-0.68

Compound	19-HBr	19-HI	19-HOtBu ^F
Crystal Habitus	colourless block	colourless block	colourless plate
Device Type	STOE IPDS-2T	STOE IPDS-2T	Bruker D8-Venture
Empirical formula	C ₄₈ H ₅₁ BrO ₃ Si	C ₄₈ H ₅₁ IO ₃ Si	C ₅₂ H ₅₁ O ₃ F ₉ Si
Moiety formula	C ₄₈ H ₅₁ BrO ₃ Si	C ₄₈ H ₅₁ IO ₃ Si	C ₅₂ H ₅₁ O ₃ F ₉ Si
Formula weight	767.88	814.88	923.01
Temperature/K	123	123	100.11
Crystal system	monoclinic	monoclinic	hexagonal
Space group	P2 ₁ /n	P2 ₁ /n	P6 ₃
a/Å	12.4322(4)	12.4133(4)	11.1007(7)
b/Å	20.9121(6)	20.9386(6)	11.1007(7)
c/Å	16.1865(4)	16.3290(5)	65.415(4)
α/°	90	90	90
β/°	105.002(2)	104.354(3)	90
γ/°	90	90	120
Volume/Å ³	4064.8(2)	4111.7(2)	6980.9(10)
Z	4	4	6
ρ _{calc} /g/cm ³	1.255	1.316	1.317
μ/mm ⁻¹	1.078	0.845	0.129
F(000)	1616.0	1688.0	2892.0
Crystal size/mm ³	0.18 × 0.06 × 0.03	0.3 × 0.2 × 0.1	0.14 × 0.12 × 0.05
Absorption correction	integration	empirical	empirical
Tmin; Tmax	0.5432; 0.7446	n.a.	0.4279; 0.7459
Radiation	MoKα (λ = 0.71073)	MoKα (λ = 0.71073)	MoKα (λ = 0.71073)
2θ range /°	5.376 to 55.996°	5.158 to 51.994°	4.236 to 55.994°
Completeness to theta	0.998	0.999	0.999
Index ranges	-16 ≤ h ≤ 16, -27 ≤ k ≤ 26, -21 ≤ l ≤ 20	-15 ≤ h ≤ 15, -25 ≤ k ≤ 25, -20 ≤ l ≤ 20	-14 ≤ h ≤ 11, -14 ≤ k ≤ 12, -86 ≤ l ≤ 85
Reflections collected	43023	56986	82463
Independent reflections	9794 R _{int} = 0.1419, R _{sigma} = 0.0903	8054 R _{int} = 0.0357, R _{sigma} = 0.0297	11115 R _{int} = 0.1161, R _{sigma} = 0.1267
Data/restraints/parameters	9794/0/500	8054/0/500	11115/212/683
Goodness-of-fit on F ²	0.988	1.253	1.048
Final R indexes [I ≥ 2σ (I)]	R ₁ = 0.0613, wR ₂ = 0.1519	R ₁ = 0.0820, wR ₂ = 0.1799	R ₁ = 0.0770, wR ₂ = 0.1326
Final R indexes [all data]	R ₁ = 0.0854, wR ₂ = 0.1647	R ₁ = 0.0936, wR ₂ = 0.1838	R ₁ = 0.1420, wR ₂ = 0.1531
Largest diff. peak/hole / e Å ⁻³	0.86/-0.67	1.97/-1.79	0.78/-0.53

Compound	19-SiHCl ₃	20-Et ₂ O	19-Cl ₂
Crystal Habitus	colourless plate	colourless block	colourless block
Device Type	Bruker X8-KappaApexII	Bruker D8 Venture	Bruker D8-Venture
Empirical formula	C ₁₈ H ₅ O ₂ Si ₂ Cl ₃	C ₅₆ H ₇₀ I ₂ O ₄ Si ₂	C ₁₈ H ₅ O ₂ SiCl ₂
Moiety formula	C ₁₈ H ₅ O ₂ Si ₂ Cl ₃	C ₂₈ H ₃₆ I ₂ O ₂ Si ₂ , C ₈ H ₁₀ O	C ₁₈ H ₅ O ₂ SiCl ₂
Formula weight	822.41	1117.10	757.87
Temperature/K	100	100.0	99.99
Crystal system	triclinic	triclinic	monoclinic
Space group	P-1	P-1	P2 ₁ /n
a/Å	12.109(2)	11.884(2)	12.5347(11)
b/Å	12.489(2)	15.337(3)	20.9468(19)
c/Å	15.639(3)	15.656(3)	16.1614(14)
α/°	77.686(8)	107.670(7)	90
β/°	88.847(8)	95.116(8)	104.614(3)
γ/°	70.382(6)	92.619(7)	90
Volume/Å ³	2173.2(7)	2700.1(9)	4106.1(6)
Z	2	2	4
ρ _{calc} /g/cm ³	1.257	1.374	1.226
μ/mm ⁻¹	0.304	1.252	0.225
F(000)	868.0	1144.0	1608.0
Crystal size/mm ³	0.27 × 0.12 × 0.02	0.25 × 0.14 × 0.12	0.22 × 0.11 × 0.06
Absorption correction	empirical	empirical	empirical
Tmin; Tmax	0.3822; 0.7461	0.5936; 0.7460	0.6881; 0.7465
Radiation	MoKα (λ = 0.71073)	MoKα (λ = 0.71073)	MoKα (λ = 0.71073)
2θ range /°	4.562 to 50.5°	4.172 to 55.998°	4.68 to 56°
Completeness to theta	0.952	0.999	0.999
Index ranges	-14 ≤ h ≤ 14, -14 ≤ k ≤ 14, -18 ≤ l ≤ 18	-15 ≤ h ≤ 15, -20 ≤ k ≤ 20, -20 ≤ l ≤ 20	-16 ≤ h ≤ 16, -27 ≤ k ≤ 27, -21 ≤ l ≤ 20
Reflections collected	52246	135361	123152
Independent reflections	7486 R _{int} = 0.0671, R _{sigma} = 0.0454	13017 R _{int} = 0.0945, R _{sigma} = 0.0456	9917 R _{int} = 0.0416, R _{sigma} = 0.0167
Data/restraints/parameters	7486/114/508	13017/50/597	9917/0/510
Goodness-of-fit on F ²	1.393	1.048	1.029
Final R indexes [I >= 2σ (I)]	R ₁ = 0.1062, wR ₂ = 0.2475	R ₁ = 0.0897, wR ₂ = 0.2535	R ₁ = 0.0362, wR ₂ = 0.0925
Final R indexes [all data]	R ₁ = 0.1140, wR ₂ = 0.2503	R ₁ = 0.1116, wR ₂ = 0.2798	R ₁ = 0.0428, wR ₂ = 0.0965
Largest diff. peak/hole / e Å ⁻³	0.80/-0.61	7.46/-2.49	0.36/-0.38

Compound	19-ZnMe ₂	19-PCl ₃	21-Cl
Crystal Habitus	colourless block	colourless plate	colourless block
Device Type	Bruker X8-KappaApexII	Bruker D8-Venture	Bruker X8-KappaApexII
Empirical formula	C ₅₀ H ₅₆ O ₂ SiZn	C ₄₈ H ₅₆ O ₂ SiPCl ₃	C ₂₃ H ₂₅ Cl ₃ OSi
Moiety formula	C ₅₀ H ₅₆ O ₂ SiZn	C ₄₈ H ₅₆ O ₂ SiPCl ₃	C ₂₃ H ₂₅ Cl ₃ OSi
Formula weight	782.40	824.29	463.88
Temperature/K	100	100	100
Crystal system	monoclinic	triclinic	monoclinic
Space group	P2 ₁ /n	P-1	P2 ₁ /n
a/Å	11.2871(10)	12.1337(6)	8.8187(5)
b/Å	19.7363(18)	12.5248(6)	26.0202(17)
c/Å	19.1096(17)	15.4971(8)	10.5303(7)
α/°	90	77.185(3)	90
β/°	91.165(3)	88.531(3)	102.112(2)
γ/°	90	70.588(3)	90
Volume/Å ³	4256.1(7)	2162.95(19)	2362.5(3)
Z	4	2	4
ρ _{calc} /g/cm ³	1.221	1.266	1.304
μ/mm ⁻¹	0.643	0.315	0.452
F(000)	1664.0	868.0	968.0
Crystal size/mm ³	0.25 × 0.22 × 0.12	0.36 × 0.15 × 0.09	0.35 × 0.15 × 0.1
Absorption correction	empirical	empirical	empirical
Tmin; Tmax	0.5804; 0.7459	0.6507; 0.7461	0.6501; 0.7460
Radiation	MoKα (λ = 0.71073)	MoKα (λ = 0.71073)	MoKα (λ = 0.71073)
2θ range /°	4.23 to 55.996°	5.234 to 56°	5.49 to 56°
Completeness to theta	0.998	0.997	0.998
Index ranges	-13 ≤ h ≤ 14, -26 ≤ k ≤ 26, -25 ≤ l ≤ 21	-16 ≤ h ≤ 16, -16 ≤ k ≤ 16, -20 ≤ l ≤ 20	-11 ≤ h ≤ 9, -34 ≤ k ≤ 34, -13 ≤ l ≤ 13
Reflections collected	72086	85648	39921
Independent reflections	10238 R _{int} = 0.1047, R _{sigma} = 0.0759	10414 R _{int} = 0.0781, R _{sigma} = 0.0532	5699 [R _{int} = 0.0351, R _{sigma} = 0.0204]
Data/restraints/parameters	10238/61/531	10414/0/508	5699/18/268
Goodness-of-fit on F ²	1.016	1.252	1.016
Final R indexes [I ≥ 2σ (I)]	R ₁ = 0.0468, wR ₂ = 0.1147	R ₁ = 0.0794, wR ₂ = 0.1523	R ₁ = 0.0334, wR ₂ = 0.0856
Final R indexes [all data]	R ₁ = 0.0768, wR ₂ = 0.1271	R ₁ = 0.0927, wR ₂ = 0.1577	R ₁ = 0.0396, wR ₂ = 0.0901
Largest diff. peak/hole / e Å ⁻³	0.34/-0.52	0.72/-0.52	0.34/-0.34

Compound	21-Br	21-I	22
Crystal Habitus	colourless block	clear colourless plate	Yellowish/colourless plate
Device Type	Bruker X8-KappaApexII	STOE IPDS-2T	Bruker D8-Venture
Empirical formula	C ₂₃ H ₂₅ BrOSi	C ₂₃ H ₂₅ IOSi	C ₂₈ H ₃₁ N ₄ O ₂ Si ₃
Moiety formula	C ₂₃ H ₂₅ BrOSi	C ₂₃ H ₂₅ IOSi	C ₂₈ H ₃₁ N ₄ O ₂ Si ₃
Formula weight	597.26	738.23	1083.74
Temperature/K	100	123	100
Crystal system	monoclinic	triclinic	monoclinic
Space group	P2 ₁ /n	P-1	P2 ₁ /c
a/Å	7.9490(4)	8.2207(3)	19.4171(10)
b/Å	12.9044(5)	11.5250(4)	14.6826(8)
c/Å	24.0091(10)	14.4153(5)	22.5945(11)
α/°	90	78.432(3)	90
β/°	97.8361(16)	74.871(3)	90.441(4)
γ/°	90	86.966(3)	90
Volume/Å ³	2439.79(19)	1291.64(8)	6441.4(6)
Z	4	2	4
ρ _{calc} /cm ³	1.626	1.898	1.118
μ/mm ⁻¹	5.022	0.163	1.017
F(000)	1184.0	2328.0	2352.0
Crystal size/mm ³	0.35 × 0.25 × 0.22	0.35 × 0.18 × 0.05	0.22 × 0.16 × 0.05
Absorption correction	empirical	integration	empirical
Tmin; Tmax	0.1655; 0.7461	0.4429; 0.7306	0.4235; 0.7533
Radiation	MoKα (λ = 0.71073)	MoKα (λ = 0.71073)	CuKα (λ = 1.54178)
2θ range /°	5.222 to 55.998°	5.96 to 56°	7.18 to 135.494°
Completeness to theta	0.998	0.999	1.000
Index ranges	-10 ≤ h ≤ 10, -17 ≤ k ≤ 17, -31 ≤ l ≤ 31	-10 ≤ h ≤ 10, -15 ≤ k ≤ 15, -19 ≤ l ≤ 19	-21 ≤ h ≤ 23, -17 ≤ k ≤ 17, -27 ≤ l ≤ 24
Reflections collected	50826	23273	81131
Independent reflections	5875 [R _{int} = 0.0826, R _{sigma} = 0.0479]	6233 R _{int} = 0.0699, R _{sigma} = 0.0499	11672 R _{int} = 0.1129, R _{sigma} = 0.0639
Data/restraints/parameters	5875/0/268	6233/0/268	11672/97/776
Goodness-of-fit on F ²	1.086	0.893	1.069
Final R indexes [I ≥ 2σ (I)]	R ₁ = 0.0387, wR ₂ = 0.0922	R ₁ = 0.0226, wR ₂ = 0.0473	R ₁ = 0.0755, wR ₂ = 0.1687
Final R indexes [all data]	R ₁ = 0.0471, wR ₂ = 0.0955	R ₁ = 0.0321, wR ₂ = 0.0487	R ₁ = 0.0992, wR ₂ = 0.1823
Largest diff. peak/hole / e Å ⁻³	0.99/-0.66	0.65/-0.66	0.72/-0.75

5.3 Supporting Crystal structures

5.3.1 $\text{SiH}[\text{SiBr}\{\text{OC}(\text{CH}_2)\text{Me}\}\text{Tbb}](\text{SIDipp})$ (4)

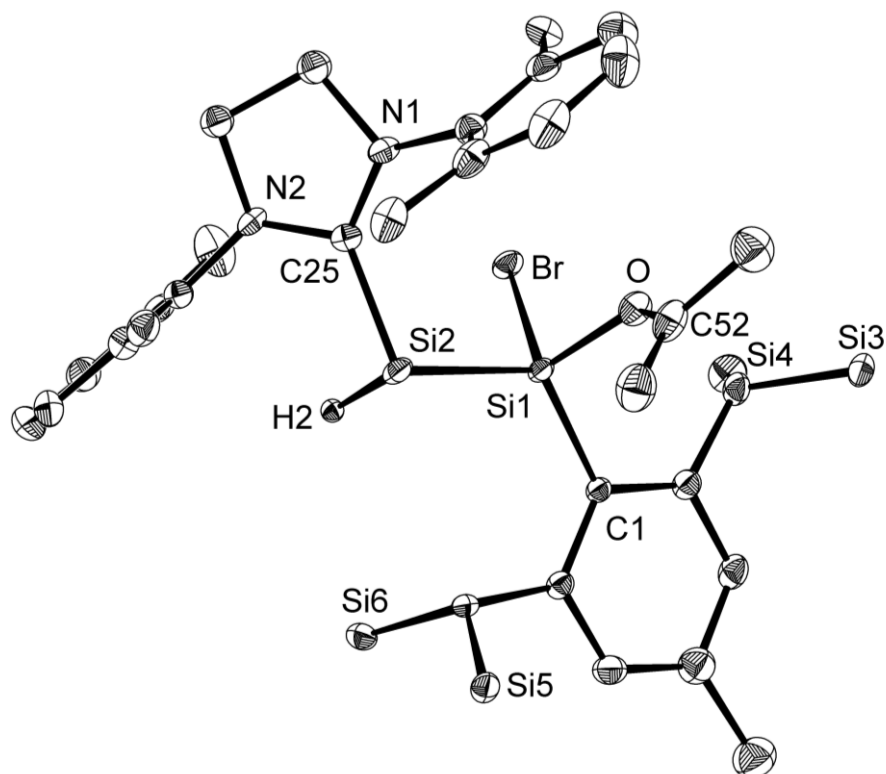


Figure 91. Molecular structure of $4\cdot(\text{C}_6\text{H}_{14})_{0.5}$. Thermal ellipsoids are set to 50 % probability; Hydrogen atoms except for H2 and the methyl groups except for that in the $\text{OC}(\text{=CH}_2)\text{Me}$ group were omitted for clarity. Selected bond lengths [Å], bond angles [°], and torsion angles [°]: Si1-Si2 2.355(2), Si1-Br 2.284(1), Si1-O 1.681(4), Si1-C1 1.921(5), Si2-C25 1.930(5); Br-Si1-Si2 106.04(6), Br-Si1-O 100.1(1), Br-Si1-C1 108.8(2), O-Si1-Si2 111.9(1), O-Si1-C1 105.4(2), C1-Si1-Si2 122.4(2), Si1-Si2-C25 103.3(2), Si1-O-C25 127.3(2); C1-Si1-Si2-C28 $-158.1(2)$. See also Scheme 14 on page 41.

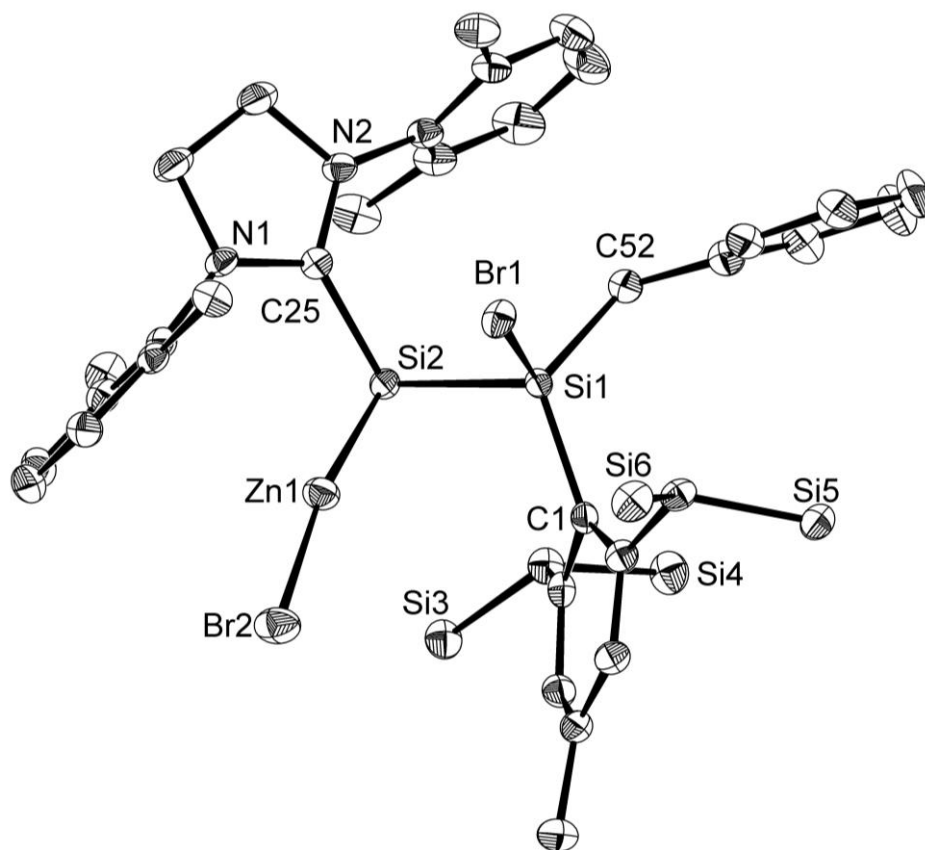
5.3.2 Si(ZnBr)(SiBrCH₂PhTbb)(SIDipp) (6)

Figure 92. Molecular structure of the monomeric moiety **6**·0.5(*n*-C₄H₉). Thermal ellipsoids are set to 50 % probability. Hydrogen atoms, the methyl groups and small side occupancies at the [Si1, Br1, C52] moiety (ca. 8 %) and at the *t*Bu group (ca. 15 %) were omitted for clarity. Selected bond lengths (Å) and angles (°): Si1–Si2 2.342(1), Si1–Br1 2.3041(9), Si1–C1 1.923(3), Si1–C52 1.888(3), Zn–Si2 2.3256(8), Zn–Br2 2.2809(5), Si2–C25 1.923(3); Si2–Zn–Br2 168.13(3), Si1–Si2–Zn 90.63(3), Zn–Si2–C25 101.12(8), Si1–Si2–C25 107.67(8), Br1–Si1–Si2 102.45(4), C1–Si1–Br1 110.18(8), Br1–Si1–C52 102.9(1), Si2–Si1–C52 111.9(1), C1–Si1–C52 119.1(1), C1–Si1–Si2 108.84(8); Zn–Si2–Si1–C52 –171.62(9), C1–Si1–Si2–C25 156.5(1). For the derivatives **5-Br**·(C₆H₅)·(*n*-C₄H₉) and **5-Cl** see Figure 23 on page 47.

5.3.3 SiHBr(OAr^{Mes})₂ (**19-HBr**) and SiHI(OAr^{Mes})₂ (**19-HI**)

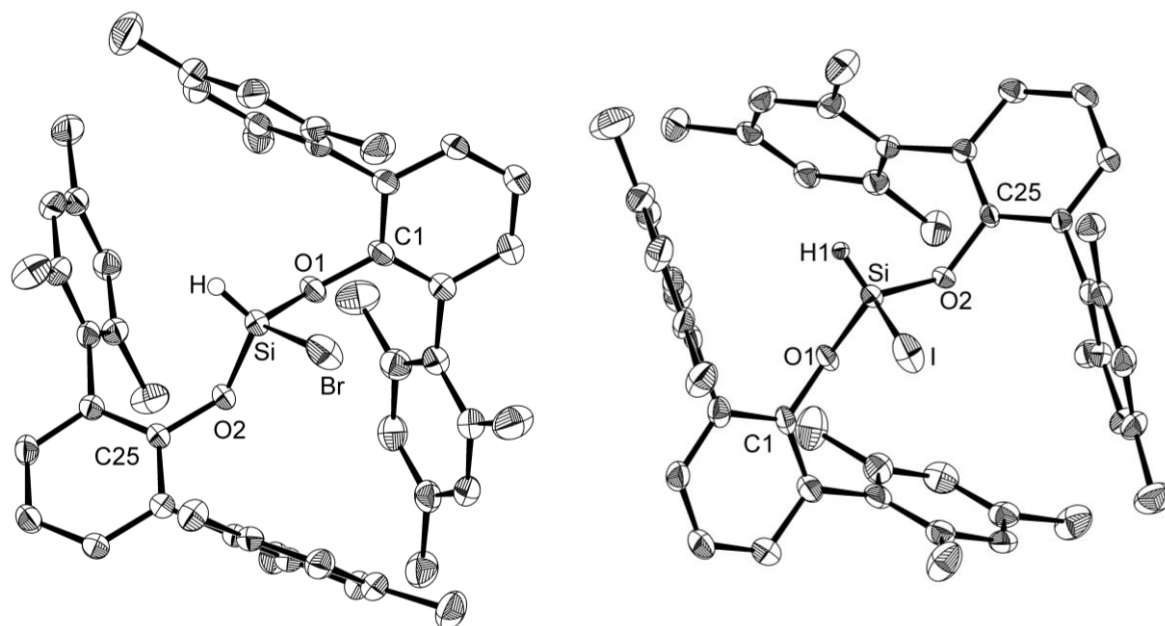


Figure 93. Molecular structure of **19-HBr** (left) and **19-HI** (right); thermal ellipsoids are set to 50 % probability and hydrogen atoms except for the Si-H atoms are omitted for simplicity. The structural data contain a crystallographic site occupancy (ca. 32 % disorder) which was solved independently. Selected bond lengths (\AA) and angles ($^\circ$): **19-HBr**: Si-Br 2.213(1), Si-O1 1.611(2), Si-O2 1.645(2), O1-C1 1.386(3), O2-C25 1.383(3); O1-Si-O2 101.9(1), O1-Si-Br 107.31(8), O2-Si-Br 112.26(8); **19-HI**: Si-I 2.415(2), Si-O1 1.625(4), Si-O2 1.633(4), O1-C1 1.384(7), O2-C25 1.384(6); O1-Si-I 107.9(2), O1-Si-O2 102.6(2), 2-Si-I 111.7(2), C1-O1-Si 134.2(4), C25-O2-Si 129.8(4).

Single crystals of the silanes **19-HBr** and **19-HI** were repeatedly obtained from solutions of **19-BBr₃** and **19-BI₃**, respectively (Figure 93). Expectedly, both compounds are isostructural to their lighter derivative **19-HCl** (see reference ^[385]) and are closely related to the other congeners **19-AB**.

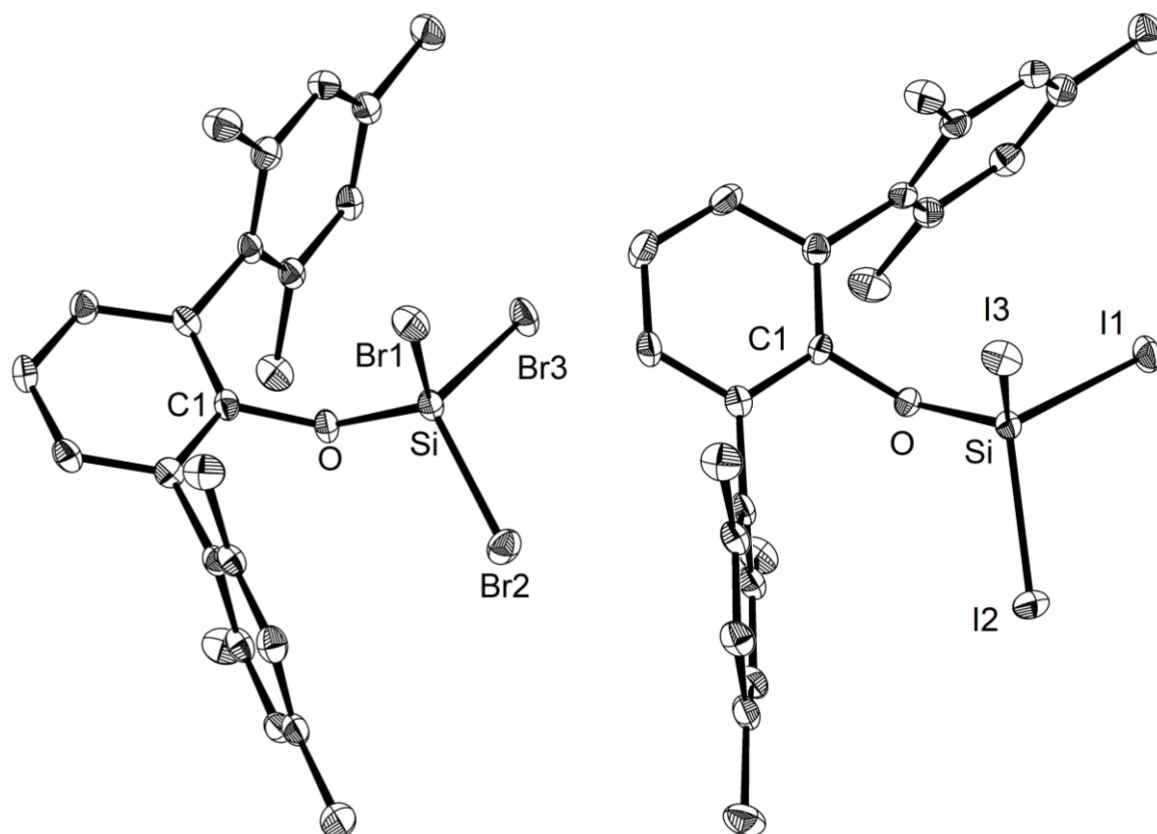
5.3.4 $\text{SiBr}_3\text{OAr}^{\text{Mes}}$ and $\text{SiI}_3\text{OAr}^{\text{Mes}}$ (**21-Br** and **21-I**)

Figure 94. Molecular structure of **21-Br** (left) and **21-I** (right). Thermal ellipsoids are set to 50 % probability; hydrogen atoms are omitted for simplicity. Selected bond lengths (\AA) and angles ($^\circ$): **21-Cl**: Si-O 1.598(1), Si-Cl1 2.0130(5), Si-Cl2 2.0157(5), Si-Cl3 2.0049(6), O-C1 1.392(2); Si-O-C1 135.31(9), Cl1-Si-Cl2 107.72(3), Cl2-Si-Cl3 108.61(3), Cl3-Si-Cl1 111.55(3), O-Si-Cl1 112.03(4), O-Si-Cl2 109.69(4), O-Si-Cl3 107.19(4); C1-O-Si-Cl1 $-4.9(1)$. **21-Br**: Si-O 1.599(2), Si-Br1 2.1886(9), Si-Br2 2.1751(9), Si-Br3 2.1911(9), O-C1 1.389(3); Si-O-C1 138.5(2), Br1-Si-Br3 109.12(4), Br2-Si-Br1 110.61(4), Br2-Si-Br3 108.37(4), O-Si-Br1 111.34(9), O-Si-Br2 108.42(9), O-Si-Br3 108.91(8); C1-O-Si-Br1 3.1(3). **21-I**: Si-O 1.609(2), I1-Si 2.4180(7), I2-Si 2.4245(7), I3-Si 2.4290(8), O-C1 1.399(3); Si-O-C1 135.9(2), I1-Si-I2 110.47(3), I1-Si-I3 110.40(3), I2-Si-I3 107.92(3), O-Si-I2 108.14(7), O-Si-I3 108.05(7), O-Si-I1 111.74(7); C1-O-Si-I1 4.0(3). For a depiction of compound **21-Cl**, see **Figure 76** on page 143.

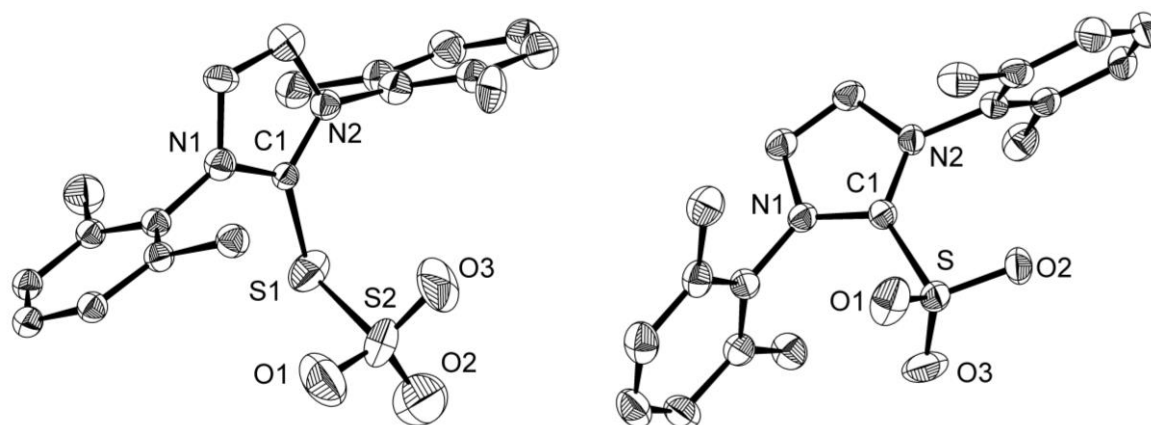
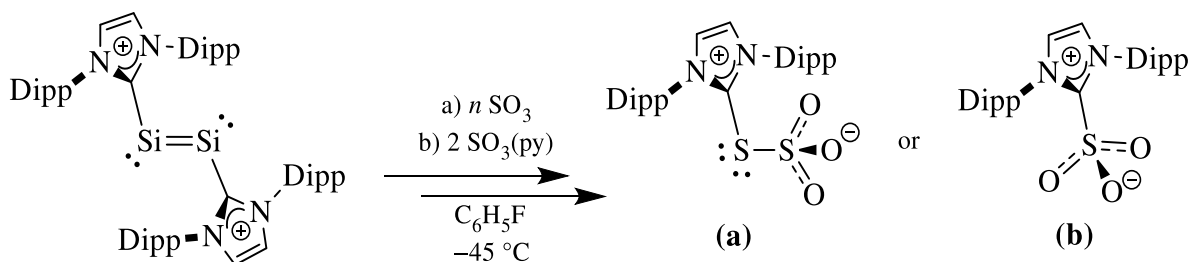
5.3.5 **S(SO₃)(IDipp)·C₆H₆ and SO₃(IDipp)**

Figure 95. Molecular structures of **S(SO₃)(IDipp)·C₆H₆** (left) and **SO₃(IDipp)** (right). Thermal ellipsoids are set to 50 % probability; peripheral methyl groups, hydrogen atoms and a cocrystallized benzene molecule are omitted for simplicity. Selected bond lengths (Å) and angles (°): **S(SO₃)(IDipp)·C₆H₆**: S1-S2 2.171(3), S1-C1 1.801(7), S2-O1 1.428(5), S2-O3 1.424(5), S2-O2 1.434(6); C1-S1-S2 104.3(3), O1-S2-S1 106.3(3), O1-S2-O2 115.0(4), O3-S2-S1 104.9(3), O3-S2-O1 116.4(4), O3-S2-O2 112.6(4), O2-S2-S1 99.3(3). **SO₃(IDipp)**: S-C1 1.818(3), S-O1 1.437(2), S-O2 1.436(2), S-O3 1.432(2); O1-S-C1 103.2(1), O2-S-O1 115.3(2), O2-S-C1 103.1(1), O3-S-O1 114.4(2), O3-S-O2 115.3(2), O3-S-C1 103.1(1).

Diluted SO₃ vapors in an argon stream were injected in a dark red, freezing fluorobenzene suspension of Si₂(IDipp)₂ at about -45 °C, whereupon the color gradually faded. Colorless crystals of **S(SO₃)(IDipp)·C₆H₆** were obtained upon workup from benzene/n-hexane mixtures. Unfortunately, no spectroscopic data can be given for certain due to the low selectivity of the rapid redox reaction. Colorless crystals of **SO₃(IDipp)** were obtained using SO₃(pyridine) instead. The fate of the silicon atoms remains elusive in either case (Scheme 42).



Scheme 69. Formation of **S(SO₃)(IDipp)** (a) and **SO₃(IDipp)** (b); py = pyridine.

S(SO₃)(IDipp) can be seen as an unprecedented complex of SO₃ and the imidazolium thione S=C{N(Dipp)CH}₂, but is better described as a zwitterionic S-alkylthiosulfate (“Bunte salt”, general formula R-S-SO₃M). Although this class of compounds is well known in the literature, the formation is in this case unexpected because it requires the full reduction of sulfur from the formal oxidation state +VI (in SO₃) to -II (arguably 0) (in S(SO₃)(IDipp)) by the Si(0) compound in presence of excess SO₃. The C1-S1 distance of 1.801(7) Å as well as the wide C1-S1-S2 angle (104.3(3)°) are indicative for a S-C single bond and stereoactive electron lone pairs with high s character at the S1 atom. Also, the S1-S2 distance (2.171(3) Å) lies well within

the range reported for Bunte salts (Table 38). The data obtained for $\text{SO}_3(\text{IDipp})$ are in between those of $\text{S}(\text{SO}_3)(\text{IDipp})$ and the smaller NHC adduct $\text{SO}_3(\text{IiPr}_2\text{Me}_2)$.^[493] Thus, no further differentiation should be done at this point. But based only on structural data, the classification of the fairly air- and water stable $\text{SO}_3(\text{IiPr}_2\text{Me}_2)$ as an “carbene adduct” of SO_3 rather than a zwitterionic molecule can be questioned.

Table 38. Structural data of $\text{S}(\text{SO}_3)(\text{IDipp})$, $\text{SO}_3(\text{IDipp})$ and related compounds from the literature.

	C1-S / Å	S1-S2 / Å	∅S-O / Å	C1-S1-S2 / °	Reference
$\text{S}(\text{SO}_3)(\text{IDipp})$	1.801(7)	2.171(3)	1.429(5)	104.3(3)	This work
$\text{SO}_3(\text{IDipp})$	1.818(3)	-	1.435(2)	-	This work
$\text{SO}_3(\text{IiPr}_2\text{Me}_2)$	1.822(2)	-	1.435(2)	-	[493]
$[\text{NH}_4][(\text{C}_6\text{F}_5)\text{SSO}_3]$	1.747(6)	2.092(2)	1.433(5)	101.7(2)	[494]
$-\text{O}_3\text{S}-\text{S}-\text{CH}_2\text{CR}_2^+$	1.810(1)	2.1907(6)	1.450(1)	97.07(6)	[495]
$\gamma\text{-SO}_3$	-	-	1.40 ^A	-	[496]

A: $\gamma\text{-SO}_3$ consists of $\mu^2\text{-O}$ bridged trimers; the average distance to the exocyclic O atoms is given.

$\text{CR}_2^+ = \text{C}\{\text{N}(\text{H})\text{CH}_2\}_2^+$

5.3.6 $[\text{Cu}(\text{IiPr}_2\text{Me}_2)(\text{SIDipp})]\text{Br}$ and $[\text{CuBr}(\text{IiPr}_2\text{Me}_2)(\text{SIDipp})]$

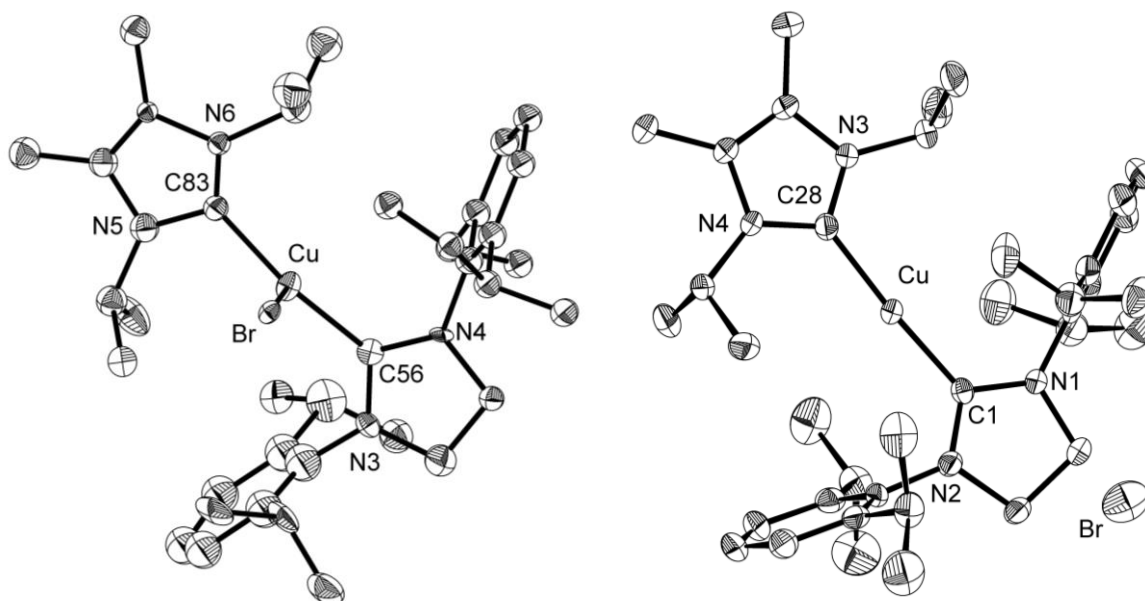


Figure 96. Molecular structures of $[\text{CuBr}(\text{IiPr}_2\text{Me}_2)(\text{SIDipp})]$ (left) and $[\text{Cu}(\text{IiPr}_2\text{Me}_2)(\text{SIDipp})]\text{Br}$ (right). $[\text{CuBr}(\text{IiPr}_2\text{Me}_2)(\text{SIDipp})]$ was obtained as a cocrystal with compound **15** (see Figure 49 on page 93) and its structural data contain crystallographic site occupancies (ca. 39 % disorder at the IiPr_2Me_2 and 44 % at one iPr group of the SIDipp) which were solved independently. Thermal ellipsoids are set to 30 % (left) or 50 % (right) probability; hydrogen atoms are omitted for simplicity. Selected bond lengths (Å) and angles (°): **$[\text{CuBr}(\text{IiPr}_2\text{Me}_2)(\text{SIDipp})]$** : Cu-Br 2.514(2), Cu-C83 1.93(2), Cu-C56 1.92(2); C83-Cu-C56 159.1(6), Br-Cu-C56 101.1(4), Br-Cu-C83 99.4(4). **$[\text{Cu}(\text{IiPr}_2\text{Me}_2)(\text{SIDipp})]\text{Br}$** : Cu-C1 1.913(3), Cu-C28 1.921(3), Cu-Br 6.4; C1-Cu-C28 175.6(2).

A low-quality structure of the neutral complex $[\text{CuBr}(\text{IiPr}_2\text{Me}_2)(\text{SIDipp})]$ was obtained from a cocrystal with compound **15** from *n*-hexane at $-30\text{ }^\circ\text{C}$. Although no close contact between the

molecules was observed,⁶⁵ independent crystallization from n-hexane at ambient temperature instead resulted in the formation of the separated ion pair [Cu(IiPr₂Me₂)(SIDipp)]Br (Figure 96). This is interpreted as a sign for some attractive interactions between compounds **14** and **15** and Cu(I) complexes that also manifested in the increased solubility. However, all obtained structural data of [CuBr(IiPr₂Me₂)(SIDipp)] and [Cu(IiPr₂Me₂)(SIDipp)]Br lie within the typical range (Table 39).

Table 39. Structural data of [CuBr(IiPr₂Me₂)(SIDipp)], [Cu(IiPr₂Me₂)(SIDipp)]Br and related complexes.

Complex	Cu-X /Å	Cu-C ^{NHC} /Å	C-Cu-C /°	Σ _{Cu} ^A /°	τ(NHC) ^B /°	Reference
[CuBr(IiPr ₂ Me ₂)(SIDipp)] ^c	2.514(2)	1.93(2), 1.92(2)	159.1(6)	359.6(5)	5.6(9)	This work
[Cu(IiPr ₂ Me ₂)(SIDipp)]Br	>6.4	1.921(3), 1.913(3)	175.6(2)	-	2.8(2)	This work
[CuCl(IiPr ₂ H ₂) ₂]	2.367(1)	1.921(4), 1.938(4)	133.5(2)	360.0(1)	97.9(2)	[304]
[CuBr(SIDipp)]	2.222(1)	1.880(7)	-	-	-	[135]

A: Sum of angles at three-coordinated Cu atoms; **B:** twist angle between the best planes of the central rings of the NHC ligands. **C:** medium-quality from a cocrystal with compound **15**, see footnote 26 on page 93.

⁶⁵ The shortest intermolecular interaction of the free bromide anion was found to be approx. 3 Å towards one CH₃ group of the SIDipp backbone of **15**, weak interactions between peripheral alkyl groups are not considered.

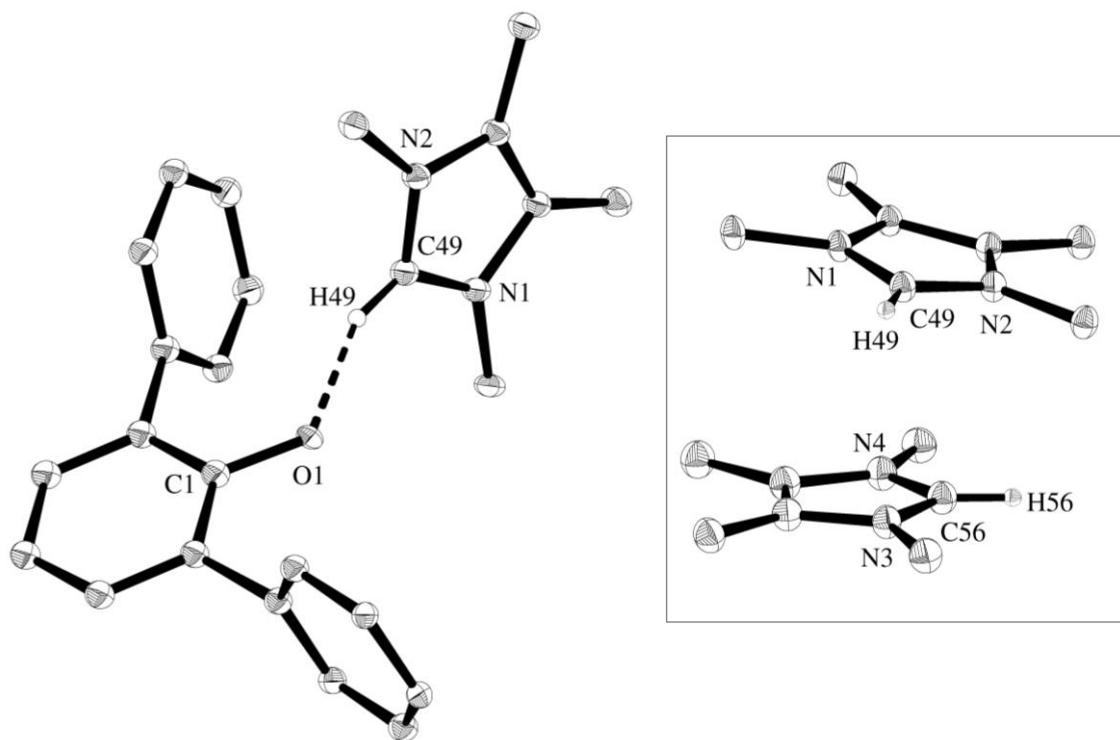
5.3.7 $[\text{H}(\text{IME}_4)][\text{OAr}^{\text{Mes}}]\cdot\text{C}_6\text{H}_6$ 

Figure 97. Molecular structure of a single $[\text{H}(\text{IME}_4)][\text{OAr}^{\text{Mes}}]\cdot\text{C}_6\text{H}_6$ unit (left) and an excerpt displaying the arrangement of the imidazolium cations (right). Thermal ellipsoids are set to 30 % probability; peripheral methyl groups of the mesityl groups as well as hydrogen atoms except for the imidazolium-bonded hydrogen atoms are omitted for simplicity. The positions of the hydrogen atoms have been calculated using standard methods. Selected bond lengths (\AA): C1-O1 1.34(1) [1.35(1)], O1-H49 1.87(1) [1.924(9)].

Yellow, medium-quality crystals of the imidazolium salt $[\text{H}(\text{IME}_4)][\text{OAr}^{\text{Mes}}]\cdot\text{C}_6\text{H}_6$ were obtained from the attempted dehydrochlorination of **19-HCl** using IME_4 as a base (see page 141). The IME_4 is oriented almost perpendicular to the central ring of the terphenyl ($\angle 78.8(5)^\circ$) and the ion pairs are interconnected by $\text{O}\cdots\text{H}$ bridges ($\text{O}\cdots\text{H}$ $1.90(1)$ \AA ; O-C-O-H-C : $171(2)^\circ$). The imidazolium cations are π -stacked in pairs of two with a plane-to-plane shifts of about 0.4 and 0.8 \AA and oriented almost parallel ($\angle 8.1(8)^\circ$). The distance between the two centroids ($3.546(9)$ \AA) lies exactly within the range observed for neighboring porphyrins (3.4 – 3.6 \AA) and is a bit larger when compared to graphite (~ 3.35 \AA).^[497] It should be noted, that the free carbene IME_4 exhibits a layered structure with immense parallel displacement but no clear π - π -interactions.^[498]

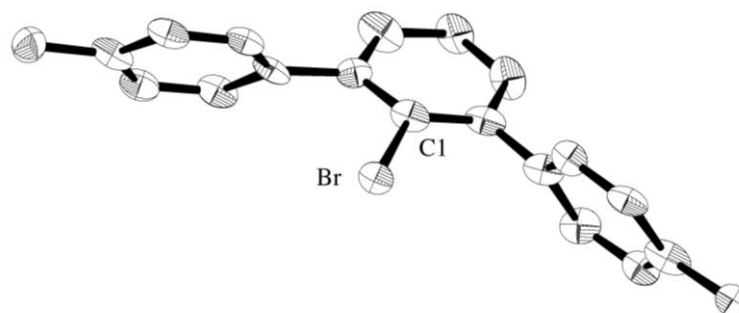
5.3.8 $\text{Ar}^{\text{pTol}}\text{Br}$ 

Figure 98. Molecular structure of $\text{Ar}^{\text{pTol}}\text{Br}$. Thermal ellipsoids are set to 50 % probability; hydrogen atoms omitted.

The terphenyl bromide $\text{Ar}^{\text{pTol}}\text{Br}$ was obtained as a colorless solid while attempting to synthesize $\text{Ar}^{\text{pTol}}\text{SiBr}_3$ from $\text{Ar}^{\text{pTol}}\text{Li}$ and SiBr_4 in ethereal solution. A similar decomposition of the closely related $\text{Ar}^{\text{Mes}}\text{SiBr}_3$ with the “loss of SiBr_2 ” under various crystallization conditions was also reported by Weidemann et al.^[413] (Table 40).

Table 40. Structural data of $\text{Ar}^{\text{pTol}}\text{Br}$ and $\text{Ar}^{\text{Mes}}\text{Br}$.

	C-Br / Å	Cone angle ^A / °	\angle (plane to plane) ^B / °	Reference
$\text{Ar}^{\text{pTol}}\text{Br}$	1.964(12) ^c	126.23(2) ^c	51.29(2) – 61.12(2)	This work
$\text{Ar}^{\text{Mes}}\text{Br}$	1.911(2)	121.5(2)	78.18(9) 88.62(9)	[413]

A: Angle between the bonds between the C^{2,6} carbon atoms and the pTol/Mes substituents.

B: Angle between the best planes of the central ring system and the aromatic substituents.

C: Two independent molecules are found in the unit cell; average values are given.

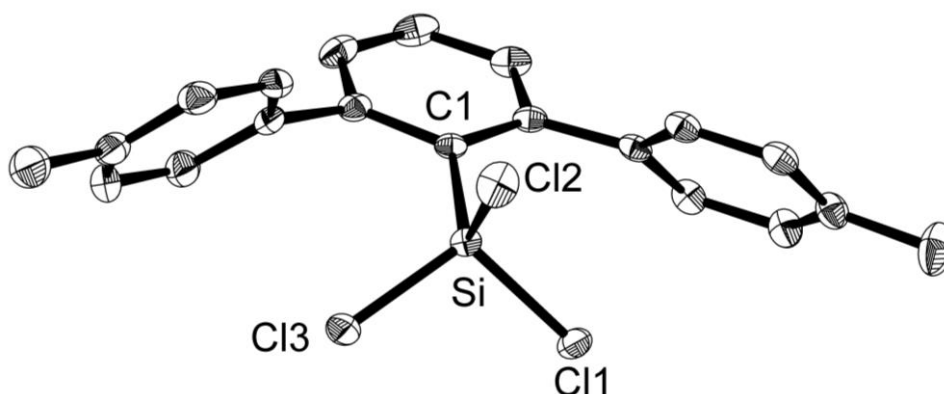
5.3.9 $\text{Ar}^{\text{pTol}}\text{SiCl}_3$ 

Figure 99. Molecular structure of $\text{Ar}^{\text{pTol}}\text{SiCl}_3$. Thermal ellipsoids are set to 50 % probability; hydrogen atoms are omitted for simplicity. Selected bond lengths (Å) and angles (°): Si-C1 1.871(1), C11-Si 2.0386(5), C12-Si 2.0367(5), C13-Si 2.0367(5); C12-Si-C11 105.88(2), C12-Si-C13 107.72(2), C13-Si-C11 102.39(2), C1-Si-C11 113.92(5), C1-Si-C12 113.84(4), C1-Si-C13 112.22(5).

The structure of $\text{Ar}^{\text{pTol}}\text{SiCl}_3$ is expectedly closely related to the one reported by Simons et al. for $\text{Ar}^{\text{Mes}}\text{SiCl}_3$ with nearly identical bond distances and -angles (Table 44).^[402] But akin to $\text{Ar}^{\text{pTol}}\text{Br}$

(vide supra), the angles between the best planes of the central ring system and the substituents ($53.35(5)^\circ$ and $60.11(5)^\circ$) deviate from the orthogonal arrangement that is commonly observed in Ar^{Mes} -containing silanes.

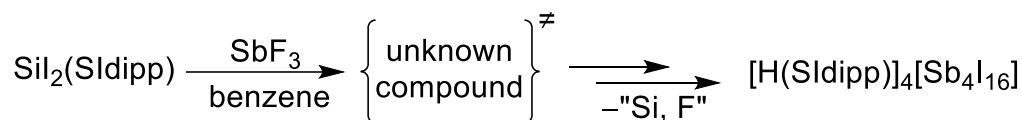
Table 41. Structural and $^{29}\text{Si}\{^1\text{H}\}$ NMR data of trihalosilanes with (oxo-)terphenyl substituents.

Compound	Si-C /Å	Si-O /Å	$\angle(\text{Si-X})$ /Å	Si-O-C /°	δ_{Si} /ppm ^A	Reference
$\text{Ar}^{\text{pTol}}\text{SiCl}_3$	1.871(1)	-	2.037(5)	-	-5.6	This work
$(\text{Ar}^{\text{pTol}}\text{SiBr}_3)$	n. a.	n. a.	n. a.	n. a.	^B	This work
$\text{Ar}^{\text{Mes}}\text{SiCl}_3$	1.872(3)	-	2.032(1)	-	-6.4	[402]
$(\text{Ar}^{\text{Mes}}\text{SiBr}_3)$	n. a.	n. a.	n. a.	n. a.	-35.7	[413]
$\text{SiCl}_3\text{OAr}^{\text{Mes}}$ (21-Cl)	2.766(1)	1.598(1)	2.0110(5)	135.31(9)	-47.5	This work
$\text{SiBr}_3\text{OAr}^{\text{Mes}}$ (21-Br)	2.796(3)	1.599(2)	2.1849(9)	138.5(2)	-87.2	This work

A: All spectra were recorded from benzene- d_6 solutions. **B:** In a $^{29}\text{Si}\{^1\text{H}\}$ zgig spectrum of the reaction mixture (containing mostly $\text{Ar}^{\text{pTol}}\text{Br}$ according to ^1H NMR spectroscopy), a weak singlet signals was observed at -70.0 ppm, but additional signals of unknown origin were detected at $\delta_{\text{Si}} = 15.0, 2.5$ and 2.1 ppm.

5.3.10 [H(SIDipp)]₄[Sb₄I₁₆]·C₆H₆

Yellow crystals of [H(SIDipp)]₄[Sb₄I₁₆] were obtained from the reaction of SiI₂(SIDipp) with solid SbF₃ in benzene (gas evolution and a small amount of a dark precipitate were observed). In situ ¹⁹F{¹H} NMR spectroscopy in benzene-d₆ solution displayed the formation of intermediates (sharp singlet signals were observed at δ_F = -95 ppm and later at -119.1 ppm), which vanished over time. No signal could be detected in the ²⁹Si NMR spectrum.



Scheme 70. Reaction leading to the formation of [H-SIDipp]₄[Sb₄I₁₆].

The molecular structure (Figure 100 on page 261) is dominated by an [Sb₄I₁₆]⁴⁻ polyanion. The polyanion consists of two central edge-shared [SbI₆] octahedrons, which each also share an edge with a [SbI₄] pyramid, resulting in an anti conformation. Generally, the Sb-I distances in the octahedrons vary from 2.8305(4) to 3.2125 (Å), with each one apical position being farther off by about 0.2 Å. As expected, the bonds towards bridging I atoms are longer than those towards terminal I atoms.

NMR data of the intermediate:

¹H NMR (500.2 MHz, benzene-d₆, 298 K): δ/ppm = 1.12 (d, 12H, ³J_{H,H} = 7.0 Hz, C^{2,6}-CHMe_AMe_B, Dipp), 1.45 (d, 12H, ³J_{H,H} = 6.8 Hz, C^{2,6}-CHMe_AMe_B, Dipp), 3.22 (sept, 4H, ³J_{H,H} = 6.8 Hz, C^{2,6}-CHMe_AMe_B, Dipp), 3.39 (s, 4H, 2 × NCH₂, SIDipp), 7.05 (d, 4H, ³J_{H,H} = 7.6 Hz, 2 × C^{3,5}-H, Dipp). The C⁴-H signal is probably hidden by the solvent residual signal (δ_H = 7.16 ppm).

¹³C{¹H} NMR (125.8 MHz, benzene-d₆, 298 K): δ/ppm = 23.4, 26.0 (each s, each 4C, 2 × CHMe_AMe_B and 2 × CHMe_AMe_B Dipp), 29.1 (s, 4C, 2 × CHMe_AMe_B, Dipp), 53.5 (s, 2C, 2 × NCH₂, SIDipp), 124.7 (s, 4C, 2 × C^{3,5}-H, Dipp), 130.3 (s, 2C, 2 × C⁴-H, Dipp), 133.8 (s, 2C, 2 × C¹, Dipp), 146.9 (s, 4C, 2 × C^{2,6}-CHMe_AMe_B, Dipp). The NCN signal was not observed. Due to the low solubility, no reliable correlation spectra could be obtained. The assignment of the ¹³C NMR data is thus only based on comparison to known compounds.

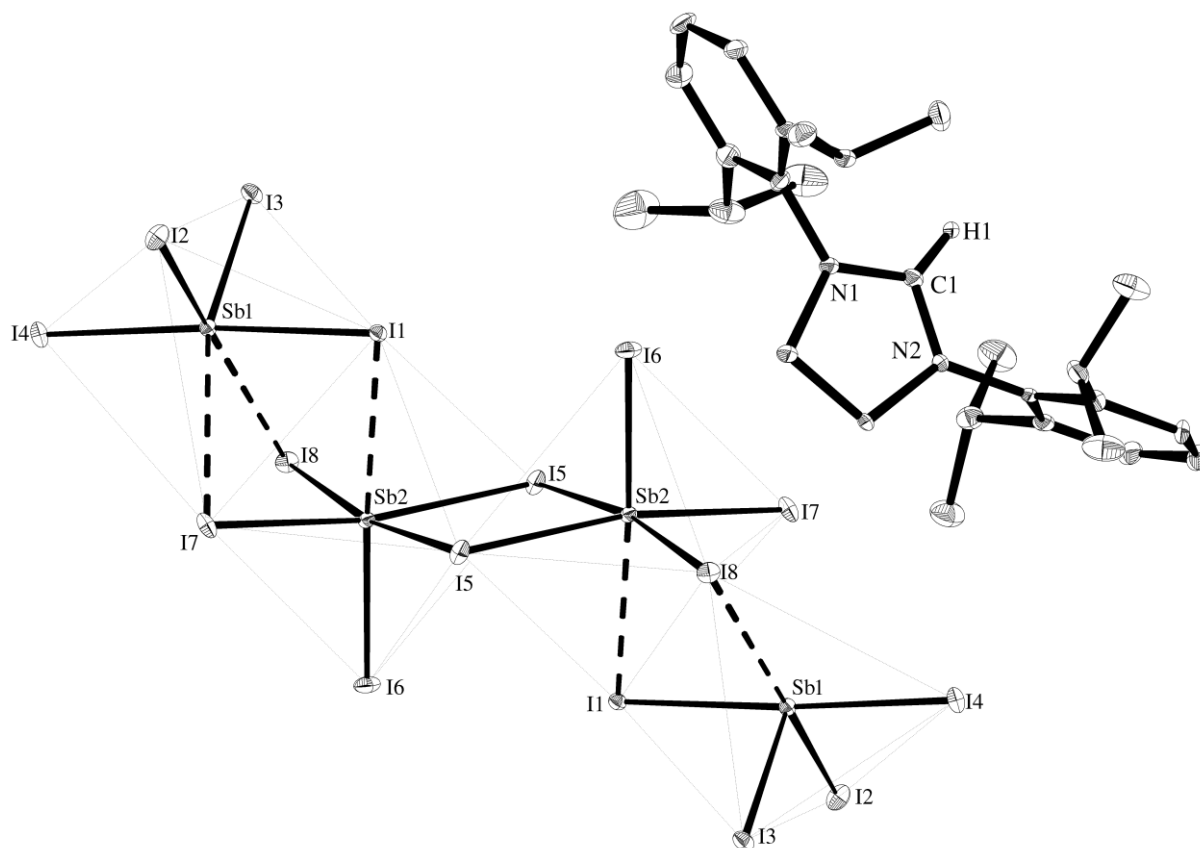


Figure 100. Molecular structures of the full polyanion $[\text{Sb}_6\text{I}_{16}]^+$ (left) and one counter cation $[\text{H-SIDipp}]^+$ (right). Thermal ellipsoids are set to 30 % probability; hydrogen atoms except H1 and a cocrystallized benzene molecule are omitted for simplicity. Selected bond lengths (\AA) and angles ($^\circ$): I1-Sb1 3.0059(4), I2-Sb1 2.8158(4), I3-Sb1 2.8039(4), I4-Sb1 2.9864(4), I8-Sb1 3.4455(2), I1-Sb2 3.2125(4), I5-Sb2 3.1190(4), I5-Sb2# 3.0806(4), I6-Sb2 2.8305(4), I7-Sb2 2.9449(4), I8-Sb2 2.9856(4), Sb2-I5# 3.0806(4).

5.4 Supporting Crystallographic data files

Compound	[H-IMe ₄][OAr ^{Me}]-C ₆ H ₆	Ar ^{Pr} TolBr	Ar ^{Tol} SiCl ₃
Crystal Habitus	yellow block	colourless block	colourless block
Device Type	Bruker D8 Venture	Bruker D8-Venture	Bruker D8-Venture
Empirical formula	C ₆₈ H ₅₂ N ₄ O ₂	C ₂₀ H ₁₇ Br	C ₂₀ H ₁₇ Cl ₃ Si
Moiety formula	2(C ₂₄ H ₂₀ O), 2(C ₇ H ₁₃ N ₂), C ₆ H ₆	C ₂₀ H ₁₇ Br	C ₂₀ H ₁₇ Cl ₃ Si
Formula weight	987.37	337.24	391.77
Temperature/K	99.99	123.05	123
Crystal system	orthorhombic	orthorhombic	monoclinic
Space group	Pca2 ₁	P2 ₁ 2 ₁ 2 ₁	P2 ₁ /c
a/Å	23.556(4)	10.1593(4)	8.8670(5)
b/Å	12.0395(18)	16.8091(7)	16.3570(10)
c/Å	41.679(7)	18.8069(7)	13.0549(9)
α/°	90	90	90
β/°	90	90	96.227(2)
γ/°	90	90	90
Volume/Å ³	11820(3)	3211.6(2)	1882.3(2)
Z	8	8	4
ρ _{calc} /g/cm ³	1.110	1.395	1.382
μ/mm ⁻¹	0.505	3.390	0.549
F(000)	4272.0	1376.0	808.0
Crystal size/mm ³	0.22 × 0.15 × 0.12	0.18 × 0.09 × 0.06	0.24 × 0.18 × 0.12
Absorption correction	empirical	empirical	empirical
Tmin; Tmax	0.3093; 0.7536	0.2754; 0.7536	0.5494; 0.7459
Radiation	CuKα (λ = 1.54178)	CuKα (λ = 1.54178)	MoKα (λ = 0.71073)
2θ range /°	4.24 to 135.498°	7.052 to 135.468°	4.98 to 55.984°
Completeness to theta	0.978	0.991	0.998
Index ranges	-26 ≤ h ≤ 28, -14 ≤ k ≤ 14, -49 ≤ l ≤ 49	-9 ≤ h ≤ 12, -20 ≤ k ≤ 16, -22 ≤ l ≤ 22	-11 ≤ h ≤ 11, -21 ≤ k ≤ 21, -17 ≤ l ≤ 17
Reflections collected	63628	11472	48223
Independent reflections	19736 R _{int} = 0.1387, R _{sigma} = 0.1207	5485 R _{int} = 0.0902, R _{sigma} = 0.1061	4551 R _{int} = 0.0581, R _{sigma} = 0.0259
Data/restraints/parameters	19736/1590/1230	5485/43/384	4551/0/219
Goodness-of-fit on F ²	1.046	1.035	1.068
Final R indexes [I ≥ 2σ (I)]	R ₁ = 0.1546, wR ₂ = 0.3856	R ₁ = 0.0998, wR ₂ = 0.2563	R ₁ = 0.0294, wR ₂ = 0.0725
Final R indexes [all data]	R ₁ = 0.1950, wR ₂ = 0.4230	R ₁ = 0.1085, wR ₂ = 0.2639	R ₁ = 0.0366, wR ₂ = 0.0768
Largest diff. peak/hole / e Å ⁻³	0.85/-0.84	2.13/-2.58	0.32/-0.37

Compound	[H-SIDipp] ₄ [Sb ₄ I ₁₆]	CuBr(SIDipp)·C ₆ H ₆	SbF ₃ (SIDipp)
Crystal Habitus	yellow plank	colourless plank	colourless block
Device Type	Bruker D8-Venture	Bruker X8-KappaApexII	Bruker D8-Venture
Empirical formula	C ₅₇ H ₈₁ I ₁₆ N ₄ Sb ₂	C ₃₅ H ₄₄ BrCuN ₂	C ₂₇ H ₃₆ Cl ₃ N ₃ Sb

Moiety formula	$\text{I}_8\text{Sb}_2, 2(\text{C}_{27}\text{H}_{38}\text{N}_2), 0.5(\text{C}_6\text{H}_6)$	$\text{C}_{27}\text{H}_{38}\text{BrCuN}_2, \text{C}_6\text{H}_6$	$\text{C}_{27}\text{H}_{36}\text{Cl}_3\text{N}_2\text{Sb}$
Formula weight	2080.95	612.15	616.68
Temperature/K	99.99	100	99.98
Crystal system	triclinic	monoclinic	monoclinic
Space group	P-1	P2/c	P2/n
a/Å	12.0277(7)	9.6387(13)	11.187(3)
b/Å	14.1581(9)	14.5900(19)	13.795(3)
c/Å	21.5556(13)	22.305(3)	18.863(4)
$\alpha/^\circ$	77.243(2)	90	90
$\beta/^\circ$	82.936(2)	95.755(4)	104.434(9)
$\gamma/^\circ$	83.234(2)	90	90
Volume/Å ³	3537.3(4)	3120.9(7)	2819.1(11)
Z	2	4	4
$\rho_{\text{calc}}/\text{g/cm}^3$	1.954	1.303	1.453
μ/mm^{-1}	4.289	2.003	1.281
F(000)	1954.0	1280.0	1256.0
Crystal size/mm ³	0.16 × 0.08 × 0.04	0.32 × 0.21 × 0.18	0.26 × 0.25 × 0.21
Absorption correction	empirical	empirical	empirical
Tmin; Tmax	0.5299; 0.7461	0.5079; 0.7462	0.4044; 0.7461
Radiation	MoK α ($\lambda = 0.71073$)	MoK α ($\lambda = 0.71073$)	MoK α ($\lambda = 0.71073$)
2 θ range /°	4.316 to 56°	5.084 to 55.996°	4.46 to 55.99°
Completeness to theta	0.997	0.998	0.992
Index ranges	-15 ≤ h ≤ 15, -18 ≤ k ≤ 18, -28 ≤ l ≤ 28	-12 ≤ h ≤ 12, -19 ≤ k ≤ 19, -29 ≤ l ≤ 29	-14 ≤ h ≤ 14, -18 ≤ k ≤ 18, -24 ≤ l ≤ 24
Reflections collected	109432	66407	61723
Independent reflections	17021 [R _{int} = 0.0411, R _{sigma} = 0.0267	7524 R _{int} = 0.1152, R _{sigma} = 0.0728	6755 R _{int} = 0.1026, R _{sigma} = 0.0484
Data/restraints/parameters	17021/30/683	7524/6/342	6755/12/306
Goodness-of-fit on F ²	1.034	1.144	1.131
Final R indexes [$I \geq 2\sigma(I)$]	R ₁ = 0.0329, wR ₂ = 0.0798	R ₁ = 0.0735, wR ₂ = 0.1659	R ₁ = 0.0830, wR ₂ = 0.2062
Final R indexes [all data]	R ₁ = 0.0437, wR ₂ = 0.0873	R ₁ = 0.0995, wR ₂ = 0.1792	R ₁ = 0.0966, wR ₂ = 0.2144
Largest diff. peak/hole / e Å ⁻³	1.93/-1.43	1.81/-1.07	5.15/-2.81

Compound	SO₃(IDipp)·(C₆H₆)₂	S(SO₃)(IDipp)·C₆H₆
Crystal Habitus	colourless block	colourless needle
Device Type	Bruker X8-KappaApexII	Bruker D8-Venture
Empirical formula	$\text{C}_{36}\text{H}_{48}\text{N}_2\text{O}_3\text{S}$	$\text{C}_{36}\text{H}_{48}\text{N}_2\text{O}_3\text{S}_2$
Moiety formula	$\text{C}_{27}\text{H}_{38}\text{N}_2\text{O}_3\text{S}, 2 \text{C}_6\text{H}_6$	$\text{C}_{27}\text{H}_{38}\text{N}_2\text{O}_3\text{S}_2, \text{C}_6\text{H}_6$
Formula weight	624.85	578.80
Temperature/K	150	100
Crystal system	monoclinic	monoclinic
Space group	P2/c	P2/n

a/Å	23.1847(7)	10.624(3)
b/Å	14.3971(4)	19.681(4)
c/Å	24.2094(7)	16.045(4)
α /°	90	90
β /°	117.5855(14)	108.84(3)
γ /°	90	90
Volume/Å ³	7162.3(4)	3175.0(14)
Z	8	4
ρ_{calc} /cm ³	1.159	1.211
μ /mm ⁻¹	1.091	1.788
F(000)	2688.0	1240.0
Crystal size/mm ³	0.08 × 0.05 × 0.03	0.18 × 0.06 × 0.05
Absorption correction	empirical	empirical
Tmin; Tmax	0.2449; 0.7533	0.369107; 0.752437
Radiation	CuK α (λ = 1.54178)	CuK α (λ = 1.54184)
2 θ range /°	7.318 to 135.488°	7.354 to 134.996°
Completeness to theta	0.997	0.999
Index ranges	-27 ≤ h ≤ 23, -17 ≤ k ≤ 17, -29 ≤ l ≤ 29	-12 ≤ h ≤ 12, -23 ≤ k ≤ 23, -19 ≤ l ≤ 19
Reflections collected	81833	83420
Independent reflections	12949 R _{int} = 0.0916, R _{sigma} = 0.0552	5733 R _{int} = 0.6320, R _{sigma} = 0.7374
Data/restraints/parameters	12949/6/815	5733/168/369
Goodness-of-fit on F ²	1.022	0.650
Final R indexes [$I \geq 2\sigma(I)$]	R ₁ = 0.0675, wR ₂ = 0.1914	R ₁ = 0.0834, wR ₂ = 0.1170
Final R indexes [all data]	R ₁ = 0.0960, wR ₂ = 0.2178	R ₁ = 0.3270, wR ₂ = 0.1460
Largest diff. peak/hole / e Å ⁻³	0.85/-0.67	0.40/-0.31

5.5 UV-vis-NIR spectra

5.5.1 (Z)-(SIDipp)Si=Si(Br)Tbb (1)

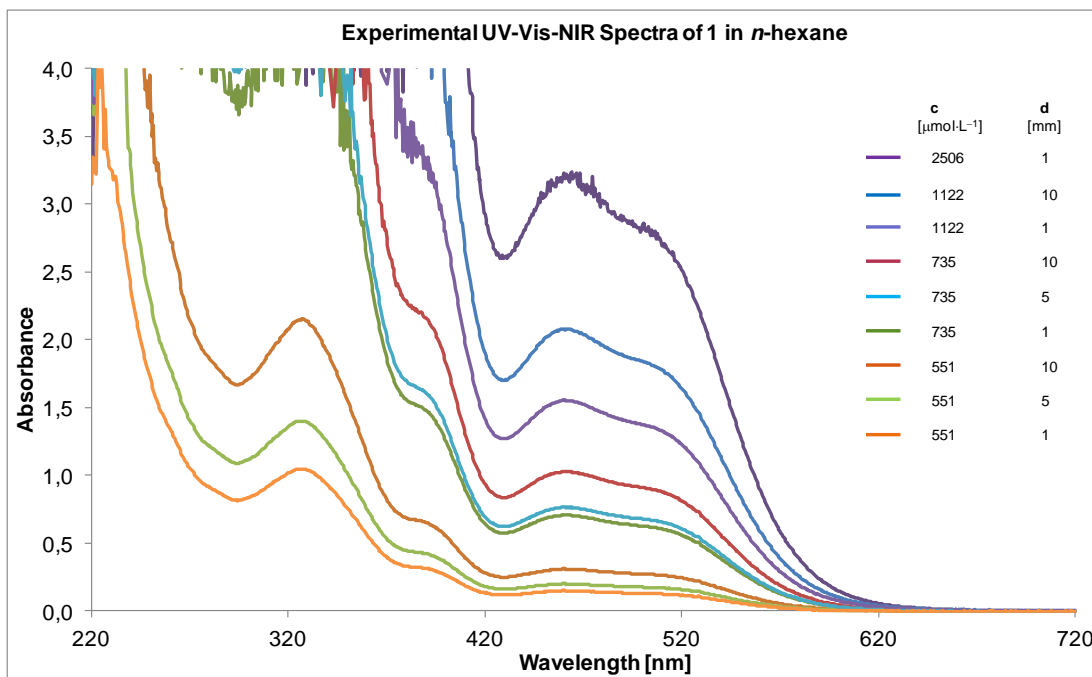


Figure 101. Experimental UV-Vis spectra of 1 in *n*-hexane from 220 – 720 nm at different concentrations *c* ($\mu\text{mol L}^{-1}$) and optical path lengths *d* [mm] of the cuvettes.

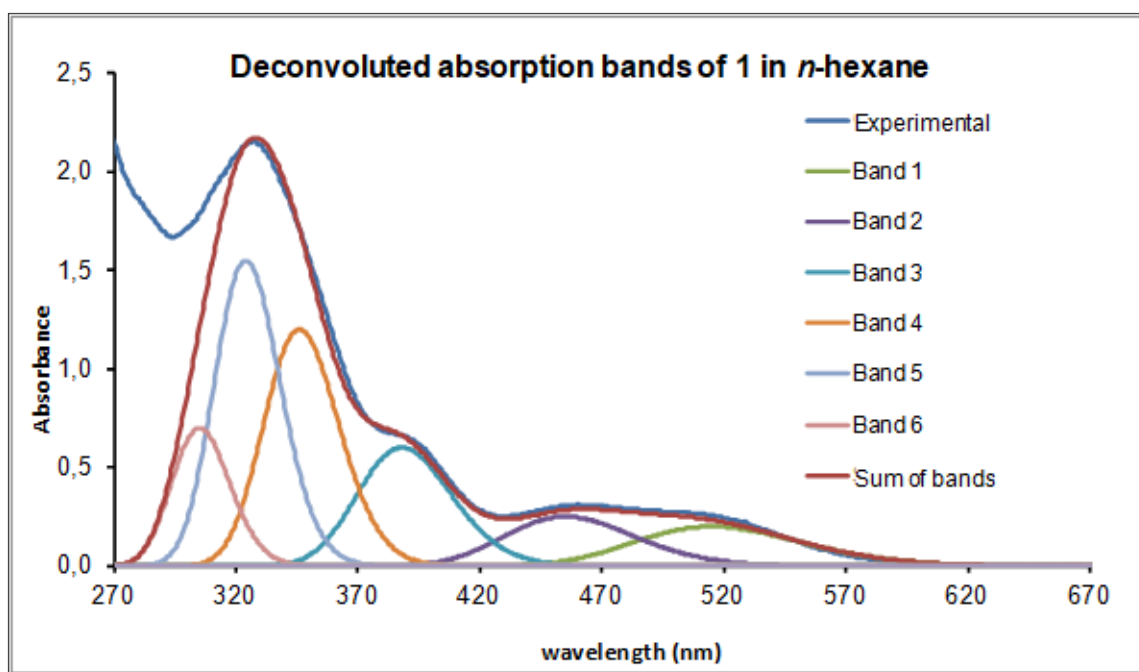


Figure 102. Deconvoluted absorption bands and experimental UV-Vis spectrum of 1 in *n*-hexane from 270 – 670 nm at $c = 551 \mu\text{mol L}^{-1}$ and $d = 10 \text{ mm}$.

5.5.2 (*E*)-(SIDipp)Si=Si(Me)Tbb (1-Me)

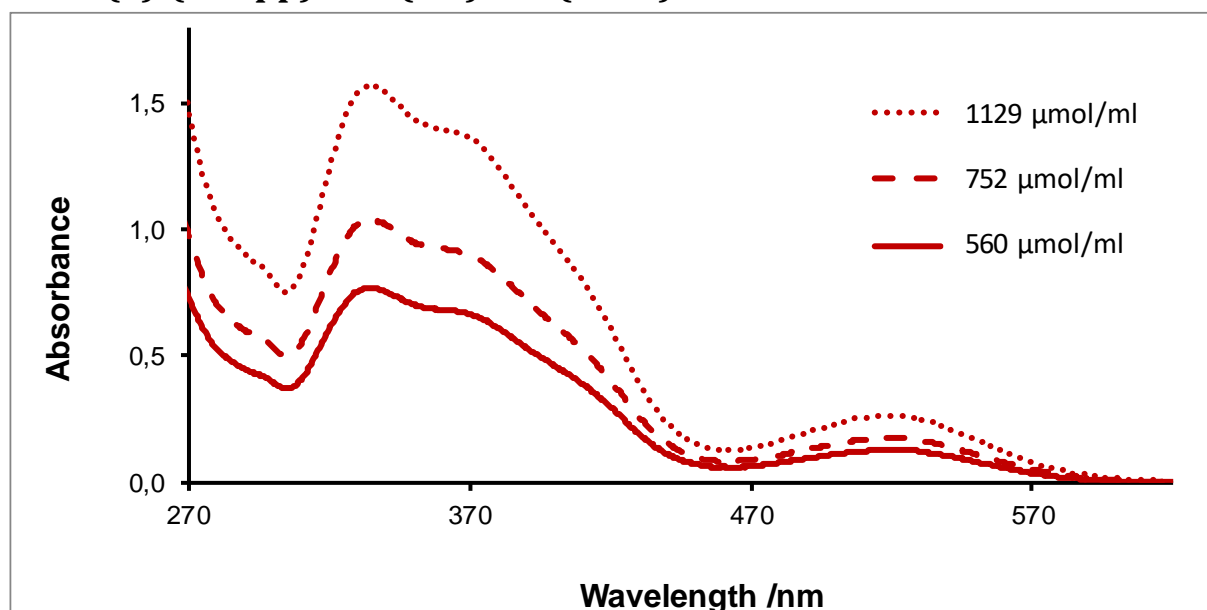


Figure 103. Experimental UV-Vis spectra of **1-Me** in n-hexane from 270 – 620 nm at different concentrations c and an optical path length $d = 1$ mm of the cuvette. See also page 26ff.

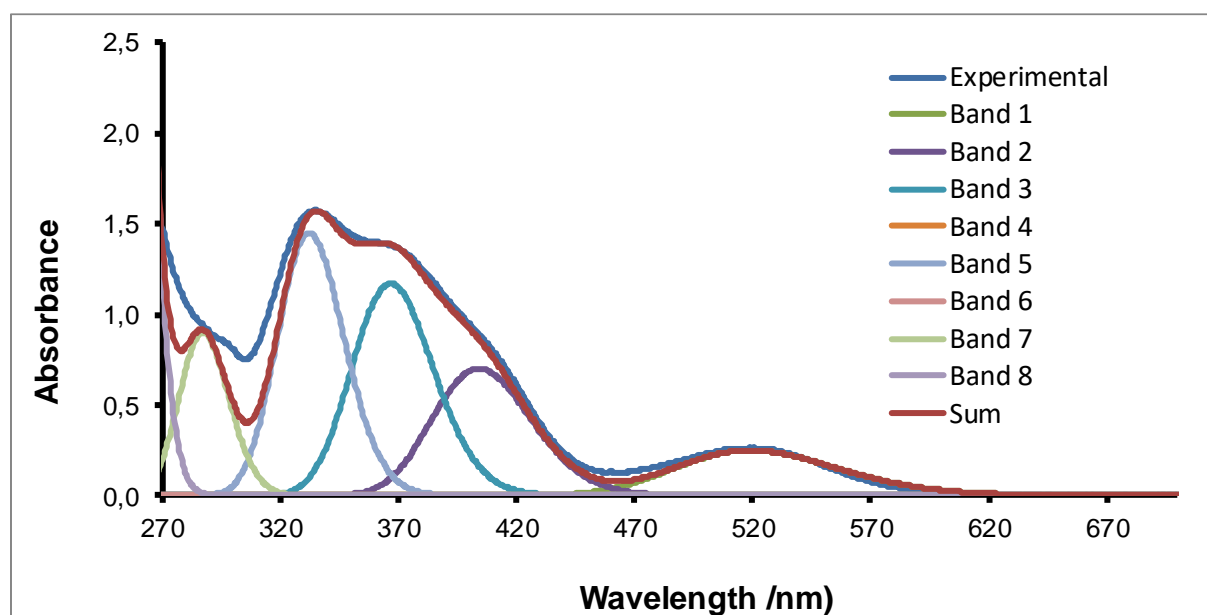


Figure 104. Deconvoluted absorption bands and experimental UV-Vis spectrum of **1-Me** in n-hexane from 270 to 670 nm at $c = 560 \mu\text{mol L}^{-1}$ and $d = 1$ mm.

5.5.3 (*E*)-(SIDipp)Si=Si(CH₂Ph)Tbb (1-CH₂Ph)

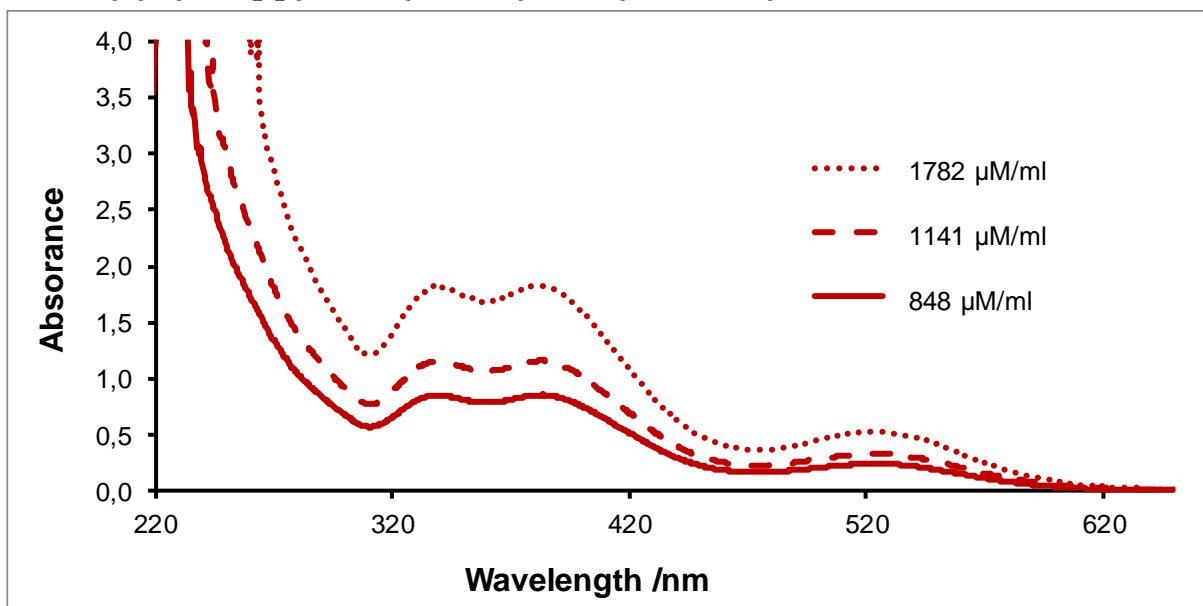


Figure 105. Experimental UV-Vis spectra of 1-CH₂Ph in n-hexane from 220 – 650 nm at different concentrations c ($\mu\text{mol L}^{-1}$) an optical path length $d = 1$ mm of the cuvette. See also page 26ff.

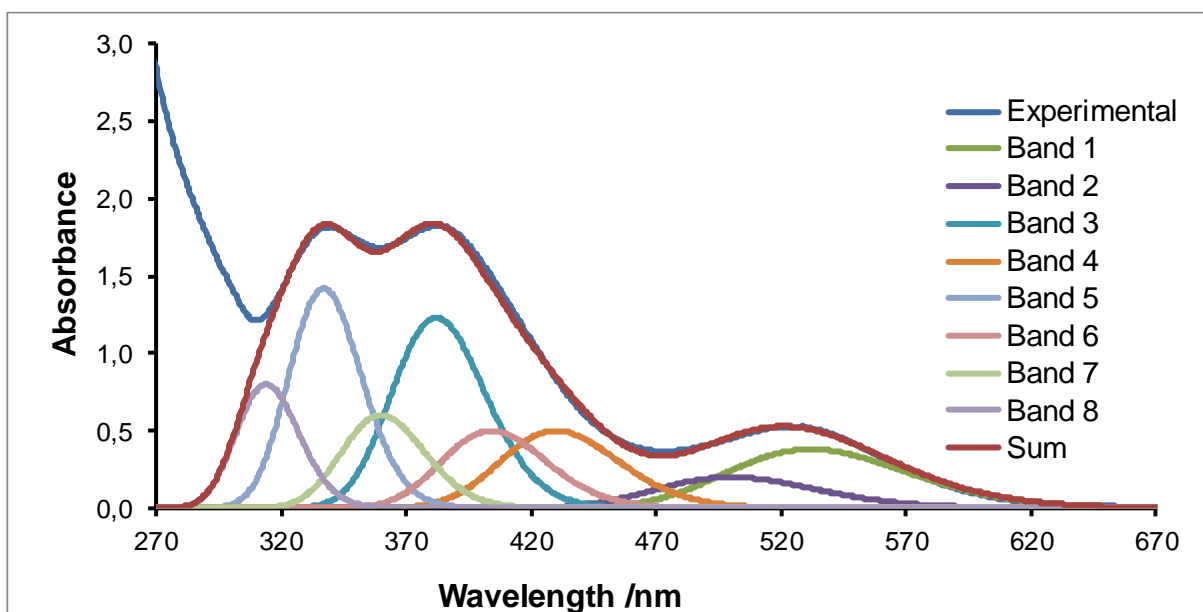


Figure 106. Deconvoluted absorption bands and experimental UV-Vis-NIR spectrum of 1-CH₂Ph in n-hexane from 270 – 670 nm at $c = 1783 \mu\text{mol L}^{-1}$ and $d = 1$ mm.

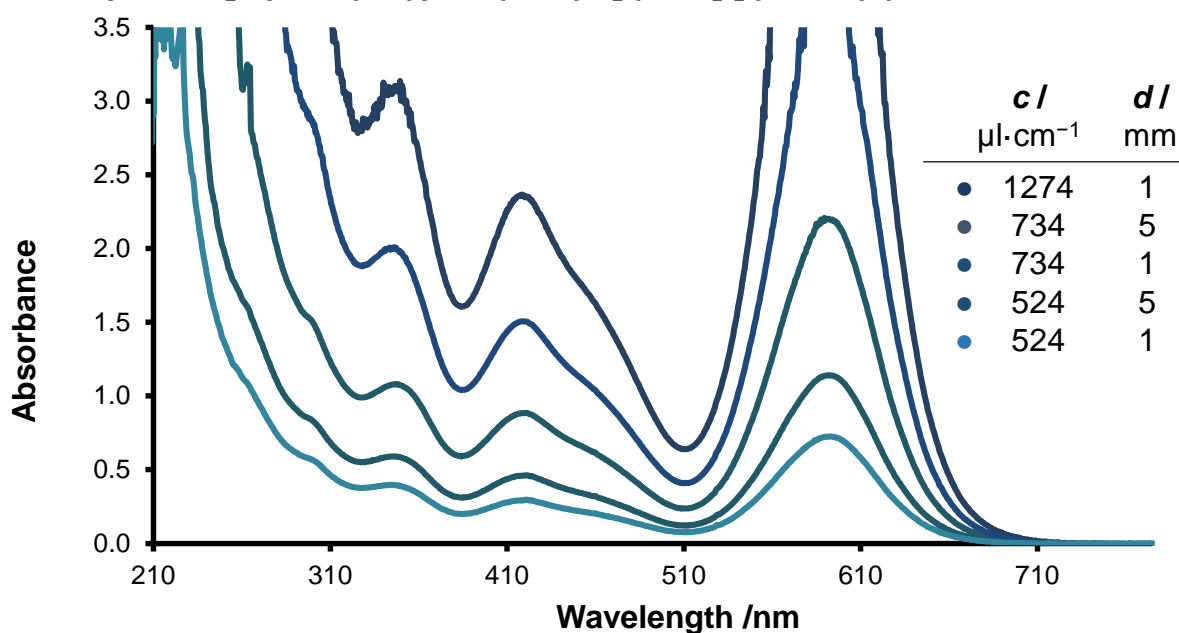
5.5.4 *cyclo-Si[C{ONa(thf)}PSi(Tbb)P](SIDipp)* (7)

Figure 107. Experimental UV-vis spectra of **7** in thf solution at 298 K from 210 – 775 nm at different concentrations c ($\mu\text{mol L}^{-1}$) an optical path length $d = 5$ or 1 mm of the cuvette. See also page 54.

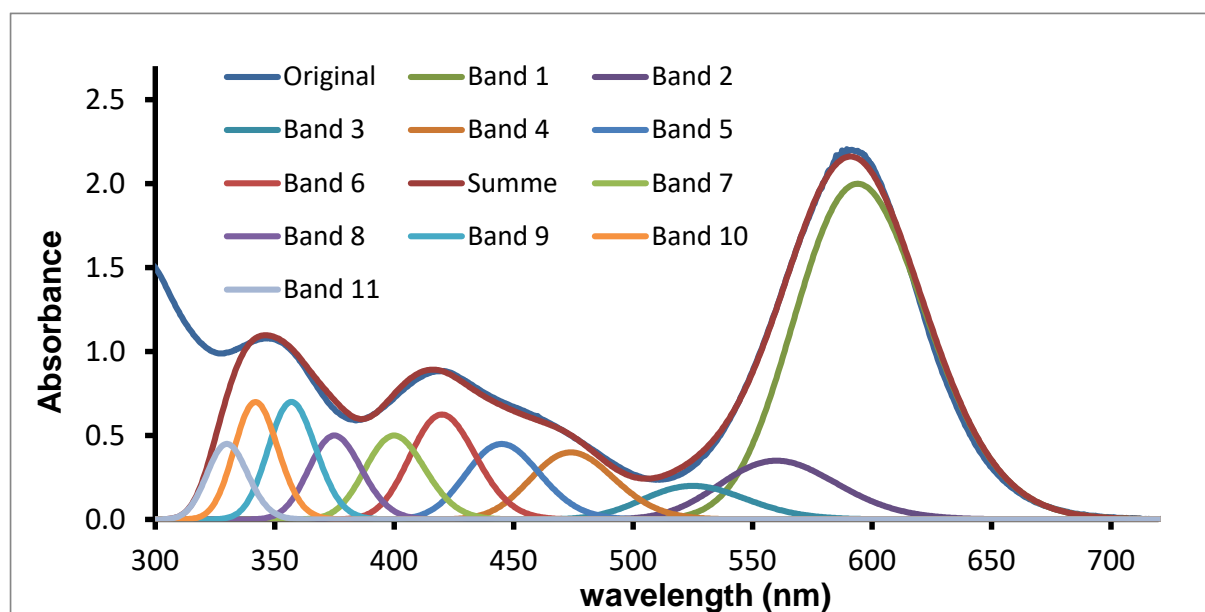


Figure 108. Deconvoluted absorption bands and experimental UV-Vis-NIR spectrum of **7** in thf solution at 298 K from 300 – 720 nm at $c = 524 \mu\text{mol L}^{-1}$ and $d = 1$ mm.

Table 42. Molar extinction coefficients ϵ_λ of **7** at the absorption maxima $\lambda = 247$ nm, 421 nm and 593 nm.

Band /nm	247	421	593
$\epsilon / \text{l}\cdot\text{mol}^{-1}\cdot\text{cm}^{-1}$	7819.6	6205.9	16435.0

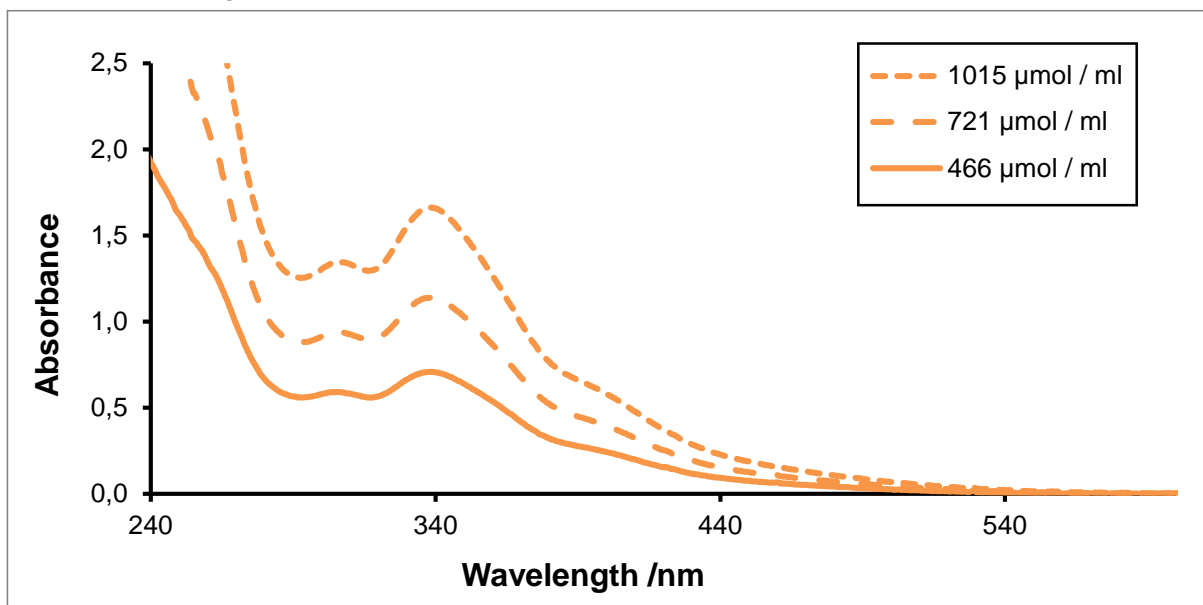
5.5.5 $\text{CuBr}\{\eta^2\text{-}(Z)\text{-(SIDipp)Si=Si(Br)Tbb}\}$ (10)

Figure 109. Experimental UV-Vis spectra of **10** in n-hexane from 240 – 600 nm at different concentrations c ($\mu\text{mol L}^{-1}$) an optical path length $d = 1$ mm of the cuvette. See also page 80.

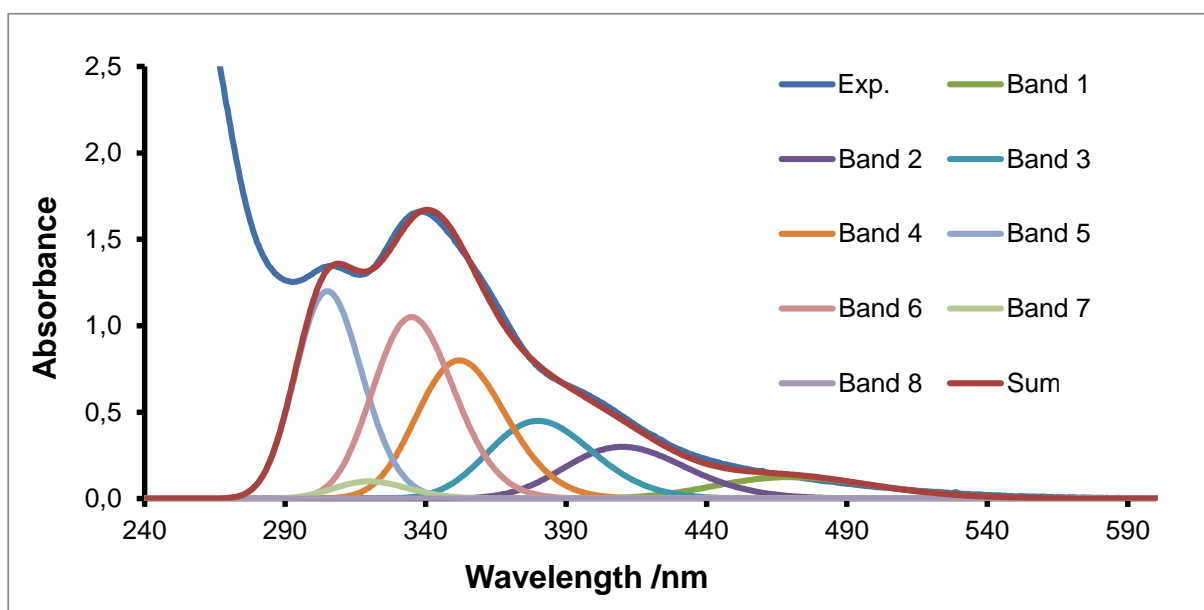


Figure 110. Deconvoluted absorption bands and experimental UV-Vis-NIR spectrum of **10** in n-hexane from 240 to 600 nm at $c = 980 \mu\text{mol L}^{-1}$ and $d = 1$ mm. See also page 80.

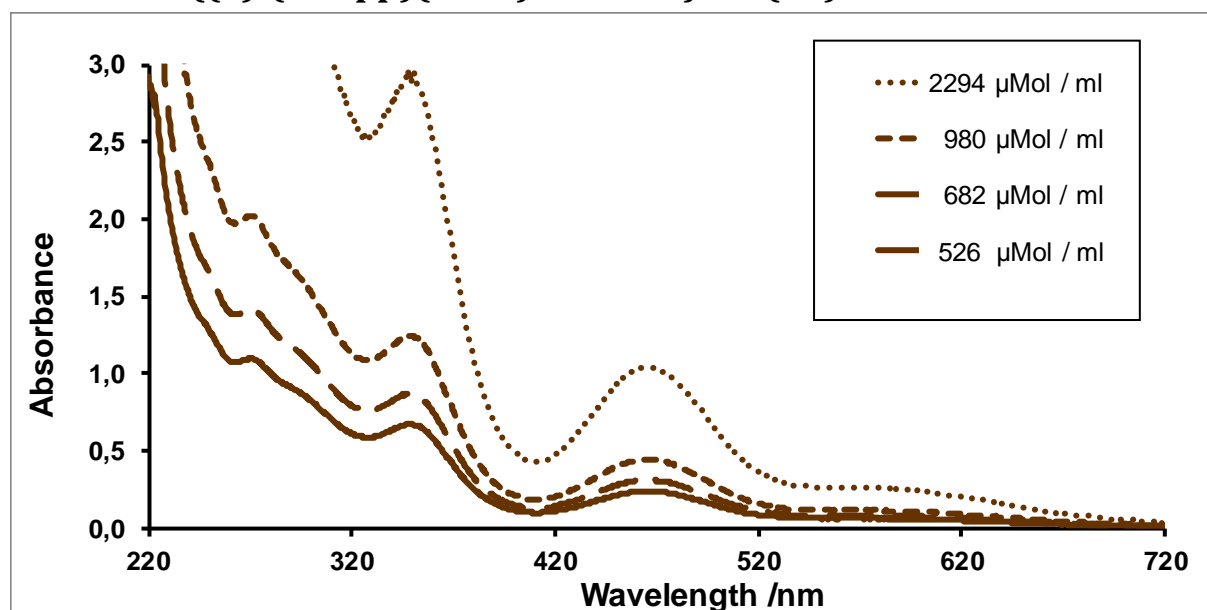
5.5.6 $\text{CuBr}\{(\text{Z})\text{-}(\text{SIDipp})(\text{OtBu})\text{Si}=\text{SiTbb}\}$ (12)

Figure 111. Experimental UV-Vis spectra of **12** in n-hexane from 220 – 720 nm at different concentrations c ($\mu\text{mol L}^{-1}$) an optical path length $d = 1$ mm of the cuvette. See also page 80.

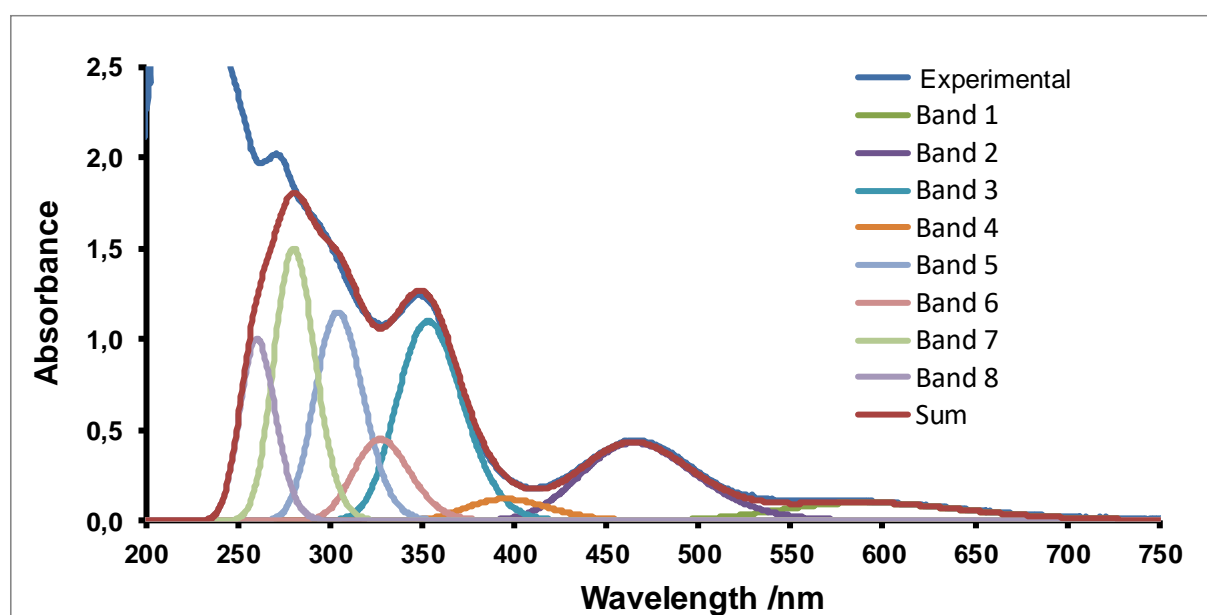


Figure 112. Deconvoluted absorption bands and experimental UV-Vis-NIR spectrum of **12** in n-hexane from 270 to 750 nm at $c = 980 \mu\text{mol L}^{-1}$ and $d = 1$ mm. See also page 80.

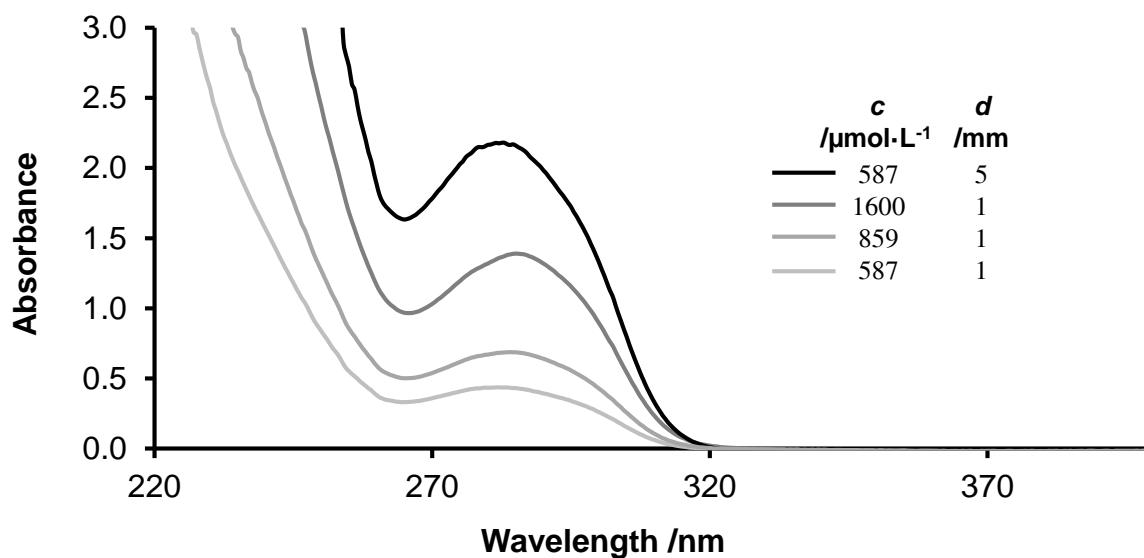
5.5.7 $\text{Si}(\text{OAr}^{\text{Mes}})_2$ (**19**)

Figure 113. Experimental UV-Vis spectra of **19** in thf from 200 – 400 nm at different concentrations (c) and optical path lengths (d) of the cuvette.

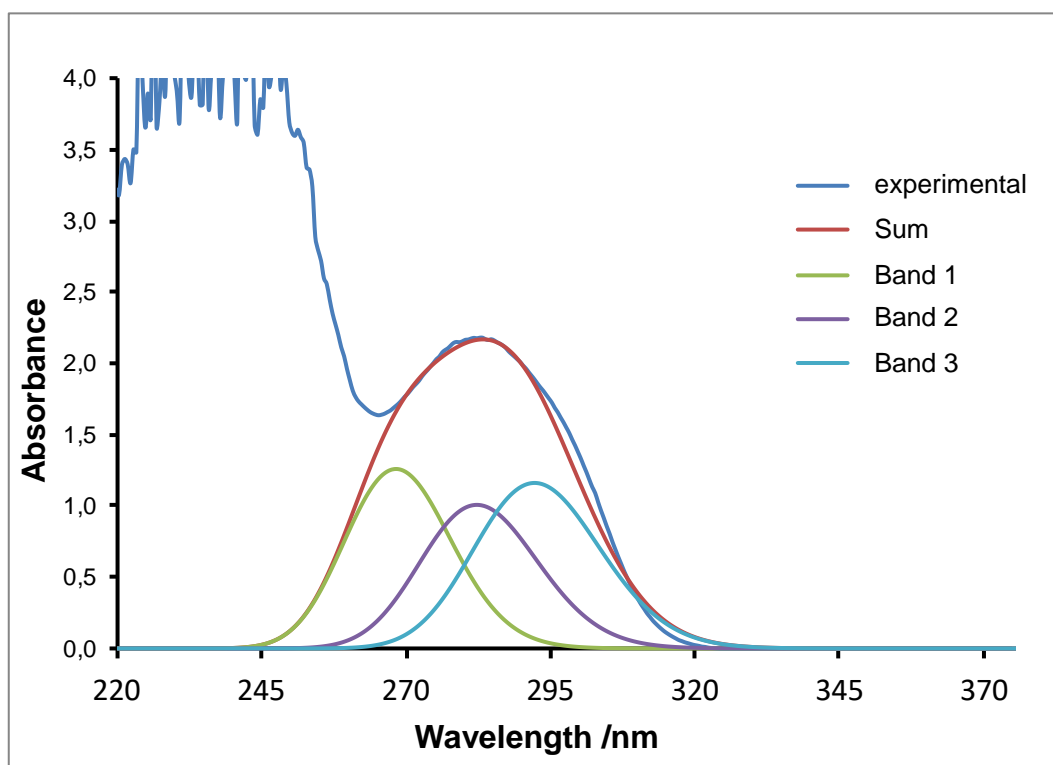


Figure 114. Experimental UV-Vis spectra of **19** in thf from 200 – 400 nm at different concentrations (c) of **1** and optical path lengths (d) of the cuvette.

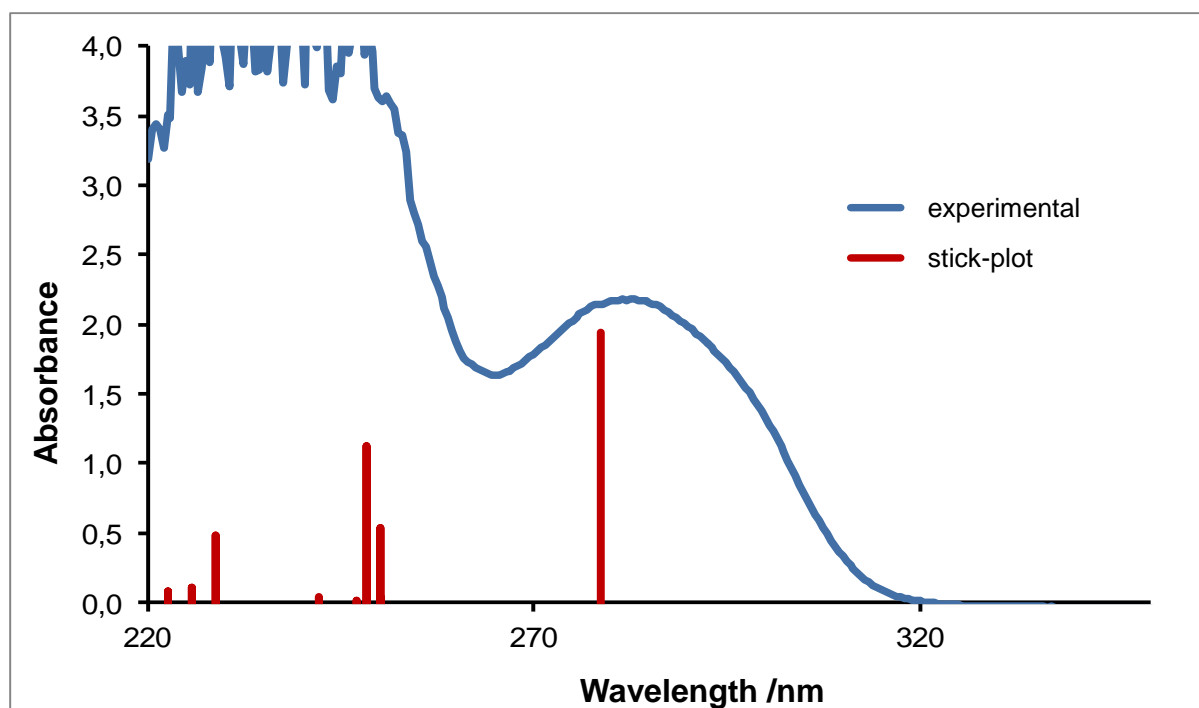


Figure 115. Comparison between the computed (stick-plot, red, CIS(D)-RI-MP2/def2-TZVP) and the experimental (blue, measured in thf) UV-vis spectrum of **19**.

Table 43. Selected transitions in the computed UV/vis spectrum of **19^{calc}** (CIS(D)-RI-MP2/def2-TZVP). Only molecular orbital contributions with more than 5 % are considered.

λ /nm	MO contribution	Contribution / %	Energy /eV	f^a
278.6	HOMO→LUMO	59.4	4.45	0.216496859
	HOMO-12→LUMO	10.0		
250.2	HOMO-1→LUMO+2	21.9	4.96	0.059423813
	HOMO-1→LUMO+2	7.4		
250.1	HOMO-6→LUMO+2	6.3	4.96	0.005352447
248.4	HOMO→LUMO+2	18.9	4.99	0.125920780
	HOMO-3→LUMO+1	9.1		
	HOMO-3→LUMO+2	6.6		
247.0	HOMO-1→LUMO+8	13.0	5.02	0.002286214
242.3	HOMO-2→LUMO+8	10.4	5.12	0.005243748
	HOMO-5→LUMO+3	6.2		
228.7	HOMO-1→LUMO+2	10.3	5.42	0.053668778
225.7	HOMO-2→LUMO+2	6.5	5.49	0.012106157

a: oscillator strength of the electronic transition

5.6 Kinetic- and variable temperature NMR studies

Variable temperature NMR spectroscopic studies (^1H , $^{13}\text{C}\{^1\text{H}\}$, ^{29}Si) of were typically carried out in toluene- d_8 or tetrahydrofuran- d_8 solutions in temperature ranges from 203 K to 373 K (BRUKER AV I-300) or 243 to 353 K (BRUKER AV III HD PRODEGY-500 NMR).

Thermodynamic activation parameters (ΔG^\ddagger , ΔH^\ddagger , ΔS^\ddagger) were determined using equations Eq. 4 and Eq. 5. based on the coalescence temperature (T_c) and the rate constants (k), which was obtained from a full line shape analysis of affected proton signals using the NMR simulation program gNMR.^[360] If no full line shape analysis could be performed, Eq. 6 was used to estimate ΔG^\ddagger from the coalescence temperature and the peak separation at low temperatures ($\Delta\nu$) instead.⁶⁶ All calculations were performed using standard methods of dynamic NMR spectroscopy.^[499]

$$\ln \frac{k}{T} = \ln \left(\frac{k_B}{h} \right) + \frac{\Delta S^\ddagger}{R} - \frac{\Delta H^\ddagger}{R} \left(\frac{1}{T} \right) \quad \text{Eq. 4}$$

$$\Delta G^\ddagger (T_c) = \Delta H^\ddagger - T_c \times \Delta S^\ddagger \quad \text{Eq. 5}$$

$$\Delta G^\ddagger = 0.0191 \times T_c \times \left[9.97 + \lg \left(\frac{T_c}{\Delta\nu} \right) \right] [\text{kJmol}^{-1}] \quad \text{Eq. 6}$$

⁶⁶ A full lineshape analysis can be impossible when 1.) the sample is contaminated with impurities (e.g. due to decomposition upon heating), 2.) additional broadening of the signals is observed (e.g. due to viscosity effects or partial precipitation at lower temperatures) or 3.) affected signals overlap with any other signals.

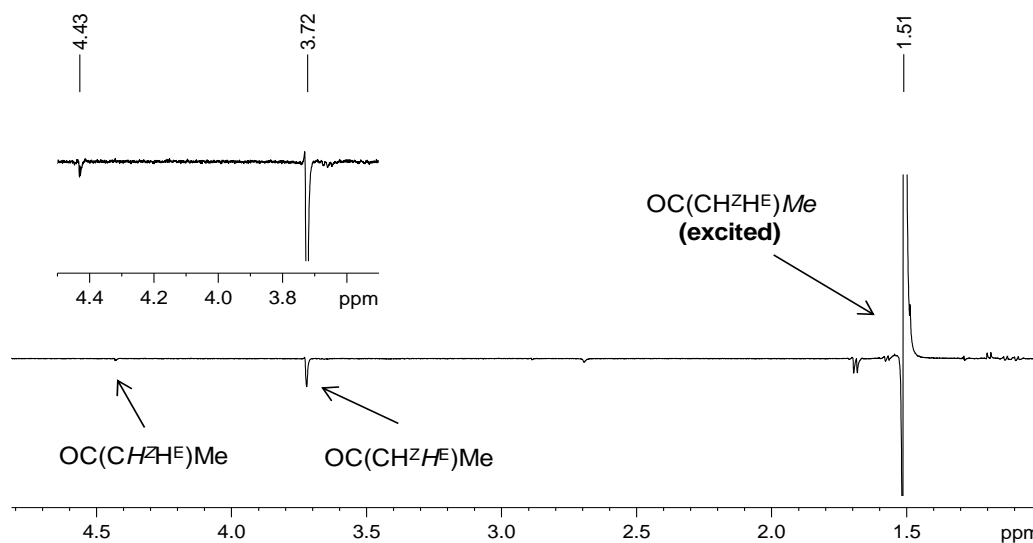
5.6.1 $\text{SiH}[\text{SiBr}\{\text{OC}(\text{CH}_2)\text{Me}\}\text{Tbb}](\text{SIDipp})$ (4)

Figure 116. Excerpt of the 1D ^1H NOESY (500.2 MHz) spectrum of 4-0.5($n\text{-C}_6\text{H}_{14}$) in benzene- d_6 at 298 K. The methyl protons of the $\text{OC}(\text{CH}_2\text{H})\text{Me}$ group were selectively excited. An enlarged excerpt of the spectrum (enlargement factor 10) with the proton signals at $\delta = 3.72$ and 4.43 ppm is shown in the inset.

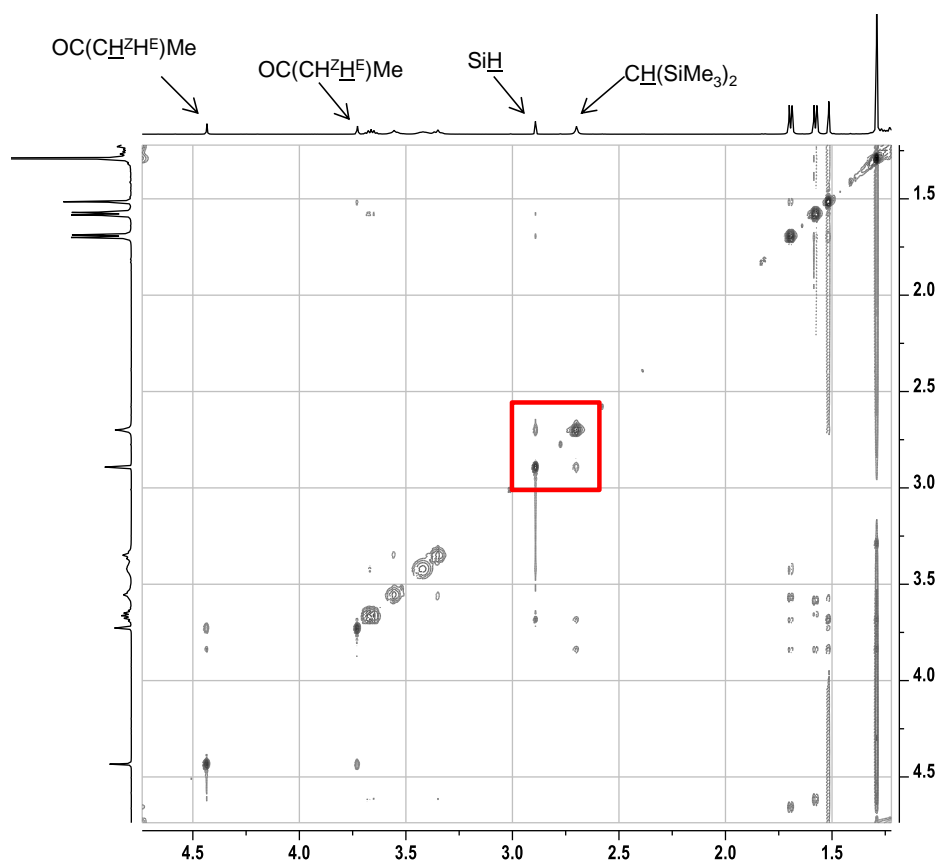


Figure 117. Excerpt of the 2D ^1H NOESY (500.2 MHz) spectrum of 4-0.5($n\text{-C}_6\text{H}_{14}$) in benzene- d_6 at 298 K. The highlighted area shows a through space correlation of the SiH and the $\text{CH}(\text{SiMe}_3)_2$ signal, but no correlation of the SiH with the $\text{OC}(\text{Me})\text{CH}_2$ group. This observation suggests the presence of a racemic mixture of the (R,S) and (S,R) stereoisomers of 4 in solution.

5.6.2 Isomerization of 14 into 15

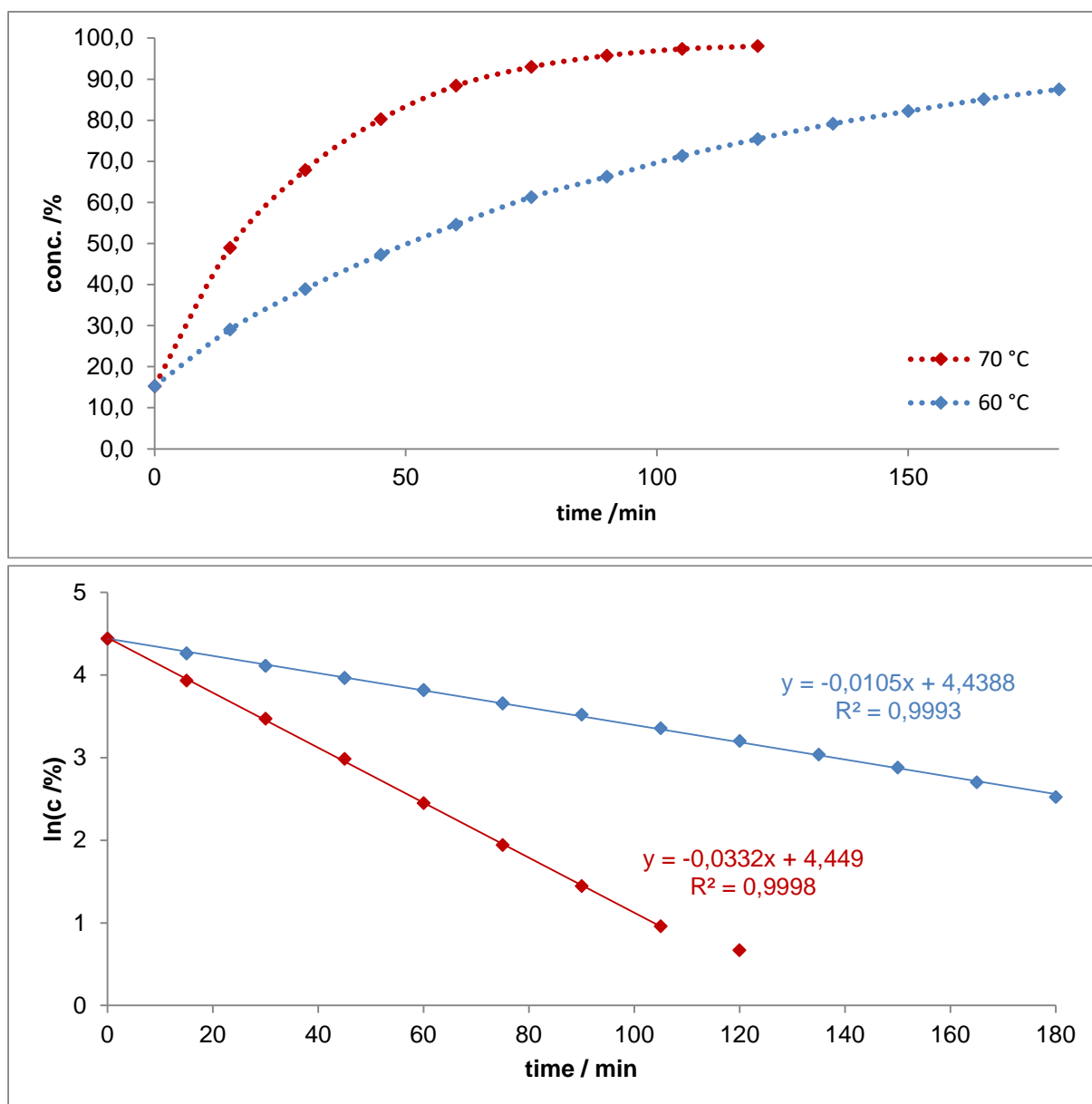


Figure 118. Conversion of 14 into 15 at $T = 60\text{ °C}$ (blue, top) and $T = 70\text{ °C}$ (red, below) and determination of k_{60} (blue, at 60 °C) and k_{70} (red, at 70 °C). The last data point at $T = 70\text{ °C}$ and $t = 120\text{ min}$ was discarded due to inaccurate integrations of the remaining isomer 14 at a conversion of $>98\%$. See also Figure 46 on page 87.

5.7 Results of quantum chemical calculations

All theoretical calculations were performed by Dr. Gregor Schnakenburg and/or Jens Rump from the Filippou group. The results presented in the following subchapters as well as support regarding specific interpretations are thankfully acknowledged.

5.7.1 (SIDipp)Si=Si(Br)Tbb and (SIDipp)Si=Si(CH₂Ph)Tbb (1 and 1-CH₂Ph)

Table 44. Results of the natural bond orbital (NBO) and natural resonance theory (NRT) analysis for **1^{calc}** (top) and **1-CH₂Ph^{calc}** (bottom).

NBO analysis of 1				NPA partial charges ^[b]		NRT analysis ^[c]	
	occ.	pol. [%]	hyb.	WBI			tot / cov / ionic
$\sigma(\text{Si1-Si2})$	1.89	57.4 (Si1) 42.6 (Si2)	sp ^{0.95} (Si1) sp ^{6.01} (Si2)	1.80	Si1 Si2	0.59 -0.02	Si1-Si2 2.09 / 1.81 / 0.28
$\pi(\text{Si1-Si2})$	1.89	51.1 (Si1) 48.9 (Si2)	p (Si1) p (Si2)				
$\sigma(\text{Si1-C}_{\text{aryl}})$	1.94	28.7 (Si1) 71.3 (C _{aryl})	sp ^{2.25} (Si1) sp ^{2.51} (C _{aryl})	0.77	C _{aryl} $\Sigma(\text{aryl})$	-0.53 -0.40	Si1-C _{aryl} 0.96 / 0.55 / 0.41
$\sigma(\text{Si2-C}_{\text{NHC}})$	1.93	22.1 (Si2) 77.4 (C _{NHC})	sp ^{7.98} (Si2) sp ^{1.33} (C _{NHC})	0.83	C _{NHC} $\Sigma(\text{NHC})$	0.16 0.19	Si2-C _{NHC} 1.07 / 0.44 / 0.64
$\sigma(\text{Si1-Br})$	1.97	26.0 (Si1) 74.0 (Br)	sp ^{4.71} (Si1) sp ^{3.85} (Br)	0.80	Br	-0.36	Si1-Br 0.79 / 0.37 / 0.41
n(Si2)	1.76		sp ^{0.3}		$\Sigma(\text{Si-Br})$	0.21	

NBO analysis of 1-CH ₂ Ph				NPA partial charges ^[b]		NRT analysis ^[c]	
	occ.	pol. [%]	hyb.	WBI			tot / cov / ionic
$\sigma(\text{Si1-Si2})$	1.91	56.2 (Si1) 43.8 (Si2)	sp ^{1.34} (Si1) sp ^{5.52} (Si2)	1.70	Si1 Si2	0.84 -0.01	Si1-Si2 1.81 / 1.60 / 0.21
$\pi(\text{Si1-Si2})$	1.74	48.8 (Si1) 51.2 (Si2)	p (Si1) p (Si2)				
$\sigma(\text{Si1-C}_{\text{aryl}})$	1.94	27.8 (Si1) 71.3 (C _{aryl})	sp ^{2.68} (Si1) sp ^{2.38} (C _{aryl})	0.79	C _{aryl} $\Sigma(\text{aryl})$	-0.52 -0.44	Si1-C _{aryl} 0.99 / 0.55 / 0.44
$\sigma(\text{Si2-C}_{\text{NHC}})$	1.92	25.9 (Si2) 74.1 (C _{NHC})	sp ^{3.01} (Si2) sp ^{3.09} (C _{NHC})	0.90	C _{NHC} $\Sigma(\text{NHC})$	0.11 0.07	Si2-C _{NHC} 1.20 / 0.48 / 0.72
$\sigma(\text{Si1-C}_{\text{Bn}})$	1.93	27.1 (Si1) 72.9 (C _{Bn})	Sp ^{2.55} (Si1) Sp ^{2.87} (C _{Bn})	0.71	C _{Bn} $\Sigma(\text{Bn})$	-0.89 -0.47	Si1-C _{Bn} 0.98 / 0.53 / 0.45
n(Si2)	1.77		sp ^{0.4}		$\Sigma(\text{Si-Bn})$	0.37	

[a]: occ.: occupancy, pol.: polarization, hyb.: hybridization, WBI: Wiberg bond index, tot / cov / ionic: total bond order / covalent bond order / ionic bond order. [b]: Partial charges obtained by natural population analysis (NPA). [c]: A local NRT analysis was carried out including the Br, Si1, Si2, N, C_{aryl} and C_{NHC} atoms.

5.7.2 SiH[SiBr{OC(CH₂)Me}Tbb](SIDipp) (4)

Table 45. Calculated structural parameters of the key species involved in the formation of **4**.

	Si1-Si2 /Å	Si1-O2 /Å	Si1-Br /Å	Si2-C25 ^{NHC} /Å	Si2...H2 /Å	C-O /Å	C-C ^α /Å
1	2.166	-	2.304	1.931	-	1.215	1.519
TS 1	2.261	2.134	2.331	1.907	5.472	1.258	1.477
Int.	2.302	1.800	2.331	1.899	5.294	1.333	1.460
TS 2	2.332	1.761	2.321	1.944	2.123	1.333	1.418
(S,S)-4	2.388	1.704	2.318	1.929	1.506	1.368	1.340
TS 3	2.298	1.690	2.312	1.813	1.475	1.371	1.341
(S,R)-4	2.371	1.696	2.327	1.917	1.500	1.371	1.340

RI-B97-D3/def2-TZVP level of theory; for the calculated mechanism, see Scheme 16 on page 45.

5.7.3 **Si(ZnBr)(SiBrCH₂PhTbb)(SIDipp) (6)****Table 46.** Selected results of the natural bond orbital (NBO) analysis for **6_{calc}** (top), **6^{TS}_{calc}** (middle) and **6'_{calc}** (bottom). Atom numbering of the experimental structures was taken over in the calculated structures.

	Orbital	occ. ^A [e]	pol. ^A [%]	hybridization		WBI ^A
				s [%]	p [%]	
compound 6_{calc}	σ(Si1-Si2)	1.89	Si1: 52.0 Si2: 48.0	32.6 13.7	66.8 85.2	1.00
	π(Si1-Si2)	-	-	-	-	
	σ(Si2-C25)	1.94	Si2: 23.7 C25: 76.3	13.6 44.2	85.7 55.6	0.98
	LP(Si2)	1.71		70.8	28.9	
	σ(Si1-Br1)	1.97	Si1: 23.7 Br1: 76.3	12.7 20.6	85.8 79.1	0.76
	σ(Zn-Br1)	-	-	-	-	
	σ(Zn-Br2)	-	-	-	-	0.35
	σ(Si2-Zn)	1.80	Si2: 63.2 Zn: 36.8	2.33 97.8	96.5 1.2	0.64
compound 6^{TS}_{calc}	σ(Si1-Si2)	1.90	Si1: 51.2 Si2: 48.8	41.1 15.5	58.4 83.2	1.33
	π(Si1-Si2)	1.59	Si1: 25.0 Si2: 75.0	0.9 0.5	98.5 99.0	
	σ(Si2-C25)	1.94	Si2: 24.4 C25: 75.6	14.5 43.8	84.7 56.1	0.96
	LP(Si2)	1.67		69.9	29.6	
	σ(Si1-Br1)	-	-	-	-	0.15
	σ(Zn-Br1)	-	-	-	-	0.23
	σ(Zn-Br2)	-	-	-	-	0.35
	σ(Si2-Zn)	-	-	-	-	0.41
compound 6'_{calc}	σ(Si1-Si2)	1.93	Si1: 48.8 Si2: 51.2	38.0 25.8	61.5 73.5	1.59
	π(Si1-Si2)	1.71	Si1: 41.1 Si2: 58.9	1.6 0.1	97.8 99.5	
	σ(Si2-C25)		Si2: 25.7 C25: 75.3	17.8 42.4	81.7 57.5	0.88
	LP(Si2)	1.67		56.6	43.2	
	σ(Si1-Br1)	-	-	-	-	0.01
	σ(Zn-Br1)	-	-	-	-	0.32
	σ(Zn-Br2)	-	-	-	-	0.33
	σ(Si2-Zn)	-	-	-	-	0.37

A: occ. = occupancy; pol. = polarization; WBI = Wiberg bond indices; B: tot. / cov. / ion. = total / covalent / ionic; LP = electron lone pair. See also Scheme 18 on page 51

5.7.4 **CuBr{(Z)-(SIDipp)Si=Si(Br)Tbb} (10) and CuBr{(Z)-(SIDipp)(OtBu)Si=SiTbb} (12)**

In order to circumvent convergence problems caused by too many resonance contributions by the substituents, a local NRT analysis involving Br1, Br2, Cu, Si1, Si2, C1 and C25 atoms was performed on the B97-D3(BJ)/def2-SVP//B97-D3(BJ)/def2-TZVP level of theory. See also Figure 42 and Figure 43 on page 78.

Table 47. Bonding parameters (calculated and experimental), Wiberg bond indices, NRT bond orders (given in total-/covalent-/ionic-contribution) and charges derived from the natural population analysis of selected bonds of **10^{calc}** and **12^{calc}**. The numbering corresponds to the numbering in the crystal structure.

compound	A-B	d(A-B) /Å	WBI	NRT-BO (tot./cov./ion.)	atom	NPA /e
10	Si1-C1	1.891	0.80	1.0/0.6/0.4	Si ^{Tbb}	+0.60
		1.898(7)				
	Si1-Br2	2.306	0.80	1.0/0.4/0.6	Si ^{NHC}	+0.04
		2.255(2)				
	Si1-Cu	2.401	0.29	0.0/0.0/0.0	Cu	+0.61
		2.411(2)				
	Si1-Si2	2.241	1.45	1.6/1.4/0.2	Br1	-0.70
		2.254(3)				
Cu-Br1	2.311	0.35	0.7/0.2/0.5	Br2	-0.36	
	2.2882(13)					
Cu-Si2	2.366	0.35	0.5/0.2/0.3	C1 ^{Tbb}	-0.56	
	2.318(2)					
Si2-C25	1.940	0.77	0.9/0.4/0.5	C25 ^{NHC}	+0.15	
	1.948(6)					
12	Si1-C1	1.931	0.78	0.9/0.5/0.4	Si1 ^{Tbb}	+0.08
		1.930(9)				
	Si2-O	1.663	0.55	1.1/0.2/0.8	Si2 ^{NHC}	+0.90
		1.631(6)				
	Si1-Cu	2.353	0.33	0.4/0.2/0.2	Cu	+0.60
		2.309(2)				
	Si1-Si2	2.243	1.59	1.8/1.4/0.4	Br1	-0.73
		2.217(3)				
Cu-Br1	2.344	0.32	0.7/0.2/0.5	O	-0.93	
	2.2859(14)					
Cu-Si2	2.446	0.23	0.1/0.1/0.0	C1 ^{Tbb}	-0.50	
	2.453(2)					
Si2-C25	1.940	0.70	0.9/0.4/0.5	C25 ^{NHC}	+0.11	
	1.936(8)					

5.7.5 (SIDipp)(*t*BuO)Si=SiTbb and (SIDipp)Si=Si(*Ot*Bu)Tbb (**14** and **15**)**Table 48.** Bonding parameters (calculated and experimental), Wiberg bond indices, NRT bond orders (given in total-/covalent-/ionic-contribution) and charges derived from the natural population analysis of selected bonds of **14** and **15** on the B97-D3(BJ)/def2-SVP//B97-D3(BJ)/def2-TZVP level of theory. The numbering corresponds to the numbering in the crystal structure.

	A–B	d(A–B) ^A /Å	WBI	NRT-BO (tot./cov./ion.)	atom	NPA /e
14	Si1–Si2	2.213 2.2243(7)	1.64	1.6/1.3/0.3	Si1 ^{Tbb}	+0.18
	Si1–C1	1.937 1.940(2)	0.77	1.0/0.5/0.5	Si2 ^{NHC}	+0.88
	Si2–O	1.679 1.651(2)	0.54	0.1/0.0/0.1	O	–0.92
	Si2–SiC29	1.896 1.891(2)	0.85	1.4/0.8/0.6	C1 ^{Tbb}	–0.50
					C29 ^{NHC}	+0.04
15	Si1–Si2	2.213 2.175(5)	1.66	1.9/1.6/0.3	Si1 ^{Tbb}	+1.14
	Si1–C1	1.903 1.915(12)	0.73	0.8/0.4/0.4	Si2 ^{NHC}	–0.11
	Si1–O	1.668 1.634(9)	0.57	1.0/0.2/0.8	O	–0.91
	Si2–SiC29	1.910 1.927(14)	0.99	1.3/0.7/0.6	C1 ^{Tbb}	–0.53
					C29 ^{NHC}	–0.07

A: Both calculated and experimental values are given.

Table 49. Comparison of experimental and calculated (B97-D3(BJ)/def2-SVP//B97-D3(BJ)/def2-TZVP) structural data of the NHC-stabilized disilyne **14**, its disilavinylidene isomer **15** and the transition state.

	Si=Si /Å	Si2··O /Å	Si1··O /Å	Si1–C1 ^{Tbb} /Å	Si2–C25 ^{NHC} /Å	O–C52 /Å
14 ^{exp}	2.225(2)	1.651(5)	3.664(7)	1.938(6)	1.901(6)	1.455(8)
14 ^{calc}	2.233	1.699	3.681	1.944	1.875	1.451
TS ^{calc}	2.392	2.576	1.772	1.966	1.873	1.447
15 ^{calc}	2.275	3.268	1.704	1.919	1.854	1.451
15 ^{exp}	2.175(5)	3.58(1)	1.634(9)	1.94(1)	1.92(1)	1.46(2)

A fully relaxed scan of the Si1-Si2-C^{NHC}-N2 dihedral angle from 0 – 180° in increments of approx. 5° gave rotation barriers of 27 kJ/mol at 84.8° (\angle NHC: 63°) for compound **14** and 46 kJ/mol at 180.0° (\angle NHC: 37°) for compound **15**.

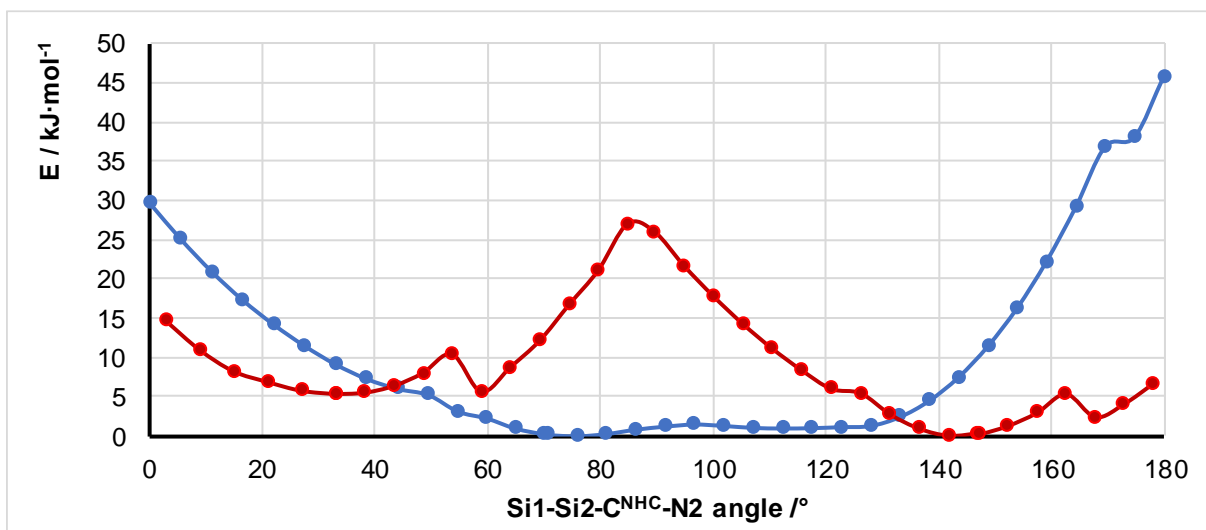


Figure 119. Rotation energies of compound **14** (red) and **15** (blue) in respect to the Si1-Si2-C^{NHC}-N2 dihedral angle, where the N2 atom is anti to the O atom in the experimental structure (see Figure 49 on page 93).

5.7.6 *cyclo-Si[C{ONa(thf)}PSi(Tbb)P](SIDipp) (7_{calc}⁻)*

For the experimental structure, see Figure 30 on page 57. For the leading NRT formulae, see Scheme 20 on page 61. For a depiction of the energy dependence of the angular deflection of the NHC, see Figure 33 on page 62.

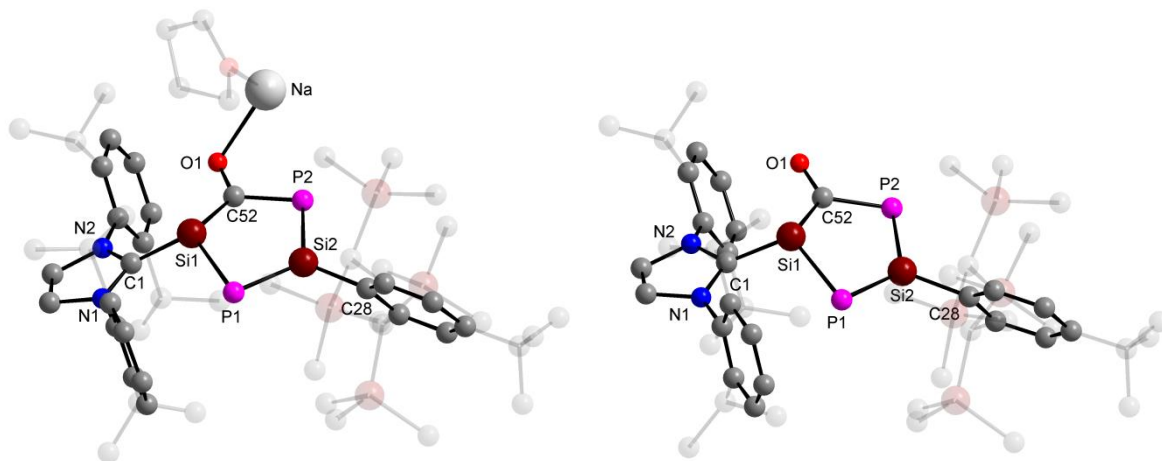


Figure 120. Comparison of the experimental structure **7·thf** (left) and the structure of the calculated anion **7_{calc}⁻** (right, RI-B97-D3/def2-TZVP). Peripheral substituents and the thf molecule are depicted transparently; hydrogen atoms are omitted for simplicity. See also Table 6 on page 60.

Table 50. Comparison of respective energies, bond lengths and the angle α at the Si1NHC atom in **7**, **7**^{-calc}, and the extreme values for maximum/minimum angular deflection (RI-B97-D3/def2-TZVP).

Cpd.	ΔE /kJ·mol ⁻¹	ϵ /°	Si1-C1 ^{NHC} /Å	Si1-P1 /Å	Si1-C52 /Å	P1-Si1-C52 /°
7 ^{exp.}	-	138.89(9)	1.875(2)	2.219(1)	1.907(2)	113.92(8)
7 ^{-calc}	0	135.96°	1.865	2.252	1.983	111.93
7 ^{-calc} ^{max}	+23.1	175.6	1.799	2.197	1.929	116.54
7 ^{-calc} ^{min}	+49.0	90.0	1.927	2.309	2.051	105.23

In the putative compound **7**^{-calc}^{max}, the imidazole ring of the NHC ligand would be in plane with the central {Si:P:C} system, while compound **7**^{-calc}^{min} features perpendicular orientation.

Table 51. Selected results of the NBO and NRT analysis of **7**^{-calc}.

orbital	occ. /e	pol. /%	hybridization		WBI	NRT		
			s /%	p /%		tot.	cov.	ion.
LP(P1)	1.926	-	63.6	36.2	-	1.35	-	-
LP(P2)	1.925	-	64.9	35.0	-	1.42	-	-
LP(P2)	1.333	-	0.00	99.9	-			
σ (P1-Si1 ^{NHC})	1.912	P: 60.09 Si: 39.01	15.61 31.84	83.00 67.61	1.00	1.03	0.78	0.25
σ (P1-Si2 ^{Tbb})	1.947	P: 58.87 Si: 41.13	20.38 35.61	78.36 63.78	1.45	1.59	1.13	0.46
π (P1-Si2 ^{Tbb})	1.914	P: 69.68 Si: 30.32	0.24 0.02	99.08 99.10				
σ (P2-Si2 ^{Tbb})	1.943	P: 55.77 Si: 44.23	17.47 35.06	81.42 64.31	1.26	1.28	1.00	0.28
σ (P2-C52 ^{Ring})	1.960	P2: 39.83 C52: 60.17	17.60 33.74	81.60 65.97	1.19	1.28	0.93	0.36
σ (Si1-C1 ^{NHC})	1.926	Si1: 26.23 C1: 73.77	27.12 39.10	72.25 60.76	1.05	1.50	0.88	0.62
π (Si1-C1 ^{NHC})	1.738	Si1: 58.57 C1: 41.43	7.76 2.90	92.10 97.01				
σ (Si1-C52 ^{Ring})	1.960	Si1: 32.77 C52: 67.23	33.28 34.78	66.27 64.99	0.90	1.00	0.62	0.38
σ (Si2-C28 ^{Tbb})	1.950	Si2: 28.40 C28: 71.60	29.14 29.45	70.26 70.41	0.77	0.97	0.55	0.42
σ (C52 ^{Ring} -O1)	1.996	O1: 65.16 C52: 34.84	37.72 31.50	61.79 68.40	1.52	1.62	1.01	0.61
π (C52 ^{Ring} -O1)	1.987	O1: 68.59 C52: 31.41	0.02 0.19	99.77 99.68				

Atom numbering of the experimental structure was taken over in the calculated structure.

occ. = occupancy; pol. = polarization; tot. / cov. / ion. = total / covalent / ionic

For the leading NRT formulae, see Scheme 20 on page 61.

5.7.7 $\text{Si}\{\text{N}(\text{Me})\text{Ar}^{\text{Mes}}\}_2$ (**18**)

For the experimental structure see Figure 63 on page 120.

Table 52. Selected results of the NBO and NRT analysis of **18^{calc}**.

orbital	occ. /e	pol. /%	hybridization		WBI	NRT		
			s /%	p /%		tot.	cov.	ion.
LP(Si)	1.91	Si: 95.5	79.5	20.4	-	-	-	-
$\sigma(\text{Si-N1})$	1.95	Si: 11.2 N: 86.5	15.6 36.7	83.1 63.2	0.62	1.49	0.30	1.19
$\sigma(\text{Si-N\#})$	1.95	Si: 11.2 N: 86.5	15.6 36.7	83.1 63.1	0.62	1.49	0.30	1.19
$\pi(\text{Si-N\#})$	1.90	Si: 7.5 N: 87.4	0.11 0.41	96.5 99.5				
LP(N)	1.76	N: 87.8 Si: 6.57	0.44 0.14	99.5 95.6	-	-	-	-
$\sigma(\text{N-C1}^{\text{Aryl}})$	1.95	N: 59.3 C: 39.7	30.3 27.9	69.5 72.0	1.01	1.00	0.80	0.20
$\sigma(\text{N-C25}^{\text{Methyl}})$	1.98	N: 60.4 C: 38.5	29.8 26.0	70.0 74.0	0.97	1.00	0.78	0.22
$\sigma(\text{N\#-C1\#}^{\text{Aryl}})$	1.98	N: 59.3 C: 39.7	30.3 27.9	69.5 72.0	1.01	1.00	0.80	0.20
$\sigma(\text{N\#-C25\#}^{\text{Methyl}})$	1.98	N: 60.4 C: 38.5	29.8 25.9	70.1 74.0	0.97	1.00	0.78	0.22

Atom numbering of the (inversion symmetric) experimental structure was taken over.

occ. = occupancy; pol. = polarization; tot. / cov. / ion. = total / covalent / ionic.

Table 53. Comparison of selected experimental bond lengths, angles and torsion angles of **18** with the calculated (RI-B97-D3/def2-TZVP) bond lengths and angles.

	Si-N /Å	N-C1 /Å	N-C25 /Å	N-Si-N# /°	C1-N-Si /°	N-Si-N#-C1# /°	N1-Si-N#-C25 /°
18	1.722(1)	1.439(2)	1.461(2)	103.38(9)	121.6(1)	-150.6(1)	33.3(1)
18^{calc}	1.755	1.434	1.466	103.8	119.4	-148.2	33.7

For the experimental structure see Figure 63 on page 120.

5.7.8 $\text{Si}(\text{OAr}^{\text{Mes}})_2$ (19)

For the computed UV-Vis-NIR spectrum of 19^{calc} see chapter 5.5.7, page 271. The calculated IR and Raman spectra are in good agreement with the experimental data. Further, the calculations have been used to assign the $\tilde{\nu}(\text{Si-O})_{\text{sym}}$ and $\tilde{\nu}(\text{Si-O})_{\text{asym}}$ vibrations observed in the experimental Raman spectrum.

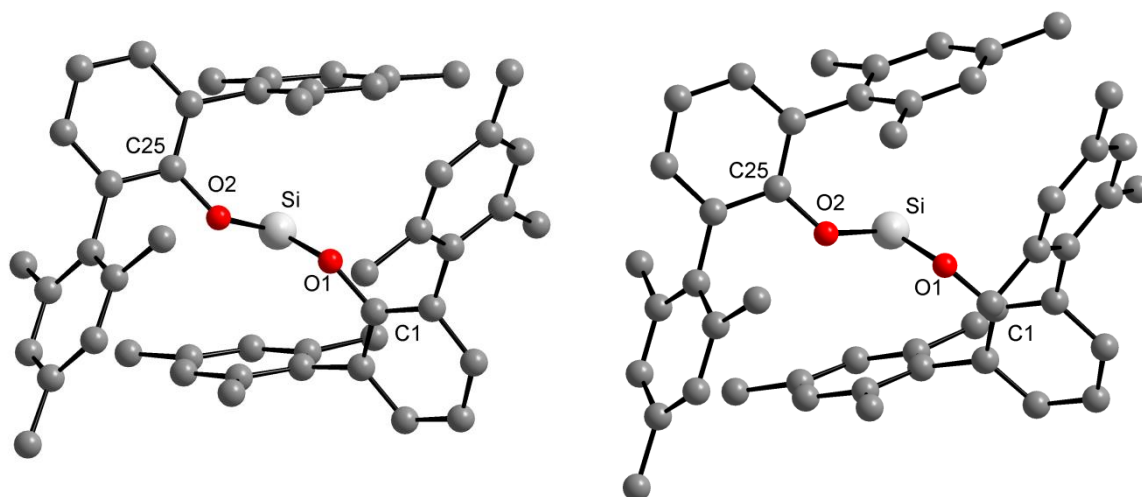


Figure 121. Comparison of the experimental (left) and calculated (right, RI-B97-D3/def2-TZVP) structure of **19**. Hydrogen atoms are omitted for simplicity.

Table 54. Comparison of selected experimental bond lengths and angles of **19** with the calculated (RI-B97-D3/def2-TZVP) bond lengths and angles.

	Si-O1 [Å]	Si-O2 [Å]	O1-C1 [Å]	O2-C25 [Å]	O1-Si1-O2 [°]	C1-O1-Si [°]	C25-O2-Si [°]
exp.	1.676(1)	1.681(1)	1.366(2)	1.368(2)	93.07(6)	131.1(1)	128.0(1)
calcd.	1.700	1.699	1.364	1.363	94.5	128.5	129.8

Atom numbering of the experimental structures was taken over in the calculated structures.

Table 55. Partial charges from natural population analysis (NPA) of 19^{calc} .

atom	Si	O1	O2	C1	C25
Partial charge	+1.14	-0.93	-0.93	+0.31	+0.31

Table 56. Selected results of the NBO and NRT analysis of **19^{calc}**.

orbital	occ. ^A [e]	Pol. ^A [%]	hybridization		WBI	NRT ^A		
			s [%]	p [%]		tot.	cov.	ion.
LP(Si)	1.958	-	86.2	13.8	-	-	-	-
LP(O1)	1.928	-	37.2	62.7	-	-	-	-
LP(O1)	1.846	-	9.2	90.6	-	-	-	-
LP(O2)	1.927	-	36.6	63.3	-	-	-	-
LP(O2)	1.846	-	9.3	90.5	-	-	-	-
σ(Si-O1)	1.936	Si: 6.95 O: 93.05	8.9	88.5	0.44	1.39	0.16	1.23
σ(Si-O2)	1.936	Si: 6.88 O: 93.12	8.7	88.7	0.44	1.39	0.16	1.23
LV(Si) ^A	0.211	-	0.0	99.0	-	-	-	-

A: occ. = occupancy; pol. = polarization; tot. / cov. / ion. = total / covalent / ionic; LV = lone vacancy.

Table 57. Experimental and computed IR and Raman bands of **19**, **19^{calc}**, Si(OCH₃)₂ and Si(OPh)₂.

Compound	ν _{symm} (Si-O)			ν _{asymm} (Si-O)		
	Band /cm ⁻¹	Intensity ^A		Band /cm ⁻¹	Intensity	
		IR	Raman		IR	Raman
19^{exp}	724 / 727 ^B	weak	weak	714	vs	-
19^{calc}	723	10.2	16.8	718	131.5	4.3
Si(OCH₃)₂	730	95.9	19.4	740	88.7	6.6
Si(OPh)₂	717	7.8	49.7	719	85.5	4.6

A: Computed relative Intensity; **B:** The symmetric stretching vibration was observed at 727 cm⁻¹ by ATR-IR spectroscopy and at 724 cm⁻¹ by Raman spectroscopy.

5.7.9 $\text{SiX}(\text{BX}_2)(\text{OAr}^{\text{Mes}})_2$ or $\text{Si}(\text{BX}_3)(\text{OAr}^{\text{Mes}})_3$: $\mathbf{19}\text{-BX}_3$ or $\mathbf{19}\cdot\text{BX}_3$?

The reaction of **19** with different trihaloboranes led to the insertion products ($\mathbf{19}\text{-BX}_3$) instead of the silylene-borane adducts ($\mathbf{19}\cdot\text{BX}_3$) as evidenced by ^{11}B NMR spectroscopy. The structures of both isomers were optimized exemplarily for the BI_3 -derivatives (see Figure 122 and Table 58 below and page 147ff. for a discussion in the main text) and were carried out at the B97-D3(BJ)^{ATM}/def2-TZVP level of theory without any symmetry restraints. The insertion product $\mathbf{19}\text{-BI}_3^{\text{calc}}$ is lower in energy by $81.1 \text{ kJ}\cdot\text{mol}^{-1}$ (Table 59) than the adduct $\mathbf{19}\cdot\text{BI}_3^{\text{calc}}$ and is therefore more likely to be formed.

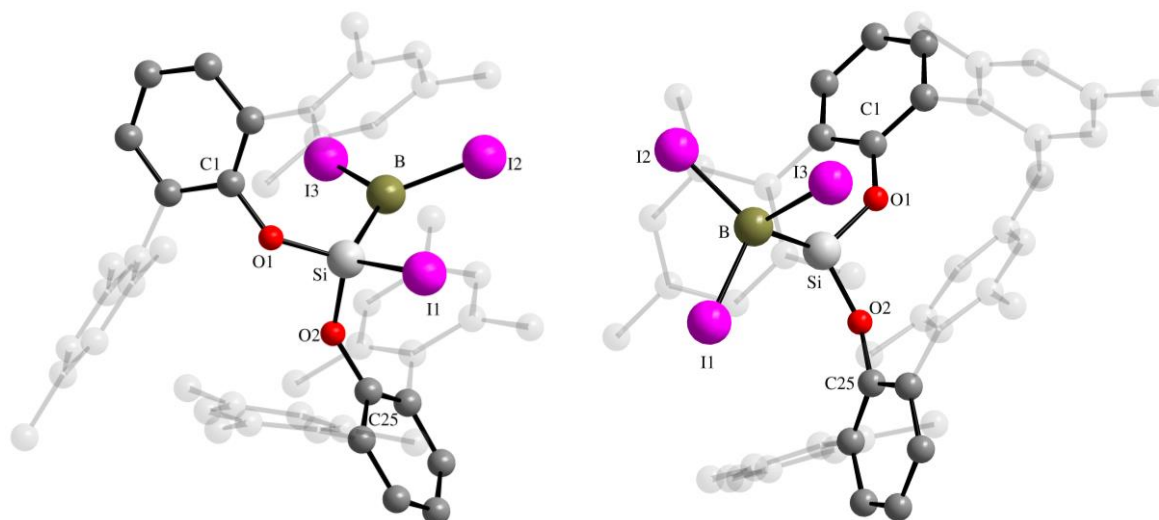


Figure 122. Comparison of the calculated (B97-D3(BJ)^{ATM}/def2-TZVP) structures of the BI_3 -insertion product $\mathbf{19}\text{-BI}_3$ (left) and the addition product $\mathbf{19}\cdot\text{BI}_3$ (right) of **19**. Hydrogen atoms are omitted for simplicity. Selected torsion angles ($^\circ$): $\mathbf{19}\text{-BI}_3^{\text{calc}}$: I2-B-Si-I1 6.6, I3-B-Si-I1 -171.1 ; $\mathbf{19}\cdot\text{BI}_3^{\text{calc}}$: O1-Si-B-I1 -169.7 , O2-Si-B-I1 -25.5 .

Table 58. Comparison of the calculated (B97-D3(BJ)^{ATM}/def2-TZVP) structures of $\mathbf{19}\text{-BI}_3^{\text{calc}}$ and $\mathbf{19}\cdot\text{BI}_3^{\text{calc}}$.

	Si-B / Å	ØB-I / Å	Si-I / Å	ØSi-O / Å	O-Si-O / $^\circ$	$\Sigma_{\text{Si}}^1 / ^\circ$	$\Sigma_{\text{B}}^2 / ^\circ$
$\mathbf{19}\text{-BI}_3^{\text{calc}}$	2.025	2.131	2.470	1.653	101.99	321.7	360.0
$\mathbf{19}\cdot\text{BI}_3^{\text{calc}}$	2.010	2.256	-	1.637	104.51	352.1	333.1

1: Sum of angles at the Si atom without consideration of the B atom in $\mathbf{19}\text{-BI}_3^{\text{calc}}$;

2: Sum of angles at the B atom without consideration of the Si atom in $\mathbf{19}\cdot\text{BI}_3^{\text{calc}}$.

Table 59. Calculated (B97-D3(BJ)^{ATM}/def2-TZVP) relative energies of **19-BI₃^{calc}** and **19-BI₃^{calc}**.

Compound	E _{el,rel}	E _{disp,rel}	U _{rel} (298.15 K)	H _{rel} (298.15 K)	S _{rel}	G _{rel} (298.15 K)
19-BI₃^{calc}	0.0	+6.4	0.0	0.0	+6.9	0.0
19-BI₃^{calc}	+81.3	0.0	+79.0	+79.0	0.0	+81.1

Although structures of acyclic silylboranes are extremely rare,⁶⁷ the structural data calculated for **19-BX₃^{calc}** and **19-BX₃^{calc}** match fairly well. Thus, no abnormal Si-B distances are predicted: in fact, the known very bulky acyclic boranes B(NiPr₂)(PPh₂){Si(SiMe₃)₃} (d_{B-Si}: 2.063(5) Å) and BX(SitBu₃)₂ (X = F: 2.102(3) or 2.126(4) Å; X = Cl: 2.127(1) Å) feature even longer distances, while the average Si-B distance in cyclic silylboranes (2.001 Å)⁶⁷ is nearly identical to the calculated values. While the elongation of the B-I bonds in **19-BX₃^{calc}** is common for acyclic, four-coordinated iodoboranes, the Si-I bond in **19-BX₃^{calc}** compares fairly well to both **19-I** (Ø2.4234(6) Å)^[385] and **19-HI** (2.415(2) Å).

⁶⁷ On the basis of a CSD 5.4.1 search. Only the three examples of acyclic silyl-substituted boranes (or boryl-substituted silanes) mentioned in the main text were found. Additionally, three iron- and manganese-complexes with silylboryl substituents were structurally characterized by the group of Braunschweig.

If cyclic compounds are included, a total of 54 structures are known. Generally, these examples feature shorter Si-B distances (average 2.001 Å) with a maximum of 2.109 Å in (Pip)B[Si(SiMe₃)₂SiMe₂]₂ (Pip = 2,6-tetramethylpiperidine) and a minimum of 1.857 Å in the bis-silylene borylene complex BrB{[Si[(NtBu)₂CPh]]₂-1,2-o-C₂B₁₀H₁₀} (where the silylenes are fused with an C₂B₁₀H₁₀ carborane cluster).

5.8 Indices

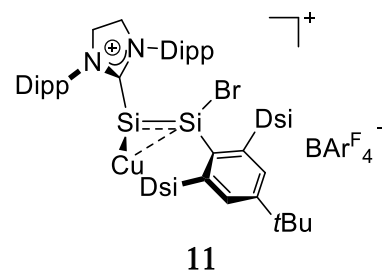
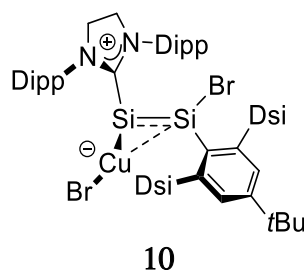
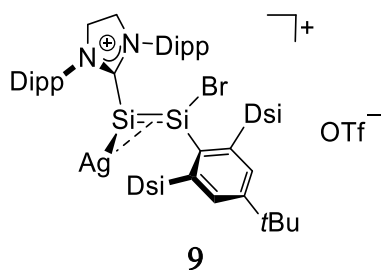
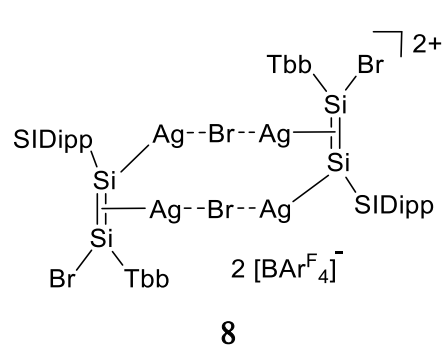
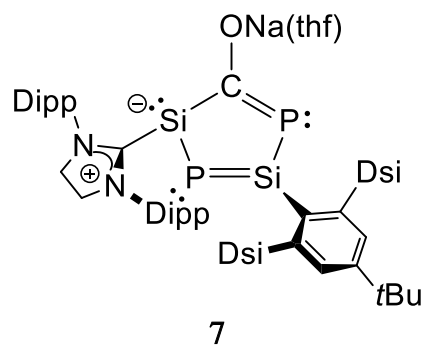
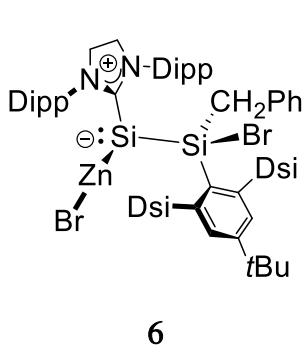
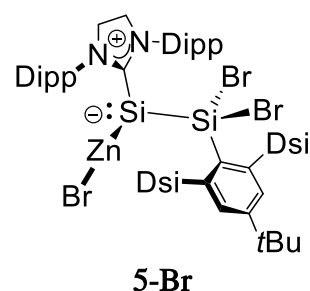
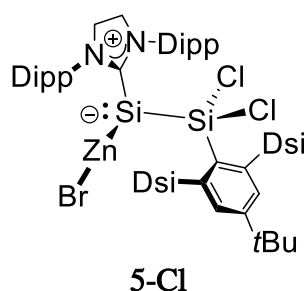
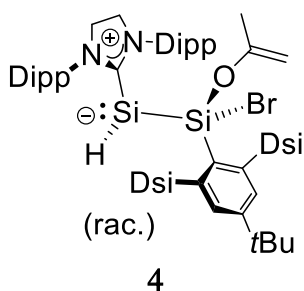
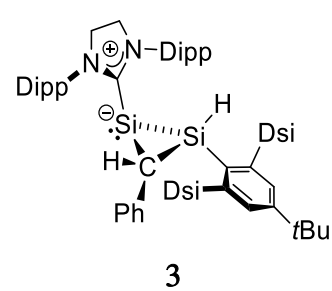
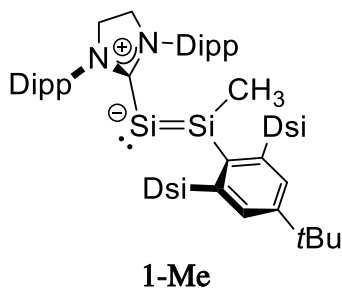
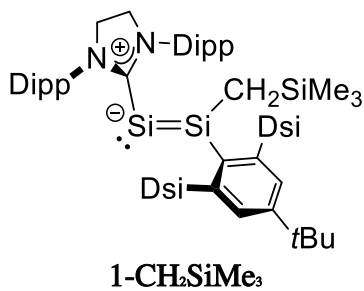
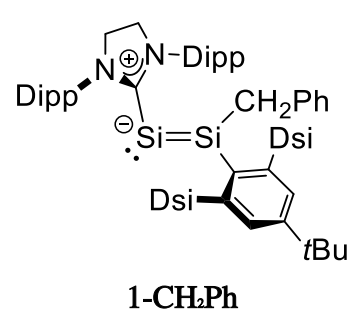
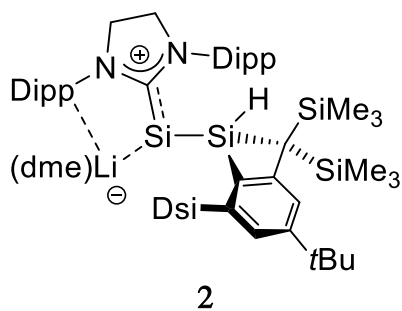
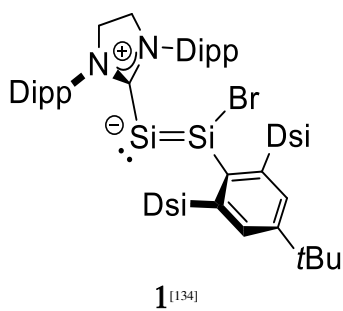
5.8.1 List of abbreviations

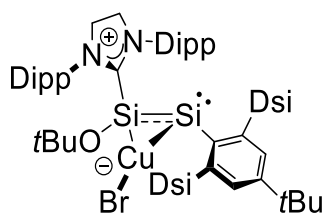
For the numeration of literature-known compounds (in roman letters) see chapter 5.8.2 below.
For the designation of signal types in NMR-, IR- or Raman spectroscopy, see chapter 4.2.

2D	Two dimensional
Ad	Adamantyl
Ar ^F	3,5-(CF ₃) ₂ -C ₆ H ₃
Ar ^{Mes}	2,6-Bis-(Mes)-C ₆ H ₃ (for a depiction see page 293)
ATR	<u>A</u> ttenuated <u>t</u> otal <u>r</u> eflection
cAAC ^R	<u>C</u> yclic <u>a</u> lkyl <u>a</u> mino <u>c</u> arbene (R = C _β substituent(s) to be defined; usually Me ₂ or cyclohexyl)
Calc.	Calculated
Cp	cyclopentadiene; η ⁵ -C ₅ H ₅
Cp*	Pentamethylcyclopentadiene; η ⁵ -C ₅ Me ₅
Cpd.	<u>C</u> ompound
CSD	<u>C</u> ambridge <u>s</u> tructural <u>d</u> atabase (for X-ray structures of compounds)
dec.	Decomposition / decet signal (in NMR spectroscopy)
DFT	<u>D</u> ensity <u>f</u> unctional <u>t</u> heory
Dipp	2,6-diisopropylphenyl
dme	<u>D</u> imethoxyethane
Dsi	Disilyl; CH(SiMe ₃) ₂
e. g.	<u>E</u> xempli <u>g</u> ratia (latin: “for example”)
equiv.	Equivalents (in reaction stoichiometry)
et al.	Et alii (and coworkers; latin: “and others”)
Exp.	Experimental
HOMO	<u>H</u> ighest <u>o</u> ccupied <u>m</u> olecular <u>o</u> rbital
IDipp	1,3-Bis(2,6-diisopropylphenyl)imidazol-2-ylidene; :C{N(Dipp)CH} ₂ (see page 293)
liPr ₂ Me ₂	1,3-Diisopropyl-4,5-dimethylimidazol-2-ylidene; :C{N(iPr)C(Me)} ₂ (see page 293)
IME ₄	1,3,4,5-Tetramethylimidazol-2-ylidene; :C{N(Me)C(Me)} ₂ (see page 293)
IR	<u>I</u> nfrared
IUPAC	<u>I</u> nternational <u>U</u> nion of <u>P</u> ure and <u>A</u> ppplied <u>C</u> hemistry
LUMO	<u>L</u> owest <u>u</u> noccupied <u>m</u> olecular <u>o</u> rbital
Mes	Mesityl; 2,4,6-trimethylphenyl
MO	<u>M</u> olecular <u>o</u> rbital
n. a.	<u>N</u> ot <u>a</u> vailable
NBO	<u>N</u> atural <u>b</u> ond <u>o</u> rbital
NHC	<u>N</u> - <u>h</u> eterocyclic <u>c</u> arbene
NHSi	<u>N</u> - <u>h</u> eterocyclic <u>s</u> ilylene
NMR	<u>N</u> uclear <u>m</u> agnetic <u>r</u> esonance (-spectroscopy)
NPA	<u>N</u> atural <u>p</u> opulation <u>a</u> nalysis
NRT	<u>N</u> atural <u>r</u> esonance <u>t</u> heory
PES	<u>P</u> otential <u>e</u> nergy <u>s</u> urface
pTol	para-Tolyl; 4-Me-C ₆ H ₄
Pyramid.	Pyramidalization of a 3-coord. atom percent $\frac{360^\circ - \text{sum of angles}}{360^\circ - 270^\circ} \times 100 \%$
r. t.	<u>R</u> oom <u>t</u> emperature (298 K; does not equal ambient temperature)
Ref.	Reference

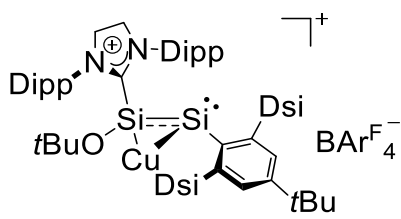
S	<u>S</u> olvent (figures of NMR spectra) / <u>s</u> inglet (in spectroscopy)
SIDipp	“Saturated IDipp” :C{N(Dipp)CH ₂ } ₂ (for a depiction see page 293)
Tbb	2,6-[CH(SiMe ₃) ₂]-4-tBu-C ₆ H ₄ (for a depiction see page 293)
TBoN	B{N(Dipp)CH ₂ } ₂ , (for a depiction see page 293)
Tbt	2,4,6-[CH(SiMe ₃) ₂] ₃ -C ₆ H ₃
T _c	Coalescence temperature
thf	<u>T</u> etrahydrofuran
Tip	2,4,6- <u>T</u> riisopropylphenyl (also commonly abbreviated as “Trip”)
Tips	<u>T</u> riisopropylsilyl; Si(iPr) ₃
TMS	<u>T</u> rimethylsilyl; SiMe ₃
Vide infra	Latin: “see below”
Vide supra	Latin: “see above”
WBI	<u>W</u> iberg <u>b</u> ond <u>i</u> ndex
XRD	<u>X</u> -ray <u>d</u> iffraction (analysis of single crystals)
Σ _x	Sum of angles around atom X (X = Si, P, N, C...)
δ _x	Chemical shift of element X (in NMR spectroscopy: d _n , δ, δ _n ...)

5.8.2 Enumeration of compounds discussed in this work

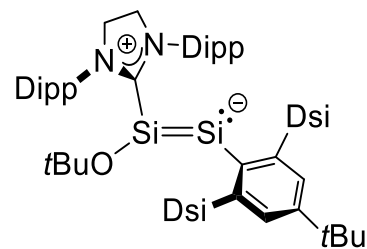




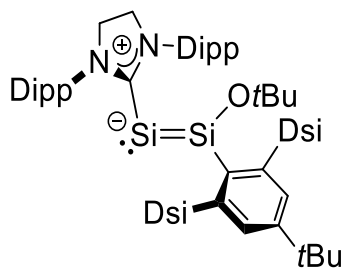
12



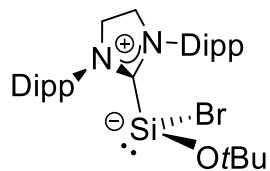
13



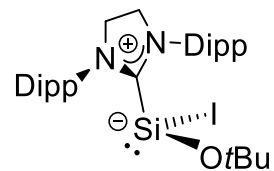
14



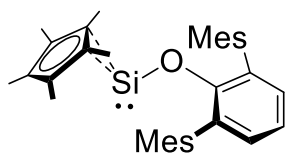
15



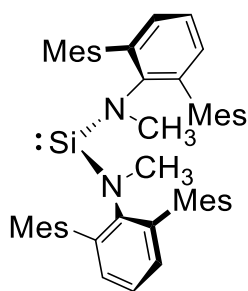
16-Br



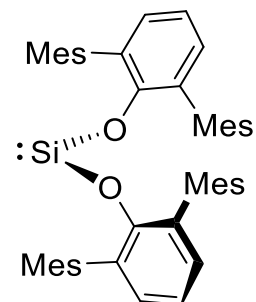
16-I



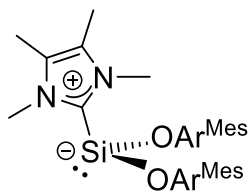
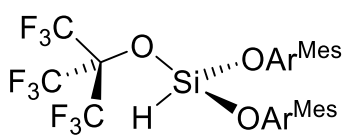
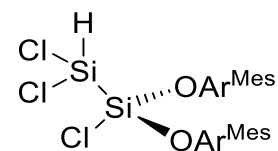
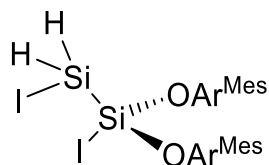
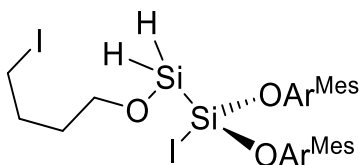
17



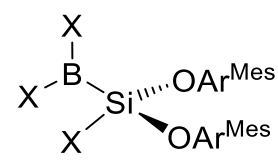
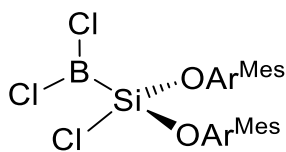
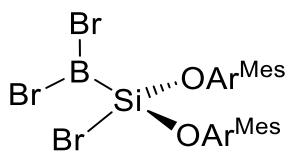
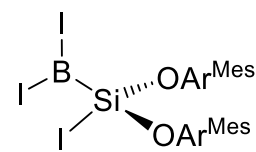
18

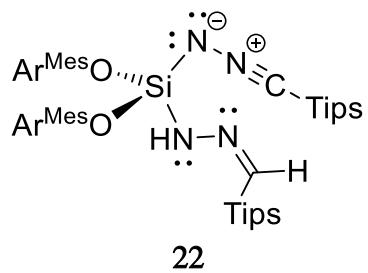
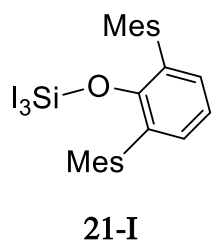
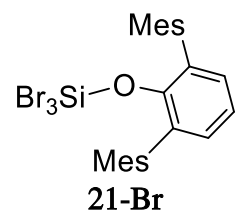
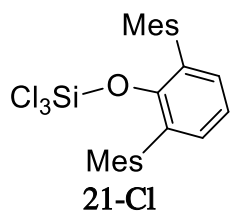
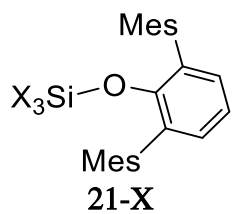
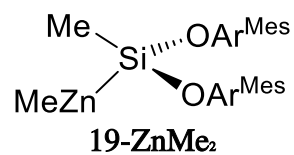
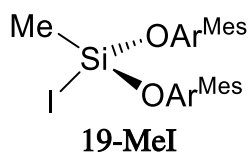
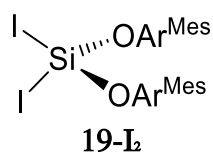
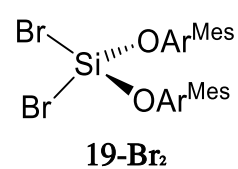
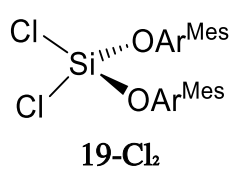
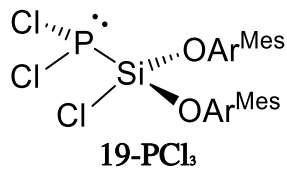
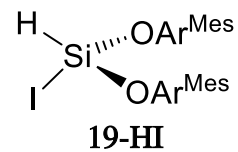
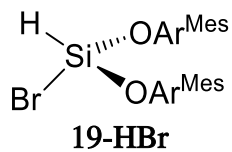
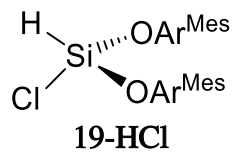


19

19-IMe₄19-HOtBu^F19-SiHCl₃19-SiHL₂

20

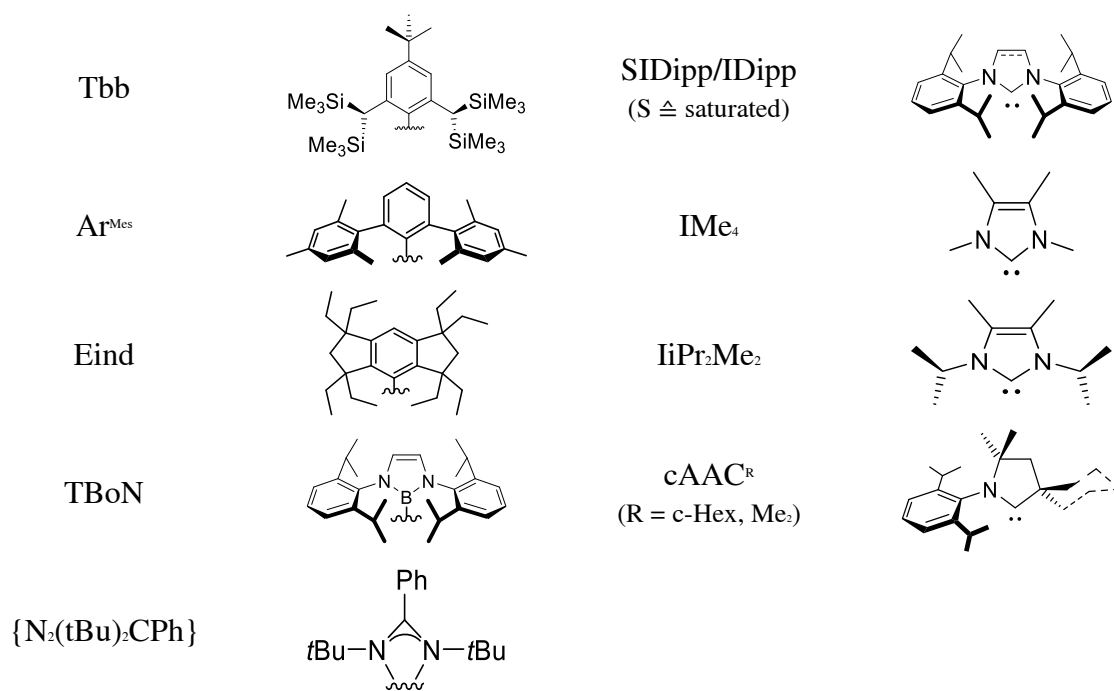
19-BX₃19-BCl₃19-BBr₃19-BI₃



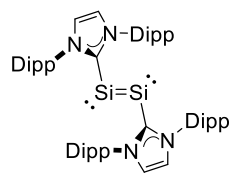
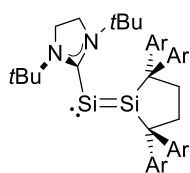
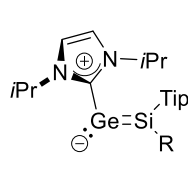
5.8.3 Abbreviation of Substituents

All formal charges are omitted for simplicity.

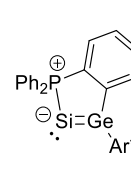
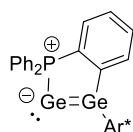
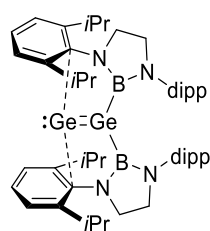
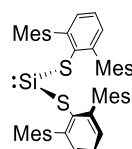
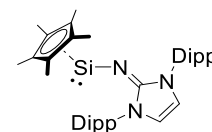
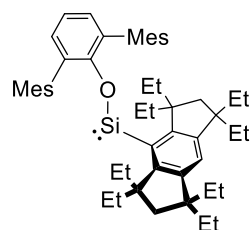
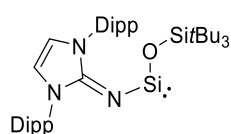
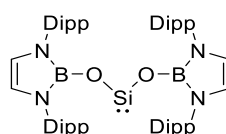
Substituents



5.8.4 Enumeration of literature-known compounds

**I**^[106]**II**^[164]**III-R**

[158–160]

**IV**^[163]**V**^[162]**VI**^[161]**VII**^[95]**VIII**^[97]**IX**^[40]**X**^[101]**XI**^[102]

5.8.5 List of tables

Table 1. Selected bond distances in disilenides $M(R^1)Si=CR^2R^3$ (with R^1 being Z to R^3).	24
Table 2. Experimental and calculated Si=Si bonding parameters of the disilavinylidenes 1 and 1-CH ₂ Ph.....	29
Table 3. Reduction potentials of 1 and 1-CH ₂ Ph and radical reduction potentials of organolithium compounds. 32	
Table 4. Selected bonding parameters and ²⁹ Si NMR spectroscopic data of compounds 1 and 5-Br – 5-Cl.....	48
Table 5. Geometrical distortion of the central ring in 7. Calculated values are given in square brackets. ^A	59
Table 6. Bond distances d, Wiberg Bond Indices and Bonding orders of 7 according to NRT.....	60
Table 7. NICS values of 7 and related compounds. ^[133,258,259,262]	61
Table 8. NPA natural charges of selected atoms in compound 7.	62
Table 9. Reactions of Ag(I) and Cu(I) compounds with 1 (overview).	68
Table 10. Selected structural and spectroscopic features of the metal complexes 9 and 10.....	70
Table 11. Calculated (B97-D3(BJ)/def2-TZVP) Cu-Si bond dissociation energies and Wiberg bond indices of the CuBr complexes 10 and 12.....	78
Table 12. Combined resonance weight of NRT formulae featuring the given bond order of 10 and 12 (B97-D3(BJ)/def2-TZVP level of theory).	79
Table 13. Absorption maxima of 10 in thf and 12 in n-hexane and their molar extinction coefficients ϵ	80
Table 14. ²⁹ Si{ ¹ H} NMR and ¹³ C{ ¹ H} carbene resonances of the copper complexes 10 – 13 and 1.....	83
Table 15. Different ligands used for the abstraction of CuBr from 12.	84
Table 16. Reaction rate constants k(T) and half life times	88
Table 17. Comparison of the ¹³ C NMR resonance of the ipso C atoms and the calculated charge of the corresponding Si atoms of compounds 12, 14, 15 and 1.	90
Table 18. Calculated ²⁹ Si NMR shielding tensors (δ_{ii}), span of the chemical shielding tensors ($\Delta\delta$), anisotropy of the chemical shift (CSA) and the calculated and experimental isotropic chemical resonances (δ_{iso}) of 12 – 15.	92
Table 19. Structural and spectroscopic data of known disilynes. Calculated data are given in parentheses.	92
Table 20. Selected structural data of 12 – 15 and 1.....	93
Table 21. High field shifts of the ¹³ C NMR NCN carbene signals of 14 and related compounds.	94
Table 22. Selected structural and spectroscopic parameters of substituted NHC-stabilized disilavinylidenes.	99
Table 23. Monomeric, heavier di(oxy)tetrylenes E(OR) ₂ (E = Ge – Pb).	105
Table 24. Selected structural and spectroscopic data of 16-Br, 16-I and their precursors.....	111
Table 25. Selected ¹³ C{ ¹ H} NMR data of 18 and related compounds.	119
Table 26. Comparison of the Δ HOMO-LUMO-gaps (in eV) of aminosilylenes. ^[40,96,98,100]	121
Table 27. Structural and ²⁹ Si NMR spectroscopic data of 19 and related silylenes (averaged values).....	124
Table 28. Calculated energy differences between the highest occupied and the lowest unoccupied molecular orbital in 19 and related silylenes reported in the literature. ^[40,95,101,102]	127
Table 29. Experimental bond energies (BE) and bond dissociation energies (BDE) from Me ₃ Si-X (X = H, Cl, I).	136
Table 30. Structural and ²⁹ Si{ ¹ H} NMR (298 K, benzene-d ₆) data of 19-X ₂ and 21-X.....	143
Table 31. Selected structural and spectroscopic data of 19 and its oxidative addition products 19-RR'	168

Table 32. Drying agents for laboratory solvents.....	174
Table 33. Deuterated solvents for NMR spectroscopy.....	175
Table 34. Referencing of NMR spectra. ^[464]	176
Table 35. Equipment of the Single crystal X-ray diffraction service.....	178
Table 36. Commercially available starting materials.	180
Table 37. Starting materials, that were generated following established procedures.	181
Table 38. Structural data of S(SO ₃)(IDipp), SO ₃ (IDipp) and related compounds from the literature.....	255
Table 39. Structural data of [CuBr(IiPr ₂ Me ₂)(SIDipp)], [Cu(IiPr ₂ Me ₂)(SIDipp)]Br and related complexes.	256
Table 40. Structural data of Ar ^{TP} Br and Ar ^{Me} Br.....	258
Table 41. Structural and ²⁹ Si{ ¹ H} NMR data of trihalosilanes with (oxo-)terphenyl substituents.....	259
Table 42. Molar extinction coefficients ϵ_{λ} of 7 at the absorption maxima $\lambda = 247$ nm, 421 nm and 593 nm.	268
Table 43. Selected transitions in the computed UV/vis spectrum of 19 ^{calc} (CIS(D)-RI-MP2/def2-TZVP). Only molecular orbital contributions with more than 5 % are considered.....	272
Table 44. Results of the natural bond orbital (NBO) and natural	276
Table 45. Calculated structural parameters of the key species involved in the formation of 4.....	277
Table 46. Selected results of the natural bond orbital (NBO) analysis for 6 _{calc} (top), 6 ^{TS} _{calc} (middle) and 6' _{calc} (bottom). Atom numbering of the experimental structures was taken over in the calculated structures.	278
Table 47. Bonding parameters (calculated and experimental), Wiberg bond indices, NRT bond orders (given in total-/covalent-/ionic-contribution) and charges derived from the natural population analysis of selected bonds of 10 ^{calc} and 12 ^{calc} . The numbering corresponds to the numbering in the crystal structure.....	279
Table 48. Bonding parameters (calculated and experimental), Wiberg bond indices, NRT bond orders (given in total-/covalent-/ionic-contribution) and charges derived from the natural population analysis of selected bonds of 14 and 15 on the B97-D3(BJ)/def2-SVP//B97-D3(BJ)/def2-TZVP level of theory. The numbering corresponds to the numbering in the crystal structure.	280
Table 49. Comparison of experimental and calculated (B97-D3(BJ)/def2-SVP//B97-D3(BJ)/def2-TZVP) structural data of the NHC-stabilized disilyne 14, its disilavinylidene isomer 15 and the transition state.	280
Table 50. Comparison of respective energies, bond lengths and the angle α at the Si1NHC atom in 7, 7 ^{-calc} ,	282
Table 51. Selected results of the NBO and NRT analysis of 7 _{calc} ⁻	282
Table 52. Selected results of the NBO and NRT analysis of 18 ^{calc}	283
Table 53. Comparison of selected experimental bond lengths, angles and torsion angles	283
Table 54. Comparison of selected experimental bond lengths and angles of 19 with the calculated (RI-B97-D3/def2-TZVP) bond lengths and angles.	284
Table 55. Partial charges from natural population analysis (NPA) of 19 ^{calc}	284
Table 56. Selected results of the NBO and NRT analysis of 19 ^{calc}	285
Table 57. Experimental and computed IR and Raman bands of 19, 19 ^{calc} , Si(OCH ₃) ₂ and Si(OPh) ₂	285
Table 58. Comparison of the calculated (B97-D3(BJ) ^{ATM} /def2-TZVP) structures of 19·BI ₃ ^{calc} and 19·BI ₃ ^{calc}	286
Table 59. Calculated (B97-D3(BJ) ^{ATM} /def2-TZVP) relative energies of 19·BI ₃ ^{calc} and 19·BI ₃ ^{calc}	287

5.8.6 List of figures

Figure 1. Expected radii (\AA) of maximum radial density r_0 of the respective s- and p-valence orbitals of group 14 elements. The values were taken from the literature. ^[5]	1
Figure 2. The first isolable silene (left) and disilene (right) are kinetically stabilized by large substituents. ^[10-13]	2
Figure 3. Double donor-acceptor bonding model (left) and valence-bond description (middle) of heavy ditetrylenes. ^[18,21,22]	3
Figure 4. Second-order Jahn-Teller distortion in heavier ditetrylenes. ^[18,21,22]	3
Figure 5. Selected examples of compounds containing Si=Si double bonds:	5
Figure 6. Selected monomeric Si(II) compounds (left); schematic orbital depiction of singlet- and triplet silylenes as well as π -donation in NHSis (right). Formal charges are omitted for simplicity.	6
Figure 7. General formulae of classical divalent N-heterocyclic silylenes (A ^[73] and B ^[83]) as well as three-coordinated amidinato-silylenes (C ^[84]), N,P-phosphonium-silylenes (D ^[86]) and cyclic alkyl(amino)silylenes (E ^[87]).	7
Figure 8. The first stable acyclic silylenes.....	8
Figure 9. The first NHC-stabilized examples of base-stabilized disilicon(0), ^[106] disilicon(I) ^[106,111] and silicon dihalides ^[112-114] each coordinated by the bulky NHC IDipp.	8
Figure 10. Selected compounds obtained from NHC-stabilized di(halo)silylenes.	9
Figure 11. Isolable base-stabilized vinylidene analogues of the heavier Group 14 elements.....	14
Figure 12. Top row: a hypervalent ferrosilylene, ^[189] a cationic chromiosilylene ^[120] and an N-hetero-Rh-metallacyclic silylene ($\text{PR}_2 = \text{cyclo-P}\{\text{N}(\text{tBu})_2\text{SiMe}_2\}$, $\text{dppe} = \text{Ph}_2\text{PC}_2\text{H}_4\text{PPh}_2$). ^[195] Bottom row: a mercury bis(silenide), ^[196] lithium silenides ($\text{R} = \text{adamantly or SiMe}_2\text{tBu}$; $\text{silyl} = \text{SiMe}(\text{tBu})_2 \text{ or SiMetBu}_2$) ^[197,198] and a cAAC-substituted potassium silenide. ^[199]	22
Figure 13. Molecular structures of 2 ·C ₆ H ₆	23
Figure 14. Proton-coupled ²⁹ Si NMR (99.34 MHz) zg30 spectrum of compound 2 in benzene-d ₆ at 298 K;.....	25
Figure 15. ²⁹ Si NMR (99.37 MHz) zgig spectrum of 1-CH₂Ph in benzene-d ₆ at 298 K.....	28
Figure 16. Molecular structures of 1-Me (left) and 1-CH₂Ph ·(C ₆ H ₆) (right).....	29
Figure 17. Selected Kohn-Sham orbitals (RI-B97-D3/def2-TZVP level of theory) of 1^{calc} (top row) and 1-CH₂Ph^{calc} (bottom row) and their corresponding energy eigenvalues;	31
Figure 18. Molecular structure of 3 ·(C ₆ H ₆).	34
Figure 19. ¹ H NMR (500.2 MHz) spectrum of 3 in benzene-d ₆ at 298 K.....	35
Figure 20. Stack-plot of the ¹ H NMR (300.1 MHz) spectra of the SiMe ₃ signals of 3	36
Figure 21. ¹ H NMR (300.1 MHz) spectrum of the crude product of the reaction of 1 with NaCH ₂ Ph	37
Figure 22. Interconversion of the (S,S)- isomer to the (S,R) isomer of 4 by a planar transition state	44
Figure 23. Molecular structure of the monomeric moiety 5-Br ·(C ₆ H ₆)·(n-C ₃ H ₇) (left) and 5-Cl (right).	47
Figure 24. Zn(II) complexes of amidinato-stabilized silylenes. R = Et, Ph or C ₆ F ₅ ; X = Cl or I.	48
Figure 25. Excerpts of the variable temperature ¹ H NMR (300.1 MHz) spectra of 6	50
Figure 26. Resonance formula of the 2-phosphaethynolate anion [$\text{P}\equiv\text{C-O}$] ⁻	52
Figure 27. Literature-known cyclic compounds featuring Si-P bonds.	54
Figure 28. ³¹ P{ ¹ H} NMR (202.5 MHz) spectrum of 7 in tetrahydrofuran-d ₈ at 298 K.	55
Figure 29. ²⁹ Si{ ¹ H} NMR (99.37 MHz) spectrum of 7 in tetrahydrofuran-d ₈ solution at 298 K.	56
Figure 30. Molecular structure of the monomeric moiety 7 ·(C ₆ H ₁₄) _{0.5}	57

Figure 31. Specification of the diverging angles α , β and φ in the central ring system of compound 7 ;	58
Figure 32. ATR-IR spectrum of 7 at ambient temperature.	60
Figure 33. Changes of the absolute energy dependent on the angular deflection of the NHC.....	62
Figure 34. Selected Kohn–Sham orbitals of 7^{calc} and their energy eigenvalues;	63
Figure 35. Selected Cu(I) complexes of silylenes, a phosphasilenyliidene and disilicon(0) (I).....	64
Figure 36. Ag(I) complexes of silylenes, a silylidene, a base-stabilized silyliumylidene ion and disilicon(0).....	65
Figure 37. Molecular structure of 9 ·(dme) _{2.5} (left) and 10 ·C ₆ H ₁₄ ·C ₅ H ₁₂ (right).	69
Figure 38. ¹ H NMR (500.1 MHz) spectra of 9 in tetrahydrofuran-d ₈ (top) and 10 in benzene-d ₆ (below)	71
Figure 39. ²⁹ Si{ ¹ H}NMR (99.37 MHz) spectrum of 9 in tetrahydrofuran-d ₈ solution at 298 K.....	72
Figure 40. Molecular structure of 12	76
Figure 41. Coordination sphere of the metal atoms in the complexes 9 , 10 and 12	77
Figure 42. Selected Kohn-Sham orbitals of complex 10 on the B97-D3(BJ)/def2-TZVP level of theory.	78
Figure 43. Selected Kohn-Sham orbitals of complex 12 on the B97-D3(BJ)/def2-TZVP level of theory.	79
Figure 44. Comparison of the UV-vis/NIR spectra of the CuBr complexes 10 in thf (orange, dashed) and 12 in n-hexane (brown, solid).	80
Figure 45. ¹ H NMR (500.1 MHz) spectra of 11 in tetrahydrofuran-d ₈	82
Figure 46. Conversion of 14 into 15 at T = 60 °C	87
Figure 47. ¹ H NMR (500.1 MHz) spectra of 14 (top) and 15 (below) in benzene-d ₆ at 298 K;	89
Figure 48. ¹ H NMR (99.36 MHz) zgig spectra of 12 (top), 14 (middle) and 15 (bottom)	91
Figure 49. Molecular structures of 14 ·C ₆ H ₆ (left, 50 % probability) and 15 (right, 50 % probability).	93
Figure 50. Known stable amino(oxy)carbenes; R/R' = Me/iPr, Me/tBu or iPr/tBu; n = 1 or 3. ^[323–325]	103
Figure 51. Different aggregation modi observed for di(oxy)tetrylenes with small substituents.	104
Figure 52. The first benzamidinato-stabilized oxysilylenes reported in the literature and a cAAC-stabilized aryloxy(bromo)silylene (right).	106
Figure 53. ¹ H NMR spectrum (500.0 MHz) of 16-I in benzene-d ₆	109
Figure 54. Excerpt of the experimental (top, benzene-d ₆) and the simulated (bottom) ¹ H NMR spectrum of 16-I	110
Figure 55. Molecular structures of 16-Br and 16-I	110
Figure 56. Selected Kohn-Sham-frontier orbitals of 16-Br and 16-I	112
Figure 57. SiCp* ₂ , [Cp*Si][B(C ₆ F ₅) ₂] ₂ and products of nucleophilic addition.	113
Figure 58. Molecular structure of 17	114
Figure 59. ¹ H NMR spectrum (500.0 MHz) of 17 in benzene-d ₆	115
Figure 60. Approximate scale of ²⁹ Si chemical shifts of acyclic silylenes and related compounds. ²⁹	116
Figure 61. Known acyclic aminosilylenes	117
Figure 62. ¹ H NMR spectrum (500.2 MHz) of 18 in benzene-d ₆	118
Figure 63. Molecular structure of 18	120
Figure 64. Selected Kohn–Sham orbitals of 18^{calc} and their corresponding energy eigenvalues;	121
Figure 65. Molecular structure of 19	123

Figure 66. ^1H NMR spectrum (500.2 MHz) of 19 in benzene- d_6	125
Figure 67. $^{29}\text{Si}\{^1\text{H}\}$ NMR spectrum (99.37 MHz) of 19 in benzene- d_6	126
Figure 68. Selected Kohn-Sham orbitals (RI-B97-D3/def2-TZVP) of 19^{calc}	127
Figure 69. TEM recordings of the Si-particles obtained from the thermolysis of 19	129
Figure 70. Molecular structure of 19-IMe₂	131
Figure 71. Excerpt of the ^1H NMR (500.2 MHz) spectrum of 19-HOtBu^F in benzene- d_6 at 298 K.....	134
Figure 72. Molecular structure of 19-HOtBu^F	135
Figure 73. Aromatic region of the ^1H NMR spectra of compound 19-SiHCl₂	137
Figure 74. Simulated signals for the $\text{C}^{3,5}\text{-H}$ and $\text{C}^4\text{-H}$ protons of 19-SiHCl₂	138
Figure 75. Molecular structures of 19-SiHCl₂ (left) and 20-Et₂O (right).....	139
Figure 76. Molecular structures of 19-Cl₂ (left) and 21-Cl (right).....	143
Figure 77. Examples of silylene/phosphane adducts or silylenes stabilized by P-bases;.....	147
Figure 78. Molecular structure of 19-PCl₂ ;.....	149
Figure 79. ^1H NMR (500.1 MHz) spectra of 19-BI₂ (top) and 19-PCl₂ (below) in benzene- d_6 at 298 K.....	150
Figure 80. $^{31}\text{P}\{^1\text{H}\}$ NMR (99.36 MHz) spectrum of 19-PCl₂ in benzene- d_6 at 298 K.....	151
Figure 81. $^{11}\text{B}\{^1\text{H}\}$ NMR (99.36 MHz) spectrum (left) and $^{29}\text{Si}\{^1\text{H}\}$ NMR (160.46 MHz) spectrum (right) of 19-BI₂ in benzene- d_6 at 298 K.....	152
Figure 82. Molecular structure of 19-ZnMe₂	155
Figure 83. Two different orientations of compound 22 are superimposed in the solid-state structure.....	158
Figure 84. ATR-IR spectrum of a solid sample of 22 at ambient temperature.....	159
Figure 85. Molecular structure of compound 22 with thermal ellipsoids set to 30 % probability.....	160
Figure 86. ^1H NMR spectra (500.1 MHz) of 22	162
Figure 87. $^1\text{H}/^{15}\text{N}$ HMBC spectrum of 22 in toluene- d_6 at 243 K.....	163
Figure 88. Exemplary side occupancy (48 %) as observed in 19-Cl₂	179
Figure 89. EDX spectrum of the Si particles obtained by the thermolysis of 19	217
Figure 90. The effect of the elimination of different symmetry operations (σ , c_2) on characteristic non-aromatic ^1H NMR signals of Tbb, SIDipp and Ar^{Mes}	237
Figure 91. Molecular structure of $4\cdot(\text{C}_6\text{H}_{14})_{0.5}$	250
Figure 92. Molecular structure of the monomeric moiety $6\cdot 0.5(\text{n-C}_6\text{H}_{14})$	251
Figure 93. Molecular structure of 19-HBr (left) and 19-HI (right);.....	252
Figure 94. Molecular structure of 21-Br (left) and 21-I (right).....	253
Figure 95. Molecular structures of S(SO₂)(IDipp)·C₆H₆ (left) and SO₂(IDipp) (right).....	254
Figure 96. Molecular structures of [CuBr(IiPr₂Me₂)(SIDipp)] (left) and [Cu(IiPr₂Me₂)(SIDipp)]Br (right).....	255
Figure 97. Molecular structure of a single [H(IMe₄)] [OAr^{Mes}] ·C ₆ H ₆ unit (left) and an excerpt displaying the arrangement of the imidazolium cations (right).....	257
Figure 98. Molecular structure of Ar^{Tol}Br . Thermal ellipsoids are set to 50 % probability; hydrogen atoms omitted.....	258
Figure 99. Molecular structure of Ar^{Tol}SiCl₂	258

Figure 100. Molecular structures of the full polyanion [Sb ₆ I ₆] ⁴⁻ (left) and one counter cation [H-SIDipp] ⁺ (right).	261
Figure 101. Experimental UV-Vis spectra of 1 in n-hexane from 220 – 720 nm at different concentrations <i>c</i> (μmol L ⁻¹) and optical path lengths <i>d</i> [mm] of the cuvettes.	265
Figure 102. Deconvoluted absorption bands and experimental UV-Vis spectrum of 1 in n-hexane from 270 – 670 nm at <i>c</i> = 551 μmol L ⁻¹ and <i>d</i> = 10 mm.....	265
Figure 103. Experimental UV-Vis spectra of 1-Me in n-hexane from 270 – 620 nm at different concentrations <i>c</i> and an optical path length <i>d</i> = 1 mm of the cuvette. See also page 26ff.	266
Figure 104. Deconvoluted absorption bands and experimental UV-Vis spectrum of 1-Me in n-hexane from 270 to 670 nm at <i>c</i> = 560 μmol L ⁻¹ and <i>d</i> = 1 mm.....	266
Figure 105. Experimental UV-Vis spectra of 1-CH₂Ph in n-hexane from 220 – 650 nm at different concentrations <i>c</i> (μmol L ⁻¹) an optical path length <i>d</i> = 1 mm of the cuvette. See also page 26ff.....	267
Figure 106. Deconvoluted absorption bands and experimental UV-Vis-NIR spectrum of 1-CH₂Ph in n-hexane from 270 – 670 nm at <i>c</i> = 1783 μmol L ⁻¹ and <i>d</i> = 1 mm.....	267
Figure 107. Experimental UV-vis spectra of 7 in thf.....	268
Figure 108. Deconvoluted absorption bands and experimental UV-Vis-NIR spectrum of 7	268
Figure 109. Experimental UV-Vis spectra of 10 in n-hexane from 240 – 600 nm	269
Figure 110. Deconvoluted absorption bands and experimental UV-Vis-NIR spectrum of 10 in n-hexane	269
Figure 111. Experimental UV-Vis spectra of 12 in n-hexane from 220 – 720 nm	270
Figure 112. Deconvoluted absorption bands and experimental UV-Vis-NIR spectrum of 12 in n-hexane from 270 to 750 nm at <i>c</i> = 980 μmol L ⁻¹ and <i>d</i> = 1 mm. See also page 80.	270
Figure 113. Experimental UV-Vis spectra of 19 in thf from 200 – 400 nm at different concentrations (<i>c</i>) and optical path lengthss (<i>d</i>) of the cuvette.	271
Figure 114. Experimental UV-Vis spectra of 19 in thf.....	271
Figure 115. Comparison between the computed (stick-plot, red, CIS(D)-RI-MP2/def2-TZVP) and the experimental (blue, measured in thf) UV-vis spectrum of 19	272
Figure 116. Excerpt of the 1D ¹ H NOESY (500.2 MHz) spectrum of 4·0.5(n-C ₆ H ₁₄) in benzene-d ₆ at 298 K.	274
Figure 117. Excerpt of the 2D ¹ H NOESY (500.2 MHz) spectrum of 4·0.5(n-C ₆ H ₁₄) in benzene-d ₆ at 298 K.	274
Figure 118. Conversion of 14 into 15	275
Figure 119. Rotation energies of compound 14 (red) and 15 (blue).....	281
Figure 120. Comparison of the experimental structure 7·thf (left) and the structure of the calculated anion 7^{-calc} (right, RI-B97-D3/def2-TZVP).	281
Figure 121. Comparison of the experimental (left) and calculated (right, RI-B97-D3/def2-TZVP) structure of 19 . Hydrogen atoms are omitted for simplicity.	284
Figure 122. Comparison of the calculated (B97-D3(BJ) ^{ATM} /def2-TZVP) structures of the BI ₃ -insertion product 19-BX₃ (left) and the addition product 19·BX₃ (right) of 19	286

5.8.7 List of schemes

Scheme 1. Synthesis of the first isolable disilyne by Sekiguchi. silyl = Si(iPr)dsi; dsi = CH(SiMe₃)₂.^[62].....5

Scheme 2. Calculated (CCSD(T)) respective energies of different Si₂H₂ isomers

Scheme 3. Reactivity of Aldridge's digermavinylidene VI . Reduction was achieved by excess KC_8 ; oxidation by $[\text{Cp}_2\text{Fe}][\text{BAr}^{\text{F}_4}]$ or $[\text{Ph}_3\text{C}][\text{B}(\text{C}_6\text{F}_5)_4]$. $\text{Ar}^{\text{F}} = 3,5\text{-(CF}_3)_2\text{-C}_6\text{H}_3$; $\text{NHC} = \text{LiPr}_2\text{Me}_2 = \text{:C}\{\text{N}(\text{iPr})\text{CMe}\}_2$	15
Scheme 4. Reactivity of Scheschkewitz's NHC-stabilized silagermenylidene III-SiTip₂Cl . ^[158–160,169–173]	16
Scheme 5. Results of the preparatory master thesis preceding to this work. $\text{IME}_4 = \text{:C}\{\text{NMeCMe}\}_2$	18
Scheme 6. Synthesis of $\text{SiBr}(\text{SiBr}_2\text{Tbb})(\text{SIDipp})$ starting from $\text{SiBr}_2(\text{SIDipp})$ and (E)- $\text{Tbb}(\text{Br})\text{Si}=\text{Si}(\text{Br})\text{Tbb}$ (path A) or TbbLi (path B) as well as the subsequent reduction to $(\text{SIDipp})\text{Si}=\text{Si}(\text{Br})\text{Tbb}$ (1). ^[134]	19
Scheme 7. Synthesis of the NHC-stabilized metalla(silyl)silylene 2 by C-H activation of the proposed lithiation intermediate $(\text{SIDipp})\text{Si}=\text{Si}(\text{Li})\text{Tbb}$ (top) or by activation of a radical species 1[•] (bottom).	21
Scheme 8. Bromide substitution of the NHC-stabilized bromo-disilavinylidene 1	26
Scheme 9. Leading natural Lewis structures (NLS) of 1 (top row) and 1-CH₂Ph (below) and their respective percentage contributions to the resonance hybrid according to local NRT analysis	30
Scheme 10. Alkali metal dependent formation of 1-CH₂Ph and/or 3 from 1 and MCH_2Ph ($\text{M} = \text{Li, Na, K}$).....	32
Scheme 11. Heavier silacyclopopylidenes described in the literature.....	33
Scheme 12. Proposed mechanism for the formation of 1-CH₂Ph and 3 from the reactions of 1 and MCH_2Ph	39
Scheme 13. Alternative, orbital-controlled mechanism for the formation of 3	40
Scheme 14. Diastereoselective reaction of 1 with acetone to the NHC-stabilized hydrido(silyl)silylene 4	41
Scheme 15. General reaction products of silylenes (top) or disilenes (below) with (non-)enolizable ketones. ^[24,27,227,230,231]	42
Scheme 16. Calculated (RI-B97-D3/def2-TZVP) mechanism of the reaction between 1 and acetone	45
Scheme 17. Syntheses of NHC-stabilized zincosilylenes 5-X and 6	46
Scheme 18. Potential energy surface (RI-B97-D3/def2-TZVP) for the dynamic process of 6 showing the global minimum structure 6_{calc} , the transition state 6^{TS}_{calc} and the local minimum structure 6'_{calc}	51
Scheme 19. Synthesis of compound 7 from 1 and $\text{NaOCP}\cdot(1,4\text{-dioxane})_{2,6}$	53
Scheme 20. Leading resonance formulae (contribution >2.5 %) of 7 as obtained from the NRT analysis.	61
Scheme 21. Reaction of 1 with $\text{Ag}[\text{BAr}^{\text{F}_4}]$ to 8 reported by Dr. P. Ghana.....	66
Scheme 22. Reactions of 1 with silver triflate and CuBr to the respective complexes 9 and 10	67
Scheme 23. Proposed η^1/η^2 -equilibrium of the metal atoms in complexes 9 and 10 in solution.	70
Scheme 24. Synthesis and structural assignment of compound 12	74
Scheme 25. Mechanism of an alkyne/vinylidene complex isomerization	74
Scheme 26. Related disilyne complexes and disilene dianions. ^[40–43,63,303]	75
Scheme 27. Bromide abstraction from the CuBr complexes 10 and 12 . Compound 13 is also available from 1 and $[\text{Cu}(\text{MeCN})_2][\text{BAr}^{\text{F}_4}]$ in fluorobenzene solution. Formal charges are omitted for simplicity.....	81
Scheme 28. Synthesis of the NHC-stabilized (oxy)disilyne 14 by abstraction of CuBr	83
Scheme 29. Unprecedented isomerization of the NHC-stabilized (oxy)disilyne 14 to the NHC-stabilized disilavinylidene 15 at elevated temperatures in solution.	85
Scheme 30. Isomerizations of heavier vinylidene derivatives.	86
Scheme 31. Calculated mechanism of the isomerization of 14 into 15 (B97-D3(BJ)/def2-TZVP).	88
Scheme 32. Reactivity of 1 towards lithium and alkyl(alkali) reagents.	96
Scheme 33. Reaction of 1 with zinc halides.	96
Scheme 34. Reaction of 1 with acetone via direct C-H activation.	97

Scheme 35. Synthesis of compound 7 by an unknown mechanism.....	97
Scheme 36. Reaction of 1 with coinage metal salts. Formal charges are omitted for simplicity.	98
Scheme 37. Liberation of a metastable NHC-stabilized oxy-disilyne 14 and its subsequent thermal isomerization to the disilavinylidene derivative 15 . Formal charges are omitted for simplicity.	98
Scheme 38. Potential synthetic strategies to obtain disilavinylidene complexes, substituted disilavinylidenes or disilynes.	100
Scheme 39. Possible reactivity studies	101
Scheme 40. Potential use of NHC-stabilized zinco(silyl)silylenes as silylene transfer reagents.	102
Scheme 41. The first unambiguously identified carbene complexes featuring alkyl(oxy)carbenes. ^[317]	103
Scheme 42. Syntheses of IX – XI reported in the literature. ^[40,101,102] Formal charges are omitted for simplicity. ...	107
Scheme 43. Synthesis of the NHC-stabilized alkoxy(halo)silylenes 16-Br and 16-I	108
Scheme 44. Synthesis of NaOAr ^{Mes}	113
Scheme 45. Synthesis of Cp*SiOAr ^{Mes} (17). Formal charges are omitted for simplicity.....	114
Scheme 46. Synthesis of the di(amino)silylene Si{N(Me)Ar ^{Mes} } ₂ (18).	118
Scheme 47. Synthesis of the first di(aryloxy)silylene Si(OAr ^{Mes}) ₂ (19 , right, X = Br or I).	122
Scheme 48. Reactivity of Inoues imino(oxy)silylene X . ^[390,391] BR ₃ = BPh ₃ or B(C ₆ F ₅) ₃ ; E = O, Se, Te.....	128
Scheme 49. The thermolysis of 19 yields Ar ^{Mes} OH and Si “nanoparticles”.....	129
Scheme 50. Reaction of 19 with IMe ₄ to the base-adduct 19-IME	130
Scheme 51. Synthesis of 19-HOtBu^F by oxidative addition of HOC(CF ₃) ₃	133
Scheme 52. Synthesis of the disilanes 19-SiHCl₂ and 19-SiHL₂ and its subsequent reaction with thf to 20	136
Scheme 53. The attempted dehydrohalogenation of 19-SiHCl₂ leads to 19-Cl₂	140
Scheme 54. Synthesis of compounds 19-X₂ and 21-X (X = Cl, Br, I).	141
Scheme 55. The reaction of 19 with SiBr ₄ only proceeds in presence of free SIDipp.	144
Scheme 56. Generation of silylene 19 by salt metathesis starting from SiX ₃ (NHC) (A), oxidation to 19-Br₂ with re-formation of SiBr ₃ (NHC) (B) and repeated generation of 19 (C).	145
Scheme 57. Exemplary reactions between an NHSi and an amidinato-supported silylene with BCl ₂ Ph reported in the literature. ^[415,416]	146
Scheme 58. Reactions of 19 with PCl ₃ (top) and boron trihalides (below).	147
Scheme 59. Reactivity studies of benzamidinato-stabilized silylenes towards various Zn(II) compounds.....	153
Scheme 60. Synthesis of compound 19-ZnMe₂	154
Scheme 61. Known reactions of silylenes with diazoalkanes.....	157
Scheme 62. Formation of compound 22 via two plausible intermediates 19-L and 22'	158
Scheme 63. Synthesis of compound 17 from [Cp*Si][Al{OC(CF ₃) ₃ } ₃] ⁺ and NaOAr ^{Mes}	165
Scheme 64. Reaction of SiX ₃ (SIDipp) with different alcoholates.....	166
Scheme 65. Synthesis of silylene 18 from SiL(SIDipp) and LiN(Me)Ar ^{Mes}	167
Scheme 66. Reactivity study of the first di(aryloxy)silylene 19	169
Scheme 67. Potential access to heteroleptic di(oxy)silylenes and metalla(oxy)silylenes.	170
Scheme 68. Potential reactions of 19 to be researched. E = chalcogen, X = halogen.....	171

Scheme 69. Formation of S(SO ₂)(IDipp) (a) and SO ₂ (IDipp) (b); py = pyridine.....	254
Scheme 70. Reaction leading to the formation of [H-SIDipp] ₄ [SbI ₆].....	260

5.9 Curriculum vitae

Personal details

Simon Schwarzwald
Born [REDACTED] in Bonn, Germany
Married (née Krämer)

Professional Career

since 06/2022 **Expert for sustainability**, REDcert GmbH, Bonn
02/2016 – 12/2021 **Research assistant** in the group of Prof. Dr. A. C. Filippou,
Institute of Inorganic Chemistry, University of Bonn

Formal Education

02/2016 – 12/2021 **PhD. Studentship** in the group of Prof. Dr. A. C. Filippou,
Institute of Inorganic Chemistry, University of Bonn
10/2013 – 12/2015 **M.Sc. in Chemistry**, University of Bonn, M.Sc. thesis in
Inorganic Chemistry “NHC-stabilisierte Disilavinylidene und Silylsilylene”, completed in the group of Prof. Dr. A. C. Filippou
10/2010 – 09/2013 **B.Sc. in Chemistry**, University of Bonn, B.Sc. thesis in
Inorganic Chemistry “Untersuchung der Reaktivität einer carbenstabilisierten Disilizium(0)-Verbindung gegenüber Übergangsmetallkomplexen”, completed in the group of Prof. Dr. A. C. Filippou
08/200 – 06/2009 **Academic high school** (Ernst-Moritz-Arndt Gymnasium Bonn, Germany)

Scientific Contributions

Publications

- [1] Y. Kim, P. Alpmann, S. Blaum-Feder, S. Krämer, T. Endo, D. Lu, D. Carson, I. G. Schmidt-Wolf, Increased in vivo efficacy of lenalidomide by addition of piroctone olamine, *In Vivo* **2011** 25, 99.
- [2] Y. Kim, P. Alpmann, S. Blaum-Feder, S. Krämer, T. Endo, D. Lu, D. Carson, I. G. Schmidt-Wolf, In vivo efficacy of griseofulvin against multiple myeloma, *Leuk Res.* **2011** 35, 1070.
- [3] S. Schwarzwald, P. Ghana, M. I. Arz, G. Schnakenburg, A. C. Filippou, The Ambiphilic Reactivity of NHC-Stabilized Disilavinylidenes: Syntheses of NHC-Stabilized Disilacyclopropylidenes, Hydrido(silyl)silylenes and Zinco(silyl)silylenes, *Chem. Sci.*, submitted.

Posters & Oral presentations

- 07/2021 19th International Symposium On Silicon Chemistry (ISOS), Toulouse, France: „From an NHC-stabilized disilavinylidene to a disilyne and back“ (Poster)
- 01/2020 Inorganic Chemistry Colloquium, Institute of Inorganic Chemistry, University of Bonn, Germany “Low-valent Si(II) Chemistry: Synthesis of the First Di(aryloxy)silylene and Reactivity Studies of an NHC-stabilized Disilavinylidene” (Talk)
- 09/2018 Summer School of the Bonn International Graduate School in Chemistry, University of Bonn, Germany: “Synthesis and Reactivity of the first stable Di(aryloxy)silylene” (Poster & Talk)
- 09/2017 Summer School of the Bonn International Graduate School in Chemistry, University of Bonn, Germany: “Reactivity Studies of an NHC-stabilized Disilavinylidene” (Poster & Talk)
- 08/2017 Anglo-German Inorganic Chemistry Meeting (AGIChem), Göttingen, Germany: “Reactivity Studies of an NHC-stabilized Disilavinylidene” (Poster)

5.10 Oath of Compliance with the Principles of Scientific Integrity

I hereby affirm that this dissertation was prepared independently at the Department of Inorganic Chemistry, University of Bonn under the supervision of Prof. Dr. A. C. Filippou, and that all references and additional sources have been appropriately cited.



Simon Schwarzwald

6 References

- [1] E. Wiberg, N. Wiberg, *Lehrbuch der anorganischen Chemie*, Walter De Gruyter, Berlin New York, **2007**.
- [2] UNEP 2019, *Sand and Sustainability: Finding New Solutions for Environmental Governance of Global Sand Resources*. GRID-Geneva, United Nations Environment Programme, Geneva, Switzerland., **n.d.**
- [3] A. Torres, J. Brandt, K. Lear, J. Liu, *Science* **2017**, 357, 970–971.
- [4] M. Karni, Y. Apeloig, J. Kapp, P. von R. Schleyer, in *The Chemistry of Organic Silicon Compounds*, John Wiley & Sons, Ltd, **2001**, pp. 1–163.
- [5] J. P. Desclaux, *Atomic Data and Nuclear Data Tables* **1973**, 12, 311–406.
- [6] P. P. Power, *Chem. Rev.* **1999**, 99, 3463–3504.
- [7] P. J. Davidson, M. F. Lappert, *J. Chem. Soc., Chem. Commun.* **1973**, 317a.
- [8] D. E. Goldberg, D. H. Harris, M. F. Lappert, K. M. Thomas, *J. Chem. Soc., Chem. Commun.* **1976**, 261.
- [9] P. P. Power, *Organometallics* **2020**, 39, 4127–4138.
- [10] A. G. Brook, F. Abdesaken, B. Gutekunst, G. Gutekunst, R. K. Kallury, *J. Chem. Soc., Chem. Commun.* **1981**, 191.
- [11] R. West, M. J. Fink, J. Michl, *Science* **1981**, 214, 1343–1344.
- [12] M. J. Fink, M. J. Michalczyk, K. J. Haller, R. West, J. Michl, *J. Chem. Soc., Chem. Commun.* **1983**, 1010–1011.
- [13] S. C. Nyburg, A. G. Brook, F. Abdesaken, G. Gutekunst, W. Wong-Ng, *Acta Crystallogr C Cryst Struct Commun* **1985**, 41, 1632–1635.
- [14] G. J. D. Peddle, D. N. Roark, A. M. Good, S. G. McGeachin, *J. Am. Chem. Soc.* **1969**, 91, 2807–2808.
- [15] D. N. Roark, G. J. D. Peddle, *J. Am. Chem. Soc.* **1972**, 94, 5837–5841.
- [16] T. Iwamoto, S. Ishida, in *Functional Molecular Silicon Compounds II* (Ed.: D. Scheschkewitz), Springer International Publishing, **2014**, pp. 125–202.
- [17] C. R. Landis, F. Weinhold, *J. Am. Chem. Soc.* **2006**, 128, 7335–7345.
- [18] R. C. Fischer, P. P. Power, *Chem. Rev.* **2010**, 110, 3877–3923.
- [19] R. A. Poirier, J. D. Goddard, *Chemical Physics Letters* **1981**, 80, 37–41.
- [20] G. Trinquier, J. P. Malrieu, *J. Am. Chem. Soc.* **1987**, 109, 5303–5315.
- [21] P. P. Power, *Nature* **2010**, 463, 171–177.
- [22] H. B. Wedler, P. Wendelboe, D. J. Tantillo, P. P. Power, *Dalton Trans.* **2020**, 49, 5175–5182.
- [23] K. L. Hurni, P. A. Rugar, N. C. Payne, K. M. Baines, *Organometallics* **2007**, 26, 5569–5575.
- [24] M. Kira, T. Iwamoto, in *Advances in Organometallic Chemistry*, Elsevier, **2006**, pp. 73–148.
- [25] T. Sasamori, N. Tokitoh, *BCSJ* **2013**, 86, 1005–1021.
- [26] C. Präsang, D. Scheschkewitz, *Chem. Soc. Rev.* **2016**, 45, 900–921.
- [27] A. Rammo, D. Scheschkewitz, *Chem. Eur. J.* **2018**, 24, 6866–6885.
- [28] M. Weidenbruch, S. Willms, W. Saak, G. Henkel, *Angew. Chem. Int. Ed. Engl.* **1997**, 36, 2503–2504.
- [29] D. Scheschkewitz, *Angew. Chem. Int. Ed.* **2004**, 43, 2965–2967.

- [30] M. Ichinohe, K. Sanuki, S. Inoue, A. Sekiguchi, *Organometallics* **2004**, 23, 3088–3090.
- [31] M. Ichinohe, K. Sanuki, S. Inoue, A. Sekiguchi, *Silicon Chem* **2007**, 3, 111–116.
- [32] R. Kinjo, M. Ichinohe, A. Sekiguchi, *J. Am. Chem. Soc.* **2007**, 129, 26–27.
- [33] T. Iwamoto, M. Kobayashi, K. Uchiyama, S. Sasaki, S. Nagendran, H. Isobe, M. Kira, *J. Am. Chem. Soc.* **2009**, 131, 3156–3157.
- [34] T. Nguyen, D. Scheschkewitz, *J. Am. Chem. Soc.* **2005**, 127, 10174–10175.
- [35] I. Bejan, D. Scheschkewitz, *Angew. Chem. Int. Ed.* **2007**, 46, 5783–5786.
- [36] D. Scheschkewitz, *Chem. Eur. J.* **2009**, 15, 2476–2485.
- [37] D. Scheschkewitz, *Chemistry Letters* **2011**, 40, 2–11.
- [38] M. J. Cowley, K. Abersfelder, A. J. P. White, M. Majumdar, D. Scheschkewitz, *Chemical Communications* **2012**, 48, 6595.
- [39] M. Majumdar, I. Omlor, C. B. Yildiz, A. Azizoglu, V. Huch, D. Scheschkewitz, *Angewandte Chemie International Edition* **2015**, 54, 8746–8750.
- [40] N. Wienkenhöver, 1,2-Dibromodisilenes: A Rich Source for Titanium Silylidyne Complexes, Acyclic Silylenes and Disilyne Dianions, Dissertation, University of Bonn, **2017**.
- [41] I. Papazoglou, Unprecedented tetrylidyne complexes of Group 6 and 10 metals **2016**.
- [42] L. Baus, unpublished results **2020**.
- [43] M. Tian, J. Zhang, H. Yang, C. Cui, *J. Am. Chem. Soc.* **2020**, 142, 4131–4135.
- [44] N. Akasaka, K. Fujieda, E. Garoni, K. Kamada, H. Matsui, M. Nakano, T. Iwamoto, *Organometallics* **2018**, 37, 172–175.
- [45] N. Wiberg, S. K. Vasisht, G. Fischer, P. Mayer, *Zeitschrift für anorganische und allgemeine Chemie* **2004**, 630, 1823–1828.
- [46] T. Sasamori, K. Hironaka, Y. Sugiyama, N. Takagi, S. Nagase, Y. Hosoi, Y. Furukawa, N. Tokitoh, *J. Am. Chem. Soc.* **2008**, 130, 13856–13857.
- [47] K. Suzuki, T. Matsuo, D. Hashizume, K. Tamao, *J. Am. Chem. Soc.* **2011**, 133, 19710–19713.
- [48] T. Agou, N. Hayakawa, T. Sasamori, T. Matsuo, D. Hashizume, N. Tokitoh, *Chemistry – A European Journal* **2014**, 20, 9246–9249.
- [49] J. S. Han, T. Sasamori, Y. Mizuhata, N. Tokitoh, *Chem. Asian J.* **2012**, 7, 298–300.
- [50] N. Hayakawa, K. Sadamori, S. Mizutani, T. Agou, T. Sugahara, T. Sasamori, N. Tokitoh, D. Hashizume, T. Matsuo, *Inorganics* **2018**, 6, 30.
- [51] D. Hoffman, Novel Synthetic Routes for Multiple Bond Formation between Si, Ge, and Sn and the d- and p-Block Elements, Dissertation, University of Bonn, **2021**.
- [52] T. Agou, T. Sasamori, N. Tokitoh, *Organometallics* **2012**, 31, 1150–1154.
- [53] I. Papazoglou, Unprecedented Tetrylidyne Complexes of Group 6 and 10 Metals, Bonn, **2016**.
- [54] A. C. Filippou, D. Hoffmann, G. Schnakenburg, *Chem. Sci.* **2017**, 8, 6290–6299.
- [55] P. Ghana, M. I. Arz, U. Chakraborty, G. Schnakenburg, A. C. Filippou, *J. Am. Chem. Soc.* **2018**, 140, 7187–7198.
- [56] T. Iwamoto, C. Kabuto, M. Kira, *J. Am. Chem. Soc.* **1999**, 121, 886–887.
- [57] T. Iwamoto, M. Tamura, C. Kabuto, M. Kira, *Science* **2000**, 290, 504–506.
- [58] S. Ishida, T. Iwamoto, C. Kabuto, M. Kira, *Nature* **2003**, 421, 725–727.
- [59] N. Wiberg, W. Niedermayer, G. Fischer, H. Nöth, M. Suter, *European Journal of Inorganic Chemistry* **2002**, 2002, 1066–1070.

- [60] M. Ichinohe, M. Igarashi, K. Sanuki, A. Sekiguchi, *J. Am. Chem. Soc.* **2005**, *127*, 9978–9979.
- [61] K. Abersfelder, A. J. P. White, H. S. Rzepa, D. Scheschkewitz, *Science* **2010**, *327*, 564–566.
- [62] A. Sekiguchi, *Science* **2004**, *305*, 1755–1757.
- [63] S. Ishida, R. Sugawara, Y. Misawa, T. Iwamoto, *Angew. Chem. Int. Ed.* **2013**, *52*, 12869–12873.
- [64] P. Jiang, P. P. Gaspar, *J. Am. Chem. Soc.* **2001**, *123*, 8622–8623.
- [65] M. Yoshida, N. Tamaoki, *Organometallics* **2002**, *21*, 2587–2589.
- [66] A. Sekiguchi, T. Tanaka, M. Ichinohe, K. Akiyama, S. Tero-Kubota, *J. Am. Chem. Soc.* **2003**, *125*, 4962–4963.
- [67] M. Ayoubi-Chianeh, *Silicon* **2022**, DOI 10.1007/s12633-021-01600-8.
- [68] C. Elschenbroich, *Organometallics*, Vieweg+Teubner Verlag, **2009**.
- [69] C. Shan, S. Yao, M. Driess, *Chem. Soc. Rev.* **2020**, *49*, 6733–6754.
- [70] P. Jutzi, D. Kanne, C. Krüger, *Angewandte Chemie International Edition in English* **1986**, *25*, 164–164.
- [71] H. H. Karsch, U. Keller, S. Gamper, G. Müller, *Angew. Chem. Int. Ed. Engl.* **1990**, *29*, 295–296.
- [72] A. J. Arduengo, R. L. Harlow, M. Kline, *J. Am. Chem. Soc.* **1991**, *113*, 361–363.
- [73] M. Denk, R. Lennon, R. Hayashi, R. West, A. V. Belyakov, H. P. Verne, A. Haaland, M. Wagner, N. Metzler, *J. Am. Chem. Soc.* **1994**, *116*, 2691–2692.
- [74] V. Nesterov, D. Reiter, P. Bag, P. Frisch, R. Holzner, A. Porzelt, S. Inoue, *Chem. Rev.* **2018**, *118*, 9678–9842.
- [75] M. Jalal, B. Hammouti, R. Touzani, A. Aouniti, I. Ozdemir, *Materials Today: Proceedings* **2020**, *31*, S122–S129.
- [76] P. Bellotti, M. Koy, M. N. Hopkinson, F. Glorius, *Nat Rev Chem* **2021**, *5*, 711–725.
- [77] B. Blom, D. Gallego, M. Driess, *Inorg. Chem. Front.* **2004**, *133*, 134–148.
- [78] B. Blom, M. Driess, in *Functional Molecular Silicon Compounds II* (Ed.: D. Scheschkewitz), Springer International Publishing, **2014**, pp. 85–123.
- [79] S. Raoufmoghaddam, Y.-P. Zhou, Y. Wang, M. Driess, *Journal of Organometallic Chemistry* **2017**, *829*, 2–10.
- [80] T. Chu, G. I. Nikonov, *Chemical Reviews* **2018**, *118*, 3608–3680.
- [81] Y. Zhou, M. Driess, *Angew. Chem. Int. Ed.* **2019**, *58*, 3715–3728.
- [82] M. Ghosh, S. Khan, *Dalton Trans.* **2021**, *50*, 10674–10688.
- [83] M. Driess, S. Yao, M. Brym, C. van Wüllen, D. Lentz, *J. Am. Chem. Soc.* **2006**, *128*, 9628–9629.
- [84] C.-W. So, H. W. Roesky, J. Magull, R. B. Oswald, *Angew. Chem. Int. Ed.* **2006**, *45*, 3948–3950.
- [85] B. Blom, D. Gallego, M. Driess, *Inorg. Chem. Front.* **2014**, *133*, 134–148.
- [86] D. Gau, T. Kato, N. Saffon-Merceron, F. P. Cossío, A. Baceiredo, *J. Am. Chem. Soc.* **2009**, *131*, 8762–8763.
- [87] T. Koike, S. Honda, S. Ishida, T. Iwamoto, *Organometallics* **2020**, *acs.organomet.9b00828*.
- [88] D. Himmel, I. Krossing, A. Schnepf, *Angew. Chem. Int. Ed.* **2014**, *53*, 370–374.
- [89] D. H. Harris, M. F. Lappert, *J. Chem. Soc., Chem. Commun.* **1974**, 895–896.
- [90] P. J. Davidson, D. H. Harris, M. F. Lappert, *J. Chem. Soc., Dalton Trans.* **1976**, 2268.

- [91] M. J. S. Gynane, D. H. Harris, M. F. Lappert, P. P. Power, P. Rivière, M. Rivière-Baudet, *J. Chem. Soc., Dalton Trans.* **1977**, 2004–2009.
- [92] J. Oláh, T. Veszprémi, *Journal of Organometallic Chemistry* **2003**, 686, 112–117.
- [93] S. Tsutsui, K. Sakamoto, M. Kira, *Journal of the American Chemical Society* **1998**, 120, 9955–9956.
- [94] R. West, G.-H. Lee, T. Müller, *J. Am. Chem. Soc.* **2003**, 125, 8114–8115.
- [95] B. D. Rekker, T. M. Brown, J. C. Fettinger, H. M. Tuononen, P. P. Power, *J. Am. Chem. Soc.* **2012**, 134, 6504–6507.
- [96] A. V. Protchenko, K. H. Birj Kumar, D. Dange, A. D. Schwarz, D. Vidovic, C. Jones, N. Kaltsoyannis, P. Mountford, S. Aldridge, *J. Am. Chem. Soc.* **2012**, 134, 6500–6503.
- [97] S. Inoue, K. Leszczyńska, *Angew. Chem. Int. Ed.* **2012**, 51, 8589–8593.
- [98] A. V. Protchenko, A. D. Schwarz, M. P. Blake, C. Jones, N. Kaltsoyannis, P. Mountford, S. Aldridge, *Angew. Chem. Int. Ed.* **2013**, 52, 568–571.
- [99] P. P. Power, B. D. Rekker, T. M. Brown, J. C. Fettinger, F. Lips, H. M. Tuononen, R. H. Herber, *J. Am. Chem. Soc.* **2013**, 135, 10134–10148.
- [100] T. J. Hadlington, J. A. B. Abdalla, R. Tirfoin, S. Aldridge, C. Jones, *Chem. Commun.* **2016**, 52, 1717–1720.
- [101] D. Wendel, D. Reiter, A. Porzelt, P. J. Altmann, S. Inoue, B. Rieger, *J. Am. Chem. Soc.* **2017**, 139, 17193–17198.
- [102] S. Aldridge, Y. K. Loh, L. Ying, M. Á. Fuentes, D. C. H. Do, *Angew. Chem. Int. Ed.* **2019**, DOI 10.1002/anie.201812058.
- [103] D. Reiter, R. Holzner, A. Porzelt, P. J. Altmann, P. Frisch, S. Inoue, *J. Am. Chem. Soc.* **2019**, 141, 13536–13546.
- [104] M. M. D. Roy, M. J. Ferguson, R. McDonald, Y. Zhou, E. Rivard, *Chem. Sci.* **2019**, 10.1039/C9SC01192G.
- [105] S. Fujimori, S. Inoue, *Eur. J. Inorg. Chem.* **2020**, 2020, 3131–3142.
- [106] Y. Wang, Y. Xie, P. Wei, R. B. King, H. F. Schaefer, P. von R. Schleyer, G. H. Robinson, *Science* **2008**, 321, 1069–1071.
- [107] W. Marco Boesveld, B. Gehrhus, P. B. Hitchcock, M. F. Lappert, P. von Ragué Schleyer, *Chem. Commun.* **1999**, 755–756.
- [108] X.-W. Li, J. Su, G. H. Robinson, *Chem. Commun.* **1996**, 2683.
- [109] Y. Wang, B. Quillian, P. Wei, C. S. Wannere, Y. Xie, R. B. King, H. F. Schaefer, P. v. R. Schleyer, G. H. Robinson, *J. Am. Chem. Soc.* **2007**, 129, 12412–12413.
- [110] D. J. D. Wilson, J. L. Dutton, *Chem. Eur. J.* **2013**, 19, 13626–13637.
- [111] M. I. Arz, D. Gei[German sz ligature], M. Stra[German sz ligature]mann, G. Schnakenburg, A. C. Filippou, *Chem. Sci.* **2015**, 6, 6515–6524.
- [112] R. S. Ghadwal, H. W. Roesky, S. Merkel, J. Henn, D. Stalke, *Angewandte Chemie International Edition* **2009**, 48, 5683–5686.
- [113] A. C. Filippou, O. Chernov, G. Schnakenburg, *Angewandte Chemie* **2009**, 121, 5797–5800.
- [114] A. C. Filippou, Y. N. Lebedev, O. Chernov, M. Straßmann, G. Schnakenburg, *Angew. Chem. Int. Ed.* **2013**, 52, 6974–6978.
- [115] R. S. Ghadwal, H. W. Roesky, C. Schulzke, M. Granitzka, *Organometallics* **2010**, 29, 6329–6333.
- [116] M. I. Arz, D. Hoffmann, G. Schnakenburg, A. C. Filippou, *Z. Anorg. Allg. Chem.* **2016**, 642, 1287–1294.

- [117] R. S. Ghadwal, H. W. Roesky, K. Pröpper, B. Dittrich, S. Klein, G. Frenking, *Angewandte Chemie* **2011**, 123, 5486–5490.
- [118] H. Tanaka, S. Inoue, M. Ichinohe, M. Driess, A. Sekiguchi, *Organometallics* **2011**, 30, 3475–3478.
- [119] A. C. Filippou, O. Chernov, G. Schnakenburg, *Chemistry – A European Journal* **2011**, 17, 13574–13583.
- [120] A. C. Filippou, B. Baars, O. Chernov, Y. N. Lebedev, G. Schnakenburg, *Angew. Chem. Int. Ed.* **2014**, 53, 565–570.
- [121] S. M. I. Al-Rafia, A. C. Malcolm, R. McDonald, M. J. Ferguson, E. Rivard, *Chem. Commun.* **2012**, 48, 1308–1310.
- [122] M. Driess, Y. Xiong, S. Yao, S. Inoue, J. D. Epping, *Angew. Chem. Int. Ed.* **2013**, 52, 7147–7150.
- [123] K. C. Mondal, P. P. Samuel, M. Tretiakov, A. P. Singh, H. W. Roesky, A. C. Stückl, B. Niepötter, E. Carl, H. Wolf, R. Herbst-Irmer, D. Stalke, *Inorg. Chem.* **2013**, 52, 4736–4743.
- [124] D. Geiß, M. I. Arz, M. Straßmann, G. Schnakenburg, A. C. Filippou, *Angewandte Chemie* **2015**, 127, 2777–2782.
- [125] T. J. Hadlington, J. A. B. Abdalla, R. Tirfoin, S. Aldridge, C. Jones, *Chem. Commun.* **2016**, 52, 1717–1720.
- [126] N. Weyer, M. Heinz, J. I. Schweizer, C. Bruhn, M. C. Holthausen, U. Siemeling, *Angew. Chem. Int. Ed.* **2021**, 60, 2624–2628.
- [127] P. Ghana, M. I. Arz, G. Schnakenburg, M. Straßmann, A. C. Filippou, *Organometallics* **2018**, 37, 772–780.
- [128] A. S. D. Stahlich, V. Huch, A. Grandjean, K. Rohe, K. I. Leszczyńska, D. Scheschkewitz, A. Schäfer, *Chem. Eur. J.* **2019**, 25, 173–176.
- [129] K. C. Mondal, H. W. Roesky, M. C. Schwarzer, G. Frenking, I. Tkach, H. Wolf, D. Kratzert, R. Herbst-Irmer, B. Niepötter, D. Stalke, *Angewandte Chemie International Edition* **2013**, 52, 1801–1805.
- [130] U. Das, unpublished results **2022**.
- [131] P. Ghana, J. Rump, G. Schnakenburg, M. I. Arz, A. C. Filippou, *J. Am. Chem. Soc.* **2021**, 143, 420–432.
- [132] S. Karwasara, L. R. Maurer, B. Peerless, G. Schnakenburg, U. Das, A. C. Filippou, *J. Am. Chem. Soc.* **2021**, 143, 14780–14794.
- [133] M. Bogner, Phosphorus-Based Substituents in Two-Coordinate Silicon Chemistry: Diphosphanosilylenes and [1.1.1]Propellanes, Dissertation, University of Bonn, **2022**.
- [134] P. Ghana, M. I. Arz, U. Das, G. Schnakenburg, A. C. Filippou, *Angewandte Chemie International Edition* **2015**, 54, 9980–9985.
- [135] S. Schwarzwald (nee Krämer), NHC-stabilisierte Disilavinylidene und Silylsilylene, master thesis, University of Bonn, **2015**.
- [136] P. Fritsch, *Justus Liebigs Ann. Chem.* **1894**, 279, 319–323.
- [137] W. P. Buttenberg, *Justus Liebigs Ann. Chem.* **1894**, 279, 324–337.
- [138] H. Wiechell, *Justus Liebigs Ann. Chem.* **1894**, 279, 337–344.
- [139] R. Knorr, *Chem. Rev.* **2004**, 104, 3795–3850.
- [140] E. J. Corey, P. L. Fuchs, *Tetrahedron Letters* **1972**, 13, 3769–3772.
- [141] D. Seyferth, R. S. Marmor, P. Hilbert, *J. Org. Chem.* **1971**, 36, 1379–1386.
- [142] M. I. Bruce, *Chem. Rev.* **1991**, 91, 197–257.

- [143] C. Bruneau, P. H. Dixneuf, *Accounts of Chemical Research* **1999**, 32, 311–323.
- [144] J. M. Lynam, *Chem. Eur. J.* **2010**, 16, 8238–8247.
- [145] S. W. Roh, K. Choi, C. Lee, *Chem. Rev.* **2019**, 119, 4293–4356.
- [146] H. Lischka, H. J. Koehler, *J. Am. Chem. Soc.* **1983**, 105, 6646–6649.
- [147] R. S. Grev, H. F. Schaefer, *The Journal of Chemical Physics* **1992**, 97, 7990–7998.
- [148] M. Karni, Y. Apeloig, J. Kapp, P. von R. Schleyer, in *The Chemistry of Organic Silicon Compounds*, John Wiley & Sons, Ltd, **2001**, pp. 1–163.
- [149] T. Yang, B. B. Dangi, R. I. Kaiser, K.-H. Chao, B.-J. Sun, A. H. H. Chang, T. L. Nguyen, J. F. Stanton, *Angewandte Chemie International Edition* **2017**, 56, 1264–1268.
- [150] B. T. Colegrove, H. F. Schaefer, *J. Am. Chem. Soc.* **1991**, 113, 1557–1561.
- [151] R. S. Grev, in *Advances in Organometallic Chemistry*, Elsevier, **1991**, pp. 125–170.
- [152] K. Kobayashi, S. Nagase, *Organometallics* **1997**, 16, 2489–2491.
- [153] S. Nagase, K. Kobayashi, N. Takagi, *Journal of Organometallic Chemistry* **2000**, 611, 264–271.
- [154] M. Lein, A. Krapp, G. Frenking, *J. Am. Chem. Soc.* **2005**, 127, 6290–6299.
- [155] R. C. Fischer, P. P. Power, *Chem. Rev.* **2010**, 110, 3877–3923.
- [156] Y. Murata, M. Ichinohe, A. Sekiguchi, *J. Am. Chem. Soc.* **2010**, 132, 16768–16770.
- [157] T. Sugahara, J.-D. Guo, D. Hashizume, T. Sasamori, S. Nagase, N. Tokitoh, *Dalton Transactions* **2018**, 47, 13318–13322.
- [158] A. Jana, V. Huch, D. Scheschkewitz, *Angew. Chem. Int. Ed.* **2013**, 52, 12179–12182.
- [159] A. Jana, M. Majumdar, V. Huch, M. Zimmer, D. Scheschkewitz, *Dalton Trans.* **2014**, 43, 5175–5181.
- [160] P. K. Majhi, M. Zimmer, B. Morgenstern, V. Huch, D. Scheschkewitz, *J. Am. Chem. Soc.* **2021**, 143, 13350–13357.
- [161] A. Rit, J. Campos, H. Niu, S. Aldridge, *Nat Chem* **2016**, 8, 1022–1026.
- [162] K. M. Krebs, D. Hanselmann, H. Schubert, K. Wurst, M. Scheele, L. Wesemann, *Journal of the American Chemical Society* **2019**, DOI 10.1021/jacs.8b13645.
- [163] C. Wilhelm, D. Raiser, H. Schubert, C. P. Sindlinger, L. Wesemann, *Inorg. Chem.* **2021**, 60, 9268–9272.
- [164] R. Kobayashi, S. Ishida, T. Iwamoto, *Organometallics* **2021**, 40, 843–847.
- [165] F. Gstrein, *Silicon Compounds in Low Oxidation States Supported by a Cyclic (Alkyl)(Amino)Carbene: Synthesis, Structure and Reactivity*, Dissertation, University of Bonn, **2022**.
- [166] A. Rit, J. Campos, H. Niu, S. Aldridge, *Nat Chem* **2016**, 8, 1022–1026.
- [167] K. M. Krebs, D. Hanselmann, H. Schubert, K. Wurst, M. Scheele, L. Wesemann, *Journal of the American Chemical Society* **2019**, DOI 10.1021/jacs.8b13645.
- [168] A. Jana, V. Huch, D. Scheschkewitz, *Angewandte Chemie* **2013**, 125, 12401–12404.
- [169] A. Jana, V. Huch, H. S. Rzepa, D. Scheschkewitz, *Angew. Chem. Int. Ed.* **2015**, 54, 289–292.
- [170] A. Jana, I. Omlor, V. Huch, H. S. Rzepa, D. Scheschkewitz, *Angew. Chem. Int. Ed.* **2014**, 53, 9953–9956.
- [171] D. Nieder, V. Huch, C. B. Yildiz, D. Scheschkewitz, *J. Am. Chem. Soc.* **2016**, 138, 13996–14005.
- [172] D. Nieder, C. B. Yildiz, A. Jana, M. Zimmer, V. Huch, D. Scheschkewitz, *Chem. Commun.* **2016**, 52, 2799–2802.

- [173] P. K. Majhi, M. Zimmer, B. Morgenstern, D. Scheschkewitz, *J. Am. Chem. Soc.* **2021**, 143, 8981–8986.
- [174] P. Ghana, unpublished results **2015**.
- [175] G. Brauer, R. F. Riley, inc Scripta Technica, Handbook of Preparative Inorganic Chemistry Volume 1 Volume 1, Academic Press, New York, **1963**.
- [176] A. J. Arduengo III, R. Krafczyk, R. Schmutzler, H. A. Craig, J. R. Goerlich, W. J. Marshall, M. Unverzagt, *Tetrahedron* **1999**, 55, 14523–14534.
- [177] K. Nagata, T. Agou, N. Tokitoh, *Angew. Chem. Int. Ed.* **2014**, 53, 3881.
- [178] I. Bejan, D. Güclü, S. Inoue, M. Ichinohe, A. Sekiguchi, D. Scheschkewitz, *Angew. Chem. Int. Ed.* **2007**, 46, 3349–3352.
- [179] I. Bejan, D. Scheschkewitz, *Angew. Chem. Int. Ed.* **2007**, 46, 5783–5786.
- [180] K. Abersfelder, D. Scheschkewitz, *J. Am. Chem. Soc.* **2008**, 130, 4114–4121.
- [181] I. Bejan, S. Inoue, M. Ichinohe, A. Sekiguchi, D. Scheschkewitz, *Chem. Eur. J.* **2008**, 14, 7119–7122.
- [182] K. Abersfelder, T. Nguyen, D. Scheschkewitz, *Z. anorg. allg. Chem.* **2009**, 635, 2093–2098.
- [183] A. Meltzer, M. Majumdar, A. J. P. White, V. Huch, D. Scheschkewitz, *Organometallics* **2013**, 32, 6844–6850.
- [184] A. Rammo, I. Bejan, A. Meltzer, K. Radacki, H. Braunschweig, D. Scheschkewitz, *Aust. J. Chem.* **2013**, 66, 1311.
- [185] P. Willmes, M. J. Cowley, M. Hartmann, M. Zimmer, V. Huch, D. Scheschkewitz, *Angew. Chem. Int. Ed.* **2014**, 53, 2216–2220.
- [186] P. Willmes, L. Junk, V. Huch, C. B. Yildiz, D. Scheschkewitz, *Angew. Chem. Int. Ed.* **2016**, 55, 10913–10917.
- [187] Y. Heider, P. Willmes, D. Mühlhausen, L. Klemmer, M. Zimmer, V. Huch, D. Scheschkewitz, *Angew. Chem. Int. Ed.* **2019**, 58, 1939–1944.
- [188] K. I. Leszczyńska, V. Huch, C. Präsang, J. Schwabedissen, R. J. F. Berger, D. Scheschkewitz, *Angew. Chem. Int. Ed.* **2019**, 58, 5124–5128.
- [189] P. Jutzi, K. Leszczyńska, A. Mix, B. Neumann, B. Rummel, W. Schoeller, H.-G. Stammler, *Organometallics* **2010**, 29, 4759–4761.
- [190] T. Kato, S. Takahashi, E. Bellan, A. Baceiredo, N. Saffon-Merceron, S. Massou, N. Nakata, D. Hashizume, V. Branchadell, *Angew. Chem. Int. Ed.* **2019**, DOI 10.1002/anie.201904594.
- [191] S. Inoue, M. Ichinohe, A. Sekiguchi, *Organometallics* **2008**, 27, 1358–1360.
- [192] T. Abe, S. Ishida, T. Iwamoto, *BCSJ* **2018**, 91, 684–686.
- [193] R. Holzner, D. Reiter, P. Frisch, S. Inoue, *RSC Adv.* **2020**, 10, 3402–3406.
- [194] F. Gstrein, unpublished results, Bonn, **2022**.
- [195] S. Takahashi, E. Bellan, A. Baceiredo, N. Saffon-Merceron, S. Massou, N. Nakata, D. Hashizume, V. Branchadell, T. Kato, *Angew. Chem. Int. Ed.* **2019**, 58, 10310–10314.
- [196] D. Bravo-Zhivotovskii, R. Dobrovetsky, D. Nemirovsky, V. Molev, M. Bendikov, G. Molev, M. Botoshansky, Y. Apeloig, *Angew. Chem. Int. Ed.* **2008**, 47, 4343–4345.
- [197] L. Zborovsky, R. Dobrovetsky, M. Botoshansky, D. Bravo-Zhivotovskii, Y. Apeloig, *J. Am. Chem. Soc.* **2012**, 134, 18229–18232.
- [198] D. Pinchuk, J. Mathew, A. Kaushansky, D. Bravo-Zhivotovskii, Y. Apeloig, *Angew. Chem. Int. Ed.* **2016**, 55, 10258–10262.

- [199] M. M. Siddiqui, S. Sinhababu, S. Dutta, S. Kundu, P. N. Ruth, A. Münch, R. Herbst-Irmer, D. Stalke, D. Koley, H. W. Roesky, *Angew. Chem. Int. Ed.* **2018**, *57*, 11776–11780.
- [200] G. Becker, H.-M. Hartmann, E. Hengge, F. Schrank, *ZAAC* **1989**, *572*, 63–74.
- [201] R. Klink, C. Schrenk, A. Schnepf, *Dalton Trans.* **2014**, *43*, 16097–16104.
- [202] F. D. Uhlig, H. C. Marsmann, in *Gelest Catalogue*, Eigenverlag, Morrisville, PA, USA, **2003**, pp. 208–222.
- [203] R. S. Simons, C. T. Haubrich, B. V. Mork, M. Niemeyer, P. P. Power, *Main Group Chemistry* **1998**, *2*, 275–283.
- [204] R. B. Bates, L. M. Kroposki, D. E. Potter, *J. Org. Chem.* **1972**, *37*, 560–562.
- [205] O. Chernov, Dissertation - Novel Molecular Si(II) Precursors for Synthesis of the First Compounds with Metal-Silicon Triple Bonds **n.d.**
- [33] For Raman data of compounds with Si=Si double bonds see: a) West, R.; Fink, M. J.; Michl, J. *Science* **1981**, *214*, 1343; b) West, R.; *Angew. Chem. Int. Ed. Engl.* **1987**, *26*, 1201; c) Leites, L. A.; Bukalov, S. S.; Garbuzova, I. A.; West, R.; Mangette, J.; Spitzner, H. J. *Organomet. Chem.* **1997**, *536–537*, 425; d) Leites, L. A.; Bukalov, S. S.; Mangette, J. E.; Schmedake, T. A.; West, R. *Mendeleev Commun.* **1998**, *8*, 43; e) Schmedake, T. A.; Haaf, M.; Apeloig, Y.; Müller, T.; Bukalov, S.; West, R. *J. Am. Chem. Soc.* **1999**, *121*, 9479; f) Wiberg, N.; Niedermayer, W.; Polborn, K.; *Z. Für Anorg. Allg. Chem.* **2002**, *628*, 1045; g) Leites, L. A.; Bukalov, S. S.; Mangette, J. E.; Schmedake, T. A.; West, R. *Spectrochim. Acta. A. Mol. Biomol. Spectrosc.* **2003**, *59*, 1975.
- [207] R. Breslow, J. L. Grant, *J. Am. Chem. Soc.* **1977**, *99*, 7745–7746.
- [208] B. Jaun, J. Schwarz, R. Breslow, *J. Am. Chem. Soc.* **1980**, *102*, 5741–5748.
- [209] J. R. Aranzaes, M.-C. Daniel, D. Astruc, *Can. J. Chem.* **2006**, *84*, 288–299.
- [38] R. Rodriguez, T. Troadec, T. Kato, N. Saffon-Merceron, J.-M. Sotiropoulos, A. Baceiredo, *Angew. Chem. Int. Ed.* **2012**, *51*, 7158–7161; *Angew. Chem.* **2012**, *124* (29), 7270–7273.
- [211] B. J. Guddorf, A. Hepp, F. Lips, *Chemistry - A European Journal* **2018**, *24*, 10334–10338.
- [43] S. Inoue, M. Ichinohe, A. Sekiguchi, *Angew. Chem. Int. Ed.* **2007**, *46*, 3346–3348; *Angew. Chem.* **2007**, *119* (18), 3410–3412.
- [213] H. Tanaka, S. Inoue, M. Ichinohe, A. Sekiguchi, *Organometallics* **2009**, *28*, 6625–6628.
- [214] N. Sigal, Y. Apeloig, *Journal of Organometallic Chemistry* **2001**, *636*, 148–156.
- [215] A. Azizoglu, C. B. Yıldız, *Journal of Organometallic Chemistry* **2012**, *715*, 19–25.
- [216] K. Leszczyńska, K. Abersfelder, A. Mix, B. Neumann, H.-G. Stammer, M. J. Cowley, P. Jutzi, D. Scheschke, *Angew. Chem. Int. Ed.* **2012**, *51*, 6785–6788.
- [217] S. Masamune, S. Murakami, H. Tobita, D. J. Williams, *Journal of the American Chemical Society* **1983**, *105*, 7776–7778.
- [218] H. A. Bent, *Chem. Rev.* **1961**, *61*, 275–311.
- [219] N. Weidemann, G. Schnakenburg, A. C. Filippou, *Zeitschrift für anorganische und allgemeine Chemie* **2009**, *635*, 253–259.
- [220] R. Ackermann, L. Lange, in *Ullmann's Encyclopedia of Industrial Chemistry* (Ed.: Wiley-VCH Verlag GmbH & Co. KGaA), Wiley-VCH Verlag GmbH & Co. KGaA, Weinheim, Germany, **2000**, p. a24_341.
- [221] D. L. Reger, S. R. Goode, D. W. Ball, *Chemistry: Principles and Practice*, Brooks/Cole, Cengage Learning, Belmont, CA, **2010**.

- [222] M. Ichinohe, R. Kinjo, A. Sekiguchi, *Organometallics* **2003**, 22, 4621–4623.
- [223] T. Yamaguchi, M. Ichinohe, A. Sekiguchi, *New J. Chem.* **2010**, 34, 1544.
- [224] A. Jana, I. Omlor, V. Huch, H. S. Rzepa, D. Scheschkewitz, *Angewandte Chemie International Edition* **2014**, 53, 9953–9956.
- [225] M. J. Fink, D. J. De Young, R. West, J. Michl, *J. Am. Chem. Soc.* **1983**, 105, 1070–1071.
- [226] A. Schäfer, M. Weidenbruch, S. Pohl, *Journal of Organometallic Chemistry* **1985**, 282, 305–313.
- [227] N. J. Mosey, K. M. Baines, T. K. Woo, *J. Am. Chem. Soc.* **2002**, 124, 13306–13321.
- [228] M. S. Samuel, H. A. Jenkins, D. W. Hughes, K. M. Baines, *Organometallics* **2003**, 22, 1603–1611.
- [229] N. Schneider, M. Finger, C. Haferkemper, S. Bellemin-Laponnaz, P. Hofmann, L. H. Gade, *Angew. Chem. Int. Ed.* **2009**, 48, 1609–1613.
- [230] D. Scheschkewitz, Ed., *Functional Molecular Silicon Compounds II*, Springer International Publishing, **2014**.
- [231] T. Veszprémi, M. Takahashi, B. Hajgató, M. Kira, *J. Am. Chem. Soc.* **2001**, 123, 6629–6638.
- [232] C. S. Cucinotta, A. Ruini, A. Catellani, A. Stirling, *ChemPhysChem* **2006**, 7, 1229–1234.
- [233] S. K. Pollack, W. J. Hehre, *J. Am. Chem. Soc.* **1977**, 99, 4845–4846.
- [234] T. Iwamoto, T. Abe, S. Ishida, C. Kabuto, M. Kira, *Journal of Organometallic Chemistry* **2007**, 692, 263–270.
- [235] J. Böhnke, T. Brückner, A. Hermann, O. F. González-Belman, M. Arrowsmith, J. O. C. Jiménez-Halla, H. Braunschweig, *Chem. Sci.* **2018**, 9, 5354–5359.
- [236] M. M. Juckel, J. Hicks, D. Jiang, L. Zhao, G. Frenking, C. Jones, *Chem. Commun.* **2017**, 53, 12692–12695.
- [237] S. Schäfer, R. Köppe, M. T. Gamer, P. W. Roesky, *Chem. Commun.* **2014**, 50, 11401–11403.
- [238] S. Schäfer, R. Köppe, P. W. Roesky, *Chemistry – A European Journal* **2016**, 22, 7127–7133.
- [239] F. M. Mück, J. A. Baus, A. Ulmer, C. Burschka, R. Tacke, *European Journal of Inorganic Chemistry* **2016**, 2016, 1660–1670.
- [240] J. A. Baus, F. M. Mück, H. Schneider, R. Tacke, *Chem. Eur. J.* **2017**, 23, 296–303.
- [241] N. Wiberg, K. Amelunxen, H.-W. Lerner, H. Nöth, A. Appel, J. Knizek, K. Polborn, *Z. Anorg. Allg. Chem.* **1997**, 623, 1861–1870.
- [242] J. Arnold, T. D. Tilley, A. L. Rheingold, S. J. Geib, *Inorg. Chem.* **1987**, 26, 2106–2109.
- [243] S. Schäfer, R. Köppe, M. T. Gamer, P. W. Roesky, *Chem. Commun.* **2014**, 50, 11401–11403.
- [244] G. Becker, W. Schwarz, N. Seidler, M. Westerhausen, *Z. Anorg. Allg. Chem.* **1992**, 612, 72–82.
- [245] M. Westerhausen, S. Schneiderbauer, H. Piotrowski, M. Suter, H. Nöth, *Journal of Organometallic Chemistry* **2002**, 643–644, 189–193.
- [246] F. F. Puschmann, D. Stein, D. Heift, C. Hendriksen, Z. A. Gal, H.-F. Grützmacher, H. Grützmacher, *Angew. Chem. Int. Ed.* **2011**, 50, 8420–8423.
- [247] D. Heift, Z. Benkő, H. Grützmacher, *Dalton Trans.* **2014**, 43, 831–840.
- [248] J. M. Goicoechea, H. Grützmacher, *Angew. Chem. Int. Ed.* **2018**, 57, 16968–16994.
- [249] L. N. Grant, D. J. Mindiola, *Chemistry – A European Journal* **2019**, 25, 16171–16178.

- [250] A. M. Tondreau, Z. Benkő, J. R. Harmer, H. Grützmacher, *Chem. Sci.* **2014**, *5*, 1545–1554.
- [251] Z. Li, X. Chen, Y. Li, C.-Y. Su, H. Grützmacher, *Chem. Commun.* **2016**, *52*, 11343–11346.
- [252] T. P. Robinson, M. J. Cowley, D. Scheschkewitz, J. M. Goicoechea, *Angew. Chem. Int. Ed.* **2014**, *50*, 12510–12513.
- [253] Y. Wu, L. Liu, J. Su, J. Zhu, Z. Ji, Y. Zhao, *Organometallics* **2016**, *35*, 1593–1596.
- [254] S. Yao, Y. Xiong, T. Szilvási, H. Grützmacher, M. Driess, *Angew. Chem. Int. Ed.* **2016**, *55*, 4781–4785.
- [255] Y. Xiong, S. Yao, T. Szilvási, E. Ballester-Martínez, H. Grützmacher, M. Driess, *Angew. Chem. Int. Ed.* **2017**, *56*, 4333–4336.
- [256] L. Rothe, Untersuchung zur Substitution von Halosilylenen und -germylenen, bachelor thesis, University of Bonn, **2017**.
- [257] A. Schäfer, M. Weidenbruch, W. Saak, S. Pohl, *Angew. Chem. Int. Ed. Engl.* **1987**, *26*, 776–777.
- [258] S. Inoue, W. Wang, C. Präsang, M. Asay, E. Irran, M. Driess, *J. Am. Chem. Soc.* **2011**, *133*, 2868–2871.
- [259] S. S. Sen, S. Khan, H. W. Roesky, D. Kratzert, K. Meindl, J. Henn, D. Stalke, J.-P. Demers, A. Lange, *Angew. Chem. Int. Ed.* **2011**, *50*, 2322–2325.
- [260] S. S. Sen, J. Hey, M. Eckhardt, R. Herbst-Irmer, E. Maedl, R. A. Mata, H. W. Roesky, M. Scheer, D. Stalke, *Angew. Chem. Int. Ed.* **2011**, *50*, 12510–12513.
- [261] S. Roy, B. Dittrich, T. Mondal, D. Koley, A. C. Stückl, B. Schwederski, W. Kaim, M. John, S. K. Vasa, R. Linser, H. W. Roesky, *J. Am. Chem. Soc.* **2015**, *137*, 6180–6183.
- [262] A. E. Seitz, M. Eckhardt, A. Erlebach, E. V. Peresyphkina, M. Sierka, M. Scheer, *J. Am. Chem. Soc.* **2016**, *138*, 10433–10436.
- [263] B. J. Guddorf, C. Mück-Lichtenfeld, A. Hepp, F. Lips, *Chem. Commun.* **2019**, *55*, 12896–12899.
- [264] V. Nesterov, N. C. Breit, S. Inoue, *Chemistry - A European Journal* **2017**, DOI 10.1002/chem.201700829.
- [265] H. Cui, J. Zhang, Y. Tao, C. Cui, *Inorg. Chem.* **2016**, *55*, 46–50.
- [266] Y. Gao, J. Zhang, H. Hu, C. Cui, *Organometallics* **2010**, *29*, 3063–3065.
- [267] Y. N. Lebedev, U. Das, O. Chernov, G. Schnakenburg, A. C. Filippou, *Chem. Eur. J.* **2014**, *20*, 9280–9289.
- [268] B. J. Guddorf, A. Hepp, F. Lips, *Chemistry - A European Journal* **2018**, *24*, 10334–10338.
- [269] K. Hansen, T. Szilvási, B. Blom, E. Irran, M. Driess, *Chemistry - A European Journal* **2015**, *21*, 18930–18933.
- [270] P. Pyykkö, *J. Phys. Chem. A* **2015**, *119*, 2326–2337.
- [271] P. von R. Schleyer, C. Maerker, A. Dransfeld, H. Jiao, N. J. R. van Eikema Hommes, *J. Am. Chem. Soc.* **1996**, *118*, 6317–6318.
- [272] Z. Chen, C. S. Wannere, C. Corminboeuf, R. Puchta, P. von R. Schleyer, *Chem. Rev.* **2005**, *105*, 3842–3888.
- [273] S. Roy, K. C. Mondal, L. Krause, P. Stollberg, R. Herbst-Irmer, D. Stalke, J. Meyer, A. C. Stückl, B. Maity, D. Koley, S. K. Vasa, S. Q. Xiang, R. Linser, H. W. Roesky, *J. Am. Chem. Soc.* **2014**, *136*, 16776–16779.
- [274] K. Wakita, N. Tokitoh, R. Okazaki, *BCSJ* **2000**, *73*, 2157–2158.

- [275] J. D. Egbert, C. S. J. Cazin, S. P. Nolan, *Catal. Sci. Technol.* **2013**, *3*, 912.
- [276] F. Lazreg, F. Nahra, C. S. J. Cazin, *Coordination Chemistry Reviews* **2015**, *293–294*, 48–79.
- [277] A. A. Danopoulos, T. Simler, P. Braunstein, *Chem. Rev.* **2019**, *119*, 3730–3961.
- [278] G. Noirbent, F. Dumur, *Catalysts* **2020**, *10*, 953.
- [279] A. G. Avent, B. Gehrhus, P. B. Hitchcock, M. F. Lappert, H. Maciejewski, *Journal of Organometallic Chemistry* **2003**, *686*, 321–331.
- [280] Y. Inagawa, S. Ishida, T. Iwamoto, *Chemistry Letters* **2014**, *43*, 1665–1667.
- [281] G. Tan, B. Blom, D. Gallego, M. Driess, *Organometallics* **2014**, *33*, 363–369.
- [282] N. Parvin, S. Pal, J. Echeverría, S. Alvarez, S. Khan, *Chem. Sci.* **2018**, *9*, 4333–4337.
- [283] A. N. Paesch, A.-K. Kreyenschmidt, R. Herbst-Irmer, D. Stalke, *Inorg. Chem.* **2019**, *58*, 7000–7009.
- [284] N. Parvin, J. Hossain, A. George, P. Parameswaran, S. Khan, *Chem. Commun.* **2020**, *56*, 273–276.
- [285] M. Chen, Y. Wang, Y. Xie, P. Wei, R. J. Gilliard, N. A. Schwartz, H. F. Schaefer, P. von R. Schleyer, G. H. Robinson, *Chem. Eur. J.* **2014**, *20*, 9208–9211.
- [286] M. I. Arz, *Molekulare Si(0)- und Si(I)-Verbindungen: Synthese, Struktur und Reaktivität*, Dissertation, University of Bonn, **2015**.
- [287] D. Geiß, *Neue Synthesestrategien für Übergangsmetallkomplexe mit ungesättigter germanium- und siliziumbasierter Ligandensphäre* **2015**.
- [288] J. D. Farwell, P. B. Hitchcock, M. F. Lappert, A. V. Protchenko, *Journal of Organometallic Chemistry* **2007**, *692*, 4953–4961.
- [289] M. J. Sgro, W. E. Piers, P. E. Romero, *Dalton Trans.* **2015**, *44*, 3817–3828.
- [290] M. Walewska, J. Hlina, W. Gaderbauer, H. Wagner, J. Baumgartner, C. Marschner, *Z. Anorg. Allg. Chem.* **2016**, *642*, 1304–1313.
- [291] F. Schödel, M. Bolte, M. Wagner, H. Lerner, *Z. Anorg. Allg. Chem.* **2020**, *646*, 264–267.
- [292] C. Boehme, G. Frenking, *Organometallics* **1998**, *17*, 5801–5809.
- [293] S. Khan, S. K. Ahirwar, S. Pal, N. Parvin, N. Kathewad, *Organometallics* **2015**, *34*, 5401–5406.
- [294] N. Parvin, R. Dasgupta, S. Pal, S. S. Sen, S. Khan, *Dalton Transactions* **2017**, *46*, 6528–6532.
- [295] N. Parvin, N. Sen, S. Tothadi, S. Muhammed, P. Parameswaran, S. Khan, *Organometallics* **2021**, *40*, 1626–1632.
- [296] T. G. Driver, K. A. Woerpel, *J. Am. Chem. Soc.* **2004**, *126*, 9993–10002.
- [297] J. A. Mayoral, S. Rodríguez-Rodríguez, L. Salvatella, *Eur. J. Org. Chem.* **2010**, *2010*, 1231–1234.
- [298] S. Díez-González, S. P. Nolan, *Acc. Chem. Res.* **2008**, *41*, 349–358.
- [299] H.-J. Liu, C. Raynaud, O. Eisenstein, T. D. Tilley, *J. Am. Chem. Soc.* **2014**, *136*, 11473–11482.
- [300] P. Frisch, S. Inoue, *Chem. Commun.* **2018**, *54*, 13658–13661.
- [301] N. A. Rajabi, C. L. McMullin, *RSC Adv.* **2021**, *11*, 11793–11803.
- [302] Y. Mutoh, K. Imai, Y. Kimura, Y. Ikeda, Y. Ishii, *Organometallics* **2011**, *30*, 204–207.
- [303] T. Yamaguchi, A. Sekiguchi, M. Driess, *J. Am. Chem. Soc.* **2010**, *132*, 14061–14063.
- [304] L. Kuehn, A. F. Eichhorn, T. B. Marder, U. Radius, *Journal of Organometallic Chemistry* **2019**, *881*, 25–33.

- [305] N. Takagi, S. Nagase, *European Journal of Inorganic Chemistry* **2002**, 2002, 2775–2778.
- [306] B. Peerless, unpublished results **2019**.
- [307] M. I. Arz, M. Straßmann, D. Geiß, G. Schnakenburg, A. C. Filippou, *J. Am. Chem. Soc.* **2016**, 138, 4589–4600.
- [308] R. Kobayashi, S. Ishida, T. Iwamoto, *Organometallics* **2021**, 40, 843–847.
- [309] S. Krämer, *NHC-stabilisierte Disilavinylidene und Silylsilylene* **2015**.
- [310] A. J. Hickman, M. S. Sanford, *Nature* **2012**, 484, 177–185.
- [311] K. Seth, S. R. Roy, A. Kumar, A. K. Chakraborti, *Catal. Sci. Technol.* **2016**, 6, 2892–2896.
- [312] I. P. Beletskaya, A. V. Cheprakov, *Organometallics* **2012**, 31, 7753–7808.
- [313] K. Sonogashira, Y. Tohda, N. Hagihara, *Tetrahedron Letters* **1975**, 16, 4467–4470.
- [314] A. V. Astakhov, S. B. Soliev, V. M. Chernyshev, *Russ Chem Bull* **2020**, 69, 2073–2081.
- [315] A. R. Jupp, M. B. Geeson, J. E. McGrady, J. M. Goicoechea, *European Journal of Inorganic Chemistry* **2016**, 2016, 639–648.
- [316] S. Yao, Y. Grossheim, A. Kostenko, E. Ballester-Martínez, S. Schutte, M. Bispinghoff, H. Grützmacher, M. Driess, *Angewandte Chemie International Edition* **2017**, 56, 7465–7469.
- [317] E. O. Fischer, A. Maasböl, *Angew. Chem. Int. Ed. Engl.* **1964**, 3, 580–581.
- [318] A. F. Hill, in *Metal–Carbon Multiple Bonding*, Royal Society Of Chemistry, Cambridge, **2007**, pp. 89–121.
- [319] G. Bertrand, Ed. , *Carbene Chemistry: From Fleeting Intermediates to Powerful Reagents*, Marcel Dekker ; FontisMedia, New York : Lausanne, Switzerland, **2002**.
- [320] K. H. Dötz, P. Tomuschat, *Chem. Soc. Rev.* **1999**, 28, 187–198.
- [321] A. Feliciano, J. L. Vázquez, L. J. Benítez-Puebla, I. Velazco-Cabral, D. Cruz Cruz, F. Delgado, M. A. Vázquez, *Chem. Eur. J.* **2021**, 27, 8233–8251.
- [322] A. J. Arduengo, D. Tapu, in *Reference Module in Chemistry, Molecular Sciences and Chemical Engineering*, Elsevier, **2013**, p. B9780124095472032000.
- [323] Roger. W. Alder, C. P. Butts, A. G. Orpen, *J. Am. Chem. Soc.* **1998**, 120, 11526–11527.
- [324] N. Merceron-Saffon, A. Baceiredo, H. Gornitzka, G. Bertrand, *Science* **2003**, 301, 1223–1225.
- [325] S. Conejero, Y. Canac, F. S. Tham, G. Bertrand, *Angew. Chem. Int. Ed.* **2004**, 43, 4089–4093.
- [326] R. W. Hoffman, H. Häuser, *Tetrahedron Letters* **1964**, 5, 197–201.
- [327] H. P. Reisenauer, J. Romanski, G. Mloston, P. R. Schreiner, *Eur. J. Org. Chem.* **2006**, 2006, 4813–4818.
- [328] B. Cetinkaya, I. Gumrukcu, M. F. Lappert, J. L. Atwood, R. D. Rogers, M. J. Zaworotko, *J. Am. Chem. Soc.* **1980**, 102, 2088–2089.
- [329] A. Meller, C.-P. Gräbe, *Chem. Ber.* **1985**, 118, 2020–2029.
- [330] M. F. Lappert, *Main Group Metal Chemistry* **1994**, 17, 183–207.
- [331] M. Grenz, E. Hahn, W.-W. du Mont, J. Pickardt, *Angew. Chem. Int. Ed. Engl.* **1984**, 23, 61–63.
- [332] T. J. Boyle, L. J. Tribby, L. A. M. Ottley, S. M. Han, *Eur. J. Inorg. Chem.* **2009**, 2009, 5550–5560.
- [333] R. A. Green, C. Moore, A. L. Rheingold, C. S. Weinert, *Inorg. Chem.* **2009**, 48, 7510–7512.

- [334] M. Novotný, Z. Padělková, J. Holeček, A. Růžička, *J. Organom. Chem.* **2013**, 733, 71–78.
- [335] C. S. Weinert, A. E. Fenwick, P. E. Fanwick, I. P. Rothwell, *Dalton Trans.* **2003**, 532–539.
- [336] T. J. Boyle, T. M. Alam, M. A. Rodriguez, C. A. Zechmann, *Inorg. Chem.* **2002**, 41, 2574–2582.
- [337] R. Gsell, M. Zeldin, *Journal of Inorganic and Nuclear Chemistry* **1975**, 37, 1133–1137.
- [338] P. B. Hitchcock, M. F. Lappert, S. A. Thomas, A. Thorne, *Journal of Organometallic Chemistry* **1986**, 315, 27–44.
- [339] P. Braunstein, M. Veith, J. Blin, V. Huch, *Organometallics* **2001**, 20, 627–633.
- [340] M. Veith, M. Ehses, V. Huch, *New J. Chem.* **2005**, 29, 154.
- [341] S. S. Karlov, G. S. Zaitseva, M. P. Egorov, *Russ Chem Bull* **2019**, 68, 1129–1142.
- [342] A. Kowalski, A. Duda, S. Penczek, *Macromolecules* **2000**, 33, 689–695.
- [343] H. Gerung, T. J. Boyle, L. J. Tribby, S. D. Bunge, C. J. Brinker, S. M. Han, *J. Am. Chem. Soc.* **2006**, 128, 5244–5250.
- [344] T. J. Boyle, T. Q. Doan, L. A. M. Steele, C. Apblett, S. M. Hoppe, K. Hawthorne, R. M. Kalinich, W. M. Sigmund, *Dalton Transactions* **2012**, 41, 9349.
- [345] T. J. Boyle, J. M. Segall, T. M. Alam, M. A. Rodriguez, J. M. Santana, *J. Am. Chem. Soc.* **2002**, 124, 6904–6913.
- [346] T. J. Boyle, T. L. Ward, S. M. De'Angeli, H. Xu, W. F. Hammetter, *Chem. Mater.* **2003**, 15, 765–775.
- [347] M. S. Hill, A. L. Johnson, J. P. Lowe, K. C. Molloy, J. D. Parish, T. Wildsmith, A. L. Kingsley, *Dalton Trans.* **2016**, 45, 18252–18258.
- [348] T. Fjeldberg, P. B. Hitchcock, M. F. Lappert, S. J. Smith, A. J. Thorne, *J. Chem. Soc., Chem. Commun.* **1985**, 939.
- [349] C. S. Weinert, P. E. Fanwick, I. P. Rothwell, *J. Chem. Soc., Dalton Trans.* **2002**, 2948–2950.
- [350] C. Stanciu, A. F. Richards, M. Stender, M. M. Olmstead, P. P. Power, *Polyhedron* **2006**, 25, 477–483.
- [351] D. A. Dickie, I. S. MacIntosh, D. D. Ino, Q. He, O. A. Labeodan, M. C. Jennings, G. Schatte, C. J. Walsby, J. A. C. Clyburne, *Can. J. Chem.* **2008**, 86, 20–31.
- [352] D. M. Barnhart, D. L. Clark, J. G. Watkin, *Acta Crystallographica Section C Crystal Structure Communications* **1994**, 50, 702–704.
- [353] B. D. Rekken, T. M. Brown, M. M. Olmstead, J. C. Fettinger, P. P. Power, *Inorganic Chemistry* **2013**, 52, 3054–3062.
- [354] K. P. Kepp, *Inorg. Chem.* **2016**, 55, 9461–9470.
- [355] C.-W. So, H. W. Roesky, P. M. Gurubasavaraj, R. B. Oswald, M. T. Gamer, P. G. Jones, S. Blaurock, *J. Am. Chem. Soc.* **2007**, 129, 12049–12054.
- [356] W. Wang, S. Inoue, S. Yao, M. Driess, *Journal of the American Chemical Society* **2010**, 132, 15890–15892.
- [357] W. Wang, S. Inoue, E. Irran, M. Driess, *Angew. Chem. Int. Ed.* **2012**, 51, 3691–3694.
- [358] F. Gstrein, Personal Communication, Bonn, **2022**.
- [359] R. Azhakar, R. S. Ghadwal, H. W. Roesky, H. Wolf, D. Stalke, *Organometallics* **2012**, 31, 4588–4592.
- [360] P. H. M. Budzelaar, *GNMR, Version 5.0.6.0*, IvorySoft, Centennial, USA, **2006**.

- [361] M. Hesse, H. Meier, B. Zeeh, *Spektroskopische Methoden in Der Organischen Chemie*, 8., Überarbeitete Auflage, Thieme Verlag, Stuttgart, **2011**.
- [362] R. S. Ghadwal, S. S. Sen, H. W. Roesky, G. Tavcar, S. Merkel, D. Stalke, *Organometallics* **2009**, 28, 6374–6377.
- [363] M. Hartmann, A. Haji-Abdi, K. Abersfelder, P. R. Haycock, A. J. P. White, D. Scheschkewitz, *Dalton Transactions* **2010**, 39, 9288.
- [364] S. Metz, C. Burschka, D. Platte, R. Tacke, *Angew. Chem. Int. Ed.* **2007**, 46, 7006–7009.
- [365] S. Metz, B. Theis, C. Burschka, R. Tacke, *Chem. Eur. J.* **2010**, 16, 6844–6856.
- [366] T. Kühler, P. Jutzi, in *Advances in Organometallic Chemistry*, Elsevier, **2003**, pp. 1–34.
- [367] P. Jutzi, *Science* **2004**, 305, 849–851.
- [368] M. Brookhart, B. Grant, A. F. Volpe, *Organometallics* **1992**, 11, 3920–3922.
- [369] C. Stanciu, M. M. Olmstead, A. D. Phillips, M. Stender, P. P. Power, *European Journal of Inorganic Chemistry* **2003**, 2003, 3495–3500.
- [370] T. Müller, *Journal of Organometallic Chemistry* **2003**, 686, 251–256.
- [371] T. J. Drahnak, J. Michl, R. West, *J. Am. Chem. Soc.* **1979**, 101, 5427–5428.
- [372] G. Maier, G. Mihm, H. P. Reisenauer, D. Littmann, *Chem. Ber.* **1984**, 117, 2369–2381.
- [373] G. Maier, H. P. Reisenauer, K. Schöttler, U. Wessolek-Kraus, *J. Organomet. Chem.* **1989**, 366, 25–38.
- [374] W. P. Neumann, *Chem. Rev.* **1991**, 91, 311–334.
- [375] A. V. Zabula, F. E. Hahn, *Eur. J. Inorg. Chem.* **2008**, 2008, 5165–5179.
- [376] Y. Apeloig, T. Mueller, *J. Am. Chem. Soc.* **1995**, 117, 5363–5364.
- [377] I. Buchem, *Homoleptische Germanium(II)-Verbindungen mit Amid-Substituenten*, diploma thesis, Humboldt-Universität zu Berlin, **2005**.
- [378] M. Hesse, U. Klingebiel, *Angew. Chem. Int. Ed. Engl.* **1986**, 25, 649–650.
- [379] N. Wiberg, K. Schurz, G. Reber, G. Müller, *J. Chem. Soc., Chem. Commun.* **1986**, 591–592.
- [380] M. Denk, R. K. Hayashi, R. West, *J. Am. Chem. Soc.* **1994**, 116, 10813–10814.
- [381] T. Iwamoto, N. Ohnishi, Z. Gui, S. Ishida, H. Isobe, S. Maeda, K. Ohno, M. Kira, *New J. Chem.* **2010**, 34, 1637.
- [382] R. Tacke, C. Kobelt, J. A. Baus, R. Bertermann, C. Burschka, *Dalton Trans.* **2015**, 44, 14959–14974.
- [383] P. Jutzi, A. Mix, B. Neumann, B. Rummel, W. W. Schoeller, H.-G. Stammler, A. B. Rozhenko, *J. Am. Chem. Soc.* **2009**, 131, 12137–12143.
- [384] L. Kong, C. Cui, *Organometallics* **2010**, 29, 5738–5740.
- [385] C. Lippmann, *Untersuchung der Reaktivität eines Bis(aryloxy)silylens*, bachelor thesis, University of Bonn, **2016**.
- [386] A. Bondi, *J. Phys. Chem.* **1964**, 68, 441–451.
- [387] I. Alvarado-Beltran, A. Rosas-Sánchez, A. Baceiredo, N. Saffon-Merceron, V. Branchadell, T. Kato, *Angewandte Chemie* **2017**, 129, 10617–10621.
- [388] A. Rosas-Sánchez, I. Alvarado-Beltran, A. Baceiredo, N. Saffon-Merceron, S. Massou, D. Hashizume, V. Branchadell, T. Kato, *Angewandte Chemie* **2017**, 129, 16132–16136.
- [389] R. Kobayashi, S. Ishida, T. Iwamoto, *Angew. Chem. Int. Ed.* **2019**, 58, 9425–9428.
- [390] D. Reiter, P. Frisch, D. Wendel, F. M. Hörmann, S. Inoue, *Dalton Trans.* **2020**, 49, 7060–7068.
- [391] D. Reiter, P. Frisch, T. Szilvási, S. Inoue, *J. Am. Chem. Soc.* **2019**, 141, 16991–16996.

- [392] K. Tokarska, Q. Shi, L. Otulakowski, P. Wrobel, H. Q. Ta, P. Kurtyka, A. Kordyka, M. Siwy, M. Vasylieva, A. Forys, B. Trzebicka, A. Bachmatiuk, M. H. Rummeli, *R. Soc. open sci.* **2020**, *7*, 200736.
- [393] P. G. Jeelani, P. Mulay, R. Venkat, C. Ramalingam, *Silicon* **2020**, *12*, 1337–1354.
- [394] N. Kuhn, T. Kratz, *Synthesis* **1993**, 1993, 561–562.
- [395] D. Hoffman, Personal Communication, Bonn, **2020**.
- [396] A. C. Filippou, O. Chernov, B. Blom, K. W. Stumpf, G. Schnakenburg, *Chemistry – A European Journal* **2010**, *16*, 2866–2872.
- [397] S. U. Ahmad, T. Szilvási, S. Inoue, *Chem. Commun.* **2014**, *50*, 12619–12622.
- [398] M. A. Brook, A. Neuy, *J. Org. Chem.* **1990**, *55*, 3609–3616.
- [399] H. A. Bent, *Chem. Rev.* **1961**, *61*, 275–311.
- [400] L. Pauling, *The Nature of the Chemical Bond and the Structure of Molecules and Crystals: An Introduction to Modern Structural Chemistry*, Cornell Univ. Press, Ithaca, NY, **2010**.
- [401] R. Walsh, *Acc. Chem. Res.* **1981**, *14*, 246–252.
- [402] R. S. Simons, C. T. Haubrich, B. V. Mork, M. Niemeyer, P. P. Power, *Main Group Chemistry* **1998**, *2*, 275–283.
- [403] J. L. Shibley, R. West, D. R. Powell, C. A. Tessier, *Heteroat. Chem.* **1994**, *5*, 205–214.
- [404] H. Cui, P. Teng, E. Zhang, J. Lu, F. Zhang, M. Wu, *Chin. J. Chem.* **2017**, *35*, 401–404.
- [405] G. R. Gillette, G. Noren, R. West, *Organometallics* **1990**, *9*, 2925–2933.
- [406] M. Ann. Pearsall, Robert. West, *J. Am. Chem. Soc.* **1988**, *110*, 7228–7229.
- [407] R. Ciriminna, A. Fidalgo, V. Pandarus, F. Béland, L. M. Ilharco, M. Pagliaro, *Chemical Reviews* **2013**, *113*, 6592–6620.
- [408] R. Schwarz, K. G. Knauff, *Z. Anorg. Allg. Chem.* **1954**, *275*, 176–192.
- [409] M. Goyal, A. Singh, *Main Group Metal Chemistry* **1996**, *19*, DOI 10.1515/MGMC.1996.19.9.587.
- [410] S. Varaprath, D. H. Stutts, *Journal of Organometallic Chemistry* **2007**, *692*, 1892–1897.
- [411] Z. Liu, C. Cui, *Journal of Organometallic Chemistry* **2020**, *906*, 121041.
- [412] H. Cui, Y. Shao, X. Li, L. Kong, C. Cui, *Organometallics* **2009**, *28*, 5191–5195.
- [413] N. Weidemann, G. Schnakenburg, A. C. Filippou, *Zeitschrift für anorganische und allgemeine Chemie* **2009**, *635*, 253–259.
- [414] J. Yang, J. G. Verkade, *Journal of Organometallic Chemistry* **2002**, *651*, 15–21.
- [415] J. Li, Y. Liu, S. Kundu, H. Keil, H. Zhu, R. Herbst-Irmer, D. Stalke, H. W. Roesky, *Inorg. Chem.* **2020**, *59*, 7910–7914.
- [416] A. Gackstatter, H. Braunschweig, T. Kupfer, C. Voigt, N. Arnold, *Chem. Eur. J.* **2016**, *22*, 16415–16419.
- [417] N. Metzler, M. Denk, *Chem. Commun.* **1996**, 2657–2658.
- [418] Y. Suzuki, S. Ishida, S. Sato, H. Isobe, T. Iwamoto, *Angewandte Chemie International Edition* **2017**, *56*, 4593–4597.
- [419] H. Wang, L. Wu, Z. Lin, Z. Xie, *J. Am. Chem. Soc.* **2017**, *139*, 13680–13683.
- [420] S. Khoo, Y.-L. Shan, M.-C. Yang, Y. Li, M.-D. Su, C.-W. So, *Inorganic Chemistry* **2018**, *57*, 5879–5887.
- [421] G. Dübek, F. Hanusch, S. Inoue, *Inorg. Chem.* **2019**, *58*, 15700–15704.
- [422] S. Khoo, C.-K. Siu, C.-W. So, *Inorg. Chem.* **2020**, *59*, 9551–9559.
- [423] M. J. Kraffuss, U. Radius, *Eur. J. Inorg. Chem.* **2021**, *2021*, 548–561.

- [424] M. K. Bisai, V. S. V. S. N. Swamy, K. V. Raj, K. Vanka, S. S. Sen, *Inorg. Chem.* **2021**, *60*, 1654–1663.
- [425] H. Braunschweig, T. Brückner, A. Deißberger, R. D. Dewhurst, A. Gackstatter, A. Gärtner, A. Hofmann, T. Kupfer, D. Prieschl, T. Thiess, S. R. Wang, *Chem. Eur. J.* **2017**, *23*, 9491–9494.
- [426] Z. Mo, T. Szilvási, Y.-P. Zhou, S. Yao, M. Driess, *Angew. Chem.* **2017**, *129*, 3753–3756.
- [427] D. W. Stephan, *Org. Biomol. Chem.* **2008**, *6*, 1535.
- [428] Z. Dong, Z. Li, X. Liu, C. Yan, N. Wei, M. Kira, T. Müller, *Chem. Asian J.* **2017**, *12*, 1204–1207.
- [429] N. Li, W. Zhang, *Chin. J. Chem.* **2020**, *38*, 1360–1370.
- [430] H. Bornemann, W. Sander, *Journal of Organometallic Chemistry* **2002**, *641*, 156–164.
- [431] P. L. Timms, *Inorg. Chem.* **1968**, *7*, 387–389.
- [432] C. Präsang, M. Stoelzel, S. Inoue, A. Meltzer, M. Driess, *Angewandte Chemie International Edition* **2010**, *49*, 10002–10005.
- [433] D. Gau, T. Kato, N. Saffon-Merceron, A. De Cózar, F. P. Cossío, A. Baceiredo, *Angewandte Chemie International Edition* **2010**, *49*, 6585–6588.
- [434] R. Rodriguez, D. Gau, Y. Contie, T. Kato, N. Saffon-Merceron, A. Baceiredo, *Angewandte Chemie International Edition* **2011**, *50*, 11492–11495.
- [435] R. Rodriguez, Y. Contie, Y. Mao, N. Saffon-Merceron, A. Baceiredo, V. Branchadell, T. Kato, *Angewandte Chemie International Edition* **2015**, n/a-n/a.
- [436] A. G. Baradzenka, M. Pilkington, A. Dmitrienko, R. Simionescu, G. I. Nikonov, *Inorg. Chem.* **2021**, *60*, 13110–13121.
- [437] N. Wiberg, A. Wrner, H. Nth, K. Karaghiosof, in *Organosilicon Chemistry II* (Eds.: N. Auner, J. Weis), Wiley-VCH Verlag GmbH, Weinheim, Germany, **1995**, pp. 195–201.
- [438] N. Wiberg, A. Wörner, H.-W. Lerner, K. Karaghiosoff, *Zeitschrift für Naturforschung, B: Chemical Sciences* **2002**, *57*, 1027–1035.
- [439] V. Cappello, J. Baumgartner, A. Dransfeld, K. Hassler, *Eur. J. Inorg. Chem.* **2006**, *2006*, 4589–4599.
- [440] L.-C. Pop, N. Kurokawa, H. Ebata, K. Tomizawa, T. Tajima, M. Saito, *Eur. J. Inorg. Chem.* **2017**, *2017*, 4969–4975.
- [441] C. Mader, O. Wunnicke, S. Martens, J. Lehmkuhl, C. Guenther, *Method for Producing Doped Polycrystalline Semiconductor Layers*, **2015**, DE 2014-102014223465.
- [442] R. Rodriguez, Y. Contie, Y. Mao, N. Saffon-Merceron, A. Baceiredo, V. Branchadell, T. Kato, *Angew. Chem. Int. Ed.* **2015**, *54*, 15276–15279.
- [443] H. Klöcker, M. Layh, A. Hepp, W. Uhl, *Dalton Trans.* **2016**, *45*, 2031–2043.
- [444] J.-C. Hierso, *Chem. Rev.* **2014**, *114*, 4838–4867.
- [445] L. D. Quin, A. J. Williams, *Practical Interpretation of P-31 NMR Spectra and Computer Assisted Structure Verification*, Advanced Chemistry Development, Toronto, **2004**.
- [446] B. Wrackmeyer, in *Modern Magnetic Resonance* (Ed.: G.A. Webb), Springer Netherlands, Dordrecht, **2006**, pp. 455–457.
- [447] J. H. Muessig, P. Lisinetskaya, R. D. Dewhurst, R. Bertermann, M. Thaler, R. Mitrić, H. Braunschweig, *Angew. Chem. Int. Ed.* **2020**, *59*, 5531–5535.
- [448] S. Yadav, E. Sangtani, D. Dhawan, R. G. Gonnade, D. Ghosh, S. S. Sen, *Dalton Trans.* **2017**, *46*, 11418–11424.
- [449] J. D. Erickson, R. D. Riparetti, J. C. Fettingner, P. P. Power, *Organometallics* **2016**, *35*, 2124–2128.

- [450] L. Rösch, G. Altnau, *Angew. Chem.* **1979**, 91, 62–62.
- [451] A. Kämpfe, E. Kroke, J. Wagler, *Organometallics* **2014**, 33, 112–120.
- [452] Y. Xiong, S. Yao, M. Driess, *Chem. Eur. J.* **2009**, 15, 8542–8547.
- [453] S. S. Sen, J. Hey, D. Kratzert, H. W. Roesky, D. Stalke, *Organometallics* **2012**, 31, 435–439.
- [454] I. Gronde, B. Neumann, A. Willner, T. Pape, N. W. Mitzel, *Dalton Trans.* **2009**, 5300.
- [455] S. P. Sarish, A. Jana, H. W. Roesky, P. P. Samuel, C. E. A. Andrade, B. Dittrich, C. Schulzke, *Organometallics* **2011**, 30, 912–916.
- [456] W. Uhl, F. Hannemann, W. Saak, R. Wartchow, *European Journal of Inorganic Chemistry* **1999**, 1999, 771–776.
- [457] In Bruker Almanac, **2012**.
- [458] A. C. Filippou, O. Chernov, K. W. Stumpf, G. Schnakenburg, *Angew. Chem. Int. Ed.* **2010**, 49, 3296–3300.
- [459] R. Pietschnig, *Chem. Commun.* **2004**, 546.
- [460] T. Müller, A. Schäfer, M. Reißmann, A. Schäfer, M. Schmidtman, *Chem. Eur. J.* **2014**, 20, 9381–9386.
- [461] B. Waerder, M. Pieper, L. A. Körte, T. A. Kinder, A. Mix, B. Neumann, H. Stammler, N. W. Mitzel, *Angew. Chem. Int. Ed.* **2015**, 54, 13416–13419.
- [462] H. Cui, M. Wu, P. Teng, *Eur. J. Inorg. Chem.* **2016**, 2016, 4123–4127.
- [463] P. Roesch, R. Müller, A. Dallmann, G. Scholz, M. Kaupp, T. Braun, B. Braun-Cula, P. Wittwer, *Chem. Eur. J.* **2019**, 25, 4678–4682.
- [464] R. K. Harris, E. D. Becker, S. M. Cabral de Menezes, P. Granger, R. E. Hoffman, K. W. Zilm, *Pure and Applied Chemistry* **2008**, 80, 59–84.
- [465] G. M. Sheldrick, *ShelXS97 and ShelXL97*, University Of Göttingen, Germany, **1997**.
- [466] Olex Sys Ltd., *Olex2*, Version 1.2.5, University Of Durham, UK, **2014**.
- [467] K. Brandenburg, *Diamond 2.1c*, Crystal Impact GbR, Bonn, Germany, **1999**.
- [468] H. Putz, K. Brandenburg, *Diamond 4.6.1*, Crystal Impact GbR, Bonn, Germany, **2019**.
- [469] T. Tsuda, T. Yazawa, K. Watanabe, T. Fujii, T. Saegusa, *J. Org. Chem.* **1981**, 46, 192–194.
- [470] J. Hicks, M. Juckel, A. Paparo, D. Dange, C. Jones, *Organometallics* **2018**, 37, 4810–4813.
- [471] J. H. Golden, P. F. Mutolo, E. B. Lobkovsky, F. J. DiSalvo, *Inorg. Chem.* **1994**, 33, 5374–5375.
- [472] R. C. Smith, J. D. Protasiewicz, *Eur. J. Inorg. Chem.* **2004**, 2004, 998–1006.
- [473] K. Ruhlandt-Senge, J. J. Ellison, R. J. Wehmschulte, F. Pauer, P. P. Power, *J. Am. Chem. Soc.* **1993**, 115, 11353–11357.
- [474] J. L. W. Pohlmann, F. E. Brinckmann, *Z. Naturforsch B* **1965**, 20, 5–11.
- [475] G. Brauer, *Handbuch der präparativen anorganischen Chemie: in drei Bänden 2. 2.*, Enke, Stuttgart, **1978**.
- [476] T. Tsuda, T. Hashimoto, T. Saegusa, *J. Am. Chem. Soc.* **1972**, 94, 658–659.
- [477] T. Tsuda, T. Takeda, A. Tsubouchi, in *Encyclopedia of Reagents for Organic Synthesis* (Ed.: John Wiley & Sons, Ltd), John Wiley & Sons, Ltd, Chichester, UK, **2009**.
- [478] A. Tudose, A. Demonceau, L. Delaude, *Journal of Organometallic Chemistry* **2006**, 691, 5356–5365.
- [479] K. Fredenhagen, G. Cadenbach, *Z. Anorg. Allg. Chem.* **1926**, 158, 249–263.
- [480] W. Rüdorff, E. Schulze, *Z. Anorg. Allg. Chem.* **1954**, 277, 156–171.

- [481] S. A. Johnson, J. J. Kiernicki, P. E. Fanwick, S. C. Bart, *Organometallics* **2015**, 34, 2889–2895.
- [482] K. Izod, D. G. Rayner, S. M. El-Hamruni, R. W. Harrington, U. Baisch, *Angewandte Chemie International Edition* **2014**, 53, 3636–3640.
- [483] E. Weiss, G. Sauermann, *Angew. Chem. Int. Ed. Engl.* **1968**, 7, 133–134.
- [484] M. Lehmann, A. Schulz, A. Villinger, *Angew. Chem.* **2009**, 121, 7580–7583.
- [485] Y. Segawa, M. Yamashita, K. Nozaki, *Science* **2006**, 314, 113–115.
- [486] S. Robinson, J. McMaster, W. Lewis, A. J. Blake, S. T. Liddle, *Chem. Commun.* **2012**, 48, 5769.
- [487] M. Hage, C. A. Ogle, T. L. Rathmann, J. L. Hubbard, *Main Group Metal Chemistry* **1998**, 21, 777–782.
- [488] M. L. Luetkens, A. P. Sattelberger, H. H. Murray, J. D. Basil, J. P. Fackler, R. A. Jones, D. E. Heaton, in *Inorganic Syntheses* (Ed.: H.D. Kaesz), John Wiley & Sons, Inc., Hoboken, NJ, USA, **2007**, pp. 7–12.
- [489] R. J. Wright, J. Steiner, S. Beaini, P. P. Power, *Inorganica Chimica Acta* **2006**, 359, 1939–1946.
- [490] P. Jutzi, D. Kanne, M. Hursthouse, A. J. Howes, *Chem. Ber.* **1988**, 121, 1299–1305.
- [491] J.-C. Hierso, D. Armspach, D. Matt, *Comptes Rendus Chimie* **2009**, 12, 1002–1013.
- [492] R. G. Bryant, *J. Chem. Educ.* **1983**, 60, 933.
- [493] N. Kuhn, K. Eichele, M. Walker, *Zeitschrift für anorganische und allgemeine Chemie* **2001**, 627, 2565–2567.
- [494] R. Boese, M. Graw, A. Haas, C. Krüger, A. Mönicke, J. Schlagheck, *Zeitschrift für anorganische und allgemeine Chemie* **1999**, 625, 1261–1272.
- [495] F. Sączewski, M. Gdaniec, K. Data, *Heterocyclic Communications* **2017**, 23, DOI 10.1515/hc-2017-0177.
- [496] R. Westrik, C. H. Mac Gillavry, *Recl. Trav. Chim. Pays-Bas* **2010**, 60, 794–810.
- [497] C. A. Hunter, J. K. M. Sanders, *J. Am. Chem. Soc.* **1990**, 112, 5525–5534.
- [498] A. J. Arduengo, H. V. R. Dias, R. L. Harlow, M. Kline, *J. Am. Chem. Soc.* **1992**, 114, 5530–5534.
- [499] J. Sandström, *Dynamic NMR Spectroscopy*, Academic Press, London ; New York, **1982**.